The petrology and geochemistry of the rossland volcanic rocks, southern British Columbia

Brett Beddoe-Stephens

THE PETROLOGY AND GEOCHEMISTRY OF THE ROSSLAND VOLCANIC ROCKS, SOUTHERN BRITISH COLUMBIA

Brett Beddoe-Stephens, B.Sc.

A thesis submitted for the degree of Doctor of Philosophy in the University of Durham

December 1977

ABSTRACT

The Rossland Volcanic Group is a dominantly clastic succession that accumulated in a back-arc sedimentary basin in Lower Jurassic time. The lava-types preserved are predominantly augite- and plagioclase-phyric basalts and low-SiO_2 andesites, but with some localised and conspicuous ankaramitic varieties. Amphibole is a less common but significant phenocryst in basaltic and andesitic compositions.

Whole-rock and primary mineral (augite and amphibole) chemical data indicate that the Rossland volcanics are of island-arc affinity. However, rather than being a normal calc-alkaline association, they compare more favourably, in some respects, with the recent, ankaramitic associations of the New Hebrides and New Georgia island-arcs. The presence of primary amphibole in the basalts, and the rare occurrence of primary biotite in one low-SiO_2 andesite, also indicate a mildly alkaline, or high-K_2O affinity.

Comparison with the sparse data on contemporaneous (Upper Triassic/Lower Jurassic) volcanics of the Canadian Cordillera, indicates that magmatism similar to that in the Rossland area was also operative along the Upper Triassic, Nicola-Takla axis. In the Lower Jurassic, the bulk of the volcanics in north-central British Columbia were somewhat different, being more evolved in nature and representing the change of the continental margin to that of an Andean type.

The chemistry of the Rossland representatives indicates an upper-mantle origin for the magmas, though only rarely were unmodified partial melts extruded. Rather, as would be expected

from the strongly porphyritic nature of the volcanics, most magmas suffered a degree of polybaric olivine fractionation (during ascent from around 30Kb) and crustal level (2-7 kb) fractionation of olivine + Cr-spinel + clinopyroxene + amphibole + Ti-magnetite + plagioclase.

Metamorphism of the volcanics occurred in Middle Jurassic time, during the early phases of the Columbian orogeny. Consideration of the secondary-mineral assemblages and chemistry, indicates that a progressive regional metamoprhism affected the volcanics, varying from the prehnite-pumpellyite facies, through the greenschist, to the epidote-amphibolite facies. This gradation is from south to north and probably culminates, north of the area, in the Valhalla gneiss dome of the Shuswap complex.

Oxygen isotope ($^{18}O/^{16}O$) data further show that during metamorphism the volcanics exchanged oxygen considerably with a pervasive hydrothermal fluid, enriching them in ^{18}O ($\delta^{18}O$ = 8-11 $^{o}/oo$) relative to their original magmatic values ($\delta^{18}O \simeq 6^{o}/oo$). The origin of the hydrothermal fluid is enigmatic, but is most probably either extremely ^{18}O-enriched meteoric water or is water released during prograde metamoprhism of deeper level sediments and which percolates upwards.

ACKNOWLEDGEMENTS

I firstly wish to thank N.E.R.C. for the award of a Research Studentship and the opportunity to visit the field area and University of Alberta in Canada.

Research facilities at Durham were made available by Professor G.M. Brown and Professor M.H.P. Bott as successive heads of department.

I am also very grateful to my supervisors, Professor G.M. Brown and Dr. J.G. Holland for various discussions and advice during the course of this research, and in particular I would like to thank Professor G.M. Brown for critically reading the manuscript.

I especially wish to thank Professor R. St.J. Lambert for his hospitality and help, in both logistical and academic matters, during my stay in Canada, and for making available laboratory facilities at the Department of Geology, University of Alberta. Dr. K. Muehlenbachs, who contributed considerable time and energy in instructing me in the theory and analysis of oxygen isotopes, receives my grateful thanks.

For instruction in the use of the electron microprobe I wish to thank Dr. A. Peckett and Dr. R.H. Pinsent, and for help in X-ray fluorescence analysis I wish to thank Dr. J.G. Holland and Mr. R.G. Hardy. Probe slides and thin sections were prepared by Mr. G. Randall and Mr. L. MacGregor, respectively, and help in the production of various photographic plates was received from Mr. G. Dresser. Mr. R. Lambert gave instruction in the methods of analysing for H_2O and FeO.

Particularly, I am grateful to Dr. R. Powell for spending time compiling thermodynamic data for my use, and for discussions on mineral equilibria in metamorphic rocks.

Less directly, help was received through discussions on many aspects of petrology from contemporaneous research students, namely Mr. I. Williamson, Miss E.A. Hoey, Mr. R.M. Forster, Mr. A.H. Al-Khamees, Mr. R.H. Hunter and Mr. T.L. Hamilton (University of Alberta).

Finally, I wish to thank Mrs. J. McArthur for patiently typing the manuscript.

LIST OF CONTENTS

LIST OF FIGURES

LIST OF TABLES

LIST OF PLATES

CHAPTER 1

INTRODUCTION

1:1 Scope of research

The Lower Jurassic Rossland volcanics of southern British Columbia are a petrologically little studied group of rocks, especially with regard to modern techniques of chemical analysis. In addition, schemes of tectonogenesis (e.g. Monger et al., 1972) are generally based on sparse data where the older volcanics of the Canadian Cordillera, such as the Rossland group, are concerned. Thus, the main purpose of this research is to investigate petrologically, the nature of the Rossland volcanics within the framework of modern ideas relating to petrogenesis and volcano-tectonic associations.

The first part of this thesis, then, deals with this aspect, whereas the second is concerned with the metamorphism of the volcanic rocks. Again, this aspect of the volcanic petrology has received only passing attention and research here is aimed at elucidating the nature of the metamorphic alteration, using, principally, mineral chemistry and oxygen isotope geochemistry.

1:2 Field-area: location, physiography and access

The Rossland volcanics form an arcuate belt, about fifty miles in length and ten miles in width, between the towns of Nelson and Rossland in the Kootenay region of British Columbia (Figs. 1.1, 1.2). The area falls within the Geological Survey of Canada 'Nelson map-area (west half)', the general geology of which is described by Little (1960).

Fig. 1.2 shows the physiographical setting of the area; the Rossland volcanics, for the most part, lying within the

Figure 1.2

Maps showing the geographical and physiographical setting of the Nelson-Rossland area.
(from Little, 1960)

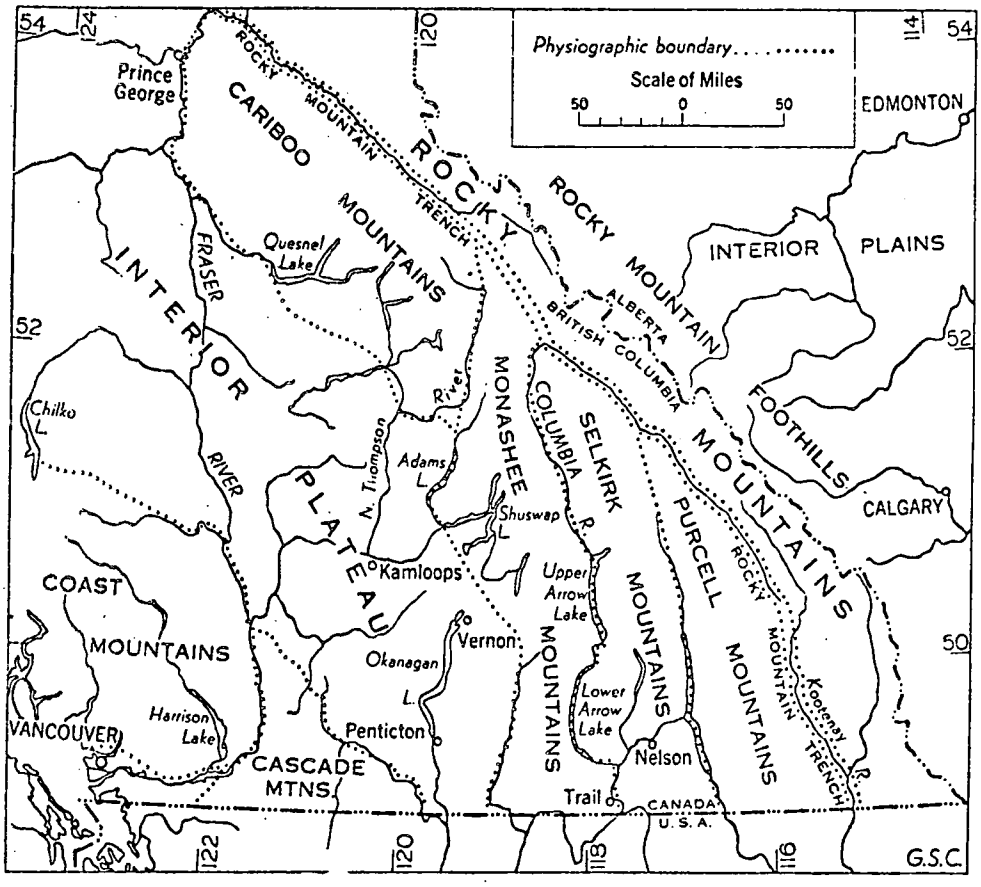
Physiographic boundary.....
Scale of Miles
50 0 50
Prince George
CARIBOO MOUNTAINS
ROCKY MOUNTAIN TRENCH
ROCKY MOUNTAINS
INTERIOR PLATEAU
INTERIOR PLAINS
FOOTHILLS
ALBERTA
BRITISH COLUMBIA
EDMONTON
CALGARY
Quesnel Lake
FRASER RIVER
Chilko L.
N. Thompson River
Adams L.
MONASHEE MTS.
COLUMBIA R.
SELKIRK MTS.
PURCELL MTS.
ROCKY MOUNTAIN TRENCH
Shuswap L.
Kamloops
Upper Arrow Lake
Lower Arrow Lake
Okanagan L.
Vernon
Penticton
Nelson
Trail
COAST MOUNTAINS
VANCOUVER
Harrison Lake
CASCADE MTNS.
Kootenay R.
CANADA
U. S. A.
G.S.C.

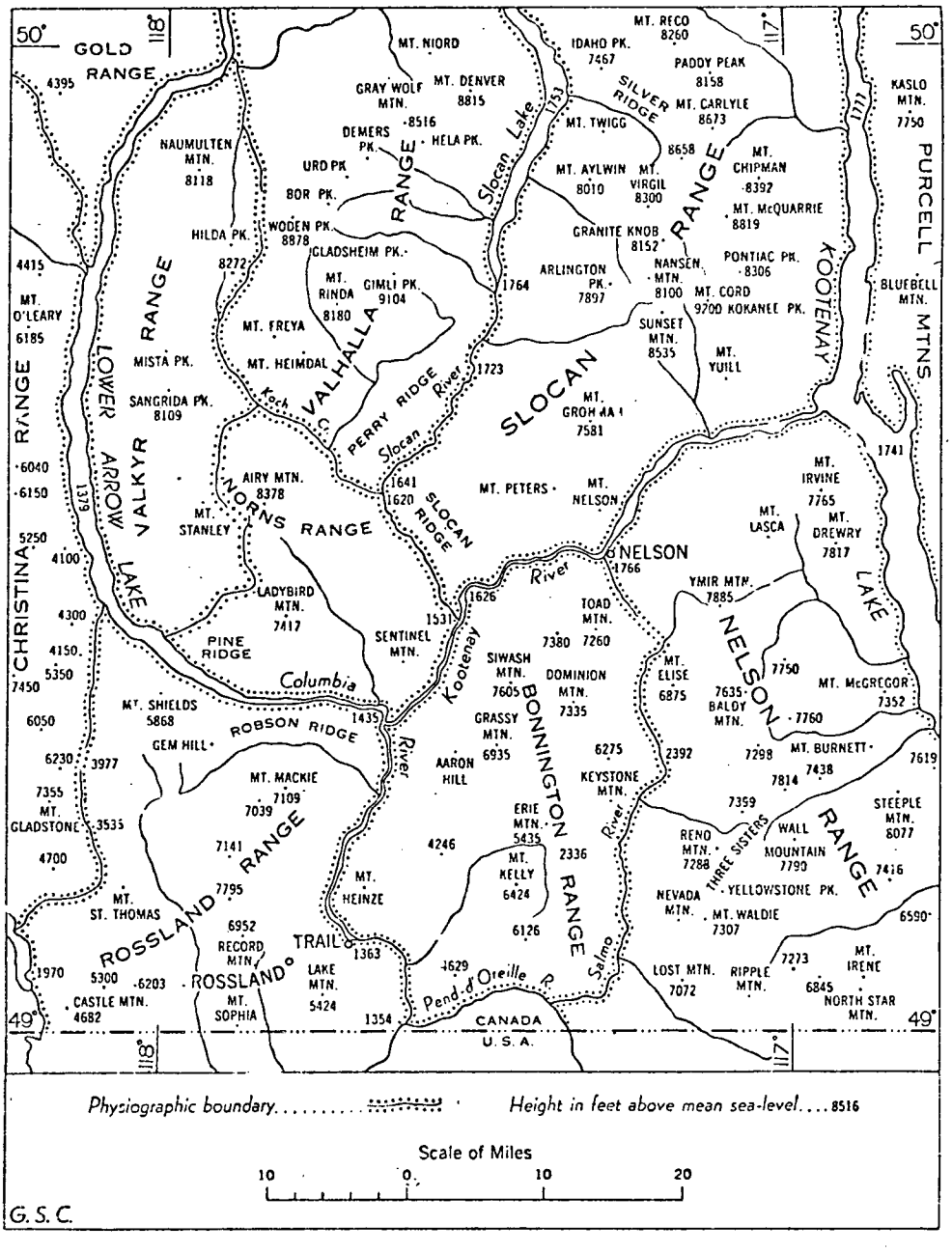
GOLD RANGE
MT. NIORD
GRAY WOLF MTN.
MT. DENVER 8815
DEMERS PK. 8516
HELA PK.
NAUMULTEN MTN. 8118
URD PK.
BOR PK.
HILDA PK. 8272
WODEN PK. 8878
GLADSHEIM PK.
MT. RINDA
GIMLI PK. 9104
8180
MT. FREYA
MISTA PK.
MT. HEIMDAL
SANGRIDA PK. 8109
LOWER ARROW LAKE
VALKYR RANGE
VALHALLA RANGE
CHRISTINA RANGE
MT. O'LEARY 6185
AIRY MTN. 8378
MT. STANLEY
NORNS RANGE
LADYBIRD MTN. 7417
PINE RIDGE
MT. SHIELDS 5868
GEM HILL
ROBSON RIDGE
MT. MACKIE 7109
7039
MT. GLADSTONE 3535
7141
ROSSLAND RANGE
MT. ST. THOMAS 7795
MT. HEINZE
ROSSLAND
6952
RECORD MTN.
TRAIL
LAKE MTN. 5424
MT. SOPHIA
CASTLE MTN. 4682
1970
5300
6203
1363
1354
Slocan Lake
Slocan River
Kootenay River
PERRY RIDGE
SLOCAN RIDGE
SLOCAN RANGE
MT. GROHMAN 7581
MT. PETERS
MT. NELSON
SILVER RIDGE
MT. RECO 8260
IDAHO PK. 7467
PADDY PEAK 8158
MT. CARLYLE 8673
MT. TWIGG
MT. AYLWIN 8010
MT. VIRGIL 8300
MT. CHIPMAN 8392
MT. McQUARRIE 8819
GRANITE KNOB 8152
ARLINGTON PK. 7897
NANSEN MTN. 8100
PONTIAC PK. 8306
MT. CORD 9700
KOKANEE PK.
SUNSET MTN. 8535
MT. YUILL
KOOTENAY RANGE
NELSON
MT. LASCA
MT. IRVINE 7765
MT. DREWRY 7817
YMIR MTN. 7885
TOAD MTN. 7260
SENTINEL MTN. 7380
SIWASH MTN. 7605
DOMINION MTN. 7335
GRASSY MTN. 6935
AARON HILL
KEYSTONE MTN. 6275
ERIE MTN. 5435
MT. KELLY 6424
BONNINGTON RANGE
MT. ELISE 6875
BALDY MTN. 7635
MT. McGREGOR 7352
MT. BURNETT 7619
RENO MTN. 7288
THREE SISTERS
WALL MOUNTAIN 7790
STEEPLE MTN. 8077
NEVADA MTN.
YELLOWSTONE PK.
MT. WALDIE 7307
LOST MTN. 7072
RIPPLE MTN.
MT. IRENE 7273
6845
NORTH STAR MTN.
KASLO MTN. 7750
PURCELL MTNS.
BLUEBELL MTN.
LAKE
Pend-d'Oreille R.
Salmo
CANADA
U. S. A.
Physiographic boundary.....
Height in feet above mean sea-level....8516
Scale of Miles
10 0 10 20
G. S. C.

Plate 1

Looking northwest towards Dominion Mountain. Upper slopes are underlain by Nelson intrusive rocks. Lower slopes by the Rossland volcanics.

Plate 2

Looking east from sample locality 4065. Wooded slopes in the foreground are underlain by volcanics. Rugged peaks in the distance form the Cambrian Quartzite range of the Kootenay Arc (Chapter 2).

Plate 3

Looking southeast from Champion Lakes. Foreground wooded area is underlain by Rossland volcanics and Archibald Formation sediments.

Plate 4

Looking south from the peak one mile southeast of Mt. Kelly (cf. sample location 4051). Wooded slopes in foreground are underlain by Rossland volcanics.

Plate 5

Summit of Mt.Kelly, looking northeast. Crags in the foreground are composed mainly of bedded and massive agglomerates and bedded,fine volcaniclastic horizons.

Plate 6

Summit of Mt.Kelly, looking northwest. Wooded slopes below crags are volcanics, underlain by Archibald Formation sediments in the valley bottom.

Bonnington Range of the southern Selkirk Mountains. The Bonnington Range is around 6,000 - 7,500 feet high, with some 3,000 - 4,000 feet of relief. Generally, to the north this range is more rugged and less vegetated, being underlain in greater part by granitic rocks (Plates 1,2), whilst to the south, the peaks are more subdued and heavily wooded, and volcanic rocks predominate (Plates 3,4).

Although highway links the towns of Nelson, Salmo, Fruitvale, Trail and Rossland (Fig.1.2), access to the areas underlain by volcanics is problematic due to the invariably dense forest cover. Locally, particularly near Mt.Kelly (G.R. 680440, Fig.1.1), exposure is reasonable and accessible by means of forestry tracks (Plates 5,6).

1:3 Sampling and analytical techniques

The samples used in this study were collected in 1974 and 1975 from throughout the area of the volcanics (Fig.1.1), together with some samples collected by Professor R. St.J. Lambert (University of Alberta) and Dr. J.G. Holland (University of Durham) in 1973. Collection was predominantly from highway and forestry road-cuts on account of the poor exposure and accessibility referred to above. An exception was the Mt.Kelly area. Appendix 1 lists descriptive and location data for the samples collected.

Samples were sectioned and crushed for petrographical and chemical study, partly at the Department of Geology, University of Alberta, and whole-rock chemical analyses made by XRF at Durham (Appendix 2). Mineral analyses were performed by electron microprobe, also at Durham (Appendix 3). Mineral separations and oxygen extractions for $^{18}O/^{16}O$ ratio determination were carried out at the University of Alberta, and mass-spectrometer runs were kindly performed by Dr. K. Muehlenbachs (Appendix 4).

CHAPTER 2

GEOLOGIC BACKGROUND

2:1 Regional geologic and tectonic setting

This section deals, primarily, with the broad geologic and tectonic environment in the Cordilleran region at the time of Rossland volcanic activity, and provides a framework within which further discussion can be based.

In sections 2:1:1 and 2:1:3 below, are discussed, briefly, the sequence of events leading up to and following on from the period of interest, namely the Upper Triassic and Lower Jurassic; whereas section 2:1:2 deals in more detail with this period.

The location of the Rossland volcanics in relation to the various large-scale, Cordilleran volcano-tectonic features discussed below, is illustrated in Figs. 2:1, 2:2 and 2:3. It can be seen that the Rossland volcanics lie well within the southern Ominica Belt and that they are apparently isolated from the main concentration of contemporaneous volcanics in the Intermontane Belt.

2:1:1 Pre-Mesozoic

From Fig.2:1 it can be seen that a number of distinct tectonic belts parallel the present-day continental margin, the Cordillera in Canada being uniformly wide. Further south, within the U.S.A., the Cordillera is considerably broader from east to west. Whilst this reflects the rather different histories of the two regions, in part this is due to the original extent of the craton about which the younger rocks of the Cordillera developed.

The edge of the basement, or craton, was established by rifting in the Precambrian and apart from southern California is situated well east of the present-day continental margin. North of 50^{o}N it is situated beneath the Rocky Mountain Trench (Fig.2:2),

Figure 2.1

Regional tectonic divisions of the Canadian Cordillera.

RV - Rossland Volcanics
RMB - Rocky Mountain Belt
OCB - Ominica Crystalline Belt
QT - Quesnel Trough
PG - Pinchi Geanticline
IB - Intermontane Belt
CPC - Coast Plutonic Complex
IN - Insular Belt

Dashed line in the USA is the division between the mio-and eugeosyncline (King, 1969).

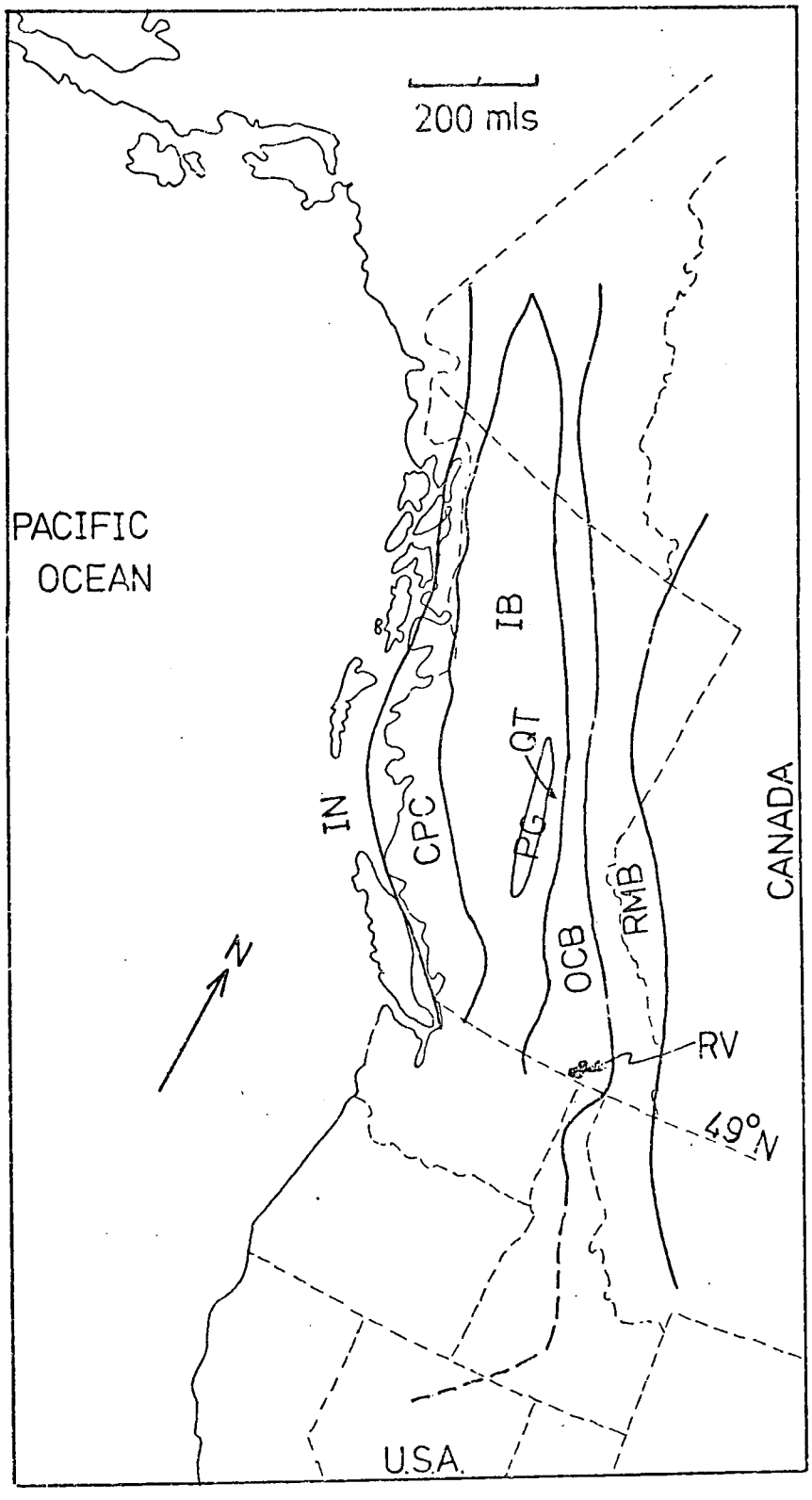
200 mls
PACIFIC
OCEAN
IB
QT
IN
CPC
PG
RMB
OCB
CANADA
N
RV
49°N
U.S.A.

Figure 2.2

Major tectonic lineaments and other features of Western North America (see text for discussion).

A Inferred edge of Archaean basement

B $^{87}Sr/^{86}Sr$ dividing line (Armstrong et al., 1977)

C Late Triassic/Early Jurassic subduction zone. (Dickinson, 1976)

D Crustal blocks (thickness in km.) deduced from gravity data (Berry et al., 1971).

RMT - Rocky Mountain Trench
PF - Pinchi Fault
YF - Yalakom-Fraser Fault system
TF - Tintina Fault
TS - Teslin Fault
SDF - Shakwak-Denali Fault system
QCF - Queen Charlotte Fault
JFR - Juan da Fuca ridge
RV - Rossland volcanics

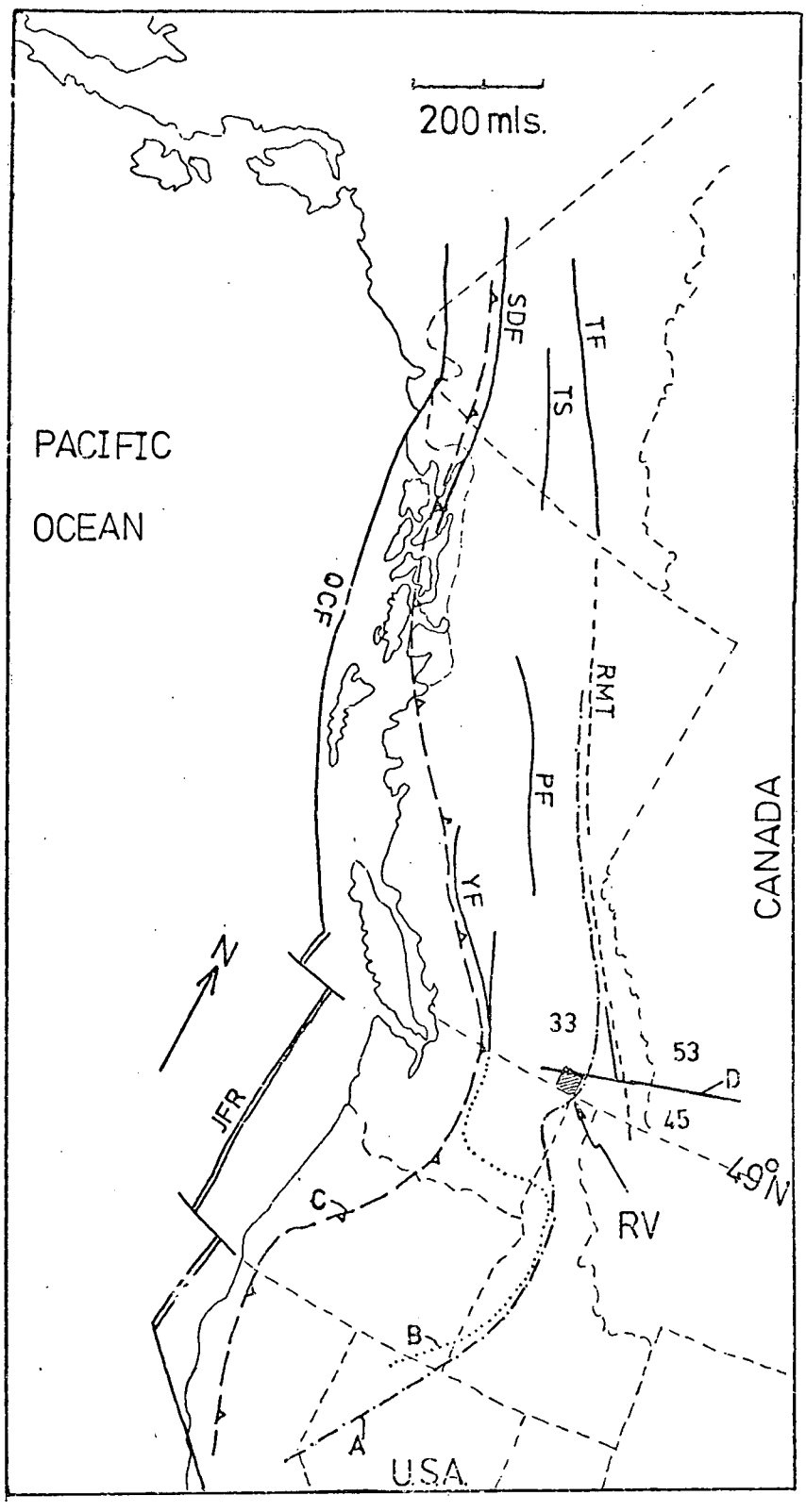
200 mls.
PACIFIC
OCEAN
SDF
TF
TS
OCF
RMT
PF
YF
CANADA
N
JFR
33
53
D
45
49°N
C
RV
B
A
USA

where crust of 50 km.thickness gives way to 35 km.-thick crust to the west (Berry et al., 1971). Near 49^{0}N, seismic refraction studies indicate the craton as extending further west beneath the Ominica Belt (Bally et al., 1966). Similarly, gravity data quoted in Berry et. al., (1971) indicate a block of 45 km.-thick crust extending from southern Alberta into British Columbia (Fig.1.2). This possible westward extension of the basement may be an offset related to the Precambrian rift-like structure identified by Kanasewich et al. (1968) in Alberta and which has been traced westward as far as the Rocky Mountain Trench (D in Fig.2.2).

Some data published by Armstrong et al. (1977) are pertinent to this problem. In the north-west U.S.A., an accurate line can be drawn between Mesozoic and Cenozoic plutons having an initial $^{87}Sr/^{86}Sr$ ratio of less than 0.7040 to the west and those with a ratio greater than 0.7055. Line B in Fig.2.2 shows the trace of this boundary and it can be seen that it crosses the International Boundary well west of the Rossland area. Though a similar line has not been drawn in Canada, consideration of the data of Petö (1974) shows it probably continues north-west into the Intermontane Belt just east of the Coast Belt intrusions which have an average initial $^{87}Sr/^{86}Sr$ of 0.7038. The Nelson Batholith, which cuts the Rossland volcanics, has a ratio of 0.7069. Armstrong et al. (1977) consider this line to represent the edge of Precambrian basement, including rocks of at least 500-1500 my. It may not, therefore, involve Archaean craton of 2000 my. and older (Gabriesle, 1972). That rocks of at least 1600 my. are enclosed to the east by this boundary, is confirmed in north-central Washington by Mattinson (1972), though these rocks may be reactivated ocean crust (Misch, 1966). Thus the Rossland volcanics may or may not overlie

cratonic basement; the data are not clear and it is hoped the study here may place some constraints.

Sedimentation in the Cordillera began some 1250 my.ago with the Purcell and Belt supergroups of the southern Omnica Belt and northern Idaho. They were followed by the Windermere supergroup at about 850 my. Both these successions in the Rossland area lie east of the volcanics as shown in Fig.2.4 and section 2:2. Gabriesle (1972) suggests both successions built out from the trailing edge of the craton, which rifted 1600 my.ago. Stewart (1972), on the other hand, suggests that rifting followed the Purcell/Belt phase and is represented by conglomerates and volcanics at the base of the Windermere group (Fig. 2.4). This episode, the East Kootenay orogeny, is seen alternatively by, for example, Monger et al. (1972), as a short-lived subduction phase.

In the late Devonian and early Mississippian, the Caribooan orogeny (Fig. 2.5) ended the Atlantic margin phase (Dickinson, 1976) of the Cordillera and recorded the obduction of ophiolitic assemblages onto the platform sediments of the miogeocline. These rocks are preserved in areas of the Ominica Belt (Monger et al., 1972). A similar event occurred in the U.S.A. during the Antler orogeny.

Following these events, late Palaeozoic volcanic arcs developed in the Ominica Belt (Monger, 1975) and in the U.S.A. (Schweickert, 1976). They were apparently situated on crust of an oceanic nature. West of the arc, oceanic rocks occur in the Intermontane Belt as represented by the Cache Creek group (Monger, 1975) and a subduction zone, causal to the volcanic arc, possibly lay along the Pinchi fault (Fig. 2.2), where localised blueschists occur (Paterson & Harakal, 1974).

2:1:2 Upper Triassic and Lower Jurassic

By this time, accumulation of material during the previous subduction episode apparently caused an oceanward stepping, or shifting, of the subduction zone to a site marked by the Fraser-Yalakom fault system in southern British Columbia. Further north, as shown by C in Fig.2.2, it transgressed the present-day Coast Plutonic Belt to link up with the Shakwak-Denali fault system (Monger, 1975; Dickinson, 1976).

Also, by this time, allochthonous arc complexes, built on Lower Palaeozoic basement, had been rafted into place in south-east Alaska (Jones et al., 1972) from a possible site in California (Schweickert, 1976).

During this period, subduction was continuous along most of the Cordillera producing the extensive and voluminous volcanics of the Nicola-Takla groups in Canada (Fig.2.3) and the various groups in the Western U.S.A. noted by Rogers et al., (1974). In the north-west U.S.A. the arc is not well defined; however, 190-210 my. plutons in Washington (Armstrong et al., 1977) record the presence of a magmatic arc in this region. Similarly, in Canada a number of ~200 my plutons lie along the Nicola-Takla axis and the Pinchi geanticline (Fig.2.1) (Douglas et al., 1970; Gabriesle & Reesor, 1974).

A problem during this period is the movement and location of the Vancouver Island segment of the Insular Belt. It is agreed that in the Upper Triassic the subduction zone responsible for the volcanic arc lay in the position indicated in Fig.2.2 (Monger et al., 1972; Monger, 1975; Dickinson, 1976; Anderson, 1976). However, the first two papers suggest that by the start of the Jurassic suturing of the Vancouver Island block to the main continent had occurred. This view is based, primarily, on the change in character of volcanism on Vancouver Island from submarine tholeiitic

type to explosive calc-alkaline, which is thought to be evidence of a further westward shift in active subduction. Dickinson (1976) notes though, that if this were so then the belt of active volcanism in southern British Columbia would be 500 km. wide, far in excess of that to the north. He suggests the arc volcanics in the Insular belt may be a northern extension of those caught up in the Sierra Foothills subduction complex of California. The identification of the Upper Triassic tholeiites of Vancouver Island as island-arc tholeiites (Souther, 1972; Griffiths, 1977), rather than ocean-basin tholeiites (Monger et al., 1972), tends to corroborate the view that two subduction zones were operative. In addition, the continuation of arc-trench gap sedimentation into the Jurassic, in southern British Columbia (Anderson, 1976), indicates the continuing presence of the Fraser-Yalakom subduction zone during the Rossland volcanic episode. Certainly, by 160 my. palaeomagnetic evidence shows Vancouver Island to be at a latitude indistinguishable from that of the mainland, whereas in the Upper Triassic this is not so (Symons, 1972; Irving & Yole, 1969). Suturing was probably complete, then, by Middle or early Late Jurassic when volcanism apparently became restricted to north-central British Columbia (J.G. Souther, in press).

The nature and distribution of volcanics (Fig.2.3) comprising the Upper Triassic/Lower Jurassic arcs is discussed, in more detail and where relevant, elsewhere in this thesis. Here it is sufficient to note that the volcanics preserved are largely fragmentary varieties developed in basins around the emerging Pinchi geanticline. Additionally, the mainly Upper Triassic Nicola-Takla rocks are predominantly basic, comprising augite-phyric basalts and basaltic andesites (Monger, 1975). By contrast, Jurassic volcanics such as the Hazelton group (Fig.2.3) are generally more differentiated, with feldspathic andesitic and dacitic varieties. This probably reflects

Figure 2.3

Distribution of Upper Triassic (black) and Lower Jurassic (horizontal shading) volcanics.

Major groups:

T Takla
H Hazelton
B Bonanza
K Karmutsen
N Nicola
RV Rossland volcanics

(mainly taken from Souther, in press).

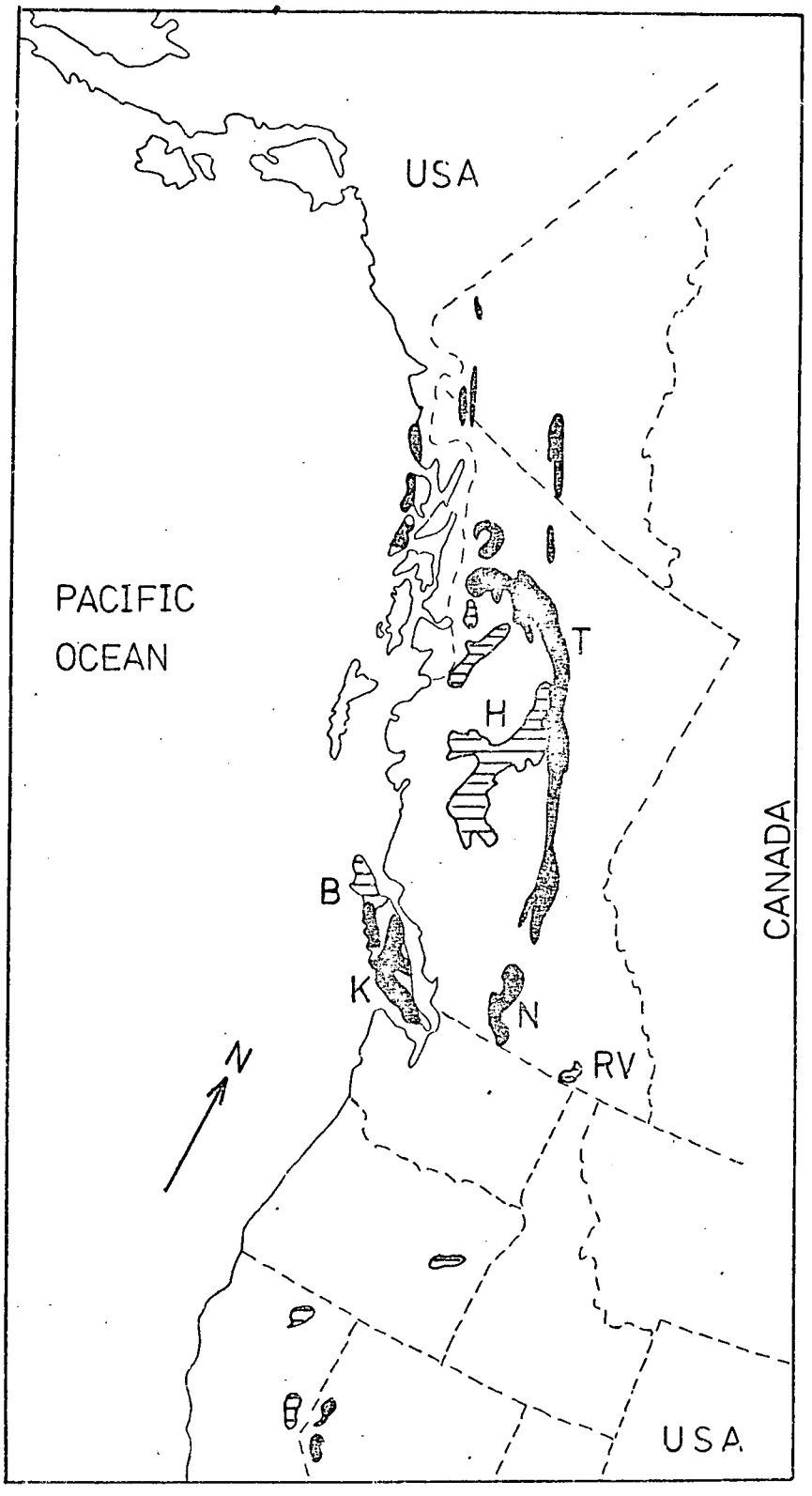
USA
PACIFIC
OCEAN
T
H
B
K
N
RV
CANADA
N
USA

the development of the Cordillera towards an Andean variety (Dickinson, 1976).

Within this tectonic framework, the Rossland volcanics (see Fig. 2.3) are somewhat anomalously situated, lying as they do east of possibly emergent areas of the Ominica belt and within the essentially non-volcanic Alberta trough (see Fig. VIII-32e of Douglas et al., 1970). Flysch-like sediments of the Slocan, Ymir and Archibald groups (see Section 2:2:2 and Fig.1.1) of the Rossland area are apparently westerly derived. However, the Rossland volcanics lie on a southerly projection of the Quesnel trough (Fig.2.1), which contains lithologically and temporally similar volcanics (Campbell & Tipper, 1971), and this belt may have been continuous.

2:1:3 Post-Lower Jurassic

Following the essentially offshore-island, volcanic-arc regime of the period described in Section 2:1:2 (see also Stanley et al., 1971), emergence of the Ominica and Coast Belts caused a restriction of the sedimentary areas and gave rise to the characteristic 'successor basin' regime (Douglas et al., 1970). By the late Cretaceous, the Cordillera was totally emergent, though active subduction continued as evidenced by the massive plutonic emplacement in the Coast Belt. Comagmatic with these plutons, highly differentiated and explosive volcanics were erupted (J.G.Souther, in press; Souther, 1967), characteristic of an Andean continental margin.

In the Ominica Belt, accompanying the intrusion of batholiths, deformation and metamorphism of the Columbian orogeny occurred (see Fig.2.4). In the south of this belt, this orogeny was heralded by the intrusion of 165 my.plutons, such as the Nelson Batholith. Migration eastwards of deformation subsequently gave

rise to the prominent décollement thrusting in the Rocky Mountain Belt in the early Tertiary (Wheeler & Gabriesle, 1972).

From the Miocene onwards, extensional rather than compressive stresses prevailed over most of the Canadian Cordillera. Reflecting this was a marked change in the character of associated volcanism from that of continental calc-alkaline to an alkaline plateau-basaltic phase. Causal to this change was the spread along the continental margin of transform motion (Queen Charlotte Fault - Fig.2.2) with active subduction being limited to the northwest U.S.A. (J.G. Souther, in press).

2:2 Local Geology

2:2:1 Pre-Mesozoic

In Fig. 1.1 it can be seen that in general, separated from Mesozoic rocks by thrust faulting, are pre-Mesozoic strata grouped under unit 1. These are the steeply dipping, tightly folded sediments of the Kootenay Arc (Ross, 1970 and Fig.2.4), which are the local representation of the early (Proterozoic to Devonian) miogeocline and the later (Permo-Trias) eugeosyncline. Fig.2.5 shows the general sequence of events in the Nelson-Rossland area.

East of the Rossland volcanics (Fig.2.4), fine-grained, siliceous clastics and carbonates of the Purcell group reach 14,000 m. in thickness and are overlain unconformably by the coarser and less mature sediments of the Windermere group. Intercalated in this succession are local, basic volcanic units, for example the Irene Formation (Rice, 1941).

The Palaeozoic was initiated during calmer sedimentary conditions (Little, 1960), with the deposition of a westerly thickening and fining sandstone, now the Cambrian Quartzite Range Formation. Further north in the Kootenay Arc, this unit is the Hamil Formation

Figure 2.4

Geology of the southern Ominica Belt showing the relation of the Rossland area to the Shuswap Complex and Kootenay Arc (from Campbell, 1966).

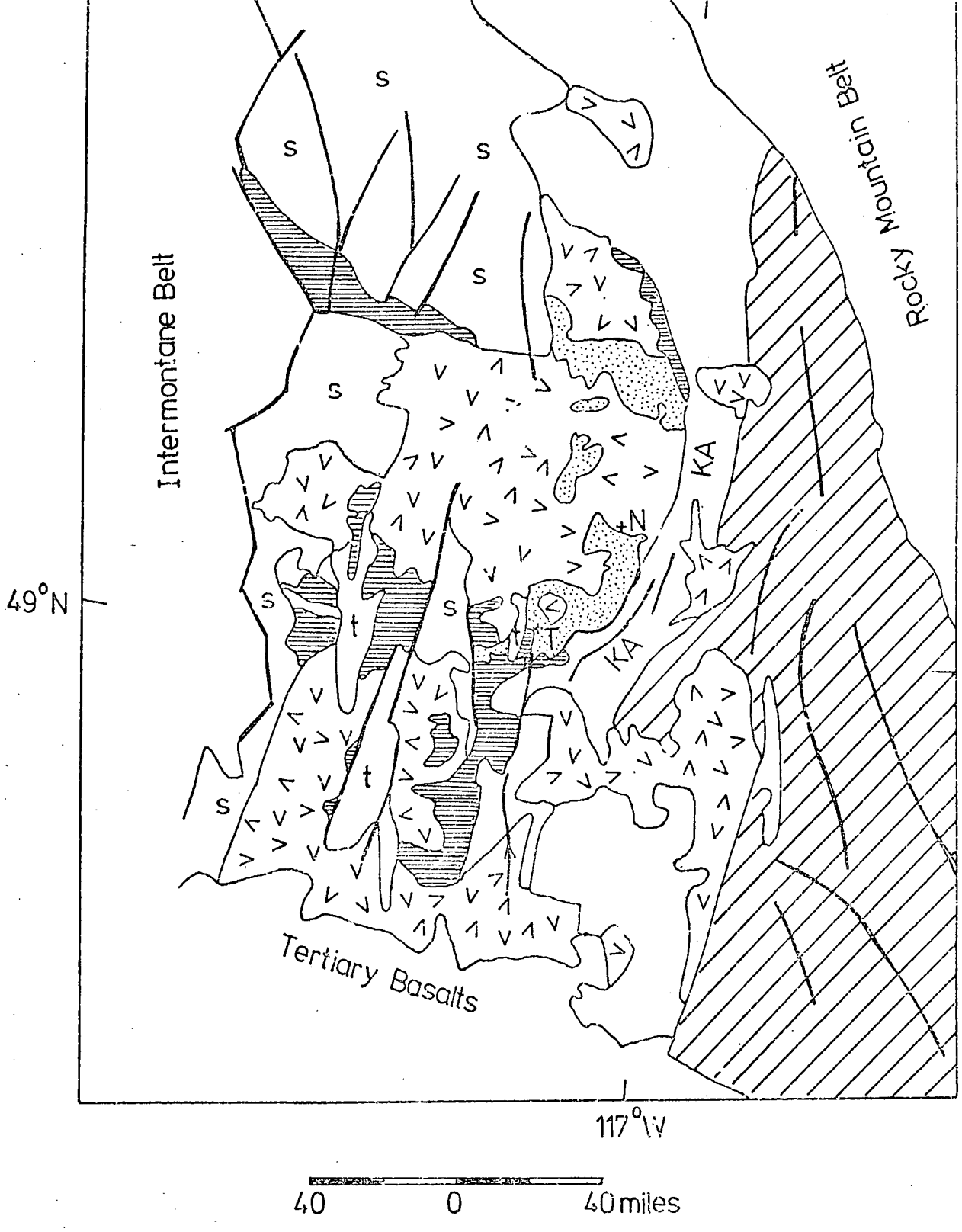
Intermontane Belt
Rocky Mountain Belt
Tertiary Basalts
KA
KA
+N
+T
s
t
49°N
117°W
40 0 40 miles
t Tertiary
U.Triassic/L.Jurassic
Carboniferous/Permian
Windermere to Devonian
Purcell
s Shuswap Complex
Batholiths (mainly Mesozoic)
+N Nelson
+T Trail
KA Kootenay Arc

Figure 2.5

Stratigraphic column for the Nelson-Rossland area of the Ominica Belt (after Douglas et al.,1970).

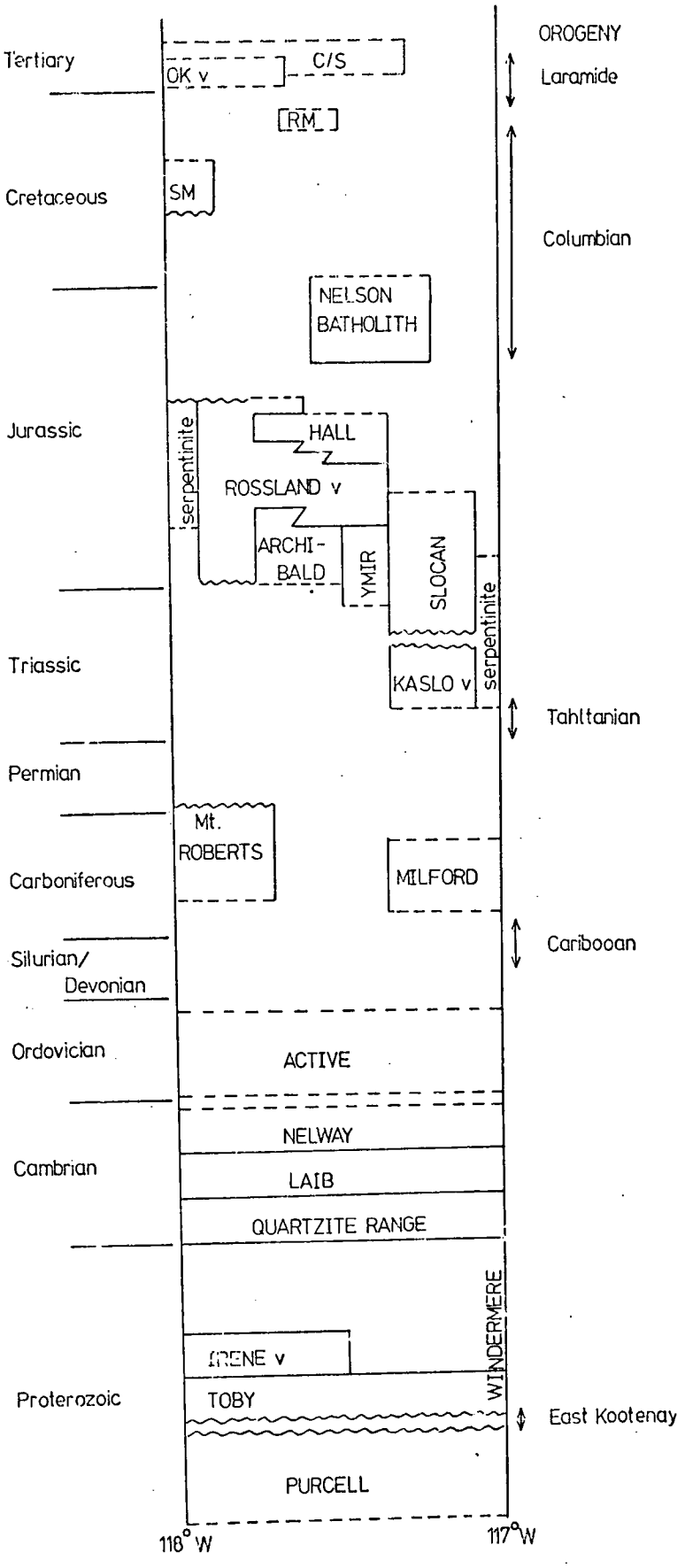
OROGENY
Laramide
Columbian
Tahltanian
Caribooan
East Kootenay
Tertiary
Cretaceous
Jurassic
Triassic
Permian
Carboniferous
Silurian/
Devonian
Ordovician
Cambrian
Proterozoic
OK v
C/S
RM
SM
NELSON
BATHOLITH
serpentinite
HALL
ROSSLAND v
ARCHI-
BALD
YMIR
SLOCAN
serpentinite
KASLO v
Mt.
ROBERTS
MILFORD
ACTIVE
NELWAY
LAIB
QUARTZITE RANGE
WINDERMERE
IRENE v
TOBY
PURCELL
118° W
117° W

(Ross, 1970). Subsequent Cambrian and Ordovician sediments comprise a similarly, easterly-derived sequence of argillites and calcareous shales.

In the southernmost end of the Canadian Kootenay Arc, deposition then apparently ceased or became very intermittent, though further north the Devonian Broadview Formation occurs (Douglas et al., 1970). Prior to the deposition of the Pennsylvanian Milford and Mt.Roberts sediments, folding, thrusting and low-grade metamorphism occurred, as shown in Fig. 2.5. The Milford and Mt.Roberts successions are broadly contemporaneous and were probably linked, the assemblage of limestones, cherts, quartzites and argillites being common to both (Douglas et al., 1970). The Mt.Roberts formation can also be linked with the Cache Creek Group of the Intermontane Belt (Campbell, 1966).

2:2:2 Mesozoic and Cenozoic

Following the Milford Group in the Kootenay Arc are the Permo-Trias Kaslo and Slocan Groups, now preserved to the north and east of the Rossland volcanics. The Kaslo Group is a succession of altered agglomerates, tuffs and flows with localised bodies of serpentinite (Rice, 1941). Monger (1975) includes this group in the late Palaeozoic to Mid-Triassic belt of volcanic-arc affinity, noted in Section 2:1:1.

The Slocan Group, overlying the Kaslo Group disconformably, consists of predominantly argillaceous sediments, containing some well-developed slaty facies, and possibly reaches thicknesses of 12,000 m. (Irwin, 1951), though this may be due to undetected folding. Further south and conformably underlying the Rossland Volcanics in the Ymir map-area (Fig.1.1) is the Ymir Group.

Despite a lack of fossil evidence (McAllister, 1951; Little, 1960), it seems that this group is an extension of the Slocan, since a discontinuous chain of roof pendants in the Nelson Batholith appear to link the two.

Underlying the Rossland volcanics in the Salmo area (Fig.1.1), the sediments are termed the Archibald Formation (Little and Frebold, 1962). These sediments, though lithologically similar to the Ymir Group, are fossiliferous, containing ammonites which date the sequence as Hettangian to Lower Sinemurian. In part they are probably correlative with the Ymir Group (see Fig.3.1). The Archibald Formation is about 4,000 feet thick in the type locality of Archibald Creek (G.R. 715 460, Fig.1.1). Lithologies in this succession include mainly argillitic siltstone and mudstone, with less common beds of greywacke, volcaniclastics and quartzite. In the coarser facies, clasts of K-feldspar, plagioclase and altered ferro-magnesian minerals occur with a relatively low abundance of quartz, indicating a volcanic and/or plutonic source terrain. In addition, the occurrence of common graded bedding, and a lack of cross bedding, suggest a distal, turbiditic sedimentary environment.

Above the Ymir and Archibald sediments is the dominantly volcanic Rossland Group or Elise Formation. This succession forms the basis of this thesis and is discussed in further chapters.

The youngest sedimentary rocks in the area, apart from the local Sophie Mountain conglomerates (Fig. 2.5), are the Hall Formation sediments which overlie, conformably, the volcanics. This sequence is Toarcian to Bajocian (Frebold, 1959; Little & Frebold, 1962). In Kelly Creek (G.R. 665 405, Fig.1.1), the Hall Formation is overlain by agglomerates and volcaniclastics of the Upper Rossland Group (Little, 1962; 1964), but in the type locality of Hall Creek (G.R. 800 700, Fig.1.1), the top is

not exposed, the Formation occupying the core of a syncline. Lithologies found in the Hall Creek locality include siltstones, greywackes and conglomerates (Mulligan, 1952). Volcanigenic components are common. The presence of cross bedding and plant remains (Little & Frebold, 1962), together with the occurrence of conglomerates suggest a shallow-water environment. This presumably reflects the beginning of emergence of the Ominica Belt during early phases of the Columbian orogeny.

Later rocks in the area are almost totally intrusive, belonging predominantly to the Nelson Batholith. This was emplaced in the Middle and Late Jurassic (Nguyen et al., 1968; Gabriesle & Reesor, 1974), clearly over a period of time, since in places the rocks are foliated parallel to the structural trend. This is particularly evident in the southern tail of the batholith and in the Silver King Porphyry (Fig.1.1; unit 8d) that intrudes the volcanics (Mulligan, 1952 and writer's observations). Younger phases of the batholith, on the other hand, are clearly discordant; for example in the Eerie Creek, Dominion Mountain area (Fig.1.1).

Petrographically, the Nelson intrusions are mainly biotite and hornblende granodiorites, usually bearing K-feldspar phenocrysts (Little, 1960; Gabriesle & Reesor, 1974). Less abundant quartz diorite and quartz monzonite facies also occur. The Silver King Porphyry, referred to above, is a distinctive rock type. It is pale-green in colour and contains rounded, milky-white to pale-green oligoclase phenocrysts about 0.5 to 1.0 cm. in diameter. Chemical analyses of samples from this body are included in Appendix 3.

Younger intrusive rocks of the Trail Batholith, Rossland Monzonite and Coryell Batholith occur southwest of Nelson Batholith

(Fig.1.1). Dates on these rocks by Fyles et al. (1973) suggest the Rossland Monzonite is at least 90 my. old, whereas the Coryell and Trail Batholiths give K-Ar biotite dates of 48-50 my. Compared to the Nelson representatives, this Tertiary suite is much more alkaline, comprising monzonites, syenites and syenodiorites (Gabriesle & Reesor, 1974). They are probably comagmatic with the OK volcanics (Fig.1.1) and lamprophyre dykes of the region, also dated around 50 my. by Fyles et al, (1973).

Other rocks in the area include a serpentinite body near the town of Rossland (G.R. 415 360, Fig.1.1) and a gabbro-syenite complex near Nelson which was named the 'Bonnington Complex' by Mulligan (1952) (G.R. 700 800, Fig.1.1, units 8a, b, c).

The former body is emplaced in the Mt.Roberts and Rossland Volcanic Groups and is apparently older than the Nelson Batholith since it is cut by porphyritic granodiorite veins. It has, generally, highly sheared contacts (J.T.Fyles, in preparation) and was probably tectonically emplaced along northeasterly striking faults called the 'Rossland Break' by Fyles (op.cit).

The Bonnington Complex includes what Mulligan (1952) calls 'pyroxene-hornblende-biotite' rock and 'pseudodiorite'. The former he believed to be a metasomatic contact facies of the volcanics. This, however, is not the case and in fact it is a clinopyroxene-rich cumulate derived from the Rossland magmas, as is shown later. The pseudodiorite is a gabbroic rock, again probably related to the volcanics. The petrography and chemistry of these rocks is discussed in chapters 4 and 5. Gradational with the pseudodiorite is a syenitic rock, though this may be a phase of the Nelson Batholith (Mulligan, 1952).

CHAPTER 3

ROSSLAND VOLCANIC GROUP:

INTRODUCTION AND GENERAL DESCRIPTION

3:1 History of research

The Rossland Volcanic Group was named initially by McConnell & Brock (1904) from exposures near the town of Rossland (Fig.1.1), to which they assigned a Carboniferous age. This was on the basis of fossils collected from the nearby Mt. Roberts Formation. A separate 'Beaver Mountain' Group was also named, by McConnell & Brock (op.cit.), for apparently fresher volcanics on Mt.Kelly (previously Beaver Mountain - Fig.1.1).

Daly (1912), in mapping the International Boundary strip, similarly divided the volcanics and also separated them from the Mt.Roberts Formation. 'Massive and schistose' volcanics near Rossland were grouped with the Carboniferous strata, whereas the apparently younger, latitic volcanics of the same area were linked with the Beaver Mountain succession, though Daly (op.cit.) noted the lack of latites in the Mt.Kelly area.

From petrographic work on the younger volcanics near Rossland, Daly (1912) recognised a diversity of lava types; olivine basalt, olivine-free basalt, augite andesite and a variety of latitic types bearing common biotite and hornblende. Analyses completed at this time, and also quoted by Little (1960), show these rocks to be alkalic, particularly in regard to K_2O. One analysis of an 'augite porphyrite' (Drysdale, 1915 and table I in Little, 1960) is substantially different in that K_2O is much less than Na_2O. The significance of this is discussed later.

Subsequently, Walker (1934), in mapping the Salmo area, thought the distinction between the Rossland and Beaver Mountain Groups too

artificial, and on the scale of one-inch-to-one-mile regarded them as a single extrusive-intrusive complex.

However, mapping in three adjacent areas by McAllister (1951), Mulligan (1952) and Little (1950) reinstated a twofold division of the volcanics, extending it to the area between Nelson and Salmo. Volcanics lying above the Ymir Group and below the Hall Formation, were regarded as older than those west of, and apparently above, the Hall sediments (Fig.1.1). In addition, sediments in Archibald Creek were mapped as Hall Formation and could be seen to underlie volcanics there. Thus, the Beaver Mountain (Mt.Kelly) Group was extended north towards Toad Mountain (G.R.763 733, Fig.1.1). The older volcanics overlying the Ymir Group were termed the Elise Formation.

Revision of this scheme came about following more detailed fossil collections in the area (Frebold, 1959; Frebold & Little, 1962). The Archibald Creek sediments were recognised as older than the Hall Formation. Subsequently, Little (1962, 1964) discovered 'Hall' rocks overlying the Beaver Mountain volcanics in Kelly Creek (Fig.1.1). Volcanic rocks, then, from throughout the Nelson-Trail belt, were henceforth regarded as of the same age and were grouped, by Little (1960), under the description 'Rossland Formation'. Later, Little (1962, 1964) reverted to the term 'Elise Formation' following the naming of the Upper Rossland Group, a localised, fault-bounded block of volcanics overlying the Hall Formation in Kelly Creek (Fig.1.1). Fig. 3.1 summarises the local stratigraphy of the area as it now stands.

While the situation, as described, now appears clear for the area between Nelson and Trail, the volcanics in the immediate vicinity of Rossland provided further controversy. Little (1960)

represented rocks on Record Ridge, OK Mountain, Grey Mountain and Old Glory Mountain (see Fig.1.1) as belonging to the Rossland Formation of Lower Jurassic age. Subsequently, Little (1963) noted the Old Glory Mountain representatives were much younger, possibly Tertiary, and distinctly more alkalic than the bulk of the volcanics. Fyles (1970; in prepn.) and Fyles et al. (1973) also rejected the Record Ridge, OK Mountain and Grey Mountain volcanics as being Lower Jurassic and renamed them the 'OK Volcanic Group'. K-Ar dates on these rocks give an age of about 51 my. (Fyles et al., 1973). It is from this group that Daly's (1912) latites were taken and analysed; thus these analyses, though occasionally quoted as belonging to the Rossland volcanics (e.g. Souther, in press), bear no relation to them. Drysdale's (1915) analysis of an augite porphyrite, though, is a Rossland volcanic representative.

3:2 Age and correlation

Resulting from the researches described above, is the fact that the Rossland volcanics were erupted and deposited between Sinemurian and Toarcian or Bajocian time. Viewed in more detail, the precise ages of the base and top of the succession vary from area to area. Fig.3.1, based on illustrations in Frebold & Little (1962) and Little (1963), shows that in the Fruitvale to Parks area, volcanics locally appear to underlie part of the Archibald Formation, whereas in Archibald Creek they occur only above it (Figs. 1.1 and 3.1). Near Rossland, the volcanics lie unconformably on the Mt.Roberts Formation (Little, 1960; Fyles, 1970), indicating a possible earlier initiation of volcanicity in this area. Also, within the volcanics here, Sinemurian sediments are intercalated.

Figure 3.1

Correlation diagram for the Mesozoic rocks of the Nelson-Rossland area.

1 Ymir Map-area
2 Keystone Mountain area
3 Mt.Kelly succession (Fig.3.2)
4 Bell Creek area
5 Blizzard Mountain - Fruitvale area
6 Rossland area

(refer to Fig.1.1 for locations)

Approximate thicknesses (where estimable) are given in thousands of feet.

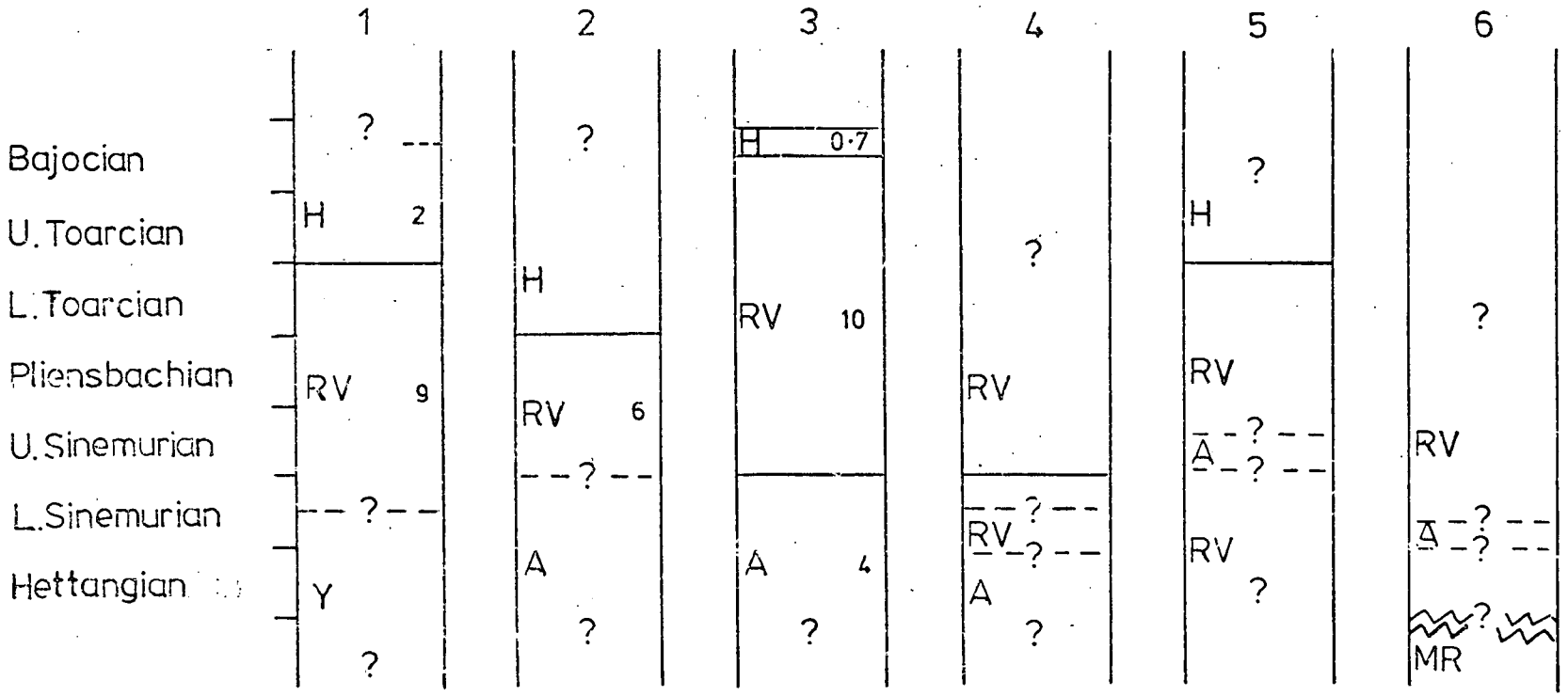

KEY

H Hall Formation

RV Rossland Volcanics

A Archibald Fm.

Y Ymir Group

MR Mt. Roberts Fm.

Similarly, the top of the volcanic succession shows transgressive time relations. In the Ymir area, where initiation of vulcanicity was possibly earlier, the Hall Formation is older (Toarcian) than in the Mt.Kelly area (Bajocian). The extent of the Upper Rossland Group is unknown.

Thicknesses of the succession vary from around 8,000 feet in the Ymir area to possibly 10,000 feet in the Mt.Kelly area.

The extent of the Rossland Volcanics south of the International Boundary is limited, and they can only be traced about ten miles south where they occur in localised, fault-bounded outcrops (Yates, 1970; Yates & Engels, 1968). To the north of Nelson there is little sign of the Rossland Volcanics, probably due to the greater intensity of uplift and metamorphism within the Shuswap Complex (Fig.2.4). However, in the Nakusp area, eighty miles north of Rossland, Hyndman (1968) correlates, tentatively, augite-bearing greenstones with the Rossland Group. It seems likely that the volcanics were originally much more widespread.

On a broader scale, similarly aged volcanic rocks are found predominantly in the Intermontane Belt of central and northern British Columbia. These are termed the Hazelton Group (Tipper, 1959; Tipper & Richards, in press). Underlying the Hazelton Group, and also occurring in the Quesnel Trough (see Figs. 2.2 and 2.3), are the predominantly Upper Triassic Takla Group. The Quesnel Trough Takla volcanics are considered, by Campbell (1960) and Campbell & Tipper (1971), to be, in part, Sinemurian in age.

The Nicola volcanics directly west of Rossland in the Intermontane Belt (Figs. 2.2, 2.3) are also predominantly Upper Triassic (Cockfield, 1948; Rice, 1947; Schau, 1970), though again the Lower Jurassic may be represented (Campbell & Tipper, 1971; Anderson, 1976).

Lower to Middle Jurassic volcanics are also found on Vancouver Island, belonging to the Bonanza Group. These are similar to the Intermontane volcanics but, as was shown in Chapter 2, are thought to be allochthonous and associated with a different subduction zone (Griffiths, 1977).

3:3 Lithological and field characteristics

A feature of the Rossland Volcanic Group, throughout the area of the map (Fig.1.1), is the high proportion of fragmentary rocks, ranging from coarse agglomerates, conglomerates and breccias to tuffaceous and fine volcaniclastic material. On the other hand, distinct, massive flows are rare. This, as will be shown, is a general characteristic of contemporaneous volcanics elsewhere in the Canadian Cordillera. Fig. 3.2 is a generalised section from Archibald Creek to Kelly Creek (see Fig.1.1) and illustrates the varieties of lithology present, and which are described in more detail below.

Though the above-named lithologies in reality form a continuum, they are described, for convenience, under separate headings below.

3:3:1 Fine-grained fragmentary rocks

In this broad group are described tuffaceous and volcaniclastic rocks with a grain-size of less than about 5 mm., and averaging around 1 mm.

These varieties occur throughout the area, but are particularly abundant near Mt.Kelly (Fig.3.2). Here, the rocks are relatively well exposed and, as is shown in Chapter 6, are comparatively texturally and mineralogically unaltered, compared to volcanics further north. Thus, most of the description below is based on samples collected in this area. Despite this, the rocks in the field are grey-green in colour and well indurated, reflecting a moderate degree of alteration.

Figure 3.2

Generalised lithological section across Mt.Kelly (see Fig.1.1) illustrating abundances of rock types discussed in Chapter 3.

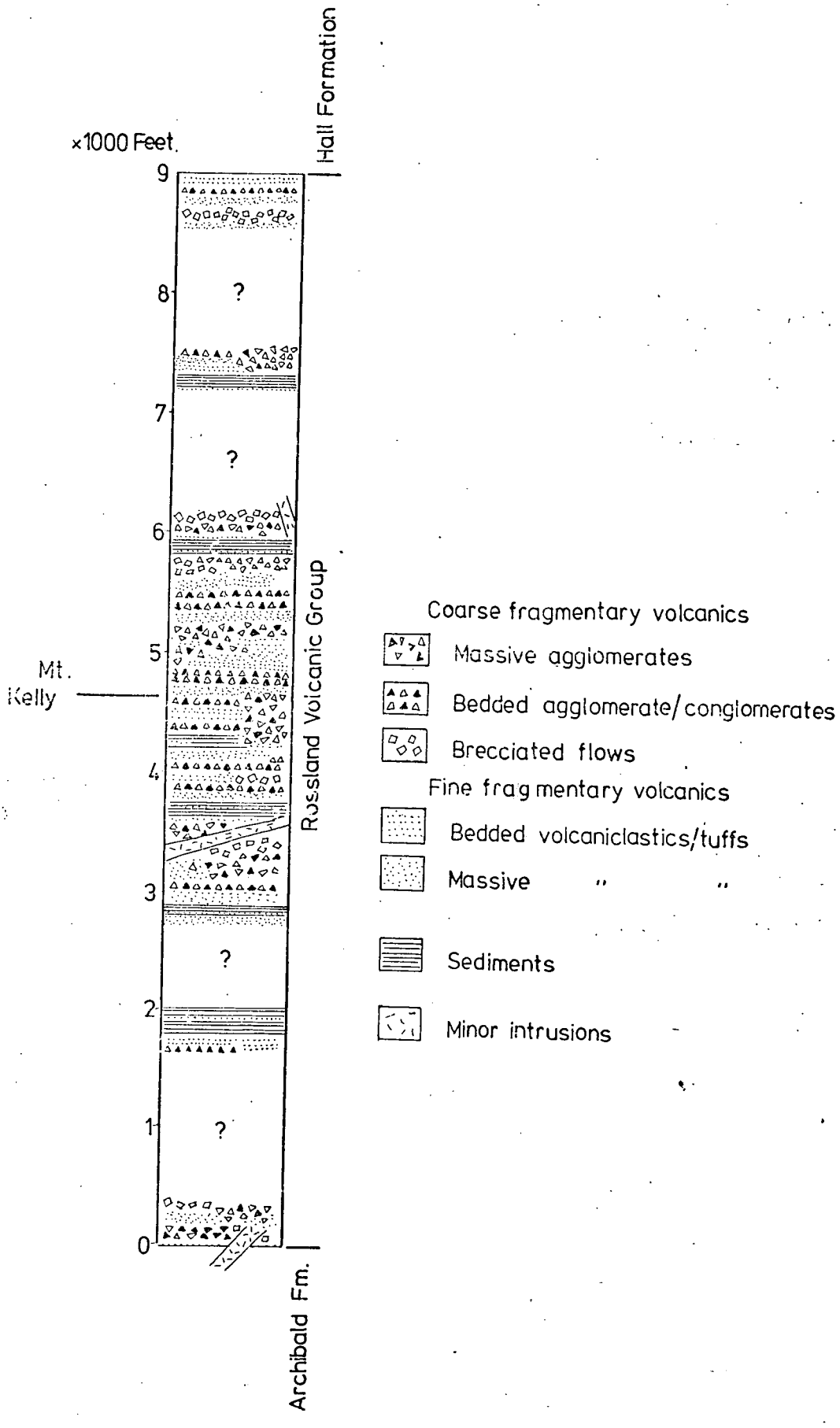
×1000 Feet.
9
8
7
6
5
4
3
2
1
0
?
?
?
?
Hall Formation
Rossland Volcanic Group
Archibald Fm.
Mt.
Kelly
Coarse fragmentary volcanics
Massive agglomerates
Bedded agglomerate/conglomerates
Brecciated flows
Fine fragmentary volcanics
Bedded volcaniclastics/tuffs
Massive " "
Sediments
Minor intrusions

Primary tuffaceous rocks occur sporadically in the section (Fig. 3.2), though they are not easily distinguishable from reworked volcaniclastics in the field. In thin-section, however, they are identifiable by being characteristically badly sorted, with broken crystal and lithic fragments set in an originally dusty matrix, though the latter is invariably chloritised or altered to clay minerals (Plate 7). Lithic fragments are almost totally volcanic, corresponding to the augite and plagioclase-phyric lava-types that characterize the area. Some of the larger fragments can be seen to be vesicular, while others are not and show evidence of derivation by explosive disintegration of previously consolidated lava. Rarely, fine, devitrified, glassy fragments are observed that show signs of being fluid or plastic during deposition (Plate 8). Crystal fragments are invariably augite, plagioclase or primary amphibole, again corresponding to the local abundance of phenocrysts. In any one sample, not all species are necessarily present. Plates 9 and 10 illustrate these characteristics. Though, in the Mt.Kelly area, augite and primary amphibole are typically unaltered (i.e. not amphibolised), those occurring as clasts in the tuffaceous (and volcaniclastic) rocks are commonly more altered along margins and fractures to chlorite and, rarely, uralite, than the same minerals in a crystalline matrix. This is a function of the ease of access of circulating fluids during hydrothermal alteration or metamorphism.

In some tuffaceous varieties, quartz grains are common (Plate 9). These are usually broken and strained, and are probably derived from underlying sediments rather than representing contemporaneous igneous phenocrysts, since they occur only as individual fragments and are not observed enclosed by any crystalline matrix.

Plate 7

Photomicrograph: Tuffaceous rock consisting principally of broken and angular plagioclase fragments with altered oxides, chloritised rock fragments and mafics. Matrix is highly altered to fine aggregates of epidote and chlorite. (Sample 5097. Field width = 4 mm.).

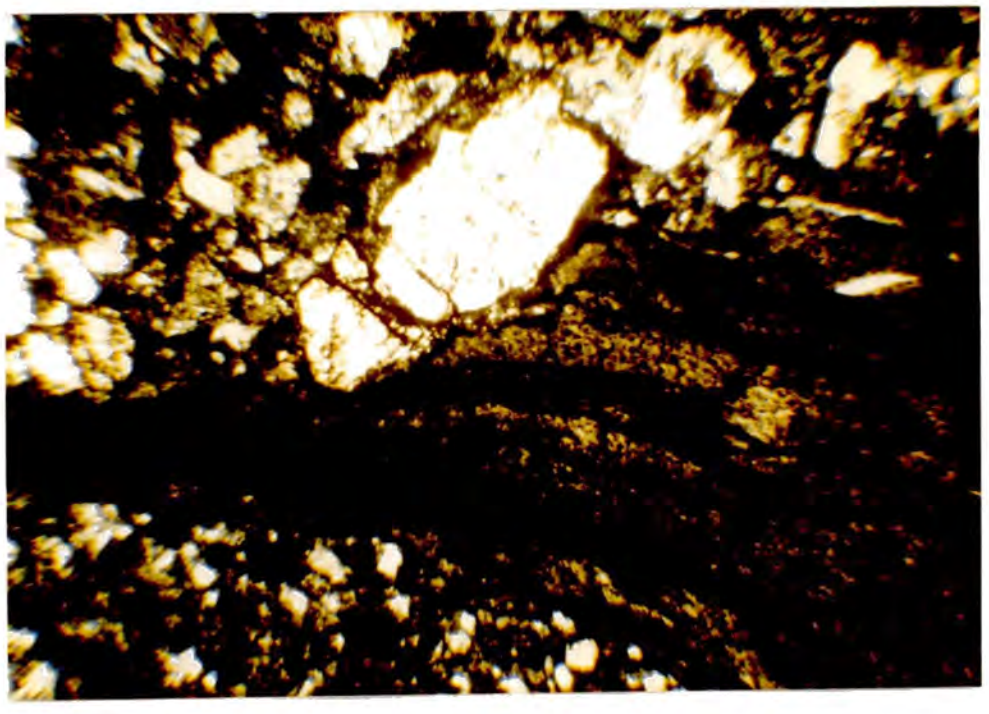

Plate 8

Photomicrograph: Glassy fragment (devitrified) in a fine agglomeratic rock, showing plastic deformation during deposition. (Sample 4076. PPL. Field width = 4 mm.).

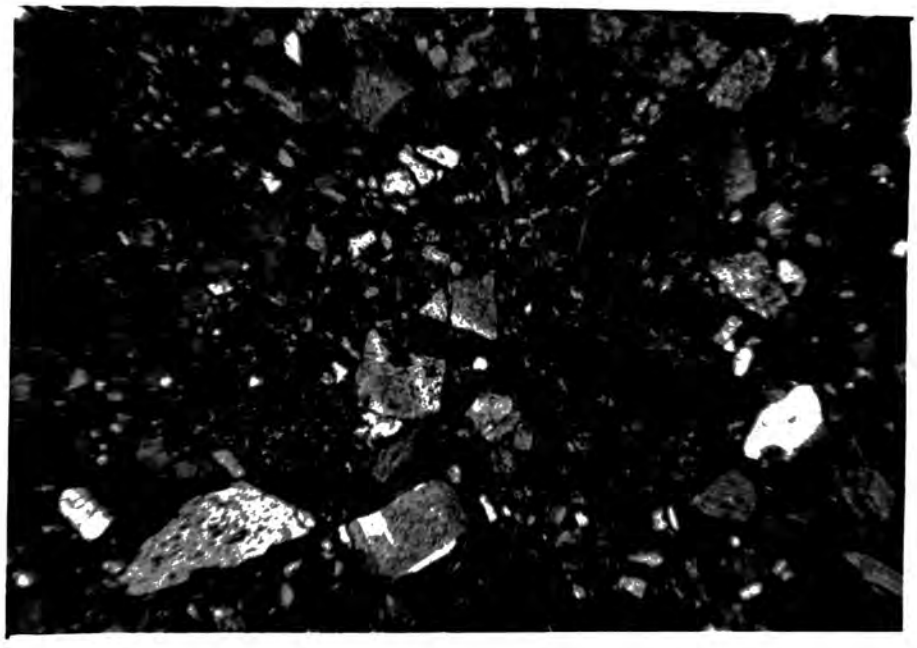

Plate 9

Photomicrograph. Tuffaceous rock consisting of plagioclase, amphibole and, less commonly, quartz grains. Chloritised rock fragments are abundant. Note the angularity and variety of size of the clasts. (Sample 5029, Field width = 4 mm.).

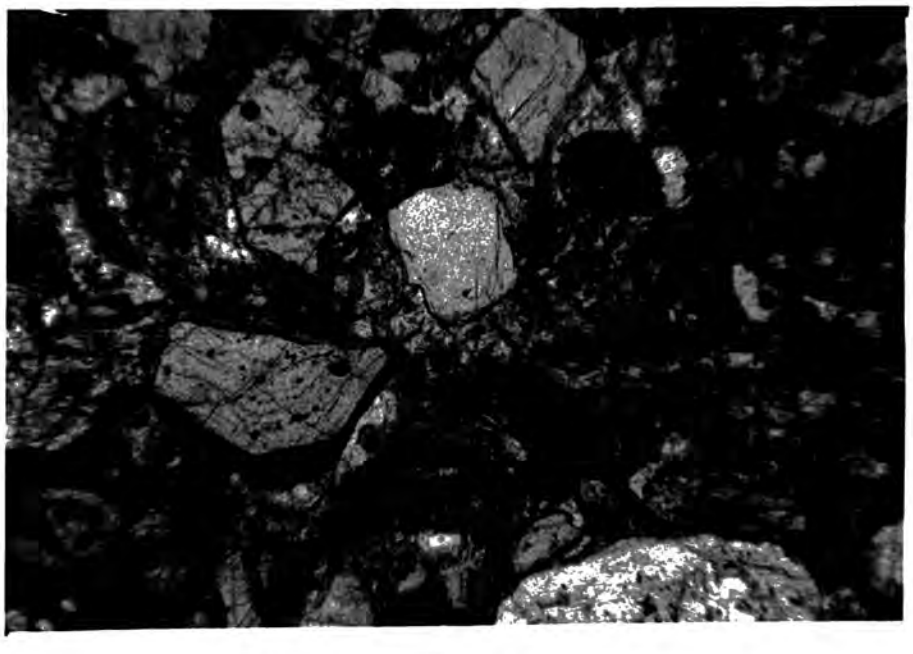

Plate 10

Photomicrograph: tuff/volcaniclastic composed of angular but slightly rounded fragments of pyroxene, plagioclase or rock. Small amount of calcite forms interstially to the fragments (Sample 5008, Field width = 4 mm.).

The tuffaceous rocks are commonly well bedded but are locally massive, lacking easily definable internal structure, and, where they are well indurated and charged with crystal fragments, can resemble porphyritic lavas or minor intrusions, especially as their field-relations are invariably obscured. Similar observations are reported by Fyles (in prepn.) on the volcanic rocks of the Rossland Camp.

No evidence was seen, either in the field or in thin-section, for the presence of ignimbritic or welded ash-flow deposits, such as characterize the continental margin calc-alkaline, andesitic to rhyolitic magmatism. Pyroclastic material, as noted, appears to be predominantly airfall deposits of cool, fragmentary debris.

In apparently greater abundance are water-reworked derivatives of primary tuffaceous material. The presence of marine sediments throughout the succession of Fig.3.2 testifies to the aqueous nature of the environment, at least at times, during the period of volcanism. It seems likely that much pyroclastic debris fell directly into the sea and was thus immediately available for reworking. In addition, the grey-green colouration of the volcanics generally, is suggestive of sub-aqueous conditions; since where the environment was subaerial at the same time, for example in the Hazelton area of British Columbia, red and purple colouration is common (Monger & Church, 1977).

Bedding in these volcaniclastic horizons is usually distinct, with fine laminations reflecting grain-size variation and the relative proportions of the constituent clasts. Whilst internal laminations are on the order of 1 to 5 cm., individual beds or units range from 1 m. to at least 10 m. As with tuffaceous horizons, thicker and more massive crystal-bearing units can resemble porphyritic crystalline rocks.

In thin-section, contrasting with primary material, fragments of the fine-grained volcaniclastics are rounded to subangular and are better sorted, indicating a tendency for any fine volcanic dust to be winnowed out (Plates 11, 12). Often a calcitic matrix infills the resultant pore space. Fragment types are generally identical to those described above. Horizons in which mafic crystal clasts are either absent or completely altered, tend to be associated with, and grade into sedimentary horizons, possibly indicating a higher degree of transport and weathering prior to deposition. On the contrary, volcaniclastic beds bearing abundant augite or amphibole fragments, tend to occur interbedded with agglomerates and conglomerates, and were rapidly buried. It is especially noticeable at the very top of the Fig.3.2 succession, and within the overlying Hall Formation, that volcaniclastics are rich in feldspathic components, augite and amphibole being quite rare (Plate 12).

In the volcanics north and north west of Salmo, where the degree of metamorphism is appreciably higher (Chapter 6), and where the rocks are locally sheared or schistose, field relations are less clear. However, it is frequently possible to detect laminated greenstones intercalated with more massive, structureless greenstones, and which are clearly original pyroclastic or volcaniclastic horizons. Apart from sporadically occurring sedimentary units, these relict beds are the only indicators of structure in this area.

3:3:2 Coarse-grained fragmentary rocks

Fragment sizes included under this heading range from around 1 cm. to 10 cm.,with, rarely, blocks in some breccias reaching 1 m.

Agglomeratic rocks commonly occur as massive, structureless units up to 25m. thick. A good locality for such lithologies, again within the Mt.Kelly area, is on the summit of the mountain

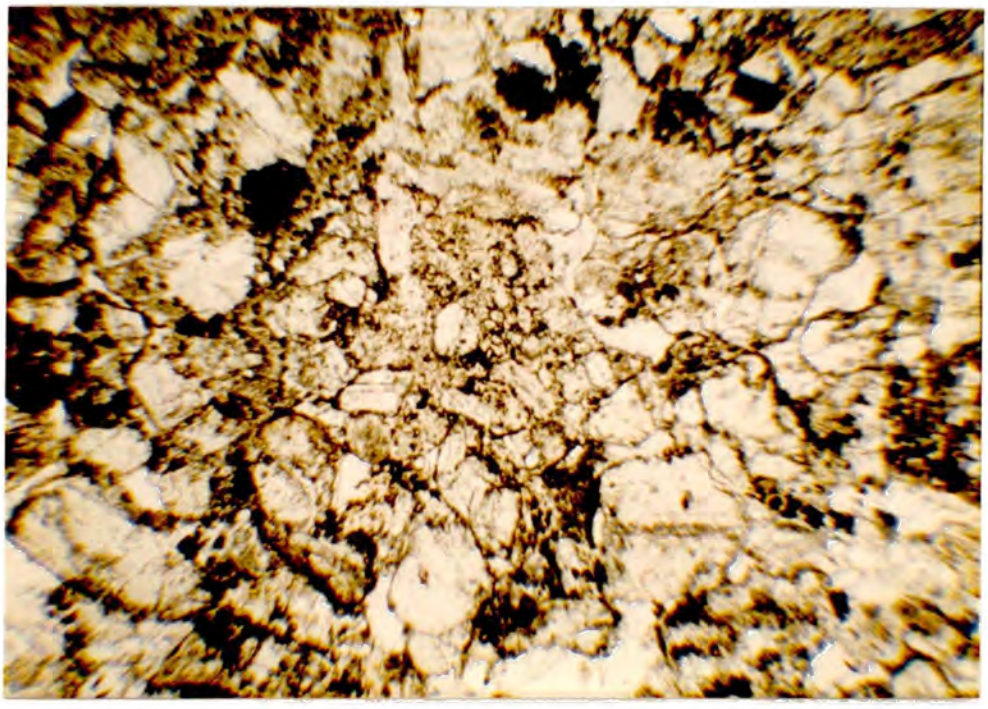

Plate 11

Photomicrograph: fine-grained volcaniclastic composed of rounded fragments of pyroxene and rock. Calcite forms interstitially to the clasts (Sample 4054. PPL. Field width = 4 mm.).

Plate 12

Photomicrograph: Volcaniclastic /fine agglomerate composed of ragged rock fragments and plagioclase clasts (Sample 5101. Field width = 4 mm.).

one mile SE of Mt.Kelly (G.R. 689 429). Here, the fabric of the rock is exposed on weathered crags, and it can be seen that the agglomerate consists, almost totally, of angular to slightly rounded blocks of augite and plagioclase-phyric volcanics (Plate 13). Variation among these fragments is evident on the basis of varying proportions of phenocrysts and different shades of weathering. Interstitial to the fragments, a small amount of tuffaceous matrix is present. Locally in this outcrop a crude, steeply inclined stratification can be discerned. In fact, the agglomerates can be traced into distinctly stratified varieties over the distance of a few metres. Plate 13 shows such an outcrop in the locality referred to above, where a coarse agglomerate grades quite sharply into finer, tuffaceous or volcaniclastic layers showing an alignment of fragments. Much of the succession on the ridge directly NE of Mt.Kelly, is similarly made up of a sequence of alternating agglomeratic and finer volcaniclastic beds from 1 to 5m. in thickness, as indicated in Fig.3.2. While some of this coarser material may have been deposited vertically as explosive debris from nearby vents, some is possibly deposited laterally in the form of massive slumps or slides down an unstable, sub-aqueous, volcanic slope.

Finer grained agglomerates, with fragments on the order of a few centimetres, noticeably occurring in Kelly Creek (Plate 14), were clearly emplaced by slumping, since the fragments are well separated by a muddy, volcaniclastic/sedimentary matrix. These rocks could be termed lahars.

As with the finer grained fragmentary rocks, distinctly reworked material, derived from rather less mature volcanic agglomerates, is common. These conglomeratic varieties show distinct rounding of the fragments to form cobbles of up to 10 cm.,

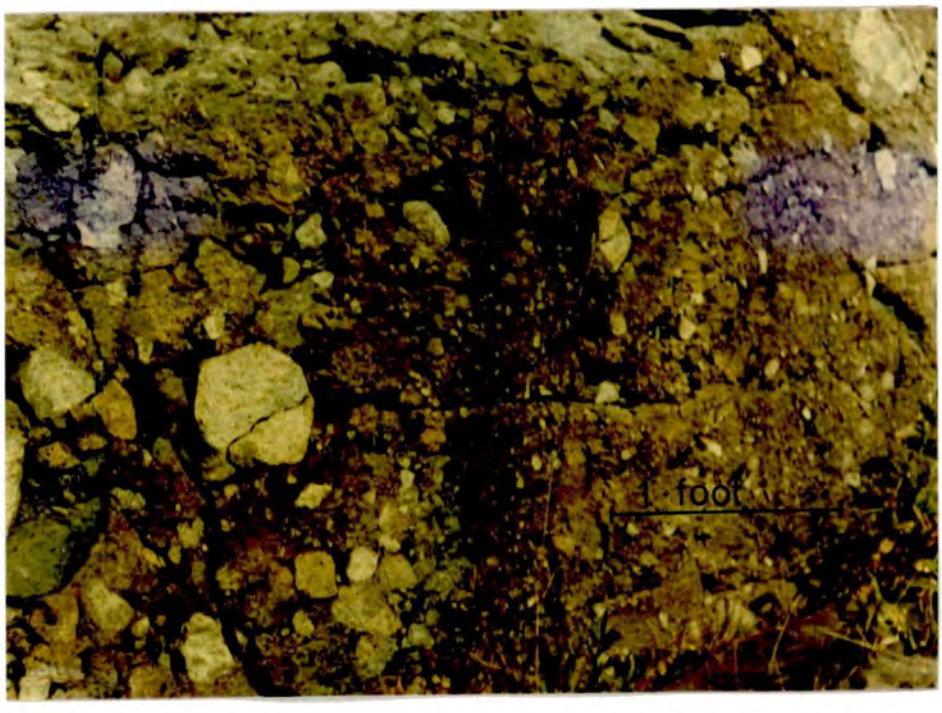

Plate 13

Vertically bedded and graded agglomerate, composed primarily of angular to sub-rounded blocks of lava in a gritty volcaniclastic or tuffaceous matrix. Sample locality 4051.

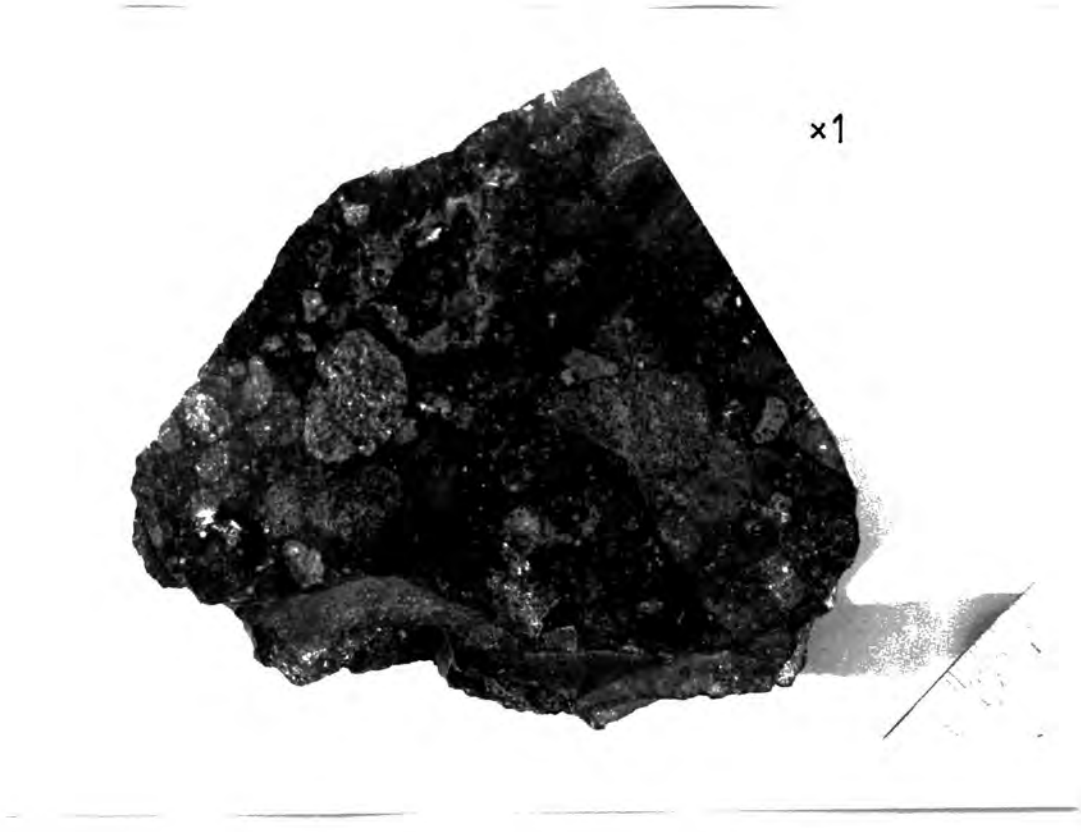

Plate 14

Hand specimen of sample 5064B: Fine conglomerate composed of sub-rounded volcanic rock fragments in a fine, muddy sedimentary matrix.

the alignment of which can define a crude bedding in places. A good locality for such lithologies is Hall Creek, west of the Hall Formation sediments (G.R. 778 704). In this locality the conglomeratic units appear to be at least 25m. thick. Quite vigorous conditions of sedimentation are implied by these deposits, and again, slumping or sliding of the fragments, down an unstable slope, appears a plausible mechanism.

Gradational with agglomerates are localised varieties resembling breccias. These, as would be expected, show a greater uniformity and angularity of fragment type, less internal structure, and are generally coarser. In one or two localities, for example, one mile NE of Mt.Kelly (G.R. 692 445), it can be inferred that the breccia is discordant relative to adjacent bedded sediments and thus may represent a vent infilling. In other cases they are possibly brecciated flows, some of which have muddy sediments forming a matrix.

In the literature (Mulligan, 1952; Little, 1960), many of the conglomerates and agglomerates referred to here are called 'flow breccias' or 'autoclastic' flows, this view being based on the similarity between matrix and fragments, and the rounding of the fragments, interpreted on a resorbtion phenomenon. However, these rocks are not apparent in the abundance implied by the above papers, the brecciated flows, referred to in the previous paragraph, being relatively scarce. This opinion is based, as Fyles (in prepn.) also notes, on the absence, in many agglomerates, of features usually associated with flow-breccias or autoclastic flows; while clastic, detrital textures are common. For example, while amygdaloidal fragments occur occasionally, the very vesicular, blocky breccias found at the flow front or at the top and base of lava flows, are not observed. Most fragments show evidence of

derivation from the massive, central portion of a pre-existing flow and are randomly mixed in with vesicular fragments. In addition, many of the agglomerates and conglomerates, as indicated in Fig.3.2, are bedded, or demonstrably associated with finer, bedded horizons. While it is also true that compositionally the matrix in these rocks is similar or identical to the fragment types, it is commonly fragmentary, in contrast with the clearly crystalline blocks or cobbles (Plate 15). Where metamorphism has strongly affected the rocks this distinction becomes blurred.

Non-volcanic fragments within the clastic rocks generally, are rare. Granite pebbles are observed infrequently in the agglomerates and conglomerates, and also rarely, shale and quartzite fragments in some of the finer rocks. Near the town of Rossland, large limestone blocks are found in agglomerates, these being derived from the underlying Mt.Roberts Formation (Little, 1960). Further east and north, where the volcanics overlie only slightly older silts, muds and greywackes, the absence of country-rock fragments is probably due to their less cohesive nature, the sediments suffering total comminution during volcanic processes, and only contributing individual grains to the pyroclastics and volcaniclastics.

3:3:3 Lavas

Lava flows are apparently rare, and the features associated with their occurrence are indistinct. Also, it is believed that many of the rocks previously identified as autoclastic flows by Little (1960), are detrital agglomerates and conglomerates. However, outcrops occur, particularly north of Ymir, where massive, non-fragmentary crystalline rocks or brecciated flows are represented. For example, on the highway six to ten miles south of Nelson

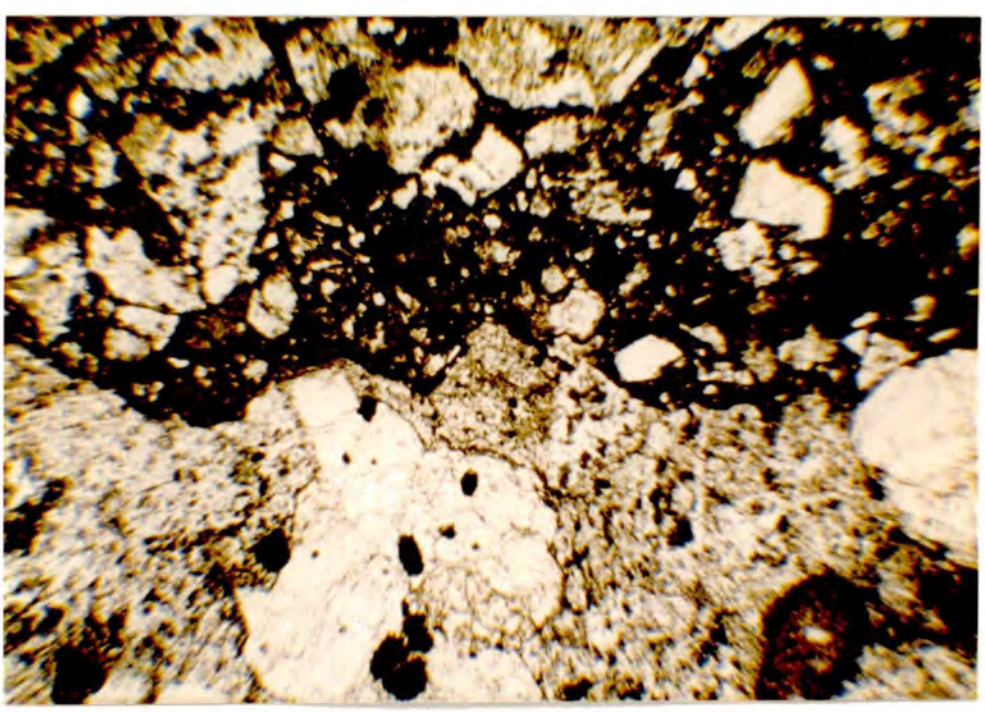

Plate 15

Photmicrograph: Interface between a large fragment in an agglomerate and the fine, fragmentary matrix which includes pyroxene clasts (Sample 4072D. PPL. Field width = 4 mm.).

(G.R. 825 745; samples 5087, 5088) there are outcrops of massive amphibolised augite-phyric basalt (ankaramite). In places it is brecciated. Determinations of structure in these outcrops is virtually impossible though, due to the fairly severe shearing and high degree of metamorphism. Accompanying sediments and volcaniclastic layers indicate a steep dip to the west (Fig. 1.1). In another locality (G.R. 828 628; samples 4105A, 5516A) an abundance of vesicular blocks in a breccia was observed, possibly indicating a flow boundary.

It is possible that some exposures generally, of non-fragmentary and invariably porphyritic volcanics are intrusive. Little (1960) notes that the augite porphyries 'appear to be mainly intrusive', and Fyles (in prepn.) maps areas of augite porphyry as sills, in one locality up to 2,500 feet thick. On the other hand, Fyles (op.cit) nowhere identifies lava flows. The problem, in this regard, is in part the lack of any continuous exposure whereby contact relations of such occurrences can be clarified.

Pillow lavas are reported to occur rarely, by McAllister (1951), in the Ymir map-area, but were not observed by the writer. If there was extensive extrusion of lava in the area, it might be expected that pillow lavas would be commonplace in view of the prevailing marine conditions.

As will be shown in Section 3:4 below, an apparent absence or scarcity of massive flows is not uncommon in the Cordilleran volcanics, and has also been described in the Ordovician Sofala volcanics of New South Wales by Barron (1976).

All the volcanics, whether derived as fragments from flows, explosively or sedimentarily; or occurring as in situ flows or intrusions, are strongly porphyritic, a feature easily seen in hand specimen. On weathered surfaces, especially in the higher-grade

metamorphosed area, augites are particularly conspicuous, occurring as dark green, equant crystals up to 1 cm., set in a pale green, weathered groundmass. In the Eerie Creek (G.R. 760 510) area and near Dominion Mountain (G.R. 771 646), plagioclase is especially conspicuous as white laths up to 2 or 3 mm. in length, contrasting with a green groundmass.

3:3:4 Minor Intrusions

Apart from the possibly intrusive nature of some augite-phyric rocks, referred to above, a few dyke-like intrusions have been observed cutting the sediments and volcanics at all levels in the succession (see Fig. 3.2). These intrusions often have distinct, lustrous black needles or laths of hornblende set in a greenish-grey matrix. It is possible they are related to the extensive lamprophyric dyke swarm of Tertiary age, but these latter dykes are usually much fresher and contain abundant biotite. They also form clear-cut little-fractured, vertical dykes, whereas the intrusions referred to here are clearly more altered and more strongly jointed or fractured, sharing features developed in the country rock. For these reasons, it seems likely that these minor intrusions are related to the volcanic episode, though clearly slightly later where they cut the youngest volcanics.

3:3:5 Sedimentary rocks

Intercalated with the volcanics are common sedimentary units. For example, in the Mt.Kelly succession (Fig.3.2), at least five such units are observable, with thicknesses up to two hundred feet. To the north of Salmo, sediments within the volcanics are less common, though a very conspicuous black shale outcrops on the highway north of Ymir (G.R. 820 672).

The sediments are predominantly hard, grey to black siltstones and shales, with less common paler and coarser greywacke bands. The shales are finely laminated on the scale of a few millimetres, with coarser horizon ranging from 1 to 50 cm. in thickness. Graded bedding is common in coarse and fine facies but, as was noted in the Archibald sediments (Section 2:2:2), small-scale cross bedding, though in evidence, is much rarer a characteristic.

Whilst the uniform laminations, bedding and fine grain-size of the sediments generally, is indicative of a distal and quiet environment of deposition, the more mixed sediments tend to show features indicative of some disturbance. These take the form of pinch-and-swell bedding, small-scale faults and slump structures, and minor wash-outs or erosional disconformities. Also, pre-diagenetic brecciation of clayey bands was observed. These features could indicate deposition on an unstable, sloping sea floor; instability perhaps being triggered by contemporaneous seismicity or volcanic eruptions.

Thin-section examination of some of the least metamorphosed sediments show them to contain abundant feldspar, some mafic crystal clasts, chloritised volcanic-rock fragments, and relatively little quartz. (Plate 16).

3: 4 Discussion

Similar assemblages of lithologies, as described for the Rossland Volcanics above, are characteristic of contemporaneous volcanic successions preserved elsewhere in the Canadian Cordillera, presumably under the same broad tectonic and sedimentological controls.

In the Takla Group of McConnell Creek, central British Columbia, is a 10,000 feet-thick assemblage of 'well layered..... volcanic rocks of which tuffs and agglomerates are by far the most abundant'

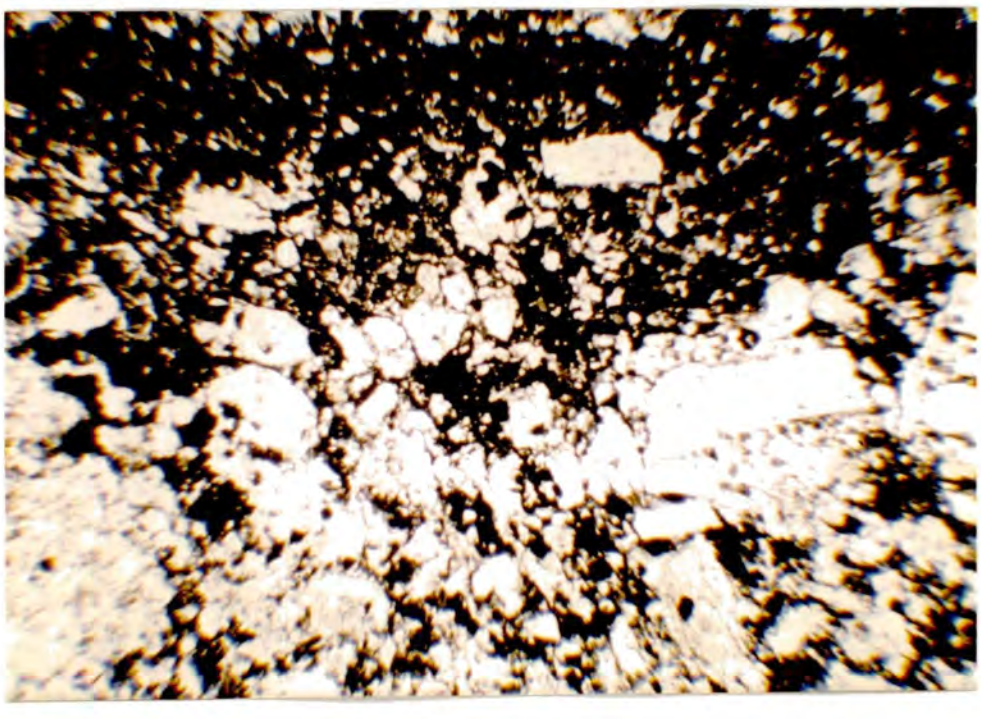

Plate 16

Photomicrograph: Graded band in sediment. Note the abundance of angular feldspathic and rock fragments in the coarse band, compared to a low abundance of quartz (Sample 5046. PPL. Field width = 4 mm.).

(Lord, 1948). Fragments of augite, plagioclase and amphibole occur within this succession. In addition, Monger & Church (1977) note the abundance of augite-phyric breccias and the presence of massive volcaniclastics, indistinguishable in the field, in places, from massive flows.

The Takla volcanics of the Aiken Lake map-area similarly contain abundant conglomerates and breccias (Roots, 1954). Roots (op.cit) also makes the observation that, despite careful examination, contacts of flows could not be definitely identified in the more massive volcanics, though he suggests flow thicknesses from 15 to 300 feet. Within the Takla successions, at all localities, common marine sediments are reported, including some limestone pods.

The overlying Hazelton Volcanics, as will be shown in Section 5:4:3, are less like the Rossland volcanics in terms of petrographic and chemical affinities, compared to the Takla Group, and this also applies to some extent in the lithological sense. However, fragmentary material of volcanic and sedimentary origin is still abundant, though a frequent red or purple colouration is indicative of subaerial conditions for part of the time (Monger & Church, 1977).

Lower Jurassic volcanics of the Bonaparte Lake and Quesnel Lake map-areas are almost totally fragmentary in nature, comprising nearly monolithologic volcanic sediments, conglomerates and breccias (Campbell & Tipper, 197; Campbell, 1960).

Also within the Bonaparte Lake area, the Nicola volcanics apparently contain no non-fragmentary flows (Campbell & Tipper, 1971). In the Nicola Lake region, the same group, whilst containing some reported flows, is predominantly a succession of tuffs, breccias and volcaniclastics, with argillites and limestones (Schau, 1970).

This abundance of fragmentary lithologics, can be related directly to the palaeoenvironment preserved and exposed at present.

In discussing the Quesnel Trough volcanics, Campbell & Tipper (1971) suggest that what is preserved is the clastic wedge built out from isolated volcanic islands. They also suggest that to provide the vast amount of coarse clastic material, volcanism was mainly explosive, and that the particularly coarse agglomerates represent the roots of volcanic edifices. Alternatively, the more massive, coherent lava flows expected near a volcanic centre may have been eroded away. Possibly, uplift along the Pinchi geanticline was responsible for this (See Fig. 2.1). Monger & Church (1977) see a similar environment for the Takla volcanics further north, with very thick massive agglomerates and flows representing volcanic islands which shed debris into the adjacent basins.

Features, such as described, are what are envisaged as typical of island arc environments by, for example, Mitchell & Reading (1971) and Dickinson (1971). Mitchell & Reading (op.cit) show that thick sequences of volcaniclastic material, much of it coarse, accumulate off both sides of an emerging and maturing arc. With distance from the arc, finer grained turbidite deposits occur. Exemplifying these characteristics are the older rocks of the New Hebrides arc in the S.W. Pacific. Here a Miocene succession of volcaniclastics, pyroclastics and immature turbidites reach several thousand metres in thickness, and which accumulated, in an entirely marine environment, in the space of 10 my. (Mitchell & Warden, 1971). This rapid rate of deposition reflects the abundant supply of detritus, as well as a tectonically emerging source region.

Conditions like these are clearly similar to those within the Rossland area in the Lower Jurassic. From early Sinemurian until the Bajocian, a period of 20 my., some 15 to 20 thousand feet of strata collected in the Rossland Trough, apparently being westerly-

derived. The axis of the arc, therefore, probably also lay to the west, the volcanics being situated on the edge of a 'back-arc' sedimentary basin. Much of the material, therefore, in the volcanic succession, particularly the finer grained volcaniclastics and sediments, is probably detritus shed off of the east side of the main arc in the form of slumps and turbiditic deposits. In addition, much is probably derived from initial pyroclastic deposits. Local volcanic islands, the presence of which is indicated by a few reported plant remains and one coquina deposit (Frebold, 1959), also contributed much of the coarser debris. Possibly, the more massive, augite-phyric agglomerates and flows, noted in the area between Ymir and Nelson, represent the location of a local volcanic centre.

The boundary of this back-arc sedimentary basin or trough is most probably represented by the 'Rossland Break' (Fyles, in prepn; Section 2:2:2), where NE-SW trending faults and sheared serpentinites occur.

Further discussion on the tectonic and palaeogeographic setting of the volcanics is deferred until the chemical evidence (Chapter 6) is considered.

CHAPTER 4

ROSSLAND VOLCANICS: IGNEOUS PETROGRAPHY AND MINERALOGY

4:1 Classification and general textural features

The scheme to be followed in this chapter is to first describe some general magmatic textural features of the rocks, primarily the volcanics, and define a preliminary classification system; then to deal more specifically with each mineral phase in terms of its mode of occurrence and chemistry.

4:1:1 Volcanics

The strongly porphyritic nature of the volcanics has already been referred to in Chapter 3. This is a feature of island-arc/calc-alkaline magmatism, as is the range of phenocrysts present. These are plagioclase, clinopyroxene, spinel (Cr-spinel and Ti-magnetite), amphibole and very rarely, biotite. Olivine and possibly orthopyroxene were also originally present. Table 4.1 shows some selected modal analyses of volcanics, where it is evident that the percentage of phenocrysts averages about 40 to 50 per cent.

Those samples in Table 4.1 subscripted A, contain secondary amphibole as pseudomorphs, primarily after Ca-clinopyroxene, and are more thoroughly metamorphosed compared to those samples with fresh igneous pyroxene (Chapter 6). For this reason, estimation of the abundance of primary amphibole and primary opaque minerals is not attempted for these samples. In the amphibolised samples (zone B, as defined in Chapter 6), primary amphibole is only rarely observed, and then only by its characteristic euhedral outlines. Opaque-oxide minerals in the amphibolised samples, where stable, are chemically altered (Chapter 6) and quite commonly they have disappeared as a result of metamorphism.

TABLE 4.1

MODAL ANALYSES OF SELECTED VOLCANICS AND MINOR INTRUSIONS (SEE TEXT FOR DISCUSSION OF CLASSIFICATION)

Non-amphibolised rocks

Sample	5006	5013	5015	5016	5032	5033	5036
Cpx.	23	21	5	26	7	-	20
Plag.	25	38	26	23	41	46	24
Amph.	-	-	18	-	-	-	-
Opaque	4	6	2	2	14(S)[4]	5(S)	4
G-mass.[1]	48	39	48	49	38	47[2]	52
Type[3]	B	B	HA	B	A	A	B

Sample	5041	5053	5054	5056	5102	5113	4051	4056
Cpx.	18	18	27	14	14	5	17	14
Plag.	12	28	26	15	23	13	19	31
Amph.	-	-	-	5	1	6	4	-
Opaque	2	1	8	1	1	3	5	5
G-mass	56	54	39	66	61	73	55	50
Type	B	B	B	HB	HB	HA	HB	A

Notes:

1. 'Groundmass' includes in some basalts possible olivine (< 5%).
2. 2% Biotite in sample 5033.
3. Types are as defined in text :
4. Opaques are sulphides.

B Basalt
HB Amphibole-bearing basalt
A Andesite
HA Amphibole-bearing andesite

TABLE 4.1 (Continued)

Amphibolised rocks

Sample	5073B[3]	5074B[3]	5085E	5087B	5088	5089
Cpx.(A)	28	41	36	37	25	23
Plag.	?	?	-	9	10	28
G-mass[1]	72	59	64	54	65	49
Type[2]	?B	?AB	AB	AB	B	B

Sample	5106A	5108	5111A	5116	5120	4007
Cpx.(A)	5	14	55	31	23	12
Plag.	31	10	-	27	20	34
G-mass	63	76	45	40	57	54
Type	A	B	AB	B	B	B/A

Sample	4013A	4016	4109B	5536	5538A	5516B
Cpx.(A)	32	25	-	36	42	43
Plag.	6	16	40	13	4	-
G-mass	58	59	60	51	54	57
Type	AB	B	A	AB	AB	AB

Notes:

1. Groundmass includes indeterminant spinel and olivine
2. Type AB = Ankaramitic basalt
3. Samples 5073B, 5074B have lost relict plagioclase due to severe recrystallization, thus type is to some extent indeterminant.

Minor Intrusions

Sample	5001B	5010	5096	5107A	5107B
Cpx.	25	19	17	16	8
Plag.	20	26	14	10	13
Amph.	-	3	12	13	12
Opaque	4(S)	6(S)	2(S)	2(S)	1(S)
G-mass	51	43	54	62	67

The presence and abundance of olivine or orthopyroxene is even more problematical, since these minerals are not stable (or relict) in any samples. The breakdown, with advancing alteration, of olivine and orthopyroxene prior to that of clinopyroxene is well documented (e.g. Barron, 1976; Hynes, 1976; Vallance, 1974). In the non-amphibolised rocks, the former presence of these minerals is evidenced by patches of chlorite and carbonate, occasionally showing euhedral control (Plates 17, 18). Since the bulk of the volcanics are basaltic (Chapter 5), most of these pseudomorphic aggregates, where they are not well defined by crystal outlines, are probably after olivine. Orthopyroxene does not occur as a significant phenocryst until more siliceous compositions, usually. For example, in the Dominican calc-alkaline suite at 54 per cent SiO_2, orthopyroxene phenocrysts are less than 2 per cent in abundance (Wills, 1974). Within the basic samples of the amphibolised zone, olivine is even harder to detect, though again occasional, well-shaped pseudomorphs occur, usually of epidote, testifying to its presence (Plate 19).

On the basis of Table 4.1, a preliminary classification for the volcanics can be proposed. In general, the abundance of clinopyroxene drops and that of plagioclase increases with differentiation, though this is not strictly so, since the phenocryst population in any magma, as well as reflecting whole-rock chemistry, depends on the crystallization stage reached on eruption. However, three main classes are proposed here, though the subject of classification will be returned to in Chapter 5. They are:-

1. Ankaramitic Basalt
2. Basalt
3. Andesite

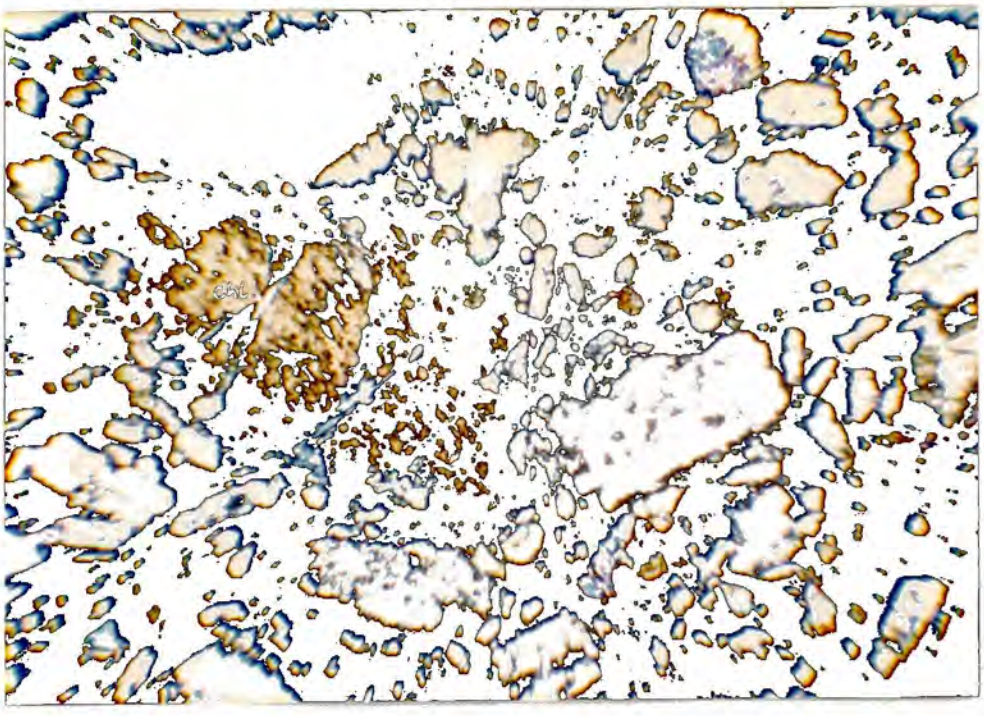

Plate 17

Photomicrograph: Chloritised pseudomorph after original olivine in a non-amphibolised basalt. Black, rounded phase in the top left of the field of view is an almost totally opacitised amphibole phenocryst (Sample 4051. XP. Field width = 4 mm.).

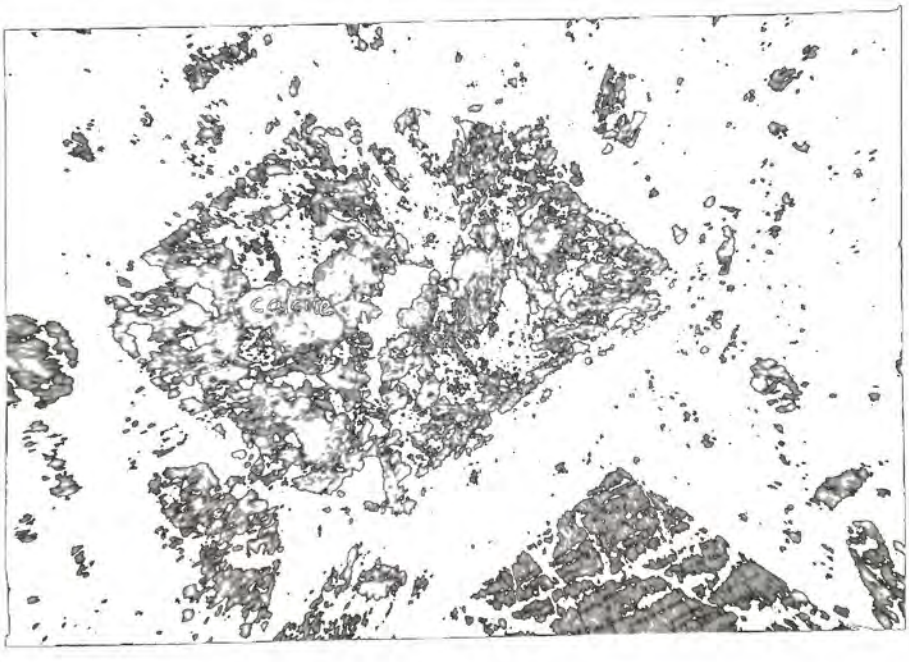

Plate 18

Photomicrograph: Calcite (with minor chlorite) pseudomorph after olivine in non-amphibolised basalt. (Sample 4070. Field width = 4 mm.).

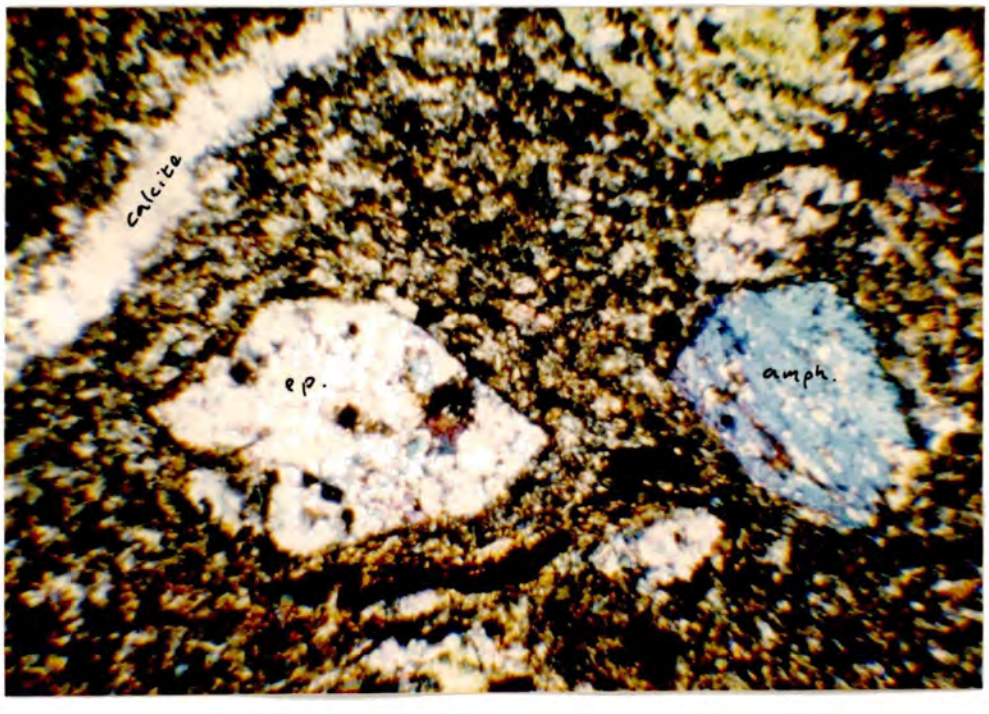

Plate 19

Photomicrograph: Epidotic aggregate pseudomorphing olivine in amphibolised ankaramitic basalt. Also evident are amphibole pseudomorphs after pyroxene that show partial internal breakdown to biotite. Note calcite vein cross-cutting the crude schistose fabric of the groundmass (Sample 5537A. XP. Field width = 4 mm.).

(1) Akaramitic Basalt

Ankaramite is a term usually reserved for basic volcanics of alkaline affinity and usually occurring in ocean-island, intraplate environments. It is defined, generally, as a basic to ultrabasic rock in which clinopyroxene is modally abundant and in excess of olivine, as opposed to picrite where the opposite is true. However, ankaramitic representatives are reported locally in the New Hebrides (Colley & Warden, 1974) and New Britain (Stanton & Bell, 1969) island-arcs. They are also reported in the supposed arc volcanics of Bridget Cove, Alaska (Irvine, 1973; Berg et al., 1972), and the Takla Group (Irvine, 1974; Table 5.4 in Chapter 5).

Since all the ankaramitic basalts of this study fall within the amphibolised zone, detailed igneous petrographic description is impossible. However, Plates 20 and 21 show some typical rocks thus classed. Clinopyroxene (amphibole pseudomorphed) is generally greater than 30 per cent in modal abundance (Table 4.1) and plagioclase ranges from 0 to 10 per cent. Olivine is present as evidenced by occasional pseudomorphs (Plates 19 , 20) but is clearly much less abundant than pyroxene. Within this rock-type, clinopyroxene attains its greatest diameter of up to 1 cm. whereas plagioclase, by comparison, is a microphenocryst occurring as laths of less than 2 mm. Evidence of primary amphibole is observed in none of the ankaramitic samples.

The groundmass of the ankaramitic basalts is completely recrystallized, but the more basic nature of the liquids they must once have represented is tentatively indicated by the low abundance of feldspar relative to actinolitic hornblende now present. Thus, although these rocks may be produced by crystal settling of pyroxene into normal basaltic liquid, it is not thought that this can explain

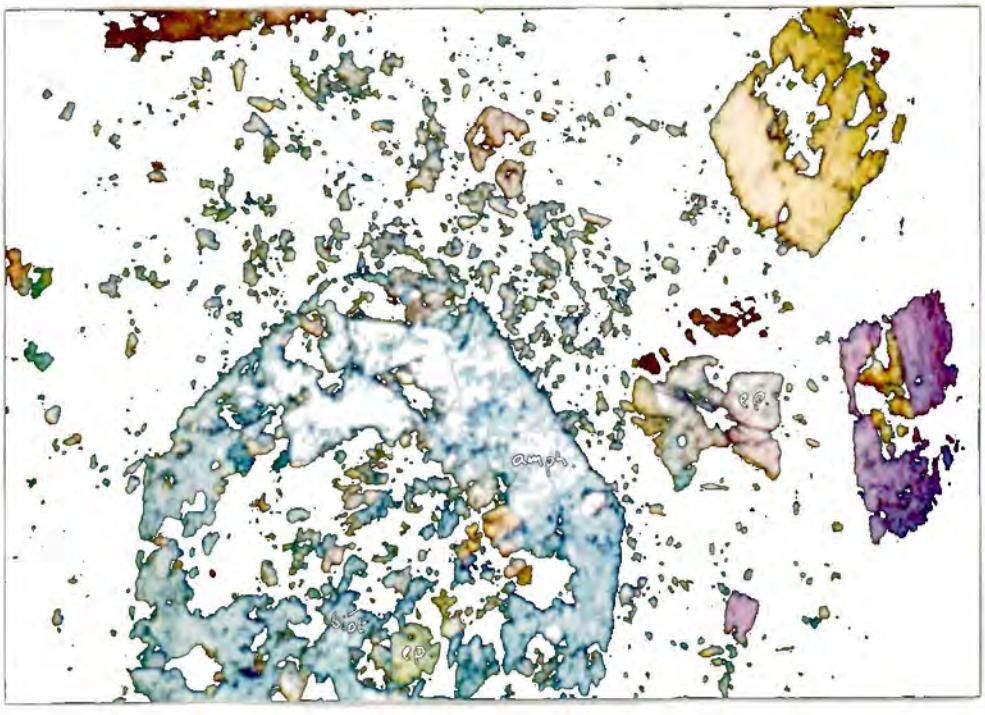

Plate 20

Photomicrograph: Amphibolised ankaramitic basalt with actinolite (pseudomorphing pyroxenes) showing partial breakdown to epidote and biotite. Epidote aggregate (left centre) possibly after olivine (Sample 5516B. XP. Field width = 4 mm.).

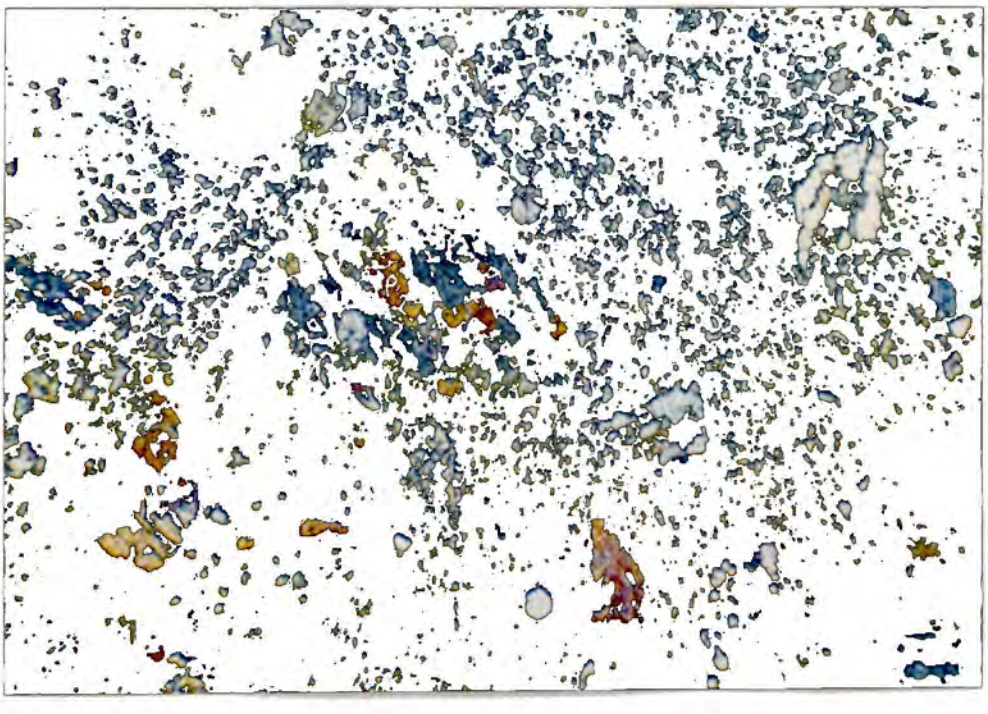

Plate 21

Photomicrograph: Amphibolised ankaramitic basalt. Actinolite pseudomorphs showing breakdown to epidote + biotite, as in Plate 20. (Sample 5111A. XP. Field width = 4 mm.).

their presence totally: basaltic rocks, as defined below, that are similarly metamorphosed, show in the groundmass a greater abundance of feldspar relative to secondary amphibole.

In addition to pyroxene, plagioclase and olivine as phenocrysts, some samples (Plate 20) show evidence of the presence of primary opaque-oxide phenocrysts, often included in pyroxene.

(2) Basalt

Basalts are defined here as those samples containing 15 to 30 per cent clinopyroxene and 10-30 per cent plagioclase. In addition, clinopyroxene/plagioclase ratios vary from 0.5 to 1.5.

Rocks, according to this definition, occur throughout the area underlain by the volcanics (Fig. 1.1). From the fresher samples it is evident that all the pyroxene is augite, there being no evidence of Ca-poor clinopyroxene and little of porphyritic orthopyroxene. Typical basalts are shown in Plates 22 and 23 . Generally, the pyroxene phenocrysts are smaller than those in the ankaramites, ranging up to 0.5 cm. Corresponding with an increase in modal abundance, plagioclase increases in size, forming laths of up to 5 mm; but is usually less than 2 mm.

Olivine is apparently a porphyritic phase as evidenced by chlorite-calcite pseudomorphs (cf. Plate 18), though there is no evidence of it being present in abundances greater than 5 per cent.

Oxide minerals (Cr-spinel and Ti-magnetite) are quite abundant, as shown in Table 4.1, ranging up to 8 per cent. They are commonly included within pyroxene (Plate 23) but also occur as indepdent, rounded to sub-euhedral crystals of up to 1 mm. in diameter.

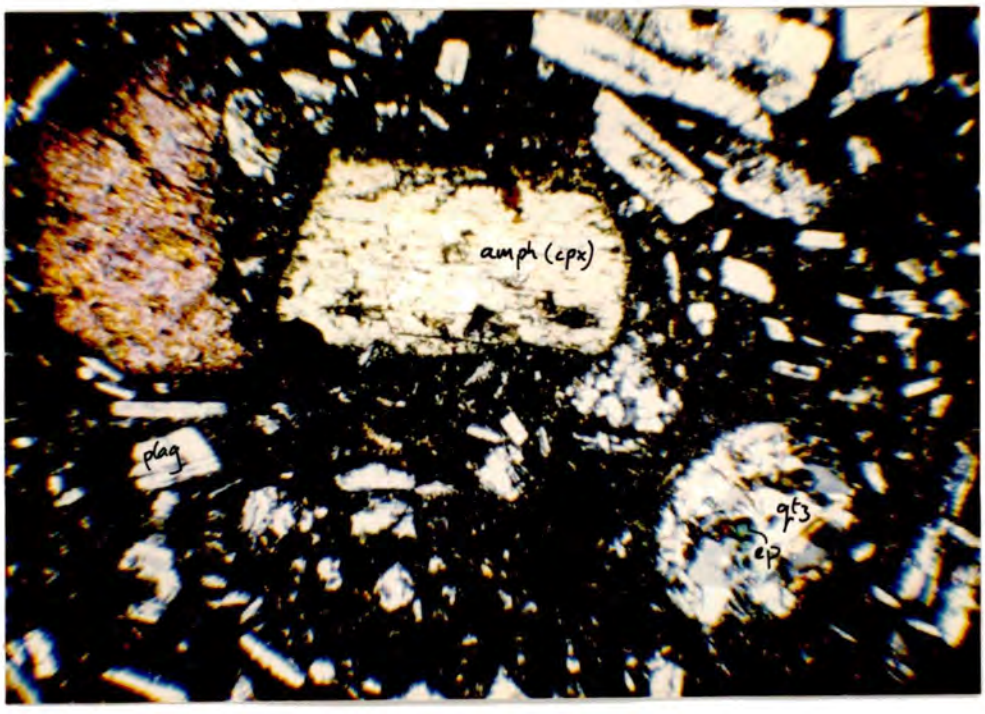

Plate 22

Photomicrograph: Amphibolised clinopyroxene and Plagioclase-phyric basalt. Vesicle (lower right) contains quartz and epidote. (Sample 4045. XP. Field width = 4 mm.).

Plate 23

Photomicrograph. Non-amphibolised basalt with single, well-developed euhedra of augite and altered plagioclase. Note the very fine groundmass, now chloritised extensively. (Sample 5016. SP. Field width = 8 mm.).

Within rocks of basaltic affinity, as defined here, primary amphibole makes an appearance. Plates 24 and 25 illustrate amphibole-bearing basalts; the amphibole occurring as 'opacitised', elongate and often resorbed phenocrysts of up to 3 or 4 mm. in length. Amphibole is apparently less than 5 per cent in abundance in the basalts.

The groundmass of these rocks is generally very fine-grained and invariably altered to turbid aggregates of chloritic minerals and sometimes brownish clay minerals (Plates 23, 24). It was clearly glassy in some samples. Where it is coarser, it apparently consists of the same phases that occur as phenocrysts; the pyroxene occurring as ragged granules or laths with interstitial plagioclase. Alternatively, plagioclase microlites occur in a glassy (now chloritic) groundmass, in which pyroxene cannot be distinguished. Small patches of quartz occur in a few samples.

The order of crystallization in these rocks can be broadly determined. Amphibole commonly shows inclusions of both plagioclase and pyroxene (Plate 26), whereas only one instance is recorded of amphibole being included in pyroxene. Clinopyroxene occasionally includes, poikilitically, plagioclase (Plate 23), though rarely is the opposite true. This may, in part, be a nucleation problem, since on the basis of the entropy of fusion (Carmichael *et al.*, 1974), pyroxene tends to grow rapidly but nucleates with difficulty compared to plagioclase, in which the opposite tends to be true. It is likely that clinopyroxene and plagioclase coprecipitated for much of the time, but on the basis of the chemistry and phase relations (Chapter 5), pyroxene was probably the earlier mineral to precipitate, at least in the more basic varieties. The common inclusion of Ti-magnetite and Cr-spinel in pyroxene indicates that these are early phases. A generalised crystallization sequence would be: Spinel-(Ti-magnetite and Cr-spinel)-pyroxene -

Plate 24

Photomicrograph: Amphibole-bearing basalt showing amphibole with thick opacite rim and several buried opacite zones. Microphenocrysts of plagioclase altered to sericite. (Sample 4051. XP. Field width = 4 mm.).

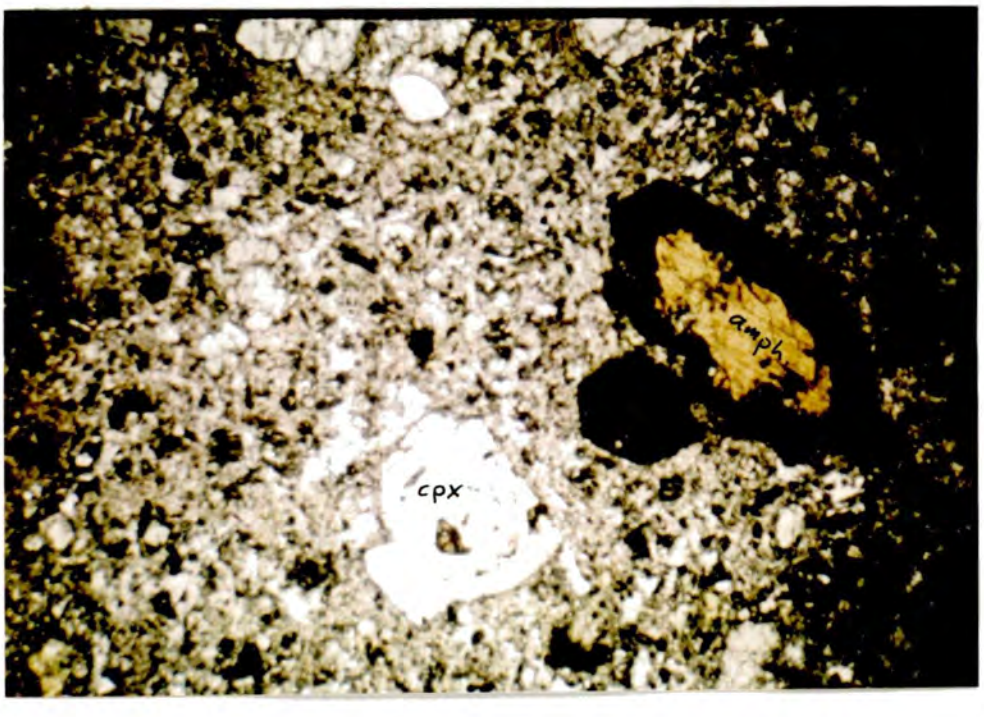

Plate 25

Photomicrograph: Amphibole-bearing basalt. Amphibole shows euhedral outline but strong development of an opacite rim. Pyroxene (lower centre) has an inclusion of olivine or liquid that has subsequently altered to chlorite. (Sample 5056. PPL. Field width = 4 mm.).

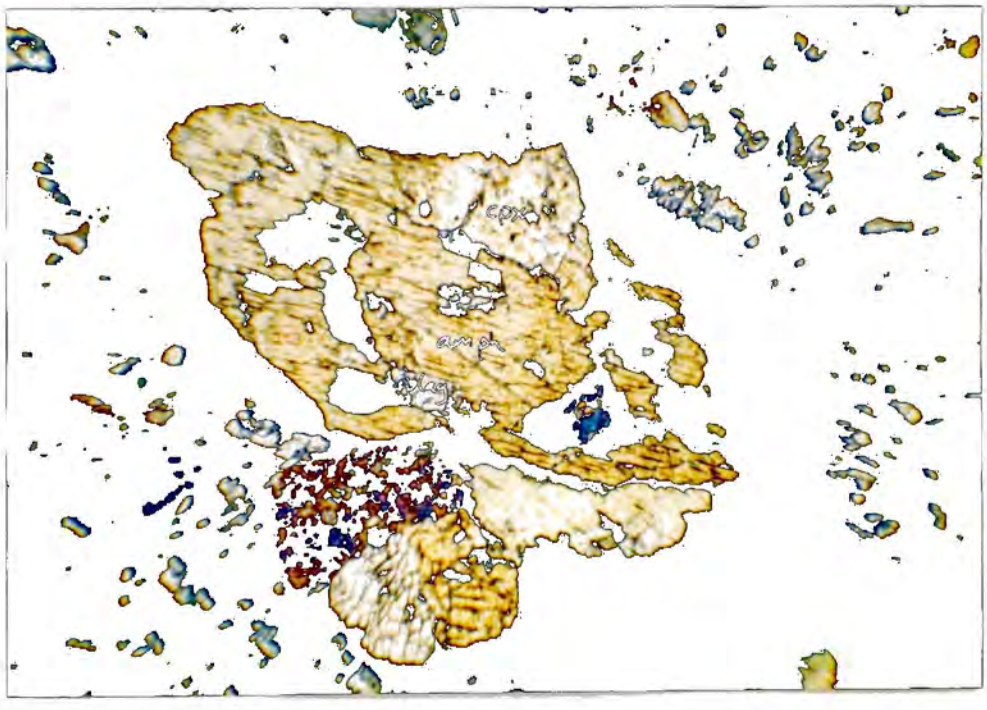

Plate 26

Photomicrograph: Amphibole phenocryst in a basalt showing poikilitic inclusions of clinopyroxene and sericitised plagioclase (Sample 4051. XP. Field width = 2 mm.).

plagioclase - amphibole. Also commonly included in pyroxene are globular-shaped, chloritic aggregates. (Plate 25). These may represent primary olivine or original trapped pockets of crystallized liquid.

(3) Andesite

This group is defined by modal clinopyroxene abundances, again all augitic, of less than 15 per cent and plagioclase abundances of greater than 30 per cent. Plates 27 and 28 illustrate andesitic varieties and show their densely porphyritic nature. Within this group, as pyroxene phenocrysts decrease in abundance, their size correspondingly decreases relative to plagioclase (compare Plates 24 and 28), indicating a change from pyroxene being the first-crystallizing phase to plagioclase.

A characteristic of these rocks, due to the high abundance of plagioclase, is the tendency to develop a trachytic texture (cf. Plate 27).

Amphibole phenocrysts are present in some andesitic representatives (Table 4.1), possibly in greater average abundance compared to amphibole basalts. In one sample (5113), these phenocrysts reach 0.8 cm. in length, though an average length for the amphibole prisms in other samples is about 2 mm.

Ti-magnetite phenocrysts are common, occurring, as in the basalts, as sub-rounded crystals included in pyroxene or amphibole and independently in the groundmass. Olivine pseudomorphs, on the other hand, are absent and possibly orthopyroxene makes an appearance in the form of rare rectangular, chloritic pseudomorphs.

One phenocryst species not observed in any basaltic samples, and observed in only one andesite (5033), is biotite. This mineral is described in more detail in Section 4:7 below, and is shown in Plate 27.

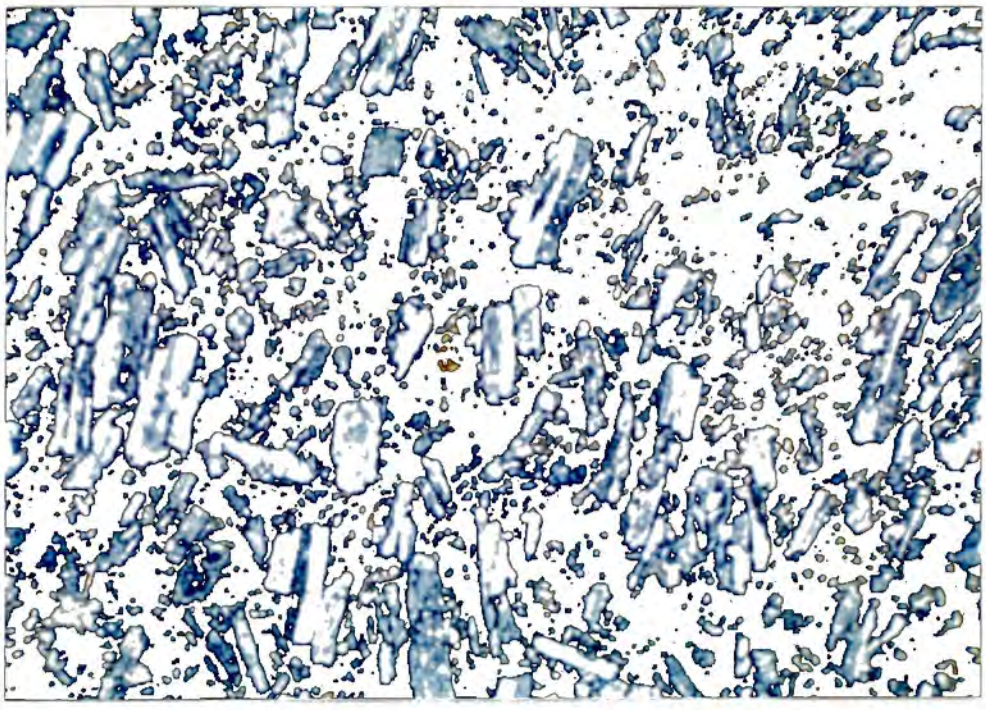

Plate 27

Photomicrograph: Andesite showing a strongly plagioclase-phyric nature with flow alignment of the plagioclase laths evident. Also evident are small biotite phenocrysts (centre) and chloritic patches probably after pyroxene (?opx). (Sample 5033. XP. Field width = 8 mm.).

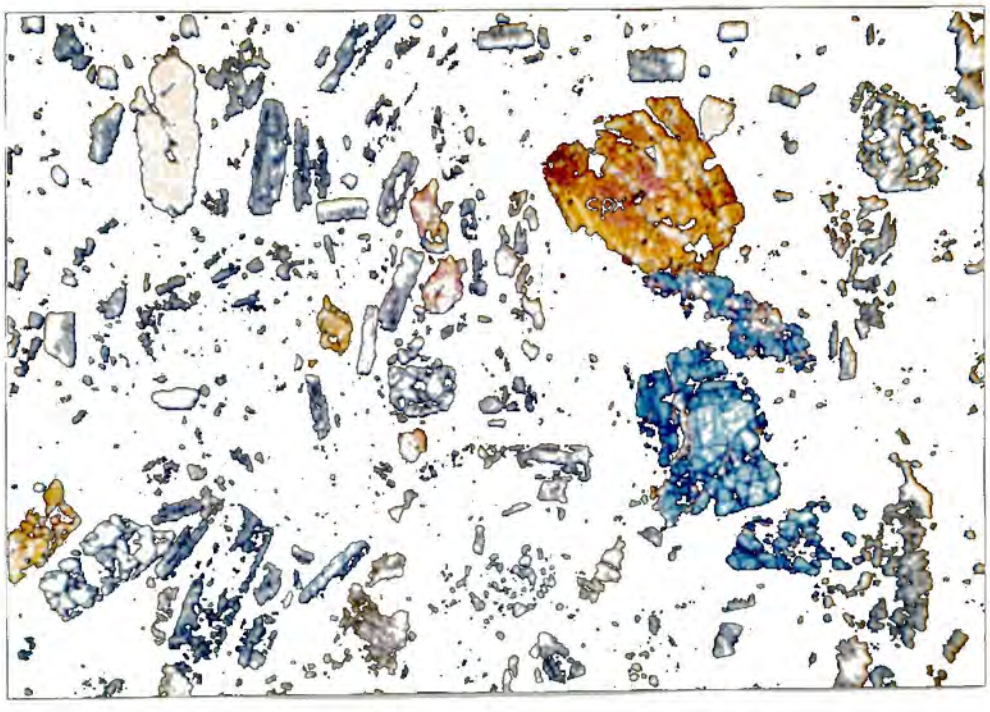

Plate 28

Photomicrograph: Andesite consisting principally of plagioclase and augite phenocrysts (Sample 4056. XP. Field width = 8 mm.).

Apatite is another mineral that apparently occurs in andesitic rather than basaltic rocks, often occurring as rounded to well-formed hexagonal prisms. These are frequently included in pyroxene (if present), sometimes associated with opaque minerals or occurring independently. Apatites are evident in Plate 29 , included in pyroxene.

The order of crystallization in the andesitic samples, as indicated by inclusion relationships, is broadly similar to the basalts; amphibole, in particular, crystallizing last. It was preceded by pyroxene or plagioclase, which again co-precipitated for some of the time. As noted above, plagioclase probably crystallised first in the most feldspathic rocks. Since both magnetite spinel and apatite occur as inclusions in pyroxene, and occasionally in plagioclase, these were the earliest phases to precipitate, albeit in small amounts.

4:1:2 Associated rocks

Under this heading are included other igneous rocks believed to have been magmatically associated with the volcanic episode. These include various amphibole-bearing minor intrusions and doleritic rocks, the pyroxenite and gabbroic rocks of the Bonnington Complex (Section 2:2:2) and, possibly, the serpentinite body near Rossland (Section 2:2:2).

(1) Minor intrusions. A few modal analyses of dyke-like minor intrusions (Appendix 1 for locations) are included under Table 4.1. A characteristic is the more abundant amphibole compared to the volcanic samples. Illustrations of samples 5010, 5107A and 5001B are shown in Plates 30 , 31 and 32 .

Generally, these rocks are similar to the volcanics in being distinctly porphyritic though, as might be expected, the groundmass is usually slightly coarser.

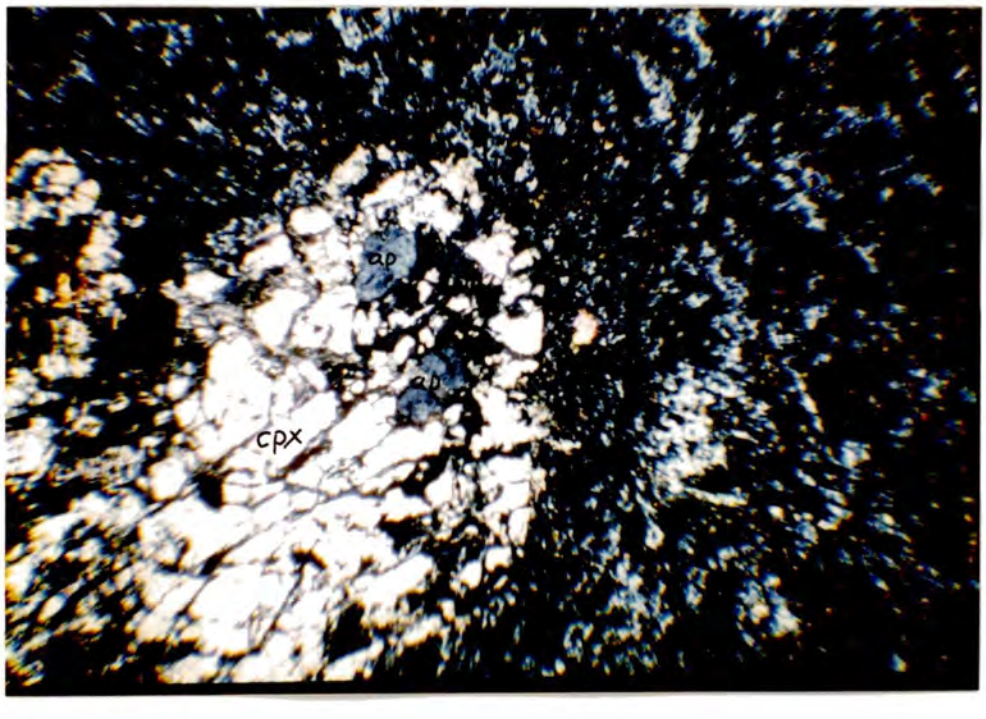

Plate 29

Photomicrograph: Rounded apatite crystals included in clinopyroxene in an andesite. (Sample 5034. XP. Field width = 4 mm.).

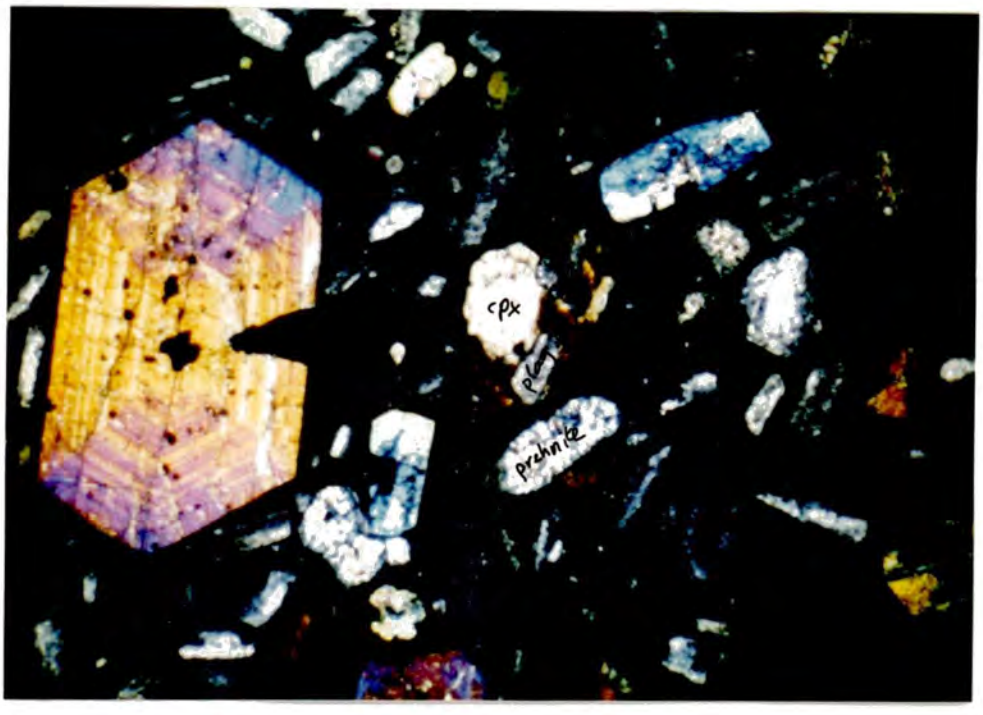

Plate 30

Photomicrograph: Large sector-zoned clinopyroxene in basaltic, amphibole-bearing minor intrusion. Also evident is an amphibole phenocryst with partial inclusion of clinopyroxene and altered plagioclase. Vesicles contain prehnite and chlorite (Sample 5010. XP. Field width = 4 mm.).

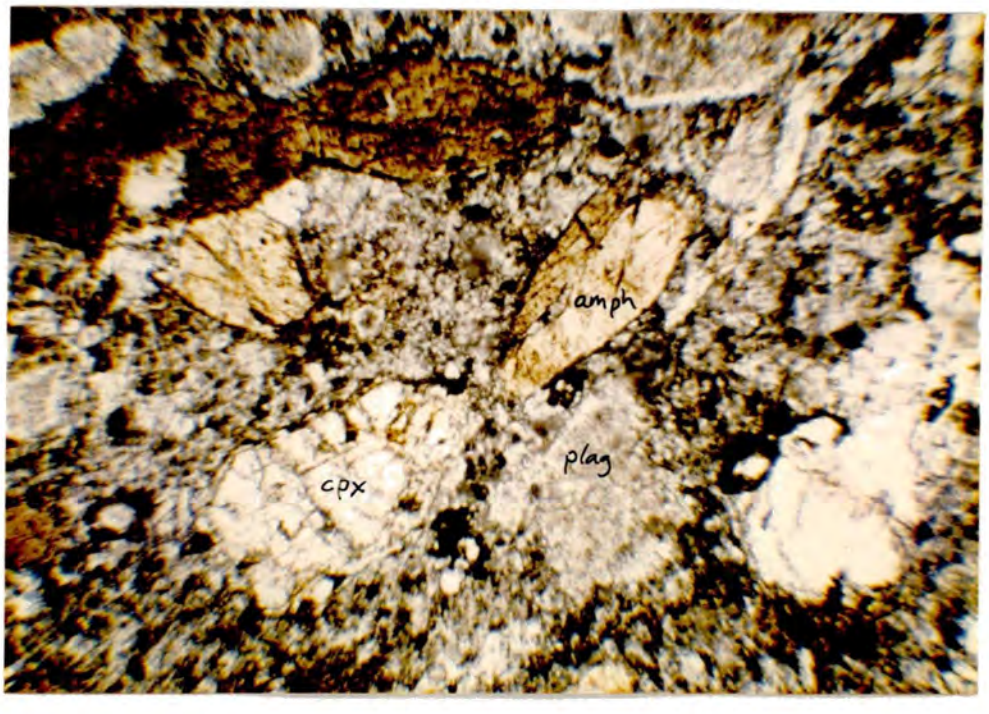

Plate 31

Photomicrograph: Amphibole-bearing minor intrusion that cuts Archibald sediments. Contains well-formed amphibole phenocrysts: clinopyroxene showing alteration, marginally and in fractures, to chlorite; and altered plagioclase phenocrysts. (Sample 5107A. PPL. Field width = 4 mm.).

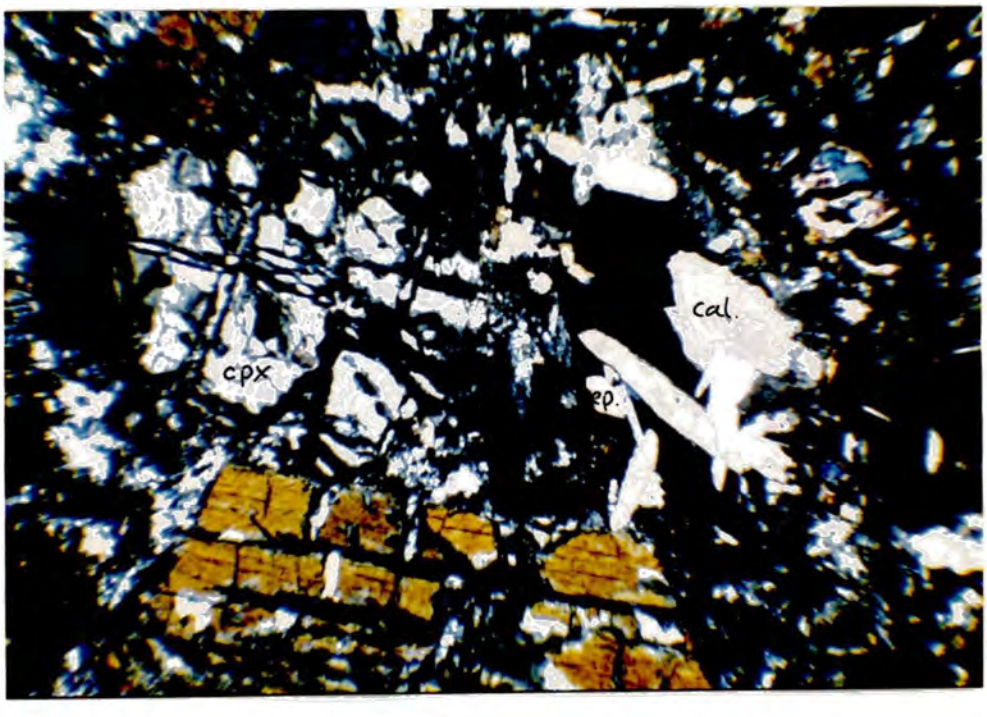

Plate 32

Photomicrograph: Fractured clinopyroxene phenocrysts in non-amphibole-bearing dyke. Note patches of chlorite (after ? vesicles) with overgrowths of calcite and epidote (right centre) (Sample 5001B. XP. Field width = 4 mm.).

Differences, excepting those of phenocryst content, are mainly in the degree of alteration; the plagioclases and pyroxenes are invariably considerably more altered to low-grade chloritic and clay minerals, and secondary sulphides are more apparent replacing primary opaques, as indicated in Table 4.1.

Apatite is a common accessory.

Samples 5031 and 5119 are doleritic intrusions (Appendix 1 for locations) within the volcanics, and judging by their similar degrees of metamorphism to the surrounding volcanics, were emplaced soon after, or during the volcanic episode. Plates 33 and 34 show these two samples, and it is evident they are broadly similar, both being composed of about 65 per cent interlocking plagioclase laths of about 2 mm. in grain-size, with ragged amphibole and biotite pseudomorphic aggregates developed after pyroxene. Sample 5119 (Plate 34) is also extensively epidotised.

(2) Bonnington Complex. An example of Mulligan's (1952) 'pyroxene-hornblende-biotite' rock is shown in Plate 35 . It is composed predominantly of about 80 per cent marginally amphibolised, equidimensional augite of 0.25 to 1 cm. in diameter. The remainder is taken up with ragged magnetite grains of 1-2 mm. and blurry, finely shredded actinolite and calcite patches that may be after olivine. Biotite (secondary) is only locally developed in this rock (Chapter 6).

Although grain-to-grain contacts are not preserved in this rock, due to the growth of actinolite, the general texture is suggestive of a clinopyroxenite cumulate, derived by settling of augite from Rossland basaltic or ankaramitic magmas.

The adjacent 'pseudodiorite' (Plate 36) is not dioritic, but

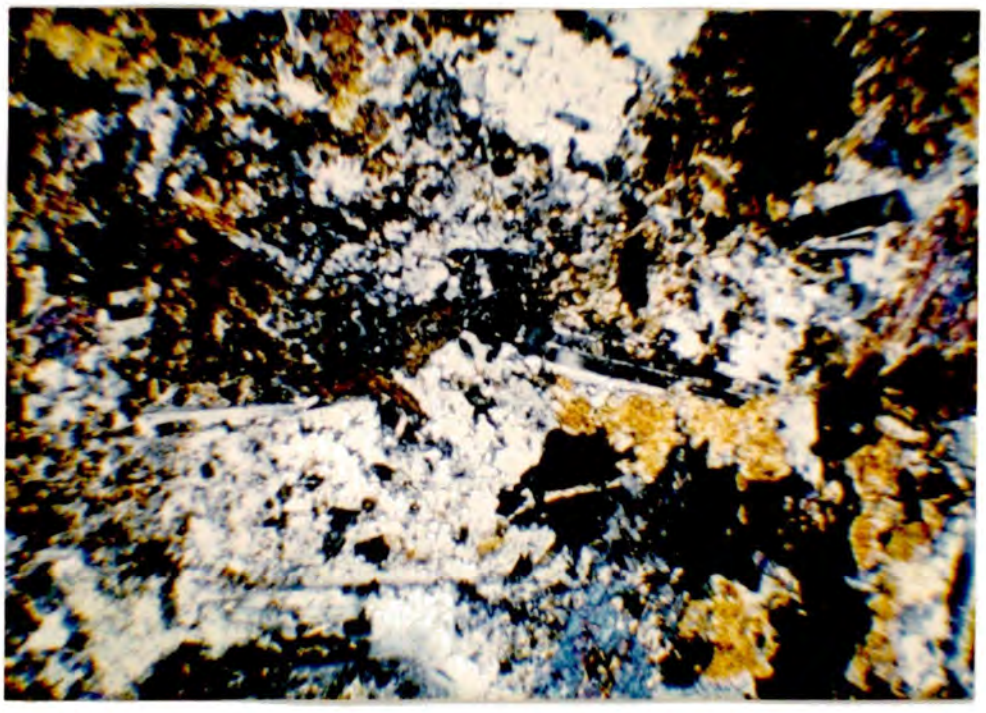

Plate 33

Photomicrograph: Doleritic minor intrusion. Note extensive alteration to amphibole and biotite (Sample 5031. XP. Field width = 4 mm.).

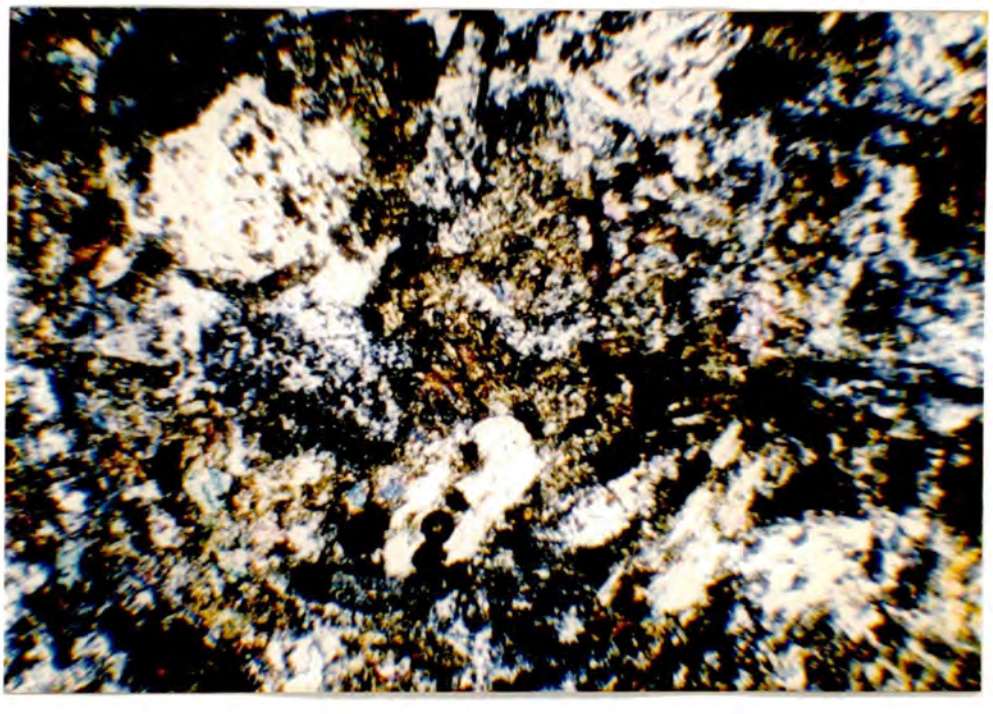

Plate 34

Photomicrograph: Doleritic minor intrusion. In addition to extensive amphibolization, epidote is abundant, often forming poikiloblastic inclusions in feldspar (Sample 5119. XP. Field width = 4 mm.).

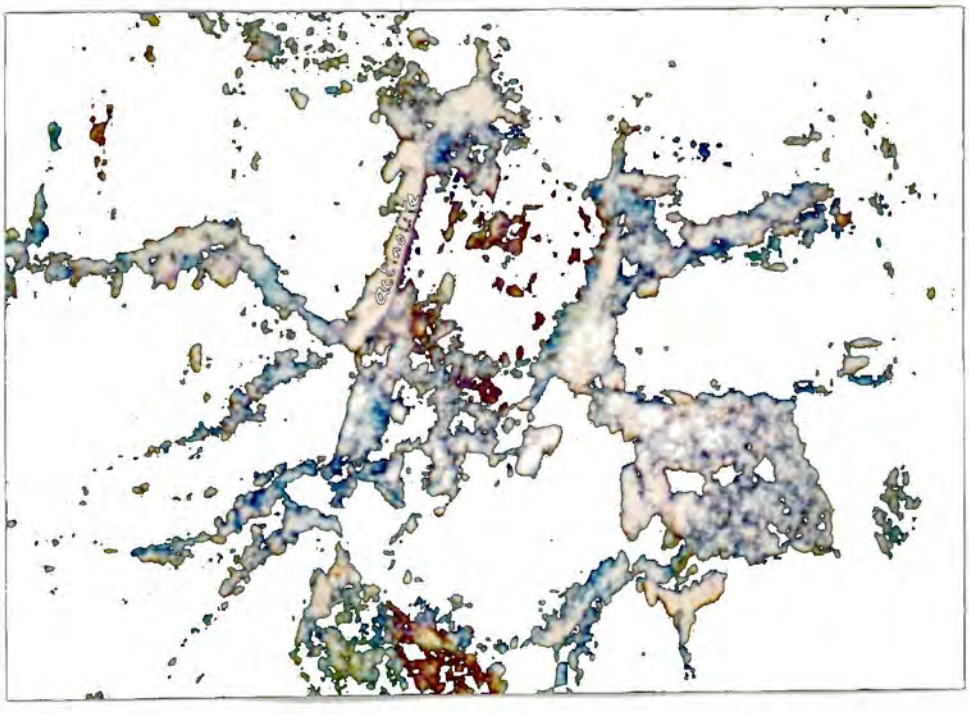

Plate 35

Photomicrograph: Clinopyroxenite cumulate. Contains rather dusty relict pyroxene altered marginally to actinolite/tremolite. Finely shredded tremolitic patches (lower right) may be after olivine. Also present are ragged, sometimes lobate, magnetite crystals (Sample 5075A. XP. Field width = 4 mm.).

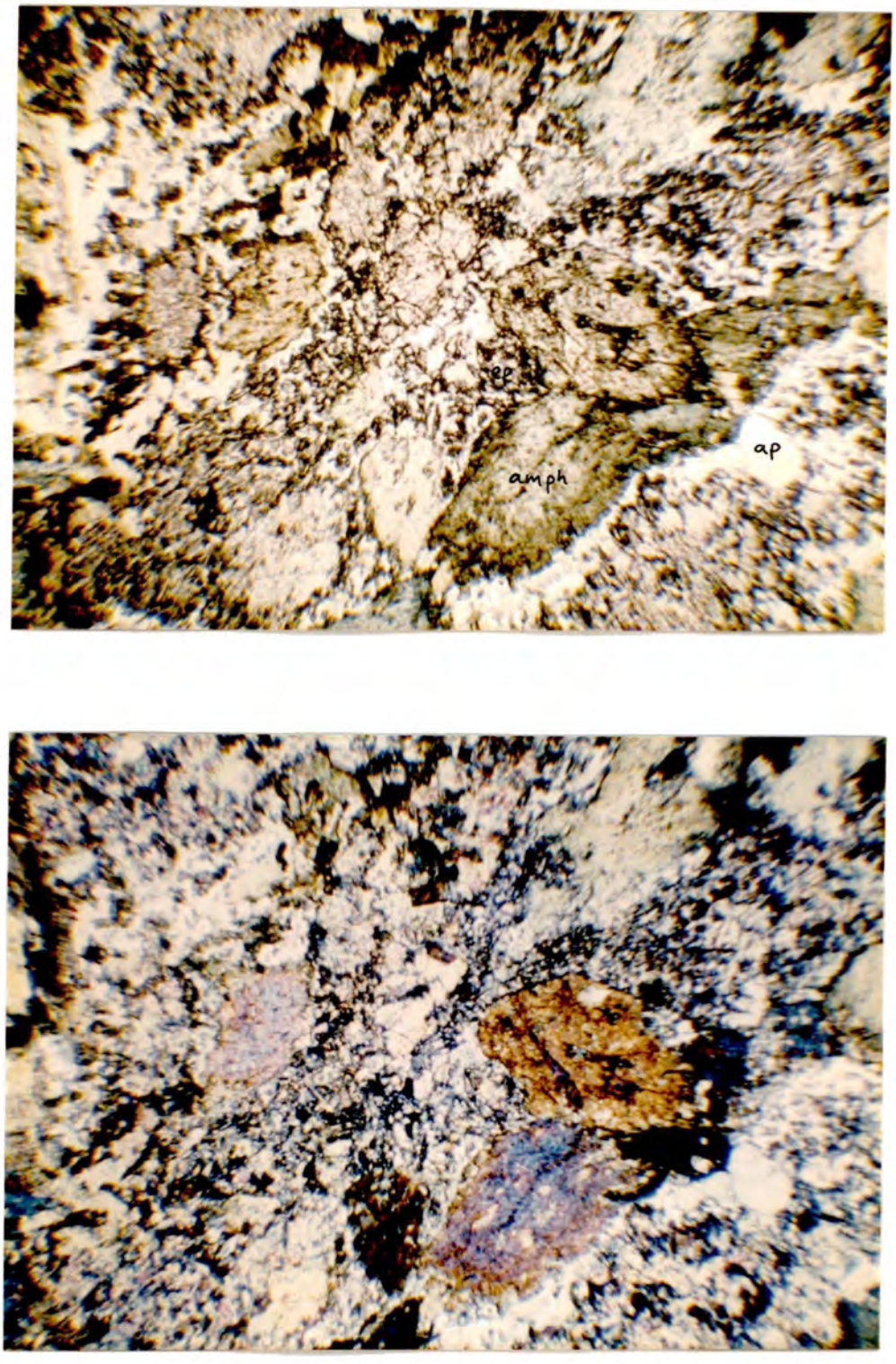

Plate 36

Photomicrographs: Doleritic rock (pseudodiorite) consisting of hornblende (amphibolised clinopyroxene) and fine granular epidote (replacing plagioclase and probably olivine). Apatite is also apparent. (Sample 7413: (A) - PPL; (B) - XP. Field width = 4 mm.).

like the doleritic rocks described above, is basic in composition (see Chapter 5). It is composed of about 50 per cent hornblende and biotite developed after pyroxene, and 50 per cent of fine, granular epidote, partly after plagioclase but also, probably, after original olivine (Plate 36). This is in view of the low SiO_2 content of this rock (sample 748, Appendix 2).

(3) Serpentinite. Thin sections examined (5132, 5133), and a brief description (Little, 1960) of the ultrabasic bodies near Rossland, show them to be almost totally altered to stringy aggregates of antigorite, with some minor talc and carbonate. Relict olivine is occasionally apparent within a network of serpentine veins. Blurred, lobate patches of brown serpentine may be after pyroxene. Also apparent are sporadic crystals of chrome spinel forming ragged grains of about 0.5 mm. or less.

The origin of these rocks is not certain, but most probably they represent ?ocean crust cumulates (olivine + Cr-spinel + ? pyroxene) that were emplaced tectonically along the 'Rossland Break'.

4:2 Clinopyroxene

Mode of occurrence. From the preceding discussion, it is evident that clinopyroxene is an almost ubiquitous phenocryst in the volcanics, absent only in the more evolved of the andesites. As a phenocryst it occurs in various habits. A common occurrence is as single, sometimes sub-rounded, euhedra up to 1 cm. in diameter (Plates 22 , 23), though an average size is nearer 0.25 cm. Clusters of several euhedra are also common, exhibiting well-developed crystal faces externally, with more irregular internal contacts. This, together with the termination of oscillatory zones by the internal contacts, indicates post-aggregation growth (Plate 37).

A further development in habit is the occurrence of glomeroporphyritic clusters of pyroxene, as shown in Plate 38 . In these clusters, the individual crystals tend to be more rounded and it seems likely that they originated by accumulation during crystal settling. They exhibit features resembling adcumulate growth, and trapped pockets of magma are indicated by interstitial chloritic patches.

As a groundmass phase, clinopyroxene occurs as small granules or rather ragged prisms, though, as noted in Section 4:1:1, the groundmass is highly altered.

In colour the pyroxenes vary from very pale-green or straw, to colourless. Occasionally, in plane-polarised light, zoning is visible, with more coloured rims surrounding a colourless core. In cross-polarised light many grains show faint to quite distinct oscillatory zoning, sometimes throughout the crystal but otherwise restricted to the outer part (Plates 37 , 39). This latter feature is also observed, in similar rocks, by Arculus (1974) and Barron (1976). Also evident in a number of cases is faint sector zoning (Plates 30 , 40).

Multiple and simple twinning parallel to {100} is a common feature.

Pyroxene phenocrysts in the minor intrusions are, as was observed above, generally less well formed (except sample 5010, Plate 30). This is due, primarily, to more extensive alteration marginally and internally along fractures and cleavage planes.

Chemistry. Chemical analyses of pyroxene, and all subsequently described minerals, were carried out by electron microprobe, the operating conditions and methods of which are detailed in Appendix 3. Appendix 3 also contains tabulations of the data discussed in this Chapter and Chapter 6.

Plate 37

Photomicrograph: Euhedral pyroxene cluster in a basalt. Note the termination of oscillatory zones by internal contacts. (Sample 4070. Field width = 4 mm.).

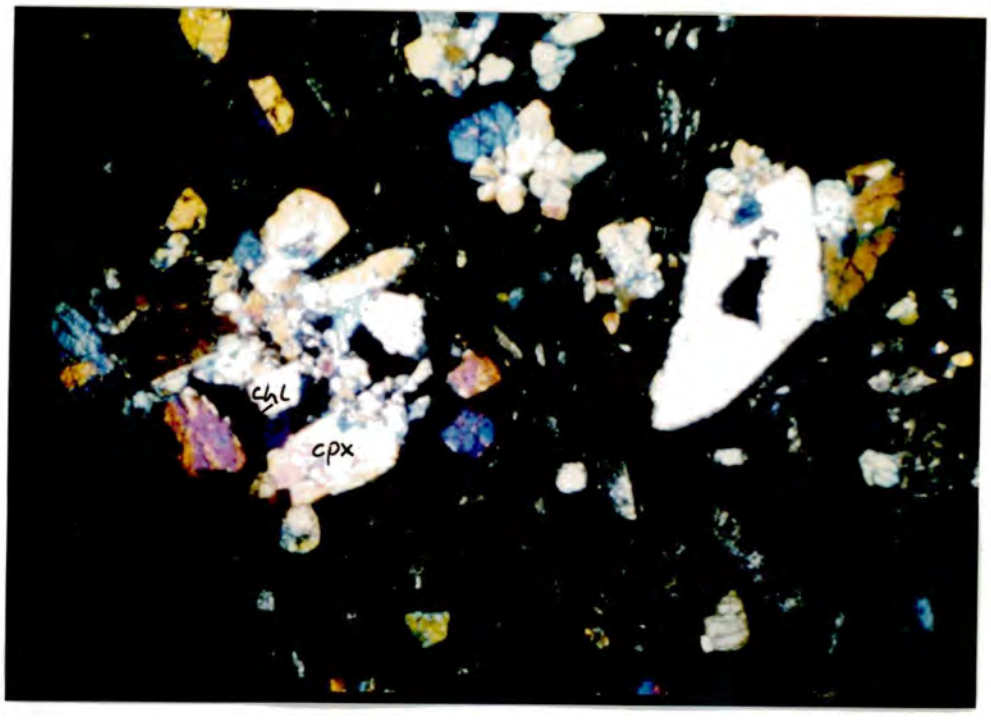

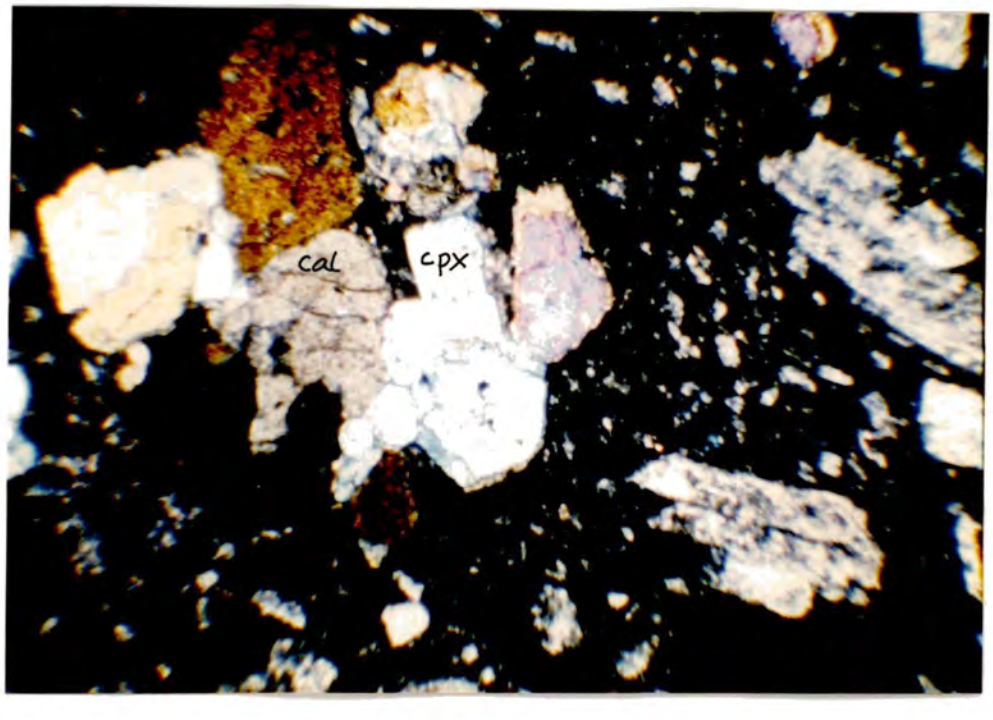

Plate 38

Photomicrographs: Glomeroporphyritic pyroxene clusters in a basalt. In particular, note in (B) trapped liquid, now chloritised, between pyroxene crystals. Also observe calcitised pyroxene in (B). (Sample 5041. XP. Field width = 4 mm. in both (A) and (B).

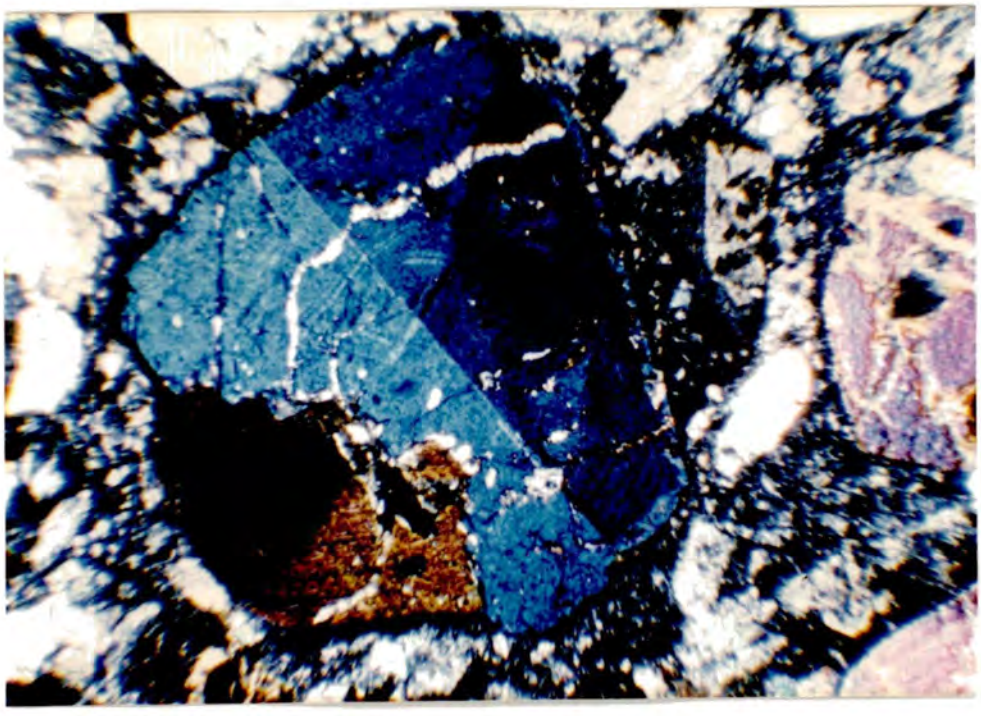

Plate 39

Photomicrograph: Augite phenocryst in basalt, showing good euhedral form. Note crenulated interface where two crystals have intergrown and which transects faint oscillatory zoning (Sample 5012. XP. Field width = 4 mm.).

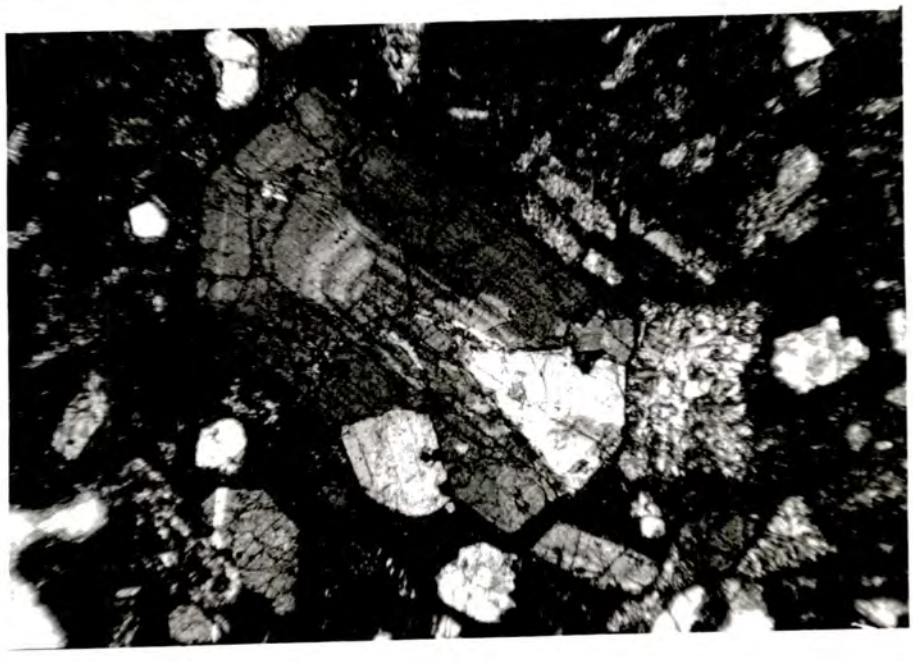

Plate 40

Photomicrograph: Sector-zoned clinopyroxene in a basalt. (Sample 5036. Field width = 4 mm.).

All the pyroxenes analysed were phenocrysts or microphenocrysts, groundmass pyroxene being too small for analysis. The analyses are plotted in Fig.4.1, the conventional pyroxene quadrilateral, from which it can be stated that all are classed as augite, salite or diopside, as defined by Deer et al. (1962). Included in the data plotted are analyses of the relict pyroxenes from the clinopyroxenite body and pyroxenes from a few minor intrusions. It is evident that there are no systematic differences between these and the volcanic pyroxenes (see also Fig.4.2).

Particularly evident in Fig.4.1 is the fact that the analyses occupy a restricted field, showing limited iron-enrichment compared to well known tholeiitic trends, such as the Skaergaard (Wager & Brown, 1967) or Thingmuli (Carmichael, 1967a). This is also true with respect to the mildly alkalic, Shiant Isles pyroxene trend (Gibb, 1973). This restricted range, whilst in part reflecting a limited range of whole-rock compositions, is also characteristic of calc-alkaline suites that exhibit a lack of absolute iron-enrichment. (see e.g. Fodor, 1971; Smith & Carmichael, 1968). That is, both FeO and mgO fall with differentiation in such a suite, in contrast to the well known Skaergaard trend, where, initially, FeO increases with differentiation; and the pyroxenes reflect this.

Variation of other components in relation to Mg-number (100 x Mg/ (Mg + Fe) atomic %), a measure of differentiation or temperature dependence, is shown in Fig.4.2. This plot shows that Al, Ti and Na all increase with decreasing Mg-number. Ca appears to go through a minimum at a Mg-number of about 75. This, however, is probably an artefact of sampling, since zoning in individual crystals show continuous Ca depletion (solid lines in Fig.4.2). The spread in Wo content, therefore, most probably reflects variable activities of

Figure 4.1

Part of the pyroxene quadrilateral (diopside-hedenbergite-enstatite- ferrosilite) showing distribution of analysed pyroxenes and amphiboles, plus tie-line relationships for average coexisting pairs. Skaergaard (SK) and Shiant Isles (SI) trends shown for comparison.

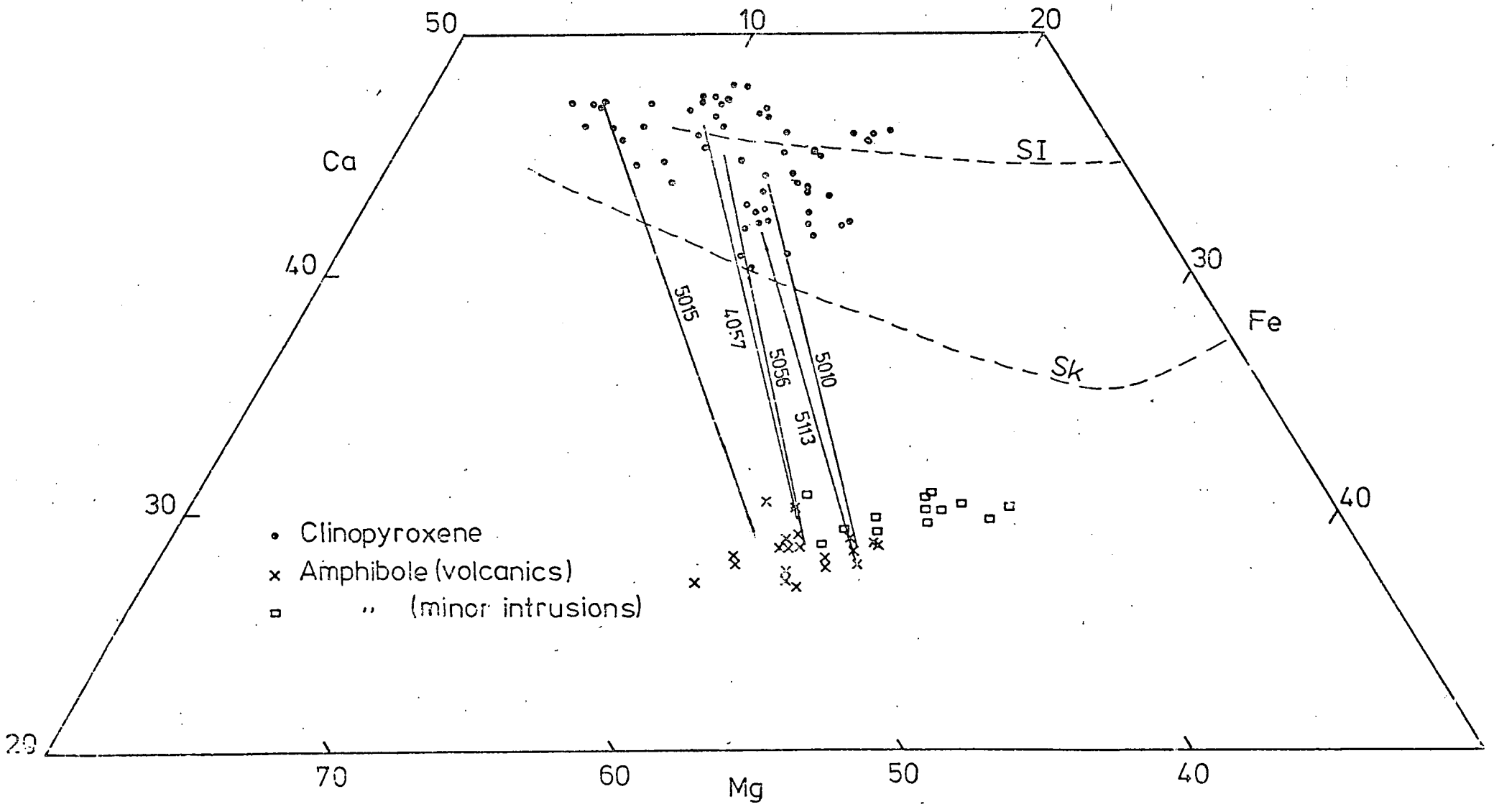
50
10
20
Ca
SI
40
30
Fe
5015
4057
5056
5113
5010
Sk
30
40
• Clinopyroxene
× Amphibole (volcanics)
▫ " (minor intrusions)
20
70
60
Mg
50
40

Figure 4.2

Variation of Na, Al, Ca and Ti with Mg-number in all Rossland volcanic pyroxenes. Solid lines join analysed cores and margins of phenocrysts, the arrows indicating the direction of overall zoning.

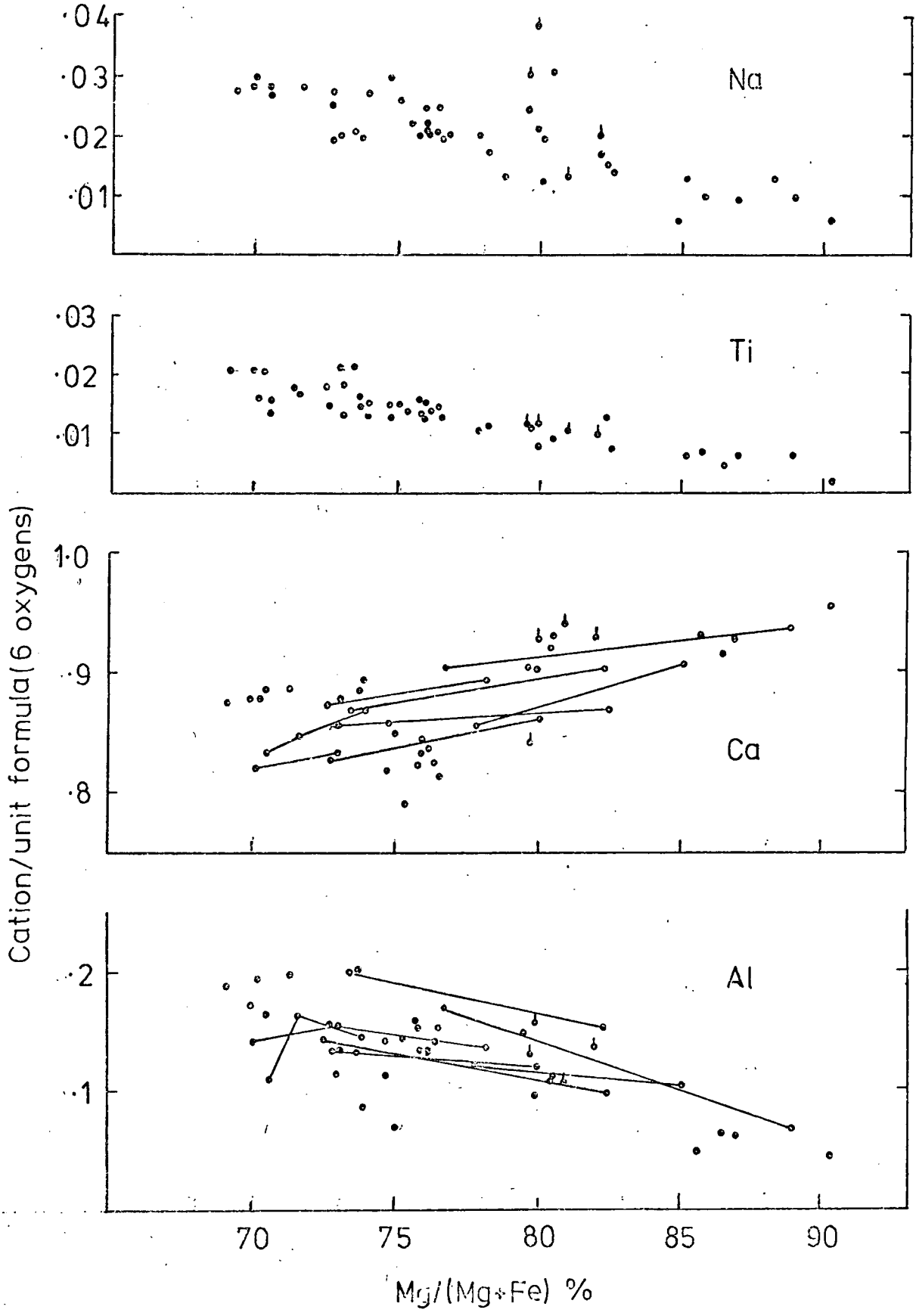

(• Pyroxenes from clinopyroxenite)

Ca, Mg and Fe in the host magmas, as well as variable external parameters, such as P_{H_2O} (Helz, 1973). Variation of pyroxene Wo content from sample to sample in a suite of rocks is evident in the data of Lowder (1970) and Smith & Carmichael (1968).

Zoning from core to rim, though oscillatory, is overall normal and parallels the overall trends æshown in Fig. 4.2. Variation within one thin section can cover almost the whole range of composition (e.g. sample CP57, Appendix 3), though it is usually less. As a result, it is found that correlation of Mg-number between whole-rock and pyroxene is very low.

In one or two cases it was observed that normally zoned crystals are bordered by a distinct rim of colourless pyroxene some 5-10μ in width. Analyses CP403A and CP403B (Appendix 3) are of such a rim and the adjacent part of the main crystal, respectively. The rim is low in Al, Ti, Na and Fe, and rich in Ca, Si and Mg and is one of the most basic compositions found. These rims may represent a quench growth similar to those produced in rapidly chilled experimental charges (Cawthorn et al., 1973). Alternatively, it may represent a new phase of growth due to the pyroxene being incorporated in a new batch of basic magma.

The chemical variations observed are governed by various coupled, or single, charge-conserving substitution reactions. Most obvious is the simple substitution:

$$Mg^{2+} \rightleftharpoons Fe^{2+}$$

Fig. 4.3 shows Si plotted against Al and indicates, as all analyses fall above the Si + Al = 2 line, Al is being incorporated in excess of that needed to fill the tetrahedral site. This effect is governed primarily by substitution of Ca-Tschermak's molecule:

$$(Mg, Fe)\ Si \rightleftharpoons Al^{vi}\ Al^{iv}$$

Figure 4.3

Al versus Si (on basis of 6 oxygen) for all analysed pyroxenes.

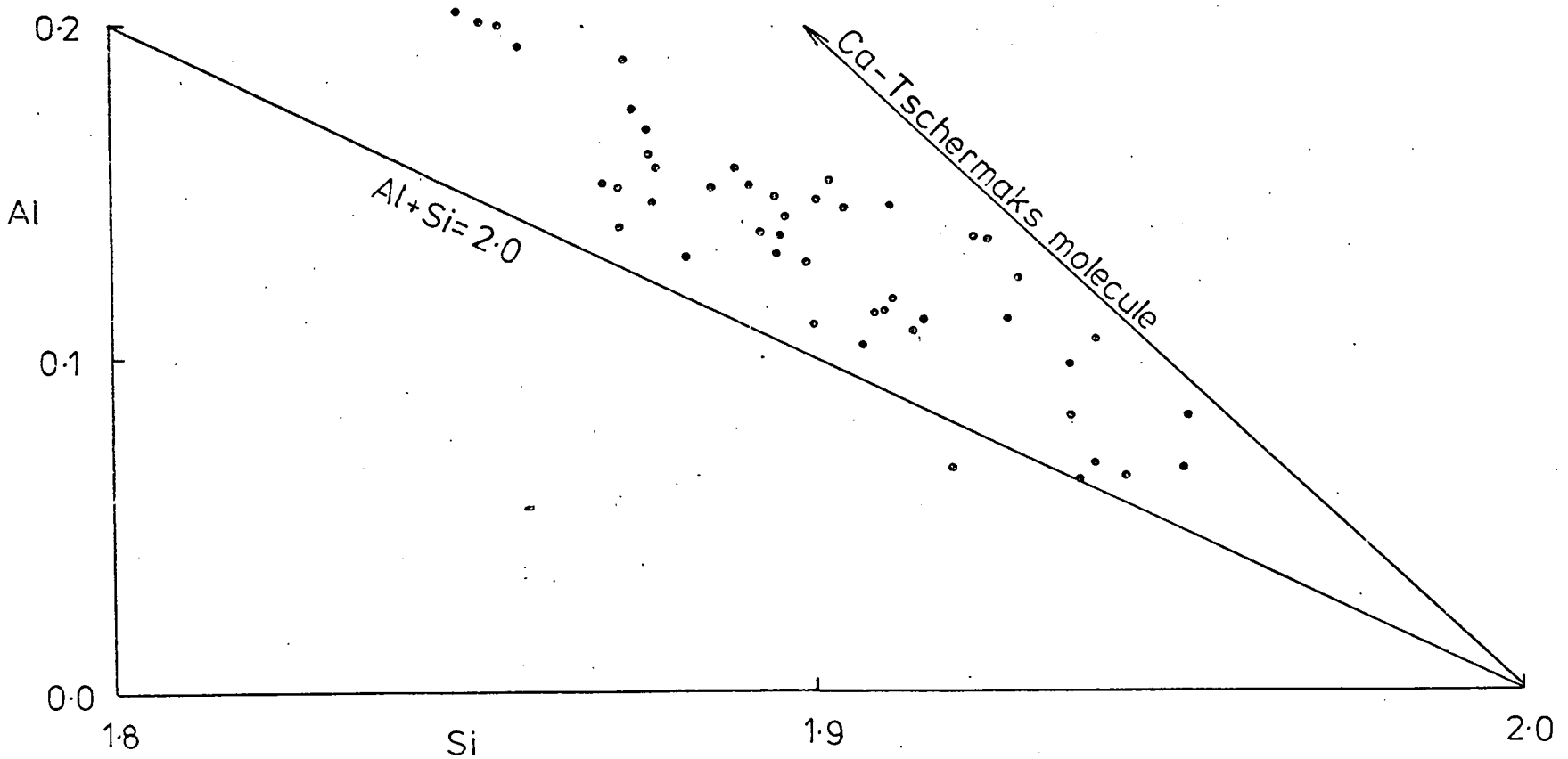
0·2
Al
0·1
0·0
1·8
Si
1·9
2·0
Al+Si=2·0
Ca-Tschermaks molecule

since the high Al/Ti ratios (about 10) for the pyroxenes preclude extensive incorporation of the molecule Ca $TiAl_2O_6$ (Yagi & Onuma, 1967). Similarly, small amounts of the acmite (Na Fe^{3+} Si_2O_6) or jadeite (Na Al Si_2 O_6) molecules are indicated by virtue of low Na/Si ratios (about 0.2). Thus, the decrease of Ca below 1 atom per formula unit, as shown by Fig. 4.2, is not compensated for by Na; rather, the negative correlation between Ca and Mg-number implies Fe^{2+} is preferentially incorporated in the M2 site compared to Mg.

Discussion

Since one of the aims of this thesis is to characterize the Rossland volcanics in terms of magmatic affinity, some attention will be paid to use of clinopyroxene chemistry in this respect.

Various schemes exist relating pyroxene chemistry to that of the host magma, for example Kushiro (1960 , Le Bas (1962) and Coombs (1963). Within the pyroxene quadrilateral, tholeiitic augite trends show strong iron-enrichment and generally low Ca/(Ca + Fe + Mg) ratios. This latter feature is particularly noticeable in groundmass pyroxenes of tholeiitic magmas, and compositions can plot within the miscibility gap between Ca-rich and Ca-poor pyroxenes, representing metastability (Carmichael et al., 1974). Strongly alkalic augite trends, by contrast, show compositions tending towards Ca/(Ca + Fe + Mg) ratios of greater than 50 per cent, and with a fractionation trend towards acmite rather than hedenbergite. Mildly alkalic trends, for example the Shiant Isles (Fig.4.1), lie in between. Differences such as these are also observable within a single magmatic environment, as Fodor et al. (1975) have demonstrated for Hawaii. The subdivisions shown in Fig.4.4 are after Le Bas (1962), where it can be seen that the Rossland analyses are mainly 'alkalic'.

Figure 4.4

Comparative diagram for clinopyroxenes from various island-arc suites (see text).

Fields 1, 2 and 3 are the sub-alkaline, alkaline and peralkaline fields, respectively, as defined by Le Bas (1962).

Source of data:-

Grenada	- Arculus	(1973)
Sofala	- Barron	(1976)
Dominica	- Wills	(1974)
Tonga	- EWart *et al.*	(1973)
Kanaga	- De Long *et al.*	(1975)
Bridget Cove	- Irvine	(1973)

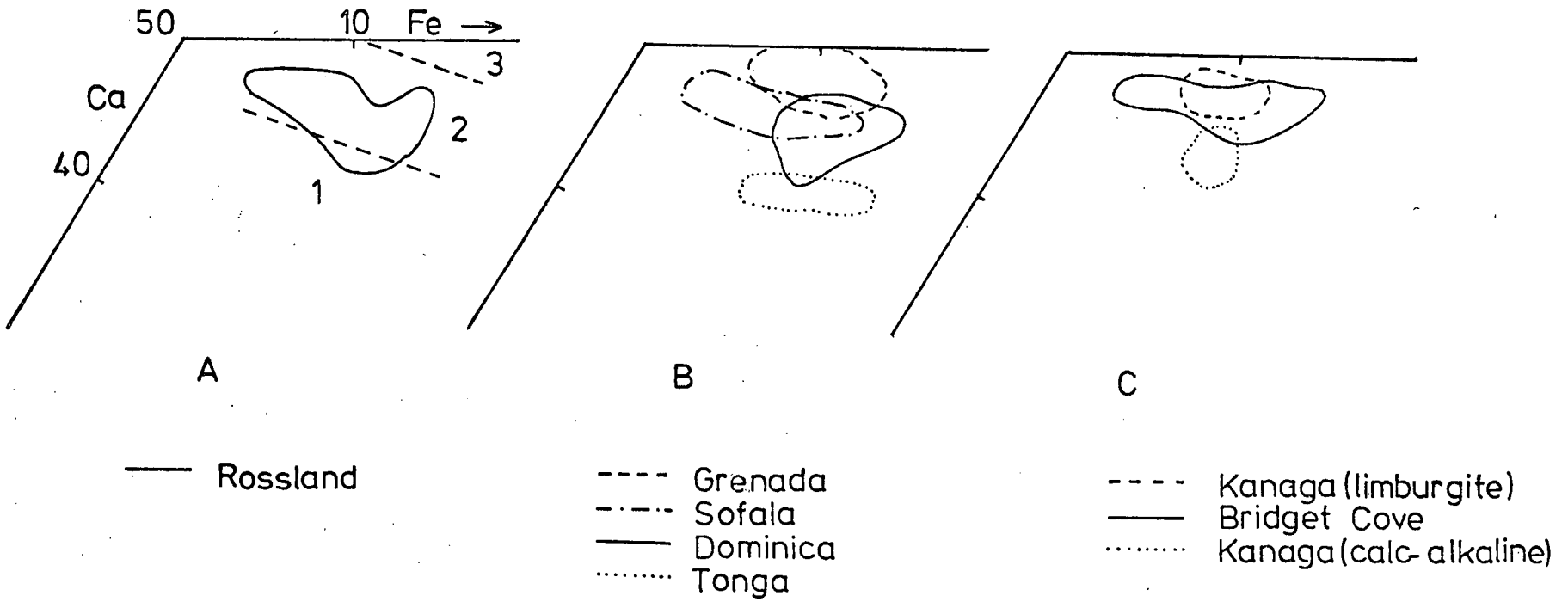
50
10
Fe →
3
Ca
2
40
1
A
B
C
Rossland
Grenada
Sofala
Dominica
Tonga
Kanaga (limburgite)
Bridget Cove
Kanaga (calc-alkaline)

However, whilst these features are generally true, they do not hold universally and considerable overlap can occur. This is especially so where calc-alkaline rocks are considered. The associations of Dominica (Wills, 1974) and Kanaga (De long et al., 1975) also plot in Le Bas' alkaline field (Fig. 4.4), whilst the coexistence of orthopyroxene with Ca-rich clinopyroxene, and other characteristics, clearly show these suites to be sub-alkaline. Similarly, data for Talasea (Lowder, 1970), which is a tholeiitic to calc-alkaline suite of rocks, transgresses the alkaline to sub-alkaline boundary. Helz (1973) has shown that the coexistence of amphibole with Ca-rich clinopyroxene shifts the pyroxene composition towards the diopside – hedenbergite join; and in general, Helz (op.cit.) notes that under hydrous conditions the distinction between pyroxenes of diverse melt compositions becomes blurred. Despite this, pyroxenes of island-arc alkaline magmas, such as the Grenadan varieties (Arculus, 1973) or the Kanaga Limburgites (De Long et al., 1975), still tend to be more Ca-rich than normal calc-alkaline pyroxenes, as shown in Fig. 4.4. Clearly, for island-arc suites, characteristically formed under hydrous conditions, the Le Bas-type boundaries need to be re-defined.

Apart from major element variations in pyroxenes, Al and Ti are frequently used as indicators (e.g. Brown, 1968). In general, Al and Ti are higher in pyroxenes derived from alkalic or low SiO_2-activity magmas. However, as for Ca, Mg and Fe, the variously defined fields are by no means exclusive. The Shiant Isles pyroxenes plot over all three fields of the SiO_2-Al_2O_3 diagrams of Le Bas (1962) and Kūshiro (1960), as do the Grenadan pyroxenes (Arculus & Curran, 1972) and the lesser Antilles plutonic-nodule pyroxenes (Lewis, 1973b). This, in part, is due to the use of phenocryst pyroxene analyses and not

just groundmass pyroxenes, as was intended. Other effects may also be operative. With respect to Ti it is clear that whole-rock TiO_2 contents are important. In TiO_2-rich alkaline rocks, correspondingly titaniferous augites are produced (e.g. Fodor et al., 1975) and chemical variations are governed more strongly by the Ca Ti Al_2 O_6 molecule as suggested by Yagi & Onuma (1967), and as seen in the Shiant Isles pyroxenes (Gibb, 1973). In such cases, Al concentrations are more effectively controlled by Ti. In TiO_2 -poor rocks, Al is incorporated primarily by Ca-Tschermak's molecule as suggested above is the case for the Rossland analyses and Al in the pyroxene is likely to be affected to a greater extent by Al_2O_3 in the melt. Thus, as suggested by Barberi et al. (1971), if plagioclase crystallizes before or during clinopyroxene precipitation, low Al levels may result, even in 'alkalic' pyroxenes. Where the reverse is true, low SiO_2-activity melts will favour high-Al pyroxenes, though not necessarily high Ti; this depending on its concentration in the magma. This effect is possibly evident in the cases of Grenada and Bridget Cove (Irvine, 1973), where Al_2O_3 in the pyroxenes, in both cases, varies from 1 to 9 weight per cent, whilst TiO_2 is less than 1.25 per cent. Both these associations are low-TiO_2, island-arc varieties, but they contain basic, under-saturated magmas in which olivine and clinopyroxene crystallization dominate. In contrast, the more siliceous, high-alumina magmas of Dominica (Wills, 1974), Santorini (Nicholls, 1971) and Kanaga (De Long et al., 1975), precipitating plagioclase readily, contain pyroxene in which Al_2O_3 does not exceed about 4 per cent.

Also effective in determining Al concentrations in clinopyroxene, are temperature and pressure. In the Lesser Antilles plutonic blocks, Lewis (1973b) and Wills (1974) have analysed pyroxenes with up to 7 per cent Al_2O_3, though these are clearly derived from sub-alkaline

magmas. Both of these authors show high Al is a function probably of temperature, Lewis (op.cit) noting a negative correlation of Fe/Mg ratio with Al. This is the opposite to what normally occurs in zoned phenocrysts (Fig. 4.2). This difference is probably due to the fact that the cumulate blocks have equilibrated at higher T and P than the volcanic phenocrysts, the pyroxene in association with other aluminous minerals such as amphibole and plagioclase; whereas phenocryst compositions in lavas are governed by complex liquid-crystal interactions.

On the basis of this discussion, and Fig.4.4, the Rossland pyroxenes show closest affinities with normal calc-alkaline volcanic pyroxenes, such as Dominica and Kanaga. They exhibit TiO_2 levels less than 1.0 per cent and Al_2O_3 levels less than 4.5 per cent. At the basic end of the pyroxene spectrum, Wo contents are quite high, greater than 45 per cent (Fig. 4.1), and thus they resemble, to some extent, the mildly alkalic affinities of the Bridget Cove (Irvine, 1973), Grenada (Arculus, 1973) and Sofala (Barron, 1976) pyroxenes. Additionally, it should be noted that the low Al concentrations of the Rossland samples also reflect the low-Al_2O_3 character of the parent magmas, contrasting with the usually high Al_2O_3, calc-alkaline magmas.

In summary, while pyroxene composition is clearly strongly dependent on bulk-magma chemistry, simple correlations between the two cannot be drawn. This is due to the influence of external parameters such as P and T of equilibration, and H_2O pressure. Additionally, crystallization sequence is important, though this is to some extent implicitly controlled by bulk chemistry. As far as can be ascertained then, the Rossland pyroxenes are indicative of normal calc-alkaline parent magmas, though extending to more Mg-rich compositions where, possibly, a mildly alkalic basalt parent is indicated.

4:3 Amphibole

Mode of occurrence. Amphibole phenocrysts are conspicuous in some volcanic samples and minor intrusions. They are also quite abundant in a few tuffaceous and volcaniclastic samples. In colour they are brown or pale brown, to shades of green-brown and they form euhedral or partly resorbed phenocrysts from 0.5 mm. to 8 mm. in length (Plates 25 , 41). The greener varieties are generally restricted to the intrusive rocks (Plate 31). Strongly pleochroic, red or dark-brown oxyhornblendes, such as reviewed by Deer et al. (1962), are not observed.

A feature of the volcanic amphiboles is their resorbed outlines and the development of 'opacite' rims, as illustrated in Plates 25 and 41 . These dusty, semi-opaque margins are probably composed mainly of iron-oxides, though optical identification is impossible. They result from the rapid transition of the amphibole-bearing magma out of the amphibole stability field (see Figs. 4.11 A,B) at relatively low temperature and P_{H_2O}. Occasionally, several buried opacite rims are observed (Plate 24), which must result from fluctuating P_{H_2O} in a sub-volcanic magma chamber. If the P-T path of the ascending magma crosses the amphibole-out curve (e.g. Figs. 4.11 A,B) at high T and P_{H_2O}, the breakdown assemblage is often coarser and can completely replace the amphibole. Such aggregates, usually containing oxides, plagioclase and pyroxenes in fairly strict proportions (Stewart, 1976), are not observed in any of the Rossland volcanic samples.

The amphiboles of the minor intrusions, as noted above, are greener in colour and do not show the degrees of resorbtion or opacite-rim development evident in the volcanic amphiboles. Presumably, this is a direct result of crystallization under moderate

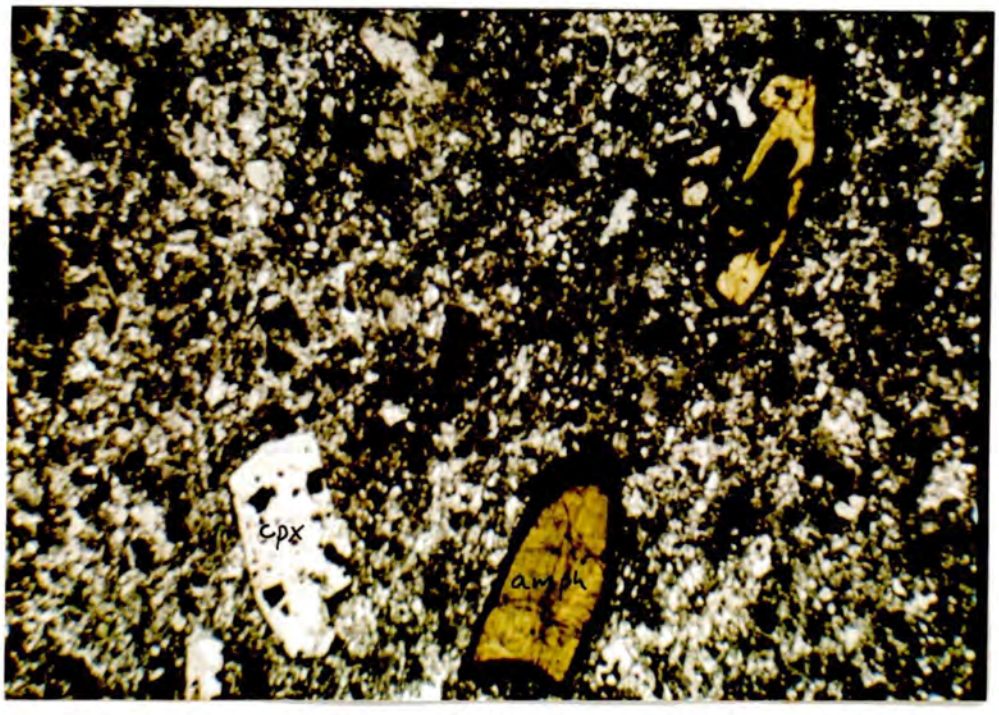

Plate 41

Photomicrographs: Amphibole phenocrysts in an andesite. Note that in addition to the opacite-rim development, the phenocrysts are also somewhat resorbed, losing their euhedral outlines.

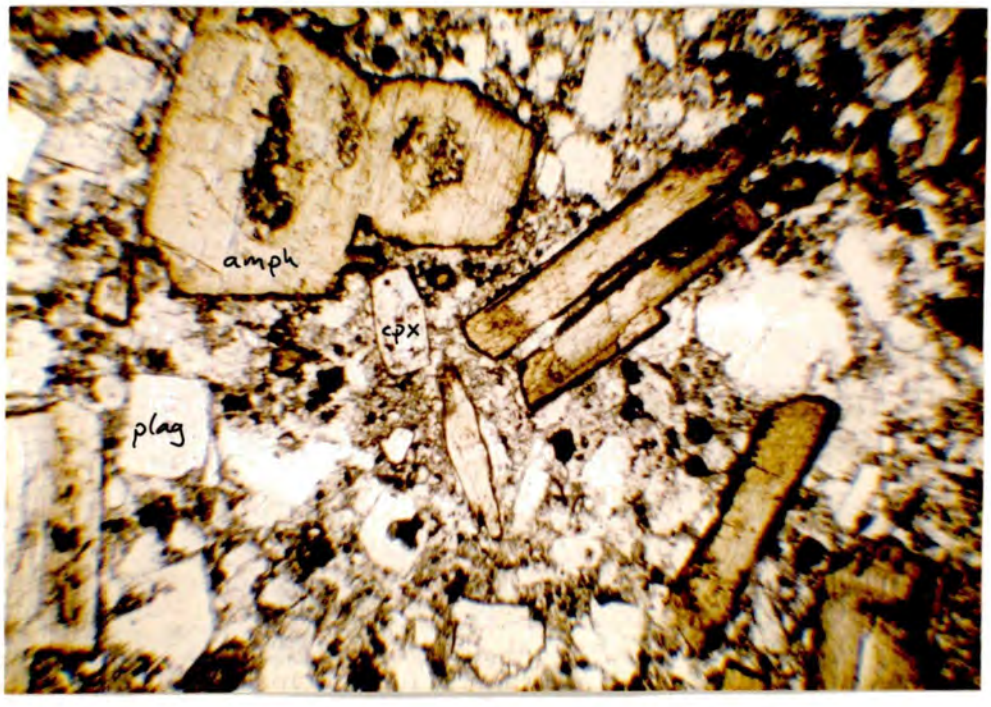

Plate 42

Photomicrograph: Amphibole-bearing andesite. Amphiboles are colour-zoned and form euhedra with only thin opacite rims. Other phenocrysts are minor clinopyroxene and plagioclase (Sample 5015. PPL. Field width = 4 mm.).

water-vapour pressures and within, or near, the amphibole stability field.

Zoning is apparent in some crystals on the basis of colour change. This is especially so in the minor intrusions, where opacite rims do not obscure the outer parts of the crystals. Usually, a paler core is surrounded by a more coloured rim. Or, in one or two cases, simple oscillatory zoning occurs, involving two or three changes (Plate 42). Fine-scale oscillatory zoning, such as characterises plagioclase or clinopyroxene, is not observed.

Amphibole, as was shown in Section 4:1, is generally the last phenocryst to precipitate, since it often contains poikilitic inclusions of magnetite , pyroxene and plagioclase (e.g. Plate 26). A late appearance of amphibole is typical in many island-arc suites (Jakeš & White, 1972a), especially in the Lesser Antilles volcanics and plutonic blocks (Wills, 1974; Lewis, 1973a; Arculus, 1973).

The significance of amphibole in the petrogenesis of the Rossland magmas is discussed later; however, it is worth making the observation here that amphibole shows very little indication of a reaction relation with clinopyroxene or olivine as is predicted by various experimental evidence at 2 - 10kb and H_2O-saturated or mildly under-saturated conditions (e.g. Cawthorn, 1976; Holloway & Burnham, 1972; Helz, 1973). Though amphibole frequently poikilitically encloses clinopyroxene, only one instance has been noted (amphibole in volcaniclastic rock) where it appears to overgrow a pyroxene in a reaction relationship. In addition, clinopyroxene phenocrysts coexisting with amphibole (e.g. Plate 24) show no sign of resorbtion.

Chemistry. Figs. 4.5 and 4.6 are two commonly used amphibole classification diagrams in which the analyses reported here (Appendix 3) are plotted. These show the variation of Al (tetrahedral) with A-site occupancy, and with Al (octahedral) + Fe^{3+} + Ti. In general, it is evident that the amphiboles are pargasitic in composition. Precise classification, however, is bedevilled by the presence of significant Fe^{3+} in these types of amphibole; microprobe analyses only returning total Fe. The effect of Fe^{3+} can be illustrated by comparing Figs. 4.5A and 4.5B and by inspection of Table 4.2. Figs. 4.5B and Fig. 4.6 are plotted assuming $Fe_2O_3/FeO = 0.68$. This value is an average taken from Wills (1974), and is based on wet chemical determinations of amphiboles by Wills (op.cit), Rea (1970) and Lewis (1964) from the Lesser Antilles. Following Ross et al. (1969), A-site occupancy is calculated by:-

$$A = Ca + Na + K + Fe\ (M4) - 2.00$$

Fe(M4) is considered as the excess over 5.00 of cations in the Y-sites. As Table 4.2 shows, increase of Fe^{3+} causes lowering of Fe(M4) and raising of Na(M4) and $Al^{iv.}$ The effect on classification is to shift compositions from pargasite towards tschermakite. The amphiboles are best described, therefore, as tschermakitic hastingsites, since Fe^{2+} replaces Mg significantly. There is also the tendency for volcanic amphiboles to plot nearer common hornblende than the minor-intrusion amphiboles (Figs. 4.5 and 4.6).

Also, it might be noted that the value of 0.68 for Fe_2O_3/FeO, whilst more or less suitable for the volcanic amphiboles - these being generally positive Fe(M4) and Na(M4) - is apparently too high for the intrusive amphiboles, where the sums of cations in Y is often less than 5.00 (negative Fe(M4)). Table 4.2 illustrates this.

Figure 4.5

Classification diagram (Al^{iv} versus A-site occupancy) for primary amphiboles.

(A) Structural formula calculated assuming all Fe as FeO

(B) Structural formula calculated assuming $Fe_2O_3/FeO = 0.68$

Crosses - amphiboles from volcanics
Squares - amphiboles from minor intrusions

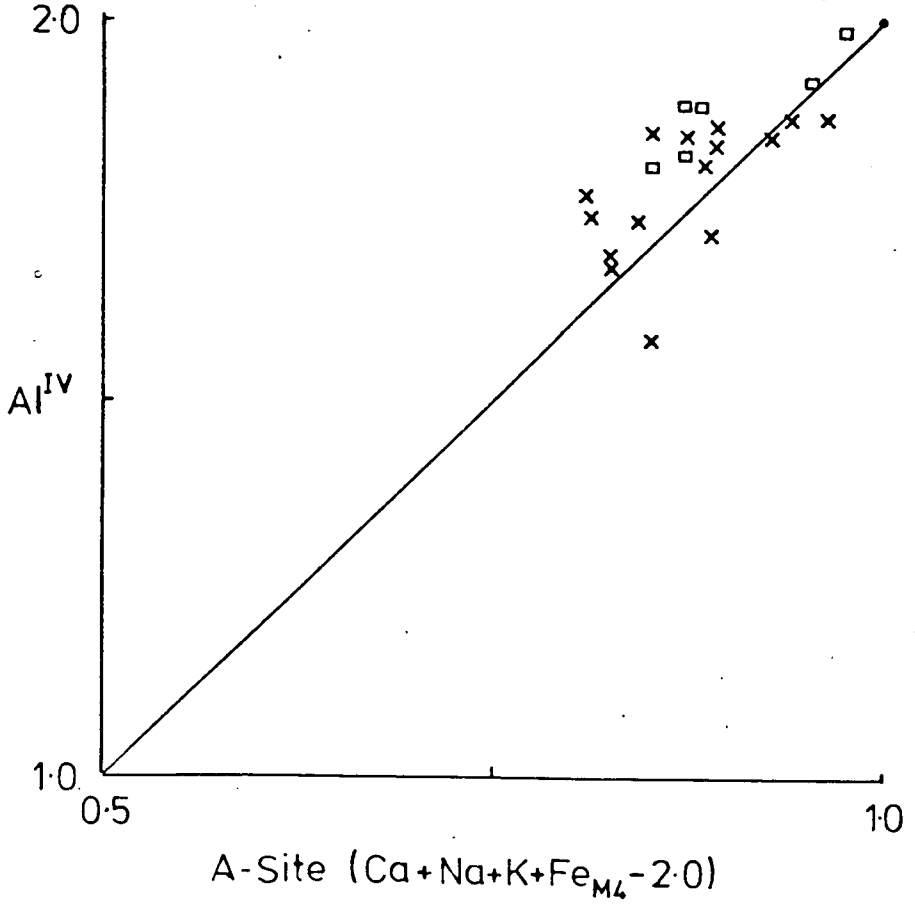
2·0
1·0
0·5
1·0
Al^{IV}
A-Site (Ca+Na+K+Fe_{M4}-2·0)

A

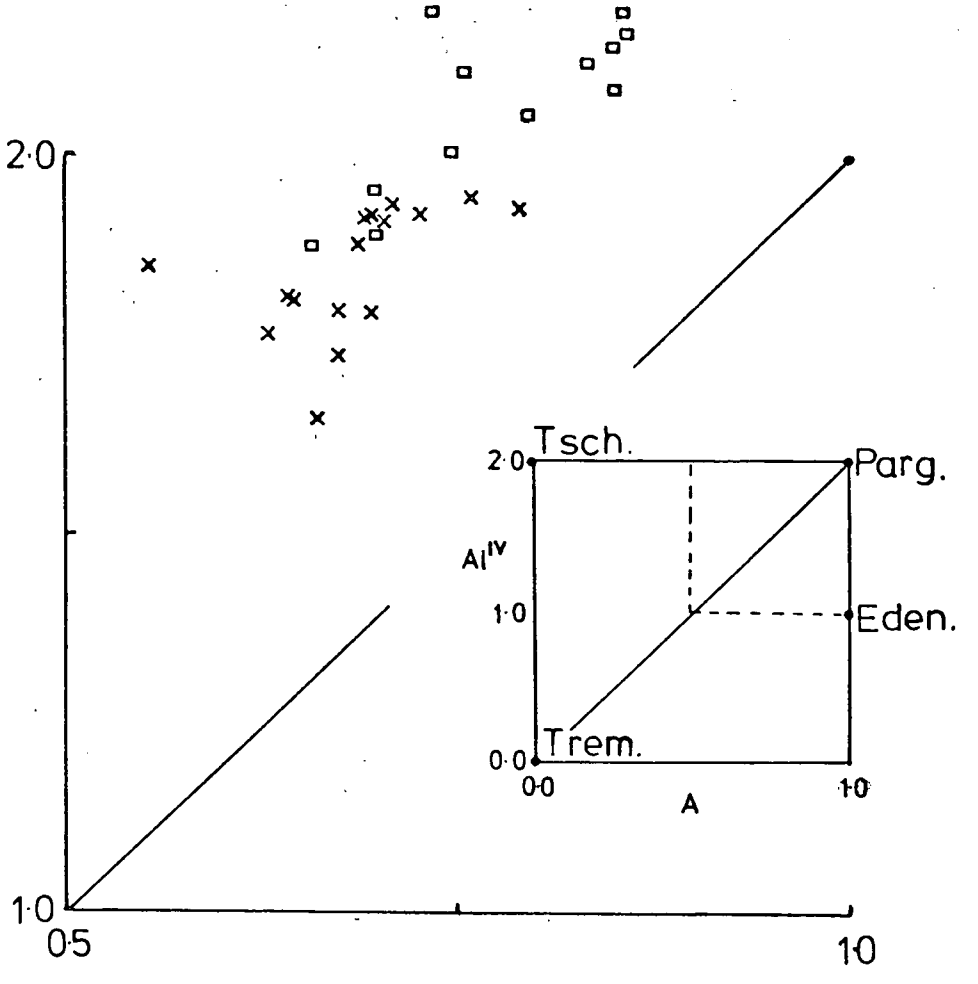
2·0
1·0
0·5
1·0
Tsch.
Parg.
Eden.
Trem.
Al^{IV}
2·0
1·0
0·0
0·0
1·0
A

B

Figure 4.6

Al^{iv} versus $Al^{vi} + Ti + Fe^{3+}$ classification diagram for primary amphiboles. $Fe_2O_3/FeO = 0.68$. (Symbols as in Fig.4.5)

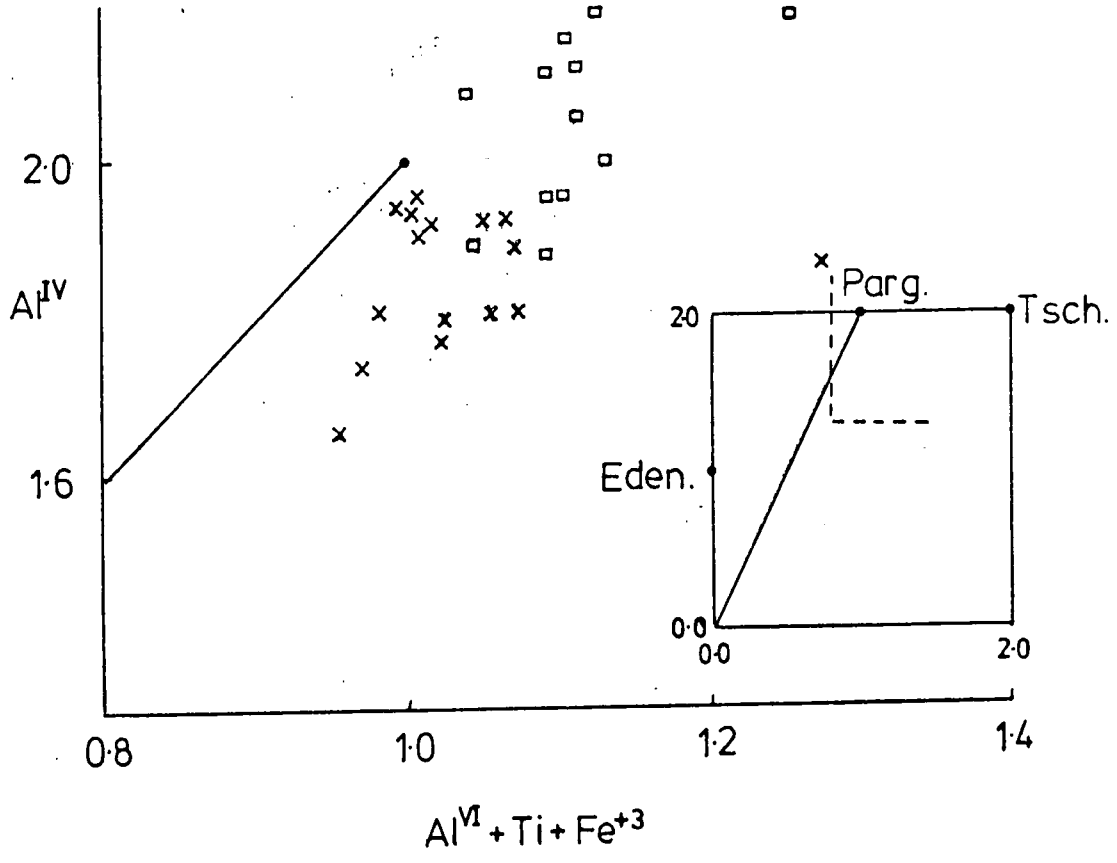
2·0
1·6
Al^{IV}
0·8
1·0
1·2
1·4
$Al^{VI} + Ti + Fe^{+3}$
Parg.
Tsch.
Eden.
2·0
0·0
0·0
2·0

TABLE 4.2

EFFECT OF Fe_2O_3 ON THE AMPHIBOLE STRUCTURAL FORMULA

	BH561		BH962	
	A	B	A	B
SiO_2	41.48	41.48	39.00	39.00
TiO_2	2.58	2.58	3.72	3.72
Al_2O_3	12.26	12.26	13.39	13.39
Fe_2O_3	-	4.80	-	5.92
FeO	11.40	7.07	14.05	8.72
Mg	0.21	0.21	0.25	0.25
MgO	14.63	14.63	11.41	11.41
CaO	11.66	11.66	11.63	11.63
Na_2O	2.18	2.18	2.37	2.37
K_2O	0.68	0.68	1.49	1.49
Total	97.16	97.56	97.31	97.90
Structural formula on the basis of 23 oxygens (anhydrous)				
Si	6.149	6.083	5.902	5.819
Al^{iv}	1.851	1.917	2.098	2.181
Al^{vi}	0.291	0.201	0.292	0.173
Fe^{3+}	-	0.530	-	0.665
Fe^{2+}	1.413	0.867	1.779	1.087
Mn	0.026	0.026	0.032	0.032
Mg	3.232	3.198	2.574	2.538
Ti	0.287	0.284	0.424	0.417
Ca	1.852	1.831	1.886	1.859
Na	0.627	0.620	0.696	0.686
K	0.129	0.127	0.288	0.283
Z	8.000	8.000	8.000	8.000
Y	5.249	5.106	5.101	4.912
A + X	2.608	2.578	2.870	2.828
Fe(M4)	0.249	0.106	0.101	-0.088
Na(M4)	-0.107	0.063	0.013	0.239

BH 561 Amphibole from 5056 (volcanics)

BH 962 Amphibole from 5096 (minor intrusion)

A Fe_2O_3 = 0, all Fe as FeO

B Fe_2O_3 = 0.68 x FeO

That Fe^{3+} is lower in the intrusive amphiboles is also indicated by the differences in colour. This also tends to confirm the suggestion, made above, that the intrusive amphiboles have not been subject to rapid removal from the amphibole stability field at low temperature, since this characteristically involves H_2O loss and oxidation (cf. Deer et al., 1962; Barnes, 1930).

Amphibole chemistry is governed by two main coupled substitutions, apart from the simple $Mg^{2+} = Fe^{2+}$ and $Na^{+} = K^{+}$ replacements. These involve incorporation of the Edenite and Tschermakite molecules. Respectively:

$$Si \rightleftharpoons NaAl^{iv}$$
$$MgSi \rightleftharpoons Al^{vi}Al^{iv}$$

From a basic tremolite formula these two produce pargasite. Most calciferous amphiboles plot in a band between tremolite and pargasite, natural edenitic or tschermakitic amphiboles being virtually unknown (Leake, 1962, 1965). Helz (1973) suggests that these two substitutions tend to occur together in order to reduce local charge imbalances, especially if Ti^{4+} is introduced.

Whilst the Al-tschermakitic substitution predominates as a mechanism for balancing the edenite molecule, it is clearly not sufficient since the amphiboles exhibit Al^{iv}/Al^{vi} of greater than 2.00, as would be required. This deficiency is made up by the presence of Ti and Fe^{3+} as is indicated by Fig. 4.6. Other minor substitutions in the amphiboles probably involve richterite ($Na(A) + Na(M4) \rightleftharpoons Ca$) or glaucophane ($Na(M4) + Al^{vi} \rightleftharpoons Ca + Mg$), since Ca is usually less than 2.00, though, as was observed above, the amounts of these molecules actually present depends critically on the accurate estimation of Fe^{3+}.

Variation within the intrusive and volcanic amphiboles is shown in Fig. 4.7. Each group shows little systematic variation. Within the volcanic group, only sample 4057 (Analyses BH 57, Appendix 3)

Figure 4.7

Variation of Al^{vi}, Ti, Al^{iv} and Ca with Mg-number in primary amphiboles.

Dashed line represents variation within sample 5015. Solid line represents zoning in one cyrstal from 5096. (Symbols as in Fig.4.5)

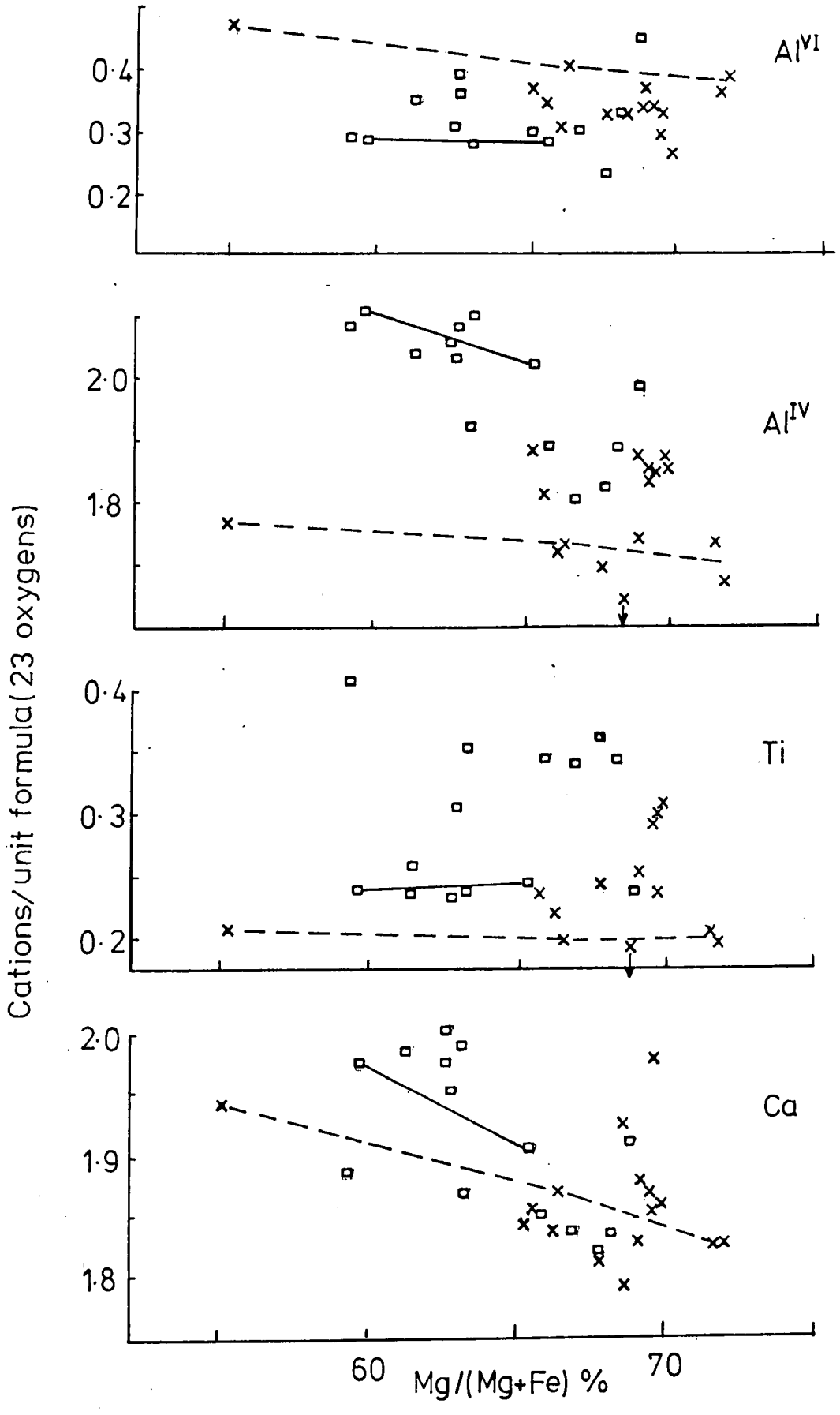
Al^VI
0·4
0·3
0·2
Al^IV
2·0
1·8
Ti
0·4
0·3
0·2
Ca
2·0
1·9
1·8
Cations/unit formula(23 oxygens)
60
70
Mg/(Mg+Fe) %

shows a wide range. Analyses from one sample tend to cluster and much of the scatter is apparently whole-rock scatter rather than individual mineral-analysis scatter; the precise chemistry of the amphibole depending, in some complex manner, on the bulk-rock chemistry. Bulk-rock chemical differences, or temperature differences, probably account for the differences between the two groups.

Where zoning is apparent (BH96, Appendix 3), or a range of compositions are obtained from one thin section (BH57), it is apparent that little variation occurs with Mg-number; Ti, Al^{vi} and Al^{iv} are roughly constant. Ca, however, tends to increase with Fe, this suggesting that deficiency in the M4 site is made up by Na rather than Fe.

Discussion

Amphiboles, similar in composition to those reported here, have been commonly described from calc-alkaline, island-arc or continental margin volcanic associations (e.g. Jakeš & White, 1972a). They have also been produced experimentally from basaltic and andesitic melts of various compositions, under hydrous conditions (Green & Ringwood, 1968; Helz, 1973; Cawthorn et al., 1974; Eggler, 1972). Precise controls of amphibole chemistry have not as yet been clearly defined, though a comprehensive study on the effects of temperature, fugacity of oxygen and whole-rock chemistry is reported by Helz (1973). In addition, Cawthorn (1976a) using data from naturally occurring samples, has shown the broad effects of whole-rock chemistry on amphibole composition, and has broadly delimited fractionation factors and distribution coefficients for the major elements.

Helz (1973) shows, for a given starting composition, that as temperature decreases so do A-site occupancy, Al^{iv} and Ti. High temperature amphiboles ($\sim$ 1000°C) plot close to the tschermakite-pargasite join. Lower temperature amphiboles plot towards common hornblende. This is in part due to the stabilization, down temperature, of Fe-Ti oxides and plagioclase. Similar temperature controls on amphibole chemistry are also typical of metamorphic amphiboles (Chapter 6).

These effects are also noticeable in natural (igneous) occurrences. Table 4.3 lists some analyses of experimentally produced amphiboles and natural samples from basalts and andesites. It is clear that those amphiboles from more evolved siliceous magmas are richer in Si, and depleted in Al, Ti and alkalis. Jakeš & White (1972a) also show that amphiboles from more siliceous continental-margin volcanics are richer in Si compared to those from less differentiated island-arc suites. From Table 4.3, Rossland volcanic amphiboles, on average, are seen to be comparable to the higher temperature amphiboles from basaltic melts. There is also evidence of the temperature effect described above. Comparison of analyses BH57 and BH56 with BH13 and BH15 (Appendix 3) show the first two, derived from basalts, to be richer in Al^{iv} compared to the latter two, derived from andesites.

Following on from these observations, a feature of island-arc occurrences of amphibole is that they are rarely reported in rocks with SiO_2 less than 55 per cent (Jakeš & White, 1972a). Furthermore, amphibole tends to make an appearance at lower SiO_2 levels in a suite, in high-K type associations, such as described by Jakeš & Smith (1970), Mackenzie & Chappell (1972), Gill (1970) or Larsen et al. (1937). Another significant fact is that normal

TABLE 4.3

COMPARATIVE DATA ON NATURALLY OCCURRING AND EXPERIMENTALLY PRODUCED AMPHIBOLES

	A	B	C	D	E	F	G	H	1	2
SiO_2	40.44	45.35	39.3	42.17	44.88	46.34	40.6	45.2	41.48	43.12
TiO_2	3.98	1.03	3.8	2.17	1.77	1.65	2.76	2.2	2.77	1.75
Al_2O_3	11.73	8.16	15.6	13.71	9.65	7.42	11.0	8.6	12.18	11.82
FeO	18.41	18.70	9.8	9.19	11.96	16.82	15.15	11.9	11.26	10.65
MnO	0.16	-	-	0.14	-	0.38	0.29	0.32	0.18	0.14
MgO	9.20	10.37	13.7	16.19	14.40	12.11	13.8	14.6	14.68	15.28
CaO	11.14	11.69	11.8	11.53	11.25	10.91	11.0	10.9	11.70	11.60
Na_2O	2.72	2.03	2.9	2.81	2.12	1.56	2.53	1.9	2.42	2.28
K_2O	0.81	0.62	0.2	0.41	-	0.34	0.28	0.36	0.58	0.69
TOTAL	98.59	97.95	97.1	98.50	96.03	97.53	98.26	96.00	97.24	97.23

A Experimentally produced amphibole, Picture Gorge tholeiite; 1000°C, PH_2O = 5 kb.(Helz, 1973)

B " " " " " " 700°C, PH_2O = 5 kb (Helz, 1973)

C " " ", High-Al,Quartz tholeiite; 1040°C, PH_2O = 9 kb (Green & Ringwood, 1968)

D Naturally occurring amphibole, transitional basalt, Grenada (Arculus, 1973)

E " " " dacite " "

F " " " dacite, Dominica (Wills, 1974)

G " " " gabbroic xenolith, Santorini (Nicholls, 1971)

H " " " dacite " "

1 Amphibole BH572, Rossland basalt

2 Amphibole BH 152A, Rossland andesite.

calc-alkaline associations, such as Santorini (Nicholls, 1971) or Dominica (Wills, 1974), whilst containing amphiboles only in andesitic or dacitic extrusives, contain amphiboles of a more 'basic' nature in cumulate blocks or gabbroic xenoliths (Table 4.3). Alternatively, basic rocks of alkaline affinities contain, more commonly, kaersutitic amphiboles (Aoki, 1964; McBirney & Aoki, 1968; Gunn, 1972). Similarly, the rarer island-arc alkaline rocks, such as those of Grenada (Arculus, 1973), Kick 'em Jenny Volcano (Sigurdsson et al., 1974), Bridget Cove (Lathram et al., 1968) and Bogoslof Island (Arculus et al., 1977) also tend to carry amphiboles in basaltic representatives. Why sub-alkaline basalts do not contain amphibole, though apparently are capable of precipitating it at depth, is somewhat enigmatic. The data of Helz (1973) and Yoder & Tilley (1962) suggest that the upper temperature of the stability field of amphibole is higher in alkalic than tholeiitic basalt. This implies that the higher alkalis of island-arc and other alkaline basalts, given sufficient P_{H_2O}, facilitates stabilization of amphibole. Cawthorn (1976) notes this tendency in synthetic melts, where amphibole stability is enhanced with increase of Na_2O in the bulk composition. Sub-alkaline basaltic magmas, therefore, must invariably erupt at temperatures above their amphibole stability field. Only those magmas retained at depth go on to precipitate the amphiboles found in nodules and xenoliths.

By inference, the presence and nature of the amphiboles within the Rossland volcanics at basaltic compositions is suggestive of relatively high alkalis, and suggests an analogy with the alkaline rocks of Grenada and Bogoslof Island. This suggestion is strengthened when consideration is made of the alkali contents of the amphiboles themselves. Helz (1973), Jakeš & White (1972a) and Wills (1974) have all shown that there is a correlation between A-site occupancy,

or alkali content, and whole-rock alkali content. This effect is particularly noticeable within the Lesser Antilles arc, where a very distinct axial change in magma type is evident (Brown et al., 1977). Fig. 4.8 shows the fields of amphiboles found in the plutonic nodules from three islands in this arc (after Wills, 1974). St.Kitts shows island-arc tholeiitic affinities, Dominica calc-alkalic and Grenada calc-alkalic/alkalic. In Fig. 4.8, together with data reported here, are plotted various amphiboles from other volcanics. The Rossland amphiboles compare well with the Grenadan plutonic and volcanic amphiboles, but have significantly higher K than the analyses from the calc-alkaline associations of Dominica and Santorini. Amphiboles from the minor intrusions are even richer in K and are comparable with the amphiboles reported from the back-arc alkaline rocks of Japan (Aoki, 1964) and Bogoslof Island (Arculus et al., 1977).

The Sofala analyses (Barron, 1976) are also K-rich (fig.4.8), and also represent amphiboles derived from basaltic rocks. It was commented upon above (Section 3:4) that these rocks are similar in many other respects to the Rossland Group.

4:4 Amphibole-Clinopyroxene Relations

It is a characteristic of coexisting amphibole and clinopyroxene that Fe/Mg ratios are distributed such that amphibole is depleted in Mg relative to clinopyroxene. It is this tendency that is the main reason for considering amphibole an important phase in producing a non-iron-enriched, calc-alkaline trend (Ringwood, 1974; Cawthorn & O'Hara, 1976).

The tie-line relationships in Fig. 4.1 show that the Rossland samples provide no exception, similar patterns being reported by Lewis (1973b), Wills (1974), Arculus (1973) and Arculus et al. (1977).

Figure 4.8

K versus Fe/Mg for primary amphiboles. Data plotted include the Rossland volcanic and minor intrusion amphiboles, plus data from the literature:-

Sofala (Barron, 1976)
Grenada (Arculus, 1973)
Kick 'em Jenny(" ")
Dominica (Wills, 1974)
Santorini (Nicholls, 1971)

A, B and C are the compositional fields of amphiboles from the plutonic nodules of Grenada, Dominica and St.Kitts, respectively. (Wills, 1974).

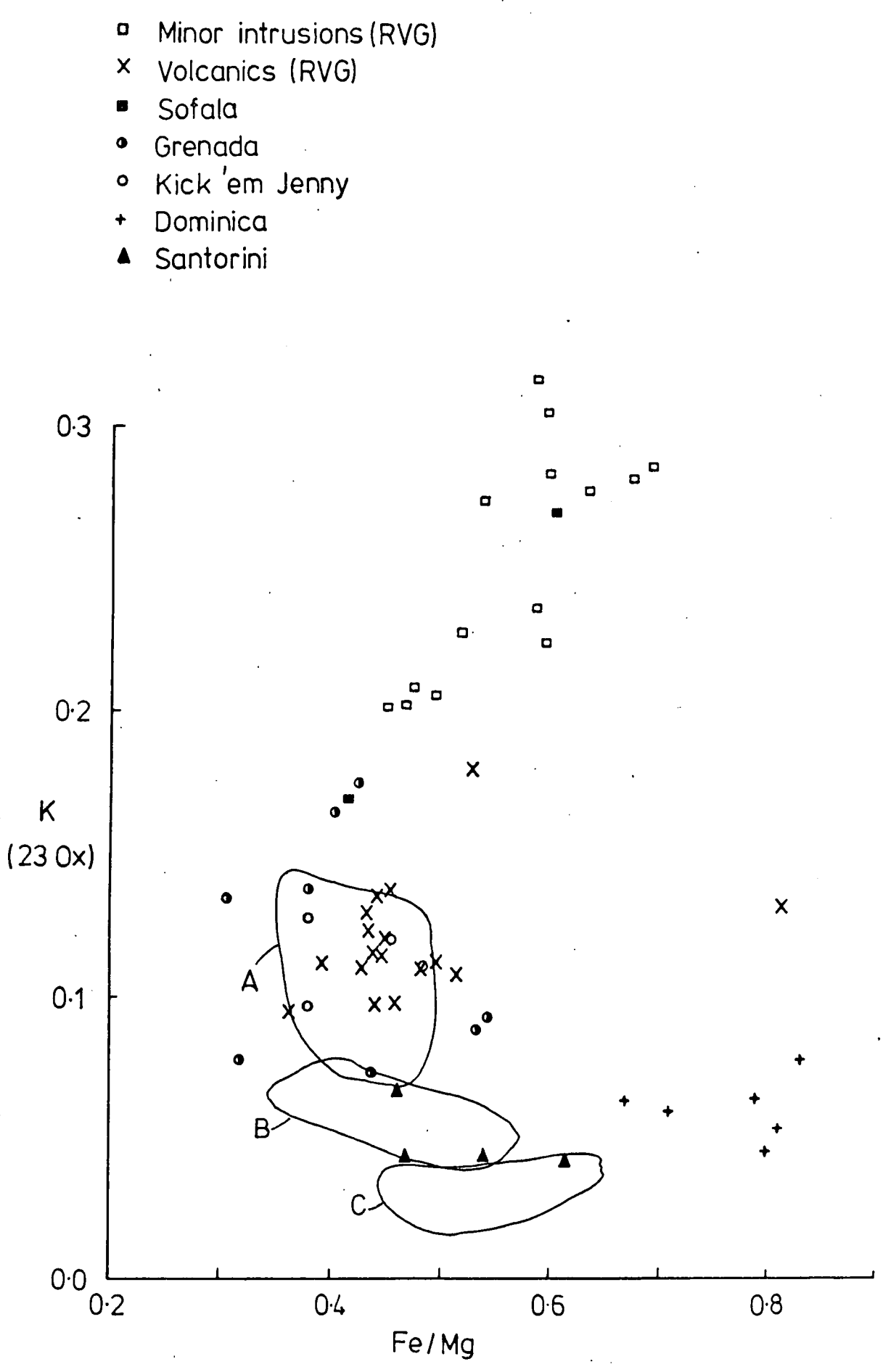
Minor intrusions (RVG)
Volcanics (RVG)
Sofala
Grenada
Kick 'em Jenny
Dominica
Santorini
0·3
0·2
0·1
0·0
K
(23 Ox)
A
B
C
0·2
0·4
0·6
0·8
Fe / Mg

The distribution coefficient governing the partitioning of Fe and Mg between these two phases, is defined:

$$K_D = (Fe/Mg)_{Amph.} \times (Mg/Fe)_{cpx}$$

Helz (1973) shows that this coefficient increases with temperature (Table 4.4). This represents a radical departure from ideality ($K_D = 1$, $T = \infty$) and is due, probably, to structural constraints. In the amphibole, as Al and alkalis increase with temperature, Fe^{2+} is favoured over Mg due to ionic-size differences.

Table 4.4 shows average K_D values for the Rossland volcanic samples, with the data of Helz (1973) for comparison. This suggests the Rossland samples equilibrated at around 930°C - 970°C, excepting sample 5015. However, this sample has only one pyroxene analysis from the core of a phenocryst, which is Mg-rich. Temperatures of about 950°C agree, generally, with those suggested in Section 4.8, on the basis of the Al^{iv} content of the amphiboles. This is a tentative indication that amphibole and clinopyroxene are in equilibrium, despite the visible reaction and resorbtion textures exhibited by the amphiboles, which are interpreted as a near-surface phenomenon.

4:5 Plagioclase

Mode of occurrence. Plagioclase, like pyroxene, occurs in virtually all rock types and is only absent, as a phenocryst, in some ankaramitic basalts. Most frequently, it occurs as discrete laths of up to 3 mm., but it can also form aggregates of several crystals joined along flat crystal faces (Plates 43 , 44). As a groundmass phase, it occurs as microlites or very small laths set in an originally glassy matrix, or it tends to form interstitially to groundmass pyroxene and oxides.

In both amphibolised and non-amphibolised rocks, plagioclase is extensively altered. Within the former samples, it is either

TABLE 4.4

Mg-Fe DISTRIBUTION COEFFICIENTS FOR CO-EXISTING AMPHIBOLE AND CLINOPYROXENE

Rossland samples		K_D Data of Helz (1973, Table 13)			
Sample No.	K_D				
5010	1.57	T^oC	PG.	1921	1801
		875	1.63	1.57	-
5056	1.70				
		930	1.58	1.50	1.52
5113	1.58				
		970	2.68	2.04	2.06
5015	2.92				
		1000	3.48	3.55	3.59
4057	1.75				

$$K_D = (Fe/Mg)_{cpx} \times (Mg/Fe)_{amph}$$

PG. Picture Gorge tholeiite

1921 1921 Kilauea olivine tholeiite

1801 1801 Hualalai alkali basalt.

inclusion-ridden with epidote, or recrystallized to relatively clear albite or oligoclase (see Chapter 6). Several X-ray diffractometer runs of the feldspars from amphibolised rocks confirm it is in the low-structural state by using the curves of Smith (1956) and Smith & Gay (1956). In the non-amphibolised rocks plagioclase is invariably altered to, or contains abundant inclusions of epidote, sericite and occasionally chlorite (e.g. Plates 43 , 45). Alternatively, it can be extensively calcitised. As a result,such features as zoning and twinning are often completely obscured. In rare cases, as shown in Plate 45 , patches of clear, unaltered plagioclase are seen and in such cases oscillatory zoning is in evidence.

Chemistry. Due to the altered nature of the plagioclases, only a few analyses, representing igneous plagioclase compositions, have been obtained. These are shown in Appendix 3 and are plotted in the ternary feldspar diagram (Fig. 4.9). Compositions lie within the andesine and sodic labradorite range. Whether or not highly calcic plagioclase, characteristic of calc-alkaline rocks, occurs is uncertain, since, as Plate 43 shows, the cores of phenocrysts are invariably altered; only the margins occasionally are capable of analysis. Since zoning is apparent, more calcic compositions would be expected.

Orthoclase contents of the plagioclases analysed are quite high, around 3-4 per cent, compared with other island-arc suites. For example, Grenadan and Dominican plagioclase compositions, reported by Arculus (1973) and Wills (1974), contain less than one per cent Or for comparable An contents. Santorini plagioclases (Nicholls, 1971) contain Or of less than 2 per cent. The Bogoslof

Figure 4.9

Analysed plagioclase phenocrysts plotted in the ternary feldspar diagram.

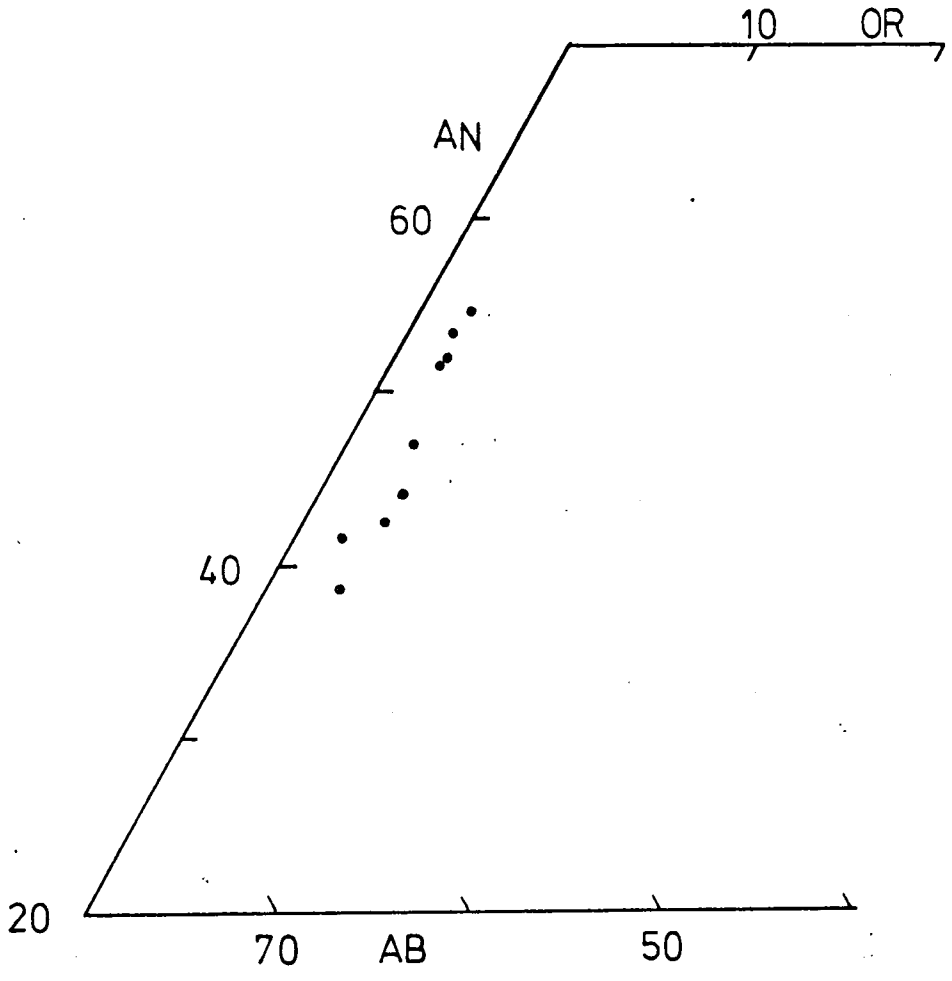
10
OR
AN
60
40
20
70
AB
50

Plate 43

Photomicrograph: Basalt showing variably sized plagioclase phenocrysts; also with phenocrysts of clinopyroxene. The plagioclase in the centre is an aggregate of several individual laths joined along crystal faces. Alteration of the feldspar to chlorite, epidote and sericite is advanced, but is least intense near the rims of the crystals. (Sample 5055. XP. Field width = 4 mm.).

Plate 44

Photomicrograph: Crystal controlled plagioclase aggregate in an andesite. Highly altered. (Sample 5034. Field width = 4 mm.).

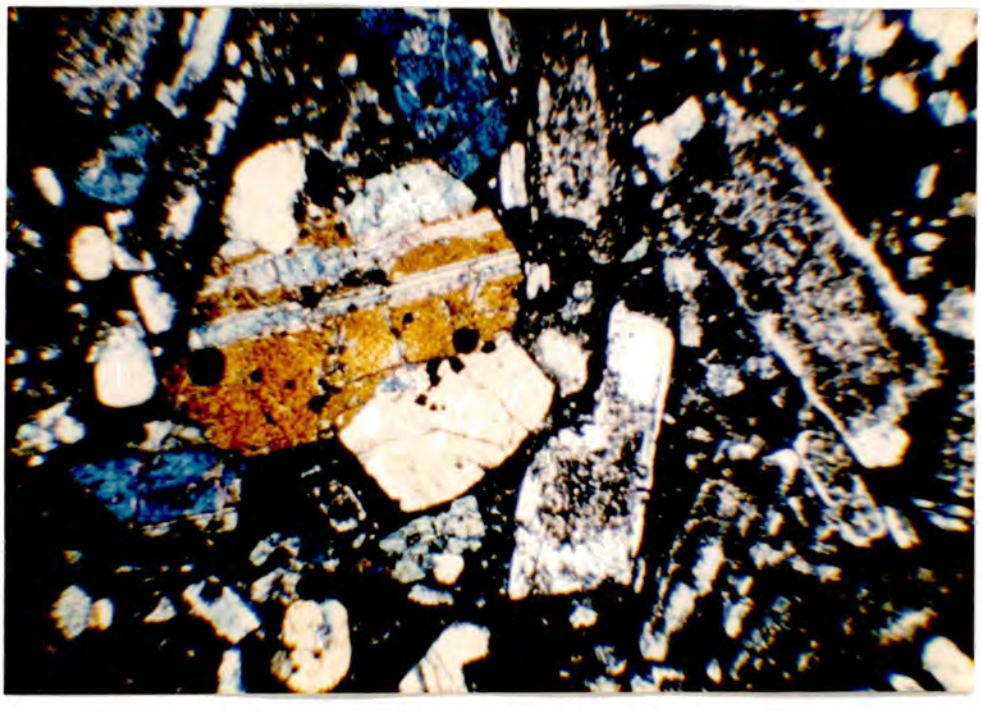

Plate 45

Photomicrograph: Basalt consisting of highly altered plagioclase (but note occasional fresh margins), and clinopyroxene phenocrysts. Large pyroxene (centre) is an aggregate of three intergrown crystals and contains rounded inclusion of spinel (Ti-magnetite mainly) (Sample 5013. XP. Field width = 4 mm.).

Island alkalic rocks contain plagioclases perhaps more comparable with the Rossland; Fig.4 of Arculus et al. (1977) shows that at a plagioclase composition of An_{40}, orthoclase content is about 4 per cent. Rossland plagioclases also compare favourably with those analysed by Gandy (1975) from the apparently mildly alkalic to calc-alkalic, Devonian Sidlaw volcanics. The Or content is, to some extent, a function of whole-rock K_2O is expected by consideration of the experimentally determined feldspar system (e.g. Carmichael et al., 1974) and is also shown to be the case in Hawaiian plagioclase feldspars (Keil et al., 1972).

4:6 Spinel

Mode of occurrence. In the non-amphibolised samples, spinels occur invariably as phenocrysts and in abundances (Table 4.1) of 1-6 per cent. They occur mainly as rounded to subhedral crystals of less than 1 mm., either enclosed by clinopyroxene or groundmass (Plates 41, 43). Only occasionally does plagioclase contain spinel inclusions.

The most common spinel is titaniferous magnetite. Ilmenite has not been observed as a separate phase. Much less common is Cr-spinel.

Alteration of magnetite is usually advanced, with, in some samples, complete replacement by turbid aggregation of ?iron hydroxides. Alternatively, sulphides (pyrite or pyrrhotite) have replaced primary magnetite, and small granules of sphene can develop as Ti is released. However, in other samples magnetite is only partially altered along fractures and margins. Smaller grains within pyroxene can even be completely fresh. In reflected light, most magnetites appear homogenous, though occasionally fine exsolution lamellae of ilmenite are observable.

Within the amphibolised rocks, no original magnetite is preserved. In many cases, secondary sulphides are the only opaque phase, and where magnetite is present and fresh it is compositionally adjusted to metamorphic conditions (see Chapter 6). Otherwise, magnetite has vanished leaving only faint turbid aggregates of ?iron hydroxides (as above) as vestiges of its presence. Thus, although porphyritic spinel was present in these rocks, abundances are not easily estimable and are not shown in Table 4.1; though it would be expected that they are similar to those calculated for the non-amphibolised volcanics.

Chemistry. Cr-spinel was, as shown above, found in a few samples and four analyses are shown in Appendix 3. They are also plotted in Fig. 4.10, with some comparative data. Three of the analyses (Fig. 4.10) have quite high Cr/(Cr + Al) ratios plotting above the field of spinels from stratiform, basic intrusions (Irvine, 1967). In analysis SP434 this may be due to the rather high SiO_2, which is a result of contamination due to the small grain-size of the analysed crystal. In the other cases these high Cr/Al ratios appear to be real. Also plotted in Fig. 4.10 are a Cr-spinel from a Grenadan alkali-basalt (Arculus, 1973), and some Cr-spinels from the Alaskan-type ultramafic bodies associated with the Nicola-Takla volcanics (Irvine, 1974; see also Section 5.4.3.)

Cr-spinel is clearly an early phase to crystallize (being included in pyroxene) and this agrees with the theories derived by Irvine (1967) who suggests that the crystallization of Cr-rich spinel, initiated at high temperature, ceases, still at quite high temperature, probably by a reaction relation with pyroxene. Certainly, there is a large compositional gap between Cr-spinel

Figure 4.10

Plot of analysed Cr-spinels with comparative data:-

Tulameen (Findlay, 1969)
Aiken Lake (Irvine, 1974)
Grenada (Arculus, 1973)

Solid lines enclose field of Cr-spinels from stratiform intrusions (Irvine, 1967).

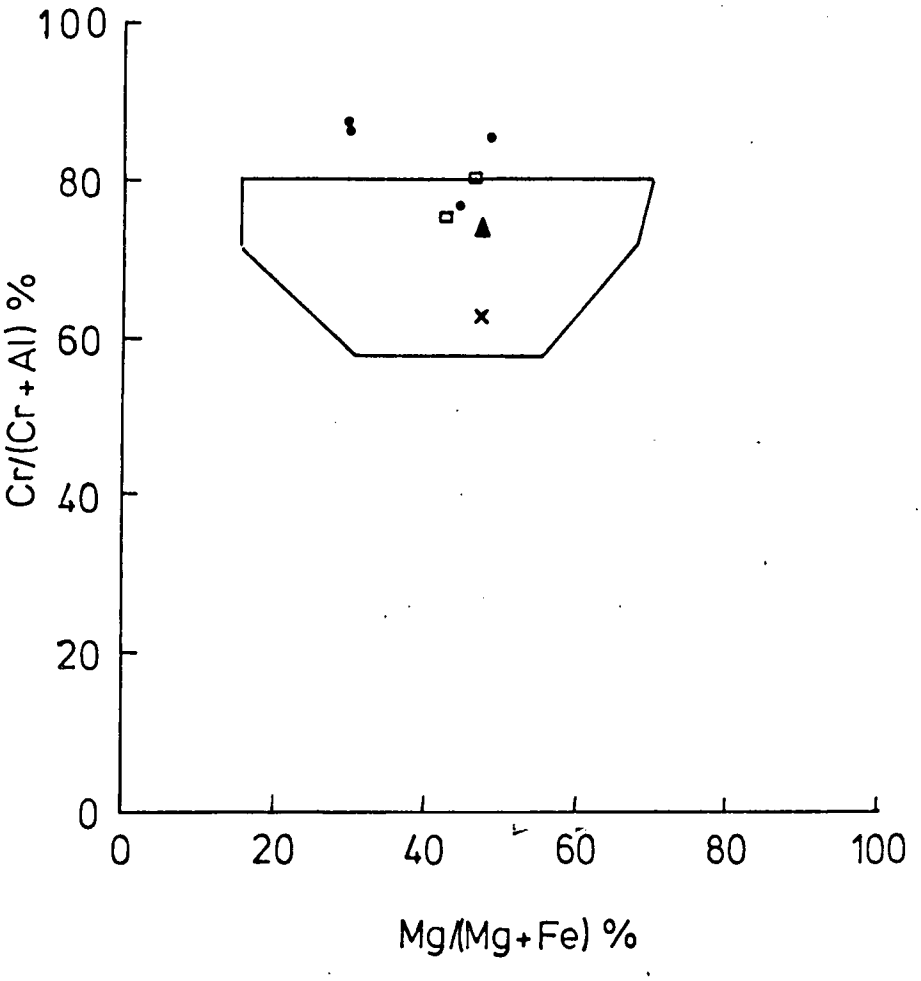

- Rossland
- Tulameen
- Aiken Lake
- Grenada

(50 per cent Cr_2O_3) and Ti-magnetite (less than 0.9 per cent Cr_2O_3).

In the magnetites, TiO_2 varies from 10.44 to 1.75 per cent and substantial amounts of Al_2O_3 also occur (0.63 - 6.00 per cent). These analyses are tabulated in Appendix 3, and they generally compare closely with magnetites from other island-arc/calc-alkaline suites, such as the Lesser Antilles (Arculus, 1973; Wills, 1974; Lewis, 1973b). The absence of ilmenite as a phenocryst is also a characteristic of low TiO_2 (island-arc) magmas (cf. Carmichael & Nicholls, 1967).

4:7 Biotite

Mode of occurrence. Biotite is observed in only one sample (5033), an andesite. It is shown in Plate 27 , where it occurs as rather ragged crystals of about 0.5 - 1 mm. Like amphibole, biotite shows evidence of marginal and internal breakdown to an assemblage involving, mainly, fine aggregates of iron oxides. This is a result of the thermal contraction of the stability field of biotite at near-surface pressures, analogously to amphibole.

Biotite phenocrysts are not unusual in calc-alkaline associations, but occur particularly in high-K suites (e.g. Mackenzie & Chappell, 1972; Gill, 1970).

Chemistry. Table 4.5 shows the two biotites analysed from sample 5033, with two comparative analyses; one from an andesite from Bogoslof Island (Arculus *et al.*, 1977) and one from the Colorado latite association described by Larsen *et al.* (1937). The igneous nature of the biotites is confirmed by their high TiO_2 content, particularly.

TABLE 4.5

ROSSLAND IGNEOUS BIOTITES WITH COMPARATIVE DATA

	1	2	A	B
SiO_2	36.93	36.48	39.14	37.41
TiO_2	5.23	4.22	4.27	4.29
Al_2O_3	14.17	14.36	13.10	14.86
FeO	13.21	16.13	16.69*	13.44
MnO	0.23	0.21	0.14	0.13
MgO	16.08	15.22	12.75	16.41
CaO	0.06	0.04	1.64	0.03
Na_2O	0.51	0.27	0.70	0.79
K_2O	8.99	8.12	6.55	8.69
Total	95.42	95.04	94.99	96.05
Structural Formula on the basis of 22 oxygens (anhydrous)				
Si	5.479	5.477	5.790	5.499
Al^{iv}	2.480	2.523	2.210	2.491
Al^{vi}	0.000	0.020	0.074	0.000
Te	1.639	2.025	1.914*	1.652
Mn	0.030	0.026	0.017	0.016
Mg	3.555	3.405	2.811	3.596
Ca	0.009	0.007	0.260	0.004
Ti	0.583	0.476	0.474	0.473
Na	0.148	0.078	0.199	0.227
K	1.701	1.556	1.236	1.628
Z	7.958	8.000	8.000	7.990
Y	5.807	5.952	5.440	5.741
X	1.858	1.640	1.700	1.859

1 BI331, Rossland andesite 5033

2 BI332, " " "

A Biotite from latite, Colorado (Larsen et al., 1935)

B Biotite from andesite, Bogoslof Island (Arculus et al., 1977)

(* Fe_2O_3 = 12.29, FeO = 5.63)

4:8 Mineral stability in basaltic and andesitic melts.

The nature and crystallization sequence of the minerals described above, can provide important constraints on the external conditions during the crystallization and eruption of the Rossland magmas. In this section, a brief discussion of recent and relevant experimental work is given, and its application to the Rossland volcanics commented upon.

Particularly significant is the presence of amphibole (and biotite), since these indicate the importance of dissolved volatiles, particularly H_2O. Figs. 4.11 A and B show experimental data taken from Eggler & Burnham (1973) and Yoder & Tilley (1962), pertaining to the stability relations of various phases in andesitic and basaltic melts, respectively, under H_2O-saturated conditions. In Fig.4.11A the oxygen fugacities were at the QFM buffer, whilst in Fig. 4.11B the oxygen fugacity, though unbuffered, was probably near to HM (Helz,1973), and Fe-Ti oxides were stable throughout the crystallization sequence. Despite these differences, and those of whole-rock composition, some features are common to both. Notably, with an increase of P_{H_2O} the upper temperature limit of amphibole stability increases, amphibole becoming a near-liquidus phase in both melts at 6-10kb. Conversely, plagioclase stability falls considerably. In the andesite (Fig.4.11A), plagioclase only precedes amphibole in the crystallization sequence below 6kb (P_{H_2O}). In the olivine tholeiite (Fig. 4.11B), compositionally closer to the bulk of the Rossland basalts, this condition occurs between 1.5 and 2kb. Similarly, in other basaltic melts experimented upon by Helz (1973) and Holloway & Burnham (1972) the crystallization sequence, plagioclase to amphibole, is only apparent at low P_{H_2O}.

Figure 4.11

(A) P_{H_2O}-T stability diagram as determined for the Mt. Hood andesite by Eggler & Burnham (1973).

(B) P_{H_2O}-T stability diagram for an olivine tholeiite as determined by Yoder & Tilley (1962).

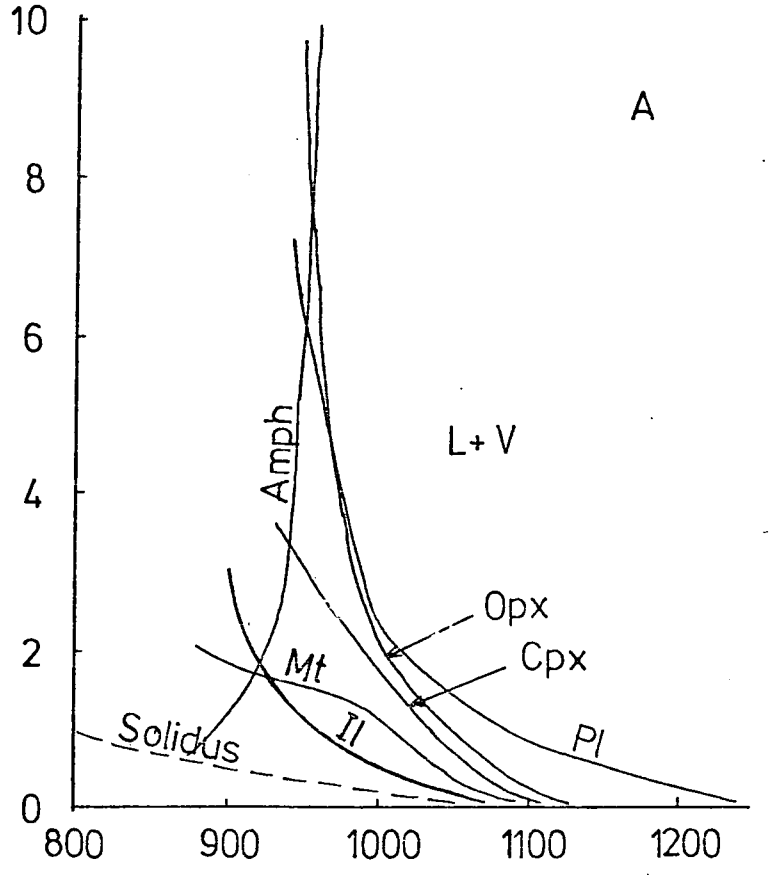
10
8
6
4
2
0
800
900
1000
1100
1200
A
Amph
L+V
Opx
Cpx
Mt
Il
Pl
Solidus

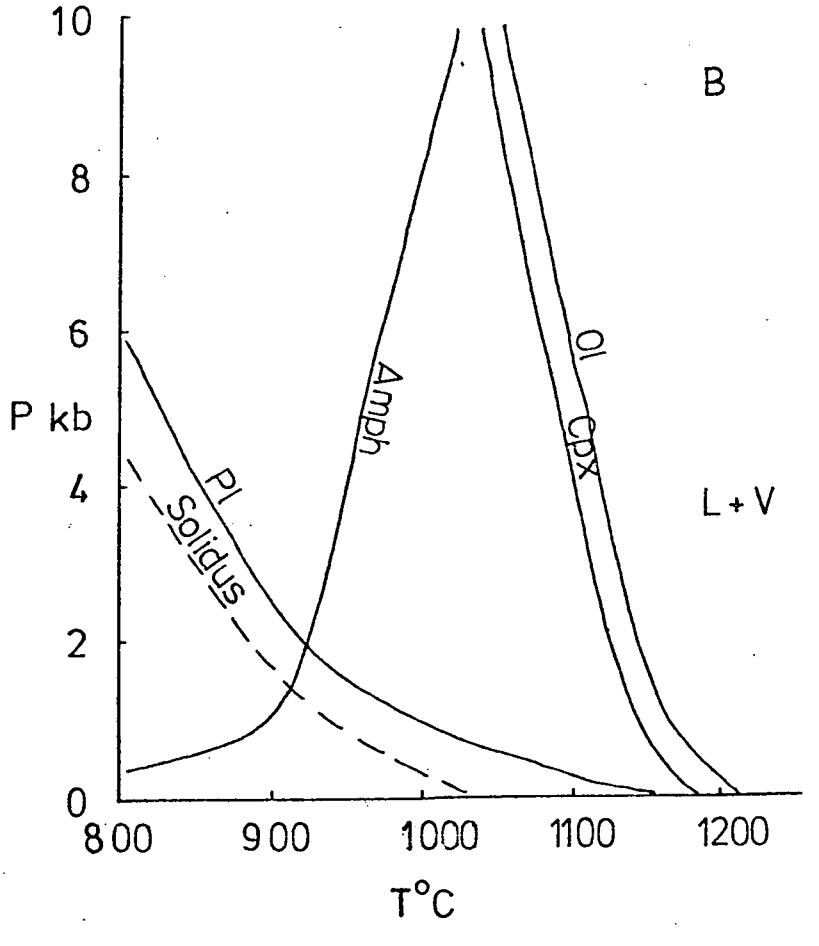
10
8
6
4
2
0
P kb
800
900
1000
1100
1200
T°C
B
Amph
Ol
Cpx
Pl
Solidus
L+V

Since it is a common feature in the volcanics bearing amphibole, that amphibole succeeds plagioclase (Section 4.1), and if $P_{tot} = P_{H_2O}$, then the magmas could have only crystallized in a small pressure range. In addition, the crystallization sequence of plagioclase followed by amphibole is also common elsewhere. In the Lesser Antilles arc, for example, in both plutonic nodules and volcanics (Lewis, 1973b; Wills, 1974; Arculus, 1973), amphibole is a late phase to appear as a phenocryst. Thus, it seems probable that a more general condition exists, other than $P_{tot} = P_{H_2O}$, whereby this crystallization sequence is not so unlikely.

Undersaturated (with respect to H_2O) melts might be expected to show a lowering of the stabilization temperature of amphibole. In fact, from $P_{H_2O} = P_{tot}$ to about $P_{H_2O} = 0.5\ P_{tot}$, the opposite is true (Eggler, 1972; Holloway, 1973). Holloway (op.cit) shows that there is an isobaric maximum in the temperature of amphibole stability at $P_{H_2O} = 0.6\ P_{tot}$ for 7.75 kb, and $P_{H_2O} = 0.4\ P_{tot}$ at 4.5 kb. For lower degrees of P_{H_2O} (relative to P_{tot}) than these, amphibole stability declines sharply. Thus, as Cawthorn & O'Hara (1976) note, slightly to moderately undersaturated melts show little difference in the relative stabilities of minerals compared with totally saturated melts. However, very low P_{H_2O} relative to P_{tot} (less than about $0.3\ P_{tot}$) will create a situation where plagioclase will precede amphibole over a broad pressure range. Fig. 4.12 illustrates this for the Mt. Hood andesite at 5kb (P_{tot}). Below H_2O contents of 2 wt.per cent, amphibole stability shows a marked decrease and the temperature difference between the plagioclase-out and amphibole-out out curves is over 200°C. At saturated conditions (9 per cent H_2O), this difference is only 50°C. A similar temperature-difference increase for the olivine tholeiite of Fig. 4.11B would permit such

Figure 4.12

H_2O content - T stability diagram for the Mt. Hood andesite at 5kb (Eggler & Burnham, 1973).

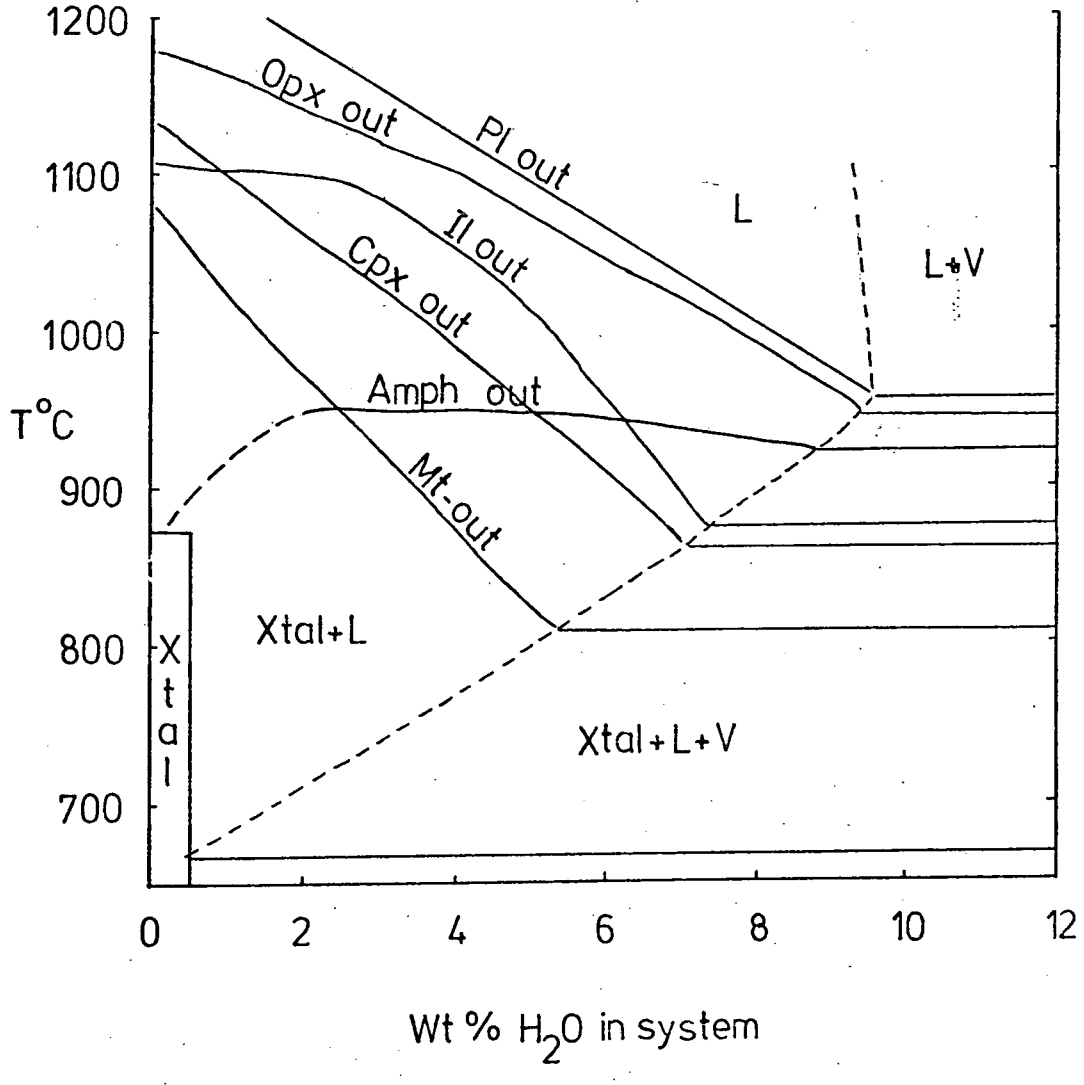
1200
1100
1000
900
800
700
T°C
Opx out
Pl out
Il out
Cpx out
Amph out
Mt-out
L
L+V
Xtal+L
Xtal+L+V
Xtal
0
2
4
6
8
10
12
Wt % H2O in system

a magma to crystallize plagioclase before amphibole up to 5 or 6 kb, or even to the upper pressure limit of plagioclase stability (7-10 kb; O'Hara, 1968).

Water contents of about 2 wt.per cent, necessary to permit the degree of water undersaturation discussed, seem a reasonable estimate, since a rising magma will then encounter saturated conditions at 1-2 kb (e.g. Hamilton & Anderson, 1968), and thus the observed crystallization sequence of plagioclase, followed by amphibole, would not be expected to change.

It is unlikely, incidentally, that a magma can ever reach water saturation, due to the presence of other volatiles and small amounts of dissolved silicates in the gas. Particularly, the low solubility of CO_2 in silicate melts, at least below 10kb (Eggler & Burnham, 1973), prevents water-vapour saturation. Nordlie (1971) has shown that most H_2O in reported volcanic-gas analyses is contamination, and in fact, $CO_2 + SO_2$ may be equally abundant to H_2O.

In Section 4:3 it was pointed out that in the Rossland volcanics, amphibole shows no reaction relationship with olivine or clinopyroxene, as is predicted for conditions of P_{H_2O} greater than $\sim$ 0.5 P_{tot} (Cawthorn et al. 1973; Helz, 1973; Holloway & Burnham, 1972). This again appears to be a feature of the Lesser Antilles volcanics, though some plutonic nodules show evidence of amphibole selectively reacting with clinopyroxene (Wills, 1974). In this latter case, this is probably due to the building up of H_2O in the trapped mesostasis, which eventually causes the clinopyroxene to react and form amphibole. More usually though, amphibole merely poikilitically encloses clinopyroxene and other phases (cf. Wills, 1974; Arculus, 1973). In the amphibole-bearing basalts of Bogoslof Island, Arculus et al. (1977) attribute the absence of olivine to the presence

of a reaction relationship between amphibole and olivine. However, Arculus et al.(op.cit) do not report clinopyroxene being affected in any way, as would be expected for high P_{H_2O}. It seems, therefore, that a consequence of low P_{H_2O} is the disappearance of reactions of the sort:

Amphibole = Olivine + Clinopyroxene + Liquid

If this is generally true for island-arc magma petrogenesis, amphibole fractionation schemes based on high P_{H_2O} ($> 0.5\ P_{tot}$) experiments, for example Cawthorn et al. (1973) or Cawthorn & O'Hara (1976), are unlikely to be realistic. That is, amphibole alone is unlikely to control a liquid line of descent, but only contribute with olivine and pyroxene, and possibly plagioclase, to the crystal extract.

Magnetite behaviour is also affected by H_2O vapour pressure. Figs. 4.11A and 4.12 show that lowering of P_{H_2O}, or H_2O per cent isobarically, causes magnetite stability to increase. Since, like plagioclase and clinopyroxene, magnetite appears in the Rossland basaltic rocks before amphibole, a low value for P_{H_2O} is again favoured; though f_{O_2} is a more important determinant of Fe-oxide stability.

At the QFM buffer, experiments by Eggler (1972) and Eggler & Burnham (1973) show magnetite to occur, in andesitic compositions well below the liquidus. In addition, ilmenite is often a separately precipitating phase before magnetite. Within the Rossland volcanics, and in many other calc-alkaline or island-arc rocks, titanomagnetite is the only Fe-Ti oxide phenocryst, apart from minor Cr-spinel (e.g. Lewis, 1973b). In part, this is due to low bulk-rock TiO_2 contents (cf. Carmichael, 1967), but as Wills (1974) shows for the Lesser Antilles plutonic nodules, Ti-magnetite + ilmenite

only stabilize together below about 940°C. Above this, titanomagnetite is the only phase. To produce a situation where Ti-magnetite is stabilized so early in the Rossland volcanics, high f_{O_2} is indicated. Helz (1973) shows that as f_{O_2} decreases from NNO to QFM buffer values, the upper temperature of magnetite stability decreases and ilmenite becomes the first-crystallizing oxide phase. Thus, in the Rossland magmas f_{O_2} was probably near NNO, which agrees with that in salic volcanics carrying amphibole and magnetite (Carmichael, 1967b)

In terms of the temperature of crystallization, amphibole chemistry is an indicator. Specifically, the Al^{iv} content is a function of temperature (Helz, 1973). The average of 1.86 Al^{iv} cations per unit formula in the analysed amphiboles suggests, by comparison with Helz's (1973) data, a temperature of about 960°C (see also Section 4:4). Thus magnetite in the Rossland magmas crystallized well above the threshold of about 940°C referred to above.

CHAPTER 5

GEOCHEMISTRY OF THE ROSSLAND VOLCANIC ROCKS

The data described in this chapter were produced by X-ray fluorescence spectrometry, the details of which, together with the data, are contained in Appendix 2. Due to the incorporation of secondary H_2O in the whole-rock samples, all analyses are normalised to 100 per cent on an anhydrous basis.

5:1 Classification

In Chapter 4 a preliminary classification of the volcanics was proposed based on phenocryst contents. Here, this is extended to take into account the geochemical variation of the rocks.

Commonly, with regard to calc-alkaline suites, SiO_2 shows a large variation and is thus frequently used as an indicator of differentiation, and used to subdivide the suite into basalt, andesite, dacite and rhyolite (cf. Taylor et al., 1969a). Alkalic suites that characteristically show a greater increase of alkalis relative to SiO_2, compared to calc-alkalic, are best subdivided using a combined indicator, such as differentiation index (normative quartz + albite + orthoclase + nepheline + leucite. Tholeiitic suites, exhibiting strong or moderate iron-enrichment, alternatively, are best illustrated by some measure of Fe/Mg ratio.

With regard to the Rossland volcanics, examination of Fig.5.1 shows SiO_2 is limited in range (coefficient of variation = 5.2 per cent). Also, since Fe, like Mg, shows a negative correlation with Si (Table 5.3), Fe/Mg ratios are of little use. The use of differentiation index is hampered by alkali mobility, as will be seen. Consequently, a classification scheme has been devised which as well as utilising SiO_2 such that comparisons can be made with other suites, uses MgO which among the major oxides shows the

Figure 5.1

Frequency distribution of MgO and SiO_2, and their covariance.

Fields 1, 2 and 3 correspond to the petrologic types; ankaramitic basalt, basalt and andesite, respectively, and as defined in the text. Open squares - pyroxenites; dots - amphibolised samples; crosses - non-amphibolised samples.

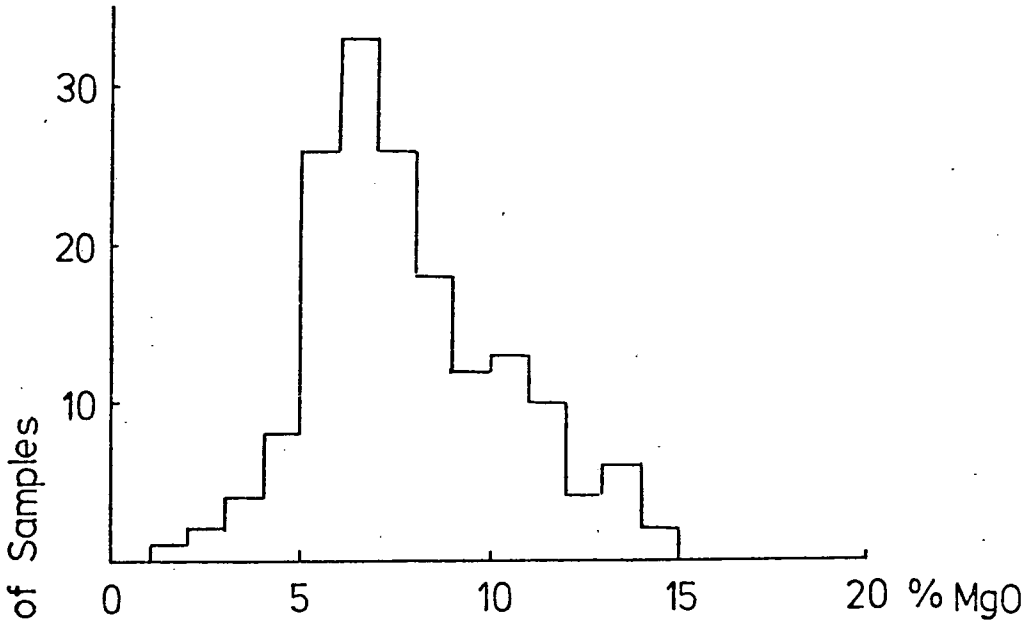
No. of Samples
30
20
10
0
5
10
15
20 % MgO

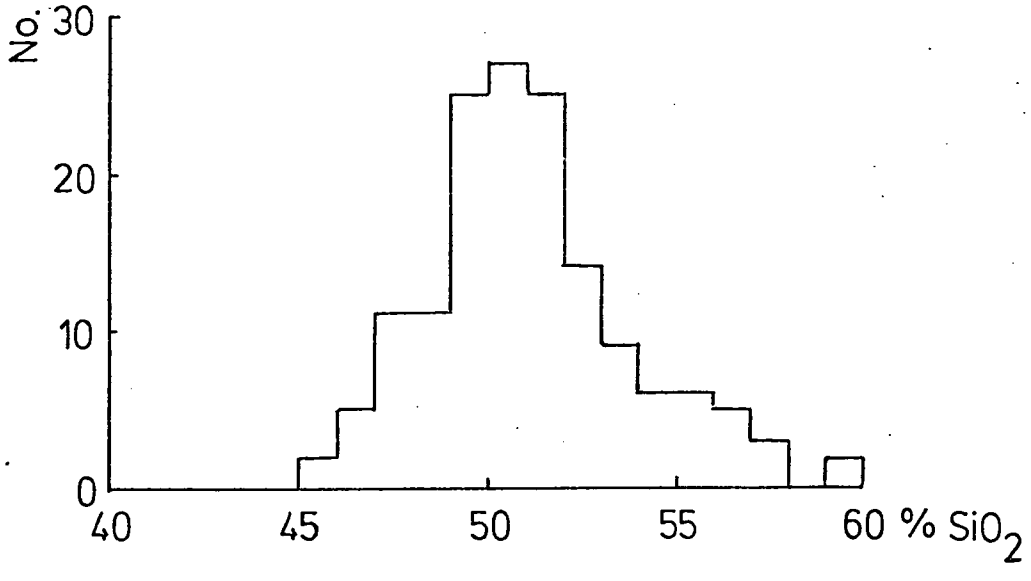
30
20
10
0
40
45
50
55
60 % SiO2

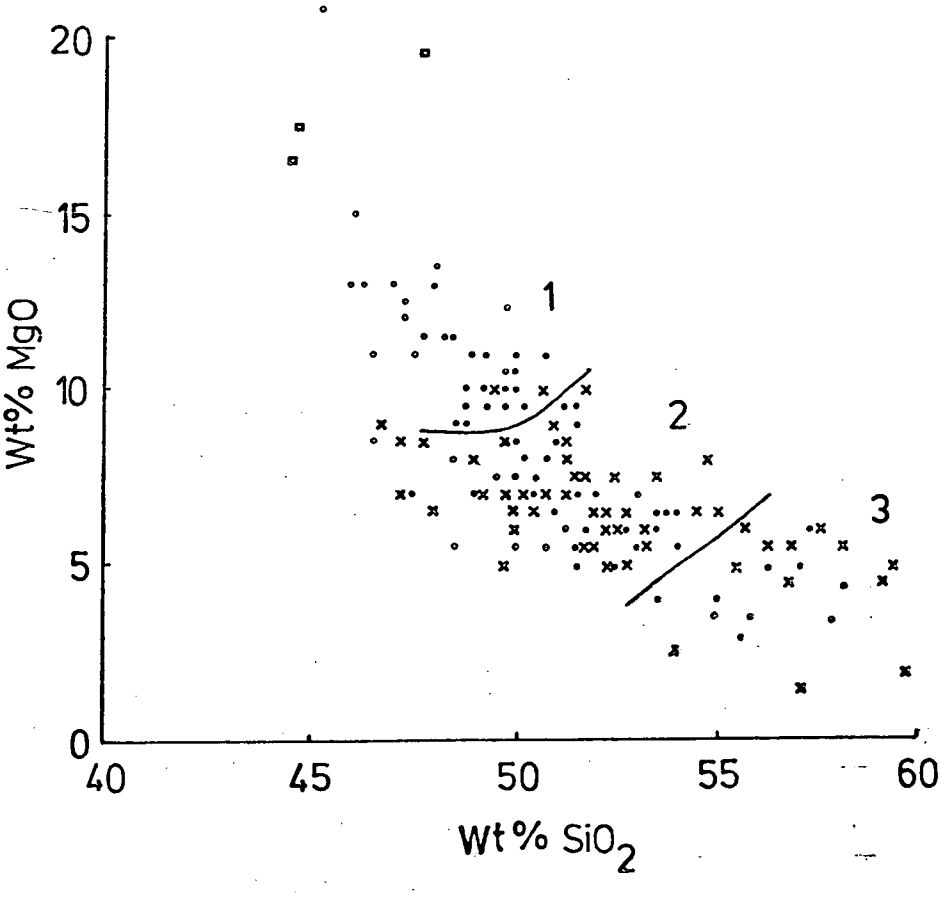
Wt% MgO
20
15
10
5
0
40
45
50
55
60
Wt % SiO2
1
2
3

highest coefficient of variation (33 per cent). This classification also permits a reasonable link with the petrographic variation already described. Fig. 5.1 shows the distribution of MgO and SiO_2, and their covariance. The MgO - SiO_2 plot (Fig. 5.1) illustrates how the series is subdivided, though somewhat arbitrarily. Together with the phenocryst abundance, the subdivisions of the series are:-

(1) Ankaramitic Basalt:

Clinopyroxene	> 30 per cent vol.	SiO_2	< 50 per cent wt.
Plagioclase	< 10 " "	MgO	> 9 " " wt.

(2) Basalt:

Clinopyroxene	15–30 " " vol.	SiO_2	48–54 " " wt.
Plagioclase	30–10 " " vol.	MgO	9– 5 " " wt.

(3) Andesite:

Clinopyroxene	< 15 " " vol.	SiO_2	> 54 " " wt.
Plagioclase	> 30 " " vol.	MgO	< 5 " " wt.

In some island-arc suites, basaltic andesite is defined between rocks of basaltic and andesite composition, and they cover a range of about 54 to 57 per cent SiO_2 (e.g. Baker, 1968a). Here, due to the relative sparsity of rocks with SiO_2 contents of over 54 per cent, no such division is made.

5:2 Element mobility in hydrothermally altered basaltic rocks

It has already been pointed out that all of the volcanics have suffered some degree of hydrothermal alteration. The nature of this is discussed in more detail in Chapters 6 and 7. However, in general, alteration varies from a relatively low-grade development of chlorite, calcite, epidote and sericite, whilst igneous clinopyroxene and amphibole are relict phases, to upper greenschist facies metamorphism. The latter degree of alteration involves

recrystallization of all primary phases to amphibole, biotite, chlorite, epidote and calcite, but retention, more or less, of igneous textures. Since many authors have shown that certain elements become mobile under these conditions, a brief review of this problem is presented here with a view to examining possible changes in the chemistry of the Rossland volcanics.

Pearce (1976), in discussing the major element patterns of basalts, delimits three major processes of alteration. These are; submarine weathering, subaerial weathering and spilitization. Table 5.1, taken from Pearce (op.cit.),shows how in general the major oxides behave during these processes.

During submarine weathering, apart from the tendencies shown in Table 5.1, trace elements such as K, Rb and Cs tend to increase rather strongly (Hart, 1969; Hart & Nalwalk, 1970; Hart et al., 1974). Enrichments for K and Rb quoted by Hart (1969) are 2.2 and 5.0, respectively. Such enrichments can occur where the basalt has been merely discoloured by weathering. Also, as would be expected, K/Rb decreases with weathering. Pillow margins and glassy phases within basaltic rocks are even more susceptible to chemical alteration, especially if palagonitization has occurred involving uptake of K and related elements (Scarfe & Smith, 1977). Sr is apparently more stable during sea-floor weathering (Hart, 1969; Cann, 1970) and would, therefore, be a safer indicator of the original, igneous abundance, though by no means totally reliable.

Subaerial weathering typically involves leaching of elements such as Ca, Mg, Na and K, whilst Fe and Al tend to remain fixed, though as a percentage would increase (Lisitsyana, 1969).

The effect of either of the above processes on the Rossland samples is hard to assess, since overprinting of higher grade alteration has occurred. Pillow lavas have not been observed

TABLE 5.1

MAJOR ELEMENT MOBILITIES DURING BASALT ALTERATION

(AFTER PEARCE,1976)

(1) Submarine weathering

very mobile	+ H_2O, + Fe_2O_3/FeO, + K_2O, - CaO, - MgO
mobile	- Na_2O, - SiO_2
slightly mobile	+ total Fe, + TiO_2
immobile	Al_2O_3

(2) Subaerial weathering

very mobile	- CaO, - Na_2O, - K_2O, - MgO, + H_2O
mobile	- SiO_2
immobile	total Fe, Al_2O_3, TiO_2

(3) Spilitization

very mobile	- CaO, - Al_2O_3, + H_2O
mobile	+ Na_2O, + SiO_2, + (MgO + FeO), - K_2O
immobile	TiO_2, Fe_2O_3/FeO

or sampled, thus problems regarding chemical heterogeneity in pillows should have been avoided. However, as was shown in Chapter 3, marine conditions were prevalent during the accumulation of the volcanics, and individual fragments in the agglomerates and conglomerates, from which many samples were taken, could have undergone low temperature chemical exchanges with sea water. $\delta^{18}O$ values for the Rossland samples (see Chapter 8) do not contradict this interpretation, showing enrichments similar to weathered oceanic basalts (Muehlenbachs & Clayton, 1972a).

Spilitization is now generally regarded as secondary hydrothermal alteration of perfectly normal basic volcanics (Vallance, 1969, 1974; Battey, 1974). The 'characteristic' Na enrichment of spilites is not in reality a general feature, spilites being better defined as mineralogical assemblages involving, typically, igneous pyroxene, chlorite and albite. Such assemblages are common in burial-metamorphosed geosynclinal sequences as described, for example, by Smith (1968) or Jolly (1970). They are also present in the oceanic crust (Cann, 1969).

The presence of abundant H_2O during low-grade spilitization processes has the effect of redistributing, sometimes quite severely, certain elements, producing patchy mineralogical zones. The mobility of Ca and Mg particularly is demonstrated by Smith (1968) and Reed & Morgan (1971) as being necessary to produce chlorite-rich epidote-rich patches in original basalt and pyroclastics. Floyd (1976) has also noted similar chemical changes in the S.W. England greenstones, associated with variations in Fe_2O_3/FeO and H_2O which tend to be antipathetic. Low H_2O, high Fe_2O_3/FeO favours epidote development and CaO concentration, whilst the opposite favours chlorite or MgO-rich concentrations.

Chemical changes during sea-floor spilitization usually involve loss of Ca, Al and K, and gain of Na, Si, Fe & Mg (Cann, 1969; Nelson & Van Andel, 1966). The reversed behaviour of K_2O, with respect to sea-floor weathering (Table 5.1), also applies to Rb and Ba. Also depleted in oceanic spilites or greenstones, when compared to fresh basalts, is $\delta^{18}O$ (Muehlenbachs & Clayton, 1972b). This is the result of relatively high temperature (300°C) interaction between large volumes of sea-water and basalt. The enriched, rather than depleted, $\delta^{18}O$ values for the Rossland samples indicate this process never occurred (Chapter 8).

Spilitization of a single lava flow in shallow-water conditions is reported by Vallance (1974). In this case K, Rb, Ba and Sr are all substantially enriched, in contrast to the sea-floor case. Enrichments reported by Vallance (op.cit.) for the above elements are, respectively, about 4, 40, 10 and 3. Much smaller enrichments, however, are reported for other situations; for example, the S.W. England greenstones (Floyd, 1976), some amphibolised gabbros (Field & Elliot, 1974) and some ophiolitic basalts (Coish, 1977).

The mineralogical assemblages for the lower-grade volcanics of the Rossland area are clearly spilitic by the above definitions. Hydration and oxidation are also comparable with other spilites (Fig.5.2). Thus, on the basis of the above discussion element mobility can be expected, particularly with regard to K, Rb and Ba.

Certain elements, however, appear to be immobile under the various conditions described above, and so long as no net loss or gain of material has occurred these should retain their igneous abundance levels. Hart et al. (1974) observed that during sea-floor weathering the elements Ti, Zr, V, Zn, Cr, Y, Nb and Sr changed little. Similarly, under higher grade processes the

Figure 5.2

Weight % H_2O versus Fe_2O_3/FeO for wet chemically analysed samples (Appendix 2). Dashed line is the field of spilites defined by Vallance (1960).

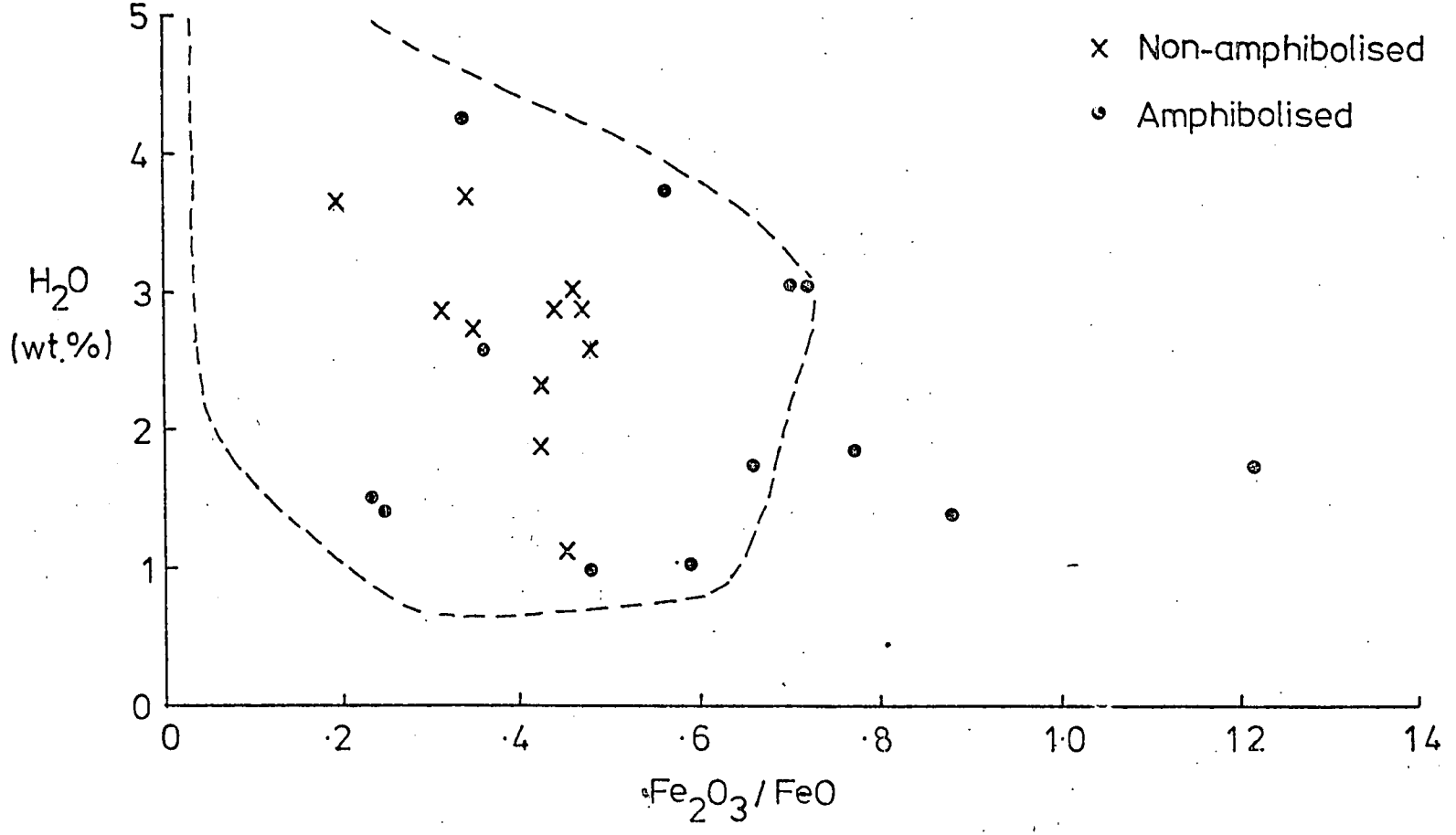
5
4
3
2
1
0
H_2O (wt.%)
0
·2
·4
·6
·8
1·0
1·2
1·4
Fe_2O_3 / FeO
Non-amphibolised
Amphibolised

elements Y, Nb, Ti and Zr are particularly stable (Cann, 1969; 1970; Coish, 1977; Vallance, 1974; Field & Elliot, 1974).

5:3 Element mobility in the Rossland volcanics

In order to gain some insight into whether the Rossland volcanics have suffered any bulk chemical changes during their alteration history, some statistical data were calculated. The volcanics sampled and analysed consist of a heterogeneous assemblage of fragments from the agglomerates and breccias, with some fine-grained tuffaceous and volcaniclastic representatives. Alteration, both texturally and mineralogically, is very variable. From this suite then, three groups were selected for intercomparison. Group A (Table 5.2) contains all volcanics from the amphibolised zone (zone A as defined in Chapter 6); Group B, those volcanics displaying 'spilitic' assemblages and representing a lower grade of alteration (zone A, Chapter 6). From groups A and B a third, C, was selected which contains samples with the least textural alteration.

Table 5.2 shows the means and standard deviations for each oxide or element for each group. Comparing initially A and B, it can be seen that all elements, except Mg , Ni and Cr, compare well in both variability and average abundance. The reasons for the higher MgO, Ni and Cr in group A is due to the fact that all ankaramitic samples contribute to this group. Slight differences in SiO_2, Al_2O_3 and Zr, for example, are also attributable to this cause. Elements that show less variation with differentiation such as TiO_2 , P_2O_5 and Y, and which are also considered immobile (Floyd & Winchester, 1975; Pearce & Cann, 1973), show almost identical abundances. There is, then, no indication in this data that the transition from spilitic to upper greenschist facies involves any significant changes. This is in contrast to the Sofala volcanics

TABLE 5.2

MEANS AND STANDARD DEVIATION OF GROUPS A,B,C AND B'

AS DEFINED IN THE TEXT(p. 128)

	A		B		C		B'	
wt.%	$\bar{x}$	s.d.	$\bar{x}$	s.d.	$\bar{x}$	s.d.	$\bar{x}$	s.d.
SiO_2	50.80	2.85	52.42	3.09	51.64	2.80	52.40	3.25
TiO_2	0.86	0.16	0.89	0.12	0.87	0.13	0.90	0.12
Al_2O_3	12.59	2.17	13.83	1.45	13.50	1.95	13.50	1.61
Fe_2O_3	12.06	1.61	11.52	1.66	11.52	1.56	11.69	1.68
MnO	0.20	0.04	0.18	0.03	0.18	0.04	0.19	0.03
MgO	8.81	3.20	7.04	1.83	7.63	2.35	7.21	1.89
CaO	9.90	2.62	9.30	2.76	9.31	2.11	9.66	3.23
Na_2O	2.66	1.07	2.80	0.88	2.91	0.86	2.67	0.86
K_2O	1.81	0.90	1.66	0.72	2.05	0.86	1.37	0.54
P_2O_5	0.31	0.11	0.29	0.08	0.32	0.09	0.27	0.07
ppm								
Cu	94	79	63	37	82	71	62	32
Ni	80	106	43	42	56	65	44	45
Cr	335	334	167	162	218	227	179	162
Ba	665	331	740	342	787	354	645	296
Nb	4	1.8	4	1.4	4	1.6	4	1.5
Zr	87	32	99	20	97	27	95	21
Y	17	3.8	17	3.8	18	3.8	17	3.9
Sr	698	274	718	272	772	225	668	285
Rb	47	30	42	17	50	28	37	17
Zn	107	51	105	48	96	19	110	59
Ce	17	10	20	10	19	7	21	11
La	4	7	8	7	7	6	8	6
V	276	75	265	69	276	61	258	79

$\bar{x}$ mean

s.d. standard deviation

* All Fe expressed as Fe_2O_3

(Barron & Barron, 1976), which have altered extensively to carbonate-tremolite-chlorite assemblages and which have lost SiO_2, CaO and alkalis, whilst MgO has increased.

Similarly, group C means and variances compare well with both A and B, bearing in mind the sampling bias referred to above. In part, this is expected since C is drawn from A and B, but it tends to indicate, nevertheless, that average abundances are retained despite varying degrees of textural disruption.

There is a slight tendency for group C to be enriched in K, Ba, Rb and Sr relative to A or B. If from B all those samples contributing to C are removed and the remainder (B′) averaged (Table 5.2), this tendency is enhanced. This suggests a preferential loss of those elements where the rock is finely brecciated, fragmentary or sheared. This could be due to leaching as a result of the easier access of the hydrothermal fluids during alteration. This loss of K, Rb and Ba is the reverse of that quoted above for low-grade submarine weathering, or spilitization of the sort reported by Vallance (1974) where these elements are strongly enriched. However, in the absence of perfectly fresh material it is impossible to prove conclusively which way, if any, the mobile elements have gone.

The immobile elements Y, Nb, Zr and Ti remain fixed in all groups, exhibiting very similar means and variances. Also apparently immobile in the three groups are the elements Mn, V, Zn, Ce and La.

Additional information concerning the secondary movement of elements can be obtained from the correlation matrices of the groups defined above. Cann (1970, 1971) showed how some elements maintain cohesion during alteration by comparing correlation matrices

for fresh and altered oceanic basalts. Again, in the absence of perfectly fresh representatives, the best that can be done is to inter-compare the various groups.

Table 5.3 shows the correlation matrices for A, B and C with all significant correlations indicated. For trace elements it is suitable to use a null model of $\rho = 0$ for significance testing, but between major elements closure problems impose negative correlation on the variables (Chayes, 1971). Significance was therefore assessed using the computer routine of Zordrow (1974), which is based on Chayes' (1971) analysis. This is not totally satisfactory but is probably a much better indication than using $\rho = 0$.

Considering firstly the elements K, Rb and Ba, a notable feature is that they correlate poorly with all other elements, but amongst themselves show significant positive correlations. This is evidence of their mobility and the fact that all three were similarly affected. Sr also shows signs of behaving analogously to K, Rb and Ba but its correlations with these elements are weaker. That Sr appears to correlate significantly with Zr in all groups, suggests it was more stable and, as suggested above, may be a more reliable indicator of magmatic abundances.

That K, Rb and Ba, despite being mobile, may have retained, on average, their igneous abundances is suggested by other evidence. In Chapter 4 it was proposed that the appearance of amphibole in rocks of basaltic composition is indicative of alkaline affinities for the volcanics. In addition, the chemistry of the amphiboles and the rare occurrence of primary biotite also implies reasonably high K_2O values in the original lavas. On the basis of Fig.4 in Jakeš & White (1972a), the K contents of the Rossland volcanic amphiboles indicate a whole-rock K_2O value of greater than 1.5 per cent. This

TABLE 5.3A GROUP A CORRELATION MATRIX(*=SIGT. AT 5%)

	SIO2	AL2O3	FE2O3	MGO	CAO	NA2O	K2O	TIO2	MNO	P2O5
SIO2	1.000	0.353	-0.814	-0.563	-0.588	0.555	0.060	-0.459	-0.522	-0.182
AL2O3	0.353*	1.000	-0.216	-0.222	-0.016	0.502	0.088	-0.060	-0.496	0.067
FE2O3	-0.814*	-0.216	1.000	0.488	0.335	-0.541	-0.291	0.544	0.597	0.084
MGO	-0.563*	-0.222	0.488*	1.000	0.117	-0.674*	-0.258	0.070	0.196	-0.209
CAO	-0.588	-0.816*	0.335*	0.117	1.000	-0.479*	0.005	0.235	0.509	0.128
NA2O	0.555*	0.502*	-0.541*	-0.674*	-0.479*	1.000	0.082	-0.129	-0.370	0.068
K2O	0.060	0.088	-0.291	-0.258	0.005	0.082	1.000	-0.322	-0.119	0.500
TIO2	-0.459*	-0.060	0.544*	0.070	0.235*	-0.129	-0.322*	1.000	0.382	-0.049
MNO	-0.522*	-0.496*	0.597*	0.196	0.509*	-0.370*	-0.119	0.382	1.000	0.226
P2O5	-0.182	0.067	0.084	-0.209	0.128	0.068	0.500*	-0.049	0.226	1.000
CU	-0.362*	-0.031	0.375*	0.243	0.178	-0.255	-0.011	-0.068	0.196	0.056
NI	-0.293*	-0.304*	0.109	0.595*	0.269*	-0.434*	-0.151	-0.056	0.031	-0.508*
CR	-0.343*	-0.357*	0.164	0.556*	0.321*	-0.395*	-0.246	-0.022	0.124	-0.266*
BA	0.104	0.077	-0.206	-0.207	0.007	0.034	0.768	-0.170	-0.075	0.442*
NB	0.291*	0.024	-0.215	-0.222	-0.137	0.212	0.020	-0.065	-0.060	-0.026
ZR	0.244	0.502*	-0.184	-0.304*	-0.338*	0.220	0.076	-0.022	-0.346	0.137
Y	0.011	0.274*	-0.003	-0.100	-0.154	0.056	0.062	0.308*	-0.080	-0.146
SR	-0.077	0.229	0.068	-0.198	0.020	-0.050	0.342*	-0.165	-0.002	0.517*
RB	0.132	0.015	-0.352*	-0.243	0.053	0.113	0.838*	-0.332*	-0.085	0.354*
ZN	0.206	0.182	0.044	-0.115	-0.294*	0.142	-0.182	0.180	0.274	-0.112
CE	-0.196	-0.044	0.364	-0.037	0.122	-0.016	-0.245	0.172	0.351	0.155
LA	-0.216	-0.032	0.258	0.148	0.022	-0.046	-0.068	-0.022	0.049	-0.192
V	-0.545*	0.067	0.658*	0.285*	0.103	-0.151	-0.062	0.441*	0.254	0.204

	CU	NI	CR	BA	NB	ZR	Y	SR	RB	ZN
SIO2	-0.362	-0.293	-0.343	0.104	0.291	0.244	0.011	-0.077	0.132	0.206
AL2O3	-0.031	-0.304	-0.357	0.077	0.024	0.502	0.274	0.229	0.015	0.182
FE2O3	0.375	0.109	0.164	-0.206	-0.215	-0.184	-0.003	0.068	-0.352	0.044
MGO	0.243	0.595	0.556	-0.207	-0.222	-0.304	-0.100	-0.198	-0.243	-0.115
CAO	0.178	0.269	0.321	0.007	-0.137	-0.338	-0.154	0.020	0.053	-0.294
NA2O	-0.255	-0.434	-0.395	0.034	0.212	0.220	0.056	-0.050	0.113	0.142
K2O	-0.011	-0.151	-0.246	0.768	0.020	0.076	0.062	0.343	0.838	-0.182
TIO2	-0.068	-0.056	-0.022	-0.170	-0.065	-0.022	0.308	-0.165	-0.332	0.180
MNO	0.196	0.031	0.124	-0.075	-0.060	-0.346	-0.080	-0.002	-0.085	0.274
P2O5	0.058	-0.308	-0.266	0.442	-0.026	0.137	-0.146	0.517	0.354	-0.112
CU	1.000	0.240	0.098	0.099	-0.234	-0.237	-0.243	0.037	-0.066	-0.156
NI	0.240	1.000	0.762*	-0.223	-0.218	-0.309	-0.018	-0.286	-0.008	-0.149
CR	0.098	0.762*	1.000	-0.302	-0.050	-0.216	-0.059	-0.247	-0.032	-0.137
BA	0.099	-0.223	-0.302*	1.000	0.043	-0.061	-0.185	0.318	0.575	-0.079
NB	-0.234	-0.218	-0.050	0.043	1.000	0.152	0.059	-0.084	0.154	0.174
ZR	-0.237	-0.309*	-0.216	-0.061	0.152	1.000	0.476	0.511	-0.026	0.087
Y	-0.243	-0.018	-0.059	-0.185	0.059	0.476*	1.000	0.074	0.067	0.134
SR	0.037	-0.288*	-0.247	0.318*	-0.084	0.511*	0.074	1.000	0.183	-0.149
RB	-0.066	-0.008	-0.032	0.575*	0.154	-0.026	0.067	0.183	1.000	-0.168
ZN	-0.156	-0.149	-0.137	-0.079	0.174	0.087	0.134	-0.149	-0.168	1.000
CE	-0.025	-0.094	-0.096	0.222*	0.225	0.274	0.146	0.159	-0.202	0.449*
LA	0.336*	0.120	0.055	-0.037	-0.209	0.026	-0.077	0.099	-0.117	-0.101
V	0.319*	0.025	0.055	-0.007	0.145	0.029	0.086	0.083	-0.127	0.328

	CE	LA	V
SIO2	-0.196	-0.216	-0.545
AL2O3	-0.044	-0.032	0.067
FE2O3	0.364	0.258	0.658
MGO	-0.037	0.148	0.285
CAO	0.122	0.022	0.103
NA2O	-0.016	-0.046	-0.151
K2O	-0.245	-0.068	-0.062
TIO2	0.172	-0.022	0.441
MNO	0.351	0.049	0.254
P2O5	0.155	-0.092	0.204
CU	-0.025	0.336	0.319
NI	-0.094	0.120	0.025
CR	-0.096	0.055	0.055
BA	-0.322	-0.037	-0.007
NB	0.225	-0.209	0.145
ZR	0.274	0.026	0.029
Y	0.146	-0.077	0.086
SR	0.159	0.099	0.083
RB	-0.202	-0.117	-0.127
ZN	0.449	-0.101	0.328
CE	1.000	0.139	0.365
LA	0.139	1.000	0.297
V	0.365*	0.297*	1.000

TABLE 5.38 GROUP B CORRELATION MATRIX(*=SIGT. AT 5%)

	SIO2	AL203	FE203	MGO	CAO	NA20	K20	TIO2	MNO	P205
SIO2	1.000	0.561	-0.786	-0.666	-0.511	0.527	0.150	0.022	-0.539	0.047
AL203	0.561 *	1.000	-0.517	-0.629	-0.775	0.724	0.308	0.373	-0.571	0.222
FE203	-0.786 *	-0.517 *	1.000	0.527	0.314	-0.559	-0.210	0.092	0.528	-0.060
MGO	-0.666	-0.629 *	0.527 *	1.000	0.200	-0.736	-0.512	-0.438	0.317	-0.356
CAO	-0.511	-0.775 *	0.314 *	0.200 *	1.000	-0.444	-0.145	-0.178	0.545	-0.087
NA20	0.527 *	0.724 *	-0.559 *	-0.736 *	-0.444 *	1.000	0.246	0.401	-0.436	0.209
K20	0.150 *	0.308 *	-0.210 *	-0.512 *	-0.145	0.246 *	1.000	0.295	-0.068	0.529
TIO2	0.022	0.373 *	0.092	-0.438 *	-0.178	0.401 *	0.295 *	1.000	-0.116	0.289
MNO	-0.539 *	-0.571 *	0.528 *	0.317 *	0.545 *	-0.436 *	-0.068	-0.116 *	1.000	-0.057
P205	0.047	0.222	-0.060	-0.356 *	-0.087	0.209	0.529 *	0.289 *	-0.057	1.000
CU	0.053	0.134	-0.002	-0.151	-0.084	0.173	0.054	0.114	0.048	0.154
NI	-0.464 *	-0.431 *	0.241 *	0.806 *	0.113	-0.547 *	-0.387 *	-0.647 *	0.095	-0.243 *
CR	-0.524 *	-0.654 *	0.349 *	0.903 *	0.288 *	-0.694 *	-0.484 *	-0.624 *	0.334 *	-0.379 *
BA	0.262 *	0.234 *	-0.222 *	-0.453 *	-0.133	0.246 *	0.631 *	0.252 *	-0.221 *	0.396 *
NB	0.389 *	0.478 *	-0.423 *	-0.331 *	-0.380 *	0.329 *	0.223 *	0.168	-0.309 *	0.265 *
ZR	0.421 *	0.467 *	-0.394 *	-0.511 *	-0.261 *	0.333 *	0.361 *	0.290 *	-0.207	0.307 *
Y	0.314 *	0.531 *	-0.319 *	-0.504 *	-0.352 *	0.490 *	0.398 *	0.557 *	-0.198	0.421 *
SR	0.347 *	0.336 *	-0.255 *	-0.610 *	-0.084	0.287 *	0.555 *	0.235 *	-0.062	0.595 *
RB	0.071	0.229 *	-0.029	-0.370 *	-0.135	0.118	0.765 *	0.183	0.050	0.360 *
ZN	-0.250 *	-0.231 *	0.313 *	0.355 *	0.022	-0.292 *	-0.171	-0.111	0.569 *	-0.154
CE	0.102	0.186	-0.093	-0.389 *	0.093	0.169	0.242 *	0.254 *	0.072	0.319 *
LA	-0.005	0.106	0.019	-0.288 *	0.102	0.094	0.269 *	0.249 *	0.114	0.281 *
V	-0.295 *	-0.110	0.351 *	0.106	0.093	-0.083	-0.052	0.389 *	0.182	0.018

	CU	NI	CR	BA	NB	ZR	Y	SR	RB	ZN
SIO2	0.053	-0.464	-0.524	0.262	0.389	0.421	0.314	0.347	0.071	-0.250
AL203	0.134	-0.431	-0.654	0.234	0.478	0.467	0.531	0.336	0.229	-0.231
FE203	-0.002	0.241	0.349	-0.222	-0.423	-0.394	-0.319	-0.255	-0.029	0.313
MGO	-0.151	0.806	0.903	-0.453	-0.331	-0.511	-0.504	-0.610	-0.370	0.355
CAO	-0.084	0.113	0.288	-0.133	-0.380	-0.261	-0.352	-0.084	-0.135	0.022
NA20	0.173	-0.547	-0.694	0.246	0.329	0.333	0.490	0.287	0.118	-0.292
K20	0.054	-0.387	-0.484	0.631	0.223	0.361	0.398	0.553	0.765	-0.171
TIO2	0.114	-0.647	-0.624	0.252	0.168	0.290	0.557	0.235	0.183	-0.111
MNO	0.048	0.095	0.334	-0.221	-0.309	-0.207	-0.198	-0.062	0.050	0.569
P205	0.154	-0.243	-0.379	0.396	0.265	0.307	0.421	0.505	0.360	-0.154
CU	1.000	-0.122	-0.215	0.086	0.091	0.035	0.152	0.063	-0.056	-0.127
NI	-0.122	1.000	0.859	-0.351	-0.214	-0.393	-0.389	-0.520	-0.278	0.105
CR	-0.215 *	0.859 *	1.000	-0.424 *	-0.337 *	-0.500 *	-0.538 *	-0.613 *	-0.334 *	0.440
BA	0.086	-0.351 *	-0.424 *	1.000	0.215	0.234	0.272	0.429	0.471	-0.220
NB	0.091	-0.214 *	-0.337 *	0.215	1.000	0.312	0.462	0.207	0.167	-0.060
ZR	0.035	-0.393 *	-0.500 *	0.234 *	0.312 *	1.000	0.601	0.599	0.204	-0.163
Y	0.152	-0.389 *	-0.538 *	0.272 *	0.462 *	0.601 *	1.000	0.372	0.281	-0.154
SR	0.063	-0.520 *	-0.613 *	0.429 *	0.207 *	0.599 *	0.372 *	1.000	0.402	-0.233
RB	-0.056	-0.278 *	-0.334 *	0.471 *	0.167	0.204	0.281 *	0.402 *	1.000	-0.359
ZN	-0.127	0.105	0.440 *	-0.220 *	-0.060	-0.163	-0.154	-0.233 *	-0.359 *	1.000
CE	0.085	-0.347 *	-0.403 *	-0.008	0.260 *	0.453 *	0.475 *	0.441 *	0.185	-0.117
LA	0.039	-0.286 *	-0.336 *	0.232 *	0.189	0.299 *	0.291 *	0.281 *	0.183	-0.020
V	-0.042	-0.075	-0.025	0.017	-0.038	-0.048	0.102	-0.115	0.067	0.077

	CE	LA	V
SIO2	0.102	-0.005	-0.295
AL203	0.186	0.106	-0.110
FE203	-0.093	0.019	0.351
MGO	-0.389	-0.288	0.106
CAO	0.093	0.102	0.093
NA20	0.169	0.094	-0.083
K20	0.242	0.269	-0.052
TIO2	0.254	0.249	0.389
MNO	0.072	0.114	0.182
P205	0.319	0.281	0.018
CU	0.085	0.039	-0.042
NI	-0.347	-0.286	-0.075
CR	-0.403	-0.336	-0.025
BA	-0.008	0.232	0.017
NB	0.260	0.189	-0.038
ZR	0.463	0.299	-0.048
Y	0.475	0.291	0.102
SR	0.441	0.281	-0.115
RB	0.185	0.183	0.067
ZN	-0.117	-0.020	0.077
CE	1.000	0.482	0.096
LA	0.482 *	1.000	0.272
V	0.096	0.272 *	1.000

TABLE 5.2C GROUP C CORRELATION MATRIX(*=SIGT. AT 5%)

	SIO2	AL203	FE203	MGO	CAO	NA2O	K2O	TIO2	MNO	P2O5
SIO2	1.000	0.456	-0.863	-0.687	-0.557	0.541	0.069	-0.137	-0.532	-0.097
AL203	0.456*	1.000	-0.449	-0.655	-0.822	0.544	0.307	0.425	-0.554	0.118
FE203	-0.863*	-0.449*	1.000	0.573	0.463	-0.554	-0.198	0.100	0.646	-0.019
MGO	-0.687*	-0.655*	0.573*	1.000	0.445	-0.712	-0.360	-0.236	0.329	-0.150
CAO	-0.557	-0.822*	0.463*	0.445*	1.000	-0.540	-0.323	-0.243	0.550	-0.056
NA2O	0.541*	0.544*	-0.554*	-0.712*	-0.540*	1.000	0.196	0.251	-0.416	0.049
K2O	0.069	0.307*	-0.198	-0.360*	-0.323*	0.196	1.000	0.094	-0.113	0.532
TIO2	-0.137*	0.425*	0.100	-0.236	-0.243*	0.251	0.094	1.000	-0.138	0.193
MNO	-0.532*	-0.554*	0.646*	0.329*	0.550*	-0.416*	-0.113	-0.138	1.000	0.068
P2O5	-0.097	0.118	-0.019	-0.150	-0.056	0.049	0.532*	0.193	0.068	1.000
CU	-0.180	-0.071	0.232	0.052	0.051	0.058	-0.029	0.059	0.286*	0.089
NI	-0.492*	-0.611*	0.364*	0.797*	0.491*	-0.577*	-0.416*	-0.381*	0.277*	-0.243
CR	-0.512*	-0.729*	0.411*	0.785*	0.609*	-0.565*	-0.459*	-0.362*	0.365*	-0.255
BA	0.188	0.404*	-0.251	-0.349*	-0.363*	0.186	0.658*	0.060	-0.202	0.523
NB	0.472*	0.442*	-0.372*	-0.412*	-0.522*	0.397*	0.158	0.230	-0.214	0.136
ZR	0.493*	0.541*	-0.458*	-0.583*	-0.374*	0.192	0.285*	0.283*	-0.290*	0.327
Y	0.362*	0.537*	-0.362*	-0.528*	-0.396*	0.247	0.293*	0.586*	-0.257	0.307
SR	0.071	0.269*	-0.085	-0.357*	-0.100	0.055	0.462*	0.115	0.009	0.597
RB	-0.052	0.211	-0.006	-0.244	-0.185	0.122	0.661*	0.067	0.088	0.346
ZN	-0.131	0.074	0.337*	-0.091	-0.014	-0.071	-0.037	0.077	0.439*	-0.150
CE	-0.037	0.223	0.045	-0.233	-0.035	0.059	0.082	0.228	0.141	0.158
LA	-0.065	0.199	0.117	-0.263	-0.062	0.125	0.217	0.204	0.140	0.161
V	-0.277*	0.054	0.371*	-0.041	0.059	0.016	-0.019	0.481*	0.199	0.266

	CU	NI	CR	BA	NB	ZR	Y	SR	RB	ZN
SIO2	-0.180	-0.492	-0.512	0.188	0.472	0.493	0.362	0.071	-0.052	-0.131
AL203	-0.071	-0.611	-0.729	0.404	0.442	0.541	0.537	0.269	0.211	0.074
FE203	0.232	0.364	0.411	-0.251	-0.372	-0.458	-0.362	-0.085	-0.006	0.337
MGO	0.052	0.797	0.785	-0.349	-0.412	-0.583	-0.528	-0.357	-0.244	-0.091
CAO	0.051	0.491	0.609	-0.363	-0.522	-0.374	-0.396	-0.100	-0.185	-0.014
NA2O	0.058	-0.577	-0.565	0.186	0.397	0.192	0.247	0.055	0.122	-0.071
K2O	-0.029	-0.416	-0.459	0.658	0.158	0.285	0.293	0.462	0.661	-0.037
TIO2	0.059	-0.381	-0.362	0.060	0.230	0.283	0.586	0.115	0.067	0.077
MNO	0.286	0.277	0.365	-0.202	-0.214	-0.290	-0.257	0.009	0.088	-0.439
P2O5	0.089	-0.243	-0.255	0.523	0.136	0.327	0.307	0.597	0.346	-0.150
CU	1.000	-0.058	-0.055	-0.049	0.162	-0.072	-0.040	0.095	-0.139	0.140
NI	-0.058	1.000	0.921	-0.422	-0.412	-0.555	-0.512	-0.465	-0.282	-0.081
CR	-0.055	0.921*	1.000	-0.503*	-0.449*	-0.549	-0.510	-0.451	-0.292	0.024
BA	-0.049	-0.422*	-0.503*	1.000	0.182	0.246	0.112	0.450	0.314	-0.165
NB	0.162	-0.412*	-0.449*	0.182	1.000	0.394	0.468	0.050	0.196	0.031
ZR	-0.072	-0.555*	-0.549*	0.246	0.394*	1.000	0.772	0.589	0.571	0.105
Y	-0.040	-0.512*	-0.510*	0.112	0.468*	0.772*	1.000	0.282	0.197	0.079
SR	0.095	-0.465*	-0.451*	0.450*	0.050	0.589*	0.282*	1.000	0.255	0.071
RB	-0.139	-0.282*	-0.292*	0.314*	0.196	0.071	0.197	0.255	1.000	0.189
ZN	0.140	-0.081	0.024	-0.165	0.031	0.105	0.079	0.071	0.189	1.000
CE	0.110	-0.220	-0.229	-0.187	0.231*	0.305*	0.285*	0.209	0.226	0.204
LA	0.167	-0.266	-0.284*	0.279*	0.085	0.213	0.091	0.327*	0.128	0.051
V	0.154	-0.293*	-0.228	0.093	0.064	-0.081	0.063	0.215	0.072	0.085

	CE	LA	V
SIO2	-0.037	-0.065	-0.277
AL203	0.223	0.199	0.054
FE203	0.045	0.117	0.371
MGO	-0.233	-0.263	-0.041
CAO	-0.035	-0.062	0.059
NA2O	0.059	0.125	0.016
K2O	0.082	0.217	-0.019
TIO2	0.228	0.204	0.481
MNO	0.141	0.140	0.199
P2O5	0.158	0.161	0.266
CU	0.110	0.167	0.154
NI	-0.220	-0.266	-0.293
CR	-0.229	-0.284	-0.228
BA	-0.187	0.279	0.093
NB	0.231	0.085	0.064
ZR	0.305	0.213	-0.081
Y	0.285	0.091	0.063
SR	0.282	0.327	0.215
RB	0.226	0.128	0.072
ZN	0.204	0.051	0.085
CE	1.000	0.258	0.292
LA	0.258	1.000	0.290
V	0.292*	0.290*	1.000

compares favourably with the XRF analyses (Appendix 2) of the amphibole-bearing rocks (e.g. samples 4051, 5056, 5113).

On the basis of Table 5.2, it was suggested above that the major elements SiO_2, Al_2O_3, FeO, MgO and CaO, since they show little difference from group to group, are not systematieally enriched or depleted. In addition, the correlations between these elements are mostly significant, an exception being Ca-Si. This may be due to the method of significance testing, or it may be indicative of Ca mobility (cf. the formation of calcite veins, amygdales etc.). However, the element pairs Ca-Mg, Ca-Fe and Ca-Al are all significant. Also, between groups the correlations for these elements are similar and they resemble expected magmatic correlations. In particular, the high correlations for Ca-Al and Fe-Si suggest only minor influence of secondary phases, these being due to primary pyroxene and magnetite control (see Section 5:5:1). The very different nature of the secondary minerals ensures correlations of magmatic origin tend to degenerate once they exert significant control on the rock chemistry. Characteristically strong, negative Fe-Si correlations in the Dominican (Wills, 1974) and Grenadan (Arculus, 1976) suites substantiate this argument.

Another interesting correlation exists between Ni and Cr, both of which also correlate positively with MgO. This is also indicative of primary magmatic control on these elements, since under hydrothermal conditions, especially if sulphide mineralizing fluids are effective, Ni and Cr might be expected to behave differently.

In conclusion then, it is thought that average element abundances are not far removed from those characterising the original lavas. The word 'average', though, is stressed since individual samples show clear evidence of chemical alteration.

Particularly, K, Rb and Ba are extremely variable. Similarly, the presence of epidotic and calcitic veins or amygdales in many samples implies CaO has been mobile. However, samples showing extreme CaO enrichment (e.g. 5014, 5042; Appendix 2) can be eliminated from further consideration. Lastly, most major elements and immobile trace elements have retained, broadly, igneous chemical patterns and thus should permit some discussion as to the petrogenesis of the Rossland suite.

5:4 Geochemical implications for the tectonic setting of the Rossland volcanics

5:4:1 General tectonic setting

On the basis of generalised palaeogeographical considerations and the nature of the lithologies in the volcanic succession, an island-arc type environment has already been considered as likely for the Rossland Group. In this section the evidence of geochemistry is considered. Firstly, the island-arc affinity for the volcanics is tested using immobile trace elements, and in subsequent sections a more detailed comparison with modern analogues and contemporaneous Cordilleran volcanics is made.

Fig. 5.3 shows the discriminatory plot of Pearce & Cann (1973) which utilises Ti, Zr and Y. Selected basalts fall clearly in the field of 'calc-alkaline' basalts. In this type of discrimination the element Ti is particularly important as shown by Chayes & Velde (1965) and Pearce (1976), and is apparently low in abundance in all varieties of destructive-margin magmatism, from tholeiitic to shoshonitic (e.g. the data of Jakeš & White, 1972b).

Fig. 5.4, another plot developed by Pearce and Cann (1973), confirms Fig. 5.3, the Rossland basalts again plotting in the calc-alkaline field. The trend of Ti-Zr in this diagram shows

Figure 5.3

Y-Zr-Ti triangular diagram (Pearce & Cann, 1973) with selected Rossland samples plotted.

Island-arc tholeiites - A + B
Ocean Floor tholeiites - B
Calc-alkali basalts - B + C
Within-Plate basalts - D

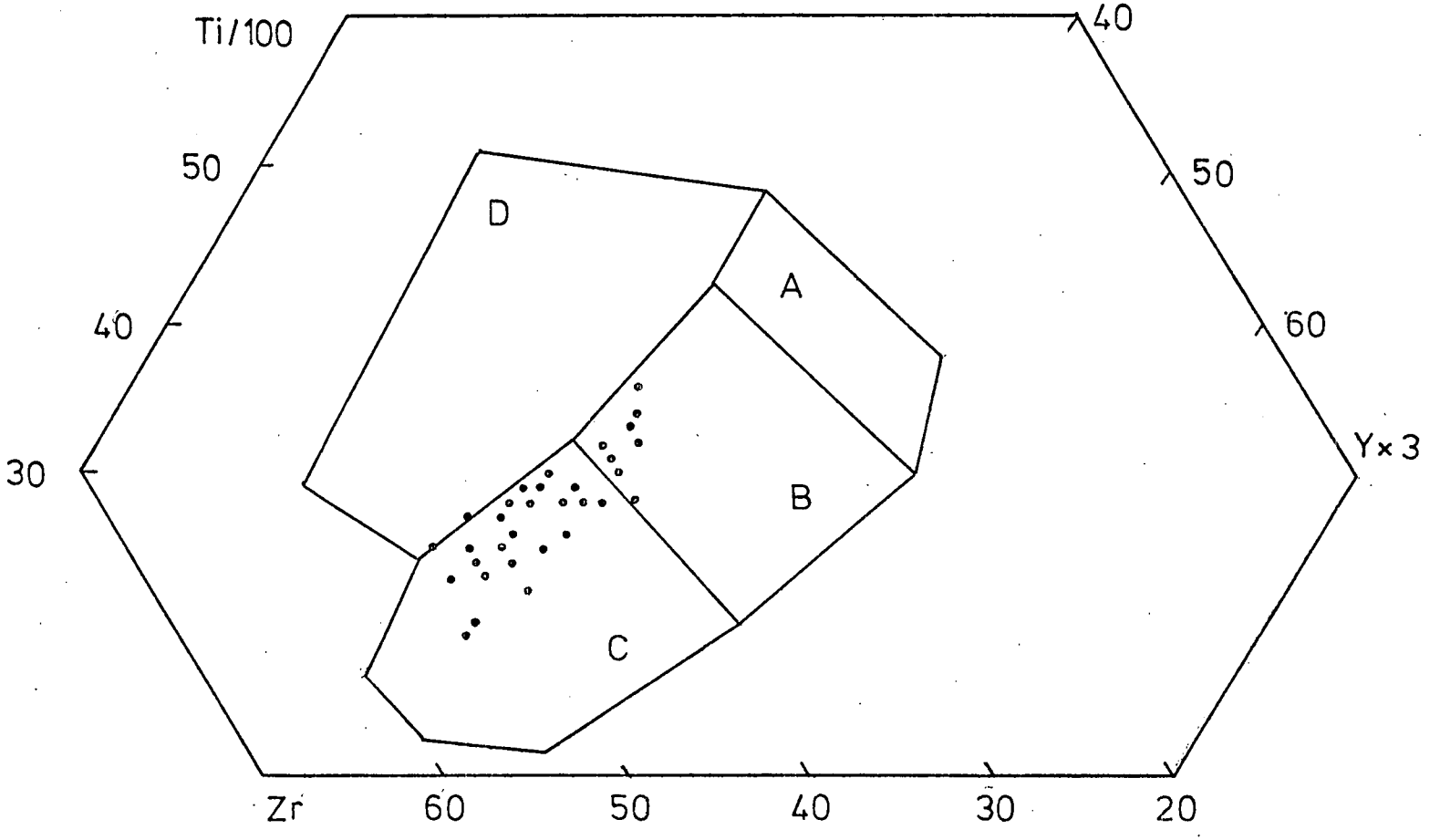
Ti/100
40
50
50
40
60
30
Y×3
D
A
B
C
Zr
60
50
40
30
20

Figure 5.4

Ti-Zr plot (Pearce & Cann, 1973) with selected Rossland ankaramites and basalts plotted.

Ocean Floor tholeiites - B + D
Island-arc tholeiites - A + B
Calc-alkali basalts - B + C

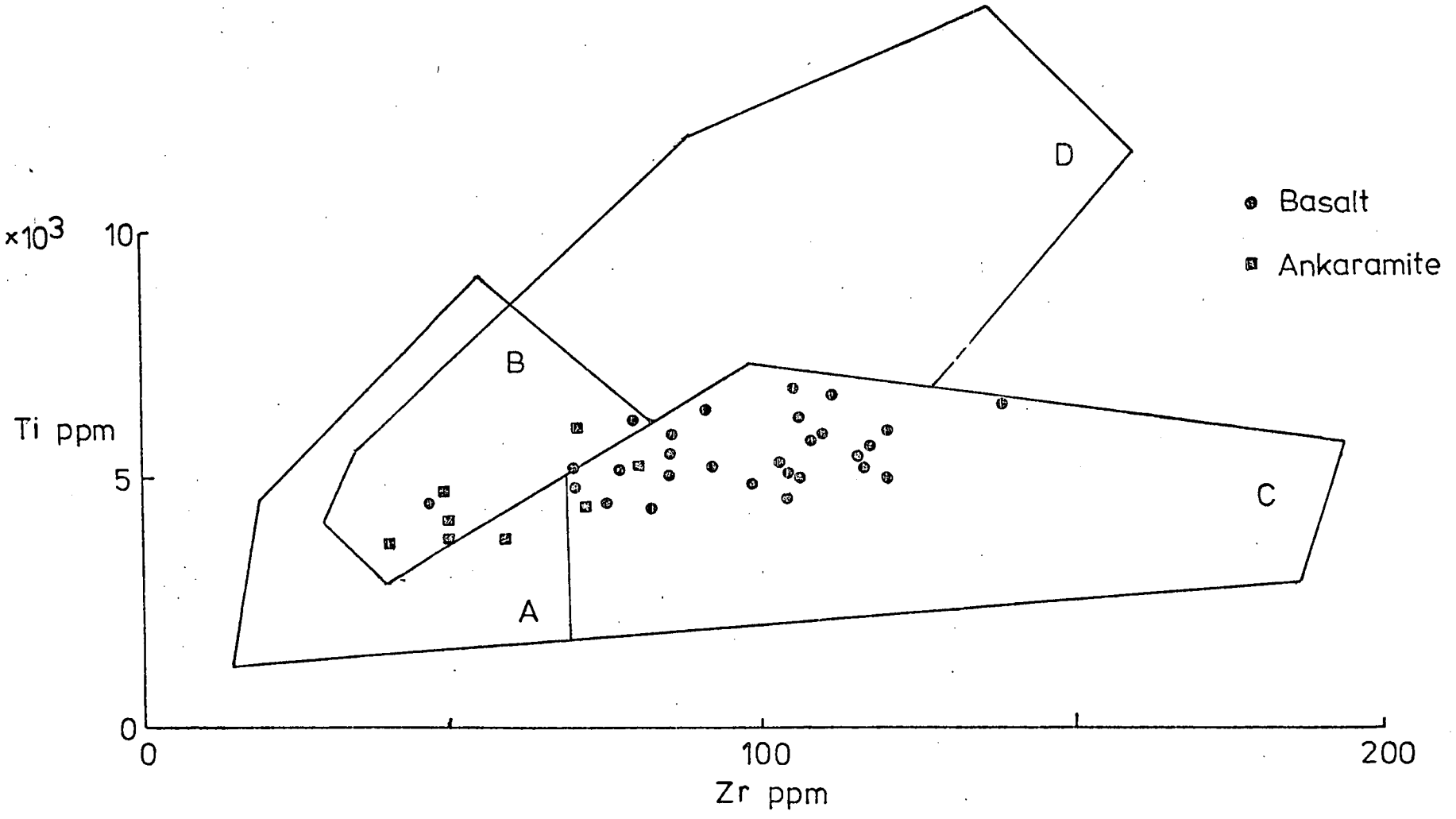
D
B
A
C
Basalt
Ankaramite
×10³
10
5
0
Ti ppm
0
100
200
Zr ppm

significant deviation from the chondritic line which characterizes ocean-floor basalts (Nesbitt & Sun, 1976), and shows that relative to Zr, Ti is not behaving incompatibly.

5:4:2 Comparison with modern island-ares

Though it was established above that the Rossland rocks are 'calc-alkalic' in affinity, the plots of Pearce & Cann (1973) are based primarily on island-arc suites, though calc-alkalic volcanism typifies continental margin environments such as the Andes and the western U.S.A. As regards the setting of the Rossland suite, it was shown in Chapters 2 and 3 that an island-arc depositional regime was operative in the Lower Jurassic, and that the development of a completely emergent continental margin occurred in the Cretaceous; but it is possible the Rossland suite overlies a crust of continental nature.

Geochemically, a continental margin site of origin is not favoured since, as Jakeš & White (1972b) show, Andean-type suites are usually highly differentiated with SiO_2 ranging from 56 to 75 per cent. As Fig.5.1 shows, this is not the case for the Rossland suite; the SiO_2 range of 45 to 60 per cent compares more favourably with that of island arcs quoted by Jakeš & White (1972).

Within island arcs, it has recently become evident that considerable variations of magma type exist, though all generally characterized by low TiO_2, as will become evident. Also, Zr and Y are not useful in discriminating, by Pearce & Cann-type diagrams, between various island-arc magmas. This feature was noted by Floyd & Winchester (1975) when trying to distinguish tholeiitic from alkalic magmas using immobile elements.

The gradational nature of magma chemistry across arcs is well defined (Kuno, 1966; Dickinson & Hatherton, 1968), with essentially

tholeiitic magmas occurring near the trench, followed by high-alumina and alkalic magmas progressively further from the trench. Temporally, a similar progression can occur (Baker, 1968a; Gill, 1970; Jakeš & White, 1969) with older tholeiites being succeeded by younger calc-alkalic and alkalic/shoshonitic varieties. Shoshonitic and alkalic magmatism also occur in the later stages of the orogenic phase of a continental margin, as in western North America. More recently, Brown et al. (1977) have documented a magmatic gradation along the axis of the Lesser Antilles island arc: tholeiites in the north grade southwards through normal calc-alkalic rocks into a mixed alkalic/calc-alkalic environment.

The limited range of SiO_2 noted above is characteristic both of the 'Island Arc Tholeiite Series' (Jakeš & Gill, 1970; Baker, 1968a) and the alkalic or shoshonitic representatives such as are found in the recent volcanics of the New Hebrides (Colley & Warden, 1974) or Fiji (Gill, 1970). Conclusions already reached above regarding the significance of amphibole and biotite, and the high K, Rb, Ba and Sr values (Table 5.2) suggest the latter alternative is more likely to be correct for the Rossland suite. In addition, the presence of clinopyroxene-rich lavas (ankaramites) is a feature found in the New Hebrides, New Georgia (Stanton & Bell, 1969) and the late-stage Fijian suites, rather than in the Tongan (Ewart et al., 1972) or St.Kitts (Baker, 1968b) tholeiitic suites. The Rossland suite also shows no tholeiitic iron-enrichment (Fig. 5.7).

Some comparative data on these ankaramitic, or strongly pyroxene-phyric lavas, from the suites mentioned above, are shown in Table 5.4. The similarities with the Rossland examples are quite apparent. All these rocks, though transitional or mildly alkalic, show the characteristic low TiO_2 of island arcs. They also exhibit low Al_2O_3, and MgO/CaO ratios of close to one.

TABLE 5.4

COMPARATIVE DATA FOR ISLAND-ARC ANKARAMITIC, OR AUGITE-RICH BASALTS

wt.%	A	B	C	D	E	1	2
SiO_2	48.59	48.68	48.97	48.37	48.1	48.54	49.42
TiO_2	0.67	0.43	0.72	0.58	0.6	0.79	0.73
Al_2O_3	11.91	12.44	12.03	12.45	11.4	11.08	10.76
Fe_2O_3*	10.33	11.10	12.54	10.81	10.7	12.93	11.87
MnO	0.19	0.20	0.17	0.20	0.2	0.21	0.18
MgO	13.18	11.36	9.88	10.53	15.3	11.64	11.32
CaO	12.31	11.17	11.52	11.65	10.5	10.67	10.90
Na_2O	2.16	1.93	2.26	1.75	2.2	2.19	2.16
K_2O	0.95	1.51	2.36	1.75	1.5	1.60	2.34
P_2O_5	0.14	0.24	0.46	0.34	0.2	0.32	0.32
Total	100.43	99.02	100.91	98.43	100.7	100.00	100.00

ppm			
Cu	120	79	129
Ni	92	147	164
Cr	360	577	587
Ba	684	577	672
Nb	-	2	3
Zr	34	48	73
Y	14	14	14
Sr	972	608	610
Rb	60	38	56
Ce	29	15	-
La	14	4	-
V	670	287	-

A Olivine-Augite basalt, Aoba, New Hebrides (Warden, 1970)

B Pyroxene-olivine basalt, New Georgia (Stanton & Bell, 1969)

C Ankaramite, Bridget Cove (Irvine, 1973)

D Pyroxene-rich basalt, Fiji (Gill, 1970)

E Ankaramite, Takla Group, Aiken Lake (Irvine, 1973)

1 Ankaramitic basalt 5538A, Rossland volcanics

2 " " 4013A, " "

Clinopyroxene is modally greater than olivine, though in the older Bridget Cove, Takla and Rossland samples alteration may have removed many traces of original olivine. Comparison of trace elements between the Fijian 'shoshonitic' representative (Table 5.4) and Rossland samples show the two to be similar, both having high Ba, Sr and Rb contents. Bearing in mind the problems of secondary alteration, this comparison shows that the high values for Sr, Ba and Rb are not unrealistic for rocks of this composition.

Comparative data for basaltic compositions are shown in Tables 5.5 and 5.6. Table 5.5 illustrates the Japanese transverse-arc gradation of basaltic magma type, with some Rossland basalts of comparable SiO_2 abundance. The actual differences between the Japanese parent magmas are slight, and involve only TiO_2 and alkalis. Taking the alkalis of the Rossland basalts at face value, clearly the best analogy is with the Japanese alkaline parent magma. Similarly, the slightly higher TiO_2 and P_2O_5 of the alkaline magma, both regarded as stable oxides , compare favourably with the Rossland samples.

Some more data for island-arc basalts are shown in Table 5.6. Here the axial-arc gradation in the Lesser Antilles (Brown et al., 1977) is apparent. The average rock composition between 50 and 52 per cent SiO_2 for the islands St. Kitts (tholeiitic), Dominica (calc-alkalic) and Grenada (alkalic/calc-alkalic) shows that the constituents Na_2O, K_2O, Ba, Rb, Sr, Ni and Cr are most abundant in Grenada. The average Rossland basalt (50-52 per cent SiO_2) is closest in composition to Grenada. Also shown in Table 5.6 is a high-Al_2O_3, high-K_2O, calc-alkaline basalt from East Papua (Jakeš & Smith, 1970). This sample also resembles the Rossland average in having high Ba, Sr and alkalis at relatively high MgO, Cr and

TABLE 5.5

COMPARATIVE DATA ON JAPANESE AND ROSSLAND BASALTS

wt.%	A	B	C	1	2	3
SiO_2	48.73	48.10	47.95	47.84	49.94	48.00
TiO_2	0.63	0.73	1.09	0.81	1.09	0.98
Al_2O_3	16.53	16.68	16.46	14.37	14.43	13.02
Fe_2O_3*	12.74	12.41	10.90	14.86	12.63	14.12
MnO	0.29	0.54	0.21	0.22	0.20	0.22
MgO	8.24	8.89	8.99	8.53	7.44	6.72
CaO	12.25	10.48	10.44	9.29	10.20	11.41
Na_2O	1.21	2.51	2.72	1.84	2.96	2.94
K_2O	0.23	0.46	1.09	1.82	0.78	2.31
P_2O_5	0.10	0.54	0.41	0.41	0.32	0.28
Total	100.95	101.34	100.26	100.00	100.00	100.00

A Tholeiitic primary magma type (Kuno, 1966)

B High Alumina " " " " "

C Alkaline " " " " "

1 Basalt 5006, Rossland volcanics

2 " 5041, " "

3 " 4070 " "

TABLE 5.6

COMPARATIVE DATA FOR ISLAND-ARC BASALTS

wt.%	A	B	C	D	E	1
SiO_2	51.02	50.90	51.13	50.59	50.89	51.09
TiO_2	0.86	0.85	0.98	1.05	0.88	0.94
Al_2O_3	17.73	19.83	19.77	16.29	16.25	13.97
Fe_2O_3*	9.14	10.25	9.47	9.30	11.53	11.57
MnO	0.16	0.19	0.18	0.17	0.21	0.17
MgO	6.23	3.74	3.92	8.96	5.41	7.65
CaO	10.44	11.10	11.09	9.50	4.02	9.44
Na_2O	3.24	2.50	3.00	2.89	5.16	2.93
K_2O	0.94	0.49	0.36	1.07	1.79	1.92
P_2O_5	0.18	0.12	0.10	0.21	0.28	0.31
Total	99.94	99.99	100.00	100.01	96.34	100.00
ppm						
Cu	98	12	60	-	-	72
Ni	129	36	11	150	-	52
Cr	285	109	17	360	-	169
Ba	398	105	126	400	-	753
Nb	6	3	2	-	-	4
Zr	96	44	65	130	-	91
Y	22	13	22	-	-	18
Sr	738	310	290	450	-	716
Rb	23	16	5	-	-	47
Zn	74	80	68	-	-	92
V	215	-	235	216	-	295

A Average basalt (50-52 per cent SiO_2), Grenada, (Brown et al., 1977).

B " " " Dominica, "

C " " " St.Kitts, "

D High-al basalt, East Papua (Jakeš & Smith, 1970)

E Pyroxene 'andesite', Sofala volcanics (Barron, 1976)

1 Average basalt (50-52 per cent SiO_2), Rossland volcanics.

Ni levels. A feature of the Rossland volcanics brought out in Tables 5.5 and 5.6 is their low Al_2O_3 content compared to many other arcs. This is a further indicator that normal calc-alkaline magmas were not erupted in the Rossland area.

Data on the more evolved andesitic (or basaltic-andesitic) compositions are shown in Table 5.7. Comparison with the Lesser Antilles again confirms the similarities deduced from the basaltic rocks, though in this case K, Rb, Ba and Sr abundances in the Rossland samples exceed those of the Grenada average. It is a fact, though, that the Grenadan suite shows a transition from alkaline to calc-alkaline with differentiation, rather than following an alkalic or shoshonitic trend (e.g. Fiji; Gill, 1970). This suggests that within the Rossland suite there is a shoshonitic trend, though as shown in Fig.5.10 some andesites exhibit low K, Rb and Ba contents. The high K, Rb and Ba contents of, for example, sample 5033 (Table 5.7) is confirmed by the presence in the rock of biotite phenocrysts.

The significance of amphibole has been stressed above. Whole-rock data for amphibole-bearing basalts from Bogoslof Island, Grenada and Kick 'Em Jenny Volcano, are shown in Table 5.8. Amphibole-bearing basaltic andesites, or andesites from the high-K or mildly alkalic suites of East Papua, New Hebrides and New Georgia, where amphibole makes a relatively early appearance in the differentiation sequence, are tabulated in Table 5.9. These data, by virtue of the comparable alkali and associated trace element contents to the Rossland examples, confirms the belief that the Rossland abundances for these mobile elements are near the original igneous values.

If a comparison is made on the basis of average values of K, Rb, Ba and Sr with the average data reported by Jakeš & White (1972b), a transitional calc-alkalic to shoshonitic affinity is indicated for the Rossland suite. K_2O/Na_2O, on average, is less

TABLE 5.7

COMPARATIVE DATA FOR ISLAND ARC ANDESITES (LOW-Si)

	A	B	C	D	1	2	3
Wt.%							
SiO_2	55.01	54.64	54.92	54.54	55.69	54.15	55.55
TiO_2	0.82	0.79	0.88	1.13	0.77	0.85	0.71
Al_2O_3	18.48	19.41	18.91	16.26	14.97	15.62	15.68
Fe_2O_{3*}	8.60	9.21	8.80	8.30	8.61	9.89	9.33
MnO	0.17	0.19	0.17	0.12	0.14	0.14	0.13
MgO	4.50	2.91	3.04	6.97	3.42	2.83	5.24
CaO	7.98	9.22	9.39	7.50	8.45	8.25	7.39
Na_2O	3.25	2.88	3.26	3.64	4.30	5.04	2.36
K_2O	0.92	0.58	0.53	1.49	3.29	2.79	3.24
P_2O_5	0.18	0.14	0.10	0.23	0.36	0.39	0.38
Total	99.91	99.97	100.00	100.15	100.00	100.00	100.00
ppm							
Cu	83	92	59	-	64	34	36
Ni	104	33	4	22	16	8	1
Cr	238	109	6	33	54	21	10
Ba	338	132	146	192	803	1190	1078
Nb	7	3	1	-	5	3	2
Zr	117	64	81	105	119	81	153
Y	24	24	24	22	19	15	23
Sr	530	280	301	358	717	868	1438
Rb	24	18	10	20	51	54	56
Zn	84	81	69	-	71	89	99
V	187	-	168	215	209	268	197

A Average andesite (54-56 per cent SiO_2), Grenada (Brown et al., 1977)

B " " " Dominica, " " "

C " " " St.Kitts, " " "

D Low-Si andesite, East Papua (Jakeš & Smith, 1970)

1 Andesite 41098, Rossland volcanics

2 " 4056 " "

3 " 5033 " "

TABLE 5.8

COMPARATIVE DATA FOR AMPHIBOLE-BEARING, ISLAND-ARC BASALTS

Wt.%	A	B	C	1	2
SiO_2	51.88	45.93	51.54	50.59	52.86
TiO_2	0.79	1.06	0.32	1.14	0.81
Al_2O_3	16.39	16.88	20.31	15.94	14.84
$Fe_2O_3^*$	8.65	10.05	8.59	11.07	10.31
MnO	0.20	0.17	0.32	0.15	0.18
MgO	9.23	11.18	3.16	6.77	5.32
CaO	9.45	12.24	9.55	9.39	9.06
Na_2O	2.53	1.84	4.29	3.30	2.28
K_2O	0.76	0.55	2.47	1.34	1.98
P_2O_5	0.11	0.11	0.57	0.27	0.23
Total	99.99	100.01	100.80	100.00	100.00
ppm					
Cu	47	88	-	62	
Ni	304	235	-	72	
Cr	-	-	-	170	
Ba	206	117	864	692	
Nb	11	5	-	3	
Zr	99	62	87	105	
Y	17	19	-	21	
Sr	401	301	815	566	
Rb	43	19	43	41	
Zn	72	72	-	100	

A Transitional basalt, Grenada (Arculus, 1973)

B Kick 'em Jenny alkaline basalt, Lesser Antilles (Arculus, 1973)

C Basalt, Bogoslof Island, Aleutian arc (Arculus et al., 1977)

1 Basalt 4051, Rossland volcanics

2 " 5056 " "

TABLE 5.9

COMPARATIVE DATA FOR AMPHIBOLE-BEARING, ISLAND ARC ANDESITES

Wt.%	A	B	C	D	E	1
SiO_2	56.18	55.45	56.08	56.43	55.60	56.81
TiO_2	0.77	0.75	0.53	0.93	0.62	0.76
Al_2O_{3*}	15.80	18.87	19.04	16.00	16.90	14.66
Fe_2O_3	7.09	6.60	7.14	6.57	7.43	9.96
MnO	0.12	0.13	0.14	0.09	0.15	0.12
MgO	7.59	4.26	3.82	6.04	5.44	4.87
CaO	7.65	5.19	8.04	5.84	6.64	7.17
Na_2O	3.81	2.55	4.18	4.05	3.63	3.56
K_2O	1.53	2.39	0.88	1.92	1.61	1.88
P_2O_5	0.22	0.44	0.16	0.99	0.23	0.22
Total	100.76	96.63	100.01	98.86	98.25	100.00
ppm						
Sr				580		535
Ba				670		686
Zr				200		106

A Augite-amphibole andesite, East Papua (Jakeš & White, 1969)

B Amphibole-augite sheshonite, East Papua (Jakeš & White, 1969)

C Augite-amphibole andesite, Guadal Canal (Jakeš & White, 1969)

D Amphibole andesite, East Papua (Jakeš & Smith, 1970)

E Hornblende basaltic andesite, New Georgia (Stanton & Bell, 1969)

1 Andesite 5113, Rossland volcanics

than 1.0 (average = 0.7) for the Rossland suite. In view of the similarities with the Grenada, New Hebrides and New Georgia 'alkalic' suites (Tables 5.4, 5.6, 5.9), a transitional affinity towards these is also indicated.

In summary, it seems clear that the Rossland volcanics are not typically calc-alkalic, though of island arc volcano-tectonic setting. A precise analogy in the present day is not evident, but various petrographic and chemical data show the Rossland suite has similarities with the generally rarer shoshonitic or alkalic rocks of young island arcs, from which most of the comparative data is drawn.

There are also comparable features with older arcs. For example, the augite-phyric volcanics of the Bridget Cove, Mesozoic arc in S.E. Alaska (Irvine, 1973) and the Sofala volcanics of New South Wales (Barron, 1976)(Tables 5.4 and 5.6).

5:4:3 Comparison with associated volcanics of the Canadian Cordillera

Lithological similarities between the Rossland and associated, or contemporaneous, volcanics of the Cordillera, notably the Takla, Hazelton and Nicola Groups, were discussed in Chapter 3. Here, the discussion is extended to chemical similarities and differences.

Within the Nicola and Takla successions there is a predominance of augite-rich, basic rock types (Monger, 1975). Chemical data for these are limited, but one analysis of a Takla ankaramite, reported by Irvine (1974), is shown in Table 5.4. Fig. 5.5 also shows the basic nature of the Takla rocks (after Monger & Church, 1977).

Souther (in press) has compiled some data for the Nicola-Takla rocks and displayed it on AFM and Alkalis-SiO_2 diagrams (Fig. 5.6). He considers this volcanic province to be alkaline on

Figure 5.5

Abundance of basalts (B), andesites (A), dacites (D) and rhyolites (R) in the Takla and Hazelton volcanic groups, based on refractive index (R.I.) measurements on fused rock samples (after Church & Monger, 1977).

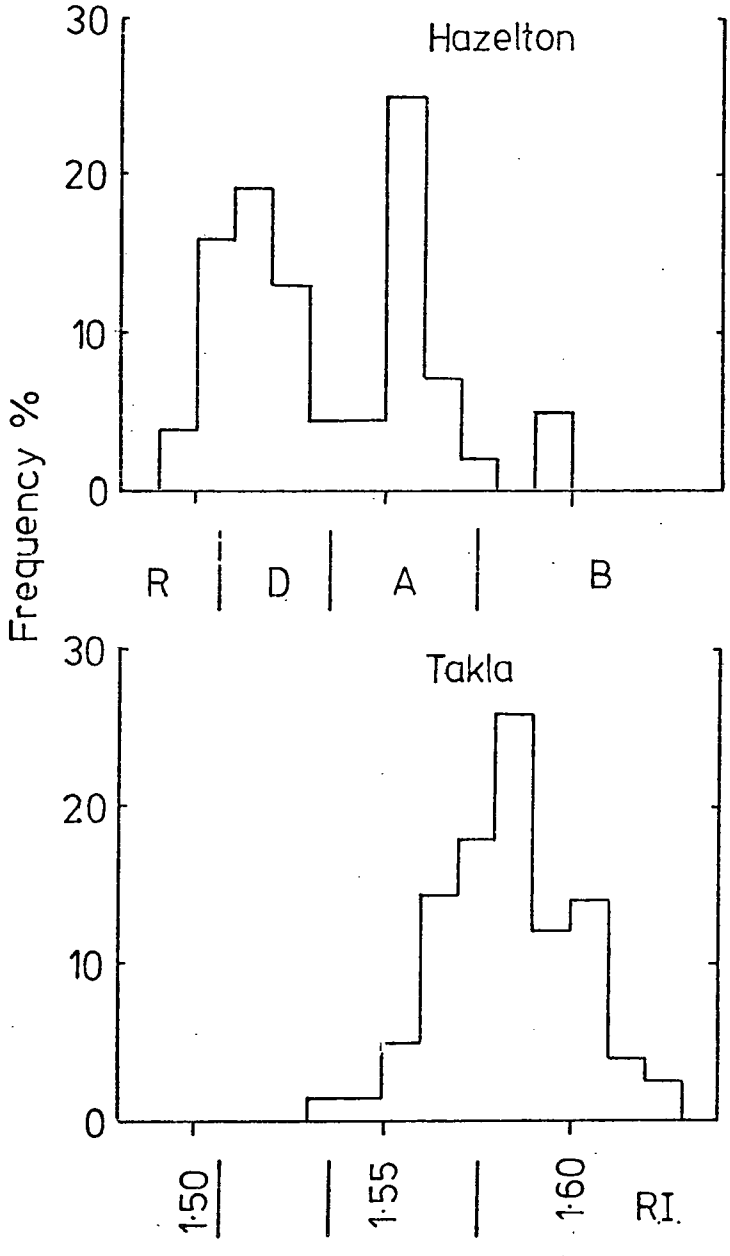
Hazelton
30
20
10
0
Frequency %
R
D
A
B
Takla
30
20
10
0
1·50
1·55
1·60
RI.

this basis, at least for the basic end of the spectrum. Other evidence for the alkalinity of the Takla-Nicola association is given by Irvine (1974). By analogy with the Alaskan ultramafic complexes and the associated ankaramites of the Bridget Cove belt (Irvine, 1973), Irvine (1974) suggests a relation between the Alaskan type Polaris and Tulameen complexes of the Intermontane Belt, and the Takla-Nicola augite porphyries. On the basis of crystallization history, such as the co-precipitation of olivine and clinopyroxene, but no orthopyroxene, and on the evidence of clinopyroxene chemistry, Irvine considers these complexes to be derived from undersaturated, ankaramitic lavas. They represent, therefore, sub-volcanic cumulates. There is an age discrepancy however, since dates on the two complexes mentioned above give Jurassic ages of 164 my. and 186 my. respectively. Other evidence of a similar nature is reported by Souther (1973) for the Stikine region, north B.C. Here, pyroxenite bodies, associated with the local augite porphyries, have fractionated to syenitic end-members. Fox (1975) also reports alkalic intrusives in the Quesnel Trough area comagmatic with the volcanics. With regard to the Rossland volcanics, the Bonnington Complex of Mulligan (1952), comprising pyroxenites, gabbros and possibly syenites, perhaps represents a similar relationship.

Hazelton volcanics, of Lower Jurassic age, are generally different from the underlying Takla rocks and, as noted above, are confined to north-central British Columbia (Fig. 5.6). Compositionally they are more differentiated than the Takla, Nicola and Rossland volcanics, being more feldspathic. Fig. 5.5 shows the frequency of the rock types basalt, andesite, dacite and rhyolite in the Hazelton succession.

Figure 5.6

Summary of the distribution and chemistry of Upper Triassic and Jurassic volcanics (from Soother, in press).

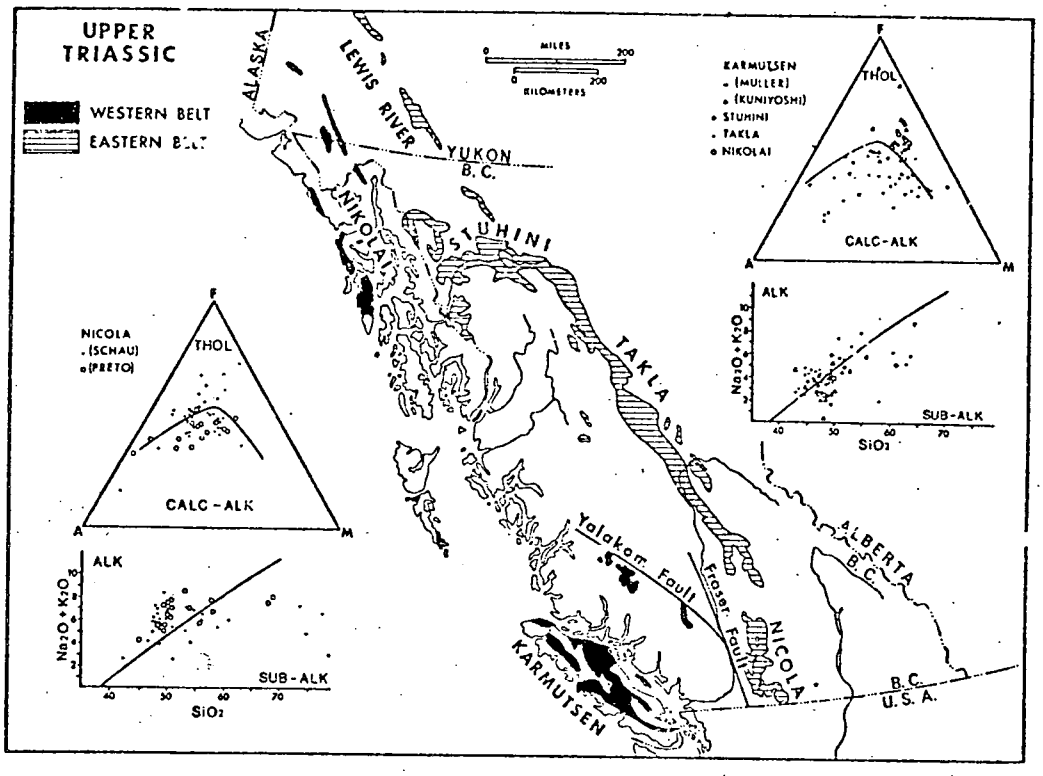
UPPER TRIASSIC
WESTERN BELT
EASTERN BELT
ALASKA
LEWIS RIVER
YUKON
B.C.
NIKOLA
STUHINI
TAKLA
Yalakom Fault
Fraser Fault
NICOLA
KARMUTSEN
ALBERTA
B.C.
B.C.
U.S.A.
MILES
KILOMETERS
KARMUTSEN
(MULLER)
(KUNIYOSHI)
STUHINI
TAKLA
NIKOLAI
NICOLA
(SCHAU)
(PRETO)
F
THOL
CALC-ALK
A
M
ALK
SUB-ALK
SiO2
Na2O+K2O

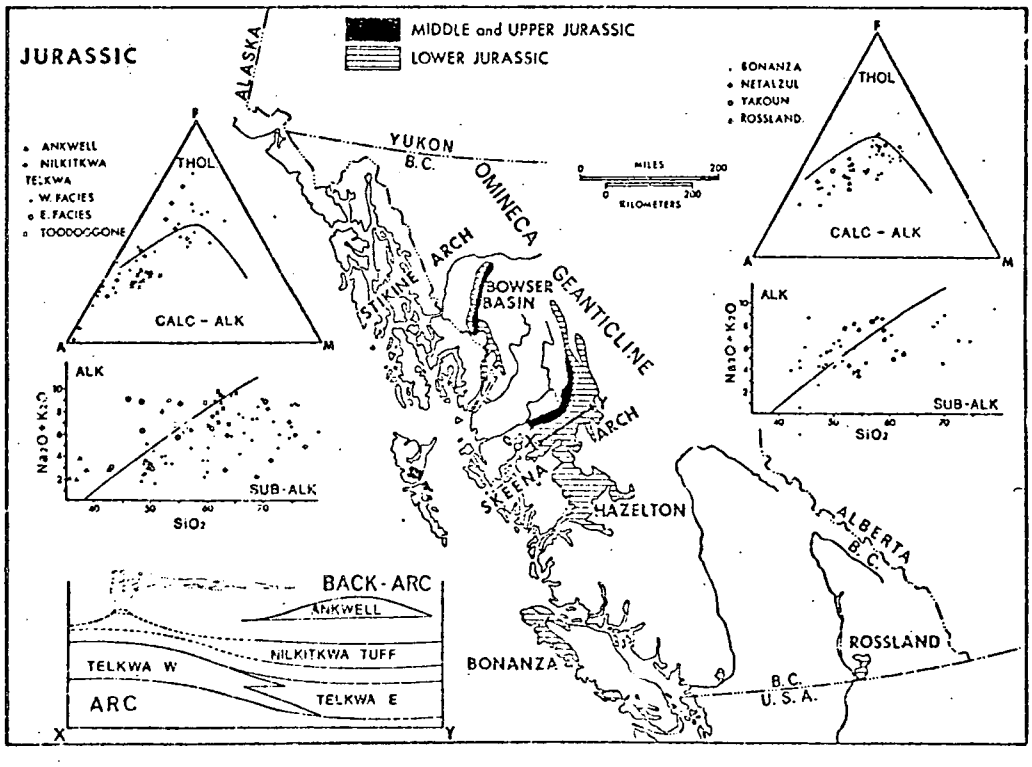
JURASSIC
MIDDLE and UPPER JURASSIC
LOWER JURASSIC
ALASKA
YUKON
B.C.
OMINECA
STIKINE ARCH
BOWSER BASIN
GEANTICLINE
SKEENA ARCH
HAZELTON
BONANZA
ROSSLAND
ALBERTA
B.C.
B.C.
U.S.A.
ANKWELL
NILKITKWA
TELKWA
W. FACIES
E. FACIES
TOODOGGONE
BONANZA
NETALZUL
YAKOUN
ROSSLAND
MILES
KILOMETERS
F
THOL
CALC-ALK
A
M
ALK
SUB-ALK
SiO2
Na2O+K2O
BACK-ARC
ANKWELL
NILKITKWA TUFF
TELKWA W
TELKWA E
ARC
X
Y

A detailed revision of the Hazelton succession has recently been completed by Tipper & Richards (in press). They distinguish a western proximal facies of mainly subaerial origin from a distal eastern facies, where clastic rocks accumulated in a subsiding, back-arc basin. Also associated with this back-arc environment are the distinctly alkalic and basic Ankwell lavas. The more alkaline nature of the eastern Hazelton rock is shown in Fig. 5.6 (after Souther, in press).

A generalised discussion of the tectonic setting, using the evidence of this and the previous two sections, is given in the final chapter.

5:5 Petrogenesis of the Rossland volcanics

5:5:1 Chemical variation within the Rossland suite

This section deals with the origin of variation within the analysed samples, whereas the subsequent section is concerned with the origin of the overall geochemical identity of the suite and of the parent magmas.

Variation within the suite is illustrated in various plots (Figs. 5.7, 5.8, 5.9, 5.10). Figs. 5.7 and 5.10 are conventional Harker plots, SiO_2 acting as the abscissa. Noticeable in all these diagrams is that there is a fair degree of scatter. Before considering the causes of the observed trends, this should be considered. Scatter in a suite of rocks can be due to:-

(1) Alteration: This is undoubtedly a causal factor here, especially with regard to K, Rb, Ba and possibly Sr. Also, oxides like MgO and CaO, that can be affected strongly by the development of secondary mineralogies, may have fluctuated. However, it is believed (Section 5:3) that most major oxides and immobile trace

Figure 5.7

Harker diagrams for the major and minor elements of the Rossland volcanic rocks.

(Crosses = pyroxenites)

Also shown are average mineral compositions estimated from the microprobe data (except olivine, FO_{80}):-

PX - Clinopyroxene

PL - Plagioclase

O - Olivine

A - Amphibole

SP - Ti-magnetite

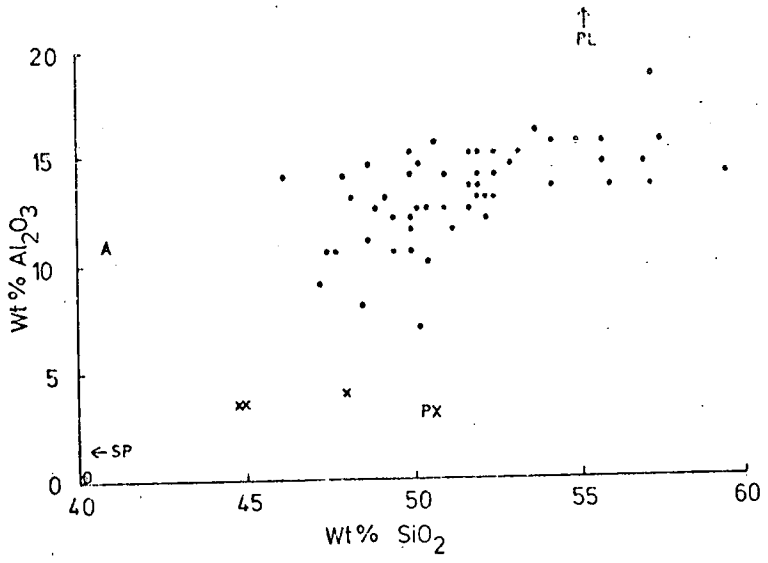
PL
20
15
10
5
0
Wt % Al_2O_3
A
PX
← SP
40
45
50
55
60
Wt % SiO_2

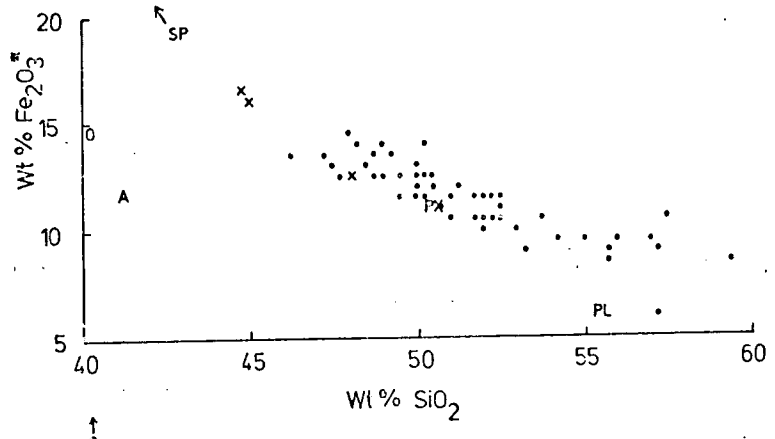
SP
20
15
10
5
Wt % $Fe_2O_3^*$
A
PX
PL
40
45
50
55
60
Wt % SiO_2

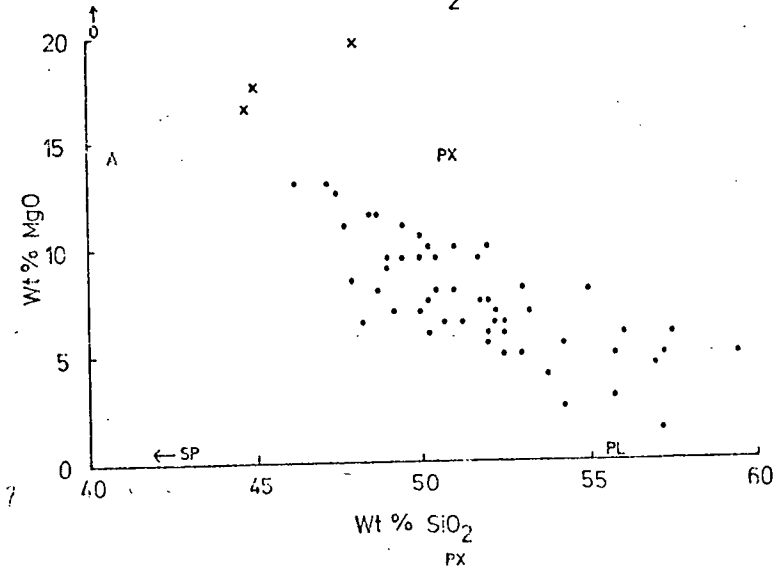
20
15
10
5
0
Wt % MgO
A
PX
← SP
PL
40
45
50
55
60
Wt % SiO_2

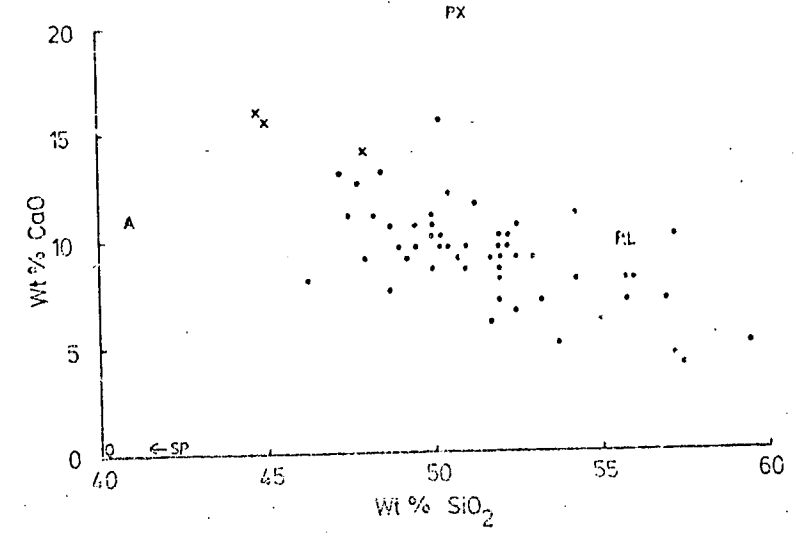
PX
20
15
10
5
0
Wt % CaO
A
PL
← SP
40
45
50
55
60
Wt % SiO_2

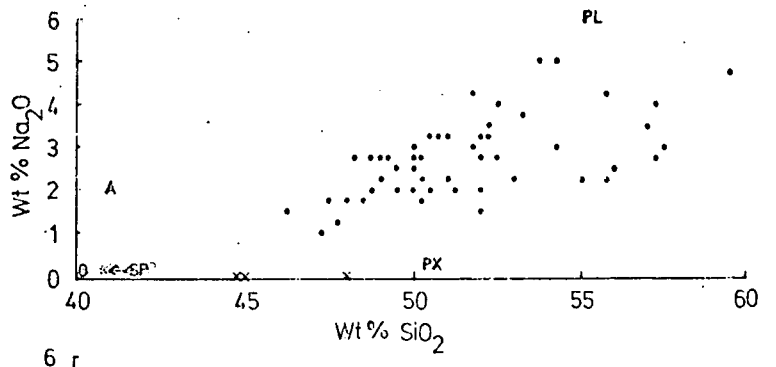
Wt % Na_2O
PL
A
PX
Wt % SiO_2

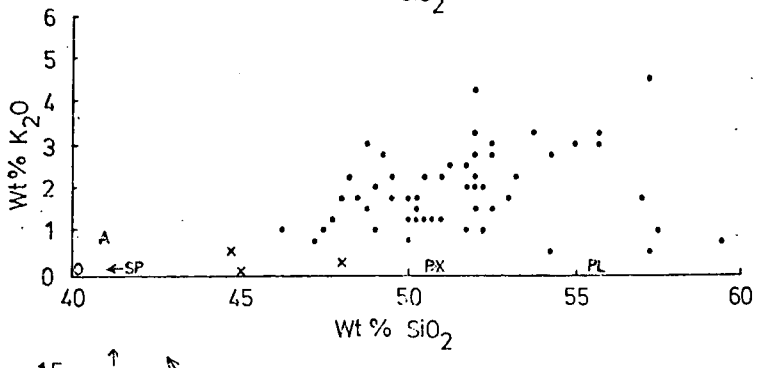
Wt % K_2O
A
SP
PX
PL
Wt % SiO_2

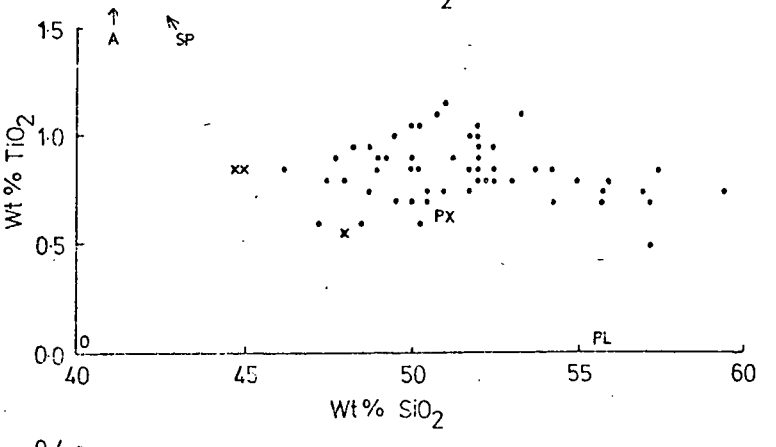
Wt % TiO_2
A
SP
PX
PL
Wt % SiO_2

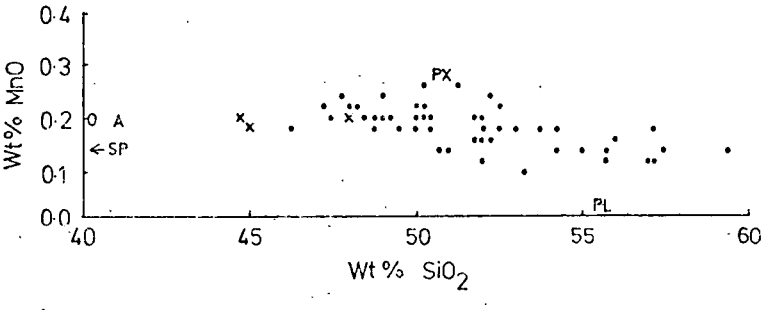
Wt % MnO
A
SP
PX
PL
Wt % SiO_2

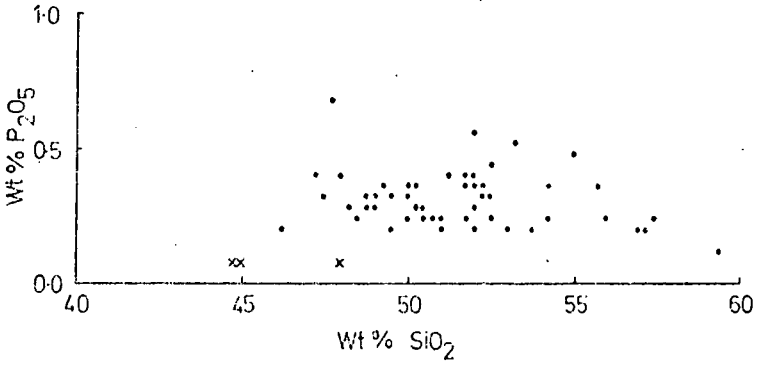
Wt % P_2O_5
Wt % SiO_2

Figure 5.8

Part of the plane nepheline - plagioclase - diopside - quartz (projected from olivine) in the normative basalt tetrahedron. Plotted points are Rossland volcanics, plus pyroxenites. Tie-lines join analysed amphiboles with the host rock. Note the Ne-normative character of the amphiboles.

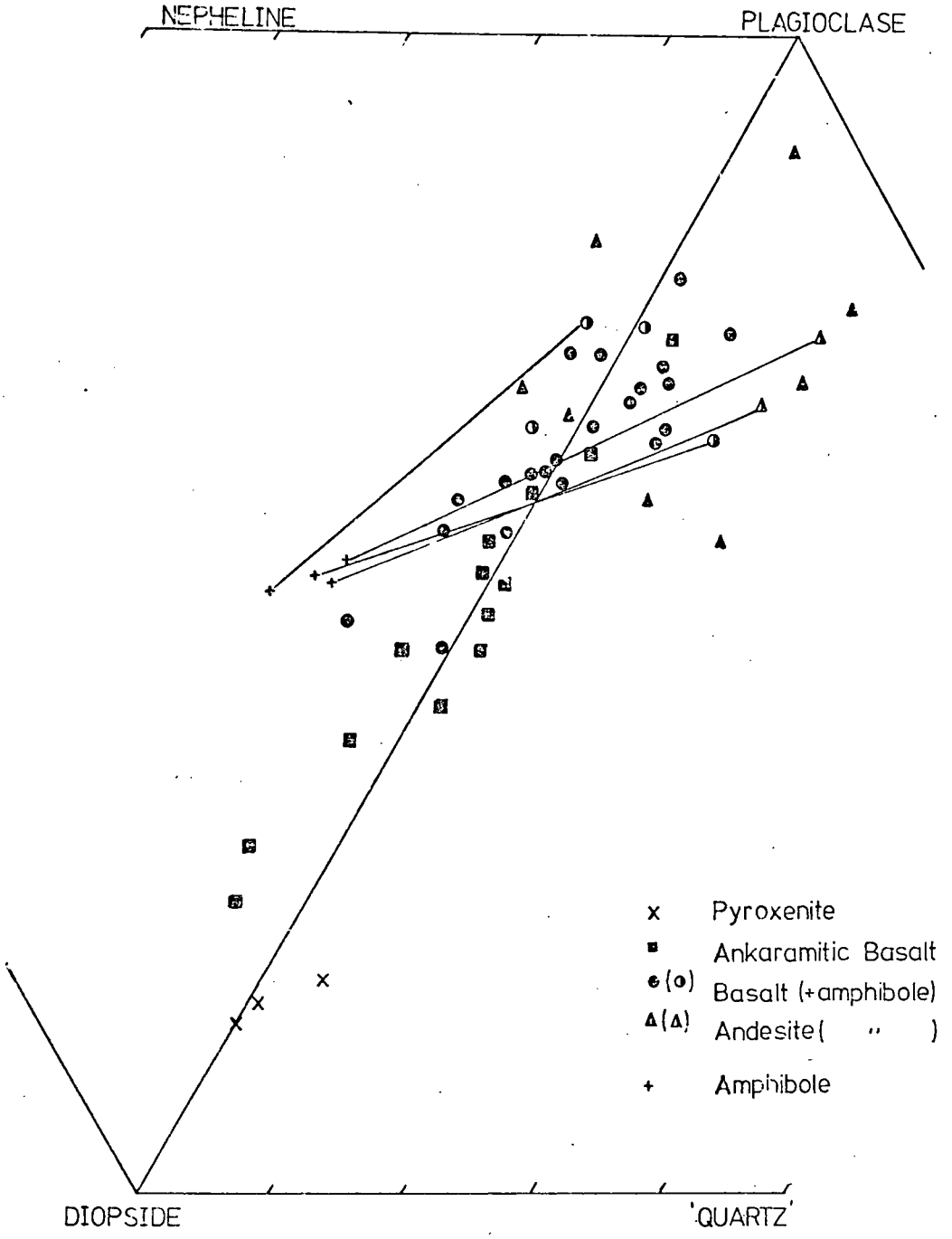
NEPHELINE
PLAGIOCLASE
DIOPSIDE
'QUARTZ'
x Pyroxenite
■ Ankaramitic Basalt
● (○) Basalt (+amphibole)
▲ (△) Andesite (")
+ Amphibole

Figure 5.9

The plane plagioclase-diopside-olivine in the normative basalt tetrahedron. ('Olivine' includes the olivine component of enstatite; i.e. projection is from quartz). Dashed lines are 1 atm. cotectics taken from Cox & Bell (1972), for natural basalts (symbols as for Fig.5.8).

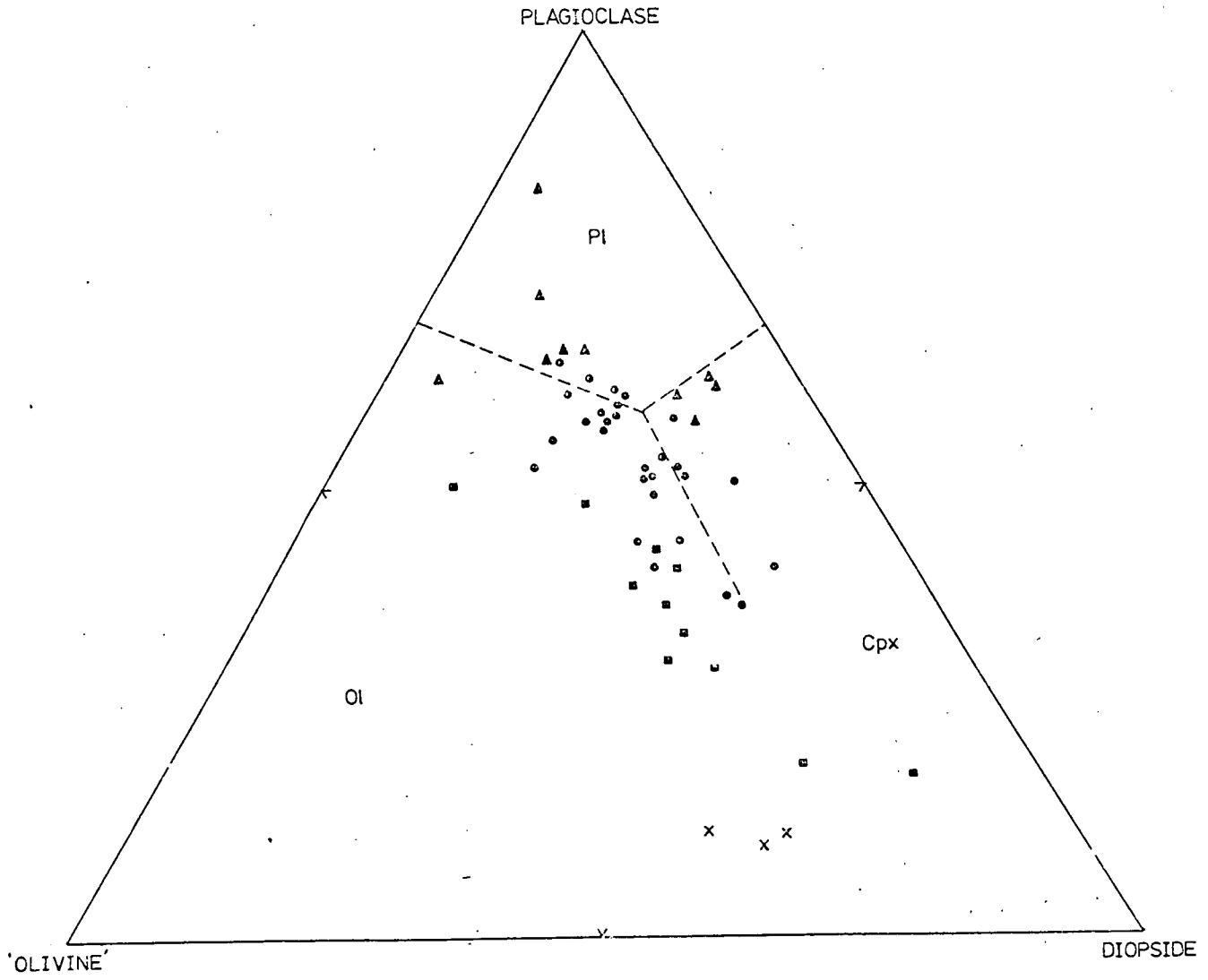
PLAGIOCLASE
Pl
Cpx
Ol
'OLIVINE'
DIOPSIDE

elements have retained, to some extent, magmatic covariances.

(2) Crystal Accumulation: The strongly porphyritic nature of the Rossland suite rocks makes it almost certain that many samples show non-liquid compositions. If the liquid line of descent, though, is controlled by the fractionation of the observed phases, then this problem may not be serious. If, however, a high-pressure crystal fractionation or partial melt trend is present, then low-pressure fractionation can seriously obscure it. It is likely that this process has occurred to a degree in the Rossland volcanics. Particularly, the variable Al_2O_3 content in the low-SiO_2 rocks (Fig.5.7) is probably due to modal variations of augite.

(3) Sampling: The rocks sampled and analysed come from a dominantly clastic sequence. Thus, a result is that temporal and spatial patterns in geochemistry have been scrambled to some extent, by sedimentary processes. It is inevitable, therefore, that although all of the volcanics come from a single magmatic province, several different volcanic centres may be represented. The broad areal differences in chemistry and rock-type suggest this. For example, ankaramitic basalts are found predominantly in the Ymir to Nelson region, whilst more feldspathic basalts and andesites are particularly common in the Eerie Creek/Keystone Mountain region (Fig.1.1).

Major and minor elements

Variation of these elements, expressed as oxides, is shown in both Harker diagrams (Fig.5.7) and normative, basalt-tetrahedron plots (Figs. 5.8, 5.9). Broadly, it is apparent that with SiO_2 increase, Na_2O and K_2O increase, whilst Fe_2O_3*, MgO, CaO and MnO decrease. Al_2O_3 shows a tendency to increase at first and then level

* All Fe as Fe_2O_3.

off. P_2O_5 and TiO_2 show a slight trend through a maximum at about 52–54 per cent SiO_2. The pyroxenite cumulates plot, in general, on a backward extension of the volcanic trends.

When plotted in the basalt tetrahedron the rocks, except at the feldspathic end of the trend, plot over the critical plane of silica-undersaturation (Fig. 5.8). A number of samples are Ne-normative, though Na_2O mobility may be partly responsible. In the plane diopside-olivine-plagioclase (the critical plane), as shown in Fig. 5.9, the suite occupies a broad band running roughly parallel to the join diopside-plagioclase. The pyroxenites plot some way from pure diopside and indicate a significant olivine component. Thus it seems that variation is broadly controlled by augite and plagioclase, the most commonly observed phases, and minor olivine. In Fig. 5.9 are also shown the 1 atm. cotectics for natural basalts (Cox & Bell, 1972), and very generally, the Rossland rocks appear to be related to these. However, they are unlikely to be strictly valid due to the influence, as shown in Chapter 4, of significant H_2O vapour pressure. This would have the effect of reducing the primary phase volume of plagioclase and introducing a phase volume of amphibole (Cawthorn, 1976a, b).

The mineralogical control on the variation can be viewed in more detail by plotting the relevant minerals in the Harker diagrams (Fig. 5.7). Considering firstly the trend from ankaramitic basalt to basalt (47–53 per cent SiO_2), it is clear that clinopyroxene (augite) cannot be solely responsible due to its high SiO_2 ($\sim$ 50 per cent). The Al_2O_3 – SiO_2 plot (Fig. 5.7) shows that olivine is most likely to be an additional controlling phase. Similarly, in Fig. 5.7, the $Fe_2O_3^*$ – SiO_2 plot indicates a contribution from magnetite, albeit a small one. Since olivine

is not abundant in the ankaramitic basalts, it is possible there is a superposition of trends here. This type of situation is described by Cox & Bell (1972) for lavas of the New Hebrides, which though lying on a strict olivine-control line, contain abundant clinopyroxene as phenocrysts. It is possible, therefore, that a series of magmas,delivered into a crystal magma chamber, showed varying degrees of olivine fractionation (cf. O'Hara, 1968) but grew and fractionated clinopyroxene at low pressure. This, in the Rossland case, has produced cross-trend scatter. Trace element evidence for the control by olivine is discussed below. Cr-spinel may have also participated in the early fractionation of the suite, being a high-temperature crystallizing phase (Irvine, 1967). The Grenadan picrite-basalt chemical trend , dooumented by Arculus (1976), is also believed to be due to Cr-spinel fractionation, in addition to pyroxene and olivine.

The more evolved end of the suite (53-60 per cent SiO_2) shows the influence of an aluminous phase. Possibilities are plagioclase and amphibole. It seems unlikely, however, that clinopyroxene and plagioclase alone can account for the observed variation, since in the different plots in Figs. 5.7 different proportions of these minerals are required. Amphibole, then, is a strong possibility as an additional controlling phase, and it also has the advantage of a low SiO_2 content. From Fig. 5.7 amphibole can be seen to plot on a backward extension of the trends, though, as was shown petrographically, it must have coexisted with clinopyroxene and plagioclase. However, the differing densities of the minerals ensure that clinopyroxene and amphibole are more likely to be effective than the modally greater plagioclase. Probably, a process as envisaged by Cox & Bell (1972) for the New Hebrides lavas was operative. That is, the bulk-rock compositions plotted

across cotectic lines due to the differential settling ability of the phenocrysts.

Another important phase to consider is titaniferous magnetite. That the $Fe_2O_3^*$ - SiO_2 trend (Fig. 5.7) plots above all the silicate phases mentioned, indicates magnetite fractionation has occurred. This is expected, especially as magnetite is often included in clinopyroxene phenocrysts. There is evidence, though, that magnetite was more effective at the evolved end of the trend, as will be shown below. Here, the tendency for TiO_2 to start to decline above about 53 per cent SiO_2 indicates the combined influence of amphibole and magnetite in controlling the variation.

Fig. 5.8 shows the effect of amphibole on composition in the basalt tetrahedron. That amphibole is Ne-normative, has caused various authors to consider it as a useful phase in producing a transition across the critical plane towards normative quartz, (e.g. Cawthorn et al., 1973; Cawthorn & O'Hara, 1976). The rare appearance of amphibole is explained by its tendency to react out as the magma ascends, as discussed in Chapter 4.

Trace elements

Fig. 5.10 shows the trace elements plotted against SiO_2. As observed above, scatter is considerable in the elements Rb, Ba and Sr, and this is mainly due to secondary mobilization. Cu, too, is variable and this may be due to the development of secondary sulphides.

As might be expected, Ni and Cr decrease with increased SiO_2, whereas Zr, Nb and Y tend to increase.

In the earlier discussion it was shown that the basic end of the trend is controlled predominantly by clinopyroxene and olivine. This fact is particularly evident in Fig. 5.11, a Ni-Cr logarithmic

Figure 5.10

Harker diagrams for the trace elements of the Rossland volcanic rocks (Crosses = pyroxenites).

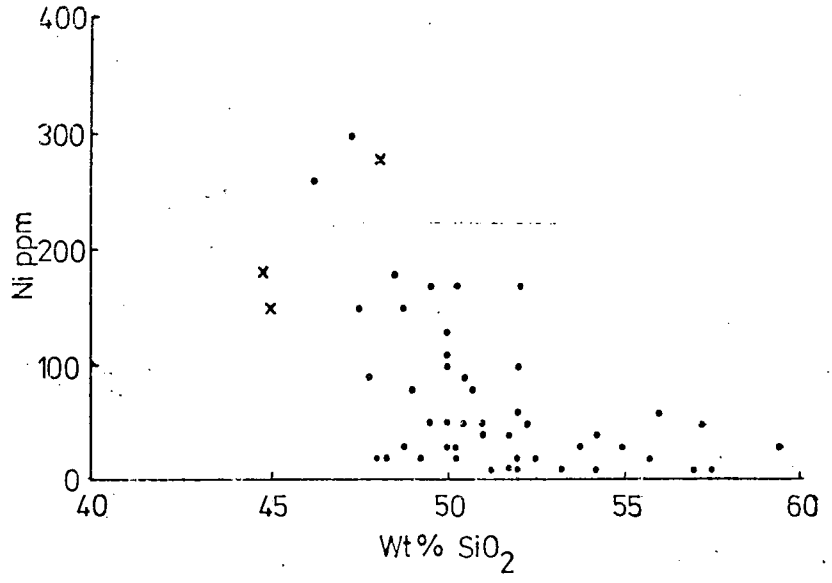
400
300
200
100
0
Ni ppm
40
45
50
55
60
Wt% SiO2

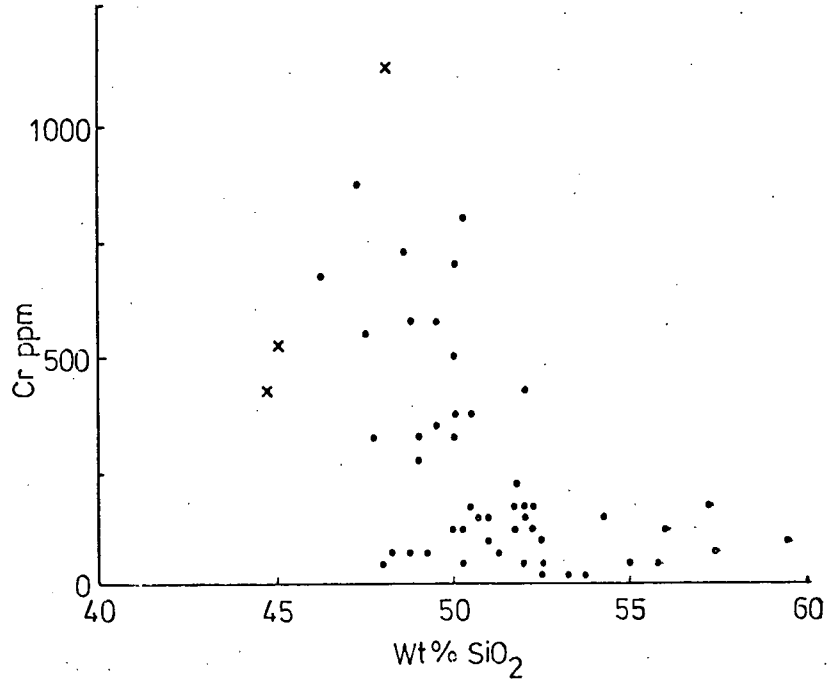
1000
500
0
Cr ppm
40
45
50
55
60
Wt% SiO2

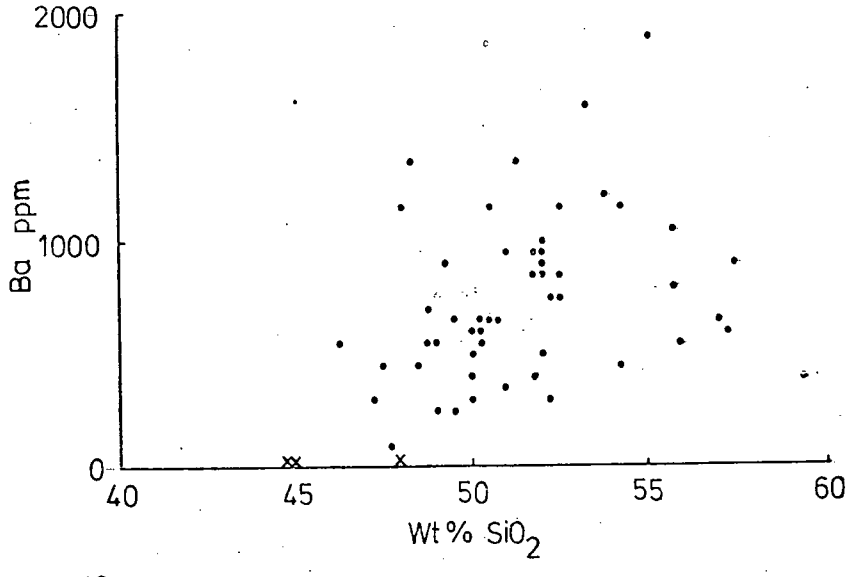
2000
1000
0
Ba ppm
40
45
50
55
60
Wt% SiO2

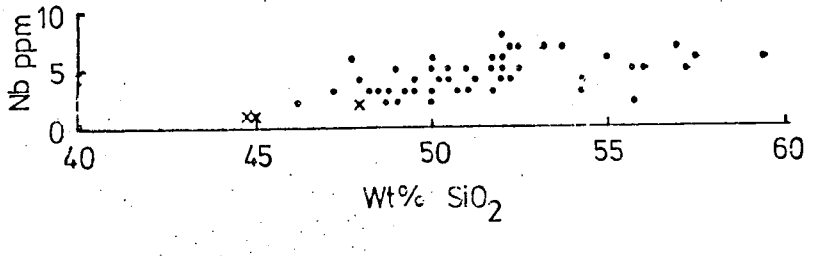
10
5
0
Nb ppm
40
45
50
55
60
Wt% SiO2

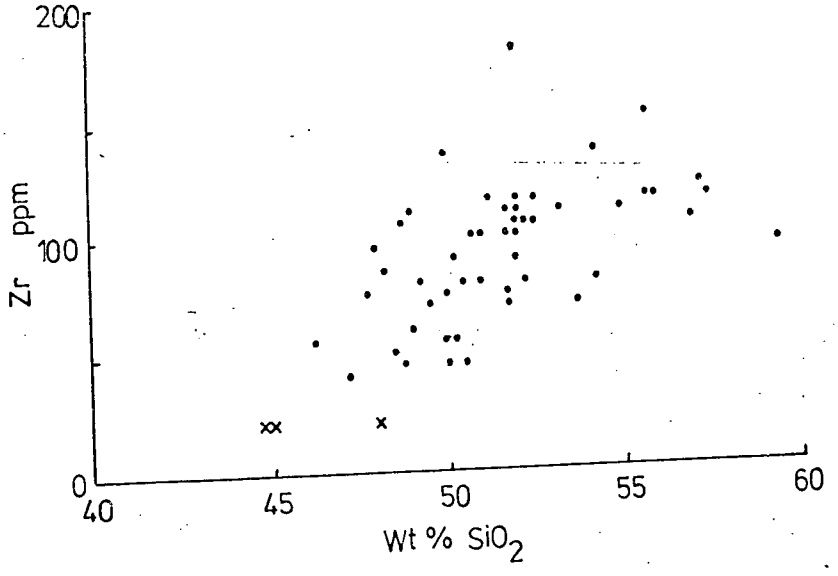
200
100
0
Zr ppm
40
45
50
55
60
Wt % SiO2

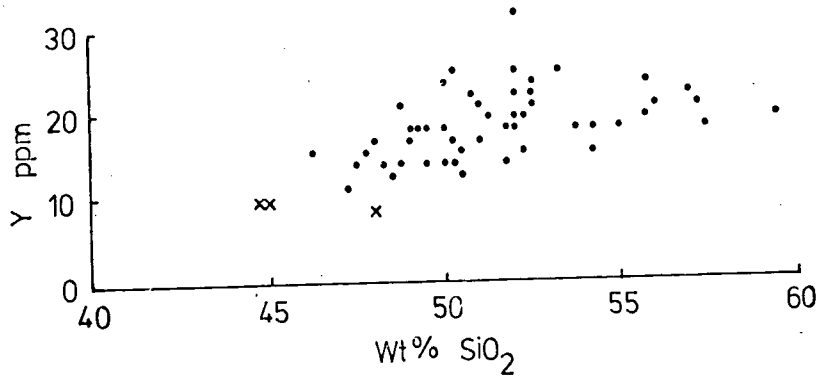
30
20
10
0
Y ppm
40
45
50
55
60
Wt % SiO2

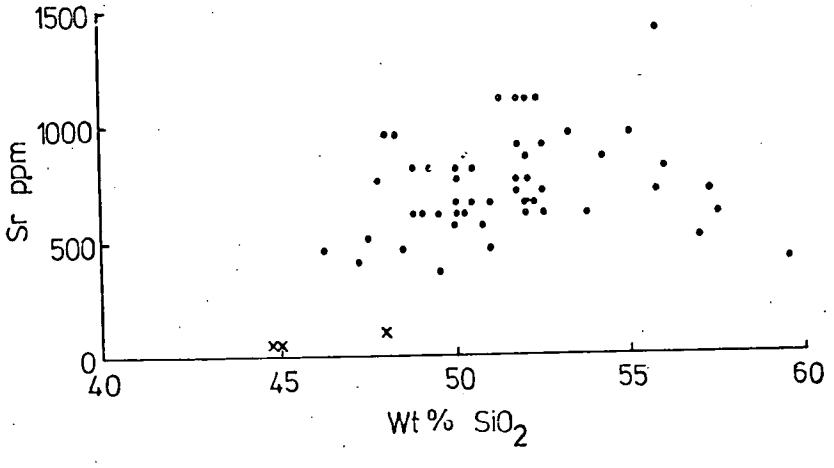
1500
1000
500
0
Sr ppm
40
45
50
55
60
Wt % SiO2

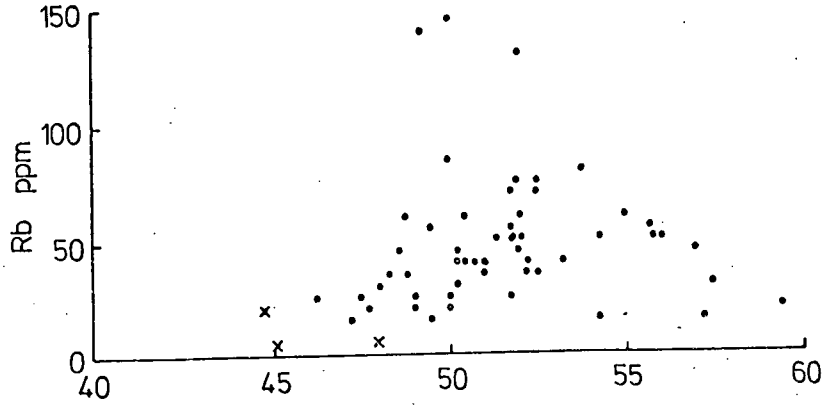
150
100
50
0
Rb ppm
40
45
50
55
60

Figure 5.11

Ni versus Cr logarithmic plot. Arrows indicate approximate fractionation paths for a liquid controlled by either olivine or clinopyroxene (see text for further discussion).

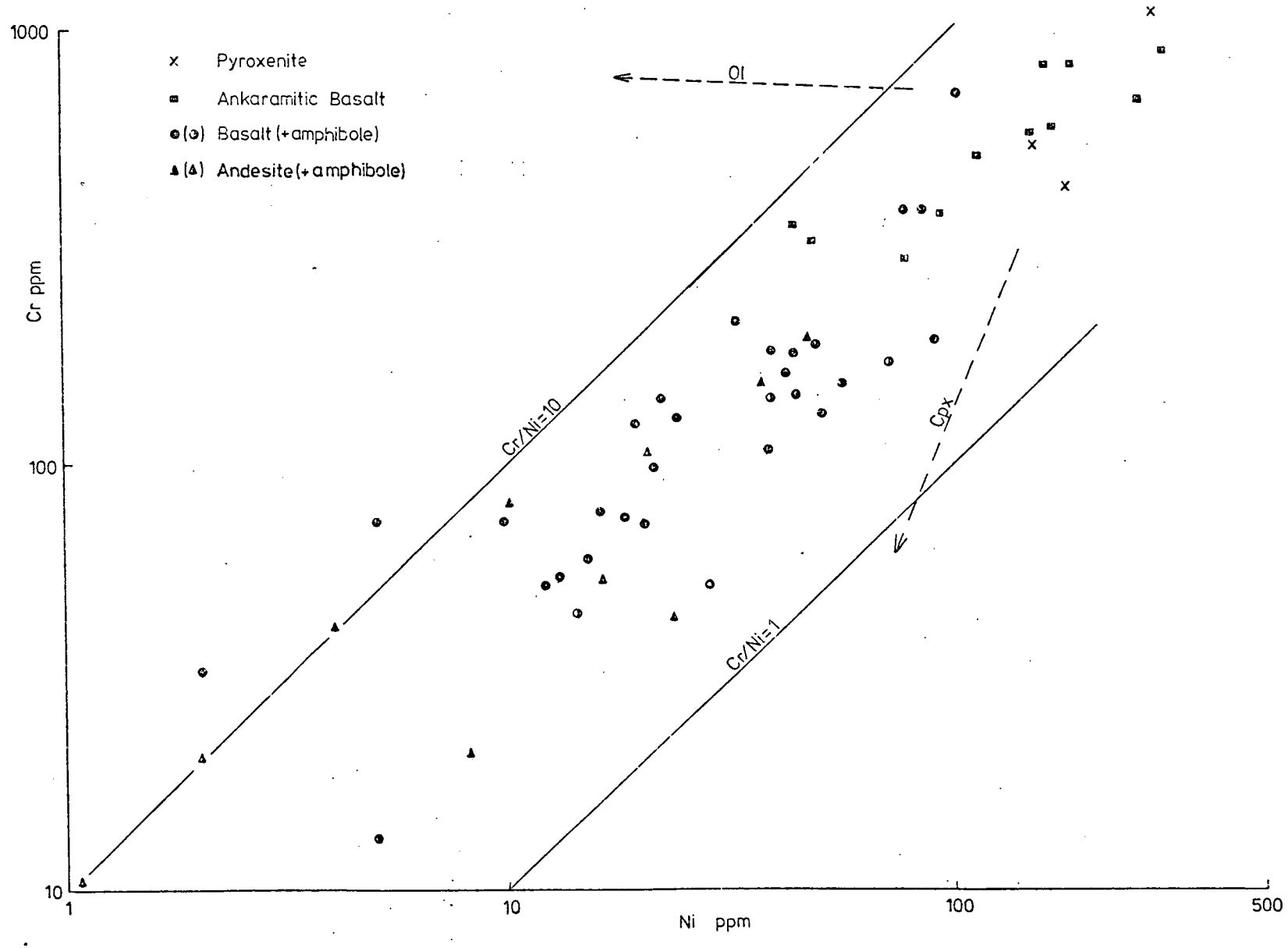
1000
100
10
Cr ppm
1
10
100
500
Ni ppm
× Pyroxenite
Ankaramitic Basalt
Basalt (+amphibole)
Andesite (+amphibole)
Ol
Cpx
Cr/Ni=10
Cr/Ni=1

plot. In this plot, trace element trends governed by a Rayleigh-type process, or an incremental fractionation process, tend to plot on a straight line. On Fig. 5.11 are shown olivine and clinopyroxene control lines based, generally, on published partition coefficient data (e.g. Flower, 1973; Henderson & Dale, 1970). Olivine itself does not readily take Cr^{3+} into its structure, though common inclusions of Cr-spinel within olivine allows it to subtract Cr from the liquid. Pyroxenes tend to incorporate both Ni and Cr preferentially, compared to the silicate melt, but strongly favour Cr. The generally constant value for Ni/Cr for the suite, as shown in Fig. 5.11, therefore indicates a degree of olivine as well as pyroxene fractionation.

The behaviour of Y is interesting in that it tends to partition into amphibole to an extent equal to, or greater than the melt (Lambert & Holland, 1974), unlike other silicate phases (except garnet) in which Y behaves incompatibly. It can be seen in Fig. 5.10 that the trend for Y tends to flatten above 53 per cent SiO_2, indicating that it is being subtracted, to some extent, from the magmas and most probably by amphibole.

V is a useful element in elucidating magnetite behaviour (cf. Taylor et al., 1969b) since it readily substitutes for Fe^{3+}. V, as is evident from Table 5.3, shows a strong correlation with Fe and Mn. Correlation of V with SiO_2, like Fe-Si, is negative, indicating magnetite fractionation. When V is plotted against MgO, however, a clearer pattern emerges (Fig. 5.12). This plot shows that at the ankaramite end of the trend V increases as MgO decreases. This does not preclude magnetite fractionation but indicates the amount of clinopyroxene and olivine was sufficient to cause a net increase; partition coefficients for these minerals relative to melt for V are less than 1. The change to V depletion with MgO decrease is

Figure 5.12

MgO versus V diagram (Symbols as in Fig.5.10).

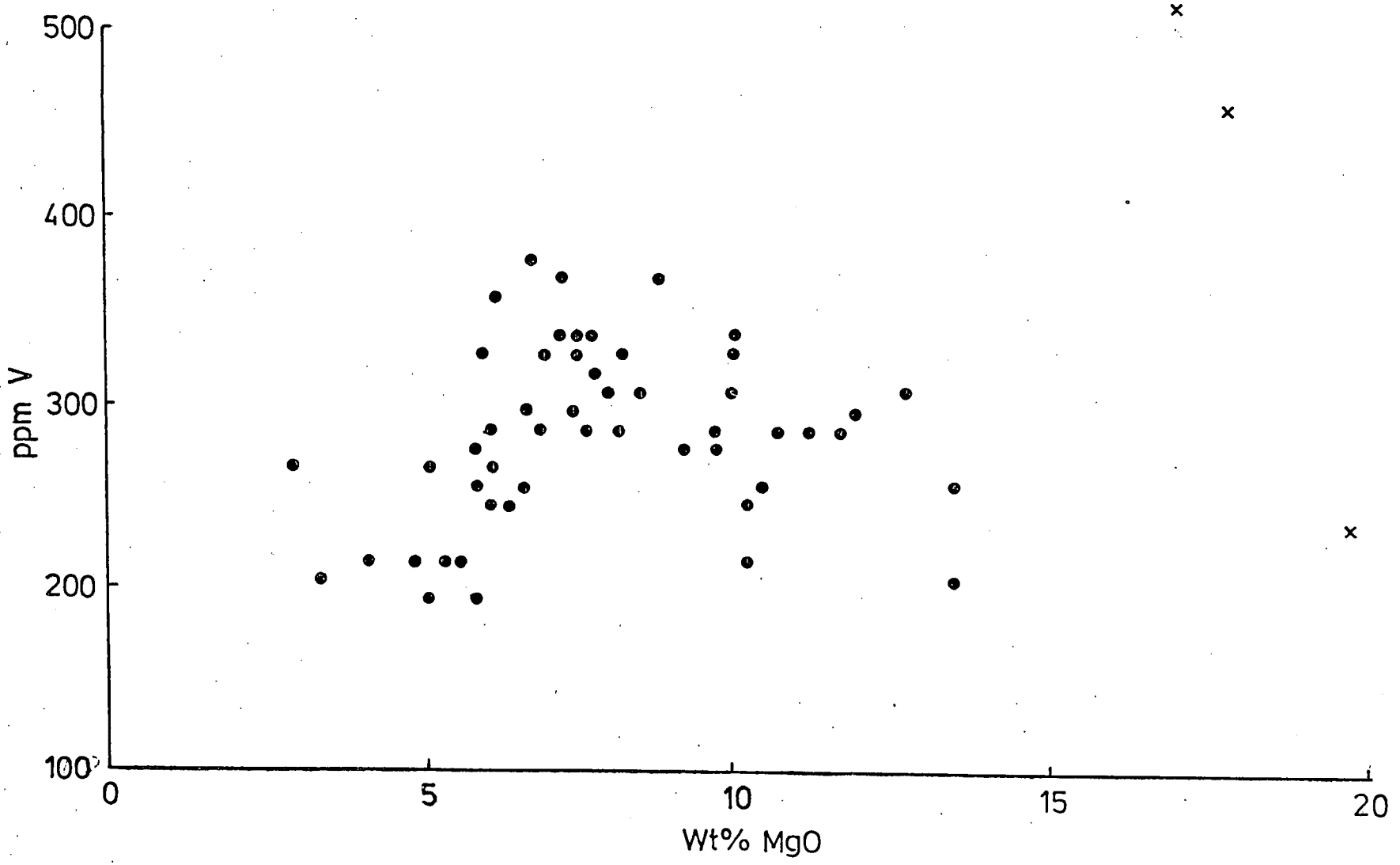
500
400
300
200
100
ppm V
0
5
10
15
20
Wt% MgO

probably due to the cessation of olivine fractionation, and the fact that magnetite becomes relatively more important. Also, the incoming of amphibole, in which significant Fe^{3+} is incorporated, may aid the decline in V.

Despite the fact that the overall trends are explicable by crystal fractionation of the observed phenocrysts, it is also evident that a number of different liquid lines of descent, and/or partial-melt variations, have been sampled. The latter effect is shown to be operative in the Grenadan Suite (Arculus, 1973), since for relatively restricted major element compositions, various incompatible or compatible trace elements can vary widely. A similar example is given by Baxter (1976) for an ocean-island suite of lavas. In these rocks a partial melt sequence is particularly well preserved, incompatible elements showing sharp enrichments with very slight increases of MgO.

That these types of chemical variation exist is to be expected then, and in the Rossland suite it is likely that a similar range of partial melts are represented, together with their respective low-pressure crystallization trends. For example, samples 5104 and 5108 (Table 5.10) have basaltic compositions in terms of major elements, but have low Ni and Cr concentrations and high K, Rb and Ba contents. Thus, compared to samples 5013 and 5055 (Table 5.10) for example, 5104 and 5108 possibly represent a lower degree of partial melting.

Differences are also apparent in the andesitic varieties. In Figs. 5.7 and 5.10 a few samples plot with anomalously low K_2O and Rb contents, lying below the main trend. These samples have possibly suffered K_2O and Rb loss due to alteration, but there is no evidence in thin-section that these samples are any more or less

TABLE 5.10

TABLE SHOWING THE RANGE IN TRACE ELEMENT CONCENTRATIONS (PARTICULARLY Ni and Cr) IN THE ROSSLAND BASALTS (SEE TEXT FOR DISCUSSION (p. 164)

Wt.%	5104	5108	5013	5055
SiO_2	51.78	53.22	51.79	51.77
TiO_2	0.99	1.11	0.91	0.85
Al_2O_3	13.62	15.30	15.16	14.16
Fe_2O_3*	11.60	9.14	10.43	11.64
MnO	0.21	0.11	0.13	0.19
MgO	5.98	7.24	5.75	7.90
CaO	8.80	7.05	10.47	7.43
Na_2O	2.21	3.87	2.87	2.78
H_2O	4.38	2.42	2.21	2.91
P_2O_5	0.43	0.54	0.28	0.37
ppm.				
Cu	56	94	114	69
Ni	5	2	56	90
Cr	73	33	152	194
Ba	950	1619	971	897
Nb	5	7	4	4
Zr	120	111	115	104
Y	24	24	21	19
Sr	1123	995	694	869
Rb	131	40	51	63
Zn	102	37	94	109
Ce	26	13	20	14
La	17	11	16	10
V	321	368	272	306

altered than any of the others. Thus, they either represent different partial melt episodes, possibly due to anomalously high H_2O pressure (cf. Kushiro, 1972; Nicholls, 1974), or derivation from basaltic compositions already depleted in K and Rb.

In summary, it is proposed that the broad chemical trend of the Rossland suite can be ascribed to the fractionation of observed phases in crustal reservoirs. Significantly, a role is assigned to amphibole which, on the basis of the discussion in Chapter 4, limits P_{H_2O} to less than 2 Kb. (2-3 wt.per cent H_2O) and total P to less than 10 Kb., the upper stability of plagioclase. In addition, it is apparent that several crystal fractionation trends exist, controlled by similar mineral phases and originating in parent melts of different composition due to varying degrees of partial melting.

5:5:2 Origin of the Rossland magmas

The origin of various island arc, and particularly andesitic magmas has been a major problem of petrogenesis, and the last ten years, particularly, have seen a considerable debate conducted. It is now generally agreed that these magmas, though possibly affected by continental crust where this is present, originate either in the mantle wedge overlying the subduction zone or in the subducted slab itself. Alternatively, as Ringwood (1974) proposes, a two-stage process is operative, the subducted slab contributing H_2O and, at greater depth, silicic melts to the overlying mantle which then partially melts. A question also surrounds the problem of whether andesitic melts are primary magmas or whether they are lower pressure fractionation products of basalt. The former view is held by, for example, Marsh & Carmichael (1974) and Kushiro (1972). Cawthorn & O'Hara (1976), on the other hand, see andesite as derived from

basalt, primarily by amphibole fractionation. They also question the probability of deriving andesite directly from either the mantle or subduction zone, unmodified.

Whether or not andesite is a primary magma, basalt, to varying degrees, is invariably associated with andesite (cf. Miyashiro, 1974) and this, too, has to be explained. To derive a basalt from the subducted slab requires, by definition, almost 100 per cent partial melting. If this is so, then it is often very hard to match the composition of island-arc basalts with the olivine-tholeiite source, especially with regard to immobile trace elements (Brown et al., 1977; Gill, 1974).

When alkalic or picritic basalts are involved, as in Grenada (Arculus, 1976), the difficulties referred to above become impossible (Arculus, 1973) and an upper mantle origin must be postulated. Since andesites within a province are, typically, compositionally gradational with associated basalts, for example in Japan (Kuno, 1966), it seems reasonable to suppose they too are mantle derived, either representing a different degree of partial melt, or a differentiation product. This idea is generally substantiated by the Rossland suite, as will be shown, which although not a typical andesitic, calc-alkaline association, is an island-arc suite.

With regard to the ankaramitic/basaltic end of the spectrum it is clear, by the same reasoning as that mentioned above, that these compositions cannot be derived by any degree of partial melting of an ocean-floor basalt. The SiO_2 content of the most basic Rossland rocks is similar to an average ocean-floor basalt, (cf. Engel & Engel, 1964) but MgO is generally higher. More importantly, Ti, Zr, Y and Nb levels in the Rossland ankaramatic basalts do not resemble ocean-floor averages (cf. Figs. 5.3, 5.4).

That TiO_2 in the Rossland basalts is lower than in the ocean-floor basalts requires this element to be refractory up to 100 per cent melting, which is most unlikely.

Thus, it is necessary to consider an upper mantle origin for the suite. A commonly used test of whether a liquid (or basalt) is in equilibrium with an olivine (or mantle), is to apply the data of Roedder & Emslie (1970) on liquid-olivine partitioning of Fe and Mg:

$$K_D = (Fe/Mg)_{ol} \times (Mg/Fe)_{Liq} = 0.3 .$$

On the assumption that upper mantle olivines have a Mg-number of $\sim$ 91 (Mysen, 1975), the corresponding Mg-number of the equilibrated liquid is 78. The most basic ankaramitic basalts show Mg-numbers of less than 68. Only one sample, 4119, which is exceptionally basic (MgO = 21 per cent, Ni = 830 ppm) has a Mg-number of 78. Unfortunately, this sample is highly altered. Thus, it would appear that nearly all of the sampled basalts and ankaramitic basalts are not unmodified partial melts from the upper mantle. Other data on K_D (defined above) reported by Nicholls & Lorenz (1973) and determined at pressures of 2-10Kb, and under hydrous conditions, give an average of 0.4. This renders the Rossland magmas even less likely to be unmodified partial melts. Although Mysen & Boettcher (1975) and Mysen (1975) have shown low Mg/Fe ratio liquids can coexist with mantle material under high f_{O_2} this requires, for the Rossland samples, Fe^{3+}/Fe^{2+} ratios of greater than 1, which is unlikely. Also, it is unlikely that f_{O_2} was above NNO during the evolution of the suite, and thus well below the f_{O_2} required by the data of Mysen (1975) for equilibrium liquids to have Mg-numbers of 65.

The conclusion reached, therefore, is that whilst the basic

Rossland rocks are mantle derived, they were not erupted unmodified. With reference to Fig. 5.13 a scheme is suggested that can explain, in terms of major oxides at least, the early petrogenesis of the suite.

Fig. 5.13 shows a number of representative basalts and ankaramitic basalts plotted in two projections within the system C-M-A-S (O'Hara, 1968). Also shown are the anhydrous phase boundaries for various pressures, taken from O'Hara (1968). The samples, in general, plot slightly to the undersaturated side of the critical plane, and in both diagrams show a very broad olivine-controlled trend. Fig. 5.13 shows, in addition, the scatter of the ankaramites, representing lower pressure accumulation or fractionation of clinopyroxene. It is evident that the samples show no simple relation to any of the five-phase invariant points, nor, as the above discussion implies, would they be expected to as they represent non-equilibrium magmas. It is envisaged that at, say, 30Kb a series of partial melts originate (a to b in Fig. 5.13) that subsequently become decoupled from the surrounding mantle. On ascent these partial melts fractionate olivine; a process, as emphasized by O'Hara (1968), that is very likely due to the rapid expansion of the olivine primary phase volume with decreasing pressure. Thus, the area compositionally represented by a to b (Fig. 5.13) would, by olivine subtraction, lead to compositions similar to the Rossland samples. At crustal levels, say 2-5Kb, the magmas would enter reservoirs and re-equilibrate, precipitating clinopyroxene and plagioclase.

It is also interesting that the partial melts represented by a-b (Fig. 5.13) are in equilibrium with garnet and would therefore have LREE enriched patterns. On average, the Rossland basalts show LREE enriched patterns. This can be seen by considering the

Figure 5.13

Projections in the C-M-A-S system of O'Hara (1968).

(A) Projection from MS (enstatite) onto the plane A_2S_3-C_2S_3-M_2S.

(B) Projection from CMS_2 (diopside) onto the plane C_3A-S-M.

Phase boundaries at various pressures are for anydrous magmas (taken from O'Hara, 1968). a-b represents possible range of partial melts parental to the Rossland volcanics (squares - ankaramites; circles - basalts).

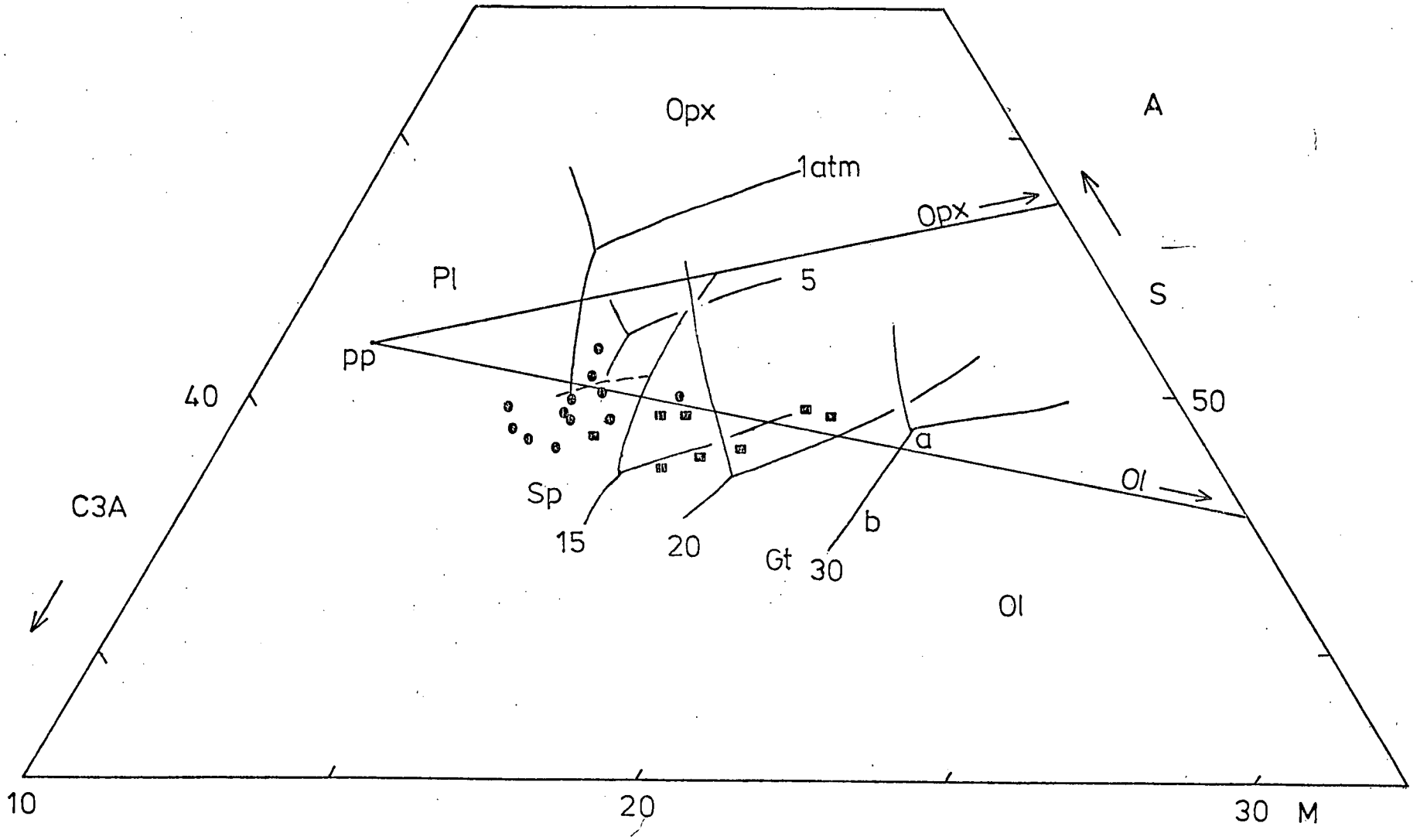
Opx
A
1atm
Opx
Pl
5
S
pp
40
50
a
Ol
C3A
Sp
15
20
Gt
30
b
Ol
10
20
30
M

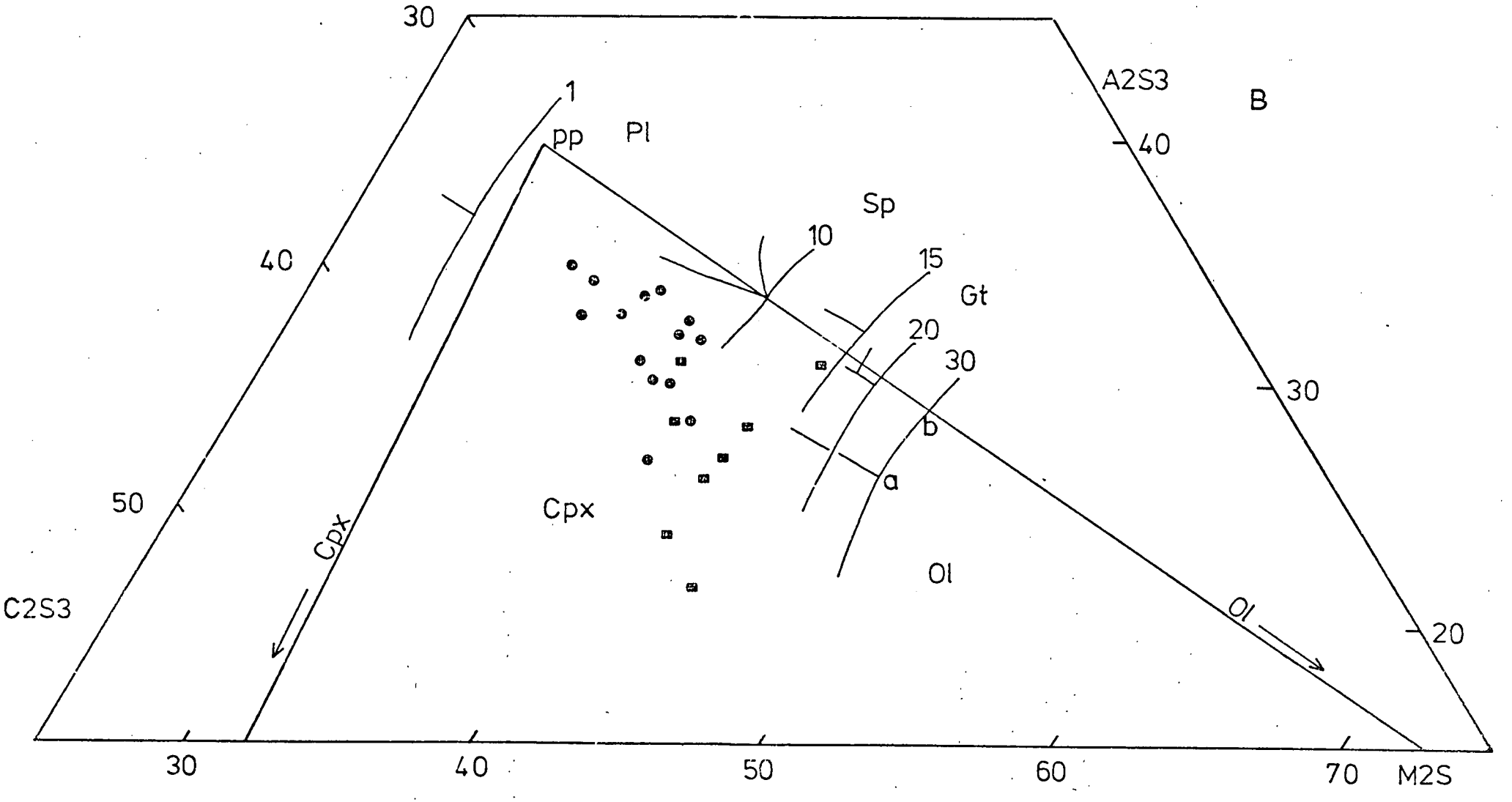
30
1
PP
Pl
A2S3
B
40
Sp
10
15
Gt
40
20
30
30
b
50
a
Cpx
Cpx
Ol
C2S3
Ol
20
30
40
50
60
70
M2S

elements La, Ce and Y, the latter behaving very similarly to the HREE (Taylor, 1965). If the average values for these elements, taken from Table 5.2, are normalised to chondrite the LREE are enriched twenty times whereas the HREE only nine times.

So far, only anhydrous conditions have been considered, as indicated by Fig. 5.13, whilst, as shown in Chapter 4, hydrous conditions were operative. However, it was suggested in Chapter 4 that at crustal levels, when amphibole was precipitating with pyroxene and plagioclase, P_{H_2O} was less than $0.5P_{tot}$. At the greater depths of partial melting and prior to any great extent of anhydrous-phase fractionation, which would increase H_2O in the melt, P_{H_2O} was even less effective. Also, under saturated H_2O conditions, contraction of the primary phase volume of olivine is severely retarded with pressure, allowing siliceous liquids to develop as partial melts (Nicholls, 1974; Nicholls and Ringwood, 1973; Mysen & Boettcher, 1975b): Such conditions are not apparent in the Rossland case. As Green (1973) and Mysen & Boettcher (1975b) show, undersaturation with respect to H_2O, due either to low H_2O contents or high activities of CO_2, restores the trend of partial melt composition, with depth, towards SiO_2 undersaturation. In fact, the role of CO_2 is only recently becoming understood and it may play as significant a role as H_2O in determining mantle-melt petrogenesis (Mysen et al., 1976). Possibly, the presence of carbonates in the oceanic crust (e.g. Scarfe & Smith, 1977) is effective in introducing CO_2 into an island-arc regime, analagous to amphibole and serpentine with respect to H_2O.

To return to the model outlined, the broad chemical consequences of such a process can be inferred by comparison with the Baffin Bay basalts (Clarke, 1970). Here, a well controlled

(olivine) group of basalts and picrites show that partial melting at about 30 kb produces a hypersthene-normative picritic liquid (Table 5.11, A), which by polybaric olivine fractionation leads to a basalt composition indicated by analysis B (Table 5.11). Subsequently, such a basalt in Baffin Bay fractionates at low pressure to other, more evolved basalts characterised by enrichment in TiO_2 and Zr. Comparison of analysis B with 2, a Rossland ankaramitic basalt (Table 5.11) shows a considerable similarity. Particularly, MgO/CaO ratios are near 1, Mg-numbers are both near 65, and TiO_2, Zr and Y levels are low. The maintenance of low TiO_2 and Y levels in the Rossland area at more evolved compositions, in contrast to the Baffin Bay case, probably reflects the more hydrous and oxidising conditions whereby amphibole and magnetite are more easily stabilised. At high pressure though, the analogy is useful. Also tabulated in Table 5.13 is the sample 4119, referred to above. Although highly altered, it is comparable in many respects to analysis A (Table 5.13), believed by Clarke(1970) to represent a nearly unmodified partial melt from about 30 kb.

Whilst the analogy with Baffin Bay holds generally for the major elements, when the elements K, Rb, Ba and Sr are considered it does not. A feature of island-arc magmatism, as seen in the data of Jakeš & White (1972b), is the ability for these elements to vary considerably, whilst the incompatible, highly-charged cations (Zr, Nb, Ti) vary comparatively little. This suggests that a constraint is placed on the primary partial melt composition at its source such that island arc magmas, when erupted, are distinguishable by these trace elements from ocean-floor or ocean-island basalts, for example. The reasons for these initial constraints could be due to either mineralogical or chemical heterogeneity in the mantle, or both.

TABLE 5.11

COMPARATIVE DATA FOR BAFFIN BAY BASALTS AND PICRITES AND SELECTED ROSSLAND SAMPLES (SEE TEXT FOR DISCUSSION p.172)

Wt.%	A	B	1	2
SiO_2	45.1	47.5	45.39	48.54
TiO_2	0.76	0.97	0.70	0.79
Al_2O_3	10.8	13.8	10.08	11.08
$Fe_2O_3^*$	10.26	9.67	11.84	10.67
MnO	0.18	0.17	0.18	0.21
MgO	19.7	11.8	21.86	11.64
CaO	9.2	11.7	8.95	10.67
Na_2O	1.04	1.53	0.42	2.19
K_2O	0.08	0.10	0.46	1.60
P_2O_5	0.09	0.10	0.20	0.30
Total	97.21	97.34	100.00	100.00
ppm				
Ni	943	314	828	147
Cr	1847	889	1820	577
Ba	55	56	153	577
Rb	2	2	13	38
Sr	186	161	135	608
Y	18	21	14	14
Zr	52	66	48	48
Mg-number	78	68	78	66

A Group II average, Baffin Island (Clarke, 1970)

B Group III " " " " "

1 'Picrite' 4119, Rossland volcanics

2 Ankaramitic basalt, 55388, Rossland volcanics

In island-arc environments the presence of H_2O, particularly, is considered important in producing hydrous phases in the source region. Jakeš & White (1970, 1972b) consider that variations in the elements K, Rb and Ba could be due to the relative stabilities of phlogopite and amphibole. As the experimental work of Forbes & Flower (1974) and Modreski & Boettcher (1972) show, phlogopite, particularly if Ti-rich, is stable to higher temperatures and pressures than amphibole. Magmas produced when amphibole, but not phlogopite, breaks down will be generally poor in incompatible elements such as K, Rb and Ba, these being strongly retained in phlogopite. At greater depths (greater than 25 Kb), amphibole is not stable and if there is no excess vapour, melting will start when phlogopite breaks down, and the first melt will be rich in incompatibles. Flower (1971) regards the differences in ocean-island basalt types to be related in this way to Ti-phlogopite control.

In order to stabilize phlogopite, however, K_2O in reasonable abundance is necessary, in addition to H_2O. This effect is shown in the experimental work of Mysen & Boettcher (1975a), where normal lherzolites with K_2O of less than 0.04 wt. per cent do not stabilize phlogopite, all K_2O going into amphibole. Thus, in addition to mineralogical differences within the mantle, if phlogopite is present, chemical differences must exist. Arculus & Curran (1972) make the point that in order to explain variations of magma type, especially in island arcs, source heterogeneity is likely as a result of the previous history of the source block of mantle. For example, lithospheric mantle near a continental margin may be enriched in certain elements due to exchange between crust and mantle. If a mantle affected in this way becomes a source for island-arc magmas, it would be expected that the magmas produced would be generally enriched in incompatibles

such as K, Rb, Ba and Sr, but otherwise normally basaltic and primitive with regard to Ni and Cr. Another possible source for these large-ion lithophile elements is the subduction zone. As Ringwood (1974) suggests, at 100 to 180 Km in the subduction zone, temperatures are high enough to promote partial melting of the slab to produce silicic magmas and to release H_2O from serpentine. If these products, over time, react with the overlying mantle they may enrich it in incompatible elements. Incompatibles such as K, Rb, Ba and Sr could be enriched in the mantle purely due to the percolation upwards of H_2O solutions, which is as suggested by Best (1975), Miyashiro (1974) and James et al. (1976) for other calc-alkalic suites.

In summary then, it is envisaged that the Rossland magmas evolved firstly by partial melting of enriched (K, Rb, Ba and Sr) upper mantle above a subduction zone. Generally, H_2O conditions were quite under-saturated. These initial partial melts rose and fractionated olivine until they entered crustal reservoirs (2-7 Kb). At this stage the basic magmas were rich in potential diopside and would occur as augite-rich ankaramitic basalts. Continued fractionation of olivine with pyroxene (and magnetite) then leads to the production of the normal basaltic varieties. A build-up of H_2O pressure and f_{O_2} by this stage also permitted the early appearance and fractionation of amphibole and Ti-magnetite, which produced the andesitic varieties. The lack of highly evolved dacitic or rhyolitic material may be, in part, due to the easy access the magmas had to the surface, possibly along the line of an old suture. (Chapter 9).

5:6 Minor intrusions

The chemistry of the few analysed minor intrusions (i.e. amphibole-bearing dykes, amphibole-free dykes, doleritic intrusions) is illustrated in Figs. 5.14 and 5.15. The fields of the volcanic rocks (cf. Figs. 5.7, 5.10) are shown for comparison. Generally,

Figure 5.14

Harker diagrams for the minor intrusions (major and minor elements). The field of the volcanics is also indicated.

Crosses - Doleritic intrusions
Triangles - Amphibole-free minor intrusions
Dots - Amphibole-bearing minor intrusions
Plus sign - 'Pseudodiorite' (74B).

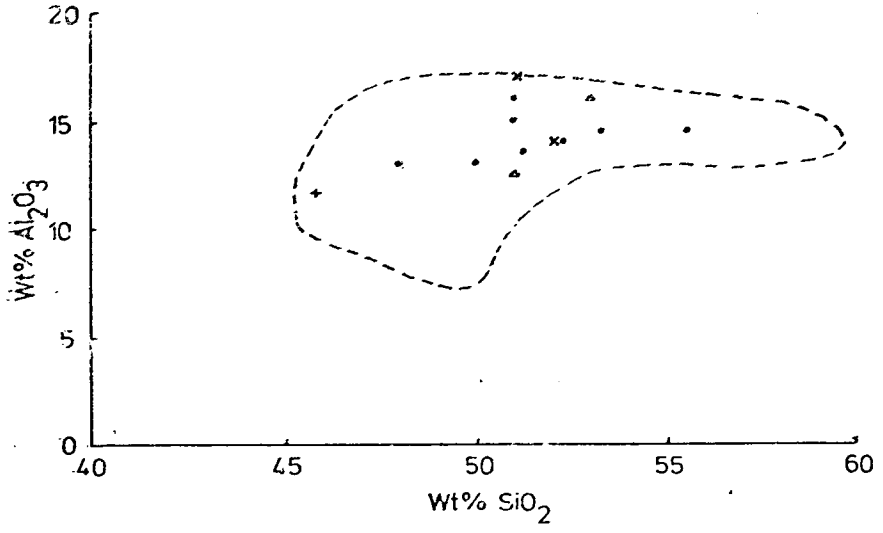
20
15
10
5
0
40
45
50
55
60
Wt% Al_2O_3
Wt% SiO_2

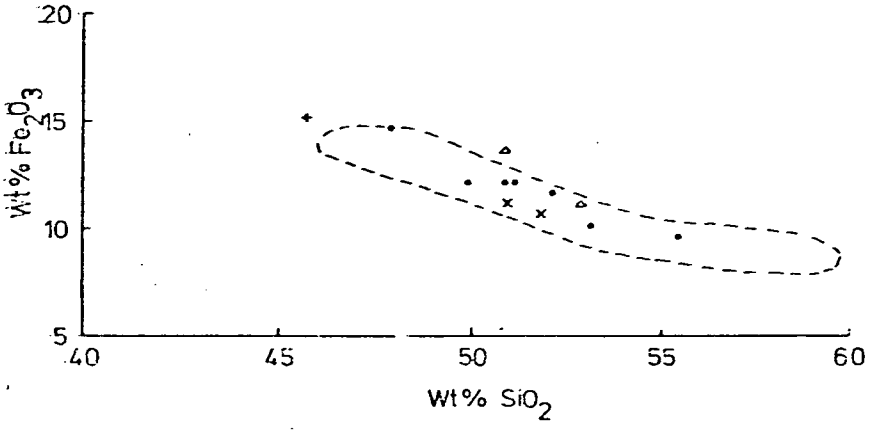
20
15
10
5
40
45
50
55
60
Wt% Fe_2O_3
Wt% SiO_2

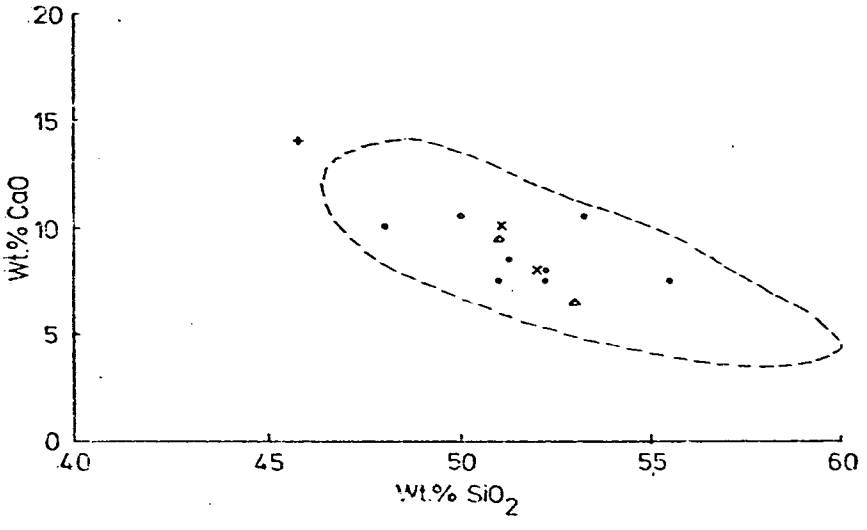
20
15
10
5
0
40
45
50
55
60
Wt.% CaO
Wt.% SiO_2

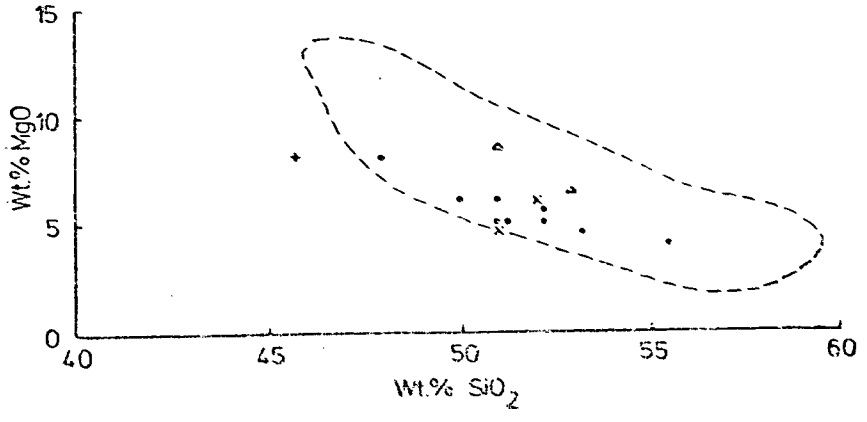
15
10
5
0
40
45
50
55
60
Wt.% MgO
Wt.% SiO_2

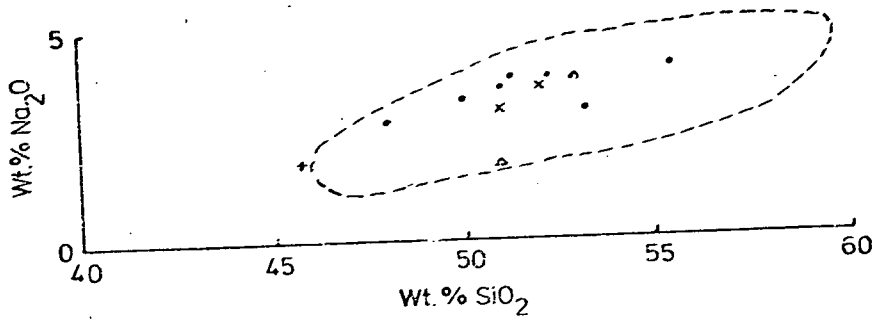
5
0
Wt.% Na_2O
40
45
50
55
60
Wt.% SiO_2

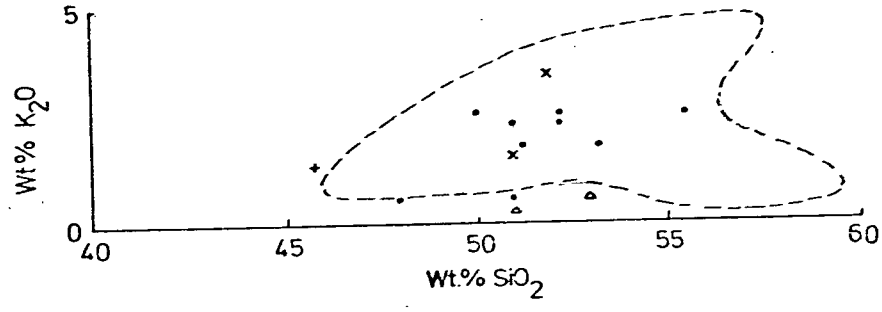
5
0
Wt% K_2O
40
45
50
55
60
Wt.% SiO_2

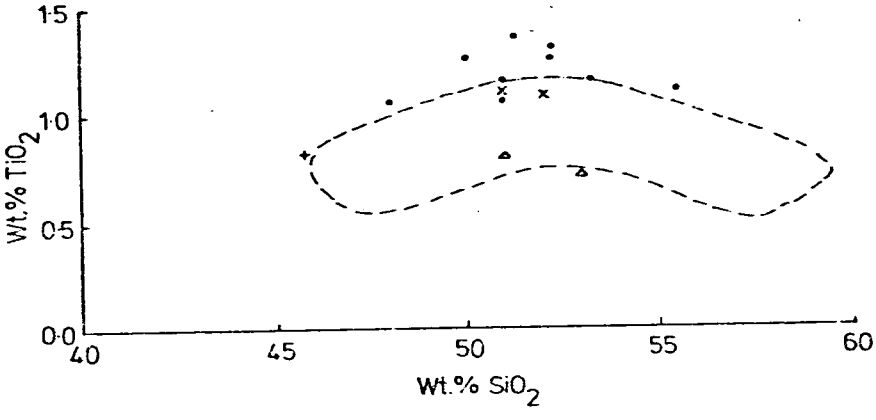
1·5
1·0
0·5
0·0
Wt.% TiO_2
40
45
50
55
60
Wt.% SiO_2

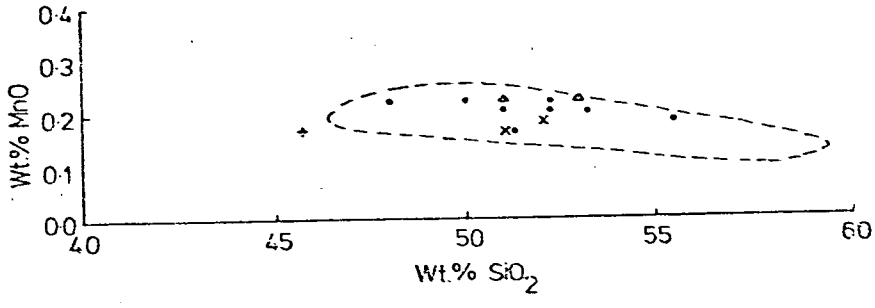
0·4
0·3
0·2
0·1
0·0
Wt% MnO
40
45
50
55
60
Wt.% SiO_2

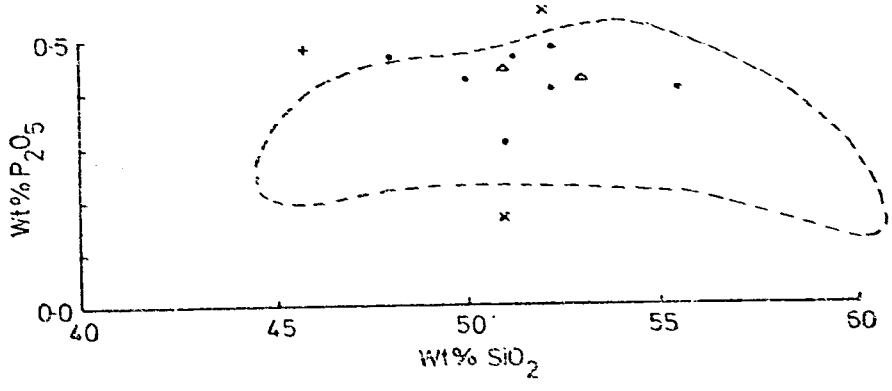
0·5
0·0
Wt% P_2O_5
40
45
50
55
60
Wt% SiO_2

Figure 5.15

Harker diagrams for the minor intrusions (trace elements). The field of the volcanics is also indicated.

Symbols as in Fig. 5.14.

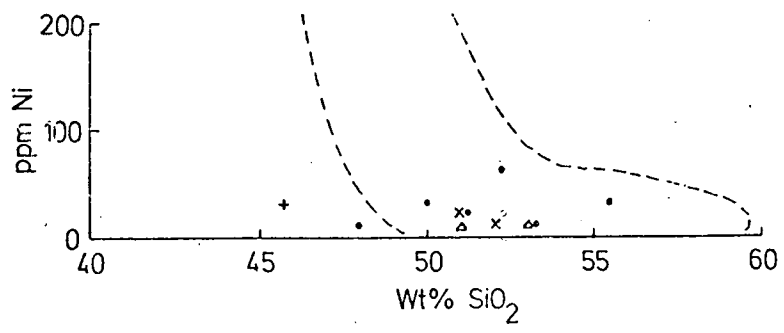
200
100
0
ppm Ni
40
45
50
55
60
Wt% SiO2

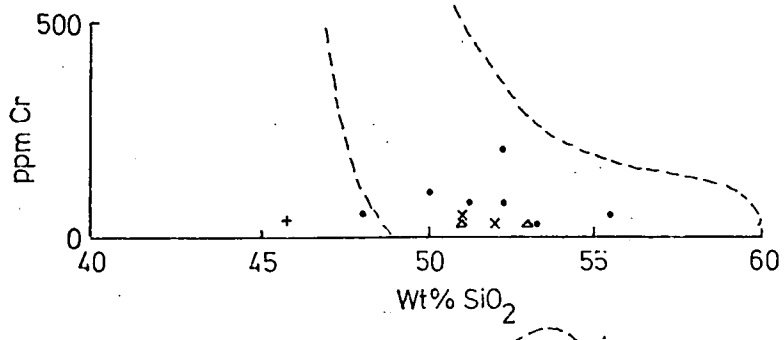
500
0
ppm Cr
40
45
50
55
60
Wt% SiO2

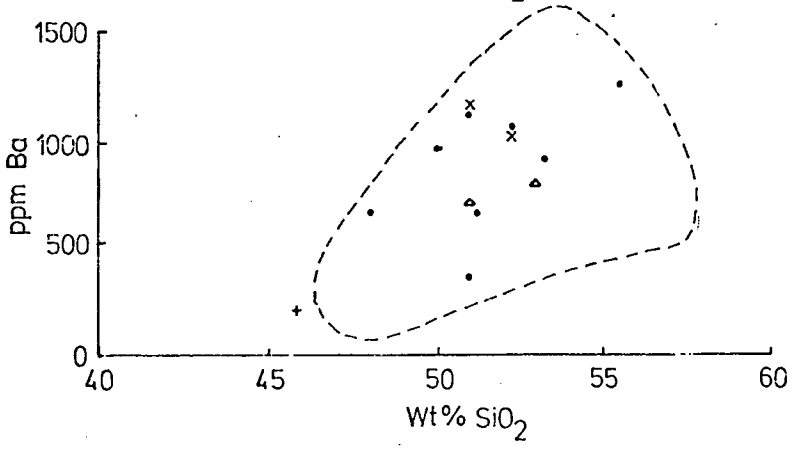
1500
1000
500
0
ppm Ba
40
45
50
55
60
Wt% SiO2

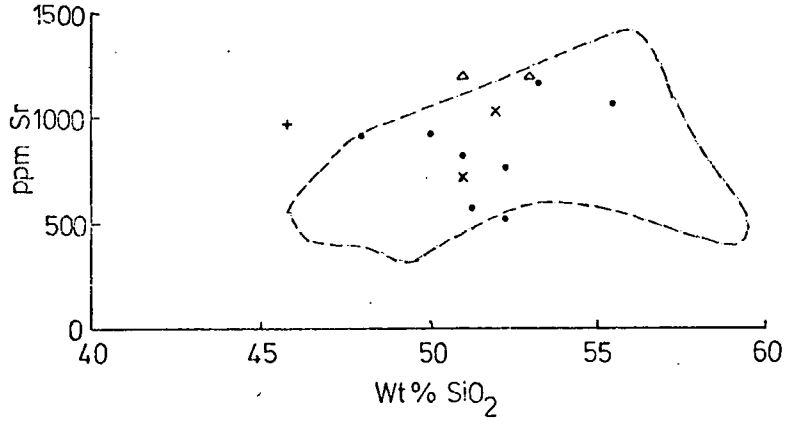
1500
1000
500
0
ppm Sr
40
45
50
55
60
Wt% SiO2

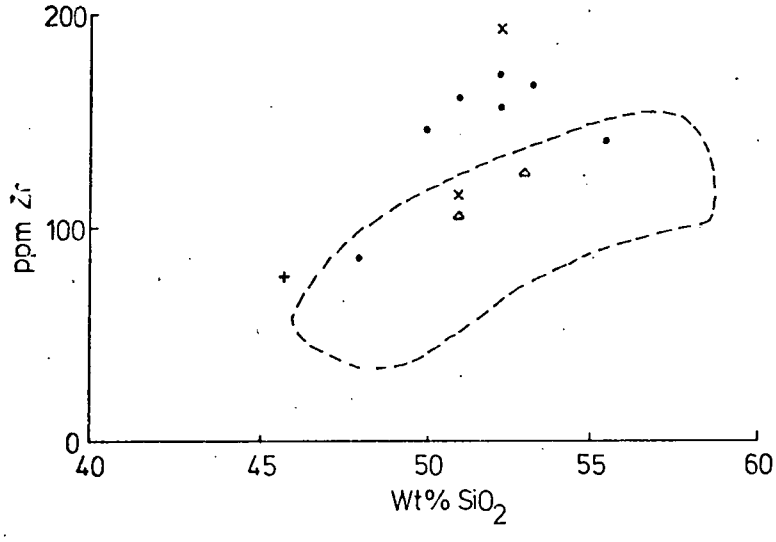
200
100
0
ppm Zr
40
45
50
55
60
Wt% SiO2

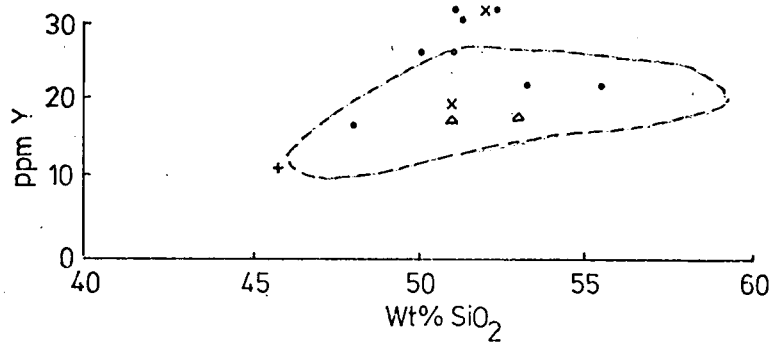
30
20
10
0
ppm Y
40
45
50
55
60
Wt% SiO2

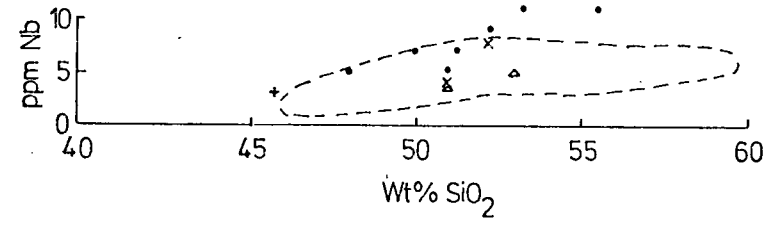
10
5
0
ppm Nb
40
45
50
55
60
Wt% SiO2

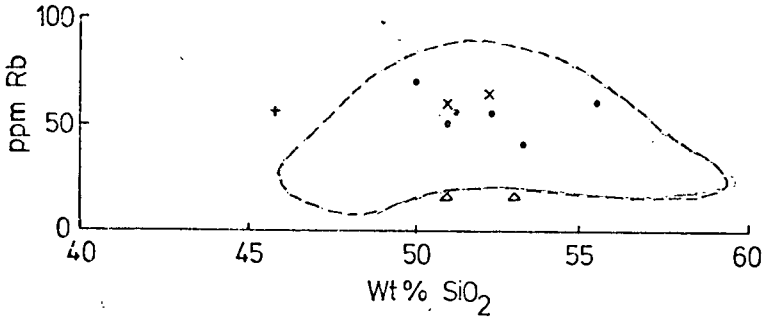
100
50
0
ppm Rb
40
45
50
55
60
Wt % SiO2

it can be seen that the chemistries of the two sets of rocks are similar. However, systematic differences in some elements are evident. Particularly, TiO_2 and Zr are enriched in the amphibole-bearing rocks. Y and Nb are also very marginally higher in the intrusive rocks. The high value of TiO_2 may be explicable if the magmas were enriched in amphibole, which is quite likely in view of their porphyritic nature (cf. Plate 31).

In contrast to the highly charged, incompatible cations (Ti, Zr, Y and Nb) mentioned above, compatible elements such as Ni and Cr are generally very low, indicating higher degrees of differentiation for these rocks. Particularly, the gabbroic sample 74B (pseudodiorite) is, though poor in SiO_2, also poor in Ni, Cr and MgO. This rock is possibly of cumulate origin, representing an aggregate of minerals (olivine, pyroxene and plagioclase) that precipitated from a fairly evolved basalt.

The minor intrusions, generally, are probably slightly later than the volcanics and could represent magmas produced in the waning stages of a thermal event. Thus they would tend to be derived by lower degrees of partial melting.

CHAPTER 6

ROSSLAND VOLCANIC GROUP:

METAMORPHIC PETROGRAPHY AND MINERALOGY

6:1 General textural features

It has been frequently commented upon earlier that the volcanics have been variably altered, both in terms of texture and mineralogy. Thus, before discussing details of mineral occurrence and chemistry, some breakdown of the area is desirable. Most conspicuous is the distribution of biotite and secondary amphibole (Figs. 6.1, 6.6), there apparently being a zone north of Salmo and Eerie Lake where these two minerals are extensively developed. In contrast, in the Mt.Kelly region, further south, these two phases do not occur. In a localised area south of Fruitvale and east of the Columbia River, amphibole and biotite reappear, most probably being related to contact metamorphism by the Coryell batholith. Amphibole and biotite are also developed west of the area shown in Fig.6.1 in the Rossland volcanics mapped by Fyles (in prepn.). As is evident, there is a broad correlation between the occurrence of amphibole and biotite and the proximity, or abundance, of intrusive rocks. Causes of metamorphism, however, are discussed in Chapter 7. Hereafter, the region around Mt. Kelly (amphibole + biotite absent) is termed zone A, and the area to the north of a line west from Salmo (amphibole + biotite present) termed zone B.

Within zone A , alteration has proceeded essentially statically: that is, secondary minerals have overprinted primary igneous textures without substantially altering them. This is evidenced by, for example, Plates 17, 23 and 45, presented in Chapter 4. Mineralogical alteration in zone A is, in addition, only partial;

metamorphic phases including chlorite, calcite, epidote, albite, prehnite and sericite.

In zone B rather more textural variation is present and zone B is further divided as is shown in Fig. 6.1. This subdivision is partly based on sampling but, as will be seen, textural and mineralogical differences are apparent.

Zone B1. In this area the volcanics are characteristically schistose and are locally thoroughly recrystallized. This is shown in Plates 46 and 47, and it is clear that metamorphic textures have substantially replaced igneous. Relict clinopyroxene phenocrysts are still evident as hornblendic aggregates, though these are sometimes drawn out and generally show no euhedral control by pyroxene. The schistose fabric in zone B1 metavolcanics is due to the alignment of chlorite or biotite flakes and hornblende prisms.

Rocks of the Bonnington Complex, though metamorphosed to similar degrees as the metavolcanics, are not schistose, however (e.g. Plates 35 , 36). This could be due to a metamorphic imprint in this area after the development of schistosity in the volcanics, which implies that rocks of the Bonnington complex were emplaced after the volcanics. Alternatively, the metavolcanics were previously bedded and easily developed an aligned metamoprhic fabric, whereas the coarse-grained Bonnington Complex rocks underwent essentially static metamorphism.

Zone B2. Rocks in this area, whilst carrying similar mineral assemblages (Chapter 7) to B1, are texturally very different. Primary magmatic textures are generally much better preserved, though clinopyroxene and plagiocalse phenocrysts are totally replaced by amphibole (actinolite or hornblende) and albite,

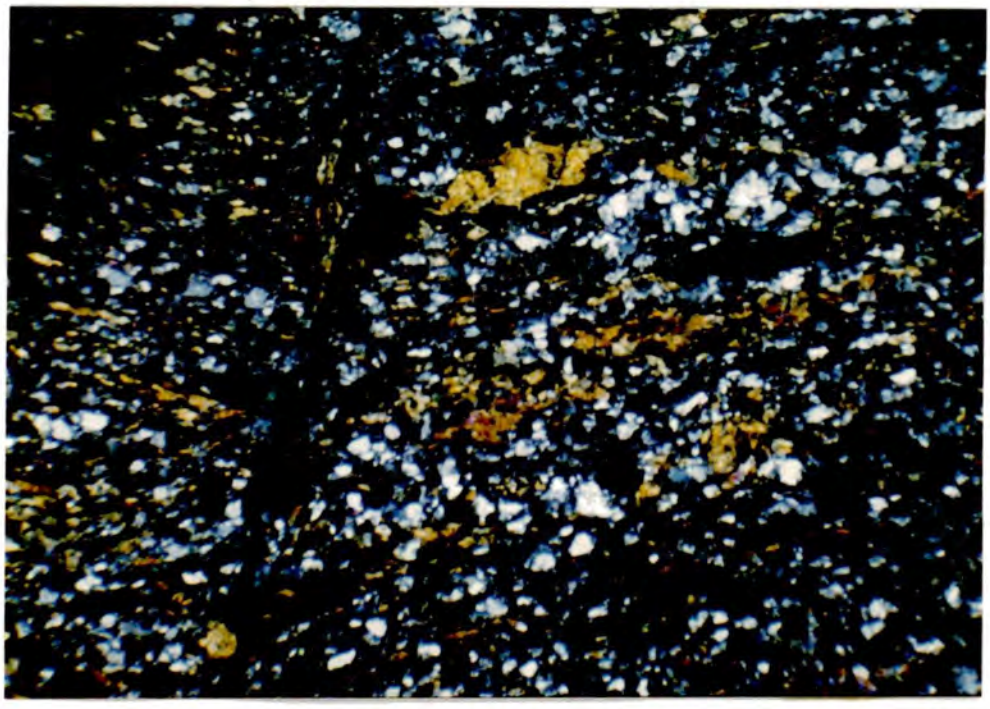

Plate 46

Photomicrograph: Schistose metabasalt from sub-zone B1. Contains aligned biotites and hornblendes with granular plagioclase and minor epidote. Note shear plane cross-cutting the schistosity (Sample 4029A. XP. Field width = 8 mm.).

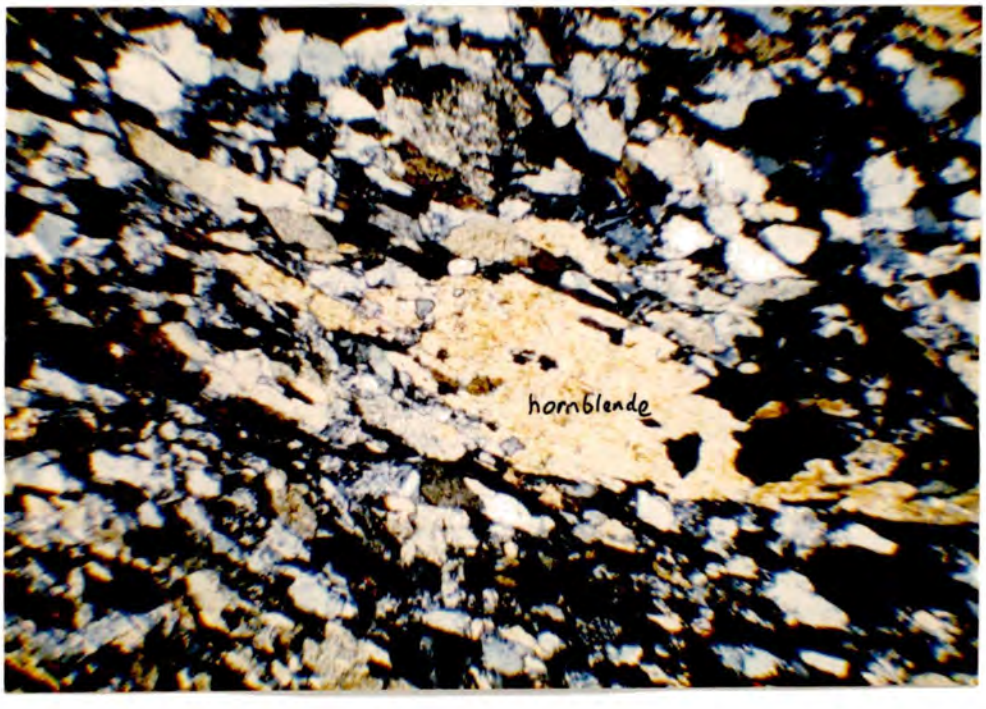

Plate 47

Photomicrograph: Schistose metabasalt from sub-zone B1. Contains aligned chlorite and hornblende, and plagioclase (sericitised in part). Large hornblende (centre) is probably a relict pseudomorph after clinopyroxene. (Sample 4029A. XP. Field width = 4 mm.).

respectively. Amphibole pseudomorphs , as shown in Plate 48, show good control by pyroxene, though occasionally secondary fringes of amphibole grow beyond the original phenocryst. However, these rocks have been quite severely sheared and brittle shattering has occurred, together with the development of a crude schistosity in the groundmass. A noticeable result of this is the development of pressure shadows around phenocrysts (Plates 48 , 49), in which secondary growths (retrograde, in some cases) of actinolite, chlorite, biotite, albite and calcite have developed.

The shearing episode responsible for these textural developments, clearly followed the initial amphibolisation of the volcanics, as is particularly well illustrated by Plate 48 . Here, the amphibole pseudomorph has been split along a cleavage plane and then prised apart. The two segments were originally in optical continuity as indicated by the polarization colours. The resulting pressure shadow, in this example, has been filled by a stringy, curvilinear aggregate of chlorite, which presumably grew synkinematically, and a granular aggregate of albite. In addition, post-kinematic needles of amphibole grew occasionally in chloritic pressure shadows..

Within zone B2 generally, several phases of metamorphic growth probably occurred. The latest phase was possibly the development of calcite, with biotite, chlorite or epidote in veins that cut the crude schistose fabric (e.g. Plate 19). The development of chlorite, biotite and calcite as breakdown products of amphibole (Plates 19 , 50) is, in addition, a late retrograde mineralogical change involving addition of H_2O and CO_2.

Zone B3. This area lies south of B2 and again mineralogical assemblages are similar. But the degree of textural reorganization, due to shearing, is less or absent. Furthermore, the abundance of chlorite has diminished as a result of the lack of shearing;

Plate 48

Photomicrograph: Sheared ankaramitic basalt. Note the amphibole pseudomorph (top left) that has been split by shearing, such that a sliver, previously in optical continuity, has been prised away from the bulk of the crystal. The resulting pressure shadow is filled with chlorite, albite and acicular actinolite. Also, note that the microphenocrysts of plagioclase have now been albitised, and despite the effects of shearing and the development of a schistose groundmass, igneous textures are well preserved. (Sample 5087B. XP. Field width = 8 mm.).

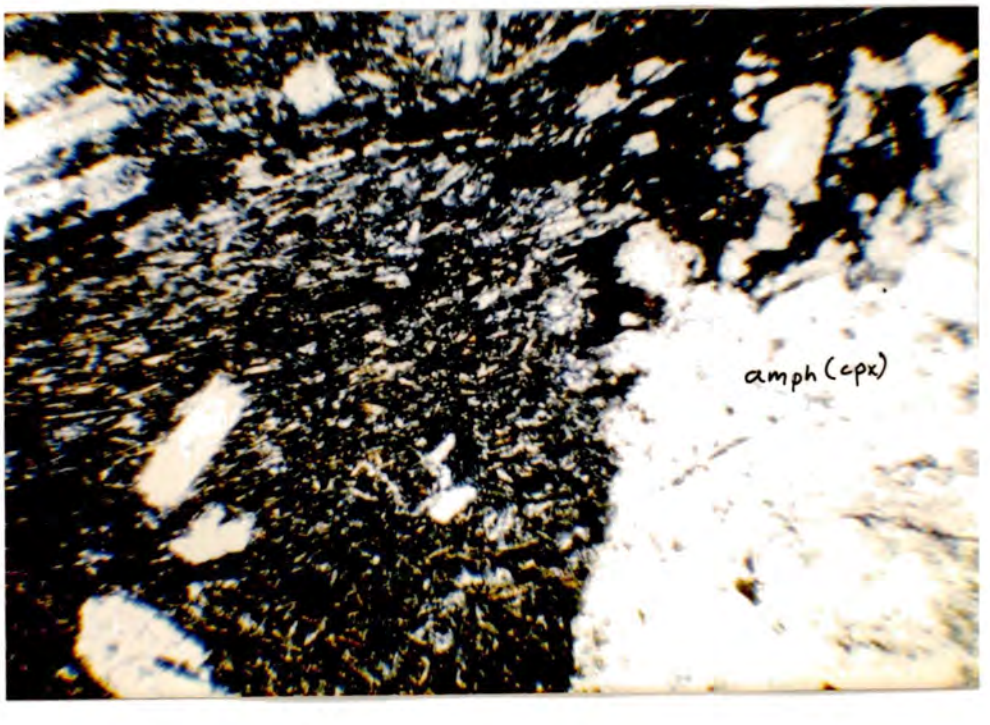

Plate 49

Photomicrograph: Ankaramitic basalt from sub-zone B2. Note the contrast in phenocryst size between pyroxene (actinolite) and plagioclase (albite). Note also the shattering of the amphibole and the development of turbid, chloritic pressure shadows (top right). Alignment in the groundmass is due to acicular actinolite mainly (Sample 5087B. XP. Field width = 4 mm.).

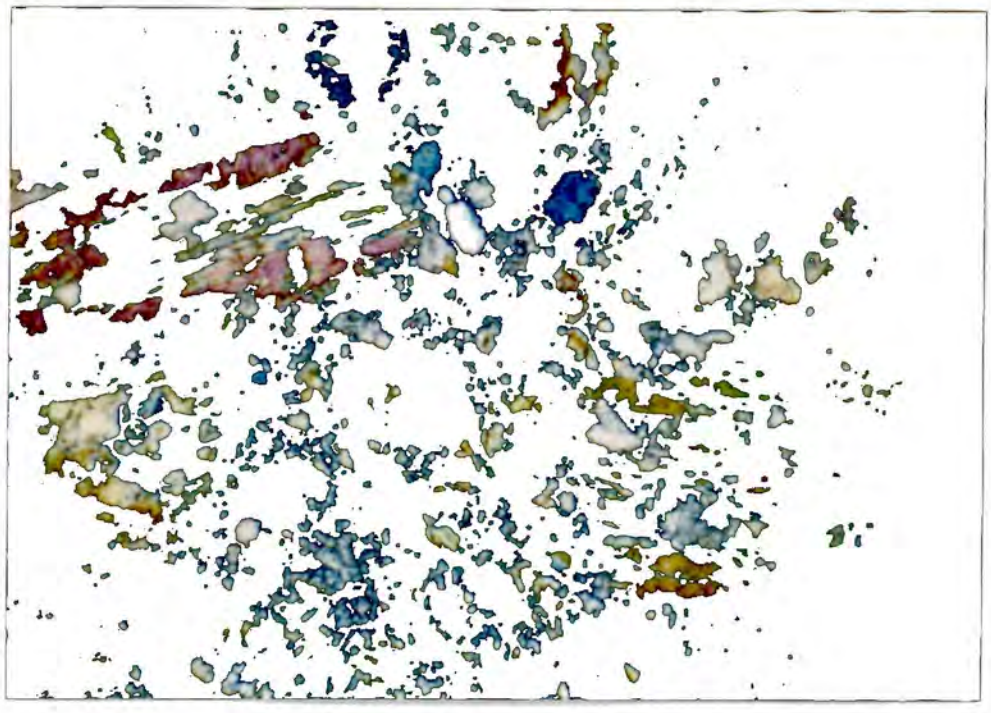

Plate 50

Photomicrograph: Ankaramitic basalt with pyroxenes pseudomorphed by actinolite, which in turn has broken down, partially, to chlorite + calcite. (Sample 5534A. XP. Field width = 8 mm.).

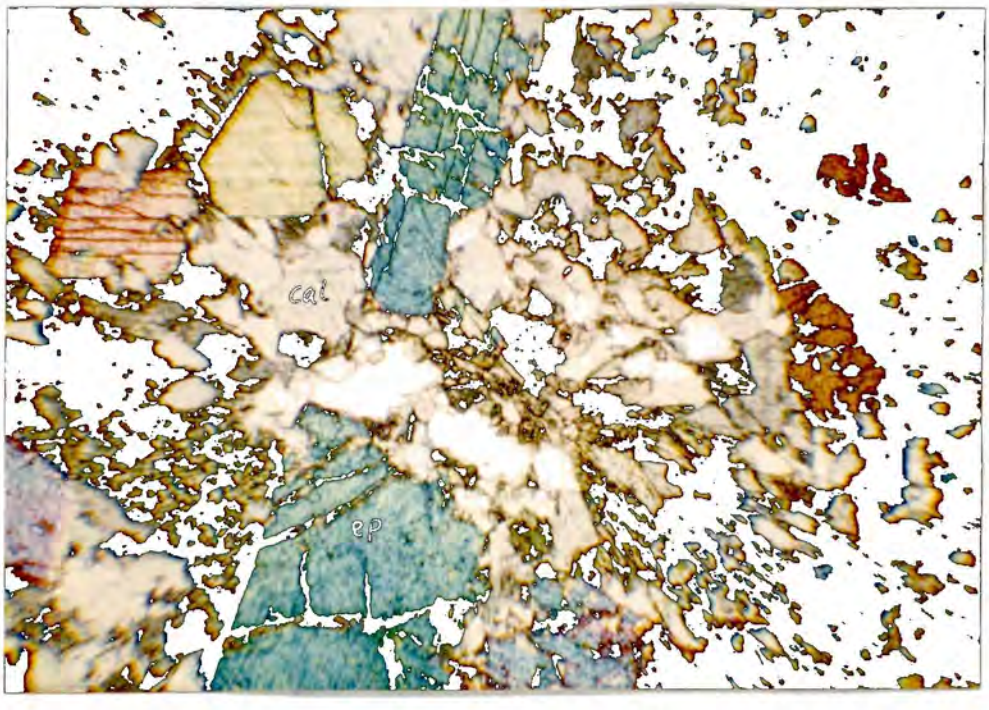

Plate 51

Photomicrograph: well-formed epidote in a calcite plus biotite vein assemblage. Host rock is an ankaramitic basalt (Sample 5516C. XP. Field width = 4 mm.).

chlorite apparently favouring areas of low stress, such as pressure shadows. Epidote, calcite and biotite occur, though, as late-stage filling of veins (cf. Plate 51).

Zone B4. This zone is also characterized by a lack of textural disruption, apart from that due to new mineral growth. Like B3, groundmass development of acicular hornblende or flaky biotite is random.

Mineralogical differences in this zone, as are emphasized in the next Chapter, are apparent, in that contact metamorphism has locally caused amphibolite facies to be represented.

A few samples in this area contain relict clinopyroxene, though invariably mantled by actinolite or hornblende (Plate 52).

Zone B5. In this area, metamorphism has again proceeded statically and as a result, relict pyroxene is common in the cores of the larger phenocrysts (Plate 53). Groundmass biotite, actinolite or hornblende also develop randomly. Sample 4003 (Plate 54), in particular, shows a 'variolitic' development of groundmass hornblende.

In general, differences between the above zones in terms of mineral assemblage, and thus grade or other conditions of metamorphism, are discussed in Chapter 7. The remainder of this Chapter deals with details of mineral occurrence and chemistry, and the mineralogical differences between the various zones.

Mineral data used in this Chapter are tabulated in Appendix 3. The samples probed and their mineral assemblages are shown in Table 6.1.

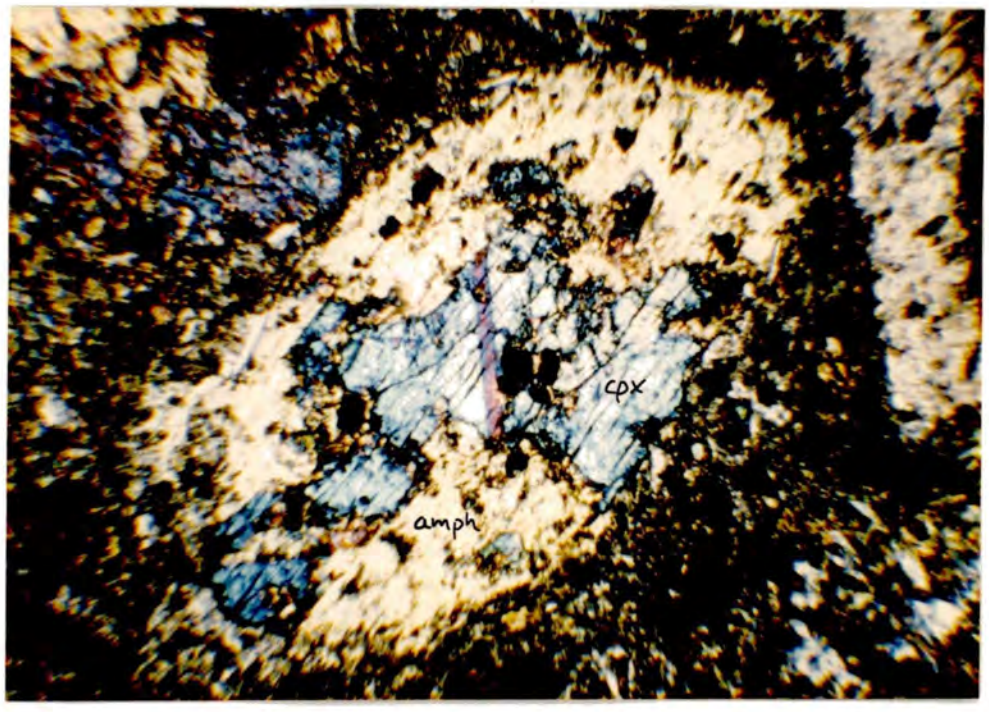

Plate 52

Photomicrograph: Partially amphibolised clinopyroxene in B4 ankaramitic basalt. Note the optical continuity of the marginal amphibole (actinolite). Opaque minerals included in the pyroxene are Ti-poor magnetites (Sample 4013A. XP. Field width = 4 mm.).

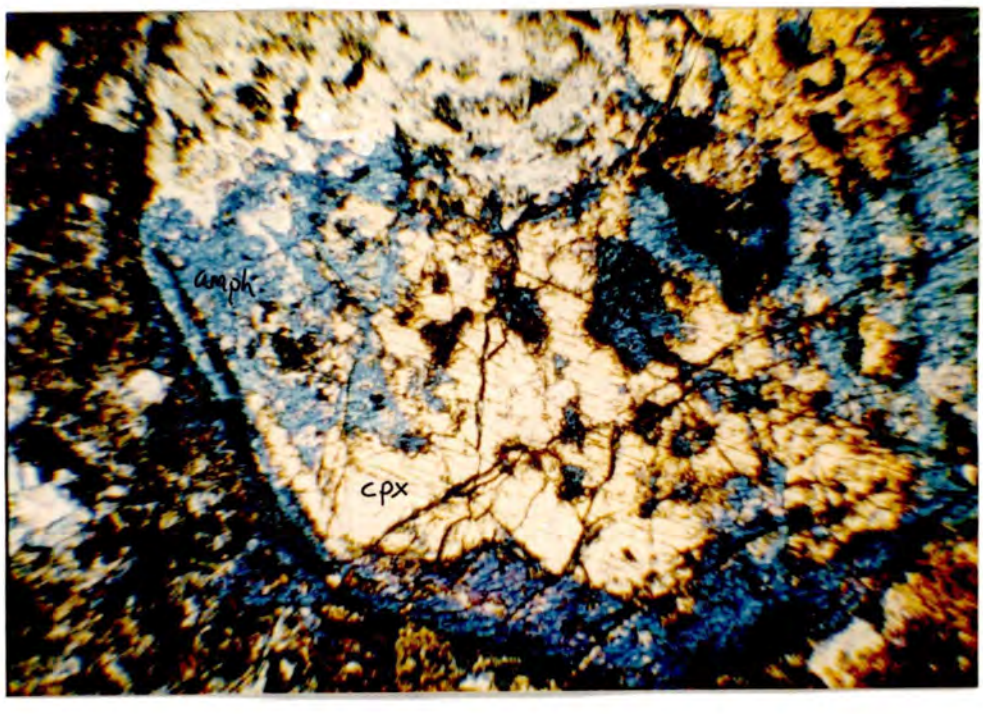

Plate 53

Photomicrograph: Partially amphibolised clinopyroxene in B5 basalt. Note the growth of an amphibole fringe beyond the margins of the original phenocryst. (Sample 4006A. XP. Field width = 4 mm.).

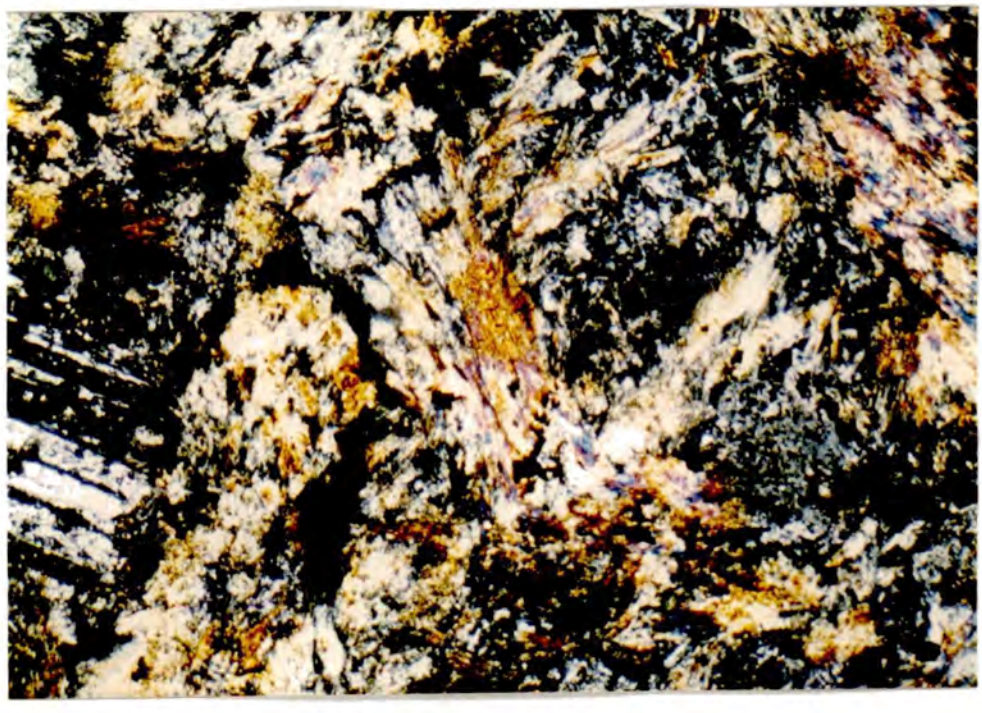

Plate 54

Photomicrograph: Shredded, acicular actinolite in the groundmass of a basalt, showing a slight radial development in patches. (Sample 4003. XP. Field width = 2 mm.).

TABLE 6.1

PROBED SAMPLES FROM ZONE B - MINERAL ASSEMBLAGES

	A	EP	BI	CH	FL	MA	Q	CC	SU	Sub-Zone
4029A	P	X		P	P	(X)				B1
4029B	P	P	P	(X)	P	X				B1
5074B	P	P	P	P	P		(X)	(X)	(X)	B1
5074C	P	X	P	P	P	(X)			(X)	B1
5075B	P	P	P	P		P		X		B1
5077	P					P		X		B1
74B	P	X	P	X	X	X			(X)	B1
4111	P	X	P		P			X		B2
5088	P	P	P	P	X			X	X	B2
5530A	P	P	P		P			X	(X)	B2
5536E	P		X	P	P			X	(X)	B2
5538B	P			X	P			X	X	B2
4105A	P	X	P		P	P		X		B3
5111B	P	P	P	P	P			X		B3
5516A	P	P	P		X	P		X		B3
5516B	P	P	P		X			(X)		B3
4013A	P	P	X		X	P		X		B4
4061	P	(X)	X		X	X				B4
5049	P				P	P	X			B4
5116	P	X	X		P					B4
4007	P	X	X		P		(X)		(X)	B5

A - Amphibole; EP- Epidote; BI - Biotite; CH - Chlorite; FL - Feldspar; MA - Magnetite; Q - Quartz; CC - Calcite; SU - Sulphides.

P Probe Analysis made

X Mineral present, but not probed. (X) only trace present.

6:2 Calcic Amphibole

Mode of occurrence. Fig. 6.1 shows the distribution of secondary amphibole where it occurs as a pseudomorph after pyroxene. This distribution also applies to its appearance as a groundmass phase.

It was noted above that amphibole does not always totally replace primary pyroxene. Where it does not, mainly in zones B4 and B5, amphibole develpps as an optically continuous overgrowth, both around the margin of the phenocryst and along fractures (Plates 52 , 53).

Complete replacement of pyroxene by amphibole results in one amphibole per pyroxene, the crystallographic axes of the two minerals being as near coincident as possible.

In some samples, it appears that amphibole has replaced pyroxene in two stages. At the interface between the continuous amphibole rim and the relict pyroxene, a new stage of growth is occasionally indicated by the development of individual blades or prisms of amphibole (Plate 55). If this process goes to completion a texture as shown in Plate 56 is developed, the regenerated or second phase of amphibole being optically and compositionally identical to the first.

Generally, the amphiboles are coloured from near colourless, through pale-green varieties to strongly pleochroic shades of blue-green or brown-green. The colour change is essentially due to the higher contents of Fe (and Fe^{3+}) and Ti in the more coloured hornblendes, compared to the less coloured actinolites. Very broadly, increased colour reflects a higher grade of equilibration (e.g.Binns, 1965).

Along with the change in colour of the amphibole is a corresponding change of habit. In samples containing actinolitic

Figure 6.1

Distribution of secondary amphibole in the Rossland volcanics. The location of zones A and B_9 and the sub-zones of B_9 are shown (see discussion in text - Section 6:1).

Also shown is the distribution of Mesozoic and Cenozoic plutonic rocks.

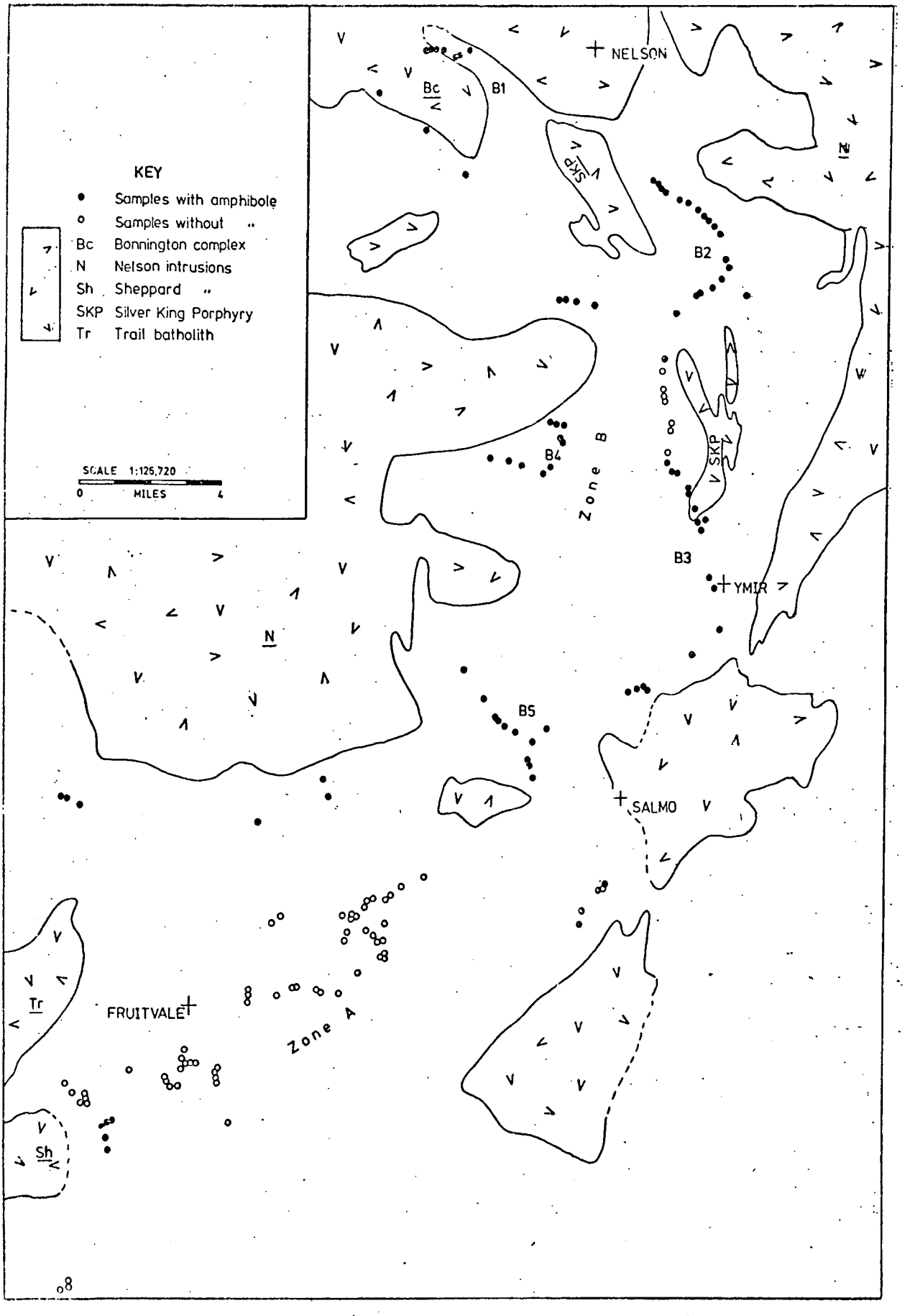
KEY
Samples with amphibole
Samples without ..
Bc Bonnington complex
N Nelson intrusions
Sh Sheppard ..
SKP Silver King Porphyry
Tr Trail batholith
SCALE 1:126,720
0 MILES 4
NELSON
YMIR
SALMO
FRUITVALE
B1
B2
B3
B4
B5
Bc
N
Sh
Tr
SKP
Zone A
Zone B

Plate 55

Photomicrograph: Interior of large clinopyroxene exhibiting a relict pyroxene core and an outer actinolitic margin. The interface between these two shows the development of discrete actinolite crystals not in optical continuity with the main overgrowth of amphibole (Sample 5088. XP. Field width = 2 mm.).

Plate 56

Photomicrograph: Pyroxene-phyric metabasalt (zone B1) showing amphibole pseudomorphs in which regenerated amphibole crystals have grown (cf. Plate 55 and discussion in text). (Sample 5074B. XP. Field width = 8 mm.).

hornblende or actinolite (zones B2, B3 and B5 particularly), the habit is usually acicular, except where amphibole growth is governed by pseudomorphic outlines. Acicular, or ragged actinolite grows randomly in zones B3 and B5, and as fringes on pseudomorphs; whereas in B2, the crude schistose fabric is in fact due to aligned, needle-like actinolite. Hornblendes in samples from zones B1 and B4, in contrast, grow as stubby, prismatic crystals (Plates 57 , 58). The more thorough recrystallization of these hornblende- (rather than actinolite) -bearing rocks, in addition, causes a loss of definition of the original phenocrysts, and aggregates of amphibole can develop where only one crystal previously existed as a replacement of pyroxene.

Zoning is apparent in some samples, typically from B1 and B4, with pale-green actinolite developing a margin of more coloured hornblende. Patchy growth of hornblende within actinolite is also evident (Plate 59). In sample 4061 (Plate 60)a sharp compositional break is apparent between the two amphiboles, as they are separated by a Becke line. In other cases, zoning is apparently continuous. Where internal patches of hornblende develop, as in 4061, they usually grow around biotite which has developed in fractures, possibly as an earlier retrograde phase (Plate 60). In 5075B, where two amphiboles occur within the area of one thin-section, the more coloured (Fe-rich) hornblende tends to develop near or around magnetite, as does biotite. These observations suggest that localised disequilibrium has occurred, brought about by local chemical differences. Possibly, reactions toward a new equilibrium, as a result of increased temperature, were not completed.

Observations of apparently coexisting calcic amphiboles, either in one crystal or within one thin-section, have been reported by

Plate 57

Photomicrograph: Schistose texture in B1 metabasalt. Note, particularly, the well-formed prismatic hornblende (contrast with Plate 54). Other phases present are biotite, plagioclase and minor epidote. (Sample 4029B. PPL. Field width = 4 mm.).

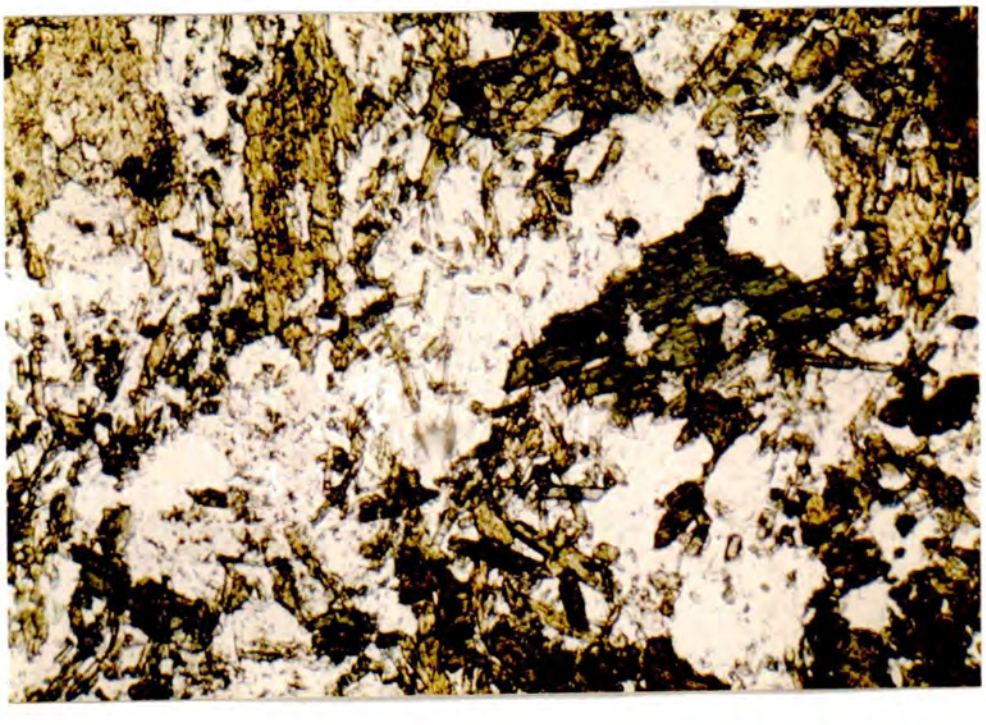

Plate 58

Photomicrograph: Hornblende in non-schistose B4 basalt, developed as stubby, prismatic crystals. The larger hornblendic patches are probably relict pseudomorphs after pyroxene. (Sample 5049. XP. Field width = 2 mm.).

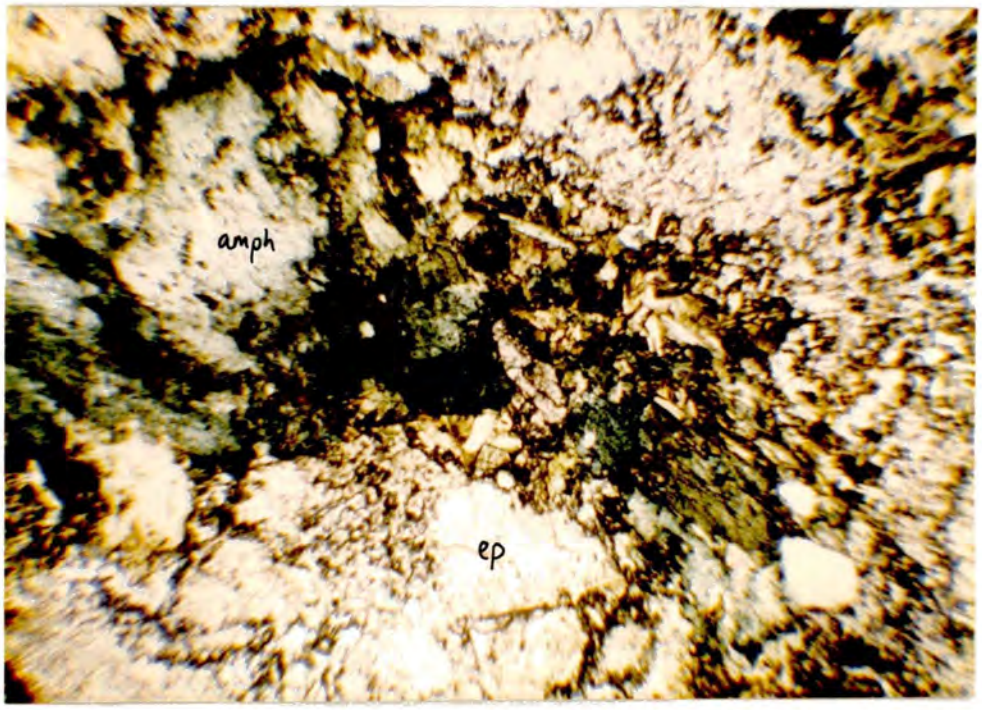

Plate 59

Photomicrograph: Zoned amphibole (actinolite to hornblende) in doleritic sample. Hornblende usually rims actinolite, but also occurs as patches within the crystal (Sample 748. PPL. Field width = 4 mm.).

Plate 60

Photomicrograph: Coexisting actinolite and hornblende. Note how internal development of hornblende (darker green) is controlled by fractures in which biotite has grown. Hornblende also forms a thin rim to the actinolite where it is juxtaposed with the groundmass. (Sample 4061. XP. Field width = 2 mm.).

various authors, for example Graham (1973), Cooper & Lovering (1970), Grapes (1975) and Hietanen (1974). This has led to a debate as to whether such relations indicate the presence of a miscibility gap, or just disequilibrium. Whether the actual compositions present are governed by a miscibility gap is hard to assess on optical evidence alone; however, the continuous zonation observed in a few samples (e.g. Plate 59) suggests it is not, and where sharp discontinuities are observed, that they are a result of disequilibrium. This topic is returned to below, when compositional evidence is discussed.

Classification and chemical variation. Inspection of Fig.6.2 shows that a considerable range of amphibole compositions are present in the Rossland volcanics. They range from actinolites (Al^{iv} less than 0.5 cations/unit formula; Grapes, 1975), through actinolitic hornblendes (Al^{iv} of 0.5 to 0.8) to hornblendes (Al^{iv} greater than 0.8). As Figs. 6.2 A, B and C show, the compositional trend is from tremolite towards pargasite (hastingsite).

The analyses in Appendix 3 are calculated assuming all Fe is FeO and Fig.6.2 is plotted on this basis. However, as was observed in discussing the primary amphiboles, Fe^{3+} can be a significant contributor to total Fe. In general, Fe^{3+} increases with total Fe and, as implied by Fig. 6.2C, is higher in the hornblendes (Grapes et al., 1977). The effect of Fe_2O_3 in abundances comparable to the data of Grapes et al. (op.cit) is shown later, in regard to estimating Na(M4).

The variation observed is predominantly due to the two coupled substitutions:

$$Na\ Al^{iv} \rightleftharpoons Si \quad \text{(Edenite)}$$

$$Al^{vi}Al^{iv} \rightleftharpoons (Mg, Fe)\ Si \quad \text{(Tschermakite)}$$

Figure 6.2

Classification diagrams for the metamorphic amphiboles.

A Al^{vi} versus Si (on basis of 23 oxygens)
B Na + K versus Al^{vi}
C Mg versus Al^{vi}

Ts	Tschermakitic	FTs	Ferrotschermakitic
Pa	Pargasite	FH	Ferrohastingsite
Ed	Edenite	FEd	Ferroedenite
Tr	Tremolite	FA	Ferroactinolite

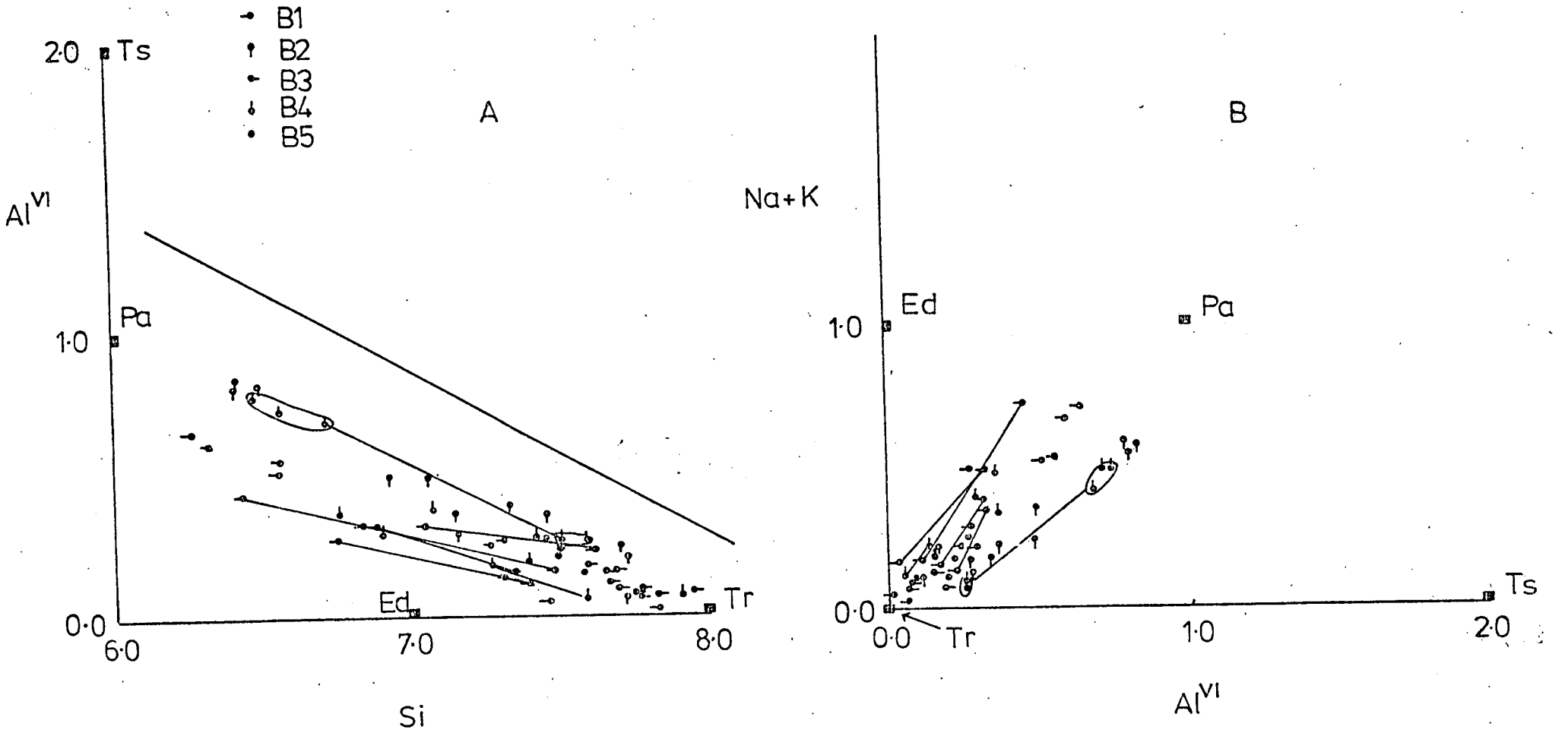
B1
B2
B3
B4
B5
A
2·0
Ts
Al^VI
Pa
1·0
0·0
6·0
7·0
8·0
Ed
Tr
Si
B
Na+K
Ed
Pa
1·0
0·0
0·0
Tr
1·0
2·0
Ts
Al^VI

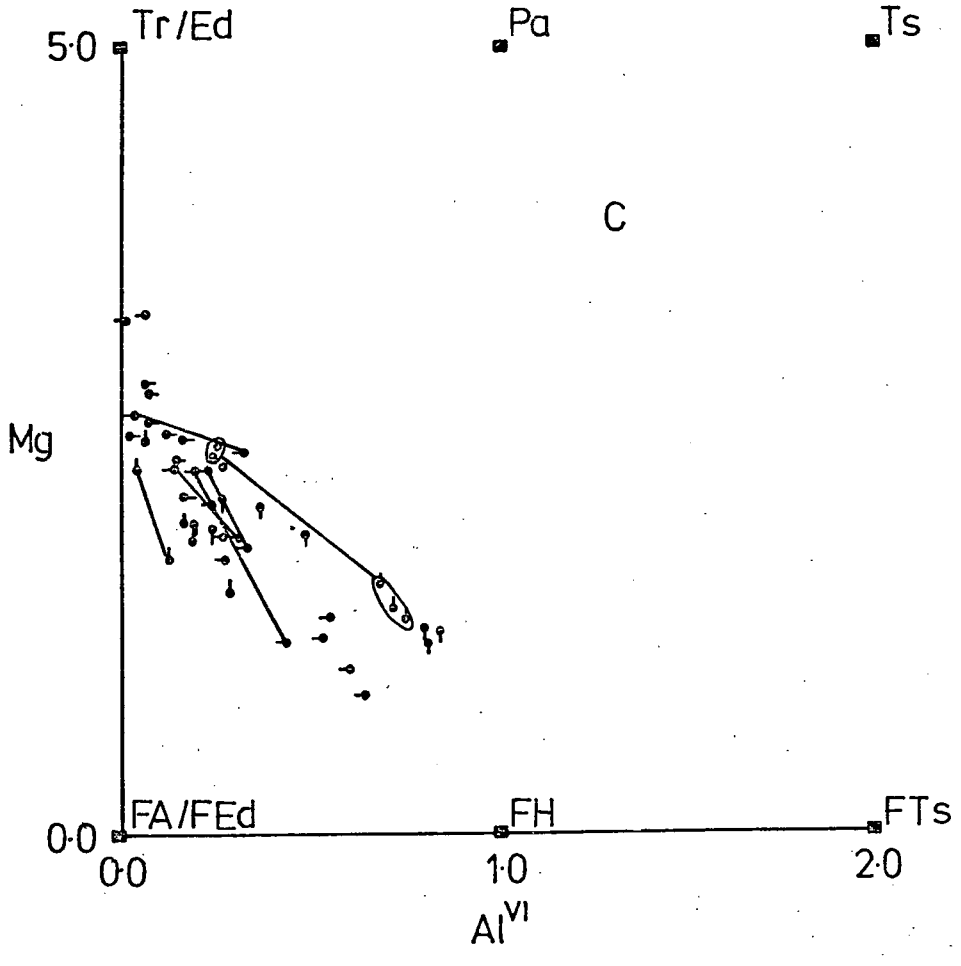
5·0
Tr/Ed
Pa
Ts
C
Mg
0·0
FA/FEd
FH
FTs
0·0
1·0
2·0
AlVI

In addition to Fe^{3+}, small amounts of Ti enter the Y sites. In the actinolites ($Al^{iv} < 0.5$) Ti is typically less than 0.01, whereas in the hornblendes ($Al^{iv} > 0.8$) Ti varies from 0.02 to 0.15. Although it is not shown graphically, Ca decreases with increase in Al, indicating incorporation of Fe and/or Na into the M4 site, both of which increase with Al.

The tendency for Fe^{2+} to increase with Al, as implied by Fig. 6.2C, is a crystal-chemical effect: since Fe and Mg differ in ionic radius, they distribute non-ideally between the sites M1, M2 and M3. Al^{vi}, which is closer in size to Mg, preferentially enters the M1 and M3 sites, rather than M2 where Fe^{2+} is concentrated (Choudhuri, 1974).

Effects of whole-rock chemistry, temperature and pressure

The effect of whole-rock chemistry on amphibole composition is strong, as shown by various authors (Leake, 1965; Graham, 1973; Grapes et al., 1977; Misch & Rice, 1975). Thus, although increasing grade of metamorphism involves an overall change from actinolite to hornblende (cf. Liou et al., 1974), the composition of an isolated amphibole is not a good indicator of temperature. Graham (1974), in particular, observes that in suitable rock compositions, hornblendic amphibole appears before the amphibolite facies in the Dalradian. Similarly, Misch & Rice (1975) show that in the upper amphibolite facies gneisses of Washington State, a complete range of amphiboles exist, varying from tremolite to hornblende.

In the Rossland area, a strong whole-rock control is evident, as shown in Fig. 6.3. At a given temperature, actinolitic hornblende or actinolite will occur in an Mg-rich, Al-poor bulk composition, whereas hornblende is more likely to stabilize where the opposite is

Figure 6.3

Whole-rock (WR) versus amphibole Mg-number correlation plot for the Rossland amphiboles.

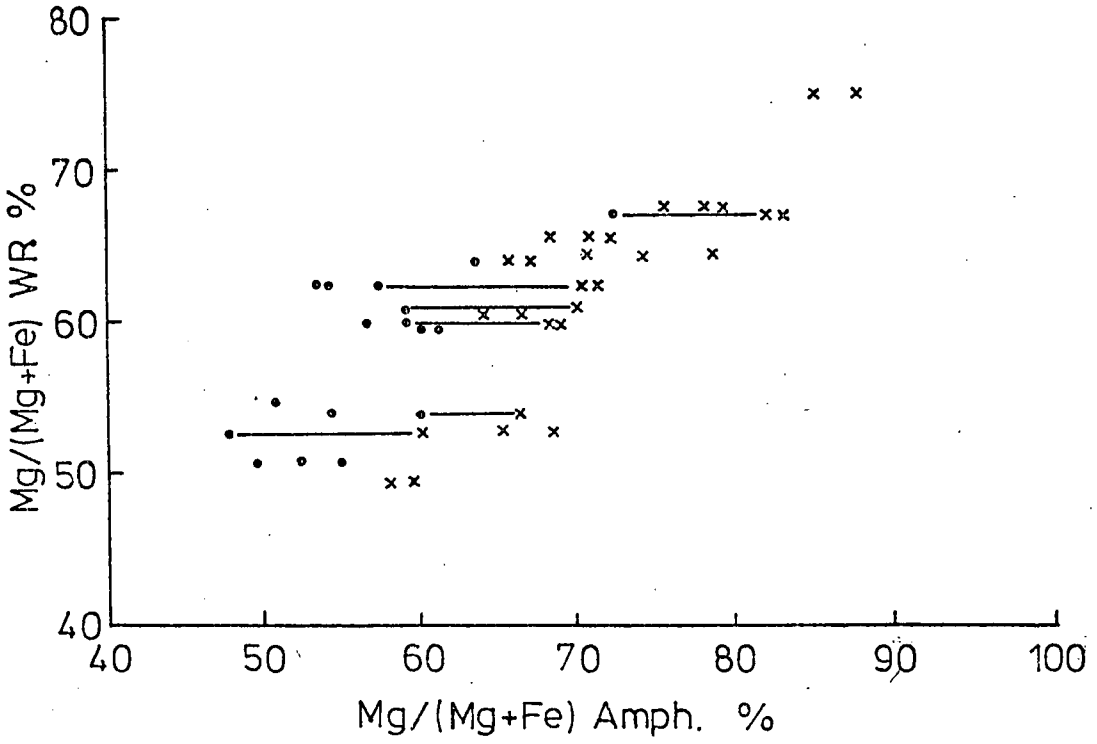
80
70
60
50
40
Mg/(Mg+Fe) WR %
40
50
60
70
80
90
100
Mg/(Mg+Fe) Amph. %

true. For example, within zone B1, clinopyroxenite (samples 5075B, 5077) develops tremolitic amphibole as an alteration product, whereas the immediately adjacent metavolcanics (e.g. samples 5074B, 5074C), high in Fe/Mg and Al_2O_3, alter to correspondingly high Al, high Fe hornblendes. In view of the correlations between the elements, Mg-Al^{vi}, Si-Al^{vi} and (Na + K) - Al^{vi} (Figs. 6.2A, B, C), it is evident that amphibole composition generally is dependent upon whole-rock chemistry, and not necessarily temperature.

Systematic changes of amphibole composition, that are apparently dependent upon grade and not bulk composition, are documented by Graham (1973, 1974), for the Dalradian metabasites. Graham (op.cit)shows that the chemical trend between the various amphiboles developed, shifts from one trending from tremolite towards edenitic pargasite at the chlorite zone, to one trending towards a hornblende richer in the tschermakite molecule at the garnet zone (Fig. 6.4). It is also apparent in Fig. 6.4 that hornblendes, rather than actinolites, are stabilized in rocks of successively higher Mg/Fe ratios as grade increases. In Fig.6.4 are plotted all the Rossland amphibole analyses and by comparison with the mineral zones established by Graham (1974) for the Dalradian, it is evident the best analogy for the Rossland data are the biotite or garnet zones of the Dalradian. Similarly, the Rossland amphiboles plot comparably with garnet isograd (lower amphibolite facies) amphiboles from Haast River (Cooper & Lovering, 1970) as plotted in Fig.3 of Harte & Graham (1975). In general, a temperature of about 500°C is indicated by comparison with data given by Winkler (1974). Misch & Rice (1975) also estimate a general temperature of 500°C for epidote-amphibolite facies rocks containing two amphiboles (see below). However, as will be seen in Chapter 7,

Figure 6.4

Plot of Rossland metamorphic amphiboles in the 'A' FM diagram of Harte & Graham (1975). Projection is from epidote. Also shown are the trends of the Dalradian amphiboles (after Graham, 1973):-

Dashes - Chlorite zone
Continuous line -Biotite zone
Dots and dashes - Garnet zone.

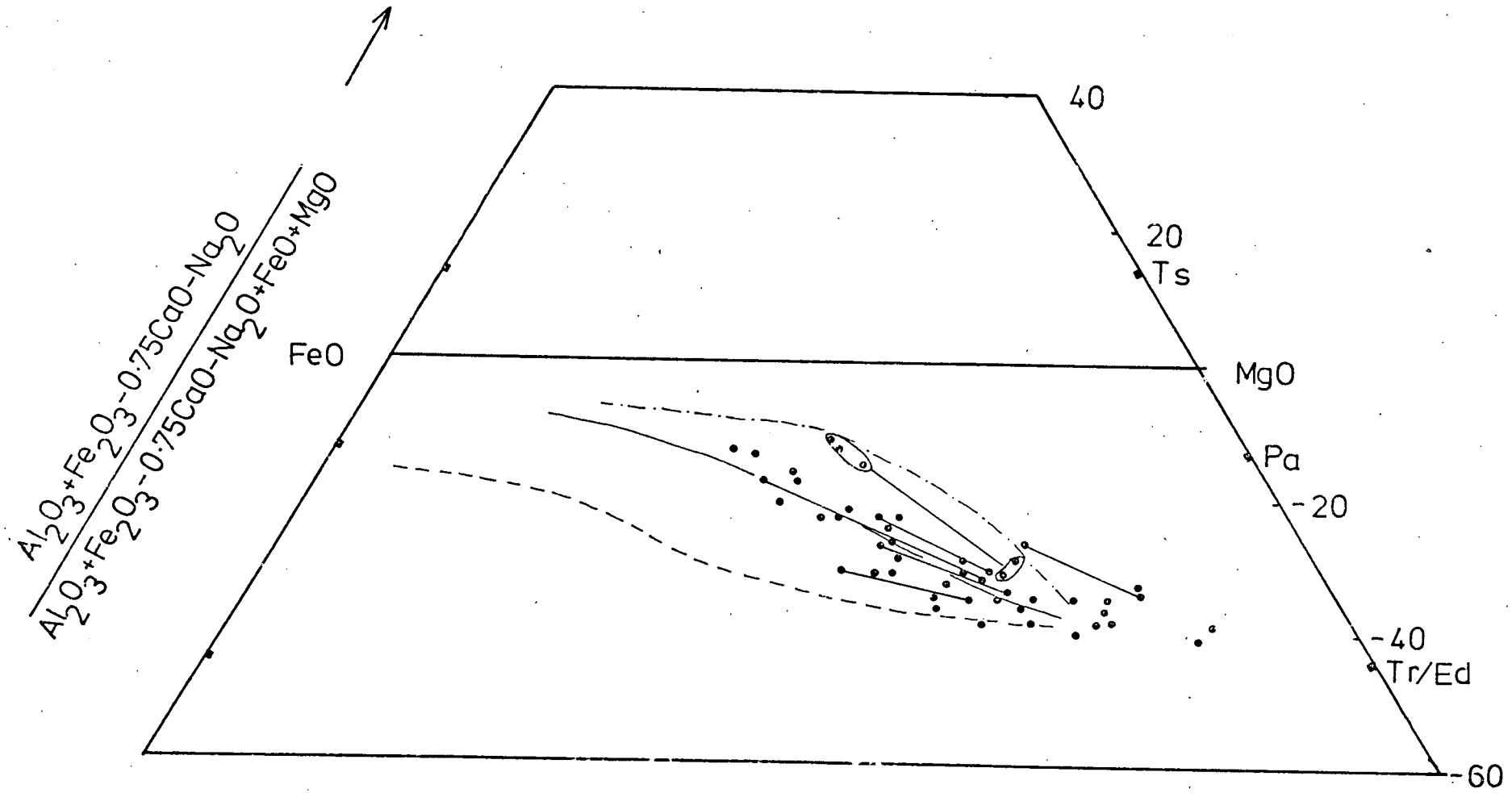
$\frac{Al_2O_3+Fe_2O_3-0.75CaO-Na_2O}{Al_2O_3+Fe_2O_3-0.75CaO-Na_2O+FeO+MgO}$
FeO
40
20
Ts
MgO
Pa
-20
-40
Tr/Ed
-60

temperature differences do occur throughout zone B and not all the amphiboles necessarily equilibrated at a single temperature; the figure of 500°C is just a generalised bulk average for the temperature of metamorphism, as indicated by the amphibole chemistry. On the basis of amphibole chemistry alone, variations in temperature between the various sub-zones within zone B is hard to evaluate, due to the masking effect of whole-rock compositional control. The schistose rocks of B1 contain the most pargasitic amphiboles (e.g. samples 4029A, B) and thus these rocks were probably metamorphosed at higher temperatures than those to the south. Though, on the other hand, these Fe-rich hornblendes also develop in Fe- and Al-rich whole-rocks (compare Figs. 6.2 and 6.3). Analyses HB07 (sample 4007) from B5 are actinolitic but still quite Fe-rich, which suggests that relative to B1 this zone equilibrated at a lower temperature. This would be expected on the basis of the broad pattern whereby lower-grade rocks in zone A become progressively higher grade northwards through zone B.

Amphibole chemistry is also considered to be indicative of pressure. Notably the presence of glaucophane or crossite in high pressure analogues of the greenschist facies is well established (cf. Turner, 1968). Within the greenschist facies, where calcic amphiboles are present, Na content or alkali content show a correlation with load pressure (Shido & Miyashiro, 1959). Brown (1977), in particular, notes this feature and shows that the crossite content of a calcic amphibole is buffered by a reaction:

$$\text{Crossite} + \text{Epidote} + H_2O = \text{Ca-amphibole} + \text{Albite} + \text{Chlorite} + \text{Iron oxide}.$$

At any T and P, the crossite component is fixed as long as the other phases in the reaction are present. With increased load pressure (P),

the crossite component (expressed as Na(M4)) increases within the Ca-amphibole. Using published analyses, Brown (op.cit) has tentatively calibrated an Al^{iv} - Na(M4) plot for pressure.

A problem with this approach is to evaluate Na(M4) which, as shown in Chapter 4, is critically dependent on correct knowledge of the Fe_2O_3 content. Table 6.2 shows several amphibole analyses from the Rossland volcanics that coexist with iron-oxide, with Na(M4) calculated on the basis that:-

(1) $Fe_2O_3 = 0.375\ (FeO - 4.00)$ (Grapes et al., 1977).

When all Fe is expressed as FeO, Na(M4) is invariably negative. Increasing Fe_2O_3 lowers the sum of elements in the Y-sites and thus restricts the amount of Fe assigned to M4. There is, therefore, a bracketing condition for Fe_2O_3 such that Fe(M4) and Na(M4) are both positive. In Table 6.2, Na(M4) is calculated by:

$Na(M4) = 2.00 - Ca - Fe\ (M4)$, if $Fe(M4) > 0$ or;

(1) $Na(M4) = 2.00 - Ca$.

Generally, it is apparent that Na(M4) is less than 0.15, which from Brown's (1977) Al^{iv} - Na(M4) plot indicates a pressure of equilibrium of no more than 3kb.

Another indicator of pressure is considered by Leake (1965) and Raase (1974) to be the amount of Al^{vi}. This, too, is controlled by the glaucophane substitution, Na(M4) Al^{vi} = Ca(Mg, Fe). In Fig. 6.2A the solid line defines the maximum Al^{vi} for all calcic amphiboles (Leake, 1965), and the dashed line represents the maximum Al^{vi} for amphiboles formed below 5kb (Raase, 1974). Again, a low-pressure origin for the Rossland samples is indicated.

Miscibility in the Ca-amphiboles. A considerable debate has continued in recent years on the subject of whether a miscibility

TABLE 6.2

Na(M4) ESTIMATES IN SELECTED AMPHIBOLES (SEE TEXT FOR DISCUSSION - p. 202)

	HB612	HB613	HB6E3	HB0A1A	HB1B1A
Si	7.456	6.398	6.354	7.655	7.911
Al^{iv}	0.544	1.602	1.646	0.345	0.089
Al^{vi}	0.204	0.674	0.751	0.179	0.042
Fe^{3+}	0.303	0.514	0.476	0.420	0.260
Fe^{2+}	1.072	1.500	1.424	1.307	0.988
Mn	0.034	0.044	0.043	0.038	0.022
Mg	3.443	2.332	2.274	2.945	3.632
Ti	0.005	0.039	0.042	0.007	0.000
Ca	1.906	1.833	1.878	1.920	1.921
Na	0.078	0.438	0.488	0.090	0.061
K	0.018	0.036	0.075	0.022	0.007
Fe (M4)	0.063	0.102	0.010	-	-
Na (M4)	0.031	0.066	0.111	0.080	0.078

Fe^{3+} is estimated by the equation (Fig.3, Grapes et al., 1977):

$$\text{wt.\% } Fe_2O_3 = 0.375\ (\text{wt.\% } FeO^{*} - 4.0)$$

FeO^{*} is total iron.

gap lies between actinolite and hornblende. Shido (1958), Klein (1969), Cooper & Lovering (1970) and Misch & Rice (1975) have argued in favour of a miscibility gap on the basis of observations of coexisting amphiboles, within one thin-section or one mineral grain, that are separated by a compositional gap. Such a gap appears to be operative, by the accounts of the above authors, into the lower amphibolite facies. Hietanen (1974) suggests the gap occurs up to around 600°C. Misch & Rice (1975), in a comprehensive survey of epidote-amphibolite and upper amphibolite facies amphiboles, show that at about 500°C a gap in Al content (per formula unit) occurs between 0.5 and 1.5. At 600°C a complete range of Al contents are found. Misch & Rice (1975) attribute this to the closure of a solvus somewhere in the region 500-600°C. However, in their samples Misch & Rice (op.cit) found no coexisting amphiboles and thus the compositional gap they defined is the maximum it could be, whereas in reality it may be considerably narrower.

Compositional gaps defined by coexisting amphiboles within one crystal, are reported by Grapes (1975) and Graham (1974); but these authors regard them as a result of disequilibrium. The compositional data, these authors observed, were chemically inconsistent with a fixed solvus, and in fact individual analyses can plot within the apparent gap. Leake (1962, 1965) also shows that although a frequency minimum, in terms of the number of analyses, occurs at Si contents (per unit formula) of about 7.2, there is a continuity of composition. Graham (1974) interprets a similar frequency minimum as a result of a rapid change in amphibole composition brought about, at the upper greenschist facies, by the disappearance of phases such as albite, chlorite and epidote, according to reactions such as:

Actinolite + Albite = Edenite + Quartz + H_2O

Chlorite + Epidote + Actinolite + Quartz = Tschermakite + H_2O

Chlorite + Epidote + Quartz = Tschermakite + Anorthite + H_2O

Experimental evidence on the greenschist to amphibolite transition (Liou et al., 1974) also indicates a sharp change in amphibole chemistry as a result of such concurrent reactions. The sluggish nature of these reactions, however, whilst releasing potential edenite and tschermakite, results in a frequent incompletion of the transition and thus produces the observed disequilibrium features.

The data presented here tend to confirm this latter view. The mineral assemblages within zone B are generally greenschist to lower amphibolite facies (Chapter 7) and a temperature of 500°C was quoted above. Unlike the data of Misch & Rice (1975), however, a complete range of Al contents are observed (cf. Figs.6.2a, 6.4). A compositional gap of the width proposed by Misch & Rice (1975) or Cooper & Lovering (1970) is not apparent. Furthermore, the generally low pressure of the Rossland metamorphism (see Chapter 7 and above), which would tend to increase the solvus width (Choudhuri, 1974; Grapes, 1975), strengthens the suggestion that the observed compositional gaps are not true solvi.

A recent paper supporting the concept of a miscibility gap (Tagiri, 1977), seeks to determine a solvus more precisely in terms of composition and temperature. Tagiri (op.cit) proposes that toward the Mg-rich end of the amphibole spectrum, the solvus width narrows and its closure temperature is lower. Thus, it could be that the appearance of a gap in some situations, whilst not in others, is compositionally dependent. Fig.6.5 shows the proposed gap of Tagiri (op.cit), with some coexisting pairs from the Rossland volcanics plotted for comparison. It is clear there

Figure 6.5

Al-Fe-Mg diagram showing the proposed miscibility gap in the calcic amphiboles of Tagiri (1977). Also plotted are coexisting actinolite-hornblende pairs analysed here.

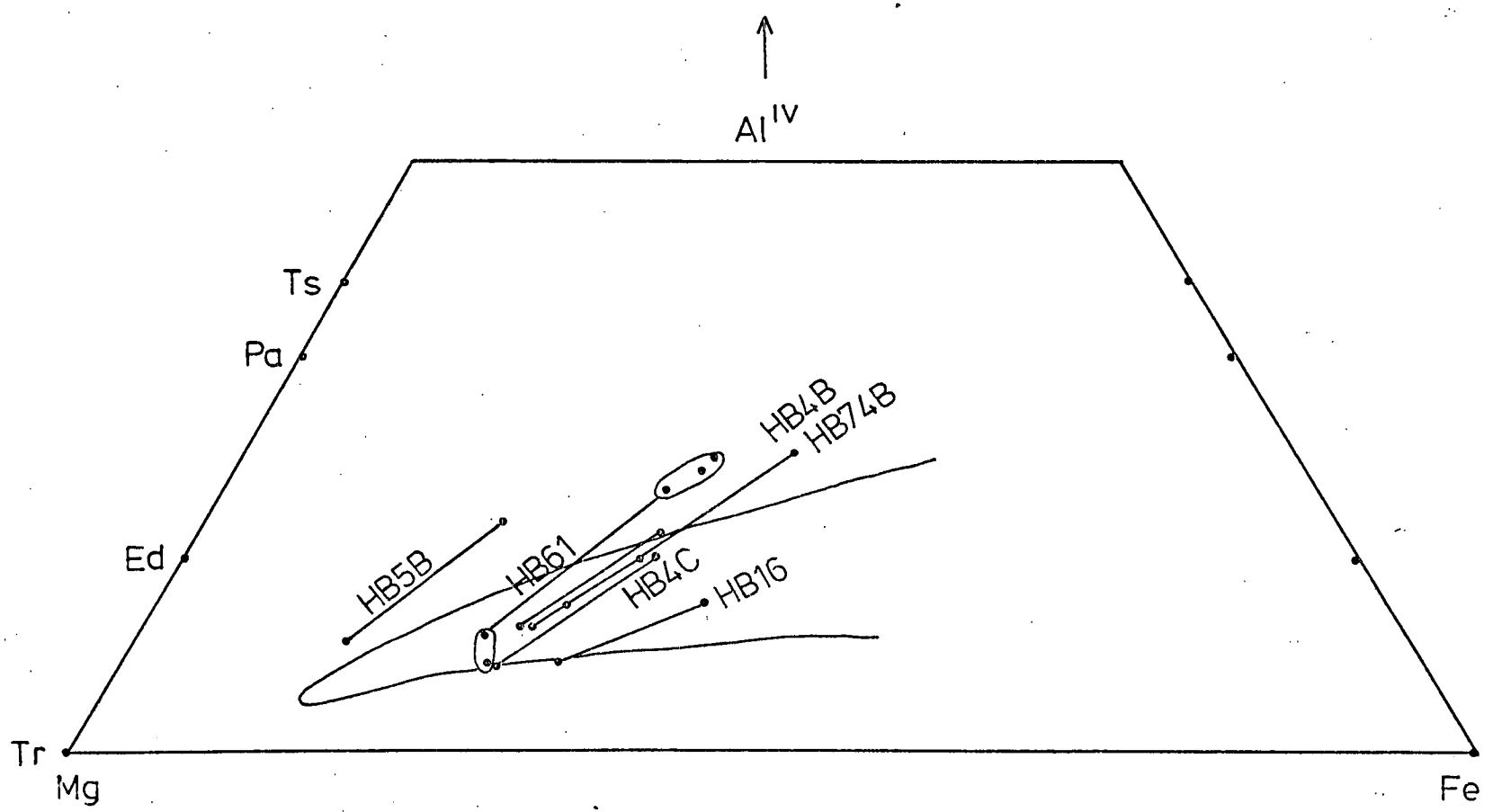
Al IV
Ts
Pa
Ed
Tr
Mg
Fe
HB4B
HB74B
HB5B
HB61
HB4C
HB16

is no simple agreement. Particularly, the analyses HB49 (sample 5049) plot in a line across this gap and represent good evidence for disequilibrium within one thin-section.

In Fig. 6.4 a small compositional gap is apparent in the area crossed by several tie-lines. However, this gap is one essentially in terms of Fe/Mg ratio, whereas the compositional gaps proposed by Misch & Rice (1975) and Tagiri (1977) are specifically in terms of Al, rather than Mg-number (cf. Fig. 6.5).

6:3 Biotite

Mode of occurrence. Fig. 6.6 shows that, like amphibole, biotite is virtually restricted to zone B. Though, unlike amphibole, it is not present invariably. It tends to show antipathetic relations with chlorite and, in addition, it is likely to be controlled by K_2O contents of the whole-rock.

In colour, biotite varies from green or green-brown to straw or brown varieties. This is a function of composition; Fe-rich varieties (and Ti-rich varieties) tend towards brown, whilst Mg-rich bioties are greener.

Biotite most commonly forms fine-grained aggregates, developed patchily or extensively in the groundmass of some samples. It is similarly developed as a breakdown (retrograde) product of amphibole (Plate 20). In some samples (e.g. 5530A), biotite has almost totally replaced amphibole pseudomorphs.

In the schistose rocks of B1, biotite is generally coarser, forming individual crystals of up to 0.5 mm. in length. Coarse, but randomly interlocking biotite also occurs in the pyroxenites and 'pseudodiorite' (Plates 59 , 61), patchily replacing, or associated with, amphibole.

Figure 6.6

Distribution of secondary chlorite and biotite in the Rossland volcanics. Zones A and B as defined in Fig. 6.1.

Also shown is the distribution of Mesozoic and Cenozoic plutonic rocks.

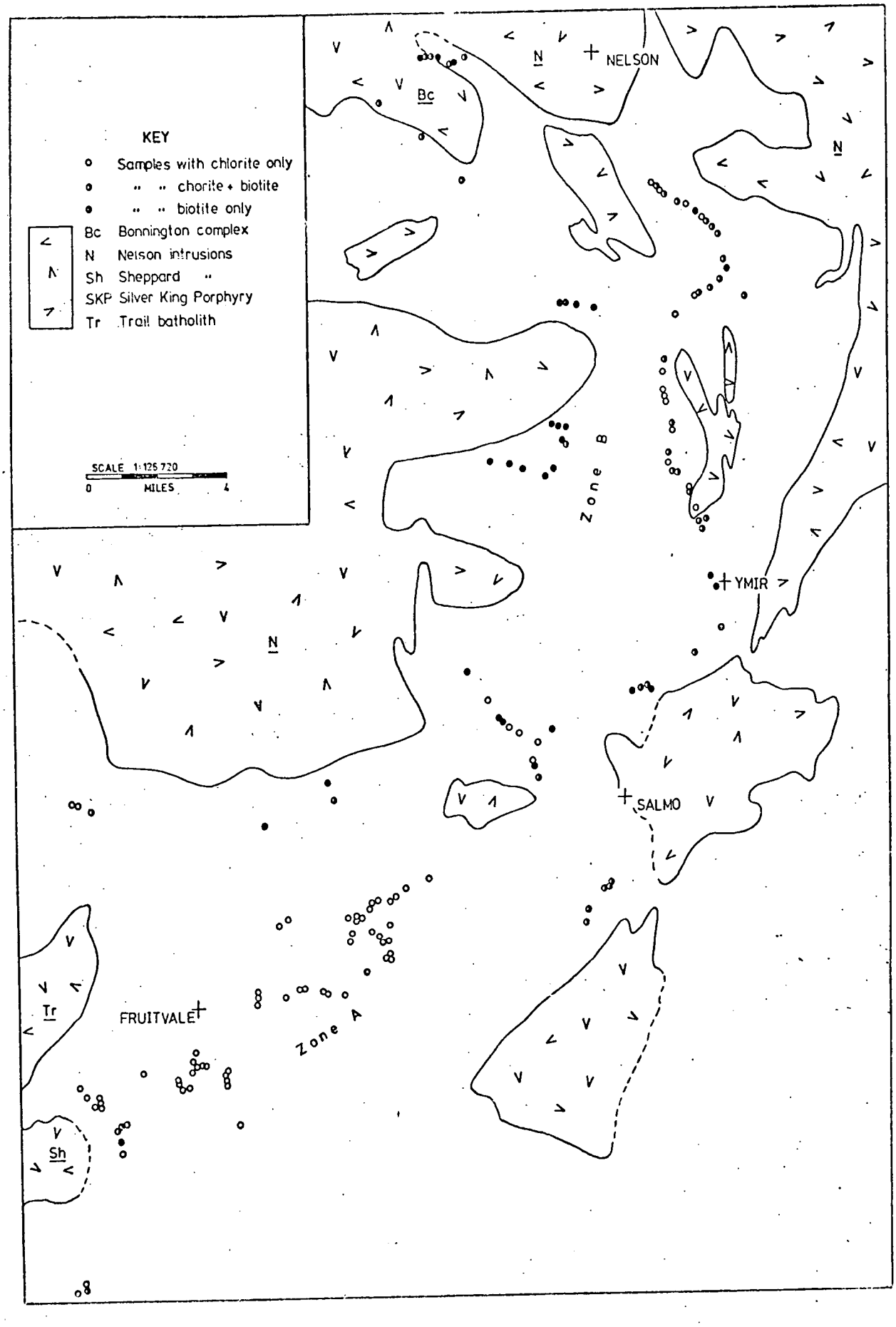
KEY
Samples with chlorite only
" " chorite + biotite
" " biotite only
Bc Bonnington complex
N Nelson intrusions
Sh Sheppard "
SKP Silver King Porphyry
Tr Trail batholith
SCALE 1:125 720
0 MILES 4
NELSON
YMIR
SALMO
FRUITVALE
Zone A
Zone B
Bc
N
Tr
Sh

Plate 61

Photomicrograph: Large magnetite grain in a pyroxenite. The margin of the magnetite is formed by a thin rim of granular sphene. Beyond this, and separating the magnetite from the fine tremolitic matrix, is a relatively coarse growth of biotite and chlorite. A large apatite crystal is also in evidence adjacent to the magnetite. At this interface no sphene has developed. (Sample 5075B. PPL. Field width = 2 mm.).

The occurrence of biotite in localised patches or aggregates, as well as in veins (Plate 51),suggests its development is partly metasomatic due to the presence of K_2O-rich fluids. As was indicated in Chapter 5, K is clearly mobile in all (zone A and B) volcanic rocks, though it is thought no significant net gain or loss occurred.

Chemistry. Biotite variation can be considered in terms of the four end-members.

Phlogopite	$K_2\ (Mg_6)\ (Si_6Al_2)\ O_{20}(OH)_4$
Eastonite	$K_2\ (Mg_5Al)\ (Si_5Al_3)\ O_{20}(OH)_4$
Annite	$K_2\ (Fe_6)\ (Si_6Al_2)\ O_{20}(OH)_4$
Siderophyllite	$K_2\ (Fe_5Al)(Si_5Al_3)\ O_{20}(OH)_4$

Fig.6.7, after Deer et al. (1962), shows the Rossland biotites plotted in terms of these components. The classification shown in Fig. 6.7 shows that some of the Mg-rich 'biotites' could be termed 'phlogopites'.

Within Fig.6.7, the analyses plot in a distinct line below, but parallel to, the phlogopite-siderophyllite join. The reason why the analyses plot below this line is in part due to the Y-site occupancies of less than 6.00. This is a common feature of biotites as noted by Deer et al. (1962), and indicates a small di-octahedral component. Another reason why the analyses plot below the theoretical line (Fig. 6.7) is due to the excess of Al^{vi} over that demanded by the substitution:

$$(Fe, Mg)\ Si \rightleftharpoons Al^{vi}Al^{iv}$$

Also apparent from Fig. 6.7 is that the substitution, $Fe^{2+} \rightleftharpoons Mg$, is coupled to the reaction above. This is analagous to the situation within the amphiboles and is probably related to an ionic-radius control.

Figure 6.7

Biotite classification diagram (see text)

Figure 6.8

Whole-rock versus biotite Mg-number correlation plot.

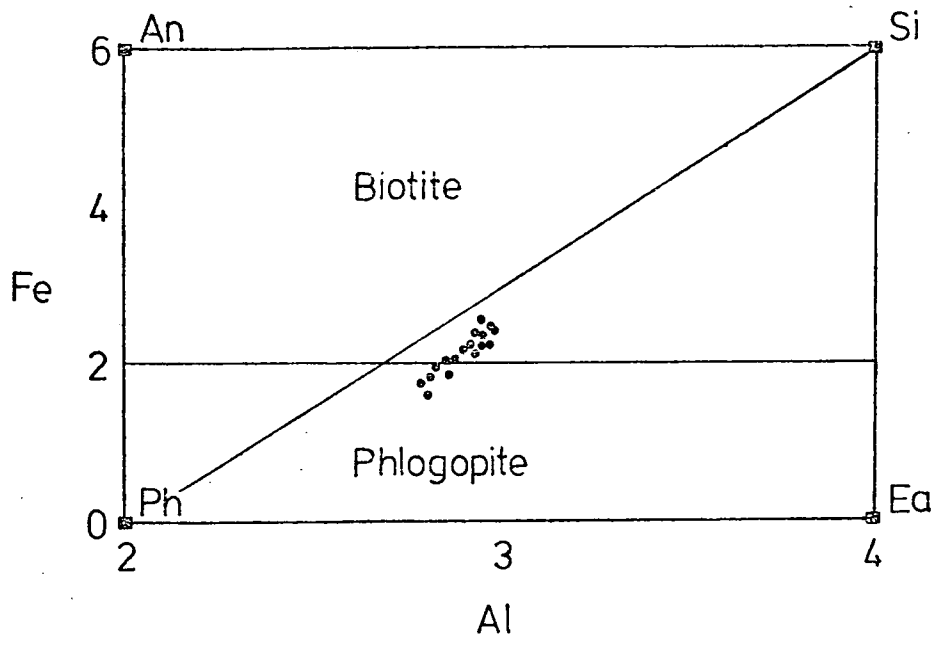
An
Si
6
4
2
0
Fe
Biotite
Phlogopite
Ph
Ea
2
3
4
Al

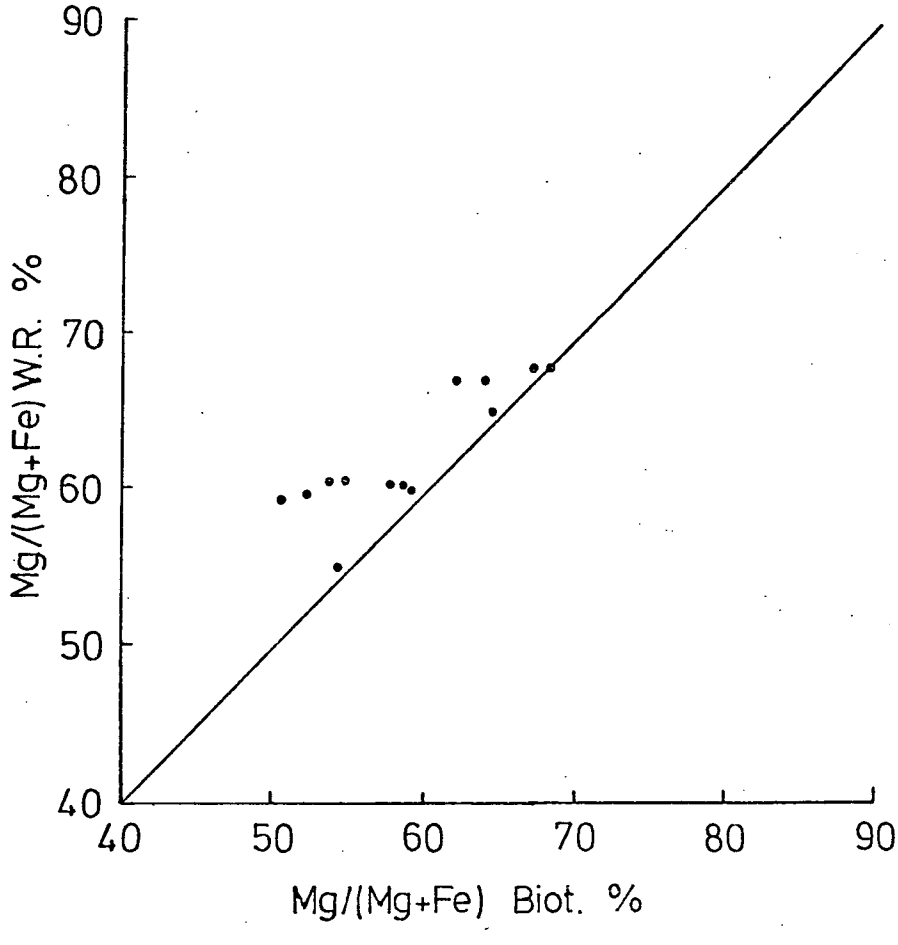
90
80
70
60
50
40
Mg/(Mg+Fe) W.R. %
40
50
60
70
80
90
Mg/(Mg+Fe) Biot. %

Other components in the biotites are minor. Ti (up to 0.19 cations/unit formula) and Mn (up to 0.038) substitute in the Y-sites, whilst Ca (up to 0.037) enters the K site. TiO_2 content is considered by Binns (1969) and Lambert (1959) to increase with grade. Binns (op.cit) quotes a value of 0.3 cations/unit formula for the greenschist facies, but the low whole-rock TiO_2 content of the Rossland volcanics most probably inhibits a value such as this from being obtained.

It can be seen in Fig. 6.8 that Mg/Fe ratio of the biotites is a strong function of whole-rock Mg/Fe ratio. Therefore, in view of the chemical coherence illustrated by Fig. 6.7, it is evident that biotite composition as a whole is largely dependent uponits chemical environment, a fact also noted by Cooper (1972) and Graham (1973). However, in Fig. 6.8 there is a tendency for those analyses which plot furthest to the left of the 1:1 line (i.e. at lower whole-rock Mg-numbers) to derive from zone B2. Biotite in this area (cf. Plate 19) is possibly retrograde, and in view of the higher temperature stability of Mg-rich biotites (pp.123-125, Turner, 1968) compared to Fe-rich biotites, a lower temperature is possibly indicated for B2. Biotite from the B1 schistose metavolcanics, though, is clearly prograde and plots at slightly higher Mg-numbers for a given whole-rock Mg-number.

6:4 Chlorite

Mode of occurrence. Chlorite, as is shown in Fig. 6.6, is distributed throughout both zones A and B, though it is generally more abundant in zone A, excepting possibly subzone B2. Chlorite abundance is generally recognised to decrease with increased grade through the greenschist facies (Cooper, 1972; Graham, 1973;

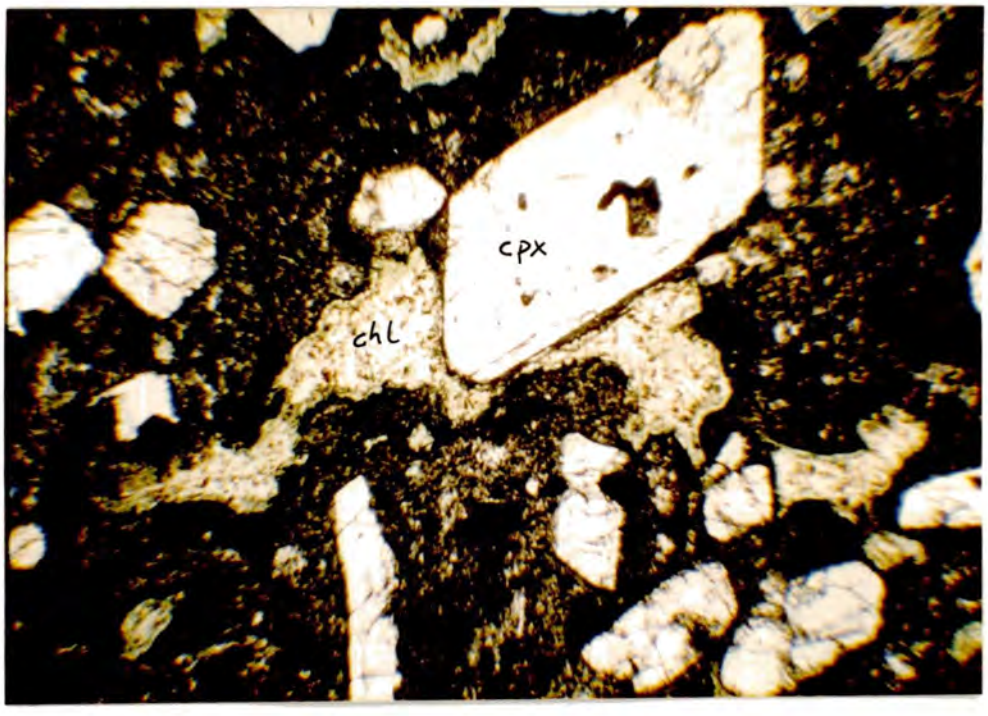

Plate 62

Photomicrograph: Basalt from zone A with somewhat rounded pyroxene phenocrysts set in a dark, turbid and fine-grained groundmass. Lobate gas cavity is filled by a flaky chloritic aggregate that is zoned outwards from a pale to a strong, green coloured variety (Sample 5036. PPL. Field width = 4 mm.).

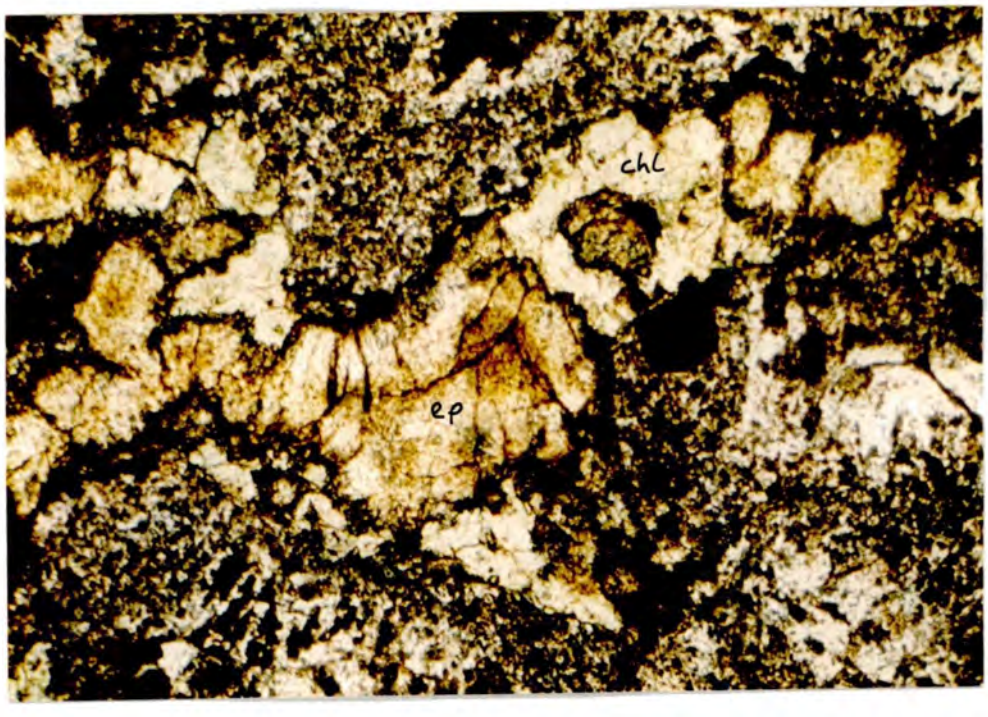

Plate 63

Photomicrograph: Cavity in zone A basalt filled with chlorite and a zoned, radiating aggregate of fine epidote.

Spinel phenocryst is also in evidence (Sample 5054. PPL. Field width = 2 mm.).

Winkler, 1974).

In zone A, chlorite is a common alteration product of mafic phases such as pyroxene and olivine (where present), as is shown by Plates 17 and 18 . It also develops commonly in gas vesicles. These are either round or form lobate amygdales (Plate 62). Amygdaloidal chlorite is often zoned, with more coloured (Fe-rich) green chlorite rimming the cavity and cored by less coloured, pale-green (Mg-rich) chlorite. Such chloritic patches are usually very fine-grained, the individual crystals occasionally being too small to see. In other cases, chlorite forms aggregates of radial sheaves(Plate 62).

Within zone B, chlorite also varies, in different rocks, form virtually colourless to pale-green or green and shows a variety of anomalous birefringence colours. Less coloured (Mg-rich) chlorites show greyish or brownish interference colours, whereas the greener (Fe-rich) chlorites exhibit dark-blue colours.

In sub-zone B2, where chlorite is especially abundant, it most characteristically develops in pressure shadows and fringing amphibole pseudomorphs. In these pressure shadows, and within the groundmass, chlorite appears as curvilinear,stringy aggregates which probably formed syn-kinematically (Plate 49). Chlorite also develops in some B2 samples as a retrogressive breakdown product of amphibole, usually associated with calcite,or less commonly epidote. As was noted above, in sub-zones B3, B4 and B5, chlorite is less common due to the absence of shearing and when it is observed it usually forms small,shapeless patches in the groundmass.

Sample 4029A (Plate 47), from B1, is conspicuous in that chlorite is well developed and with hornblende defines the rock's

schistosity. However, sample 4029B (Plate 57), that is immediately adjacent in the field to 4029A, has no chlorite, only biotite. It seems as though chlorite in 4029A is retrograde after biotite, or variations in H_2O have promoted a reaction from biotite to chlorite. This is also evidenced by the presence of chlorite in veins, or shear zones, cross-cutting the schistosity in B1 rocks; and in the presence, in sample 5075B (Plate 61), of biotitic aggregates associated with chlorite. In this latter case, the two minerals are interlayered, the chlorite obviously replacing the biotite. In the samples 4029A and 4029B, the released K_2O, resulting from the breakdown of biotite, is apparently taken up in increased sericitization of the plagioclase.

Chemistry. Fig. 6.9 shows the chlorites analysed from both zones A and B (Appendix 3) plotted in a classification diagram based on the scheme of Hey (1954). Zone B chlorites are, on average, slightly more Mg-rich (which is mainly a bulk-rock compositional effect) and Al-rich compared to zone A. Zone A chlorites plot as brungsvigites or pycnochlorites and zone B chlorites as Mg-rich ripidolites or pycnochlorites, by this scheme.

The main controlling substitution reaction in the chlorite series is:-

$$(Mg, Fe)\ Si \rightleftharpoons Al^{vi}\ Al^{iv},$$

and Fig.6.9 is based on this fact. That the chlorites as a whole obey this relation is shown by Fig. 6.10, though two analyses plot somewhat below the 'antigorite' - 'amesite' join: One (CH882) is anomalously high in TiO_2 and has a low Y-site occupancy, suggesting minor contamination, whilst the other (CH441) has an excess of Al^{vi}.

Figure 6.9

Chlorite classification diagram (after Hey, 1954): Si versus Mg and Mg-number.

TC	Talc-chlorite
Pn	Penninite
C	Clinochlore
S	Sheridanite
Di	Diabantite
P	Pycnochlorite
B	Brungsvigite
R	Ripidolite
D	Daphnite

Figure 6.10

Mg + Fe versus Al diagram (Plotted symbols as in Fig.6.9).

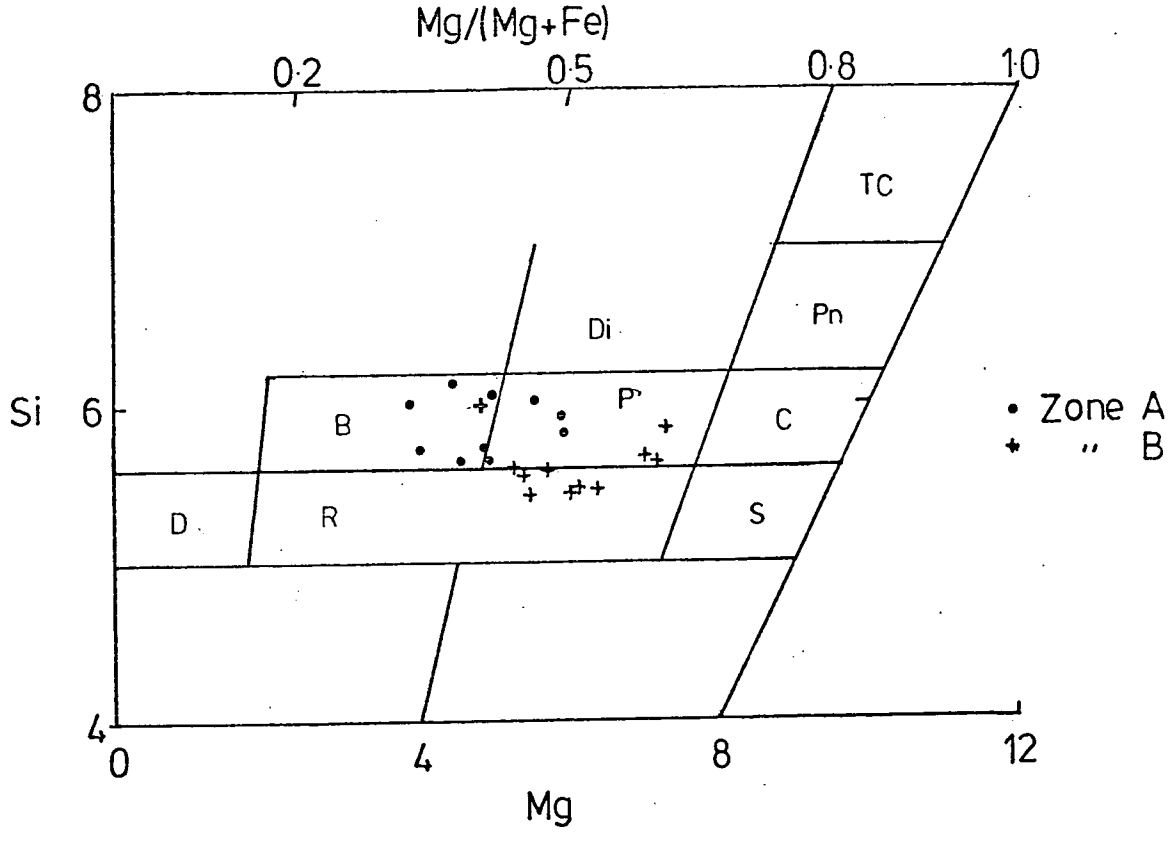
Mg/(Mg+Fe)
0·2
0·5
0·8
1·0
8
6
4
Si
0
4
8
12
Mg
TC
Pn
Di
P
B
C
D
R
S
• Zone A
+ " B

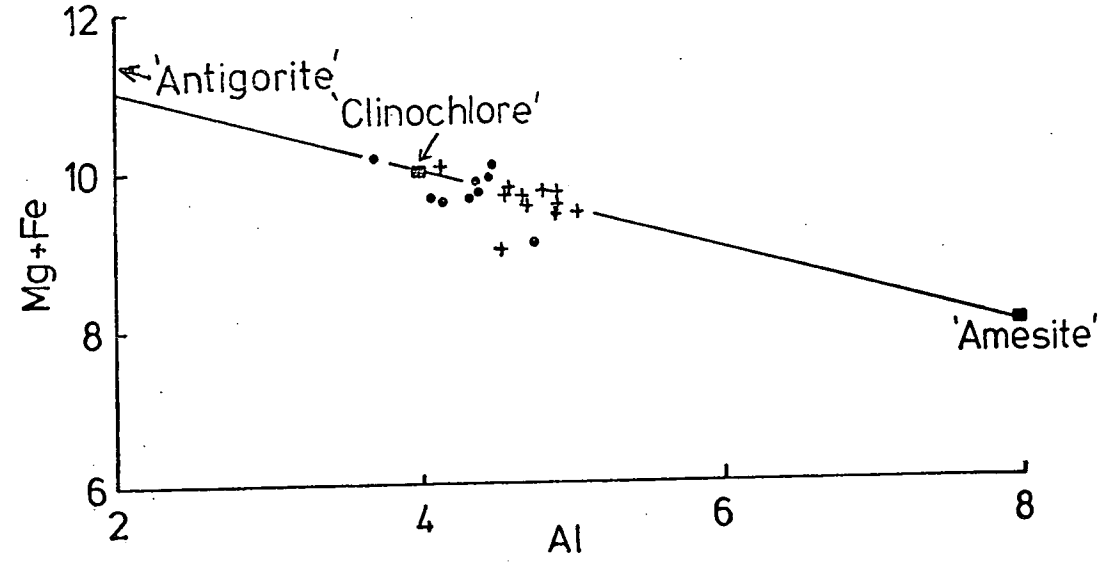
12
10
8
6
Mg+Fe
2
4
6
8
Al
'Antigorite'
'Clinochlore'
'Amesite'

Comparing Figs. 6.9 and 6.10 shows that substitution of Fe for Mg is not strongly coupled to the above substitution reaction. If anything, Mg tends to increase with Al. This is the opposite to that which occurs in the amphiboles and biotites, suggesting ionic-size controls are less effective in the chlorite case. It appears reasonable that the increased amesite (Al) content of zone B chlorites (Fig. 6.10) is due to the increased metamorphic grade, whereas the Fe-Mg differences are a function of bulk-rock compositions, as shown in Fig. 6.11. Increase of Al-content with grade is also reported by Pinsent (1976) and Kuniyoshi and Liou (1975).

Although Mg-chlorites are stable to higher temperatures than Fe-chlorites (Turnock ., 1959, 1960; Fawcett & Yoder, 1966), the chlorites analysed by Kuniyoshi & Liou (1975) show an increase of Fe/Mg with grade. In the Haast River schists, Mg/Fe in chlorite increases with grade. This appears to emphasize the effect of whole-rock chemistry in controlling chlorite Mg/Fe, an effect also noted by Graham (1973).

6:5 Epidote

Mode of occurrence. Epidote minerals occur throughout zones A and B, but are better developed and generally more common in zone B, though are not present in all samples (Fig. 6.12).

Within zone A, epidotes are usually fine-grained, forming small aggregates of less than 0.1 mm. (cf. Plate 45). Apart from small aggregates such as these, which are developed essentially in the groundmass, epidote is also developed associated with chlorite in gas-cavity fillings. Here, epidote occurs as small granules, rimming the amygdale or as small, well-formed prisms. Another habit of epidote in this situation is shown in Plate 63 , where

Figure 6.11

Chlorite versus whole-rock Mg-number correlation plot. (Symbols as in Fig.6.9).

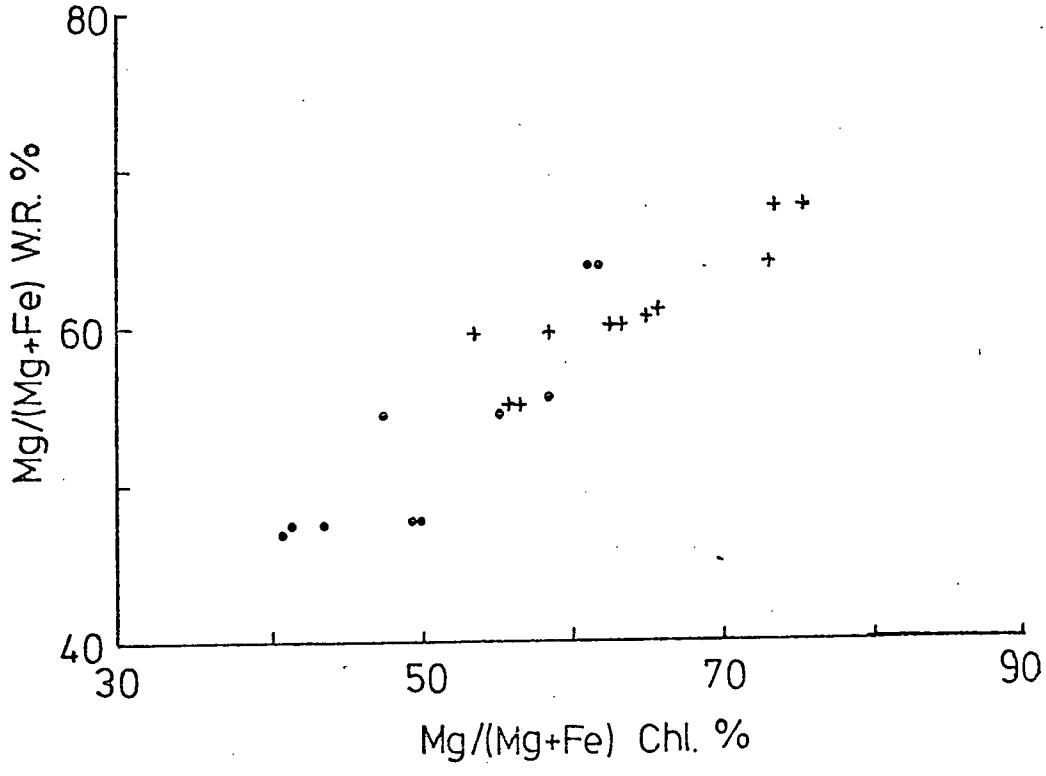
80
60
40
30
50
70
90
Mg/(Mg+Fe) W.R. %
Mg/(Mg+Fe) Chl. %

Figure 6.12

Distribution of epidote in the Rossland volcanics. Zones A and B are as defined in Fig.6.1.

Also shown is the distribution of Mesozoic and Cenozoic plutonic rocks.

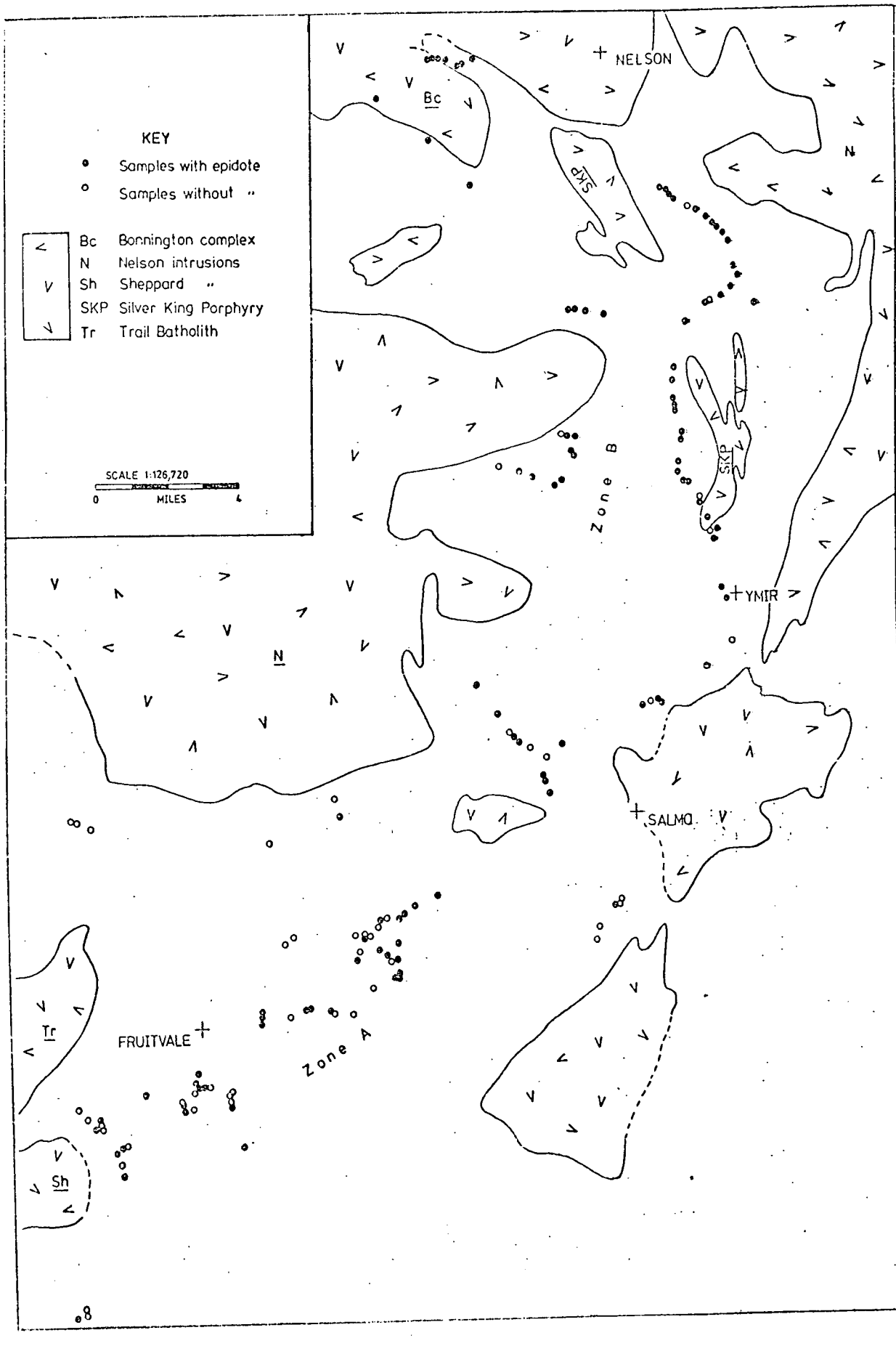
KEY
Samples with epidote
Samples without "
Bc Bonnington complex
N Nelson intrusions
Sh Sheppard "
SKP Silver King Porphyry
Tr Trail Batholith
SCALE 1:126,720
0 MILES 4
NELSON
Bc
SKP
N
Zone B
YMIR
SALMO
Tr
FRUITVALE
Zone A
Sh
8

it forms radiating aggregates. Plate 32 shows epidote associated with calcite as well-formed laths or prisms set in a turbid chloritic pool.

Fine saussuritic epidote is also responsible, in part, for the cloudy, inclusion-ridden alteration of plagioclase feldspar. Individual crystals, in these cases, are too fine to identify definitely, but the high relief of these small inclusions suggest an epidote mineral (although pumpellyite may be a contributing phase).

Usually, epidotes in Zone A are pistacite rich, as judged from birefringence colours. An exception (see below) is the epidote shown in Plate 32 (5001B) which is clinozoisite-rich.

Zone B epidotes occur most prominently as porphyroblastic or granoblastic aggregates containing several well-formed crystals (Plate 64), and which occasionally represent pseudomorphs (cf. Plate 65). Samples 5516A and B contain particularly well-developed and abundant epidotes of this nature, either in calcitic veins (Plate 51) or growing within the groundmass or amphibole pseudomorphs. The epidotes in Plate 51 reach 2 mm. in diameter.

Less conspicuously, but more commonly, epidote is smaller and more ragged or granular in appearance, and forms dusty aggregates, occasionally after olivine (Plate 19).

In colour, generally, epidote varies from relatively colourless to distinctly pleochroic, yellow varieties. There is a corresponding increase in birefringence from first or second order, or sometimes anomalous colours, to third and fourth order colours. Within a single grain, birefringence is characteristically quite variable and often a slight zonation is apparent from high-order cores to a rim of lower order. This represents a decrease of Fe^{3+} outwards and is a common feature, reported by Graham (1973) and Cooper (1972).

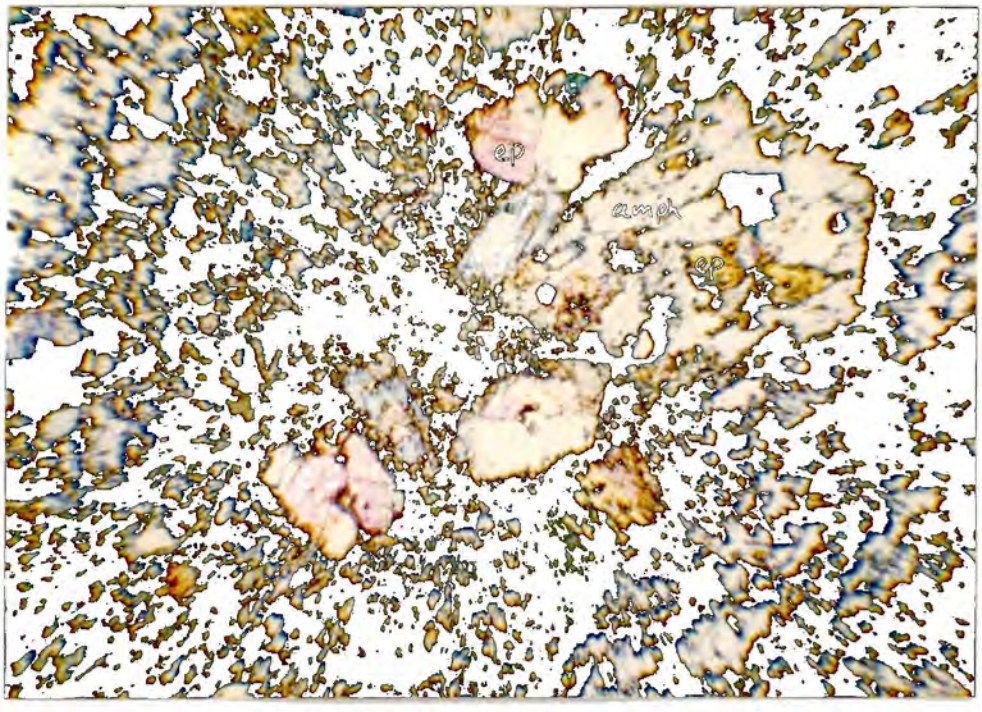

Plate 64

Photomicrograph: Porphyroblastic aggregates of epidote in Zone B basalt. Some possibly pseudomorphing olivine. Poikiloblastic epidote is also apparent within actinolite pseudomorphs (Sample 4044. XP. Field width = 4 mm.).

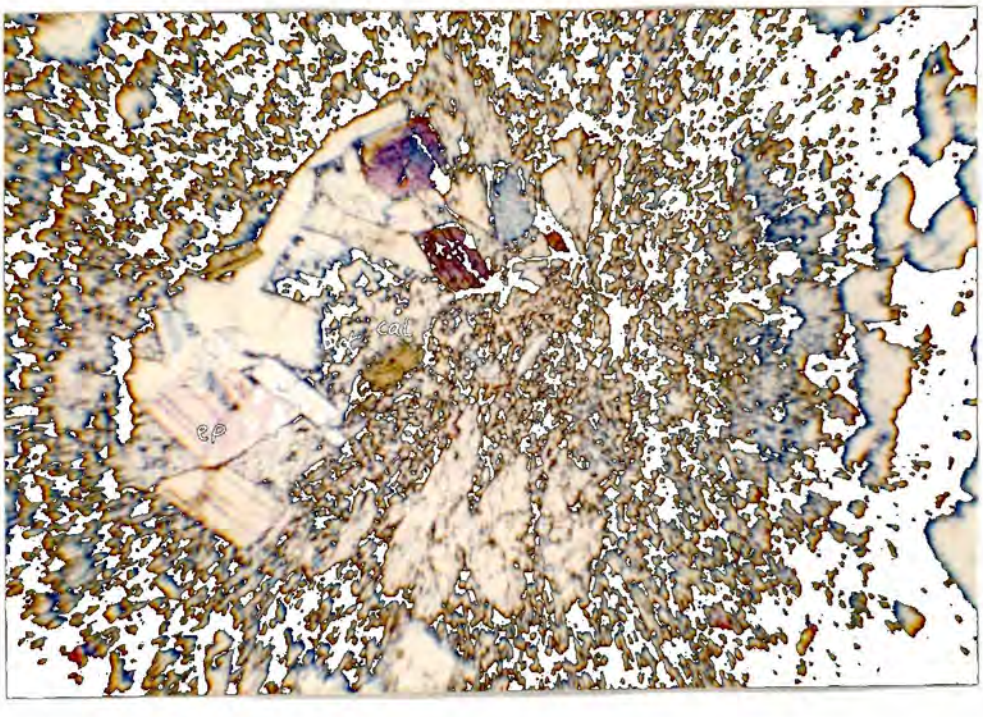

Plate 65

Photomicrograph: Aggregate of coarse, well-formed epidote associated with finer grained calcite and biotite. Possibly a composite pseudomorph after olivine or pyroxene. (Sample 5530A. XP. Field width = 4 mm.).

This zonation is not necessarily a prograde chemical change, but may result from the kinetics of crystal growth, whereby Fe^{3+} is rapidly taken up initially, depleting the immediate surrounds of the crystal (Graham, 1973).

Chemistry. Variation in the epidote series is simply a result of the substitution:-

$$Fe^{3+} \rightleftharpoons Al,$$

this rarely exceeding a value of 1 Fe^{3+} cation in the basic zoisite formula (i.e. Ps = 33%).

The distinction between epidote and clinozoisite is somewhat arbitrary, though Deer et al. (1962) indicate a value of Ps = 15%, above which 2V about Z exceeds 90^{o}. Holdaway (1972) regards Ps = 10% as a subdivision. By either of these schemes, the epidotes analysed here are not 'clinozoisite', the Ps range being from 14.5 to 32 per cent. Zoisite (Ps < 3%) has not been observed.

Variation of epidote composition with temperature is complex. Miyashiro & Seki (1958) noted that with increased grade the compositional range of epidote was extended from Ps near to 33 per cent at low temperature, to encompass more Al-rich clinozoisitic varieties at higher temperatures. Similarly, Kuniyoshi & Liou (1976) observed a slight decrease in Ps content from around 30 at prehnite-pumpellyite facies to about 26 at epidote - amphibolite facies. Holdaway (1965) documents somewhat more complex variation with grade: At the chlorite zone (greenschist facies) he reports a compositional gap between Ps = 16 and Ps = 29. At slightly higher grade, only Ps of greater contents than 20 per cent occurs, and finally, at epidote-amphibolite facies, the epidotes all contain Ps of less than 22 per cent. These relations possibly suggest the

presence of a solvus as proposed by Strens (1965), though it is probably asymmetrical with the apex at about Ps = 22 per cent as suggested by Holdaway (1972). Thus, the compositional gap near the top of the solvus involves Ps contents higher than those lower down.

Though the presence of a solvus explains the increased spread of compositions at higher temperatures, it does not explain the actual shifting of composition away from high Ps values as reported, and noted above, by Kuniyoshi & Liou (1976) and Holdaway (1965). On the contrary, as Liou (1973) and Holdaway (1972) show, Fe-rich epidote is thermally more stable than clinozoisite, both at high and low temperature, given suitably high f_{O_2}. Thus, where all epidotes tend towards clinozoisite as temperature increases, it is likely this is due to decreasing f_{O_2}. This is seen in the data of Cooper (1972), where oligoclase-zone, amphibolite facies epidotes, although only containing Ps contents of 17 per cent compared to biotite-zone, greenschist facies epidotes with Ps = 28-30 per cent, occur in much less oxidised rocks. That is, there is a direct correlation between Ps content and whole-rock oxidation ratio.

Epidotes analysed here are plotted in Fig. 6.13, a plot of Ps% versus whole-rock $Fe^*/(Fe^* + Al)$. There is a slight correlation, as might be expected. However, what is important, as suggested in the previous paragraph, is Fe^{3+}/Al and not Fe^*/Al in the rock. Where the samples probed have been analysed for FeO wet chemically, as well as for Fe_2O_3 by XRF (Appendix 2), oxidation ratio is indicated in Fig. 6.13. Also shown, is the presence of coexisting magnetite, which as Holdaway (1972) notes, represents excess Fe^{3+} and means epidote composition is a function of f_{O_2} only. Thus, the relationship between f_{O_2} and Ps% is apparent in the Rossland

Figure 6.13

Whole-rock Fe/(Fe + Al) versus Ps% in epidote. Underlined symbols indicate epidote coexists with magnetite. Numbers adjacent to some points are the $Fe_2O_3/(Fe_2O_3 + FeO)$ ratios of the host rocks.

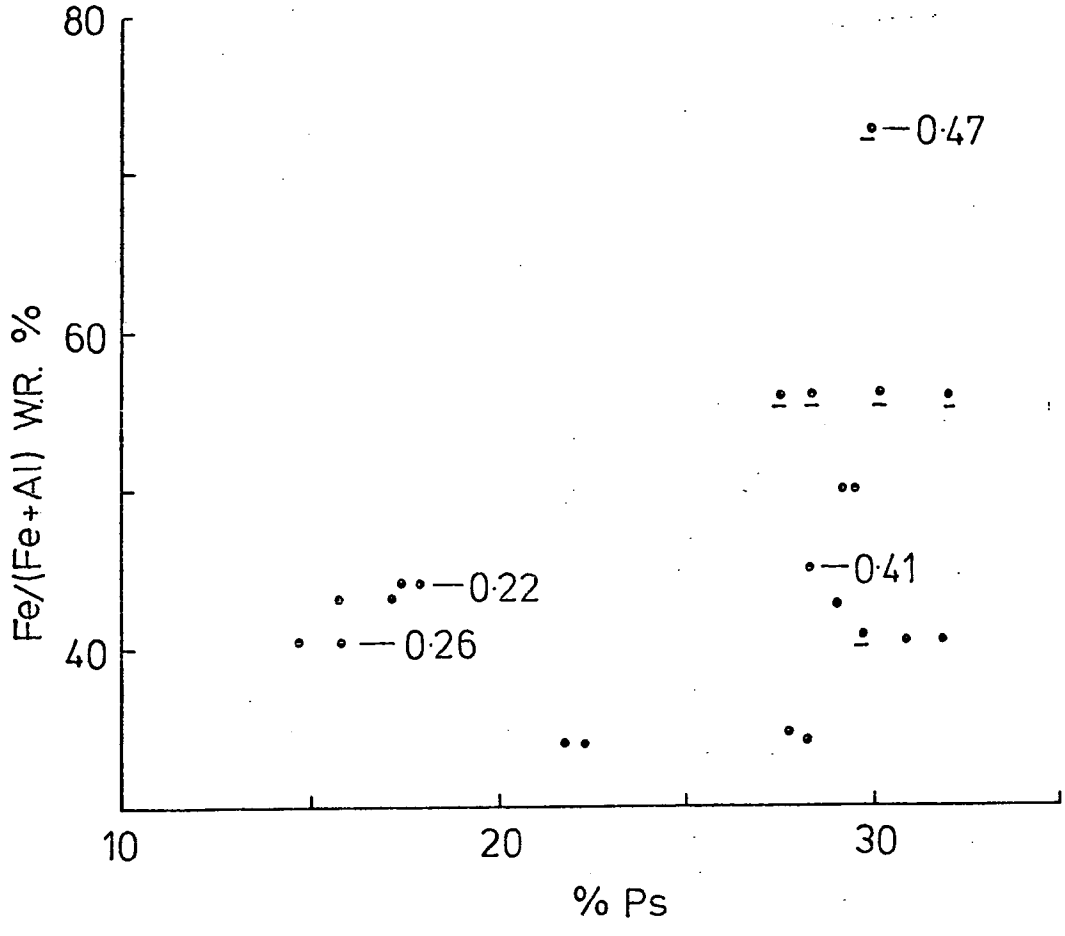
80
60
40
Fe/(Fe+Al) W.R. %
10
20
30
% Ps
0·47
0·41
0·22
0·26

data. In addition, there is no reason to suppose zone B (representing higher grade) has epidotes lower in Ps than zone A. That is, given sufficiently high f_{O_2}, Ps-rich epidotes are stable into the upper greenschist facies (zone B - samples 5075B, 5516A, for example).

On the basis of Liou's (1973) paper, a Ps content of 33 per cent appears at a f_{O_2} value near the HM buffer, whilst Ps = 25 per cent is produced at the QFM buffer. Samples 5088 and 5530A, whose epidotes are low in Ps (EP88, EP0A, Appendix 3), notably do not contain magnetite, but sulphides, indicating a lower f_{O_2}. Samples 5075B and 5516B, containing magnetite and Ps-rich epidotes (EP5B, EP16B), probably had a f_{O2} somewhere between QFM and HM.

The data in Fig. 6.13 suggest a compositional gap may lie between Ps = 22 and Ps = 28 per cent, and possibly the solvus referred to above was operative. Strens (1965) suggested the epidote solvus closed at about 550°C. Also a compositional gap of about 22 to 26 (Ps%) is apparent in the data of Cooper (1972) and Brown (1967) for similar grade (greenschist facies) rocks of the Southern Alps.

6:6 Feldspar

Mode of occurrence. Zone A feldspar was described briefly in Chapter 4, since it occasionally occurs with relict patches of clear primary plagioclase. Otherwise, the extreme clouding of the phenocrysts (cf. Plates 43 , 45) by sericitic and saussuritic alteration, or by carbonates, makes the determination of composition, optically and by microprobe, extremely difficult. X-ray diffractometer runs of feldspar separates from two samples, however, show the feldspar to be generally in the low structural state, by using the peak-separation curves of Smith (1956) and Smith & Gay (1956). The

altered feldspar in these rocks is, therefore, probably albite. Relatively coarse and clear patches of albite were observed in one sample (5038), associated with quartz and epidote. Generally, though, secondary feldspar only occurs replacing primary feldspar in zone A, and does not cause destruction of igneous textures.

Feldspar in zone B assumes, essentially, two common habits. Most frequently, metamorphic plagioclase has replaced igneous plagioclase occurring as lath-like phenocrysts. In sub-zone B2 the plagioclase is usually albite (e.g. Plate 49), whereas in samples (e.g. 5116, 5049) from B4 the composition is more anorthitic. Invariably, lath-like plagioclase contains inclusions of either epidotic minerals or, less commonly, actinolite needles. Compared to zone A, however, the plagioclases are generally much clearer except where retrograde development of sericite has occurred.

Apart from assuming igneous textures, plagioclase also develops as recrystallized aggregates showing no crystal form at all. These aggregates are particularly common in the sheared and shattered rocks of B2. Plates 66 and 67 show albite feldspar aggregates forming in pressure shadows. These show rather dusty interiors and uneven extinction. Similar albitite aggregates occur in undeformed vesicles in samples from B3 (e.g. 5516A, 4105A).

In zone B1, where metamorphic recrystallization has been severe, no laths of relict igneous habit exist. All the feldspar forms a granular mosaic as shown in Plate 47 . This plagioclase is generally quite clear except where some sericitization has developed.

K-feldspar is also rarely observed. Where it is identified, it usually forms very small, clear grains or aggregates associated with albite.

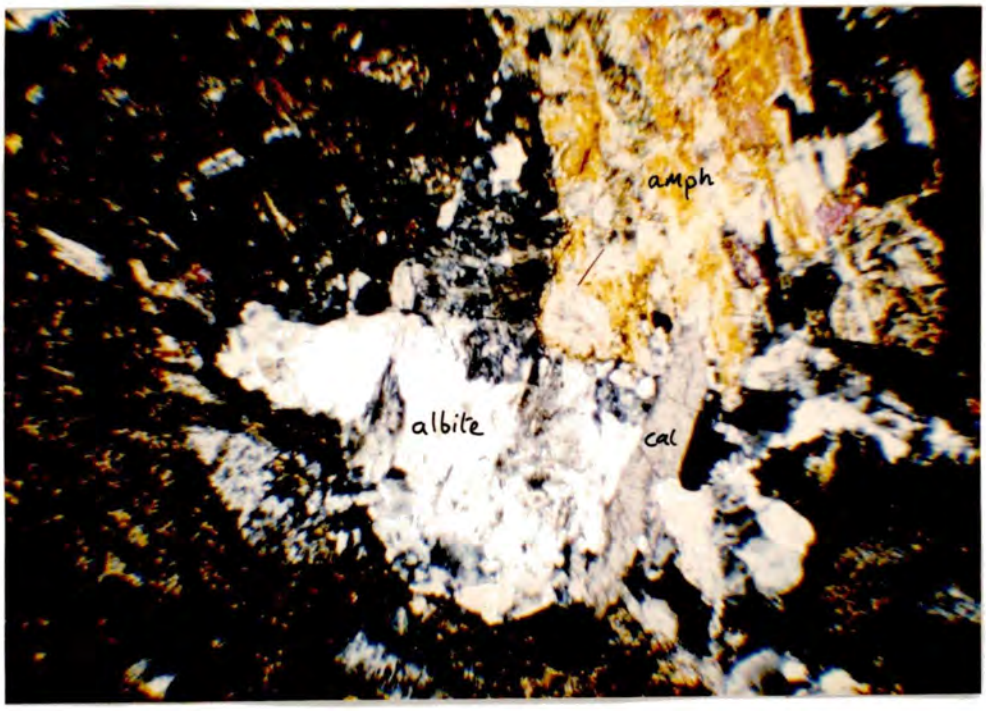

Plate 66

Photomicrograph: Sub-zone B2 sample showing the development of albitic aggregates, partly pseudomorphing amphibole, and partly developed in a pressure shadow. Calcite is also present associated with albite (Sample 5530A. XP. Field width = 4 mm.).

Plate 67

Photomicrograph: Calcite + albite aggregates resulting from shearing in sub-zone B2 (Sample 5538A. XP. Field width = 4 mm.).

Chemistry. Plagioclase composition in the greenschist and lower amphibolite facies is, as is well known, controlled at the Na-rich end of the spectrum by the peristerite solvus. Generally, albite is believed characteristic of the greenschist facies, whereas with increased grade a jump in plagioclase composition from about An_5 to An_{17} occurs (Winkler, 1974). The reason for this change is the tendency for epidote to react with albite to form a more calcic plagioclase. This type of reaction, however, appears to vary with pressure. As Graham (1973, 1974) and Winkler (1974) suggest, albite persists to higher grade (amphibolite) at high P, whereas at lower P, for example during contact metamorphism (Kuniyoshi & Liou, 1976), albite readily transforms to oligoclase at about the temperature that actinolite goes to form hornblende.

In general, within the Rossland zone B area, the occurrence of Al-rich hornblende in sub-zones B1 and B4 is associated with a plagioclase more anorthithite than An_{17}; for example, samples 4029A, 4029B (B1) and 5049, 5116 (B4). On the opposite side of the peristerite solvus, albite in sub-zones B2 and B3 tends to be associated with actinolitic hornblende (e.g. 5538B, 4105A), Exceptions to this occur, as pointed out in Chapter 7, but nevertheless, this would seem to indicate that low pressures . . . occurred during the Rossland metamorphism, in contrast to the Dalradian Barrovian metamorphism, for example, where albite persists in metabasites well up into the garnet-zone Amphibolite facies (Graham, 1973). This agrees with other evidence, such as the Na(M4) contents of the amphiboles (Section 6.2).

Analysis of albite (Appendix 3) show An content varies from less than one per cent to about 5 per cent, whereas the higher grade plagioclase compositions of B1 and B4 have An contents ranging from 17 to 60 per cent.

Three K-feldspar analyses are also tabulated in Appendix 3. Two are from 5538B and have Ab contents of less than 3 per cent, whereas one from 4007 has an Ab content of 11 per cent.

6:7 Opaque Minerals

It was shown in Chapter 4 that within zone A , relict Ti-magnetite is present in some samples, but that in others primary spinels have altered to sulphides or indeterminate, turbid aggregates of alteration products, possibly iron hydroxides and sphene. In zone B, no relict igneous spinel has been identified. Here, it has either vanished during metamorphic recrystallization, or it has formed sulphides. Where fresh magnetite is apparent, it is compositionally adjusted to metamorphic conditions. Analyses of magnetite (Appendix 3) show it is virtually pure Fe_3O_4 with very little Ti or Al.

Magnetite is observed in sub-zones B1 (5075B, 5077), B3 (5516A, B, 4105A) and B4 (4013A), whereas in B2,sulphides tend to develop, particularly in the sheared rocks near to the Silver King porphyry.

Examples of magnetite are seen in Plates 20 and 21 , where they form small inclusions in pseudomorphic amphibole or rounded crystals in the groundmass. In these cases they probably represent pseudomorphs after primary spinel.

Sulphides, pyrite or chalcopyrite, usually form ragged patches that may have developed over primary spinel, but equally are likely to be new growths. Occasionally they form conspicuous clusters of well-formed cubic minerals, easily visible in hand specimen; and, as noted, form particularly near the outcrop of the Silver King Porphyry (unit 8d in Fig.1.1) which, as Mulligan (1952) observes, appeared to be a locus or cause of mineralization.

Haematite is occasionally observed forming translucent, red rims to magnetite. It seems likely that f_{O_2} varied considerably during the alteration history of the volcanics.

6:8 Carbonate

Carbonate is a prolific phase in the volcanics, occurring in both zones. In zone A it is locally abundant, typically forming in cavities (Plates 23 , 32). Alternatively, it forms as a breakdown product of plagioclase,sometimes replacing it completely. Carbonate also pseudomorphs olivine (Plate 18) and occasionally pyroxene, sometimes together with chlorite. It is curious that in some samples,pyroxene can be both totally fresh or totally replaced by carbonate - an example is shown in Plate 38B . Another characteristic habit of carbonate, as noted in Chapter 3, is its formation as a cement or matrix in volcaniclastic rocks (Plate 11). Zone A carbonate is apparently all calcite. The presence of dolomite or ankerite was tested for by a qualitative determination of Fe and Mg with the microprobe, and by examination of X-ray diffraction patterns of several samples.

In zone B, calcite is again the only carbonate observed, or detected, and in general it is less abundant. As noted in Section 6:1, calcite (with chlorite) is most abundant in zone B2. Here it can form as aggregates in veins and cavities, associated with either albite (Plate 66), biotite, epidote (Plate 65) or chlorite. Where calcite replaces amphibole in a retrogressive manner, it is usually associated with chlorite (cf. Plate 50).

In the other B sub-zones calcite is generally less abundant, although in B3 it can be common in a few veined or vesicular samples,

(Plate 51). The presence of carbonate, as is the case with chlorite, is aided by the creation of spece during shearing or brittle fracturing.

6:9 Accessory and other minerals

Apart from the minerals described above, others appear occurring only in small amounts, or, whilst being quite common, are low in abundance and fine-grained. These include quartz, prehnite, apatite, muscovite and sphene.

Due to the basic nature of the volcanics, free quartz is never very abundant - invariably much less than 1%. It also occurs as very small crystals in the groundmass or associated with epidotic veins and patches. Sometimes, small quartz crystals can be observed included poikiloblastically in amphibole.

Prehnite occurs sporadically in zone A rocks, but not zone B, principally as a vesicle filling but possibly also as an alteration product of feldspar, though in this case it is generally far too fine-grained to identify optically. As a cavity filling, prehnite occurs as aggregates of radial sheaves. It is colourless with moderate (2nd order) polarization colours. Invariably, prehnite in this mode is surrounded by chlorite of a similar habit, though this mineral is green and shows anomalous or first-order polarization colours (Plate 30).

Two analyses of prehnite from sample 5063, where it is well-developed, are tabulated in Appendix 3. These compare very closely with prehnites from the Karmutsen Group, Vancouver Island, reported by Surdam (1969) and Kuniyoshi & Liou (1974, 1976).

The presence of apatite, presumably of igneous origin, was reported in Section 4:1:1 from zone A. Apatite is also apparent in zone B, where it similarly occurs included in pyroxene

(amphibole pseudomorphs), or independently in the groundmass, as sub-euhedra of up to 0.5 mm. In one sample, a prism of apatite was observed, enclosed by amphibole, which reached 1 mm. in length. Plate 36 shows a rounded apatite crystal in sample 748. Apatite in zone B is probably a relict igneous phase.

Sphene is a commonly reported accessory phase in metabasites (e.g. Kuniyoshi & Liou, 1976; Graham, 1973; Smith, 1969; Floyd, 1976), where it evolves due to the release of TiO_2 when titaniferous igneous minerals (augite, magnetite, ilmenite) breakdown. Similarly, in the Rossland volcanics sphene is present as minute granules scattered in the groundmass or included in amphibole. Plate 61 shows an occurrence of fine, granular sphene rimming a Ti-free magnetite.

Muscovite, in the form of sericite, is quite a commonly occurring phase, especially in zone A where it replaces primary feldspar (cf. Plate 17). Within zone B it is less common and where it does occur, it is a retrograde alteration product. A localised area between zones B2 and B3 (samples 5519, 5520, 5521) is particularly rich in sericite, and coarse muscovite is occasionally seen in veins, associated with calcite and chlorite. Coarse muscovite is also a characteristic mineral replacing feldspar in the Silver King porphyry rocks (unit 8d in Fig.1.1).

6:10 Fe-Mg partitioning between phases

A frequently used test for equilibrium amongst mineral assemblages is to consider the distribution of elements between pairs of minerals. (e.g. Cooper, 1972; Saxena, 1969; Ernst et al., 1970). A distribution coefficient, K_D , is defined thus:

$$(6:1) \qquad K_D{}_A^{\alpha-\beta} = \frac{X_A^{\alpha}\,(1 - X_A^{\beta})}{X_A^{\beta}\,(1 - X_A^{\alpha})}$$

where X_A^{α} is the atomic fraction of element A in phase α. For a given temperature and pressure, it would be expected that minerals in equilibrium should define a line when the denominator of equation 6:1 is plotted against the numerator. Ideally, this should be a straight line originating at zero.

If the ion-exchange reaction;

$$Fe_{\alpha} + Mg_{\beta} \rightleftharpoons Fe_{\beta} + Mg_{\alpha},$$

is considered, then equation 6:1 would reduce to:

(6:2) $K_{D\ Mg/Fe}^{\alpha-\beta} = (Mg/Fe)_{\alpha} \times (Fe/Mg)_{\beta}$

That is, $X_{Mg} = Mg/(Mg + Fe)$.

Using equation 6:2, plots of coexisting chlorite-biotite, chlorite-amphibole and biotite-amphibole pairs have been produced.

6:10:1 Chlorite-Biotite

It is evident from Fig.6.14A that the few samples analysed with coexisting chlorite and biotite plot along a straight line, nearly, with a K_D value of 1.33. It is reasonable to assume that equilibrium was more or less attained. A best-fit straight line, however, does not pass through the origin but rather, at high Mg/Fe, chlorite is preferentially enriched in Mg relative to biotite. This effect is only slight and may not be significant.

Good coherence between biotite and chlorite is also observed by Cooper (1972), though he used equation 6:1 above. Cooper (op.cit) also notes an increase in K_D with increased grade, due to a tendency, noted in Section 6:4, for Mg/Fe to increase in chlorite with increased grade, whereas biotites do not show this feature. The somewhat differing behaviour of chlorite and biotite chemistry, pointed out in Section 6:4, may be the cause of the slight deviation in Fig.6.14A referred to in the previous paragraph.

Figure 6.14

(A) Mg/Fe distribution between chlorite and biotite (K_D as defined in equation 6.2 in the text).

(B) Mg/Fe distribution between chlorite and amphibole.

(C) Mg/Fe distribution between biotite and amphibole. (Some samples numbered where referred to in text).

(D) Fe distribution between biotite and amphibole (K_D defined by equation 6.1 in text).

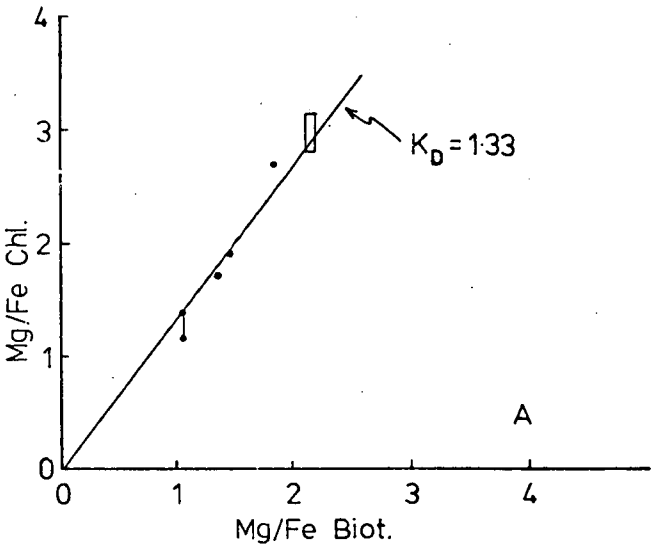
Mg/Fe Chl.
Mg/Fe Biot.
$K_D = 1{\cdot}33$
A

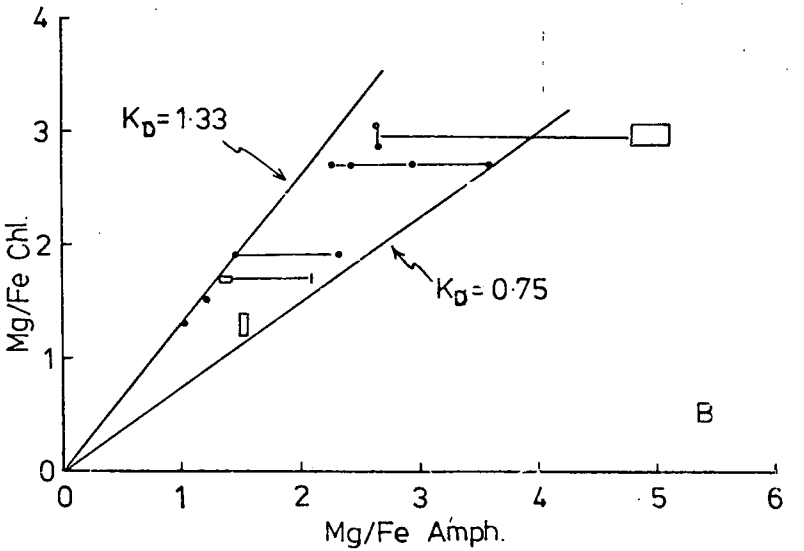
Mg/Fe Chl.
Mg/Fe Amph.
$K_D = 1{\cdot}33$
$K_D = 0{\cdot}75$
B

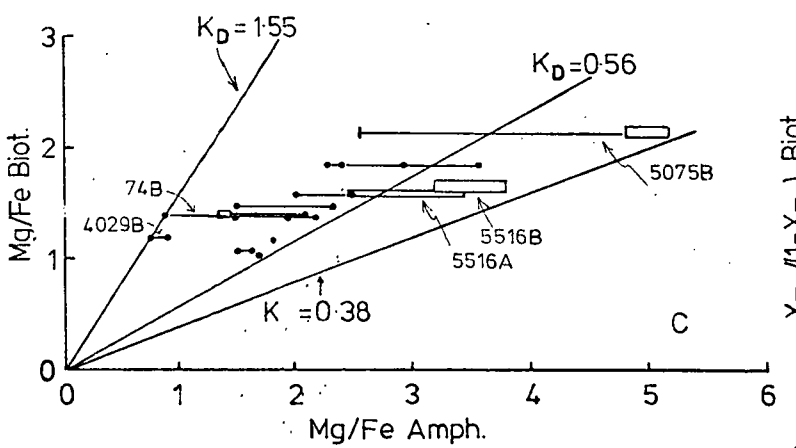
Mg/Fe Biot.
Mg/Fe Amph.
$K_D = 1{\cdot}55$
$K_D = 0{\cdot}56$
74B
4029B
5075B
5516B
5516A
K = 0·38
C

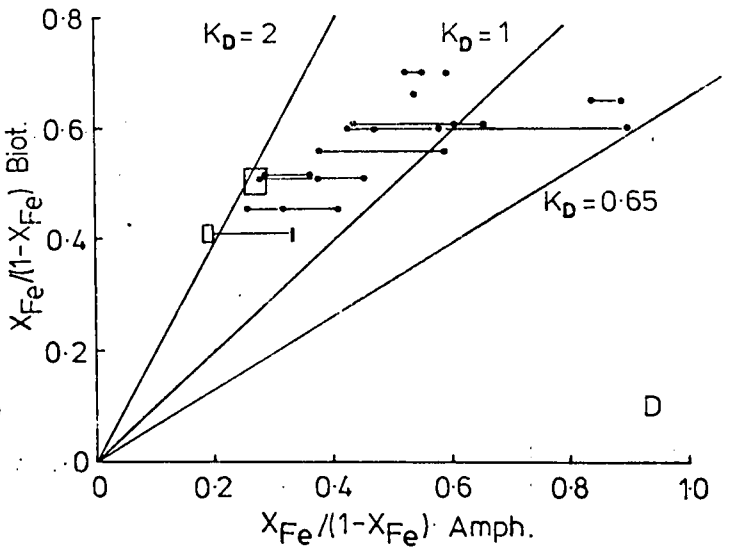
$X_{Fe}/(1-X_{Fe})$ Biot.
$X_{Fe}/(1-X_{Fe})$ Amph.
$K_D = 2$
$K_D = 1$
$K_D = 0{\cdot}65$
D

6:10:2 Chlorite-Amphibole

Clearly (Fig. 6.14B), this mineral pair behaves somewhat differently to chlorite-biotite, although a broad positive correlation through zero is evident. The reason for the scatter is due to the variable amphibole composition, thought in part to reflect disequilibrium (Section 4:2). The tendency for hornblende to have higher Fe/Mg ratios than coexisting chlorite, whereas actinolite has a lower ratio, is a fact also reported by Graham (1973, 1974), Hietanen (1974) and Cooper (1972). This reflects the non-ideal mixing between the M1, M2 and M3 sites, which in turn reflects the variable amounts of Al^{vi}. Also, Fe^{3+} is effective in introducing deviations from a straight line in Fig. 6.14B. If ideal mixing takes place between the M1, M2 and M3 sites, Mg/Fe would not vary, though X_{Mg} would decrease (i.e. $Mg/(Mg + Fe + Al^{vi})$). Alternatively, if Al only replaced Mg in the M2 site, Mg/Fe would decrease, as it does, and so would X_{Mg}. However, in this latter case X_{Fe} would remain constant. As Cooper (1972) shows, X_{Fe} in fact increases as Al^{vi} increases, which reflects Fe^{3+} incorporation concurrently with Al^{vi}. This effect is also evident in Fig.6.14D, which shows X_{Fe} variation in amphibole, but relative to biotite. As Graham (1973) notes, using Fe/Mg ratios in complex minerals -like amphibole in which other elements interfere - to demonstrate equilibrium or disequilibrium is not easy.

However, K_D values shown in Fig. 6.14B are comparable to those quoted by Hietanen (1974) for greenschist facies, of 0.7 to 1.2, with one value of $K_D = 1.9$ near a granite contact. Probably, therefore, equilibrium between amphibole and chlorite is not far from the truth, except perhaps in the case of 5075B (Fig.6.14B), where the Mg-rich amphiboles plot at very low K_D.

6:10:3 Biotite-Amphibole

The behaviour of this mineral pair is similar to that of chlorite-amphibole. There is, however, an apparent bulk shift of K_D as Mg/Fe varies (Fig. 6.14C), rather than a scattered correlation originating at zero. The most Fe-rich amphiboles have K_D values up to 1.55 (samples 4029B, 74B), whereas the most Mg-rich amphiboles (5075B, 5516B) produce K_D values near to 0.4. That samples 4029B, 74B and 5075B all come from sub-zone B1 indicates a degree of disequilibrium, particularly, as noted in Section 6:9:3, with regard to 5075B. By comparison, Choudhuri (1974) reports K_D values for this mineral pair between about 1.50 and 1.00 in rocks of upper greenschist to hornblende-hornfels facies. Fig.6.14D, which is plotted with regard to equation 6.1 above, and for the element Fe only, shows a similar distribution of points as Fig.6.14C. Using K_D as defined in Fig. 6.14D, Cooper (1972) reports values of 1.61 at the biotite-zone (greenschist facies) and 0.77 at the oligoclase-zone (amphibolite facies). That K_D values for the bulk of the Rossland samples are similar to these other examples, suggests equilibrium was on average attained, but the more extreme samples (see Fig.6.14C) that give K_D values more or less than other reported examples probably represent localised disequilibrium, or possibly temperature differences. The samples 5516A, 5516B and 4105A, particularly, indicate disequilibrium since they all occur within a localised area (see Fig.1.1) and contain biotites of constant composition. Sample 4029B, alternatively, may reflect a higher temperature of equilibration, though since its K_D is so different from the bulk of the other samples, this is unlikely to be wholly the case.

Another possible cause of variation in K_D is pressure. Hietanen (1971) considered that the difference between K_D values of 0.65 and 0.8 (cf. equation 6:2) for amphibole-biotite pairs in diorites, reflected a pressure difference of greater than 1 Kb, higher pressures favouring lower K_D. But in the Rossland case the complexity of the data does not allow resolution of this sort.

CHAPTER 7

METAMORPHISM OF THE ROSSLAND VOLCANIC ROCKS

In the first part of this chapter, discussion is centred around the conditions of metamorphism, namely T, P and X_{CO_2}, as deduced from the nature of the secondary mineral assemblages developed. The latter part of the chapter deals with the causes of the metamorphism and the relation of the volcanics to the regional metamorphic picture.

7:1 Conditions of metamorphism

7:1:1 Zone A

The characteristic mineral assemblage in this zone is:

Chlorite + Calcite + Albite + Epidote ± Prehnite. (1)

Other phases include sericite, sulphides and possibly secondary quartz. Also, in view of the presence of prehnite, the mineral pumpellyite may be present (cf. Coombs, 1960), although it has not been positively identified. Pumpellyite, where it is reported (e.g. Jolly, 1970; Jolly & Smith, 1972), typically occurs as a cavity filling or as an alteration product after plagioclase. In zone A samples, pumpellyite has not been observed as a cavity filling, whereas chlorite, calcite, epidote and prehnite have. However, plagioclase (Section 6:5) is commonly altered to fine, high-relief alteration products that may include pumpellyite. X-ray diffractometer runs of various samples, split gravitationally and magnetically, gave inconclusive results; the problem being that due to the minor amounts of pumpellyite, if it existed, its peaks are swamped by chlorite, calcite and feldspar peaks. Other reasons could account for the absence or very low abundance of pumpellyite, such as low pressure or high X_{CO_2}.

The assemblage (1), defined above, by virtue of the lack of zeolites or actinolite, places zone A in the prehnite-pumpellyite metagreywacke facies (Turner, 1968) or the very-low-grade zone of Winkler (1974). Similar mineral assemblages are reported by Smith (1969), Levi (1969) and Kuniyoshi & Liou (1974) in burial metamorphosed sequences of volcanics and sediments. Assemblage (1) compares well with descriptions of zones 1 and 2 of the New South Wales sequence described by Smith (1969). Here, pumpellyite is apparently absent due to temperatures and pressures below its stability field. In zone 3, as defined by Smith (op.cit) and which is of slightly higher grade, pumpellyite makes an appearance. Similarly, in the sequence in Chile described by Levi (1969), rocks with the assemblage:-

Albite + Epidote + Calcite + Chlorite,

but without pumpellyite or prehnite, lie directly over lower greenschist facies rocks. Thus prehnite and pumpellyite are not invariably present in all low-grade rocks at the P and T of prehnite-pumpellyite facies. Hashimoto (1972) notes that within the pumpellyite zone of the Tamba district of Japan, pumpellyite is not always present and shows an antipathetic relationship with calcite.

Both prehnite and pumpellyite are limited by the reactions:-

$$\text{Prehnite} + CO_2 = \text{Calcite} + \text{Clinozoisite} + \text{Quartz} + H_2O \quad (2)$$

$$\text{Pumpellyite} + CO_2 = \text{Chlorite} + \text{Calcite} + \text{Clinozoisite} + \text{Quartz} + H_2O \quad (3)$$

Thus, the presence of these two minerals becomes increasingly restricted to low X_{CO_2} as T increases. At 350°C to 400°C (P_{fluid} = 2Kb), X_{CO_2}, defined by (2), is about 0.01 (Fig.10.2 in Winkler, 1974). In the Sanbagawa terrain, pumpellyite and lawsonite-bearing rocks were

formed at X_{CO_2} = 0.03 or less and in the Franciscan terrain X_{CO_2} was less than 0.01 (Ernst, 1972). That calcite is quite abundant in some zone A samples suggests that CO_2 activity may have been high enough to cause reaction (3) and possibly (2) to proceed from left to right. The reaction:-

Clinozoisite + CO_2 = Anorthite + Calcite + H_2O (4)

similarly limits epidote stability and at 350-400°C (P_{fluid} = 2kb) defines X_{CO_2} at 0.03 (Storre & Nitsch, 1972). A condition may be possible, then, where X_{CO_2} is bounded by these reactions such that epidote rather than pumpellyite is stable, although T is still within the range of very low-grade metamorphism.

In zone A the influence of a significant activity of CO_2 is seen by the occurrence of reactions such as:-

Diopside + H_2O + CO_2 = Chlorite + Calcite + Quartz (5)

(cf. Plate 18), and:-

Diopside + CO_2 + H_2O = Actinolite + Calcite + Quartz (6) .

Reaction (6) particularly is favoured by high X_{CO_2} (Hashimoto, 1972).

As already implied, temperatures within zone A are on the order of 300 to 400°C. This temperature range defines, for pressures less than about 3kb, an area in P-T space where zeolites are unstable and where actinolite has still to be stabilised (see compilation of experimental data by Winkler, 1974). More specifically, it is observed, by for example Smith (1969), that laumontite (not observed in zone A) disappears when prehnite and possibly pumpellyite become stable. Liou (1971) shows that at 3kb. and 300°C, laumontite breaks down. Below 2Kb, and above about 310-340°C, prehnite is stable but not necessarily pumpellyite; and above 350-370°C, actinolite may be expected to start forming (Fig.12.11 in Winkler, 1974). Thus low P, and T in the region 320°C to 370°C, appear reasonable

for the zone A volcanics. Above 3-4kb the assemblage actinolite + pumpellyite ± lawsonite is stabilised and prehnite is not observed. The earlier appearance of actinolite at these higher pressures, and its ability to coexist with pumpellyite is pointed out by Hashimoto (1972), Seki (1969) and Kuniyoshi & Liou (1976).

Stratigraphical considerations also limit the load pressure (P). The Mt. Kelly section (Fig. 3.2) of the volcanics is about 30 thousand metres thick. Deposition of the Hall Formation and the Upper Rossland Group provide at least another 1,500 metres. But since by this time (Bajocian) the Ominica Belt was rapidly emerging, it is unlikely that much more sedimentation occurred. Probably, therefore, at the very base of the volcanic succession, the overburden was not much greater than 7,000 metres. This corresponds to about 2kb. A similar pressure estimate is made by Kuniyoshi & Liou (1974, 1976) for the prehnite-pumpellyite facies Karmutsen volcanics of Vancouver Island.

7:1:2 Zone A to B transition

This transition is not exposed in the field, since it occurs along the valley west from Salmo (Fig.1.1). It is possible this is fault-controlled as suggested by Frebold & Little (1962). The incoming of amphibole south of Fruitvale (Fig.6.1), however, is quite abrupt.

The conspicuous habit of amphibole as a pseudomorph after pyroxene is probably governed by a generalised reaction:-

$$H_2O + \text{Chlorite}_1 + \text{Diopside} = \text{Chlorite}_2 + \text{Actinolite} \quad (7)$$

In this case, chlorite_2 is more aluminous than chlorite_1 (cf. Section 6:4). This type of reaction, though, does not define an isograd or an equilibrium assemblage. Amphibole (actinolite)

is also produced by:

Prehnite + Chlorite + Quartz = Epidote + Actinolite + H_2O (8),

though large amounts of prehnite are required (Hashimoto, 1972). Thus, although this reaction is unlikely to be responsible for much actinolite, it does define a temperature near which zone A is transformed to zone B. A more general reaction that is likely to occur in the Rossland volcanics is:

Chlorite + Calcite + Quartz = Tremolite + Clinozoisite + H_2O + CO_2 (9)

This last reaction (9) is proposed by Hashimoto (1972) to occur in the low-P metamorphism of the Tamba district, Japan. At higher pressure the incoming of actinolite does not replace pumpellyite, and as might be expected, actinolite + pumpellyite assemblages have not been observed in any Rossland rocks. On the contrary, Fe-poor epidote is apparently readily stabilised in zone B, this only occurring when other Ca-Al hydrous silicates have broken down (Winkler, 1974).

Reaction (8) is experimentally estimated to occur at about 350°C ($P_{fluid} < 2kb$) (Nitsch, 1971) and reaction (9) has been calculated (Fig.7.1) to occur at similar temperatures for X_{CO_2} less than 0.2.

Biotite-forming reactions must also have continued at roughly the same temperature as those forming actinolite. Most probably, as Smith (1969) suggests, biotite creation involves sericitic muscovite. The reaction:

Muscovite + $Chlorite_1$ = Biotite + $Chlorite_2$ + Quartz (10)

(Winkler, 1974) is probably realistic, as this reaction, like (7), involves the production of a more Al-rich chlorite (cf.Section 6:4).

This reaction, however, has not been specifically recognised but is regarded as likely by Winkler (op.cit) on the basis that it involves commonly occurring greenschist-facies minerals, especially in pelitic rocks. Biotite in the Rossland rocks probably also evolved by alteration of a K-rich igneous matrix. Stabilization of biotite in pelitic rocks is shown to occur at 400-430°C by Winkler (1974).

7:1:3 Zone B

Mineral assemblages in this zone are quite varied (Table 7.1), though they all indicate metamorphism within the greenschist and lower amphibolite facies. It is evident from Table 7.1 that differences are also apparent between zones, a fact noted previously. Particularly, calcite and chlorite are not essential constituents of sub-zones B1, B4 and B5 but are ubiquitous in sub-zone B2. It was suggested in Chapter 6 that calcite and chlorite represent retrograde minerals whose development is facilitated by shearing. These minerals also show an antipathy with epidote and biotite (cf. B2(1) and B2(4), Table 7.1).

Another feature, also noted in Chapter 6, is the tendency for either hornblende + plagioclase or actinolite + albite to occur. However, some samples disobey this generalization, for example 5536E (assemblage B1(2) in Table 7.1) and 5074B (B1(3)). This suggests that although albite reacts to form plagioclase, and actinolite reacts to form hornblende simultaneously in low-P greenschist metamorphism, the decomposition of albite to provide Na for the edenite molecule is not essential. Thus to some extent, especially in B1, a transitional albite - epidote - hornblende facies is developed. In B2 the textures of the rocks allow the possibility that disequilibrium

TABLE 7.1

MINERAL ASSEMBLAGES IN ZONE B METAVOLCANICS

B1

(1) Hornblende + Epidote + Chlorite + Plagioclase

(2) Hornblende + Epidote + Biotite + Plagioclase

(3) Actinolite/Hornblende + Chlorite + Biotite + Albite

± minor calcite, quartz, magnetite and sulphides.

B2

(1) Actinolite + Epidote + Biotite + Albite + Calcite

(2) Actinolite/Hornblende + Epidote + Biotite + Chlorite + Calcite + Albite

(3) Actinolite/Hornblende + Biotite + Chlorite + Albite + Calcite

(4) Actinolite + Chlorite + Albite + Calcite

± minor quartz, K-feldspar. Sulphides common.

B3

(1) Actinolite + Epidote + Biotite + Albite + Calcite

(2) Actinolite + Epidote + Chlorite + Biotite ± Calcite

± minor quartz, ? K-feldspar. Magnetite common; sulphides rare.

B4

(1) Actinolite + Epidote + Biotite + Albite (+ Calcite)

(2) Hornblende + Biotite + Plagioclase

(3) Hornblende + Plagioclase + Quartz

(4) Actinolite + Hornblende +Epidote + Biotite + Plagioclase

± very rare chlorite, calcite. ± Magnetite.

B5

(1) Actinolite + Epidote + Biotite + Albite

(2) Actinolite/Hornblende + Chlorite + Epidote + Albite

(3) Actinolite/Hornblende + Biotite + Plagioclase

(4) Actinolite/Hornblende + Chlorite + Calcite

± minor quartz, K-feldspar, sulphides.

may be present with calcite occurring as a relict phase.

In general, there are three causes of mineralogical variation, given a fixed or limited pressure:

(1) Bulk-rock composition. In the text on Metamorphism by Winkler (1974), variation of mineral assemblage in mafic rocks is considered in terms of essentially only four components: CaO, FeO + MgO, Al_2O_3 and SiO_2. Most naturally occurring minerals in metabasites fall within this tetrahedron. One common mineral in the Rossland rocks does not, however: That is biotite. Clearly, the amount of biotite is a function of K_2O, whether this is original or introduced. Biotite in some samples, for example the B1 pyroxenites, was almost certainly introduced as noted in Chapter 6 (Section 6:3). Similarly, biotite growth in veins and as a replacement of amphibole in some B2 and B3 rocks indicates local K redistribution.

Another component, Fe_2O_3, is also unconsidered in the C-M-A-S tetrahedron referred to above, and as shown in Section 6:5, epidote is a function of oxidation ratio.

More generally, however, it was observed earlier that the common phases chlorite, biotite and amphibole, particularly the latter, are chemically controlled, to an extent, by whole-rock compositions. The generalised reaction:

$$\text{Chlorite} + \text{Albite} + \text{Actinolite} + \text{Epidote} = \text{Plagioclase} + \text{Hornblende} + H_2O \qquad (11)$$

(cf. Liou et al., 1974), although proceeding to the right with increased T, depends on Mg/Fe ratios in the whole-rock. In Mg-rich whole-rocks, actinolite persists to higher temperature and thus the transition to amphibolite is retarded.

Much of the variation in zone B, therefore, can be attributed to this effect, certainly within any of the B sub-zones, and possibly between them.

(2) Temperature. Superimposed upon bulk-rock control is the effect of temperature. Over an area as large as zone B, especially since the area is riddled with intrusive rocks, temperature variation is expected. However, since the bulk-rock effect is so evident (cf. Figs. 6.3, 6.8, 6.11), temperature could not have varied greatly.

Locally, where exposure permits, the effects of a superimposed contact metamorphism are demonstrable. Since the shearing episode which affected the rocks in B1, B2 and, in part, B3 predates the Nelson intrusion, and since the early amphibolization stages preceded shearing (and probably the folding) of the volcanics, the Nelson Batholith was not totally responsible for the metamorphism of the volcanics. The superimposed contact metamorphism is thus restricted, since the volcanics were already within the greenschist facies.

In sub-zone B4, near Dominion Mountain (Fig.1.1), it can be seen that a seemingly vertical granite contact cross-cuts the volcanics. Sample 5049, taken from within 100m. of the contact, shows a true amphibolite assemblage (B4(3) - Table 7.1). At about 250m., sample 5048 shows the appearance of epidote and an actinolitic hornblende. Further still from the contact (e.g. samples 4016, 4013A; $\sim$ 500m.) calcite, epidote and biotite occur. Similarly, the sequence of samples 4060-4066 (Fig.1.1) show that within 200m. the assemblage consists of essentially hornblende + biotite + plagioclase (4060). Within 500 m (4061), minor epidote

appears and the amphiboles are zoned from actinolite to hornblende. (This two-amphibole assemblage, evident in Plate 60 , probably reflects the two-stage metamorphism of the volcanics; regional followed by contact metamorphism). Beyond this distance the minerals amphibole (actinolite or hornblende), biotite, epidote and feldspar (albite or plagioclase) occur, with minor chlorite and calcite.

Temperature differences also probably exist between zone B1 rocks and those further south, as suggested in Chapter 6. Despite the whole-rock control on mineral assemblages, the Al-and Fe-rich hornblendes and calcic plagioclases in zone B1 suggest higher grades of metamorphism compared to B2, B3 and B5. Possibly, this is a contact metamorphic effect due to the proximity of large masses of intrusive rocks ardund B1. Alternatively, as is indicated in Section 7:4 below, this reflects a south to north increase in regional metamorphic grade.

In general, however, mineral assemblages are definitive of greenschist to lower amphibolite, or transitional epidote-amphibolite facies. Temperatures thus indicated lie within a range of about 400°C to 525°C at P_{fluid} 2-3kb . Low pressures, such as these, are indicated by amphibole chemistry (Section 6:2). 400°C is the average temperature, as considered by Winkler (1974), where low-grade (greenschist) metamorphism starts, as heralded by the appearance of actinolite and Fe-poor epidotes. The upper temperature of low-grade metamorphism Winkler (op.cit) indicates to be about 500-525°C, which is when amphibole becomes hornblendic and, in rocks of suitable composition, when diagnostic minerals such as almandine and staurolite appear. Liou et al. (1974) show that chlorite starts to disappear (at P_f = 2kb) at about 470°C, finally

vanishing at about 540°C. In addition, epidote is unstable above 500°C at the QFM buffer and at 620°C at the HM buffer (Liou, 1973). The occurrence of epidote together with hornblende in B1 suggests quite high f_{O_2} (between QFM and HM), unless P_f is greater than 3-4 kb (Liou et al., 1974).

(3) Fluid Composition. If $P_{fluid} = P_{solid}$, a common assumption and probably a realistic one (Winkler, 1974), then the only way in which the fluid can alter the mineral paragenesis is to vary in composition. Since the fluid dominantly is a mixture of CO_2 and H_2O (cf. Greenwood, 1976), X_{CO_2} is usually considered.

In a simple dehydration reaction, an increase in X_{CO_2} in the ambient fluid phase lowers the temperature of the reaction. For a dehydration and decarbonation reaction, the maximum temperature will be achieved when the ambient fluid phase has an X_{CO_2} equal to that produced by the reaction. Thus, it can be seen that at a constant T, a variety of mineral parageneses can be produced, simply by varying X_{CO_2}.

To demonstrate the combined effect of T and X_{CO_2} in the Rossland volcanics, Fig.7.1 has been constructed. This illustrates the P-T-X_{CO_2} dependancy of mineral assemblages amongst the minerals quartz (q), calcite (cc), anorthite (an), clinochlore (clin), clinozoisite (cz) and tremolite (tr). Reactions between phases are:

1. $2cz + CO_2 = 3\ an + cc + H_2O$ (12)
2. $6cz + 1\ clin + 7q = 10an + 1tr + 6H_2O$ (13)
3. $3cc + 1\ clin + 7q = 1\ an + 1tr + 3H_2O + 3CO_2$ (14)
4. $3clin + 10cc + 21q = 3tr + 2cz + 10CO_2 + 8H_2O$ (15)

In order to calibrate these reactions for T and X_{CO_2}, thermodynamic data were used. The method of calculation and the data used are modified versions (R.Powell , pers.comm.) of those

Figure 7.1.

$T-X_{CO_2}$ cross-section (see text for discussion on its construction and use). $I_{2,4}$ refers to the pressure (2,4 kb) of the invariant point. Bracketed numbers refer to equations in Chapter 7 and unbracketed numbers refer to the fields bounded by the various reactions.

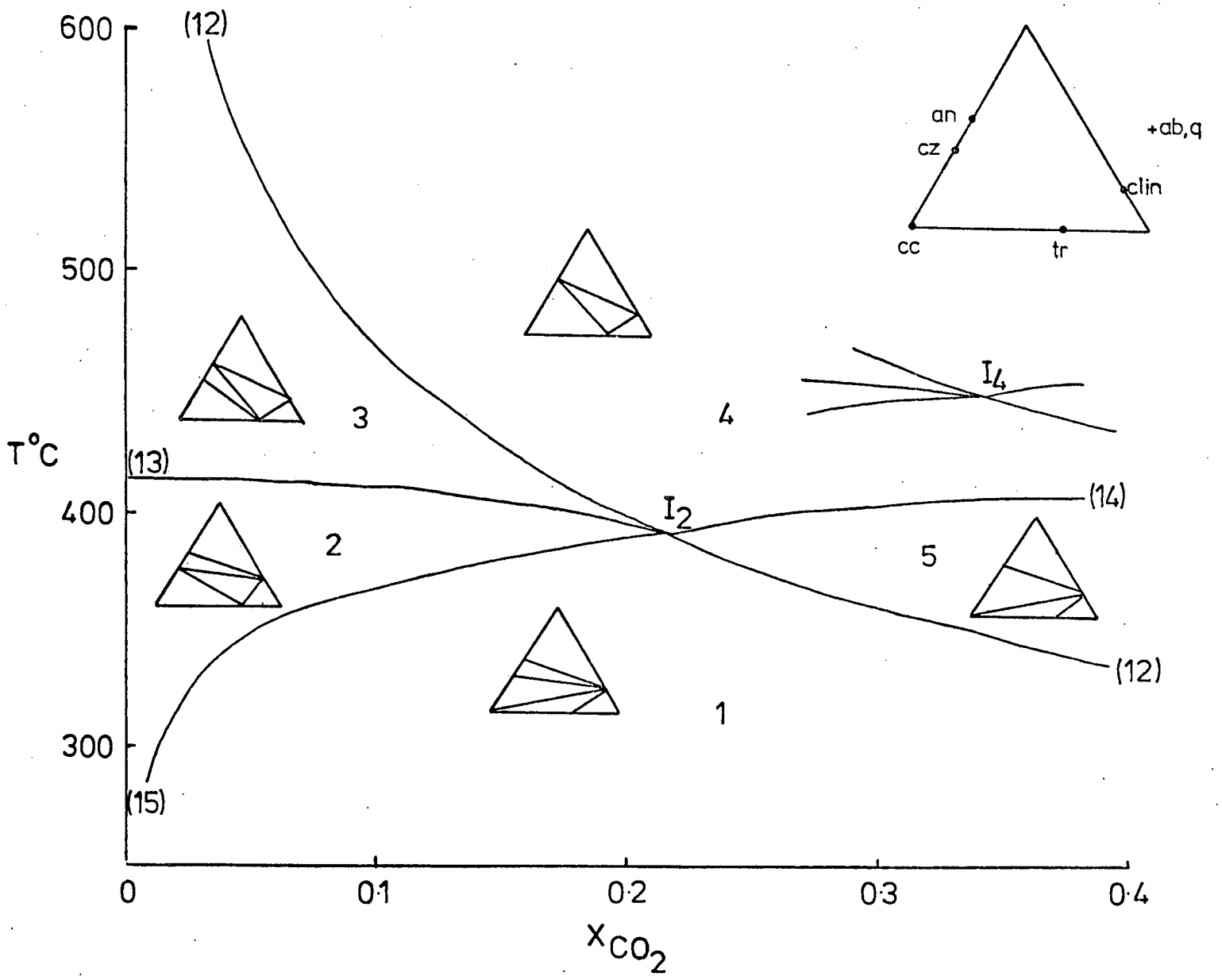
600
500
400
300
T°C
(12)
(13)
(14)
(15)
(12)
I2
I4
1
2
3
4
5
0
0·1
0·2
0·3
0·4
x_{CO_2}
an
cz
cc
tr
clin
+ab,q

described in Richardson & Powell (1976). The fluid composition was assumed to be an ideal mixture of CO_2 and H_2O.

In relating such a model to the real situation, the following should be noted:

(1) Only end-member mineral compositions are considered. Introduction of activity or mole-fraction terms was found not to affect greatly the $T-X_{CO_2}$ pattern or the temperatures of the reactions, lowering the T of the I_2 invariant point (Fig.7.1) only 10 or 20°C. For the purposes of this discussion, in which Fig.7.1 is only used to illustrate the effect and general value of X_{CO_2}, this is not critical.

(2) More important is the fact that variables such as K_2O and Fe_2O_3 are not considered, thus Fe-rich epidote and biotite cannot be plotted in the C-M-A-S projection used. Albite, however, can be considered as in excess (either as pure albite or as a component in plagioclase), together with quartz.

(3) This leads on to another problem; that is, the fact that quartz is not always visibly in excess. However, quartz is apparent in small quantities in a number of samples and the mineral assemblages in these samples are generally the same as those in which no quartz was identified. Thus, although it is not strictly valid, in order to simplify the discussion, Fig.7.1 is constructed assuming projection from quartz.

Particularly important in defining the magnitute of X_{CO_2}, is reaction (9). By comparison, Storre & Nitsch (1972) show that between 500 and 600°C, this reaction is almost vertical at $X_{CO_2} = 0.02$. The gentler slope and higher X_{CO_2} shown for (9) in Fig.7.1, may be due to the non-ideality of the fluid. Thus, the presence of epidote

(clinozoisite) in greenschist facies rocks indicates an X_{CO_2} restricted to quite low values, though, as Fig.7.1 shows, an increase in pressure shifts the invariant point to higher X_{CO_2}.

Reaction (15) is significant since it was quoted before ((9) - Section 7:1:2) as a reaction defining the A-B transition, which is thought to occur at about 350°C. This agrees reasonably with Fig.7.1 when X_{CO_2} is slightly greater than zero. It can also be seen that chlorite and calcite tend not to coexist in the greenschist facies (i.e. above reaction (15)) if clinozoisite is stable. Thus the presence of abundant chlorite and calcite in some samples in B1, B2 and B3 (Table 7.1), indicates a possible retrograde rise in X_{CO_2}; that is, a transition from field 2 to field 1 (Fig.7.1).

At this stage, in fields 1 and 2, although anorthite is represented, albite is usually the only feldspar, and plagioclase does not appear until temperatures lie above reaction (13). Thus, (13) is an analogue for transition to the amphibolite facies in that amphibole and plagioclase are produced at the expense of chlorite and epidote. Within field 3 generally, the amphibole should become hornblendic due to reactions such as quoted in Section 6:2. Field 3 would be analogous to zone B1, though again with the retrograde production of chlorite and calcite, for example in samples 74B and 5075B of the Bonnington complex, involving increased X_{CO_2} and the partial transition back to field 2. Field 5 may be represented in some B2 samples (Table 7.1) in which epidote is absent, though in this case a calcic plagioclase would be expected. More probably, epidote is absent due to whole-rock compositional effects or low f_{O_2}.

That epidote is present to quite high grades in the zone B volcanics suggests that unless X_{CO_2} was initially low (less than 0.1 in Fig.7:1), then X_{CO_2} must have decreased as grade increased, possibly being buffered by reaction (12). Either way, if the data of Storre & Nitsch (1972) on this reaction (see above), is correct, then X_{CO_2} was probably less than 0.01 in the B1 metavolcanics, and possibly up to 0.03 (see Section 7:1:1) in zone A. As Harte & Graham (1975) show, low X_{CO_2} produces calcite as the sole carbonate phase. Higher X_{CO_2} has the tendency of producing ankerite-bearing assemblages. That calcite only is present in Rossland volcanics is, therefore, a further indication of low X_{CO_2} values.

7:2 Causes and timing of metamorphism

Metamorphism of the Rossland volcanics was not a one-stage process, but within zone B involved two or more stages. Prior to the shearing and folding episode, which correlates with F3 in the adjacent Kootenay arc (Ross, 1970), amphibolization of zone B pyroxenes had occurred. The emplacement of plutons into the volcanics, presumably at quite high levels (P of metamorphism = 2-3 kb), then locally caused a contact-metamorphic upgrading of the rocks. Later retrogressive metamorphism has been shown to occur, involving introduction of CO_2 and H_2O into the rocks.

That the zones A and B are separated by quite a sharp temperature gradient, while both are temporally identical, also shows that the metamorphism was not burial in nature. Probably, localised high heat-flow regions developed, heralding the emplacement of the later plutons, which caused the initial amphibolization of zone B. Zone A, however, has all the

characteristics associated with burial metamorphism, and temperatures and pressures indicated above are similar to those developed during the burial metamorphism of the Karmutsen Group (Kuniyoshi & Liou, 1976). However, the P and T of the zone A alteration indicates a high geothermal gradient, about $40^{\circ}C/Km$, and thus these rocks were also exposed to the high heat-flow attending the initiation of the metamorphic and plutonic episode.

7:3 Regional metamorphic setting

Metamorphism of the volcanics occurred post-Lower Jurassic and before and during the intrusion of the Nelson Batholith. An apparent south to north increase in grade from prehnite-pumpellyite facies (zone A), through greenschist, to lower amphibolite facies (zone B) was imposed. Further north of zone B1 the Valhalla gneiss dome of the Shuswap complex is encountered, in which sillimanite-grade gneisses occur (Reesor, 1965). This suggests the Rossland volcanics were metamorphosed at the same time as the Shuswap complex to which a Jurassic age is generally assigned (Wheeler & Gabrielse, 1972). This interpretation agrees with that of Hyndman (1968) for the Nakusp area, fifty miles north of Rossland. Here, (?) Rossland Group volcanics, which are metamorphosed to greenschist facies, grade into higher grade gneisses of the Shuswap complex. On this basis Hyndman assigned a post-Lower Jurassic age to Shuswap metamorphism.

The south to north increase in grade established in the Salmo to Nelson area is also noticed in the Rossland area by Fyles (in prepn.). Here, greenschist-metamorphosed Rossland volcanics grade just north of Trail into garnet-amphibolite facies meta-sediments (unit A in Fig. 1.1). Similarly metamorphosed sediments occur just west of sub-zone B1 (Mulligan, 1952) and confirm the degree of metamorphism

inferred for the volcanics.

The general metamorphic setting of the Rossland volcanics is shown in Fig.7.2 which is taken from Monger & Hutchinson (1968). It is clear that the greenschist and amphibolite-facies rocks of the Ominica belt grade very sharply into very low-grade (prehnite-pumpellyite or zeolite facies) rocks in the Intermontane Belt, and eastwards into virtually unmetamorphosed sediments of the Rocky Mountain Belt. This is a result of the uplift of the Ominica Belt, faulting-out isograds on either side, and causing them to dip essentially vertically at the margins of the Belt.

It can be seen that Monger & Hutchinson (1968) have placed the whole of the Mesozoic Belt in the prehnite-pumpellyite facies (Fig.7.2), while it is clear that this is not so, as shown here, since zone B lies well within the greenschist facies. The preservation of the lower-grade (zone A) rocks within an essentially higher-grade terrain is due to structural controls; the Jurassic rocks occupying a structural depression. The eastern edge of the Mesozoic belt is generally a thrust fault (Fig.1.1) which dips east and has allowed older, higher-grade rocks of the Kootenay Arc to be juxtaposed with the volcanics.

In summary, the Rossland volcanics, being the youngest unit to have suffered a degree of metamorphism in the area, are generally of lower grade than the older rocks in the Shuswap Complex and Kootenay Arc. That they were variably metamorphosed along their strike, however, indicates that they are not a simple burial metamorphosed sequence overlying an older basement, but were actively involved in a culmination involving all the rocks of the area, which was most probably centred on the Valhalla gneiss dome.

Figure 7.2

Metamorphic map of the southeastern part of the Canadian Cordillera (after Monger & Hutchinson, 1971). The Rossland volcanics (RV) lie within the area designated 2 by Monger & Hutchinson).

Key. (Facies after Turner, 1968).

(1) Unmetamorphosed: (1a) Transitional facies (in non-volcanic lithologies) to (2) and (4).

(2) Prehnite -Pumpellyite metagreywacke facies and zeolite facies. Some primary mineral preserved.

(2a) As 2 but transitional towards (3).

(2b) As 2 but transitional towards (4).

(3) Glaucophane-Lawsonite facies. Primary minerals extremely rare.

(4) Greenschist facies. Primary minerals extremely rare.

(5) Amphibolite facies. Appearance of 'regional' garnet.

(6) Granitic.

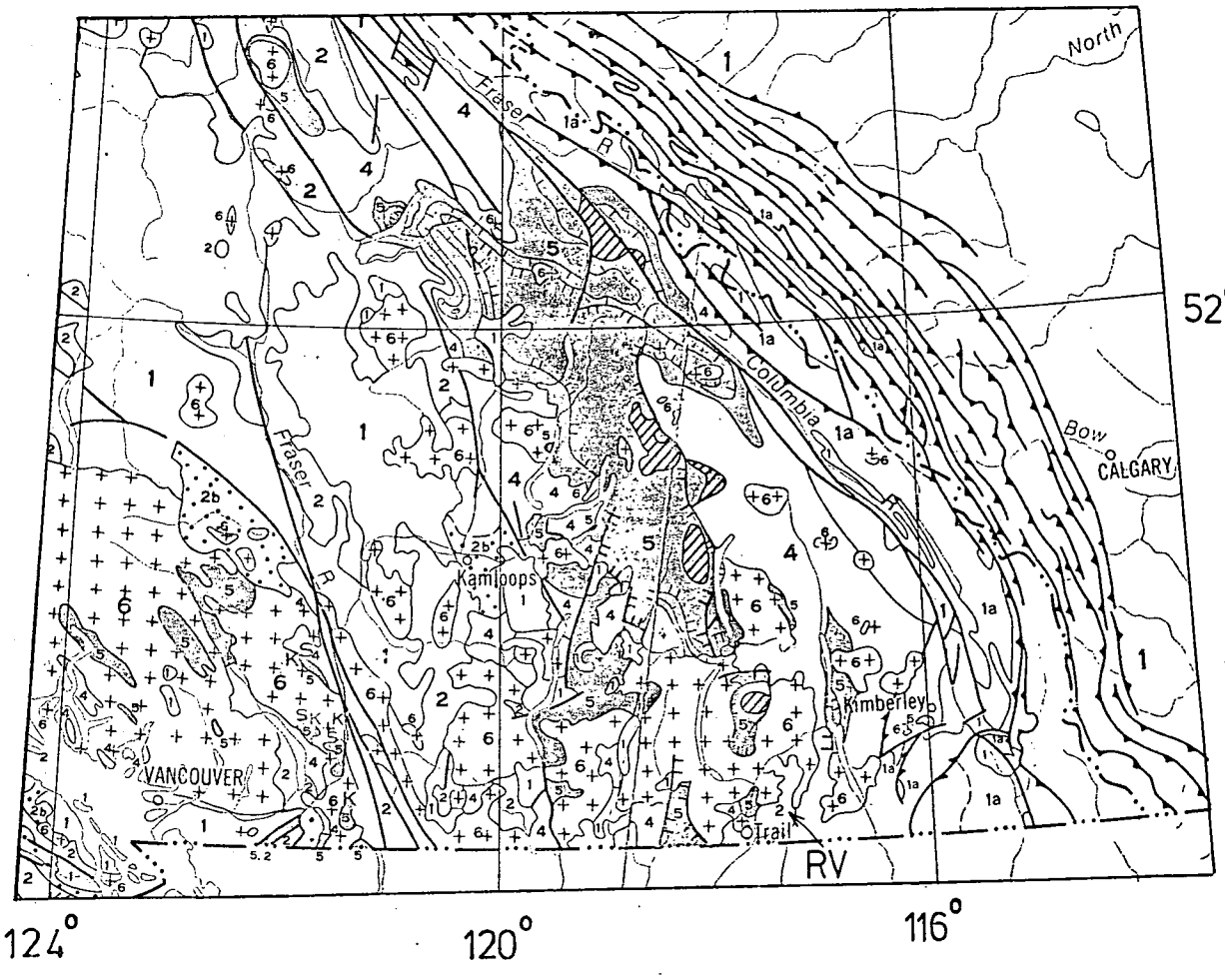

Metamorphic map of part of the Canadian Cordillera (Monger & Hutchinson, 1971)

MILES
100 0 100

Scale 1:5,000,000

CHAPTER 8

OXYGEN ISOTOPE GEOCHEMISTRY OF THE ROSSLAND VOLCANIC ROCKS

8:1 Introduction

Oxygen isotope ratios, while relatively insensitive indicators at the high temperatures of igneous processes, are useful when dealing with metamorphic or lower-grade hydrothermal alteration of rocks. In an ideal situation, information can be obtained from isotopic data on the temperatures of the hydrothermal alteration; the presence or absence of equilibrium between minerals; the isotopic character and hence the origin of the fluid involved; and the relative abundances of fluid compared to rock. Not all of these necessarily can be determined from the isotopic data alone, but where a variable, say temperature, is known from other lines of evidence, then the presence or absence of isotopic equilibrium between the constituent minerals of a rock can be assessed.

It is likely, therefore, that the oxygen isotope data reported here can add information as to the nature of the metamorphic processes affecting the volcanics, additional to that deduced from more conventional mineralogical data described in earlier chapters.

The method of analysis for $^{18}O/^{16}O$ ratios is described in Appendix 4. All analyses are reported in the usual 'del' notation, with Standard Mean Ocean Water (SMOW) as a standard (Craig, 1961):

$$\delta^{18}O = \frac{^{18}O/^{16}O_{Q} - ^{18}O/^{16}O_{SMOW}}{^{18}O/^{16}O_{SMOW}} \times 1000 \qquad (1)$$

Figure 8.1

Mineral - H_2O fractionations ($\Delta = \delta^{18}O_A - \delta^{18}O_{H_2O}$ per mille). Taken from Taylor (1974).

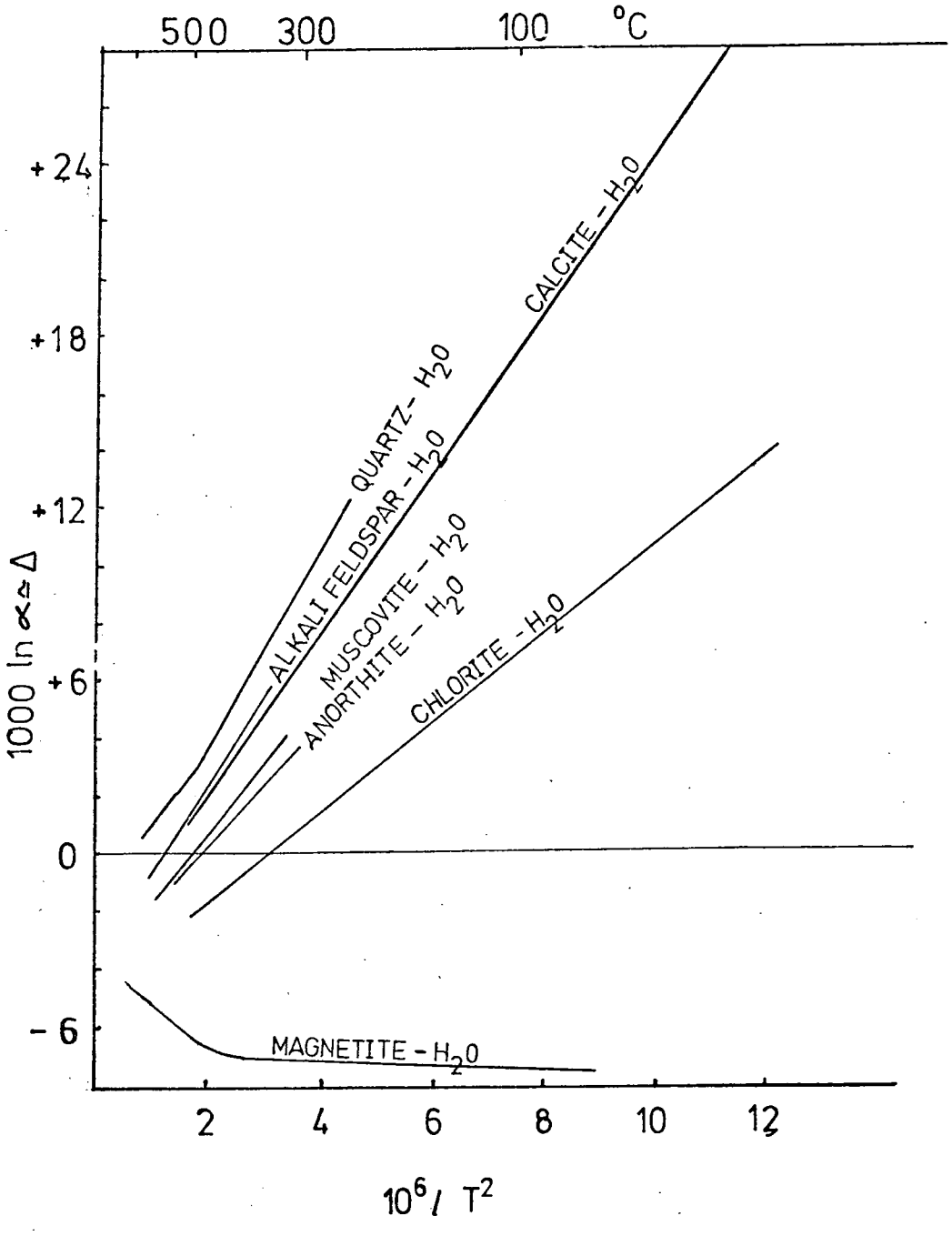
500
300
100
°C
+24
+18
+12
+6
0
- 6
1000 ln α≃Δ
QUARTZ - H2O
ALKALI FELDSPAR - H2O
MUSCOVITE - H2O
ANORTHITE - H2O
CALCITE - H2O
CHLORITE - H2O
MAGNETITE - H2O
2
4
6
8
10
12
10^6 / T^2

Thus, $\delta^{18}O$ represents the 'per mille' difference in ^{18}O between the sample (Q) and SMOW.

If the fractionation of $^{18}O/^{16}O$ between two phases A and B is defined as

$$\alpha^{A-B} = \frac{^{18}O/^{16}O_A}{^{18}O/^{16}O_B} \quad , \qquad (2)$$

then a useful simplification arises from the $\delta^{18}O$ definition: That is, α shows a temperature dependance of the sort

$$1000 \ln \alpha = A/T^2 + B \qquad (3)$$

(cf. Clayton, 1963) and since α is usually very close to 1.00:

$$1000 \ln \alpha \simeq \delta^{18}O_A - \delta^{18}O_B \equiv \Delta (A, B) \qquad (4)$$

Fig. 8.1 shows this temperature dependance (equations 3 and 4) for various mineral-water fractionations (from Taylor, 1974). Thus, in an ideal situation any mineral pair can be calibrated for temperature, from data on naturally occurring minerals, given two reliable and accurate laboratory calibrations of mineral - H_2O fractionations with temperature. That is:

$$\Delta(A,B) = \Delta(A,H_2O) - \Delta(B, H_2O) \qquad (5)$$

Bottinga and Javoy (1975), using this type of approach, have compiled various equations for commonly occurring minerals, and these are used in the discussion below.

8:2 Discussion of results

8:2:1 Whole-rock data

Before the significance of these data can be discussed, it is necessary to define the original $\delta^{18}O$ of the lavas. It is found that worldwide, basic extrusive rocks have a very limited range of isotopic composition, $\delta^{18}O$ between 5.0 and 7.0 per mille

(Anderson et al., 1971; Taylor, 1968). Fresh ocean-floor basalts are even more restricted in composition, varying between 5.5 and 5.9 (Muehlenbachs and Clayton, 1972a). Exceptions to this generalization do occur, rarely, for example low - ^{18}O lavas from Iceland, described by Muehlenbachs et al. (1974). Compared to these 'primary' values it is clear that the Rossland samples are all considerably enriched in ^{18}O. That they did not originally have these anomalous values, is shown by the pyroxene analyses in Table 8.1. At igneous extrusive temperatures the various inter-mineral fractionations are low, as would be expected from inspection of equation 3 above. From the data reported by Anderson et al. (1971) the $\delta^{18}O$ of pyroxene is within 1 per mille of the whole-rock value. Thus, the original Rossland lavas had $\delta^{18}O$ within the normal range of 5.0 to 7.0. That relict pyroxenes maintain their igneous $^{18}O/^{16}O$ ratios is also shown by the data of Muehlenbachs & Clayton (1972b) for ^{18}O depleted oceanic green-stones. At some stage, then, both zone A and zone B rocks have exchanged ^{18}O with an external reservoir of oxygen, most probably in the form of a pervasive hydrothermal fluid. The stage when this ^{18}O enrichment took place in the history of the volcanics, is difficult to assess. It was commented upon in Chapter 5 that the volcanics are likely to have been through more than one period of alteration. One possibility is that both zone A and B rocks were enriched in ^{18}O by an early, low-T submarine or subaerial weathering. In this case the $\delta^{18}O$ of the water involved is likely to be less than 0.00 (SMOW), since nearly all meteoric waters have negative $\delta^{18}O$ (Craig, 1961), but the large positive mineral - H_2O fractionations of the derivative

TABLE 8.1

WHOLE-ROCK AND MINERAL $^{18}O/^{16}O$ DATA (REPORTED AS $\delta^{18}O$ ‰ RELATIVE TO SMOW)

Zone A analyses

Sample	Cpx.	Plag.	Mgt.	Cal.	W.R.
4051	4.8		5.0		10.3
4054	5.8			14.1	10.7
4056	6.5	11.3	5.2		10.1
4070				13.7	
5010					10.4
5033				13.4	11.6
5036				13.6	10.2

Zone B analyses

Sample	Amph.	Plag.	Mgt.	Ep.	Cal.	W.R.
5516B			3.6	9.0		
5516C	9.4		4.5	8.8	13.1	
5529A	9.5	11.6*		7.6	11.6	
4040	8.6	10.5				8.7
4062	8.7	10.8				9.0
4044	7.8					
5111A						9.5
5116					13.2	7.9
5120						9.8

* Minor quartz contamination.

clay minerals (Savin & Epstein, 1970a) at low temperatures, push the whole-rocks to higher $\delta^{18}O$ than the normal 5.7 (cf. Muehlenbachs, 1976). If, subsequent to this early enrichment, the rocks acted as a closed system, then although new minerals would have crystallized they will internally adjust about the whole-rock value which itself would not change. In this case, it would not be expected that there would be an average difference in whole-rock values between zones A and B. From Table 8.1, however, it is clear that zone A rocks are enriched compared to zone B by about 1.5 per mille. This suggests that the difference in $^{18}O/^{16}O$ is due to the different grade of metamorphism attained. That is, up to the grade of metamorphism now preserved in the rocks, ^{18}O was freely exchanged with a substantial volume of water. The lower values of whole-rock $\delta^{18}O$ in zone B, therefore, is a function of the higher temperatures of this zone, and the lower mineral - H_2O fractionations.

Similar observations of decreasing whole-rock $\delta^{18}O$ with grade, have been reported in other regional metamorphic terrains (e.g. Garlick & Epstein, 1967; Black, 1974). On the other hand, Anderson (1967) reports very limited isotopic exchange in some metamorphosed rocks, suggesting that in other situations a pervasive fluid phase was not available.

Implicit in the argument above is that the temperature at which the rocks exchanged ^{18}O is that, more or less, at which they were metamorphosed, and as deduced in Chapters 6 and 7. In North-Central British Columbia, Takla volcanic rocks east of the Pinchi fault are enriched similarly to the Rossland volcanics (Magaritz & Taylor, 1976). However, west of the Pinchi fault, similar

rocks are generally lower in $\delta^{18}O$ (5-10 per mille). Magaritz & Taylor (op.cit) ascribe this to the fact that the eastern rocks were altered (silicified, albitised and chloritised) at lower temperatures ($\simeq 100^{o}C$) with variable amounts of low-^{18}O water, whereas the western rocks were altered at higher temperatures with similar water. The argument put forth below in more detail, contrary to that by Margaritz & Taylor (op.cit.) for the Takla rocks, is that similar degrees of enrichment in ^{18}O can be obtained at higher temperatures (greenschist facies) but with ^{18}O-rich water, and as exemplified by the Rossland rocks.

8:2:2 Mineral data

Mineral separate analyses are shown in Table 8.1. Apart from pyroxene, the three analyses of which compare with pyroxenes in fresh extrusive rocks, all the other phases show evidence of ^{18}O exchange during alteration.

Plagioclase in zone A (sample 4056) shows a 4.8 per mille enrichment relative to pyroxene, which is far too high for equilibrium at igneous-extrusive temperatures. The status of magnetite in zone A is less certain. In 4051 the negative pyroxene-magnetite fractionation suggests the magnetite has exchanged ^{18}O, since pyroxene-magnetite fractionations in fresh extrusive rocks are positive, with $\delta^{18}O$ of magnetite usually falling below 4.5 per mille (Anderson et al., 1971). This is somewhat unusual since zone A magnetites are 'igneous' in terms of their major element composition. It is possible that ^{18}O diffusion has occurred through the magnetite due to the presence of H_2O. Calculations by Bottinga & Javoy (1975) show that wet magnetite may theoretically exchange ^{18}O down to about $550^{o}C$ for grain sizes of 1 mm.

Zone A calcite is apparently quite constant in composition and tends to indicate that it has equilibrated with a regionally present, and compositionally constant hydrous fluid, as inferred in 8:2:1. In Chapter 7, zone A temperatures were estimated to be of the order 250-300^{o}C, and also that the CO_2/H_2O molecular ratio was low; then, to a first approximation the fluid can be considered to be H_2O only. From the data of O'Neil et al. (1968), and also from Fig.8.1, the composition of the water in equilibrium with calcite of $\sim$13.5 per mille, is about 7.5 per mille. Thus, the water involved is not pristine meteoric water, or sea water.

Within zone B all the minerals are demonstrably secondary in origin and thus during their formation will have inherited ^{18}O according to the T and $\delta^{18}O$ of the oxygen reservoir, be it water or rock. Inspection of Table 8.1 shows the order of enrichment in ^{18}O to be: calcite, plagioclase, amphibole, epidote, magnetite. Consideration of data compiled by Garlick & Epstein (1967) and Bottinga & Javoy (1975) indicates this is the expected equilibrium order of enrichment. Some idea of the temperature of equilibrium may be obtainable, therefore, using published isotopic geothermometers.

Unfortunately, the lack of quartz in the rocks prevents use of the quartz-magnetite geothermometer, as used, for example, by Schwarz et al. (1970) and Black (1974). This mineral pair shows the greatest fractionation of any two commonly occurring minerals, and is thus potentially the most sensitive indicator of temperature. From the compilation of mineral-mineral fractionations by Bottinga & & Javoy (1975) the following data, relating to amphibole (A), feldspar (F) and magnetite (MA), can be used.

$$\Delta (A, MA) = 0.3 + 2.422 \times 10^6 \times T^{-2} \quad (6)$$

$$\Delta (F,A) = -0.3 + (2.178 - 1.04b) \times 10^6 \times T^{-2} \quad (7)$$

$$\Delta (F,MA) = (4.6 - 1.046) \times 10^6 \times T^{-2} \quad (8)$$

In these equations, b is the mole per cent of anorthite in plagioclase (F). The following results can be obtained from equations 6, 7 and 8 and the data of Table 8.1:

Sample	Mineral-Mineral	Δ	T°C	
5516C	A - MA	4.9	452	
5529A	F - A	2.1	668	(531)
4040	F - A	1.9	673	(567)
4062	F - A	2.1	632	(531)
Average	F - MA	6.9	524	(486)

These temperatures are not concordant and apart from 5516C are unrealistically high. Paradoxically, if instead of the actual plagioclase compositions, An_{60} is used, then the bracketed temperatures are derived, which are more reasonable. Possibly, feldspar has exchanged ^{18}O with low- ^{18}O water to lower temperatures than amphibole or magnetite. This effect also is apparent in the Takla rocks where in one sample analysed by Magaritz & Taylor (1976) there is feldspar-actinolite fractionation of 2.1 per mille, which implies a much higher temperature than was ever attained in these rocks. Discordant temperatures are quite common in metamorphic rocks, though, and are attributed by Bottinga & Javoy (1975) to retrograde exchanges and grain-size diffusion effects. Also, little is known about $\delta^{18}O$ variation in compositionally complex minerals such as amphibole where, like the plagioclases, Al can substitute greatly for Si.

Despite the somewhat anomalous temperatures calculated above, the minerals amphibole, feldspar and magnetite, together with epidote,

are probably not far removed from their equilibrium $\delta^{18}O$ values and some estimate of H_2O composition can be made. Inspection of the data presented by Garlick & Epstein (1967) shows that hornblende generally has a $\delta^{18}O$ value between that of chlorite and muscovite, and as shown, below that of sodic plagioclase. From Fig.8.1, therefore, at 400°C the equilibrium water is about 2 per mille less than the $\delta^{18}O$ of hornblende. Magnetite, at 400°C, is about 6 per mille depleted relative to H_2O (Fig.8.1). Thus, a fluid composition of between 7 and 10 per mille is indicated. This agrees with that deduced above as coexisting with zone A calcite. Zone B calcite from Fig.8.1 also indicates a fluid H_2O of $\delta^{18}O$ equal to about 9 per mille. In fact, calcite does not appear to have exchanged ^{18}O to significantly lower temperatures than the other minerals, as it is prone to do. Schwarz et al. (1970) and Black (1974) record anomalous quartz-calcite temperatures that they attribute to retrograde exchange by calcite. Above about 500°C, quartz-calcite fractionations do not 'remember' temperatures of equilibrium (Schwarz et al., 1970).

Data on epidote are limited. If the $\delta^{18}O$ of the H_2O is about 9 per mille then Δ(EP, H_2O) is slightly less than, or near to zero for a temperature of 400°C. An epidote-H_2O fractionation of zero for 300°C (K.Muehlenbachs, pers. comm.) is thus reasonable. An epidote analysed by Muehlenbachs & Clayton (1972b) has a value of 2.6, and this demonstrably equilibrated with seawater ($\delta^{18}O$ = 0.0) at 200-300°C. Thus, the epidotes analysed here are more or less in equilibrium with the other minerals and the pervasive fluid.

8:3 Discussion and conclusions

It has been shown that the original Rossland lavas had 'normal' $\delta^{18}O$ values of around 5-7 per mille, and that the volcanics were subsequently enriched in ^{18}O during hydrothermal alteration.

The first conclusion from this is that relatively pristine meteoric water was not involved, as is the case in the ^{18}O-depleted rocks adjacent to the epizonal plutons of the Scottish Tertiary district (e.g. Forester & Taylor, 1977). In those environments, permeable, flat-lying country rocks exchanged ^{18}O with circulating meteoric water of low ^{18}O content, up to five miles from the intrusive contact. Samples 4062 and 4040, collected from within 500 - 700 m of a Nelson Batholith contact, show no sign of a significant decrease of $\delta^{18}O$ compared to other zone B, or zone A, samples. The situation in the Rossland area is analogous, therefore, to the contact metamorphic effects documented by Shieh & Taylor (1969) for deeper level plutons than those in the Scottish Hebrides. Here, ^{18}O exchange due to localised upward and pluton-ward movement of H_2O is restricted to a zone only a few feet from the contact. The Rossland volcanics have been essentially unaltered, isotopically, by contact metamorphism but have retained $\delta^{18}O$ values imprinted during the earlier regional metamorphism.

The decrease of whole-rock $\delta^{18}O$ with increase in grade noted here, and recognised as a fairly general feature of regionally metamorphosed rocks (Shieh & Taylor, 1969), indicates exchange of ^{18}O with a substantial amount of water. This does not imply that abundant water was available at any stage, but that small amounts of fluid continually percolated through the rocks. The origin of the water is problematic, since pristine meteoric water (< 0 per mille)

is ruled out by the mineral data. However, in geothermal areas meteoric water can be shown to have undergone a positive "^{18}O-shift" due to reaction over time with ^{18}O-rich sediments at elevated temperatures. An ^{18}O-shift is invoked by Magaritz & Taylor (1977) to explain the high ^{18}O values of rocks in north-central British Columbia. However, even at 300°C in rocks both east and west of the Pinchi fault, Magaritz & Taylor (op.cit) envisage the modified H_2O as having a composition of about 0.0 per mille, modified from an original (meteoric) composition of -16 per mille. The waters in equilibrium with the Rossland volcanics are inferred to be 8 - 10 per mille, which is somewhat higher. This could also be meteoric water that has undergone an extreme ^{18}O-shift, due to prolonged contact with ^{18}O-rich silicates and carbonates. This value of 8 - 10 is comparable with 'metamorphic' water (see Taylor, 1974) whose composition is calculated from mineral data. Metamorphic water has never been directly collected, though White et al. (1971) have documented unusual ^{18}O-rich waters that may have such a metamorphic component. Thus, another origin for the ^{18}O-rich water could be upward percolating 'metamorphic' water that is released by prograde, dehydration reactions. During dehydration reactions water/rock volume ratios are low, and the H_2O composition will be largely controlled by the reservoir of oxygen bound in the rock. Thus, water produced by dehydration of ^{18}O-rich sediments, by progressive burial and temperature increase, would itself be ^{18}O-rich. If an average shale has a $\delta^{18}O$ of 20 per mille (Savin & Epstein, 1970b), then taking muscovite-H_2O (Fig.8.1) as a crude model of rock - H_2O fractionation, at about 200°C the required $\delta^{18}O$ H_2O of $\sim$10 per mille is obtained. It is significant that H_2O in coexistence with

burial-metamorphosed members of the Belt (Purcell) supergroup has a calculated $\delta^{18}O$ of 7 to 11 per mille (Eslinger & Epstein, 1973). Since the Rossland volcanics overlie and are now closely related to a large mass of eugeosynclinal and miogeoclinal sediments (Chapter 2), it is possible they were metamorphosed in the presence of H_2O released during the dehydration of these rocks, and which was continually percolating upwards. The original water, then, either incorporated in pores of sediments or bound in clay minerals, may have been substantially marine.

CHAPTER 9

GEOLOGIC HISTORY OF THE ROSSLAND VOLCANICS: SUMMARY AND CONCLUSIONS

9:1 Volcano-tectonic history

In Section 5:4:2 it was shown that there is an analogy between the Rossland volcanics and the rather more unusual or rarer varieties of modern island-arc volcanics, exemplified by the New Hebrides and New Georgia ankaramitic associations, and possibly the alkalic or shoshonitic rocks of Grenada, East Papua and Fiji. It was further suggested that similar rocks to those found in the Nelson-Rossland area also characterize the Nicola-Takla Belt volcanics of British Columbia.

The modern analogies referred to generally form as the late-stage products of their respective arcs, or occur distal to the trench. Grenada is one exception occurring equidistant to the trench, and contemporaneous with more 'normal' volcanics (Brown et al., 1977). De Long et al. (1975) have suggested that localised tectonic anomalies are causal to these alkalic-trending arc volcanics. They suggest the presence of a gash or fault in the subducted ocean crust, or proximity to the edge of the subducted plate, where hinge faulting occurs, are possible mechanisms or causes. However, other factors may be effective. Particularly, in the cases of the New Georgia and New Hebrides, unusual subduction-zone configurations are apparent. In the former case, Mitchell & Warden (1971) have shown that the polarity of the arc has probably changed, with the subduction trench switching from one side of the arc to the other. In the latter case, Cox & Bell (1972) note that the occurrence of a near-vertical subduction may have been effective petrogenetically.

Certainly, the Rossland volcanics do characterize the latter stages of the Nicola-Takla arc and also occur, relative to the Nicola Group, towards a 'back-arc' setting. As Douglas et al. (1970) note, they appear to be related to the flexure between a subsiding basin (back-arc) and a rising belt to the west, which is now the Shuswap Complex (Fig.9.1).

However, the situation is not this simple since it was suggested above that the Rossland volcanics are similar to the main arc rocks of the Nicola-Takla belt. So what processes produced the Rossland volcanics probably operated the length of the arc, and thus localised subduction of faults, or hinge faulting cannot really be invoked as an explanation. It is interesting that the late Mesozoic arc in S.E. Alaska, to which the Bridget Cove ankaramites belong, is also anomalous by present-day standards, and is comparable, as Irvine (1974) notes, to the Nicola-Takla belt. Possibly, therefore, the complex tectonic history of Western Canada -that of continued oceanward stepping of subduction zones with suturing events - has produced this situation. In the Nicola-Takla case, it may be significant that prior to the arc's initiation, subduction shifted from the Pinchi fault to the Fraser-Yalakom fault zone. This shift, incidentally, may have been in response to an early rifting phase of the North Atlantic, pushing the North American craton westwards and thus sealing off the old subduction zone (cf. Monger et al., 1972).

In the Lower Jurassic the relative uniformity of magmatism along the length of the Cordillera was disrupted, and an apparent gradation was imposed, in terms of magma type and intensity of volcanism. To the north, Upper Triassic Takla rocks were overlain

by more evolved andesitic/dacitic varieties. A localised back-arc basin in north-central British Columbia (see Fig.5.6) allowed the persistence of more basic, alkalic magmas. In Southern British Columbia this situation did not occur and volcanism was less intense. Andesitic or dacitic volcanics, comparable to the Hazelton rocks, do not succeed the Nicola rocks. Rather,a similar form of volcanism and magmatism to that characterizing the Upper Triassic, persisted in the Rossland and Quesnel troughs until late Lower Jurassic.

These changes must reflect the complex tectonics of this period (Chapter 2) in that suturing was occurring in the south and the Fraser-Yalakom subduction zone was becoming less active. Further north, subduction continued along a similar line to that of the Upper Triassic. That the focus of magmatism in the south of British Columbia shifted eastwards (from the Nicola to the Rossland area) may be a manifestation of the growth of the arc-trench gap with time (Dickinson, 1974). Alternatively, as was suggested above, westward movement of the American craton in response to early rifting in the North Atlantic may be responsible. However, this last process was probably not great in significance since arc-trench gap sedimentation was continuing uninterrupted west of the arc (Anderson, 1976).

A further influence on the nature and setting of the Rossland volcanics is the extent of the Archaean craton. In Chapter 2 it was shown that its westward extent in Southern British Columbia is not well known. From the geochemistry of the volcanics, however, there is no evidence of cratonic influence, the arc to which the Rossland volcanics belong probably being built on the

thin end of the wedge of miogeoclinal sediments, and thus ultimately over oceanic crust, albeit modified. The similar chemistry of the Nicola rocks, which were almost certainly built on Cache Creek oceanic assemblages (see Fig.2 of Monger et al., 1972), confirms this. Permo-Carboniferous rocks similar to the Cache Creek assemblage are traceable (see Fig. 2.4) through the Southern Shuswap complex as far as the Mt.Roberts succession.

The 'Rossland Break' has been mentioned above (Chapter 3) as possibly being a significant boundary between the Rossland/ Lardeau trough to the east, in which the bulk of the volcaniclastic succession accumulated, and the positive area to the west now underlain by Cache Creek and Shuswap assemblages. This fault zone, along which serpentinites are emplaced, could therefore represent a line of weakness along which Rossland magmas were focussed. There is also the possibility that the Rossland Break is a southward continuation of the Pinchi-fault suture zone and thus represents the site of subduction causal to the Late Palaeozoic, Ominica Belt volcanic-arc, locally represented by the Kaslo volcanics (Chapter 2). If this is the case, continental crust of Archaean age cannot plausibly extend further west than the Rossland area. This idea of the Rossland volcanics relating to the old Pinchi fault-Rossland Break suture also fits in with the observed similarity, in age, chemistry and lithology, with the Quesnel trough volcanics described by Campbell & Tipper (1971).

Fig. 9.1, taken from Douglas et al. (1970), shows several schematic sections through the Cordillera for the early Mesozoic. The back-arc setting of the Rossland volcanics (9.1a) and the Quesnel trough (9.1b) is evident with, in both cases, seemingly

Figure 9.1

Schematic cross sections through the Canadian Cordillera in the early Mesozoic. RB is the position of the Rossland Break and SZ the position of the trench where east dipping subduction was believed to be taking place up to the Middle Jurassic (see text for discussion).

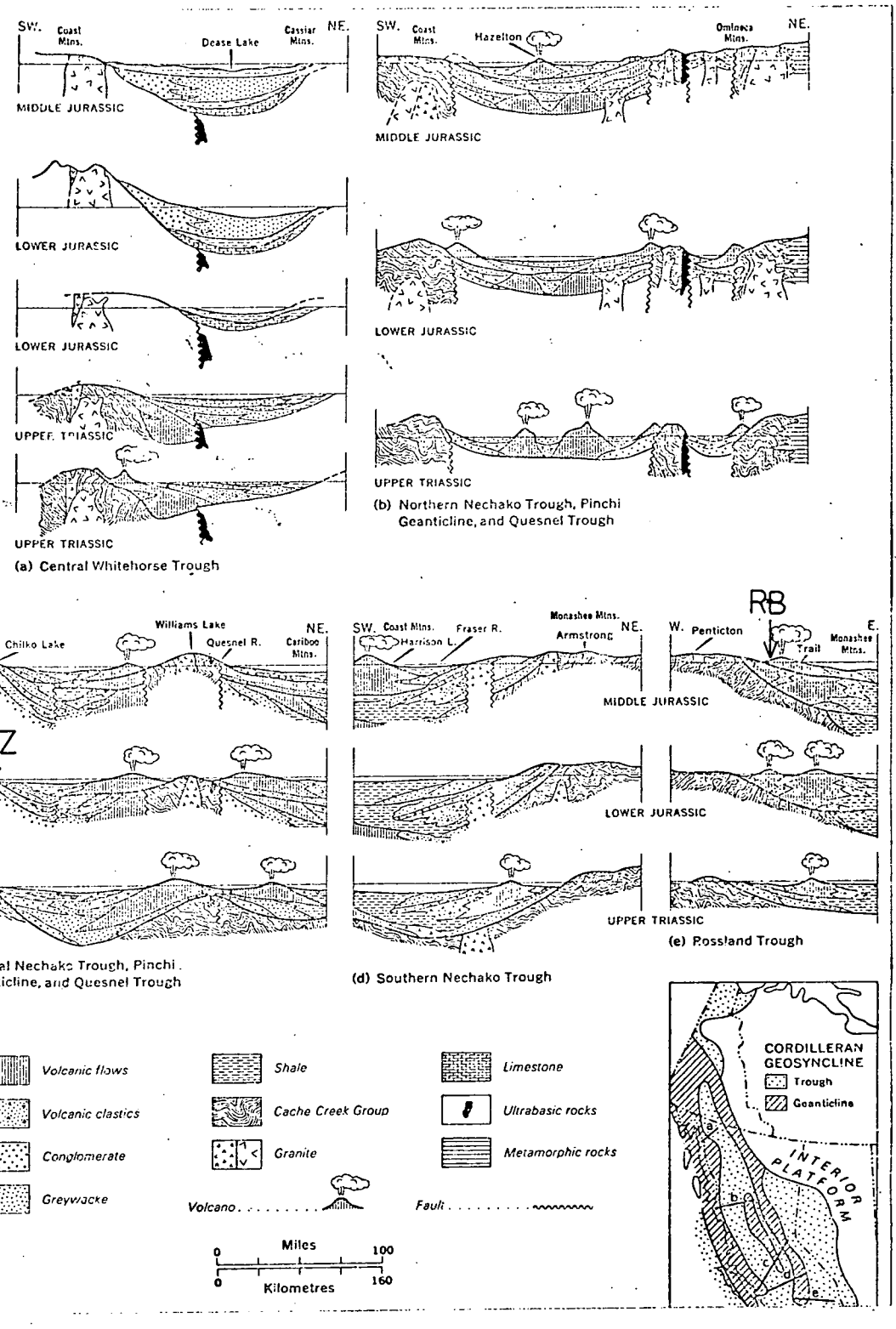
SW.
Coast Mtns.
Dease Lake
Cassiar Mtns.
NE.
MIDDLE JURASSIC
LOWER JURASSIC
LOWER JURASSIC
UPPER TRIASSIC
UPPER TRIASSIC
(a) Central Whitehorse Trough
SW.
Coast Mtns.
Hazelton
Omineca Mtns.
NE.
MIDDLE JURASSIC
LOWER JURASSIC
UPPER TRIASSIC
(b) Northern Nechako Trough, Pinchi Geanticline, and Quesnel Trough
SW.
Coast Mtns.
Chilko Lake
Williams Lake
Quesnel R.
Cariboo Mtns.
NE.
MIDDLE JURASSIC
SZ
LOWER JURASSIC
UPPER TRIASSIC
(c) Central Nechako Trough, Pinchi Geanticline, and Quesnel Trough
SW.
Coast Mtns.
Harrison L.
Fraser R.
Monashee Mtns.
Armstrong
NE.
MIDDLE JURASSIC
LOWER JURASSIC
UPPER TRIASSIC
(d) Southern Nechako Trough
RB
W.
Penticton
Trail
E.
Monashee Mtns.
MIDDLE JURASSIC
LOWER JURASSIC
UPPER TRIASSIC
(e) Rossland Trough
Volcanic flows
Volcanic clastics
Conglomerate
Greywacke
Shale
Cache Creek Group
Granite
Limestone
Ultrabasic rocks
Metamorphic rocks
Volcano
Fault
0
Miles
100
0
Kilometres
160
CORDILLERAN GEOSYNCLINE
Trough
Geanticline
INTERIOR PLATFORM
a
b
c
d
e

emergent land to the west. However, it is envisaged here that these emergent areas may have been the actual loci of the arc volcanics; not as shown, since what is preserved in the troughs are, in high proportion, volcaniclastic debris (Chapter 3). The position of the Rossland Break is indicated by 'RB' in Fig.9.1e. Another difference between the sections in Fig.9.1 and what is envisaged here is that a subduction zone was operative, located near 'SZ'.

In Chapter 5 it was proposed that the Rossland magmas are mantle-derived and it seems likely that this is the case generally for the Nicola-Takla arc, in view of the basic nature of the volcanic products. The parental partial melts are thought to have been picritic and fractionated olivine on ascent, giving rise to a series of augite-rich or ankaramitic basalts. Crustal level fractionation, of an oxidising and hydrous nature, resulted in the fractionation of clinopyroxene, spinel (magnetite), amphibole and plagioclase to give rise to a series of low-TiO_2 basalts and andesites characteristic of island-arcs. It was also suggested that the high concentration of elements such as K, Rb and Ba is a result of their enrichment in the source mantle by hydrous fluids, possibly derived from the subduction zone. It is thought that partial melts derived from the subducted slab had little influence on the petrogenesis of the magmas. Possibly this is one reason why there is a lack of highly evolved magmas in the Nicola-Takla Belt generally.

9:2 Metamorphic history

Following the eruption and deposition of the volcanics, in quite rapid succession, they were metamorphosed, locally up to lower amphibolite facies. As shown in Chapters 2 and 3, uplift in the Southern Ominica Belt started around the Middle Jurassic in response to accompanying plutonism, deformation and metamorphism.

The volcanics were demonstrably metamorphosed at relatively low pressures, as would be expected from the time considerations, and they also exhibit a variation in grade along strike, indicating that localised hot spots were responsible. It is thought the south to north increase in grade from prehnite-pumpellyite facies to lower amphibolite facies is related to the metamorphic culmination centred on the Valhalla gneiss dome, north of the area of the Rossland volcanics.

This metamorphic hot spot also represented the focus for the Nelson Batholith which generally intrudes the northern half (zone B) of the volcanics to a greater extent than the southern (zone A). Prior to the intrusion of the bulk of the Nelson Batholith, folding of the volcanics about north-south axes and localised shearing had occurred, which in turn succeeded an early phase of greenschist metamorphism. Thus, although the Nelson rocks cause local contact metamorphism, they are not directly responsible for the 'regional' metamorphism of the volcanics. The Silver King Porphyry body shares various shearing structures with the volcanics, and this body probably was related to the earlier stages of the metamorphic episode.

From consideration of the oxygen isotope data it is clear that the volcanics were not metamorphosed or altered by circulating meteoric water, as are, for example, basalts in the British Tertiary Province. Rather, the volcanics were enriched in ^{18}O by exchange, over time, with a reservoir of ^{18}O-enriched water, probably resulting from dehydration metamorphic reactions continuing at depth and percolating surface-wards.

The last event to have any significant effect on the petrogenesis of the volcanics is the emplacement of the Tertiary Trail, Sheppard

and Coryell Batholiths. These have locally contact-metamorphosed the volcanics. This is reported in the Rossland area by Fyles (in prepn.) and is observed by the development of amphibole locally, south of Fruitvale (Fig.6.1), near the eastern margin of the Sheppard intrusion.

LIST OF REFERENCES

Anderson, A.T., 1967. The dimensions of oxygen isotope equilibrium attainment during prograde metamorphism. J.Geol., 75, 323-332.

Anderson, A.T., Clayton, R.N., & Mayeda, T., 1971. Oxygen isotope thermometry of mafic igneous rocks. J.Geol., 79, 715-729.

Anderson, P., 1976. Oceanic crust and arc-trench gap tectonics in southwestern British Columbia. Geology, 4, 443-446.

Aoki, K., 1963. The Kaersutites and oxykaersutites from alkalic rocks of Japan and surrounding areas. J. Petrol., 4, 198-210.

Arculus, R.J., 1973. The alkali-basalt, andesite association of Grenada, Lesser Antilles. Unpub. Ph.D. thesis, University of Durham.

Arculus, R.J., 1976. Geology and geochemistry of the alkali-basalt, Andesite association of Grenada, Lesser Antilles island arc. Geol. Soc.Am.Bull., 87, 612-624.

Arculus, R.J., De Long, S.E., Kay, R.W., Brooks, C., & Sun, S.S., 1977. The alkalic rock suite of Bogoslof Island, Eastern Aleutian Arc, Alaska. J.Geol., 85, 177-186.

Arculus, R.J., & Curran, E.B., 1972. The genesis of the calc-alkaline rock suite. Earth. Planet. Sci.Lett., 15, 255-262.

Armstrong, R.L., Tanbeneck, W.H., & Hales, P.O., 1977. Rb-Sr and K-Ar geochronology of Mesozoic granitic rocks and their Sr isotopic composition, Oregon, Washington, and Idaho. Geol .Soc. Am.Bull., 88, 397-411.

Baker, P.E., 1968a. Comparative volcanology and petrology of the Atlantic island-arcs. Bull.Volcanol., 32, 189-209.

Baker, P.E., 1968b. Petrology of Mt.Misery volcano, St.Kitts, West Indies. Lithos, 1, 124-150.

Bally, A.W., Gordy, P.L. & Stewart, G.A., 1966. Structure, seismic data and orogenic evolution of southern Canadian Rocky Mountains. Bull. Can. Petrol.Geol., 14, 337-381.

Barberi, F., Bizonard, H., & Varet, J., 1971. Nature of clinopyroxene and iron-enrichment in alkali and transitional basaltic magmas. Contr.Mineral.Petrol., 33, 93-107.

Barron, B.J., 1976. Recognition of the original volcanic suite in altered mafic volcanic rocks at Sofala, New South Wales, Am.J.Sci., 276, 604-636.

Barron, B.J., & Barron, L.M., 1976. A model for greenschist facies equilibria in altered mafic volcanic rocks at Sofala, New South Wales. Am.J. Sci., 276, 637-669.

Battey, M.H., 1974. Spilites as weakly metamorphosed tholeiites, in G.C. Amstutz (ed.)., Spilites and spilitic rocks. Springer Verlag, Heidelberg.

Baxter, A., 1976. Geochemistry and petrogenesis of primitive alkali basalt from Mauritius, Indian Ocean. Geol.Soc.Am. Bull., 87, 1028-1034.

Berg, H.C., Jones, D.L., & Richter, D.H., 1972. Gravina-Nutzotin belt; tectonic significance of an Upper Mesozoic sedimentary and volcanic sequence in southern and southeastern Alaska. U.S.Geol. Surv. Prof.Paper 800D, D1-D24.

Berry, M.J., Jacoby, W.R., Niblett, E.R., & Stacey, R.A., 1971. A review of geophysical studies in Canadian Cordillera. Can. J.Earth.Sci., 8, 788-801.

Best, M.G., 1975. Migration of hydrous fluids in the upper mantle and potassium variation in calc-alkalic rocks. Geology, 3, 429-432.

Binns, R.A., 1965. The mineralogy of metamorphosed basic rocks from Willyama Complex, Broken Hill district, New South Wales. Part I: Hornblendes. Min.Mag., 35, 306-326.

Binns, R.A., 1969. Ferromagnesian minerals in high grade metamorphic rocks. Geol.Soc. Australia. Spec.pubs. 2,323-332.

Black, P.M., 1974. Oxygen isotope study of metamorphic rocks from the Onega district, New Caledonia. Contr.Mineral. Petrol., 47, 197-206.

Bottinga, Y, & Javoy, M., 1975. Oxygen isotope partitioning among the minerals in ingeous and metamorphic rocks. Revs. Geophys. Space Physics, 13, 401-418.

Brown, E.H., 1967. The greenschist facies in part of eastern Otago. Contr.Mineral. Petrol., 14, 259-292.

Brown, E.H., 1977. The crossite content of Ca-amphibole as a guide to pressure of metamorphism. J.Petrol. 18, 53-72.

Brown, G.M., 1968. The mineralogy of basaltic rocks in H.H.Hess and A. Pldervaart (eds.)., Basalts, The Poldervaart treatise on rocks of basaltic composition, 1, 103-162.

Brown, G.M., Emeleus, C.H., Holland, J.G., and Phillips, R., 1970. Petrographic, mineralogic and X-ray fluorescence analysis of lunar igneous-type rocks and spherules. Science 167, 559-601.

Brown, G.M., Holland, J.G., Sigurdsson, H., Tomblin, J.F., & Arculus, R.J., 1977. Geochemistry of the Lesser Antilles volcanic island arc. Geochim.et Cosmoctim. Acta. 41, 785-801.

Campbell, R.B., 1961. Quesnel Lake, west half, British Columbia. Geol.Surv.Canada, Map 3 - 1961.

Campbell, R.B., 1966. Tectonics of the south central Cordillera of British Columbia. Can.Inst.Mining & Metallurgy, Spec. vol. 8, 61-71.

Campbell, R.B., & Tipper, H.W., 1971. Geology of Bonaparte Lake map-area, British Columbia. Geol. Surv.Can.Mem. 363.

Cann, J.R., 1969, Spilites from the Carlsberg ridge. J.Petrol., 10, 1-19.

Cann, J.R., 1970. Rb, Sr, Y, Zr and Nb in some ocean floor basaltic rocks. Earth. Planet. Sci.Lett. 10, 7-11.

Cann, J.R., 1971. Major element variations in ocean floor basalts. Phil.Trans.R.Soc. London, 268, 495-505.

Carmichael, I.S.E., 1967a. The mineralogy of Thingmuli, a Tertiary volcano in Eastern Iceland. Am.Mineral., 52, 1815-1841.

Carmichael, I.S.E., 1967b. The iron-titanium oxides of salic volcanic rocks and their associated Fe-Mg silicates. Contr. Mineral. Petrol., 14, 36-64.

Carmichael, I.S.E., & Nicholls, J., 1967. Iron-titanium oxides and oxygen fugacities in volcanic rocks. J. Geophys. Res., 72, 4665-4681.

Carmichael, I.S.E., Turner, F.J., & Verhoogen, J., 1974, Igneous Petrology. McGraw Hill, New York.

Cawthorn, R.G., Ford, C.E., Biggar, G.M. Bravo, M.S., & Clarke, D.B., 1973. Determination of the Liquid composition in experimental samples; discrepancies between microprobe analysis and other methods. Earth.Planet.Sci. Lett., 21, 1-5.

Cawthorn, R.G., 1976a. Some chemical controls on igneous amphibole compositions. Geochim.et Cosmochim. Acta, 40, 1319-1328.

Cawthorn, R.G., 1976b. Melting relations in part of the system $CaO-MgO-Al_2O_3 - SiO_2 - Na_2O - H_2O$ under 5 kb pressure. J.Petrol., 17, 44-72.

Cawthorn, R.G., & O'Hara, M.J., 1976. Amphibole fractionation in calc-alkaline magmas genesis. Am.J.Sci., 276, 309-329.

Chayes, F., 1971. Ratio Correlation. Univ. of Chicago Press, Chicago.

Chayes, F., & Velde, D., 1965. On distinguishing basaltic lavas of circumoceanic and ocean island type by means of discriminant functions. Am.J.Sci. 263, 206-222.

Choudhuri, A., 1974. Distribution of Fe and Mg in actinolite, hornblende and biotite in some Precambrian metagreywackes from Guyana, South America. Contr.Mineral. Petrol, 44, 45-55.

Clarke, D.B., 1970. Tertiary basalts of Baffin Bay: Possible primary magmas from the mantle. Contr. Mineral. Petrol., 25, 203-224.

Clayton, R.N., 1963. Oxygen isotope geochemistry: Thermometry of metamorphic rocks. In D. Shaw (ed.): Studies in analytical geochemistry. Univ. of Toronto press., 42-57.

Clayton, R.N., & Mayeda, T.K., 1963. The use of Bromine Pentafluoride in the extraction of oxygen from oxides and silicates for isotopic analysis. Geochim. et Cosmochim. Acta, 27, 43-52.

Cockfield, W.E., 1948. Geology and mineral deposits of Nicola map-area. Geol. Surv. Can.Mem. 249.

Colley, H., & Warden, A.J., 1974. Petrology of the New Hebrides. Geol.Soc.Am. Bull., 85, 1635-1646.

Coish, R.A., 1977. Ocean floor metamorphism in the Betts Cove Ophiolite, Newfoundland. Contr. Mineral. Petrol., 60, 225-270.

Coombs, D.S., 1960. Lower Grade mineral facies in New Zealand. Rep.Int.Geol. Congr. 21st Session, Norden. Pt. XIII, 339-351.

Coombs, D.S., 1963. Trends and affinities of basaltic magmas and pyroxenes as illustrated on the di-ol-q3 diagram. Min.Soc.Am. Spec. Paper 1, 227-250.

Cooper, A.F., 1972. Progressive metamorphism of metabasic rocks from the Haast Schist Group of Southern New Zealand. J.Petrol., 13, 457-492.

Cooper, A.F., & Lovering, J.F., 1970. Greenschist amphiboles from Haast River, New Zealand, Contr.Mineral. Petrol., 27, 11-24.

Cox, K.G., & Bell, J.D., 1972. A crystal fractionation model for the basaltic rocks of the New Georgia Group, British Solomon Islands. Contr. Mineral. Petrol. 37, 1-13.

Craig, H., 1957. Isotopic standards for carbon and oxygen and the correction factors for mass spectrometric analysis of CO_2. Geochim. et Cosmochim. Acta, 12, 133-149.

Craig, H., 1961. Standards for reporting concentrations of deuterium and oxygen -18 in natural water. Science, 133, 1833-1834.

Daly, R.A., 1912. North America Cordillera, Forty-ninth Parallel. Geol. Surv. Can.Mem. 38.

Deer, W.A., Howie, R.A., & Zussman,J., 1962. Rock forming minerals. Longmans, London.

De Long, S.E., Hodges, F.N., & Arculus, R.J., 1975. Ultramafic and mafic inclusions, Kanaga Island, Alaska and the occurrence of alkaline rocks in island arcs. J.Geol., 83, 721-736.

Dickinson, W.R., 1971. Plate tectonic models of geosynclines. Earth Planet. Sci.Lett., 10, 165-174.

Dickinson, W.R., 1974. Width of modern arc-trench gaps proportional to past duration of igneous activity in associated magmatic arcs. J.Geophys.Res., 78, 3376-3389.

Dickinson, W.R., 1976. Sedimentary basins developed during the evolution of Mesozoic-Cenozoic arc-trench systems in western North America. Cam.J.Earth.Sci. 13, 1268-1287.

Dickinson, W.R., & Hatherton, T., 1967. Andesitic volcanism and seismicity around the Pacific. Science, 157, 801-803.

Douglas, R.J.W., Gabriesle, H., Wheeler, J.O., Stott, D.F., & Belyea, H.R., 1970. Geology of western Canada. In R.J.W. Douglas (ed.): Geology and economic minerals of Canada. Geol.Surv.Can.Economic Geology rept. 1.

Drysdale, C.W., 1915. Geology and ore deposits, Rossland, British Columbia. Geol.Surv.Can.Mem. 77.

Eggler, D.H., 1972. Water-saturated and undersaturated melting relations in a Paracutin andesite, and an estimate of water content of the natural magma. Contr.Mineral.Petrol., 34, 261-271.

Eggler, D.H., & Burnham, C.W., 1973. Crystallization and fractionation trends in the system. Andesite- H_2O - CO_2 - O_2 at pressures to 10kb. Geol.Soc.Am.Bull. 84, 2517-2532.

Engel, A.E.J., & Engel, C.G., 1964. Composition of basalts from the mid-Atlantic ridge. Science, 144, 1330-1333.

Ernst, W.G., 1972. CO_2-poor composition of the fluid attending Franciscan and Sanbagawa low-grade metamorphism. Geochim. et Cosmochim. Acta, 36, 497-504.

Ernst, W.G., Seki, Y., Onuli, H., & Gilbert, M.C., 1970. Comparative study of low-grade metamorphism in California coast Ranges and outer metamorphic belt of Japan. Geol.Soc. Am.Mem. 124.

Ewart, A., Bryan, W.B., & Gill, J.B., 1973. Mineralogy and geochemistry of the younger volcanic islands of Tonga, S.W. Pacific. J.Petrol., 14, 429-465.

Fawcett, J.J. & Yoder, H.S., Jnr., 1966. Phase relationships in the chlorites in the system $MgO - Al_2O_3 - SiO_2 - H_2O$. Am. Mineral., 51, 353-380.

Field, D. & Elliot, R.B., 1974. The chemistry of gabbro/amphibolite transitions in South Norway. II: Trace elements. Contr. Mineral. Pet., 47, 63-76.

Flower, M.F.J., 1971. Evidence for the role of phlogopite in the genesis of alkali basalts. Contr.Mineral. Petrol., 32, 126-137.

Flower, M.F.J., 1973. Trace element distribution in lavas from Anjouan and Grand Comore, Western Indian Ocean. Chem.Geol., 12, 81-98.

Floyd, P.A., 1976. Geochemical variation in the greenstones of S.W. England. J.Petrol. 17, 522-545.

Floyd, P.A., & Winchester, J.A., 1975. Magma type and tectonic setting discrimination using immobile elements. Earth.Planet. Sci. Lett., 27, 211-18.

Fodor, R.V., 1971. Fe content in pyroxenes from a calc-alkaline volcanic suite in New Mexico, USA. Earth Planet.Sci.Lett., 11, 385-390.

Fodor, R.V., Keil, K., & Bunch, T.E., 1975. Contribution to the mineral chemistry of Hawaii rocks. IV: Pyroxenes in rocks from Haleakala and West Mauai volcanoes, Mauai, Hawaii. Contr. Mineral. Petrol, 50, 173-195.

Forbes, W.G., & Flower, M.F.J., 1974. Phase relations of titan-phlogopite K_2Mg_4 $TiAl_2Si_6O_{20}$ $(OH)_4$: A refractory phase in the upper mantle. Earth. Planet. Sci.Lett. 22, 60-66.

Forester, R.W. & Taylor, H.P., Jr., 1977. $^{18}O/^{16}O$, D/H and $^{13}C/^{12}C$ studies of the Tertiary igneous comples of Skye, Scotland. Am.J. Sci. 277, 136-177.

Fox, P.E., 1975. Alkaline rocks and related mineral deposits of the Quesnel trough, British Columbia. (abs.) Geol.Assoc. of Canada, Symposium on intrusive rocks and related mineralization of the Canadian Cordillera. Program and abs. p.12.

Frebold, H., 1959. The marine Jurassic rocks in Nelson and Salmo areas, southern British Columbia. Geol.Surv. Can. Bull. 51.

Frebold, H., & Little, H.W., 1962. Palaeontology, stratigraphy and structure of the Jurassic rocks in Salmo Map-area, British Columbia. Geol. Surv. Can. Bull. 81,
o

Fyles, J.T., 1970. Rossland: British Columbia Department of Mines, Petroleum and Resources, preliminary Map No.4.

Fyles, J.T., in preparation. Bulletin to accompany preliminary Map 4 of the Rossland area. British Columbia Department of Mines, Petroleum and Resources.

Fyles, J.T., Harakal, J.E. & White, W.H., 1973. The age of sulphide mineralization at Rossland, British Columbia. Econ. Geol. 68, 23-33.

Gabriesle, H., 1972. Younger Precambrian of the Canadian Cordillera. Am.J. Sci., 272, 521-536.

Gabriesle, H., & Reesor, J.E., 1974. The nature and setting of granite plutons in the central and eastern parts of the Canadian Cordillera. Pacific Geol. 8, 109-138.

Gandy, M.K., 1975. The petrology of the Lower Old Red Sandstone lavas of the eastern Sidlaw Hills, Perthshire, Scotland. J.Petrol., 16, 189-211.

Garlick, G.D. & Epstein, S., 1967. Oxygen isotope ratios in coexisting minerals of regionally metamorphosed rocks. Geochin. et Cosmochim. Acta, 31, 181-214.

Gibb, F.G.F., 1973. The zoned clinopyroxenes of the Shiant Isles sill, Scotland. J. Petrol. 14, 203-230.

Gill, J.B., 1970. Geochemistry of Viti Levu, Fiji, and its evolution as an island arc. Contr. Mineral. Petrol., 27, 179-203.

Gill, J.B., 1974. Role of underthrust oceanic crust in the genesis of a Fijian calc-alkaline suite. Contr. Mineral. Petrol. 43, 29-45.

Graham, C.M., 1973. Chemical petrology of metamorphosed basic rocks of the Dalradian series, with particular reference to the Knapdale area of Argyll. Unpub. Ph.D. thesis, Univ. of Edinburgh.

Graham, C.M., 1974. Metabasite amphiboles of the Scottish Dalradian. Contr.Mineral. Petrol. 47, 165-185.

Grapes, R.H., 1975. Actinolite-hornblende pairs in metamorphosed gabbros, Hidaka Mountains, Hokkaido. Contr.Mineral. Petrol, 49, 125-140.

Grapes, R.H., Hashimoto, S., & Miyashita, S. 1977. Amphiboles of a metagabbro-amphibolite sequence, Hidaka metamorphic belt, Hokkaido. J.Petrol. 18, 285-318.

Green, D.H., 1973. Experimental melting studies on a model upper mantle composition at high pressure and under water-saturated and undersaturated conditions. Earth.Planet. Sci.Lett., 19, 37-53.

Green, T.H., & Ringwood, A.E., 1968. Genesis of the calc-alkaline igneous rock suite. Contr.Mineral. Petrol., 18, 105-162.

Griffiths, J.R., 1977. Mesozoic-early Cenozoic volcanism, plutonism and mineralization in southern British Columbia; A plate tectonic synthesis. Can.J.Earth. Sci, 14, 1611-1614.

Gunn, B.M., 1972. The fractionation effect of kaersutite in basaltic magmas. Can.Mineral., 11, 840-850.

Hamilton, D.L., & Anderson, L.M., 1968. Effects of water and oxygen pressure on the crystallization of basaltic magmas. In H.H. Hess and A.Poldernart (eds.). Basalt. The Poldervaart treatise on rocks of basaltic composition. 1, 445-482.

Hart, S.R., 1969. K, Rb, Cs contents and K/Rb, K/Cs ratios of fresh and altered submarine basalts. Earth Planet. Sci. Lett. 6, 295-303.

Hart, S.R., & Nalwalk, A.J., 1970. K, Rb, Cs and Sr relationships in submarine basalts from Puerto Rico trench. Geochim et Cosmochim. Acta, 34, 145-155.

Hart, S.R., Erlank, A.J. & Kable, J.D., 1974. Sea floor basalt alteration: Some chemical and Sr isotope effects. Contr. Mineral. Petrol, 44, 219-230.

Harte, B., & Graham, C.M., 1975. The graphical analysis of greenschist to amphibolite facies mineral assemblages in metabasites. J.Petrol., 16, 347-370.

Hashimoto, M., 1972. Reactions producing actinolite in basic metamorphic rocks. Lithos, 5, 19-31.

Helz, R.T., 1973. Phase relationships of basalts in their melting range at P_{H_2O} = 5 kb. as a function of oxygen fugacity. Part I: Mafic phases. J.Petrol. 14, 249-302.

Henderson, P. & Dale, I.M., 1970. The partitioning of selected transition element ions between olivine and groundmass of oceanic basalts. Chem. Geol. 5, 267-274.

Hietanen, A., 1971. Distribution of elements in biotite-hornblende pairs and in an orthopyroxene-clinopyroxene pair from zoned plutons, northern Sierra Nevada, California. Contr. Mineral. Petrol. 30, 161-176.

Hietanen, A., 1974. Amphibole pairs, epidote minerals, chlorite and plagioclase in metamorphic rocks, northern Sierra Nevada, California. Am. Mineral., 59, 22-40.

Holdaway, M.J., 1965. Basic regional metamorphic rocks in part of the Klamath Mountains, Northern California. Am.Mineral., 50, 953-977.

Holdaway, M.J., 1972. Thermal stability of Al-Fe epidote as a function of f_{O_2} and Fe content. Contr.Mineral. Petrol. 37, 307-340.

Holland, J.G., & Brindle, D.W., 1966. A self-consistent mass absorption correction for silicate analysis by X-ray fluorescence. Spectrochim. Acta. 22, 2083-2093.

Holloway, J.R., 1973. The system pargasite - H_2O-CO_2: A model for melting of a hydrous material with mixed-volatile fluid. I: Experimental results to 8kB. Geochim. et Cosmochim.Acta, 37, 651-666.

* Hey, M.H., 1954. A new review of the chlorites. Min. Mag, 30, 277.

Holloway, J.R., Burnham, C.W., 1972. Melting relations of basalt with equilibrium water pressures less than total pressure. J.Petrol. 13, 1-29.

Hyndman, D.W., 1968. Petrology and structure of the Nakusp Map-area, British Columbia. Geol.Surv. Can.Bull. 161.

*

Irvine, T.N., 1967. Cr-spinel as a petrogenetic indicator. Part II: Petrologic applications. Can.J.Earth. Sci, 4, 71-103.

Irvine, T.N., 1973. Bridget Cove volcanics, Junean area, Alaska; Possible parental magma of Alaskan type ultramafic complexes. Carnegie Inst. Washington Yearbook 72, 478-491.

Irvine, T.N., 1974. The Duke Island ultramafic complex, south east Alaska. Geol.Soc.Am. Mem. 138.

Irwin, A.B., 1951. Mapping complex folds in the Slocan Series, British Columbia. Trans. Can.Inst. Mining and Metallurgy, 54, 494-501.

Jakeš, P., & Smith, I.E., 1970. High potassium calc-alkaline rocks from Cape Nelson, Eastern Papua. Contr.Mineral. Petrol., 28, 259-271.

Jakeš, P. & White, A.J.R., 1969. Structure of the Melanesian arcs and correlation with distribution of magma types. Tectonophysics, 8, 223-236.

Jakeš, P. & White, A.J.R., 1972a. Hornblendes from calc-alkaline volcanic rocks of island arcs and continental margins. Am. Mineral. 57, 887-902.

Jakeš, P. & White, A.J.R., 1972b. Major and trace elements abundances in volcanic rocks of orogenic regions. Geol. Soc.Am. Bull., 83, 29-40.

* Hynes, A. 1976. Magmatic affinity of Ordovician volcanic rocks in northern Maine, and their tectonic significance. Am. J. Sci 276, 1208-1224

James, D.E., Brooks, C. & Cuyubamba, A., 1976. Andean Cenozoic volcanicsm: magma genesis in the light of strontium isotopic composition and trace element geochemistry. Geol.Soc. Am. Bull. 87, 592-600.

Jenkins, R. & DeVries, J.L., 1970. Practical X-ray spectrometry. Macmillan Press, London.

Jolly, W.T., 1970. Zeolite and prehnite-pumpellyite facies in South Central Puerto Rico. Contr. Mineral. Petrol, 27, 204-224.

Jolly, W.T. & Smith, R.E., 1972. Degradation and metamorphic differentiation of the Keweenan tholeiitic lavas of northern Michigan, U.S.A. J. Petrol., 13, 273-309.

Jones, D.L., Irwin, W.P. & Ovenshine, A.T. Southeast Alaska - a displaced continental fragment? U.S. Geol.Surv. Prof. Paper 800B, B213-B219.

Kaneswich, E.R., Clowes, R.M., & McCloughan, C.H. 1968. A buried Precambrian rift in western Canada. Tectonophysics, 8,513-527.

Keil, K., Fodor, R.V., & Bunch, T.E., 1972. Contribution to the mineral chemistry of the Hawaiian rocks. II: Feldspars and interstitial material in rocks from Haleakala and West Mauai volcanoes, Manai, Hawaii. Contr. Mineral. Petrol., 37, 253-275.

King, P.B., 1969. Tectonic map of North America. U.S. Geol. Surv., scale 1:5,000,000.

Klein, C.R., Jr., 1969. Two amphibole assemblages in the system actinolite-hornblende-glaucophane. Am.Mineral., 54, 212-237.

Kuniyoshi, S. & Liou, J.G., 1974. Burial metamorphism of the Karmutsen Volcanics, Vancouver Island. Am.Geophys. Union. Trans. 56, 1199.

Kuniyoshi, S., & Liou, J.G., 1976. Contact metamorphism of the Karmutsen Volcanics, Vancouver Island, British Columbia. J. Petrol. 17, 73-99.

Kuno, H., 1966. Lateral variation of basalt magma across continental margins and island arcs. Bull. Volcanol., 29, 195-222.

Kushiro, I., 1960. Si-Al relations in clinopyroxenes from igneous rocks. Am.J.Sci., 258, 548-554.

Kushiro, I., 1972. Effect of water on the composition of magmas formed at high pressures. J.Petrol., 13, 311-334.

Lambert, R. St.J. & Holland, J.G., 1974. Yttrium geochemistry. Geochim. et Cosmochim. Acta, 38, 1393-1414.

Larsen, E.S., Gonyer, F.A., Irving, J. & Larsen, E.S., 3rd 1937. Petrologic results of a study of the minerals from tertiary volcanic rocks of the San Juan region, Colorado. Am.Mineral. 22, parts 5 & 6, 889-905.

Lathram, E.H., Pomeroy, J.S., Berg, H.S., & Loney, R.A., 1968. Reconnaisance geology of Admiralty Island, Alaska. U.S. Geol.Surv. Bull.1178.

Leake, B.E., 1962. On the non-existence of a vacant area in the Hallimond calciferous amphibole diagram. Jap. Jour. Geol. Geog., 33, 1-13.

Leake, B.E., 1965. The relationship between tetrahedral aluminium and the maximum possible octahedral aluminium in natural calciferous amphiboles. Am.Mineral. 50, 843-851.

Le Bas, M.J., 1962. The role of aluminium in igneous clinopyroxenes with relation to their parentage. Am.J.Sci. 260, 267-288.

Levi, B., 1969. Burial metamorphism of a Cretaceous volcanic sequence west from Santiago, Chile. Contr.Mineral. Petrol., 24, 30-49.

Lewis, J.F., 1964. Mineralogical and petrological studies of plutonic blocks from the Soufriere volcano, St. Vincent, British West Indies. D.Phil.thesis, Univ. of Oxford.

Lewis, J.F., 1973a. Petrology of the ejected plutonic blocks of the Soufriere Volcano, St.Vincent, West Indies. J.Petrol., 14, 81-112.

Lewis, J.F., 1973b. Mineralogy of the ejected plutonic blocks of the Soufriere Volcano, St.Vincent: Olivine, pyroxene, amphibole, and magnetite paragenesis. Contr. Mineral. Petrol. 38, 197-220.

Liou, J.G., 1971. P-T stabilities of Caumontite, wairakite, lawsonite and related minerals in the system Ca $Al_2Si_2O_8$ - SiO_2 - H_2O. J. Petrol., 12, 379-411.

Liou, J.G., 1973. Synthesis and stability relations of epidote, $Ca_2Al_2FeSi_2O_{12}(OH)$. J. Petrol. 14, 381-413.

Liou, J.G., Juniyoshi, S. & Ito, K., 1974. Experimental studies of the phase relations between greenschist and amphibolite in a basaltic system. Am.J. Sci. 274, 613-632.

Lisitsyana, N.A., 1968. Geochemistry of weathering zones of basic rocks. Geochim.Int., 5, 210-244.

Little, H.W., 1950. Salmo Map-area, British Columbia. Geol. Surv. Can. Paper 50-19.

Little, H.W., 1960. Nelson Map-area, west half, British Columbia. Geol.Surv. Can.Mem., 308.

Little, H.W., 1962. Trail Map-area, British Columbia. Geol. Surv. Can.Paper 62-5.

Little, H.W., 1963. Rossland Map-area, British Columbia. Geol. Surv., Paper 63-13.

Little, H.W., 1964. Geology of Salmo Map-area. Geol. Surv. Can., Map 1145A.

Lord, C.S., 1948. McConnell Creek Map-area, Cassiar district, British Columbia, Geol. Surv.Can.Mem., 251.

Lowder, G.G., 1970. The volcanoes and caldera of Talasea, New Britain: Mineralogy. Contr. Mineral. Petrol., 26, 324-340.

MacKenzie, D.E. & Chappell, B.W., 1972. Shoshonitic and calc-alkaline lavas from the highlands of Papua, New Guinea. Contr. Mineral. Petrol., 35, 50-62.

Magaritz, M. & Taylor, H.P., Jr., 1976. $^{18}O/^{16}O$ and D/H studies along a 500 km. traverse across the Coast Ranges Batholith and its country rocks, central British Columbia. Can.J. Earth Sci., 13, 1514-1537.

Marsh, B.D. & Carmichael, I.S.E., 1974. Benioff zone magmatism. J. Geophys. Res. 79, 1196-1206.

Mattinson, J.M., 1972. Age of zircons from the northern Cascade Mountains, Washington. Geol. Soc. Am. Bull., 83, 3769-3784.

McAllister, A.L., 1951. Ymir Map-area, British Columbia. Geol. Surv. Can.Paper 51-4.

McBirney, A.R., & Aoki, K., 1968. Petrology of the Island of Tahiti. Geol. Soc. Am. Mem., 116, 523-556.

McConnell, R.G. & Brock, R.W., 1904. West Kootenay Sheet, British Columbia, Geol. Surv. Can. Map 792.

McCrea, J.M., 1950. The isotopic chemistry of carbonates and a palaeotemperature scale. J. Chem. Phys., 18, 849-857.

McKinney, C.R., McCrea, J.M., Epstein, S., Allen, H.A., & Urey, H.C., 1950. Improvements in mass spectrometers for the measurement of small differences in isotopic abundance ratios. Revs. Sci. Instruments, 21, 724-730.

Melson, W.G. & Van Andel, Tj.H., 1966. Metamorphism in the Mid-Atlantic Ridge, 22°N latitude. Marine Geol. 4, 165-186.

Misch, P., 1966. Tectonic evolution of the Northern Cascades province of Washington State. Can.Inst. Mining and Metallugry, Spec. vol. 8, 101-148.

Misch, P. & Rice, J.M., 1975. Miscibility of tremolite and hornblende in progressive Skagit metemorphic suite, North Cascades, Washington. J. Petrol. 16, 1-21.

Mitchell, A.H. & Reading, H.G., 1971. Evolution of island arcs. J. Geol. 79, 253-284.

Mitchell, A.H. & Warden, A.J., 1971. Geological evolution of the New Hebrides island-arc. J. Geol. Soc. London., 127, 501-530.

Miyashiro, A., 1974. Volcanic rock series in island-arcs and active continental margins. Am.J. Sci. 274, 231-355.

Miyashiro, A. & Seki, Y., 1958. Enlargement of the compositional field of epidote and piemontite with rising temperature. Am. J.Sci. 256, 423-430.

Medreski, P.J. & Boettcher, A.L., 1972. The stability of phlogopite and enstatite at high pressures: a model for micas in the interior of the Earth. Am.J. Sci., 272, 852-869.

Monger, J.W.H., 1975. Correlation of eugeosynclinal tectono-stratigraphic belts in the North American Cordillera. Geoscience Canada, 2, 4-10.

Monger, J.W.A., Souther, J.G., & Gabriesle, H., 1972. Evolution of the Canadian Cordillera: A plate tectonic model. Am.J. Sci., 272, 577-602.

Monger, J.W.H., & Hutchinson, H.W., 1970. Metamorphic map of the Canadian Cordillera. Geol.Surv. Can. Paper 70-33.

Monger, J.W.H., & Church, B.N., 1977. Revised stratigraphy of the Takla Group, north-central British Columbia. Can.J. Earth Sci. 14, 318-326.

Muehlenbachs, K., 1976. Oxygen isotope geochemistry of DSDP leg 34 basalts. Initial Repts. of the Deep Sea Drilling Project. 34, 337-339.

Muehlenbachs, K., & Clayton, R.N., 1972a. Oxygen isotope studies of fresh and weathered submarine basalts. Can.J. Earth Sci., 9, 172-184.

Muehlenbachs, K. & Clayton, R.N., 1972b. Oxygen isotope geochemistry of submarine greenstones. Can.J. Earth Sci., 9, 471-478.

Muehlenbachs, K., Anderson, A.T., & Sigvaldasson, G.E., 1974. Low ^{18}O basalts from Iceland. Geochim. et Cosmochim. Acta., 38, 577-588.

Mulligan, R., 1952. Bonnington Map-area, British Columbia. Geol. Surv. Can.Paper 52-13.

Mysen, B., 1975. Partitioning of iron and magnesium between crystals and partial melts in peridotite upper mantle. Contr. Mineral. Petrol., 52, 69-76.

Mysen, B. & Boettcher, A.L., 1975a. Melting of a hydrous mantle. I: Phase relations of natural peridotite at high pressures and temperatures with controlled activities of water,carbon dioxide and hydrogen. J. Petrol. 16, 520-548.

Mysen, B. & Boettcher, A.L., 1975b. Melting of a hydrous mantle. II: Geochemistry of crystals and liquids formed by anatexis of mantle peridotite at high pressures and temperatures of water, hydrogen and carbon dioxide. J. Petrol. 16, 549-593.

Nicholls, I.A., 1971. Petrology of Santorini Volcano, Cyclades, Greece. J. Petrol. 12, 67-121.

Nicholls, I.A., 1974. Liquids in equilibrium with peridotitic mineral assemblages at high water pressure. Contr.Mineral. Petrol., 45, 289-316.

Nicholls, I.A., & Lorenz, V., 1973. Origin and crystallization history of Permian tholeiites from the Saar-Nake trough, S.W. Germany. Contr. Mineral. Petrol. 40, 327-344.

Nicholls, I.A., & Ringwood, A.E., 1973. Effect of water on olivine stability and the production of silica-saturated magmas in the island-arc environment. J. Geol., 81, 285-300.

Nitsch, K.H., 1971. Stabilitätsbeziehungen von prehnitund pumpellyithaltigen paragenesen. Contr. Mineral. Petrol. 30, 240-260.

Nordlie, B.E., 1971. The composition of the magmatic gas at Kilanea and its behaviour in the near-surface environment. Am.J. Sci. 271, 417-463.

O'Hara, M.J., 1968. The bearing of phase equilibria studies in synthetic and natural systems on the origin and evolution of basic and ultrabasic rocks. Earth Sci. Revs., 4, 69-133.

Paterson, I.A., & Harakal, J.E., 1974. K-Ar dating of blueschists from Pinchi Lake, central British Columbia. Can.J. Earth Sci., 11, 1007-1012.

Pearce, J.A., 1976. Statistical analysis of major element patterns in basalts. J. Petrol., 17, 15-43.

Pearce, J.A., & Cann, J.R., 1973. Tectonic setting of basic volcanic rocks determined using trace element analysis. Earth Planet. Sci. Lett. 19, 290-300.

* O'Neil J.R., Clayton, R.N., & Mayeda T, 1969. Oxygen isotope fractionation in the divalent metal carbonates. J. Chem. Physics, 51. 5547-5558.

Petö, P., 1974. Plutonic evolution of the Canadian Cordillera. Geol. Soc. Am. Bull. 85, 1269-1276.

Pinsent, R.H., 1974. The emplacement and metamorphism of the Blue River ultramafic body, Cassiar district, British Columbia, Canada. Unpub. Ph.D. thesis, Univ. of Durham.

Raase, P., 1974. Al, Ti content of hornblende, indicators of P and T of regional metamorphism. Contr. Mineral. Petrol., 45, 231-236.

Rea, W.J., 1970. The geology of Montserrat, British West Indies. Unpub. D.Phil. thesis, Univ. of Oxford.

Reed, J.C., Jr., & Morgan, B.A., 1971. Chemical alteration and spilitization of the Catocin Greenstones, Shenandoah National Park, Virginia. J. Geol., 79, 526-548.

Reesor, J.E., 1965. Structural evolution and plutonism in Valhalla gneiss complex, British Columbia. Geol. Surv. Can. Bull. 129.

Reeves, M.J., 1971. Geochemistry and mineralogy of British Carboniferous seatearths from morthern coalfields. Unpub. Ph.D. thesis, Univ. of Durham.

Rice, H.M.A., 1941. Nelson Map-area, east half, British Columbia. Geol. Surv. Can. Mem. 228.

Rice, H.M.A., 1947. Geology and mineral deposits of the Princeton Map-area, British Columbia. Geol. Surv. Can. Mem. 243.

Richardson, S.W., & Powell, R., 1976. Thermal causes of the Dalradian metamorphism in the central Highlands of Scotland. Scott. J. Geol. 12, 237-268.

Riley, J.P., 1958. Simultaneous determination of water and carbon dioxide in rocks and minerals. Analyst, 83, 42-49.

Ringwood, A.E., 1974. The petrological evolution of island-arc systems. J. Geol. Soc.London. 130, 183-204.

Roedder, P.L., & Emslie, R.F., 1970. Olivine-liquid equilibrium. Contr. Mineral. Petrol. 29, 275-269.

Rogers, J.J.W., Burchfiel, B.C., Abbot, E.W., Anepohl, J.K., Ewing, A.H., Koenken, P.J., Novitsky-Evans, J.M., & Talnkdar, S.Cr., 1974. Palaezoic and Lower Mesozoic volcanism and continental growth in the western United States. Geol. Soc. Am. Bull. 85, 1913-1924.

Roots, E.F., 1954. Geology and mineral deposits of Aiken Lake Map-area, British Columbia. Geol. Surv. Can. Mem., 274.

Ross, J.V., 1970. Evolution of the Kootenay Arc, south eastern British Columbia. Geol. Assoc. Can. Spec. Paper 6, 53-65.

Savin, S.M., & Epstein, S., 1970a. The oxygen and hydrogen isotope geochemistry of clay minerals. Geochim. et Cosmochim. Acta, 34, 25-42.

Savin, S.M., & Epstein, S., 1970b. The oxygen and hydrogen isotope geochemistry of ocean sediments and shales. Geochim. et Cosmochim. Acta 34, 43-63.

Saxena, S.K., 1969. Distribution of elements in coexisting minerals and the problems of chemical disequilibrium in metamorphosed basic rocks. Contr. Mineral. Petrol., 20, 177-197.

Scarfe, C.M., & Smith, D.G.W., 1977. Secondary minerals in some basaltic rocks from DSDP leg 37. Can.J. Earth. Sci. 14, 903-910.

Schau, M., 1970. Stratigraphy and structure of the type area of the Upper Triassic Nicola Group in south-central British Columbia. Geol. Assoc. Can. Spec. Paper 6, 123-135.

Schwarz, H.P., Clayton, R.N., & Mayeda, T.K., 1970. Oxygen isotope studies of calcareous and pelitic metamorphic rocks, New England. Geol. Soc. Am. Bull., 81, 2299-2316.

Schweickert, R.A., 1976. Early Mesozoic rifting and fragmentation of the Cordillera orogen in the western USA. Nature, 260, 586-591.

Seki, Y., 1969. Facies series in low-grade metamorphism. J.Geol. Soc. Japan, 75, 255-266.

Shido, F., 1958. Plutonic and metamoprhic rocks of the Makoso and Iritoro districts in the Central Abukuma Plateau. J. Fac. Sci. Tokyo Univ. Sec.2, 11, 132-217.

Shido, F., & Miyashiro, A., 1959. Hornblendes of basic metamorphic rocks. J. Fac. Sci. Tokyo Univ. sec. 2, 12, 85-102.

Shieh, Y., & Taylor, H.P., Jr., 1969. Oxygen and hydrogen isotope studies of contact metamoprhism in the Santa Rosa Range and other areas. Contr. Mineral. Petrol., 20, 306-356.

Sigurdsson, H., & Shepherd, J.B., 1974. Amphibole-bearing basalts from the submarine volcano Kick 'em Jenny in the Lesser Antilles. Bull. Volcanol., 38, 891-910.

Smith, A.L., & Carmichael, I.S.E., 1968. Quaternary lavas from the southern Cascades, western USA. Contr. Mineral. Petrol., 19, 212-238.

Smith, R.E., 1968. Redistribution of major elements in the alteration of some basic lavas during burial metamorphism. J. Petrol. 9, 191-219.

Smith, R.E., 1969. Zones of progressive regional burial metamorphism in part of the Tarman geosyncline, eastern Australia. J. Petrol. 10, 144-163.

Smith, J.V., 1956. The powder patterns and lattice parameters of plagioclase feldspar. I: The soda-rich plagioclases. Min. Mag., 31, 47-68.

Smith, J.V., & Gay, P., 1956. Powder patterns and lattice parameters of plagioclases. Min. Mag. 31, 744-762.

Souther, J.G., 1967. Acid volcanism and its relationship to the tectonic history of the Cordillera of British Columbia, Canada. Bull. Volcanol., 30, 161-176.

Souther, J.G., 1972. Mesozoic and Tertiary volcanism of the western Canadian Cordillera. Dept. Energy Mines and Resources, Ottawa, Canada. Earth Physics Branch publication. 42, 59-64.

Souther, J.G., 1973. Tahltan syenite stock. In the Cordilleran Volcanic Project report; Geol. Surv. Can. Paper 74-1, 39.

Souther, J.G., in press. Volcanism and tectonic environments of the Canadian Cordillera - A second look. Geol. Assoc. Can.

Stanley, K.O., Jordan, W.M., & Dott, R.H., Jr., 1971. New hypothesis of Early Jurassic palaeogeography and sediment dispersal for western United States. Assoc. Am. Petrol. Geol., 55, 10-19.

Stanton, R.L., & Bell, J.D., 1969. Volcanic and associated rocks of the New Georgia Group, British Solomon Islands Protectorate. Overseas Geol. Min. Res. (G.B.) 10, 113-145.

Stewart, D.C., 1975. Crystal clots in calc-alkaline andesites as breakdown products of high-Al amphiboles. Contr. Mineral. Petrol., 53, 195-204.

Stewart, J.H., 1972. Initial deposits of the Cordillera geosyncline. Evidence of a late Precambrian continental separation. Geol. Soc. Am. Bull. 83, 1345-1360.

Storre, B., & Nitsch, K.-H., 1972. Die reaktion: 2 Zoisit + 1 CO_2 = 3 Anorthit + 1 Calcit + H_2O. Contr. Mineral. Petrol, 35, 1-10.

Strens, R.G., 1965. Stability and relation of the Al-Fe epidotes. Min. Mag. 35, 464-475.

Surdam, R.C., 1969. Electron microprobe study of prehnite and pumpellyite from the Karmutsen Group, Vancouver Island, British Columbia. Am. Mineral., 54, 256-266.

Sweatman, T.R., & Long, J.V.P., 1969. Quantitative electron probe microanalysis of the rock forming minerals. J.Petrol., 10, 332-379.

Tagiri, M., 1977. Fe-Mg partition and miscibility gap between coexisting calcic amphiboles from the southern Abukuma Plateau, Japan. Contr. Mineral. Petrol, 62, 271-282.

Taylor, H.P., Jr., 1968. The oxygen isotope geochemistry of igneous rocks. Contr. Mineral. Petrol., 19, 1-71.

Taylor, H.P., Jr., 1974. The application of oxygen and hydrogen isotope studies to problems of hydrothermal alteration and ore deposition. Econ. Geol., 69, 843-883.

Taylor, H.P., Jr., & Epstein, S., 1962. Relationship between $^{18}O/^{16}O$ ratios in coexisting minerals of igneous and metamorphic rocks. Part 1: Principles and experimental results. Geol. Soc. Am. Bull., 73, 461-480.

Taylor, S.R., 1965. The application of trace element data to problems in petrology. Phys. Chem. Earth, 6, 133-213.

Taylor, S.R., Capp, A.C., Graham, A.L., & Blake, D.H., 1969a. Trace element abundances in andesites. Part II: Saipan, Bouganville and Fiji. Contr. Mineral. Petrol., 23, 1-26.

Taylor, S.R., Kaye, M., White, A.J.R., Duncan, A.R., & Blake, D.H., 1969b. Genetic significance of Co, Dr, Ni, Sc and V content of andesites. Geochim. et Cosmochim. Acta, 33, 275-286.

Tipper, H.W., 1959. Revision of the Hazelton and Takla Groups of central British Columbia. Geol.Surv. Can.Bull., 47.

Tipper, H.W., & Richards, T.A., in press. Jurassic stratigraphy and history of north-central British Columbia. Geol.Surv.Can.

Turnock, A.C., 1959. Stability range of iron chlorite. Geol. Soc.Am.Bull., 70, 1690-1691.

Turnock, A.C., 1960. The stability of iron chlorites. Carnegie Inst. Washington Yearbook, 59, 98-103.

Turner, F.J., 1968. Metamorphic petrology. McGraw Hill, New York.

Vallance, T.G., 1960. Concerning spilites. Proc.Linnean Soc. New South Wales, 85, 7-52.

Vallance, T.G., 1969. Spilites again: some consequences of the degradation of basalts. Linnean Soc. New South Wales. Proc. 94, 8-50.

Vallance, T.G., 1974a Spilitic degradation of a tholeiitic basalt. J.Petrol., 15, 79-96.

*

Wager, L.R.,& Brown, G.M., 1967. Layered igneous rocks. Oliver and Boyd, Edinburgh.

Walker, J.F., 1934. Geology and mineral deposits of the Salmo map-area. Geol.Surv.Can.Mem. 172.

Wheeler, J.O. & Gabriesle, H., 1972. The Cordilleran structural province. In: Variations in tectonic style in Canada. Geol.Assoc.Can.Spec.Paper 11. (R.A.Price & R.J.W. Douglas, eds.).

* Vallance, T.G., 1974b. Pyroxenes and the basalt-spilite relation. in G.C. Amstutz (ed.), Spilites and spilitic rocks. Springer Verlag, Heidelberg.

White, D.E., Barnes, I., & O'Neil, J.R., 1973. Thermal and mineral waters of non-meteoric origin, California Coast Rangers. Geol. Soc. Am. Bull., 84, 547-560.

Wills, K.J.A., 1974. The geological history of southern Dominica and the plutonic nodules from the Lesser Antilles. Unpub. Ph.D. thesis, Univ. of Durham.

Wilson, A.D., 1955. A new method for the determination of ferrous iron in rocks and minerals. Bull. Geol. Soc. Great Britain, 9, 56-58.

Winkler, H.G.F., 1974. Petrogenesis of metamorphic rocks. Springer Verlag, New York.

Yates, R.G., 1969. Geologic background of the Metaline and North port mining districts, Washington. State of Washington Dept. of Nat. Resources, Div. of Mines and Geology. Bull. 61, 17-40.

Yates, R.G., & Engels, J.C., 1968. Potassium-argon ages of some igneous rocks in northern Stevens County, Washington. U.S. Geol. Surv. Prof. Paper 600D.

Yoder, H.S., Jr., & Tilley, C.E., 1962. Origin of basalt magmas: An experimental study of natural and synthetic rock systems. J. Petrol., 3, 342-532.

Yagi, K., & Onuma, K., 1967. The join $CaMgSi_2O_6$ - $CaTiAl_2O_6$ and its bearing on the titanaugites. J. Fac. Sci. Hokkaido Univ. ser 4. 8, 463-483.

Zodrow, E., 1974. Note on closure correlation. Can.J. Earth Sci. 11, 1616-1619.

ADDITIONAL REFERENCES

Barnes, V.E., 1930. Changes in hornblende at about 800°C. Am. Min., 15, 393-417.

Flanagan, F.J., 1973. 1972. Values for international geochemical reference standards. Geochim. et Cosmochim. Acta., 37, 1189-1200.

Irving, E. & Yole, R., 1972. Palaeomagnetic criterion for the recognition of ancient oceanic crust. Can. Dept. Energy, Mines and Resources. Earth Phys. Br. Publ. 42, 87-96.

Lambert, R. St.J., 1959. The mineralogy and metamorphism of the Moine schists of the Morar and Knoydart districts of Inverness-shire. Trans. Roy. Soc. Edin., 63, 553.

Nesbitt, R.W., & Sun, S-S, 1976. Geochemistry of Archaean spinifex textured peridotites and magnesian and low-magnesian tholeiites. Earth. Planet. Sci.Lett., 31, 433-453.

Nguyen, K.K., Sinclair, A.J, & Libby, W.G., 1968. Age of the northern part of the Nelson Batholith . Can.J. Earth Sci., 5, 955-957.

Ross, M., Papike, J.J., & Shaw, K.W., 1969. Exsolution textures in amphiboles as indicators of subsolidus thermal histories. Spec. Paper, Min.Soc.Am. 2, 275-299.

Symons, D.T.A., 1971. Palaeomagnetism of the Jurassic Island Intrusions of Vancouver Island, British Columbia. Geol. Surv. Can. Paper 70-63.

APPENDIX 1

SAMPLE LOCATIONS AND FIELD DATA

Brief descriptions of the samples and their six-figure grid references are given in Table A1.1.

Sample numbers beginning 55 are rocks collected by Professor R. St.J. Lambert; the others by the writer. All grid references (column 2) fall within the One-Thousand metre Universal Transverse Mercator Grid zone 11. The 100,000 m,M-square identification is ME (see Fig.1.1). Column three, entitled 'Field Occurrence', gives a brief description of the field relations. Abbreviations used are:-

AF	Archibald Formation
V-Clastic	Volcaniclastic deposit
X	Sample is a fragment from an agglomerate or conglomerate
HF	Hall Formation
YG	Ymir Group
SKP	Silver King Porphyry

'Hand Spec. Desc.' (column 4, Table A1.1) gives an indication of obvious hand specimen petrographical features:-

HP	Amphibole-phyric
FP	Feldspar-phyric
PP	Pyroxene-phyric
PX	Pyroxene
XTLS	Crystals
(A)	Amphibolised pyroxene.

The dip and strike of the locality, if any, is recorded in column 5 (cf. Fig.1.1). Lastly, column 6 gives the petrologic lava-type to which certain samples belong, as defined in Chapters 4 and 5.

AK	Ankaramitic Basalt
B	Basalt
HB	Amphibole Basalt
A	Andesite
HA	Amphibole Andesite
PT	Pyroxenite

Only the samples thus designated were considered geochemically in Chapter 5 (Sections 5:4, 5:5) regarding the petrogenesis of the volcanics. Associated minor intrusions are also indicated by MI, with a prefix A if amphibole-bearing.

TABLE A1.1 SAMPLE DATA AND LOCATIONS

SAMPLE	GRID REF.	FIELD OCCURENCE	HAND SPEC DESC.	DIP STRIKE	TYPE
5001A	710 454	DYKE IN AF	FP		
5001B	710 454	DYKE IN AF	PP		
5003	561 361	BEDDED V-CLASTIC		70NW 45	
5006	697 448	?INTRUSION/FLOW	PP		B
5007	693 445	BEDDED V-CLASTIC	GRADED	62SW 160	
5008	685 434	MASSIVE V-CLASTIC	SHALE INCLUSIONS	20SW 150	
5009	686 440	BEDDED V-CLASTIC		50SE 30	
5010	690 443	MASSIVE INTRUSION	PP		
5011	690 443	BRECCIATED FLOW	FP		
5012	682 442	AGGLOMERATE		22SW 115	
5013	682 442	?FLOW	PP		B
5014	684 444	BEDDED V-CLASTIC	ABUNDANT PX XTLS	40SW 160	
5015	687 440	MINOR INTRUSION	PP		HA
5016	688 440	AGGLOMERATE X	PP		B
5017A	839 605	SKP	FP		
5017B	839 605	SKP	FP		
5017C	839 605	SKP	FP SHEARED		
5018	839 605	MASSIVE GREENSTONE	PYRITISED		
5019	839 605	SKP	FP		
5020	839 605	SKP	FP		

TABLE A1.1 SAMPLE DATA AND LOCATIONS

SAMPLE	GRID REF.	FIELD OCCURENCE	HAND SPEC DESC.	DIP STRIKE	TYPE
5021	839 605	SKP	FP		
5022	839 605	MASSIVE GREENSTONE	PYRITISED		
5023	838 617	SKP	FP SHEARED		
5024	833 620	MASSIVE GREENSTONE			
5025	832 621	SKP	FP		
5027	832 621	SKP	FP		
5028	632 401	TUFF	FELDSPATHIC		
5029	632 404	TUFF	FELDSPATHIC		
5030A	632 406	BEDDED V-CLASTIC		45SW 140	
5031	630 495	DOLERITIC INTRUSION			MI
5032	686 431	BRECCIA X	FP		A
5033	687 429	BRECCIA X	FP		A
5034	692 423	BRECCIA X	FP		A
5036	693 420	AGGLOMERATE X	PP		B
5038	693 419	AGGLOMERATE	EPIDOTISED		
5039	691 421	BEDDED V-CLASTIC		50W 175	
5040	678 439	AGGLOMERATE X	PP		
5041	673 437	BRECCIA X	PP		B
5042	673 428	BEDDED V-CLASTIC		35SW 130	
5044	692 435	V-CLASTIC			

TABLE A1.1 SAMPLE DATA AND LOCATIONS

SAMPLE	GRID REF.	FIELD OCCURENCE	HAND SPEC DESC.	DIP STRIKE	TYPE
5045	689 432	AGGLOMERATE			
5046	685 432	CARBONACEOUS SHALE	PYRITISED	90W 30	
5048	762 655	AGGLOMERATE	PP(A)		
5049	767 653	BRECCIATED FLOW	PFP(A)		
5050	770 652	AGGLOMERATE	PFP(A)		
5051		SKP	FP		
5052	601 382	V-CLASTIC		30SW 130	
5053	601 380	BRECCIATED FLOW			B
5054	605 375	?FLOW			B
5055	605 376	?FLOW			B
5056	608 376	?FLOW			HB
5058	598 370	MASSIVE FLOW	PP		B
5060	605 365	COARSE AGGLOMERATE			
5062	604 367	DYKE	HP		AMI
5063	650 406	MASSIVE ?FLOW	PP		B
5064A	655 407	V-CLASTIC			
5064B	655 407	FINE CONGLOMERATE	MUDDY MATRIX		
5065	655 407	BEDDED V-CLASTIC		40W 20	
5066	844 561	ARGILLITE YG	SILICEOUS 2CM BANDS	80E 160	
5067	851 587	ARGILLITE YG		30SE 20	

TABLE A1.1 SAMPLE DATA AND LOCATIONS

SAMPLE	GRID REF.	FIELD OCCURENCE	HAND SPEC DESC.	DIP STRIKE	TYPE
5068	852 590	ARGILLITE YG			
5069	859 589	ARGILLITE YG			
5070	855 591	ARGILLITE YG		60E 170	
5071	850 585	ARGILLITE YG		40E 0	
5073B	717 811	GREENSTONE	SCHISTOSE	20S 90(S)	B
5074A	715 811	GREENSTONE	SCHISTOSE		
5074B	715 811	GREENSTONE	SCHISTOSE PP(A)		B
5074C	715 811	GREENSTONE	PP(A) +COARSE BIOTITE		
5075A	713 811	PYROXENITE	(A)		PT
5075B	713 811	PYROXENITE	(A)		PT
5077	711 810	PYROXENITE	(A)		PT
5078	666 490	AGGLOMERATE	FELDSPATHIC		
5079	664 505	BRECCIATED ?FLOW	FP		
5080A	665 515	BRECCIATED ?FLOW	FP		
5080B	665 515	BRECCIATED ?FLOW	FP		
5081A	572 350	BRECCIA	PP(A)		
5082	572 349	BEDDED V-CLASTIC		80NE 30	
5083A	568 347	AGGLOMERATE X	PP(A)		
5084	569 345	MASSIVE FLOW	PP(A)		
5085A	832 611	MASSIVE GREENSTONE			

TABLE A1.1 SAMPLE DATA AND LOCATIONS

SAMPLE	GRID REF.	FIELD OCCURENCE	HAND SPEC DESC.	DIP STRIKE	TYPE
5085B	832 611	MASSIVE GREENSTONE	PYRITISED		
5085C	832 611	MASSIVE GREENSTONE	LINEATED		
5085E	832 611	MASSIVE GREENSTONE	PP(A)		AB
5086A	823 634	SKP	FP		
5086B	823 634	MASSIVE GREENSTONE	EPIDOTE VEINED		
5087A	829 749	MASSIVE GREENSTONE	PP(A)		
5087B	829 749	MASSIVE GREENSTONE	PP(A)		AB
5088	824 745	MASSIVE GREENSTONE	PP(A)		AB
5089	835 741	MASSIVE GREENSTONE	PP(A)		B
5093	860 559	ARGILLITE YG	PERMEATED BY GRANITE	70E 170	
5094	858 559	ARGILLITE YG	PERMEATED BY GRANITE	70E 170	
5095	856 559	ARGILLITE YG		80E 10	
5096	657 407	MINOR INTRUSION	HP		AMI
5097	658 407	V-CLASTIC/TUFF			
5099	664 405	BEDDED V-CLASTIC(HF)			
5100	664 405	BEDDED V-CLASTIC(HF)		35W 160	
5101	664 406	V-CLASTIC			
5102	650 406	?FLOW	PP		A
5103	763 515	BRECCIATED ?FLOW	FPP		
5104	763 515	BRECCIATED ?FLOW	FPP		B

TABLE A1.1 SAMPLE DATA AND LOCATIONS

SAMPLE	GRID REF.	FIELD OCCURENCE	HAND SPEC DESC.	DIP STRIKE	TYPE
5105	760 510	V-CLASTIC			B
5106A	764 526	BRECCIATED ?FLOW	FPP(A)		A
5106B	764 526	BRECCIATED ?FLOW	FPP(A)		B
5107A	641 441	MINOR INTRUSION(AF)	HP		AMI
5107B	641 441	MINOR INTRUSION(AF)	HP		AMI
5107D	638 446	BEDDED V-CLASTIC	GRADED	45SE 85	
5108	809 540	BRECCIATED FLOW	PP(A)		B
5109	808 542	AGGLOMERATE	EPIDOTISED		
5110	806 540	BEDDED V-CLASTIC		80E 170	
5111A	826 626	MASSIVE GREENSTONE	PP(A)		AB
5111B	826 626	MASSIVE GREENSTONE	PP(A)		AB
5111C	826 626	BEDDED V-CLASTIC	PYRITISED&FINELY LAMINATED	80W 170	
5112	690 443	BRECCIATED ?FLOW	FP		
5113	676 430	COARSE AGGLOMERATE X	HP		HA
5114A	712 456	V-CLASTIC BED IN AF		38W 40	
5115	771 646	AGGLOMERATE X	PP A)		
5116	771 646	AGGLOMERATE X	FPP(A)		B
5117A	832 622	SKP	FP SHEARED		
5117B	832 622	SKP	PYRITISED		
5117C	832 622	SKP	FP SHEARED		

TABLE A1.1 SAMPLE DATA AND LOCATIONS

SAMPLE	GRID REF.	FIELD OCCURENCE	HAND SPEC DESC.	DIP STRIKE	TYPE
5118	804 540	MASSIVE GREENSTONE	PP(A) EPIDOTISED		
5119	804 540	INTRUSION	DOLERITIC TEXTURE		MI
5120	804 540	BRECCIATED FLOW	PP(A) EPIDOTISED		B
4001	727 549	MASSIVE GREENSTONE	PYRITISED/EPIDOTISED		B
4002	739 533	AGGLOMERATE			
4003	743 527	BRECCIATED ?FLOW	FPP(A)		
4004	744 525	BRECCIATED ?FLOW	FFP(A)		
4005	745 525	MASSIVE GREENSTONE	PP(A)		
4006A	749 519	AGGLOMERATE	(A)		
4007	757 500	BRECCIATED FLOW	PFP(A)		B
4009	757 501	AGGLOMERATE			
4010	757 501	AGGLOMERATE			
4011	757 501	SKP?	FHP		
4012B	833 552	MASSIVE GREENSTONE	PP(A) SHEARED		
4013	771 649	AGGLOMERATE/CONGLOMERATE X	PFP(A)		B
4013A	771 649	AGGLOMERATE/CONGLOMERATE X	PFD(A)		AB
4015	771 645	AGGLOMERATE			
4016	771 651	AGGLOMERATE X	PP(A)		B
4017	721 764	MASSIVE GREENSTONE			
4018	721 764	V-CLASTIC	(A)		

TABLE A1.1 SAMPLE DATA AND LOCATIONS

SAMPLE	GRID REF.	FIELD OCCURENCE	HAND SPEC DESC.	DIP STRIKE	TYPE
4019	721 764	MASSIVE GREENSTONE			
4020	721 764	GREENSTONE	SCHISTOSE		
4021	721 764	GREENSTONE	SCHISTOSE & PYRITISED		
4022	721 764	GREENSTONE	SCHISTOSE		
4023	721 764	BRECCIA	PP(A)		HB
4024A	721 764	MASSIVE GREENSTONE			
4024B	721 764	BRECCIATED ?FLOW	PP(A)		
4025	712 775	MASSIVE GREENSTONE	FP PYRITISED		
4026	723 807	MASSIVE GREENSTONE	PP(A)		
4027	724 807	MASSIVE GREENSTONE			
4028	724 808	GREENSTONE	SCHISTOSE		
4029A	729 810	GREENSTONE	SCHISTOSE		B
4030	729 810	MASSIVE GREENSTONE	PP(A) SCHISTOSE		
4031	556 483	V-CLASTIC			
4032	554 485	MINOR INTRUSION?			
4033	551 486	AGGLOMERATE	QUARTZITIC INCLUSIONS		
4034	551 486	MINOR INTRUSION			
4036	551 487	AGGLOMERATE X	PP(A)		
4040	779 703	MASSIVE ?FLOW	FPP(A)		
4042	778 704	BRECCIATED ?FLOW	FP		A

TABLE A1.1 SAMPLE DATA AND LOCATIONS

SAMPLE	GRID REF.	FIELD OCCURENCE	HAND SPEC DESC.	DIP STRIKE	TYPE
4044	772 704	AGGLOMERATE	PP(A)		
4045	772 703	AGGLOMERATE X	PP(A)		B
4047	787 702	AGGLOMERATE/CONGLOMERATE	PP(A)		
4048	859 705	BEDDED V-CLASTIC			
4049	859 705	MASSIVE GREENSTONE	PP(A) SCHISTOSE		
4051	690 429	COARSE AGGLOMERATE X	PP		HB
4052	689 428	MASSIVE ?FLOW	PFP		
4053	687 428	BRECCIA	FP		
4054	680 439	V-CLASTIC			
4056	682 417	AGGLOMERATE X	FP		A
4057	674 406	BRECCIATED ?FLOW	PP		HB
4058	665 405	AGGLOMERATE/V-CLASTIC			
4060	739 638	MASSIVE GREENSTONE			
4061	749 637	BEDDED V-CLASTIC	(A)	50E 170	
4062	749 637	BRECCIATED FLOW	PP(A)		B
4063	754 635	BEDDED V-CLASTIC	(A)	40E 20	
4065	704 632	MASSIVE GREENSTONE			
4066	766 633	BRECCIA	FPP(A)		
4068A	598 398	SHALE HF			
4068B	598 398	MINOR INTRUSION IN HF			AMI

TABLE A1.1 SAMPLE DATA AND LOCATIONS

SAMPLE	GRID REF.	FIELD OCCURENCE	HAND SPEC DESC.	DIP	STRIKE	TYPE
4068C	598 398	MINOR INTRUSION IN HF				AMI
4068D	598 398	MINOR INTRUSION IN HF				AMI
4070	576 368	BRECCIATED ?FLOW	PP			B
4072A	558 357	FINE AGGLOMERATE/V-CLASTIC		90W	30	
4072B	558 357	V-CLASTIC				
4072C	558 357	V-CLASTIC				
4072D	558 357	AGGLOMERATE	PP FRAGMENTS			
4073B	552 364	BRECCIA	PP			
4076	618 372	BRECCIATED ?FLOW	PP			
4077	617 371	BRECCIATED ?FLOW	PP			B
4078	617 368	AGGLOMERATE				
4079	618 365	V-CLASTIC				
4082	623 349	AGGLOMERATE				
4099	845 563	BRECCIA	PP(A)			
4100A	842 585	BRECCIA	PP(A)			
4100B	842 585	GREENSTONE	SCHISTOSE			
4101A	837 606	SKP	FP			
4101B	837 606	SKP	FP			
4102A	834 615	MASSIVE GREENSTONE	EPIDOTISED			
4102B	834 615	MASSIVE GREENSTONE	EPIDOTISED			

TABLE A1.1 SAMPLE DATA AND LOCATIONS

SAMPLE	GRID REF.	FIELD OCCURENCE	HAND SPEC DESC.	DIP	STRIKE	TYPE
4103	832 620	SKP	FP			
4104	839 609	SKP	FP			
4105A	828 628	MASSIVE GREENSTONE	PP(A) AMYGDALOIDAL			
4105B	828 628	BEDDED V-CLASTIC	FINELY LAMINATED	90W	5	
4109B	821 678	BRECCIATED ?FLOW	FP			A
4110	834 703	MASSIVE GREENSTONE	PP(A) SHEARED			AB
4111V	850 715	MASSIVE GREENSTONE	PP(A) SHEARED			AB
4111S	850 715	ARGILLITE RUG	FINELY LAMINATED			
4112	594 398	MINOR INTRUSION	HP			
4113	835 741	MASSIVE GREENSTONE	PP(A)			
4114	843 732	MASSIVE GREENSTONE	PP(A)	70W	10	
4115	781 435	BEDDED V-CLASTIC		70E	30	
4117	792 449	MASSIVE GREENSTONE				
4118	793 451	V-CLASTIC				
4119	793 452	V-CLASTIC?	SHEARED			

TABLE A1.1 SAMPLE DATA AND LOCATIONS(CONT.)

SAMPLE NO.	GRID REF.	ROCK TYPE
5132	386 353	SERPENTINITE
5133	386 353	SERPENTINITE
5512	842 583	RVG
5513	835 609	SKP
5514	834 614	SKP
5515	832 621	SLP
5516	827 626	RVG
5517	815 629	RVG
5518	813 638	RVG
5519	824 648	RVG
5520	824 651	RVG
5521	822 656	RVG
5522	822 660	RVG
5523	822 662	RVG
5524	821 672	RVG
5525	828 678	RVG
5526	828 697	RVG
5527	833 702	RVG
5528	841 707	RVG
5529	848 711	RVG

TABLE A1.1 SAMPLE DATA AND LOCATIONS(CONT.)

SAMPLE NO.	GRID REF.	ROCK TYPE
5530	850 716	RVG
5531	848 721	RVG
5532	842 733	RVG
5533	837 739	RVG
5534	836 739	RVG
5535	834 741	RVG
5536	832 742	RVG
5537	822 746	RVG
5538	822 747	RVG
5539	821 746	RVG

APPENDIX 2

WHOLE-ROCK CHEMICAL DATA AND METHOD OF ANALYSIS

A2:1 X-ray fluorescence analysis

Samples were fragmented and stripped of weathering, using a Cutrock Engineering hydraulic splitter. Further fragmentation to an aggregate of ~ 1 cm. chips was achieved with a Sturtevant 2" x 6" Roll Jaw Crusher. Grinding of this aggregate to a fine powder was accomplished in a Tema Laboratory Disc Mill with a tungsten-carbide grinding barrel. Grinding took 1-4 minutes.

Several grams of powder were then compressed into bricquettes using a hydraulic press operated at 800-900 Kg/cm^2 (5-6 $tons/inch^2$). A few drops of an inert organic binding agent (Mowiol) was added to the powder, prior to compression, to aid cohesion.

Major and trace elements were analysed on a Philips PW1212 automatic spectrometer, into which the bricquettes were loaded by a Torrens Industries TE108 Automatic Sample Loader. Routine operating conditions for this machine are given by Reeves (1971).

The major and minor elements Si, Al, Fe, Ca, Mg, Na, K, Ti and P were determined using a Cr target and an evacuated tube. Mn was determined separately using W radiation. The accumulation of counts for the unknowns was based on a 'fixed count' time for a monitor. This minimizes machine drift or instability.

Data handling was performed using an iterative procedure described by Holland & Brindle (1966) and Reeves (1971). Standards used in the calibration were the international standards G1, G2, W1, T1, S1, GR, GA, AGV-1, GSR-1, BCR-1, PCC-1 and DTS-1 (for composition see Flanagan, 1973).

The trace elements Ba, Nb, Zr, Y, Sr, Rb, Zn, Cu, Ni and Cr were determined using W radiation. Peaks and backgrounds obtained for standards and unknowns were converted to the function (P/B - 1). This function, when plotted against standard concentrations, produces a straight line from which unknown concentrations can be directly obtained. This calculation was performed using the program TRATIO (written by R.C.O. Gill). Mass absorption and matrix effects are compensated for by the (P/B-1) function using scattered background radiation as an internal standard. TRATIO also allows correction for the interferences of SrK_β on ZrK_α, RbK_β on YK_α, and YK_β on NbK_α using experimentally determined interference factors.

The standards used were synthetic, spiked glasses produced by the Pilkington Research Laboratory for use in lunar investigations (Brown et al., 1970).

Vanadium was determined differently owing to the very strong interference of TiK_β on VK_α. The method used was devised by D.J. Hughes, G.C. Brown and J. Esson (Manchester University) and programmed in PLI by J.G. Fitton (Edinburgh University). Standards used in this procedure are synthetically prepared, Ti-free vanadium standards, and V-free titanium standards that cover the range of expected values. For the data here, a 1000 ppm V standard and two Ti standards, with 2.84% TiO_2 and 0.28% TiO_2, were prepared, the matrix being specpure Al_2O_3. Using these standards, the mutual interferences of V and Ti can be calculated and applied to the unknowns in an iterative manner. In addition to producing V concentrations in ppm, TiO_2 contents are also calculated. Mass absorption coefficients (from Jenkins &

De Vries, 1970) were also applied to correct for differences between unknown and standard compositions. Thus, the major element composition of the sample being analysed should preferably be known first.

Using international standards and TiO_2 contents determined on K_β, precision and accuracy can be assessed. Compared with TiO_2 determined on K_α, TiO_2 on K_β differed by less than 0.015 wt.% about the average of the two values. V calculated for the international standards BCR-1, BR and W-1 were always within 10 ppm of the true quantities.

La and Ce were determined analogously to Ba-Zn, but using L radiation and international standards. Generally, precision is not good owing to near-detection level sample concentrations and other element interferences. Precision and accuracy as judged from running samples several times is on the order of $\pm$ 50%; thus the La and Ce data reported can only be treated with caution.

All XRF data are tabulated in Table A2.1, with Fe_2O_3 representing total Fe. Also, the analyses, due to the presence of secondary H_2O, are recalculated to 100% (anhydrous).

Table A2.2 contains selected data from Table A2.1 recast into normative minerals. Fe_2O_3/FeO was somewhat arbitrarily set at 0.3, but this is a similar value to those used by Arculus (1973), Wills (1974) and Brown et al. (1977) for generally similar, but fresher rocks.

A2:2 H_2O and FeO determination

Total H_2O was determined by a gravimetric method similar to that described by Riley (1957). Water is driven off the

specimen by heating to 1100–1200°C and flushed by nitrogen through an absorption tube filled with $CaCl_2$. The tube is weighed before and after water absorption.

FeO was determined for selected rocks using the Ammonium Metavanadate method described by Wilson (1955).

H_2O and FeO data are given in Table A2.3.

TABLE A2.1 MAJOR AND TRACE ELEMENT ANALYSES(RVG).

	4001	4003	4004	4004B	4005	4006A	4007	4008	4009	4010
WEIGHT % OXIDE										
SIO2	49.02	51.65	56.49	50.61	50.24	50.81	51.61	46.53	54.21	46.16
AL203	13.39	13.13	15.31	11.97	13.07	9.87	14.92	9.30	10.95	7.45
FE203*	13.77	11.83	9.40	12.91	11.50	11.85	11.60	13.90	13.01	10.08
MGO	7.23	9.09	5.15	7.88	11.41	11.37	5.80	8.62	11.89	6.07
CAO	9.41	10.22	7.90	10.56	9.14	12.05	8.51	18.08	7.41	23.43
NA20	2.90	2.47	3.97	3.03	2.43	2.12	3.45	0.65	0.38	2.74
K20	2.77	0.36	0.79	1.58	1.02	0.68	2.68	1.49	1.02	2.71
TIO2	0.91	0.84	0.67	0.83	0.81	0.79	0.84	0.85	0.73	0.81
MNO	0.20	0.19	0.14	0.21	0.19	0.17	0.19	0.26	0.20	0.24
P205	0.39	0.22	0.17	0.38	0.18	0.23	0.41	0.28	0.19	0.29
PPM										
CU	20	34	57	134	63	36	216	71	75	99
NI	16	99	41	53	141	179	10	37	59	40
CR	78	453	150	182	630	869	141	351	519	389
BA	901	174	757	741	337	569	959	647	307	854
NB	3	4	5	4	4	2	3	3	5	3
ZR	85	99	104	53	68	66	115	74	60	82
Y	18	18	15	15	17	16	18	18	12	13
SR	810	729	939	827	349	435	1145	579	258	796
RB	145	12	21	36	19	16	59	44	46	44
ZN	80	89	84	95	89	115	99	97	124	77
CE	23	19	22	0	13	22	33	29	20	33
LA	5	5	7	0	3	3	13	10	8	22
V	339	300	200	0	258	301	259	293	292	256

TABLE A2.1 MAJOR AND TRACE ELEMENT ANALYSES(RVG).

	4012	4013	4013	4015	4016	4018	4021	4023	4029A	4030
WEIGHT % OXIDE										
SIO2	49.19	50.33	49.42	51.03	51.78	48.15	49.02	51.62	49.77	54.23
AL203	12.68	12.74	10.76	11.75	15.37	13.09	12.30	13.54	15.30	8.84
FE203*	12.83	12.25	11.87	12.39	10.80	12.66	13.34	10.62	12.06	10.94
MGO	11.13	8.06	11.32	6.74	5.92	13.49	8.55	7.66	7.35	10.57
CAO	8.55	9.81	10.90	12.83	9.34	7.54	10.47	9.48	8.95	11.25
NA2O	2.76	3.29	2.16	2.95	2.89	1.85	2.56	4.27	3.21	1.79
K2O	1.36	2.28	2.34	0.99	2.32	1.63	2.29	1.23	1.96	1.36
TIO2	1.04	0.76	0.73	0.84	1.04	0.86	0.96	1.02	0.86	0.62
MNO	0.17	0.18	0.18	0.21	0.17	0.18	0.19	0.16	0.22	0.19
P2O5	0.29	0.27	0.32	0.26	0.36	0.56	0.33	0.36	0.32	0.21
PPM										
CU	99	88	129	17	24	181	106	94	26	3
NI	100	44	164	87	13	281	99	39	22	95
CR	402	180	587	391	55	804	386	145	142	752
BA	519	1158	672	463	857	525	754	415	503	718
NB	2	5	3	4	4	4	5	3	6	2
ZR	97	47	73	84	106	69	76	78	77	49
Y	20	12	14	15	22	15	14	18	18	13
SR	521	806	610	714	755	457	423	950	767	471
RB	36	63	56	14	49	34	48	29	150	51
ZN	100	100	84	82	91	112	105	73	138	81
CE	16	13	0	21	21	0	0	23	27	0
LA	6	7	0	9	7	0	0	5	11	0
V	302	286	0	299	326	303	321	338	321	246

TABLE A2.1 MAJOR AND TRACE ELEMENT ANALYSES(RVG).

	4031	4032	4034	4036	4040	4042	4045	4049	4050	4051
WEIGHT % OXIDE										
SIO2	58.16	52.74	50.41	52.04	49.81	53.64	50.19	48.18	47.72	50.59
AL203	16.51	13.73	14.75	13.68	11.34	16.39	11.15	11.56	10.84	15.94
FE203*	8.58	9.09	11.07	9.61	12.72	10.79	12.89	12.45	12.87	11.07
MGO	4.87	8.51	8.14	8.57	10.20	4.11	10.78	13.76	11.11	6.77
CAO	3.58	9.71	9.45	8.03	9.74	5.33	10.21	10.61	12.90	9.39
NA20	6.40	2.33	2.35	2.32	2.88	5.10	2.02	1.60	1.39	3.30
K20	0.79	2.40	1.90	3.90	2.01	3.37	1.71	0.73	1.31	1.34
TIO2	0.84	0.95	1.13	1.09	0.79	0.87	0.85	0.91	0.93	1.14
MNO	0.10	0.16	0.18	0.16	0.23	0.19	0.20	0.20	0.25	0.15
P205	0.16	0.39	0.63	0.59	0.26	0.23	-	-	0.68	0.27
PPM										
CU	16	26	39	0	84	170	101	92	83	62
NI	31	21	17	39	52	23	119	59	85	72
CR	212	398	124	246	218	44	538	468	347	170
BA	863	1396	1772	1933	912	1241	478	257	136	692
NB	5	12	25	29	1	7	3	5	6	3
ZR	100	165	160	207	49	70	89	55	79	105
Y	23	15	17	20	15	17	15	15	15	21
SR	376	853	854	1485	551	624	817	385	768	566
RB	26	70	71	115	57	81	41	10	20	41
ZN	153	119	138	106	108	108	101	70	96	100
CE	0	49	61	63	12	17	18	12	0	19
LA	0	27	37	34	5	9	8	4	0	7
V	238	179	205	179	328	218	305	297	285	287

TABLE A2.1 MAJOR AND TRACE ELEMENT ANALYSES(RVG).

	4052	4053	4054	4055	4056	4058	4060	4061	4062	4063
WEIGHT % OXIDE										
SIO2	59.73	53.25	52.52	47.45	54.15	56.27	49.36	48.95	50.93	51.69
AL203	12.10	14.00	10.31	11.26	15.62	14.99	13.70	13.77	12.78	15.47
FE203*	5.21	10.54	12.76	11.97	9.89	11.00	11.47	12.29	11.79	10.35
MGO	2.35	6.34	7.57	8.81	2.83	5.81	10.08	10.35	8.20	7.08
CAO	12.92	9.42	14.56	15.52	8.25	6.08	9.37	9.30	9.87	8.32
NA2O	3.54	3.10	1.67	1.73	5.04	3.48	3.41	2.51	3.46	4.59
K2O	2.98	2.10	0.96	1.69	2.79	1.18	1.40	1.38	1.34	0.98
TIO2	0.60	0.76	1.11	1.11	0.85	0.91	0.81	1.04	1.19	0.98
MNO	0.19	0.18	0.23	0.19	0.14	0.16	0.17	0.18	0.14	0.16
P2O5	0.34	0.31	0.32	0.26	0.39	0.12	0.18	0.24	0.27	0.33
PPM										
CU	68	33	62	42	34	55	77	64	85	66
NI	41	11	71	37	8	19	96	94	42	61
CR	80	28	0	307	21	86	308	287	162	146
BA	1368	1279	653	1021	1190	1093	927	234	388	556
NB	4	6	4	4	3	5	4	4	5	11
ZR	77	81	66	95	81	91	67	97	81	75
Y	12	17	19	20	15	16	21	17	20	18
SR	858	1229	468	645	868	721	394	751	452	48
RB	83	57	24	36	54	34	0	37	38	28
ZN	67	89	98	75	89	140	93	99	92	110
CE	0	18	21	15	15	19	13	25	27	18
LA	0	7	5	6	0	13	6	4	0	7
V	0	201	310	261	268	266	257	309	321	309

TABLE A2.1 MAJOR AND TRACE ELEMENT ANALYSES(RVG).

	4065	4066	4068B	4068C	4068D	4070	4072B	4072C	4072D	4073B
WEIGHT % OXIDE										
SIO2	49.64	55.00	52.11	52.19	51.05	48.00	52.62	49.26	51.31	51.42
AL203	15.52	12.44	14.28	14.44	13.89	13.02	12.01	15.05	14.18	13.78
FE203*	12.38	10.69	11.84	11.58	12.14	14.12	13.71	13.06	13.05	11.49
MGO	7.68	6.79	5.71	5.17	5.02	6.72	7.93	7.30	7.21	8.47
CAO	7.26	9.08	7.71	8.16	8.91	11.41	10.59	9.07	8.75	9.73
NA2O	4.36	2.86	3.97	3.94	3.92	2.94	1.69	3.12	2.51	2.42
K2O	1.52	1.78	2.49	2.52	1.85	2.31	1.05	1.57	1.60	1.54
TIO2	1.13	0.82	1.28	1.33	1.38	0.98	0.95	1.09	0.91	0.79
MNO	0.19	0.18	0.22	0.20	0.17	0.22	0.22	0.22	0.22	0.19
P2O5	0.31	0.36	0.41	0.49	0.46	0.28	0.24	0.25	0.26	0.18
PPM										
CU	147	108	119	70	76	154	53	34	130	93
NI	46	15	55	17	14	18	52	8	9	115
CR	274	89	203	75	83	75	200	14	52	669
BA	636	838	1057	1049	668	1359	635	404	512	460
NB	3	5	8	9	7	3	0	4	1	5
ZR	94	117	160	174	167	86	56	94	95	87
Y	23	17	31	31	30	13	13	23	20	18
SR	464	1161	500	767	553	984	477	549	583	651
RB	62	32	55	65	55	35	28	38	39	62
ZN	99	97	167	95	70	84	116	120	129	76
CE	13	0	24	25	30	17	0	20	23	0
LA	4	0	13	15	10	43	0	3	6	4
V	309	255	292	306	304	371	0	329	302	239

TABLE A2.1 MAJOR AND TRACE ELEMENT ANALYSES(RVG).

	4075	4077	4078	4079	4081	4082	4090	4092	4095	4099
WEIGHT % OXIDE										
SIO2	57.54	50.10	52.26	50.05	55.28	51.06	51.52	50.59	50.08	49.77
AL203	15.33	14.54	12.72	13.11	14.79	10.59	12.97	13.23	14.09	11.64
FE203*	9.89	14.07	11.67	12.68	9.64	11.94	11.69	13.66	12.50	11.54
MGO	6.35	6.13	6.64	6.64	4.37	9.41	7.71	7.01	5.77	10.66
CAO	4.73	9.79	10.66	11.69	7.61	13.38	9.45	10.27	10.44	11.11
NA20	3.93	2.34	2.75	2.84	4.07	1.44	3.11	2.58	3.59	2.06
K20	0.98	1.44	1.92	1.43	2.52	0.83	2.14	1.25	2.01	1.91
TIO2	0.91	1.07	0.88	0.93	1.10	0.78	0.79	0.80	0.88	0.74
MNO	0.14	0.21	0.19	0.21	0.19	0.23	0.20	0.18	0.22	0.20
P205	0.22	0.30	0.31	0.41	0.40	0.34	0.42	0.43	0.42	0.37
PPM										
CU	27	68	105	117	131	18	55	293	65	66
NI	6	12	31	35	22	36	32	3	7	123
CR	64	52	254	138	56	531	232	87	60	508
BA	377	596	629	866	1283	455	963	880	630	635
NB	6	4	5	5	11	5	5	5	4	2
ZR	122	91	83	64	142	78	70	97	114	48
Y	19	24	17	0	22	13	14	18	20	13
SR	487	639	693	384	1067	600	714	823	1094	614
RB	32	34	58	35	62	24	70	34	73	86
ZN	107	106	94	96	91	96	93	78	106	131
CE	19	19	22	20	14	28	30	31	38	13
LA	16	6	4	7	11	9	12	15	15	41
V	232	350	297	335	228	298	281	306	284	280

TABLE A2.1 MAJOR AND TRACE ELEMENT ANALYSES(RVG).

	4100A	4102A	4102B	4105B	4107F	4109B	4110	4111V	4112	4113
WEIGHT % OXIDE										
SIO2	49.86	54.02	49.99	46.67	49.76	55.69	48.88	49.50	59.94	50.58
AL203	12.27	12.77	13.34	8.92	16.57	14.97	12.89	10.95	13.68	14.11
FE203*	11.53	10.65	13.12	15.70	13.20	8.61	14.20	13.04	7.62	11.59
MGO	9.92	6.85	5.34	11.03	8.64	3.42	9.85	10.27	4.96	7.07
CAO	10.62	10.00	9.27	11.94	7.50	8.45	9.97	10.58	6.64	9.32
NA2O	2.59	2.99	4.46	2.32	2.71	4.30	2.29	2.64	2.60	3.96
K2O	1.80	1.31	2.89	1.52	0.11	3.29	1.01	1.73	3.55	1.83
TIO2	0.92	0.88	1.01	1.32	0.94	0.77	0.91	0.78	0.67	0.82
MNO	0.19	0.24	0.27	0.24	0.20	0.14	0.21	0.20	0.14	0.16
P2O5	0.32	0.29	0.31	0.35	0.36	0.36	0.30	0.32	0.20	0.50
PPM										
CU	72	487	199	80	64	64	131	139	11	104
NI	91	27	29	38	16	16	77	69	12	31
CR	380	120	66	176	54	54	291	310	261	136
BA	438	816	1022	869	93	803	270	423	1050	691
NB	3	3	3	4	2	5	5	3	15	4
ZR	57	96	95	70	142	119	112	55	162	56
Y	17	21	22	22	18	19	16	15	15	14
SR	576	676	942	386	1642	717	1220	577	718	758
RB	89	29	101	35	3	51	23	41	92	33
ZN	93	95	98	136	115	71	116	100	97	90
CE	0	22	14	20	36	26	33	23	51	14
LA	0	6	3	39	13	10	10	4	31	7
V	0	254	318	531	276	209	339	307	127	296

TABLE A2.1 MAJOR AND TRACE ELEMENT ANALYSES(RVG).

	4115	4117	4118	4119	0074B
WEIGHT % OXIDE					
SiO_2	51.43	49.12	47.52	45.39	45.60
Al_2O_3	11.24	13.26	14.54	10.08	11.88
Fe_2O_3*	11.59	13.02	15.70	11.84	15.02
MgO	15.41	11.03	7.02	21.86	8.47
CaO	7.58	8.12	8.86	8.95	14.40
Na_2O	1.01	2.30	2.95	0.42	1.94
K_2O	0.70	1.75	1.95	0.46	1.49
TiO_2	0.67	0.98	0.93	0.01	0.82
MnO	0.18	0.21	0.19	0.18	0.17
P_2O_5	0.18	0.21	0.34	0.20	0.49
PPM					
Cu	64	65	122	96	7
Ni	313	88	24	828	22
Cr	1021	380	89	1820	47
Ba	383	712	857	153	240
Nb	4	4	2	4	3
Zr	71	94	98	48	75
Y	15	13	15	14	11
Sr	224	878	711	135	960
Rb	13	41	35	13	56
Zn	112	143	139	85	63
Ce	13	8	11	5	17
La	4	1	16	4	3
V	263	285	364	240	468

TABLE A2.1 MAJOR AND TRACE ELEMENT ANALYSES(RVG).

	5001A	5001B	5006	5008	5009	5010	5012	5013	5014	5015
WEIGHT % OXIDE										
SIO2	52.88	50.86	47.84	49.74	50.72	50.99	53.60	51.79	43.21	59.35
AL203	16.12	12.99	14.37	13.23	13.78	16.15	13.30	15.16	6.34	14.37
FE203*	11.36	13.99	14.86	12.41	12.50	12.08	11.03	10.43	13.18	8.83
MGO	6.85	8.59	8.53	10.31	13.42	5.50	7.69	5.75	8.93	5.50
CAO	6.87	9.73	9.29	9.24	6.60	7.51	9.16	10.47	25.47	5.13
NA2O	3.98	1.83	1.84	1.91	0.91	3.58	2.56	2.87	1.47	4.87
K2O	0.57	0.49	1.82	1.85	1.05	2.33	1.46	2.21	0.14	0.86
TIO2	0.72	0.83	0.81	0.93	0.68	1.19	0.82	0.91	0.83	0.78
MNO	0.23	0.23	0.22	0.17	0.18	0.20	0.16	0.13	0.23	0.15
P2O5	0.42	0.44	0.41	0.19	0.15	0.48	0.23	0.28	0.19	0.15
PPM										
CU	114	176	207	69	98	117	78	114	54	46
NI	5	13	15	103	145	3	181	56	207	21
CR	40	48	60	371	435	11	419	152	672	112
BA	825	729	1158	772	353	1149	721	971	339	409
NB	5	4	4	4	3	5	1	4	3	6
ZR	129	118	98	69	58	163	96	115	58	100
Y	18	17	16	16	14	31	21	21	15	19
SR	1216	1243	996	330	306	834	558	694	358	409
RB	17	6	31	37	32	52	39	51	6	21
ZN	102	113	105	86	94	114	123	94	83	79
CE	33	31	22	12	9	20	21	20	37	8
LA	13	14	6	5	23	30	21	16	4	6
V	252	322	360	308	270	284	262	272	257	217

TABLE A2.1 MAJOR AND TRACE ELEMENT ANALYSES(RVG).

	5016	5018	5024	5028	5029	5031	5032	5033	5034	5036
WEIGHT % OXIDE										
SIO2	55.95	48.58	54.18	56.99	55.17	50.96	54.88	55.53	57.17	52.30
AL203	13.67	10.82	14.61	14.81	16.62	17.03	15.63	15.68	18.54	13.46
FE203*	9.96	13.83	10.62	11.07	10.97	11.04	9.98	9.33	6.06	11.37
MGO	6.26	8.47	6.84	5.69	6.64	4.53	8.32	5.24	1.99	5.12
CAO	8.43	13.48	8.40	5.25	4.13	10.18	6.28	7.39	4.56	10.65
NA20	2.68	2.42	3.19	3.69	3.96	3.16	2.28	2.36	4.12	2.81
K20	1.79	1.07	0.93	1.05	1.14	1.67	3.17	3.24	4.66	2.95
TIO2	0.84	0.85	0.77	0.96	0.94	1.06	0.80	0.71	0.51	0.83
MNO	0.17	0.25	0.21	0.25	0.15	0.20	0.15	0.13	0.13	0.18
P205	0.25	0.22	0.26	0.24	0.29	0.16	0.50	0.38	0.22	0.32
PPM										
CU	79	60	14	33	50	165	67	36	0	39
NI	51	54	20	5	10	14	28	0	0	19
CR	130	245	58	23	89	59	52	10	0	124
BA	571	117	317	683	689	1176	1921	1078	0	876
NB	5	2	5	7	4	4	6	2	0	7
ZR	119	65	128	100	106	106	112	153	0	120
Y	20	17	18	19	17	17	17	23	0	20
SR	814	417	1100	436	489	732	962	1438	0	949
RB	53	51	42	26	24	61	64	56	0	77
ZN	84	110	97	434	99	122	81	99	0	101
CE	21	20	21	53	13	9	5	21	0	20
LA	8	7	24	1	0	0	0	8	0	0
V	241	316	257	262	267	294	302	197	0	263

TABLE A2.1 MAJOR AND TRACE ELEMENT ANALYSES(RVG).

	5038	5039	5040	5041	5042	5043	5044	5045	5048	5049
WEIGHT % OXIDE										
SIO2	52.69	53.40	47.48	49.94	42.43	46.77	52.77	51.26	53.58	53.04
AL203	12.61	14.66	10.07	14.43	5.66	11.58	13.52	14.03	12.58	13.47
FE203*	13.44	12.28	13.14	12.63	12.01	13.66	10.92	11.28	11.28	11.39
MGO	6.19	5.54	7.12	7.44	6.67	9.48	6.59	8.76	6.99	5.88
CAO	11.12	9.22	17.21	10.20	29.49	14.94	10.48	8.90	9.78	9.99
NA20	1.24	1.95	1.89	2.96	1.20	1.29	3.91	2.63	2.53	2.37
K20	1.49	1.52	1.51	0.78	1.09	0.88	0.69	1.99	2.02	2.48
TIO2	0.77	0.97	1.06	1.09	0.99	0.98	0.72	0.75	0.79	0.82
MNO	0.18	0.18	0.26	0.20	0.25	0.20	0.15	0.17	0.18	0.19
P205	0.28	0.28	0.26	0.32	0.20	0.21	0.24	0.29	0.27	0.36
PPM										
CU	71	64	52	41	41	75	87	74	101	74
NI	18	22	55	103	25	137	66	79	42	22
CR	109	68	282	709	328	382	246	213	171	92
BA	775	568	767	341	375	459	109	751	581	831
NB	5	6	5	5	3	4	4	4	4	6
ZR	139	102	88	137	80	89	90	95	96	108
Y	14	21	18	23	19	18	16	16	17	17
SR	1278	927	660	813	524	498	414	697	855	934
RB	26	43	32	28	25	27	29	51	48	50
ZN	97	109	89	136	74	101	92	103	99	113
CE	33	30	26	22	47	25	29	15	19	5
LA	12	5	6	7	34	5	11	7	0	11
V	262	315	308	291	261	299	242	218	285	288

TABLE A2.1 MAJOR AND TRACE ELEMENT ANALYSES(RVG).

	5050	5052	5053	5054	5055	5056	4057	5058	5062	5063
WEIGHT % OXIDE										
SIO2	53.90	37.93	50.84	52.17	51.77	52.86	52.36	51.77	49.83	52.47
AL203	13.89	6.56	14.16	13.10	14.16	14.84	15.21	13.22	13.16	14.12
FE203*	9.64	10.97	10.54	10.98	11.64	10.31	10.94	10.98	12.36	11.90
MGO	6.66	17.42	10.02	6.94	7.90	5.32	6.01	10.12	6.27	6.51
CAO	9.70	25.80	8.55	9.54	7.43	9.06	6.74	9.58	10.64	9.11
NA20	3.19	-	2.42	3.73	2.78	2.28	4.02	1.51	3.26	2.77
K20	1.58	0.11	2.34	2.16	2.91	1.98	3.20	1.68	2.53	1.64
TIO2	0.94	0.79	0.76	0.84	0.85	0.81	0.87	0.84	1.29	0.99
MNO	0.15	0.23	0.14	0.17	0.19	0.18	0.22	0.19	0.22	0.23
P205	0.35	0.18	0.23	0.38	0.37	0.23	0.44	0.21	0.43	0.26
PPM										
CU	44	11	36	21	69	0	53	75	93	43
NI	63	50	38	44	90	0	14	163	30	20
CR	199	168	113	145	194	0	44	441	106	72
BA	688	42	959	761	897	0	1167	535	970	787
NB	5	3	3	4	4	0	5	6	7	5
ZR	99	64	104	106	104	0	116	93	147	109
Y	19	12	16	15	19	0	23	18	26	22
SR	635	520	675	1120	869	0	730	607	932	619
RB	33	5	40	44	63	0	74	47	74	38
ZN	75	74	72	93	109	0	118	84	121	101
CE	17	40	15	18	14	28	28	40	28	18
LA	7	3	2	7	10	6	12	3	13	8
V	296	246	217	325	306	0	260	246	295	255

TABLE A2.1 MAJOR AND TRACE ELEMENT ANALYSES(RVG).

	5073B	5074A	5074B	5074C	5075A	5075B	5076	5077	5079	5081A
WEIGHT % OXIDE										
SIO2	52.07	57.98	50.49	49.67	44.94	44.53	55.84	47.82	59.00	50.99
AL203	12.45	16.98	10.11	9.35	3.96	3.93	16.14	4.07	13.80	13.63
FE203*	11.91	7.96	12.81	13.14	16.35	16.53	7.27	12.97	7.75	12.43
MGO	7.31	3.92	9.74	10.35	17.64	16.97	3.75	19.52	4.74	7.32
CAO	10.13	6.03	12.09	13.30	15.87	16.25	6.81	14.26	8.32	10.24
NA20	3.45	3.13	2.11	1.62	0.04	0.02	3.99	0.21	4.14	3.29
K20	1.24	2.71	1.40	1.33	0.07	0.62	4.94	0.28	1.19	0.75
TIO2	0.84	0.89	0.74	0.74	0.86	0.87	0.65	0.58	0.74	0.90
MNO	0.25	0.11	0.21	0.23	0.19	0.21	0.18	0.21	0.13	0.18
P205	0.35	0.28	0.30	0.26	0.08	0.09	0.41	0.09	0.20	0.28
PPM										
CU	477	249	89	51	3	9	16	30	26	109
NI	48	2	85	114	149	177	0	277	9	56
CR	187	17	387	467	534	431	10	1132	84	156
BA	314	986	684	649	17	46	867	30	512	420
NB	7	5	4	4	0	1	6	2	5	5
ZR	85	120	82	75	20	21	139	23	132	93
Y	19	19	15	14	10	9	18	8	17	17
SR	685	620	696	673	78	77	1184	122	351	695
RB	36	72	43	40	0	21	143	8	42	21
ZN	121	86	104	108	70	91	86	95	115	73
CE	23	17	20	20	13	14	12	19	27	30
LA	7	11	4	0	0	1	10	4	9	9
V	335	223	281	278	459	518	237	233	164	318

TABLE A2.1 MAJOR AND TRACE ELEMENT ANALYSES(RVG).

	5081B	5083A	5084	5085A	5085C	5085D	5085E	5086B	5087A	5087B
WEIGHT % OXIDE										
SIO2	50.39	49.97	49.17	45.31	46.29	47.30	50.06	50.00	51.25	49.42
AL203	14.01	13.15	13.00	7.26	10.43	9.20	7.40	15.08	11.78	12.39
FE203*	12.21	13.07	13.60	14.44	15.89	14.53	11.89	12.35	13.51	12.64
MGO	7.43	5.08	8.06	19.74	13.45	12.06	10.35	5.71	9.55	9.92
CAO	10.33	12.14	10.14	12.12	10.67	12.25	15.57	9.19	8.82	9.73
NA20	3.04	3.17	2.19	0.01	0.24	0.30	1.87	3.32	2.87	2.51
K20	1.19	1.85	2.31	0.01	1.73	3.06	1.68	2.70	0.88	1.97
TIO2	0.91	0.87	1.05	0.58	0.77	0.80	0.64	1.11	0.86	1.00
MNO	0.19	0.24	0.20	0.38	0.23	0.22	0.26	0.25	0.18	0.19
P205	0.30	0.44	0.30	0.18	0.29	0.28	0.28	0.29	0.31	0.23
PPM										
CU	130	23	20	0	2	64	21	137	109	83
NI	45	14	22	184	260	189	168	5	83	43
CR	158	66	141	1780	969	842	819	18	377	355
BA	521	517	1030	0	200	1899	653	547	546	299
NB	5	4	4	3	4	3	0	3	3	4
ZR	103	109	98	43	56	52	57	99	85	70
Y	18	17	19	10	17	14	13	23	18	18
SR	811	945	702	224	363	474	612	601	625	397
RB	37	48	80	2	80	123	46	65	45	18
ZN	83	85	125	536	203	149	112	166	91	88
CE	32	44	25	5	15	4	11	22	12	15
LA	17	14	13	3	4	10	1	9	3	1
V	329	284	358	286	364	327	258	335	301	321

TABLE A2.1 MAJOR AND TRACE ELEMENT ANALYSES(RVG).

	5088	5089	5096	5097	5098	5100	5101	5104	5105	5106A
WEIGHT % OXIDE										
SIO2	49.96	50.09	53.09	52.01	54.50	58.17	57.39	51.78	51.80	57.22
AL203	10.79	13.00	14.65	13.11	14.88	15.95	15.74	13.62	15.13	13.51
FE203*	13.16	12.96	10.26	10.77	11.43	10.47	10.86	11.60	10.58	9.19
MGO	9.87	7.56	4.61	5.90	6.92	5.87	6.14	5.98	9.54	5.36
CAO	11.38	10.12	10.52	6.34	6.65	3.83	4.34	8.80	6.26	10.13
NA20	2.24	2.97	3.12	2.89	3.13	3.23	3.15	2.21	3.09	2.81
K20	1.26	1.83	1.97	1.00	1.07	1.21	1.08	4.38	2.58	0.67
TIO2	0.87	0.88	1.15	0.97	1.00	0.88	0.89	0.99	0.88	0.70
MNO	0.19	0.22	0.21	0.16	0.16	0.14	0.14	0.21	0.17	0.18
P205	0.27	0.36	0.42	0.27	0.28	0.24	0.25	0.43	0.27	0.22
PPM										
CU	137	104	55	15	34	35	31	56	89	58
NI	48	24	7	0	15	10	10	5	39	47
CR	329	138	29	15	106	74	81	73	183	196
BA	331	607	947	166	667	978	918	950	878	607
NB	2	4	11	5	5	5	6	5	6	5
ZR	79	92	169	104	114	115	116	120	103	122
Y	17	16	22	20	17	14	17	24	18	20
SR	689	875	1195	443	845	685	604	1123	760	741
RB	23	40	40	11	35	30	30	131	52	17
ZN	90	95	86	109	95	128	132	102	90	87
CE	10	23	5	20	22	7	16	26	21	23
LA	3	11	10	8	1	9	11	17	9	6
V	302	310	205	175	281	261	282	321	275	211

TABLE A2.1 MAJOR AND TRACE ELEMENT ANALYSES(RVG).

	5106B	5107A	5107B	5108	5109	5110	5111A	5113	5115	5116
WEIGHT % OXIDE										
SIO2	54.20	47.76	50.84	53.22	52.86	55.01	48.35	56.81	47.50	48.60
AL203	13.94	13.44	15.25	15.30	12.67	12.75	8.20	14.66	8.57	14.59
FE203*	9.84	14.74	12.36	9.14	12.15	10.93	13.33	9.96	12.26	13.51
MGO	5.82	8.45	6.07	7.24	6.26	4.32	11.93	4.87	7.76	8.08
CAO	11.32	10.25	10.06	7.05	9.51	9.53	13.33	7.17	18.25	7.76
NA20	3.12	2.85	3.14	3.87	1.65	3.17	1.97	3.56	2.24	2.79
K20	0.60	0.72	0.71	2.42	3.39	2.78	1.80	1.88	2.21	3.15
TIO2	0.70	1.09	1.10	1.11	0.97	0.87	0.64	0.76	0.75	0.98
MNO	0.19	0.22	0.22	0.11	0.15	0.23	0.20	0.12	0.20	0.19
P205	0.27	0.47	0.31	0.54	0.38	0.42	0.25	0.22	0.25	0.35
PPM										
CU	45	153	61	94	49	22	115	17	90	108
NI	36	8	0	2	9	4	179	2	77	21
CR	152	63	4	33	35	42	738	21	396	98
BA	491	675	378	1619	1485	770	474	686	654	720
NB	4	5	5	7	5	2	3	7	2	3
ZR	139	87	119	111	135	144	50	106	75	108
Y	18	16	26	24	19	21	12	22	13	20
SR	883	936	724	995	1424	1130	463	535	848	819
RB	17	6	17	40	98	55	45	48	43	63
ZN	95	101	117	37	73	114	96	103	97	135
CE	21	27	21	13	19	47	13	15	23	29
LA	8	6	11	11	4	13	5	6	7	11
V	194	419	265	368	323	257	291	217	307	288

TABLE A2.1 MAJOR AND TRACE ELEMENT ANALYSES(RVG).

	5118	5119	5120	5519A	5519B	5519C	5526A	5528A	5528B	5531A
WEIGHT % OXIDE										
SIO2	51.31	51.78	51.06	51.50	52.66	50.79	48.68	53.56	51.17	48.98
AL203	14.62	14.09	11.55	16.41	16.44	18.10	11.28	14.21	11.52	12.85
FE203*	11.25	10.97	12.18	10.94	9.88	10.68	13.28	12.12	12.50	12.59
MGO	6.47	6.22	6.66	5.32	5.30	5.60	9.07	6.13	8.55	9.22
CAO	7.24	8.25	11.90	7.72	6.83	6.75	12.52	7.22	10.31	9.99
NA2O	3.58	3.38	2.25	3.60	4.30	2.83	2.05	2.78	1.77	2.87
K2O	3.60	3.49	2.75	3.05	3.24	3.74	1.56	2.60	2.60	2.05
TIO2	1.06	1.07	0.94	0.86	0.83	0.88	0.91	0.82	0.84	0.87
MNO	0.21	0.18	0.27	0.17	0.17	0.17	0.20	0.15	0.20	0.24
P2O5	0.64	0.58	0.42	0.38	0.31	0.41	0.43	0.39	0.49	0.33
PPM										
CU	97	123	93	38	34	70	81	131	89	112
NI	15	5	10	15	18	9	62	22	49	74
CR	15	13	80	61	69	68	314	89	231	337
BA	878	1025	1373	939	904	963	483	503	1290	566
NB	10	8	4	4	3	4	6	4	5	2
ZR	187	183	117	82	87	119	68	93	73	64
Y	33	31	19	18	17	22	17	18	14	18
SR	1212	1150	1144	1064	735	1236	644	910	1112	644
RB	80	78	50	69	89	96	38	55	60	27
ZN	121	89	126	123	133	143	94	134	97	127
CE	59	25	15	0	0	0	0	30	23	15
LA	12	13	8	0	0	0	0	12	11	12
V	256	244	293	0	0	0	0	0	264	276

TABLE A2.1 MAJOR AND TRACE ELEMENT ANALYSES(RVG).

	5531C	5532A	5533	5534A	5536	5537A	5537B	5538A	5538B	5539B
WEIGHT % OXIDE										
SIO2	46.20	47.92	47.23	50.54	46.22	50.14	48.70	48.54	47.29	49.58
AL203	12.97	9.35	9.23	12.91	14.04	12.92	13.64	11.08	10.96	11.99
FE203*	12.94	13.41	13.75	11.53	14.00	12.75	13.48	12.93	13.29	13.57
MGO	15.11	11.76	13.47	7.63	13.34	8.63	5.97	11.64	12.60	10.22
CAO	8.67	12.69	13.14	9.99	8.34	8.79	9.98	10.67	11.34	9.34
NA20	2.54	1.49	1.04	2.98	1.69	3.21	4.46	2.19	1.98	2.56
K20	0.29	1.71	0.83	2.91	1.06	1.97	2.05	1.60	1.16	1.38
TIO2	0.74	0.87	0.61	0.77	0.87	1.02	1.10	0.79	0.82	0.84
MNO	0.29	0.21	0.23	0.29	0.19	0.19	0.20	0.21	0.21	0.19
P205	0.23	0.61	0.42	0.42	0.20	0.32	0.41	0.30	0.35	0.32
PPM										
CU	105	106	10	147	84	0	94	79	77	138
NI	193	52	298	78	257	81	36	147	143	63
CR	780	419	889	292	689	329	0	577	571	350
BA	65	1396	344	1114	579	505	604	577	476	550
NB	3	4	3	3	2	1	4	2	0	0
ZR	52	58	40	63	57	68	89	48	223	43
Y	13	13	11	13	15	16	19	14	13	10
SR	314	346	400	618	491	700	642	608	518	449
RB	4	49	17	62	29	46	44	38	25	32
ZN	109	87	64	171	108	94	109	85	91	98
CE	0	0	18	0	8	8	0	15	17	4
LA	0	0	8	0	2	1	0	4	8	5
V	0	0	252	0	203	296	0	287	300	328

TABLE A2.1 MAJOR AND TRACE ELEMENT ANALYSES(SKP).

	4014	4101B	4103C	4107C	4104	5004	5017A	5017B	5019	5020
WEIGHT % OXIDE										
SIO2	63.34	64.59	62.36	61.93	63.07	64.89	63.28	62.04	65.81	65.07
AL2O3	15.34	15.21	17.39	13.87	15.75	14.67	15.59	16.31	16.16	15.86
FE2O3*	5.40	4.37	5.07	6.27	5.24	5.08	5.99	5.45	4.34	4.16
MGO	2.92	2.04	1.85	4.82	2.06	3.29	2.67	2.51	1.66	1.72
CAO	5.26	5.93	4.99	5.47	5.73	4.09	5.61	6.22	4.11	5.01
NA2O	4.70	5.32	3.93	2.87	4.94	3.10	4.07	3.15	5.00	5.14
K2O	2.10	1.69	3.54	3.44	2.28	3.95	1.79	3.45	2.19	2.25
TIO2	0.58	0.46	0.57	0.95	0.57	0.58	0.60	0.54	0.49	0.50
MNO	0.13	0.15	0.10	0.08	0.13	0.09	0.16	0.16	0.09	0.10
P2O5	0.22	0.23	0.21	0.25	0.16	0.25	0.23	0.18	0.15	0.18
PPM										
CU	10	4	1	14	12	0	1	0	0	0
NI	5	0	0	36	4	15	0	1	0	0
CR	425	2	5	281	12	99	20	33	14	14
BA	506	630	586	1400	606	1502	500	718	469	539
NB	9	14	11	22	12	41	11	11	11	11
ZR	197	213	234	256	197	199	258	208	249	236
Y	23	27	31	16	25	19	28	30	24	22
SR	871	794	763	1289	1167	641	1700	615	1349	1198
RB	53	43	101	92	77	139	58	103	66	54
ZN	74	130	32	92	84	50	136	143	60	56

TABLE A2.1 MAJOR AND TRACE ELEMENT ANALYSES(SKP).

	5027	5047	5051	5072	5086A	5090	5117A	5117B
WEIGHT % OXIDE								
SIO2	63.94	62.77	61.59	63.68	63.13	62.92	62.50	62.88
AL203	15.42	15.51	15.03	15.12	15.85	14.92	16.08	16.61
FE203*	5.28	5.22	6.20	6.09	5.41	6.56	4.80	5.07
MGO	2.09	2.26	3.32	2.60	2.36	2.53	2.44	2.22
CAO	5.65	5.76	6.24	5.23	5.99	5.55	5.16	4.78
NA20	5.45	3.86	3.90	3.03	2.19	3.16	6.84	5.44
K20	1.32	3.63	2.63	3.04	4.19	3.14	1.23	2.08
TIO2	0.48	0.52	0.64	0.80	0.56	0.81	0.58	0.52
MNO	0.10	0.15	0.15	0.11	0.12	0.10	0.13	0.13
P205	0.25	0.31	0.30	0.29	0.19	0.30	0.24	0.26
PPM								
CU	3	0	8	5	106	1	0	0
NI	0	0	5	0	1	0	3	0
CR	26	5	16	3	23	9	6	1
BA	457	1044	664	893	1084	1185	436	442
NB	11	10	8	12	11	18	13	12
ZR	256	150	202	191	149	256	217	232
Y	28	20	27	18	16	28	30	31
SR	1377	883	955	664	591	905	456	1150
RB	33	130	85	140	110	112	33	54
ZN	50	80	73	111	84	111	87	67

TABLE A2.2 SELECTED NORMS(FE203/FEO=0.3)

NORMCAL .. R.C.O.GILL

SUMMARY NORM TABLE

	5006	5013	5015	5016	5032	5033	5034	5036	5041	5053	5054	5055
QUARTZ	0.0	0.0	7.0	6.6	1.4	5.0	1.1	0.0	0.0	0.0	0.0	0.0
ORTHOCLASE	10.9	13.2	5.1	10.7	18.5	19.3	28.2	17.6	4.7	13.9	12.9	17.4
ALBITE	15.8	24.5	41.5	22.9	19.1	20.1	35.8	24.0	25.3	20.6	28.7	23.7
ANORTHITE	25.9	22.1	14.9	20.1	22.8	22.8	18.8	15.5	24.0	21.0	12.7	17.7
NEPHELINE	0.0	0.0	0.0	0.0	0.0	0.0	0.0	0.0	0.0	0.0	1.7	0.0
DIOPSIDE	14.8	23.2	7.9	16.6	3.9	9.5	2.4	29.4	20.4	16.3	26.5	13.9
HYPERSTHENE	12.8	5.1	18.9	17.8	28.7	18.1	10.2	0.3	11.2	8.6	0.0	10.3
OLIVINE	12.8	6.2	0.0	0.0	0.0	0.0	0.0	7.3	7.6	14.2	11.6	10.9
MAGNETITE	4.6	3.2	2.7	3.1	3.0	2.9	1.9	3.5	3.9	3.3	3.4	3.6
ILMENITE	1.6	1.7	1.5	1.6	1.5	1.4	1.0	1.6	2.1	1.5	1.6	1.6
APATITE	1.0	0.7	0.4	0.6	1.2	0.9	0.5	0.8	0.8	0.5	0.9	0.9
DIFF. INDEX	26.6	37.7	53.6	40.1	39.0	44.4	65.1	41.6	30.0	34.6	43.3	41.1
NA/(NA+K)	0.61	0.66	0.90	0.69	0.52	0.53	0.57	0.59	0.85	0.61	0.72	0.59
(NA+K)/AL	0.35	0.47	0.62	0.46	0.46	0.47	0.64	0.58	0.40	0.46	0.65	0.55
F3/(F2+F3)	0.21	0.21	0.21	0.21	0.21	0.21	0.21	0.21	0.21	0.21	0.21	0.21

TABLE A2.2 SELECTED NORMS(FE2O3/FEO=0.3)

NORMCAL .. R.C.O.GILL

SUMMARY NORM TABLE

	5056	4057	5058	5063	5073B	5074B	5085E	5087B	5088	5089	5101	5104
QUARTZ	4.7	0.0	1.1	0.9	0.0	0.0	0.0	0.0	0.0	0.0	12.3	0.0
CORUNDUM	0.0	0.0	0.0	0.0	0.0	0.0	0.0	0.0	0.0	0.0	2.1	0.0
ORTHOCLASE	12.1	19.1	10.0	9.8	7.4	8.4	10.0	11.8	7.5	10.9	6.4	26.1
ALBITE	19.9	30.5	12.9	23.7	29.5	18.0	9.3	21.4	19.2	24.9	26.9	18.9
ANORTHITE	25.1	14.1	24.5	21.4	15.0	14.1	6.9	16.9	15.8	16.9	20.1	14.4
NEPHELINE	0.0	2.1	0.0	0.0	0.0	0.0	3.6	0.0	0.0	0.3	0.0	0.0
DIOPSIDE	16.1	13.7	17.8	18.4	27.3	36.1	56.0	24.6	32.0	25.7	0.0	22.0
HYPERSTHENE	16.7	0.0	28.2	19.6	6.8	8.1	0.0	0.0	8.2	0.0	26.5	0.9
OLIVINE	0.0	14.5	0.0	0.0	7.9	9.1	8.6	18.9	10.9	14.7	0.0	11.2
MAGNETITE	3.3	3.4	3.4	3.7	3.7	4.0	3.7	3.9	4.1	4.0	3.4	3.6
ILMENITE	1.6	1.7	1.6	1.9	1.6	1.4	1.2	1.9	1.7	1.7	1.7	1.9
APATITE	0.6	1.1	0.5	0.6	0.8	0.7	0.7	0.6	0.6	0.9	0.6	1.0
DIFF. INDEX	36.7	51.6	24.0	34.3	36.9	26.4	22.9	33.2	26.7	36.1	45.6	45.0
NA/(NA+K)	0.64	0.66	0.58	0.72	0.81	0.70	0.63	0.66	0.73	0.71	0.82	0.43
(NA+K)/AL	0.40	0.66	0.33	0.45	0.56	0.49	0.66	0.51	0.47	0.53	0.40	0.62
F3/(F2+F3)	0.21	0.21	0.21	0.21	0.21	0.21	0.21	0.21	0.21	0.21	0.21	0.21

TABLE A2,2 SELECTED NORMS(FE2O3/FEO=0.3)

NORMCAL .. R.C.O.GILL

SUMMARY NORM TABLE

	5105	5106A	5106B	5108	5111A	5113	5116	5119	5120	4001	4007	4013
QUARTZ	0.0	10.7	3.9	0.0	0.0	5.7	0.0	0.0	0.0	0.0	0.0	0.0
ORTHOCLASE	15.4	4.0	3.6	14.4	10.7	11.2	18.8	20.8	16.4	16.5	16.0	13.6
ALBITE	26.4	24.0	26.6	33.0	8.2	30.4	18.2	24.9	19.1	18.0	28.5	21.3
ANORTHITE	20.0	22.4	22.4	17.3	8.3	18.6	18.2	13.1	13.4	15.5	17.5	13.4
NEPHELINE	0.0	0.0	0.0	0.0	4.7	0.0	3.1	2.1	0.1	3.7	0.5	3.7
DIOPSIDE	7.7	21.9	26.5	11.6	46.0	13.0	15.1	19.9	35.6	23.9	18.4	27.7
HYPERSTHENE	9.0	12.3	12.0	7.4	0.0	16.1	0.0	0.0	0.0	0.0	0.0	0.0
OLIVINE	16.0	0.0	0.0	10.0	16.1	0.0	19.8	12.3	8.8	15.4	12.9	14.4
MAGNETITE	3.3	2.9	3.1	2.8	4.2	3.1	4.2	3.4	3.8	4.3	3.6	3.8
ILMENITE	1.7	1.3	1.3	2.1	1.2	1.5	1.9	2.0	1.8	1.7	1.6	1.5
APATITE	0.6	0.5	0.6	1.3	0.6	0.5	0.8	1.4	1.0	0.9	1.0	0.6
DIFF. INDEX	41.7	38.6	34.1	47.4	23.6	47.2	40.1	47.8	35.6	38.3	45.0	38.6
NA/(NA+K)	0.65	0.86	0.89	0.71	0.62	0.74	0.57	0.60	0.55	0.61	0.66	0.69
(NA+K)/AL	0.52	0.40	0.41	0.59	0.63	0.54	0.55	0.66	0.58	0.58	0.57	0.62
F3/(F2+F3)	0.21	0.21	0.21	0.21	0.21	0.21	0.21	0.21	0.21	0.21	0.21	0.21

TABLE A2,2 SELECTED NORMS(FE2O3/FEO=0.3)

NORMCAL .. R.C.O.GILL

SUMMARY NORM TABLE

	4013	4016	4023	4029A	4042	4050	4051	4056	4062	4070	4077	4090
ORTHOCLASE	14.0	13.8	7.3	11.7	20.1	7.8	8.0	16.6	8.0	13.8	8.6	12.8
ALBITE	14.9	24.7	31.9	25.7	35.0	11.9	28.2	34.3	29.5	12.5	20.0	26.6
ANORTHITE	12.9	22.3	14.3	21.8	12.0	19.7	24.9	11.9	15.5	15.7	25.2	15.2
NEPHELINE	1.9	0.0	2.4	0.9	4.6	0.0	0.0	4.7	0.0	6.8	0.0	0.0
DIOPSIDE	32.0	18.1	25.0	17.1	10.9	32.7	16.5	22.5	26.1	32.7	18.1	23.9
HYPERSTHENE	0.0	9.7	0.0	0.0	0.0	6.9	5.8	0.0	0.0	0.0	20.4	2.9
OLIVINE	18.5	5.2	12.9	16.6	11.8	13.6	10.3	4.4	14.2	11.5	0.5	12.5
MAGNETITE	3.7	3.4	3.3	3.8	3.4	4.0	3.4	3.1	3.7	4.4	4.4	3.6
ILMENITE	1.4	2.0	2.0	1.6	1.7	1.8	2.2	1.6	2.3	1.9	2.1	1.5
APATITE	0.8	0.9	0.9	0.8	0.5	1.6	0.6	0.9	0.6	0.7	0.7	1.0
DIFF. INDEX	30.8	38.5	41.7	38.3	59.7	19.7	36.2	55.7	37.5	33.2	28.6	39.3
NA/(NA+K)	0.58	0.65	0.84	0.71	0.70	0.62	0.79	0.73	0.80	0.66	0.71	0.69
(NA+K)/AL	0.57	0.47	0.62	0.48	0.73	0.34	0.43	0.72	0.56	0.56	0.37	0.57
F3/(F2+F3)	0.21	0.21	0.21	0.21	0.21	0.21	0.21	0.21	0.21	0.21	0.21	0.21

TABLE A2.2 SELECTED NORMS(FE203/FEO=0.3)

NORMCAL .. R.C.O.GILL

SUMMARY NORM TABLE

	4099	4100A	4109B	4110	5533	5536	5538A	5538B	5531A	5075A	5075B	5077
ORTHOCLASE	11.4	10.7	19.6	6.0	5.0	6.3	9.6	6.9	12.2	0.4	0.0	1.7
ALBITE	17.6	21.3	35.4	19.5	8.9	14.5	18.0	15.5	18.9	0.3	0.0	1.8
ANORTHITE	17.0	16.7	11.9	22.0	18.3	27.9	15.8	17.8	16.3	10.6	8.9	9.4
LEUCITE	0.0	0.0	0.0	0.0	0.0	0.0	0.0	0.0	0.0	0.0	2.9	0.0
NEPHELINE	0.0	0.4	0.6	0.0	0.0	0.0	0.4	0.8	3.0	0.0	0.1	0.0
DIOPSIDE	29.2	27.8	23.1	21.0	36.2	10.2	28.8	29.7	25.7	55.3	55.8	49.1
HYPERSTHENE	3.2	0.0	0.0	11.9	8.7	11.3	0.0	0.0	0.0	3.2	0.0	14.4
OLIVINE	15.7	16.9	4.3	12.8	16.5	23.3	21.1	22.8	17.5	23.3	24.3	18.2
CAL ORTHOSIL	0.0	0.0	0.0	0.0	0.0	0.0	0.0	0.0	0.0	0.0	0.9	0.0
MAGNETITE	3.6	3.6	2.7	4.4	4.3	4.4	4.0	4.1	3.9	5.1	5.2	4.0
ILMENITE	1.4	1.8	1.5	1.7	1.2	1.7	1.5	1.6	1.7	1.7	1.7	1.1
APATITE	0.9	0.8	0.9	0.7	1.0	0.5	0.7	0.8	0.8	0.2	0.2	0.2
DIFF. INDEX	29.0	32.5	55.7	25.5	13.9	20.8	28.0	23.2	34.2	0.8	3.0	3.5
NA/(NA+K)	0.62	0.69	0.67	0.78	0.66	0.71	0.68	0.72	0.68	0.46	0.05	0.53
(NA+K)/AL	0.47	0.51	0.71	0.38	0.28	0.28	0.48	0.41	0.54	0.04	0.18	0.16
F3/(F2+F3)	0.21	0.21	0.21	0.21	0.21	0.21	0.21	0.21	0.21	0.21	0.21	0.21

TABLE A2.3

FeO and H_2O wet chemical determinations

Sample	Weight % Fe_2O_3	FeO	H_2O (total)
5001A	1.67	8.73	3.65
5001B	3.33	9.60	3.79
5006	3.04	10.64	
5010	3.56	7.68	2.63
5013	2.88	6.80	2.34
5016	2.05	7.13	2.73
5031	1.94	8.20	1.54
5033	2.06	6.55	2.82
5036	3.08	7.47	1.88
5041	3.58	8.15	2.92
5053	1.69	7.97	
5054	3.19	7.02	1.17
5055	3.45	7.38	2.93
5056	2.13	7.36	
5062	2.31	9.05	
5073B	3.62	7.47	1.54
5074B	3.42	8.46	
5075A	7.05	8.38	
5075B	7.39	8.23	1.34
5077	5.37	6.85	1.78
5085E	3.84	7.25	
5087B	1.67	9.88	
5088	2.64	9.48	
5089	3.01	8.96	
5096	2.15	7.31	
5104	2.39	8.30	1.54
5106A	2.96	5.61	
5107A	4.32	9.57	3.17
5107B	4.47	7.11	
5111A	4.59	7.86	1.02
5113	3.15	6.14	
5115	6.44	5.23	

TABLE A2.3 (Cont'd)

Sample	Fe_2O_3	FeO	H_2O (total)
5116	4.89	7.77	1.75
5119	4.63	5.82	1.70
5120	6.39	5.22	1.76
4001	3.68	9.09	
4013	5.35	6.22	
4016	2.22	7.72	2.19
4023	4.32	5.68	
4042	2.65	7.33	
4051	4.61	5.82	
4056	4.78	4.61	
4062	4.62	6.45	3.19
4068D	2.94	8.28	
4070	3.15	9.88	
4077			
4090	2.39	8.38	
4110	4.80	8.47	3.76
5536	3.30	9.64	4.30
5538A	3.18	8.78	2.63

Note:-

Fe_2O_3 calculated from total Fe_2O_3 determined by XRF and FeO determined wet-chemically. (see text).

APPENDIX 3

ELECTRON PROBE MICROANALYSIS

The machine used was Cambridge Instrument Company 'Geoscan - Mark II' operated at an accelerating voltage of 15kV and a specimen current of 40 nanoamps. The focussed beam diameter is on the order of 2-5 μ .

Samples were prepared as polished thin sections and, where possible, simultaneously carbon-coated with the standards (Table A3.1).

Most analyses were made on a wavelength dispersive system (WDS) using one spectrometer and three analysing crystals; LiF, K.A.P. and P.E.T. The general analysing conditions for each element are shown in Table A3.1.

Data handling follows the general method described by Sweatman & Long (1969), and was performed by an on-line Varian 620 L/100 computer. The program TIM 3 (written by Dr.A. Peckett) performs a ZAF (Atomic number, Mass absorption, Fluorescence) correction on peak and background data for standards and sample. In general, 4 to 6 ten-second count accumulations are obtained and averaged for each peak and background position, for each element.

Detection limits (calculated) for the elements in Table A3.1 are on the order of 200-500 ppm. Overall accuracy for the major constituents is estimated to be $\pm$ 2%.

A few analyses (asterisked) were made with a recently developed energy dispersive system (EDS), which uses a Si(Li) detector. A single count-accumulation time of 100 seconds is used for each analysis (represents about 300,000 counts). The resulting energy spectrum is processed in the L/100 by software

TABLE A3.1

OPTIMUM ANALYSING CONDITIONS AND STANDARDS

USED IN ELECTRON PROBE ANALYSIS

Z	Element	Line	Analysing Crystal	Counter	Peak	Background*	Standard
11	Na	K_{α_1}	K.A.P.	Flow	$53^{o}14'$	$\pm 2^{o}$	Jadeite
12	Mg	"	"	"	$43^{o}42'$	"	MgO
13	Al	"	"	"	$36^{o}32'$	"	Al_2O_3
14	Si	"	"	"	$31^{o}02'$	$+2^{o}$	Wollastonite
19	K	"	P.E.T.	"	$50^{o}20'$	$\pm 2^{o}$	K-feldspar
20	Ca	"	LiF	"	$113^{o}02'$	"	Wollastonite
22	Ti	"	"	"	$86^{o}05'$	"	TiO_2
24	Cr	"	"	"	$69^{o}16'$	"	Cr_2O_3
25	Mn	"	"	"	$62^{o}48'$	"	Rhodonite
26	Fe	"	"	"	$57^{o}20'$	"	Fe
28	Ni	"	"	"	$48^{o}34'$	"	Ni

*Backgrounds were in some cases determined by analysing a material with the same average atomic number, but free of the element in question.

devised by Dr. A. Peckett and an analysis produced in 5-6 minutes. In cases where elements are low in abundance (< 0.5%) these can be separately determined by the WDS and included in the final ZAF correction. Precision in the EDS is generally less than the WDS and totals are more variable about 100%; however, all elements are similarly affected.

The mineral analyses made are tabulated below. Table A3.2 is a guide to probe analysis numbers and the corresponding sample number. For example, BH57xx refers to a primary amphibole in sample 4057. XX contains either one number or one number and one letter, e.g. BH571A. The 1A means analysis 1 of 4057 and A the first analysis of a specific crystal.

TABLE A3.2

GUIDE TO MICROPROBE ANALYSIS NUMBERS

Zone A

Sample No.	Cpx.	Amph.*	Fel.	Sp.	Ep.	Chl.	Biotite*	Prehnite
4057	CP57	BH57		SP57				
4077	CP477							
5001B	CP1B				EP1B			
5010	CP10	BH10				CH10		
5013	CP13		FL13	SP13		CH13		
5015	CP15	BH15						
5016	CP16							
5028		BH28						
5032	CP32							
5033			FL33				BI33	
5036	CP36					CH36		
5938	CP38				EP38	CH38		
5040	CP40							
5043	CP43		FL43		EP43			
5044				SP44	EP44	CH44		
5054				SP54	EP54	CH54		
5055				SP55				
5056	CP56	BH56						
5058	CP58					CH58		
5062		BH62						
5063								PR63
5096		BH96						
5104			FL04					
5107A	CP7A	BH7A						
5113	CP13	BH13	FL113	SP113				

(*Amphibole and biotite as primary phases)

TABLE A3.2 (Cont'd)

Zone B

Sample No.	Cpx.	Amph.*	Biotite*	Chl.	Ep.	Fel.	Magnetite
4007		HB07				FL07	
4013A	CP3A	HB3A			EP3A		MG3A
4029A		HB29A		CH29A		FL7A	
4029B		HB29B	BI29B		EP29B	FL9B	
4061		HB61					
4105A		HB5A	BI5A			FL5A	MG5A
4111	CP11	HB11	BI11			FL11	
5049	CP49	HB49				FL49	MG49
5074B		HB4B	BI4B	CH4B	EP4B	FL4B	
5074C		HB4C	BI4C	CH4C		FL4C	
5075B	CP5B	HB5B	BI5B	CH75B	EP5B		MG5B
5077	CP77	HB77					MG77
5088	CP88	HB88	BI88	CH88	EP88		
5111B		HB1B	BI11B	CH11B	EP11B		
5116		HB16				FL16	
5516A		HB16A	BI6A		EP6A		
5516B		HB16B	BI6B		EP6B		
5530A		HB0A	BI0A		EP0A		
5536E		HB6E		CH6E		FL6E	
5538B		HB8B				FL8B	
74B		HB74B	BI74B				MG74B

(*Biotite and amphibole on secondary phases)

TABLE A3.3 CLINOPYROXENES

	CP571B	CP572A	CP572B	CP151	CP3A1	CP111	CP431	CP321	CP322	CP882
WEIGHT % OXIDE										
SIO2	51.19	50.07	52.30	53.37	49.92	52.86	52.15	51.05	50.64	49.16
TIO2	0.46	0.64	0.24	0.26	0.41	0.05	0.25	0.40	0.54	0.57
AL203	3.53	3.83	1.57	2.00	4.09	1.03	2.08	3.30	3.32	4.57
FEO	5.84	7.66	3.78	3.96	8.35	3.37	6.85	6.70	7.48	8.84
MNO	0.15	0.18	0.11	0.13	0.24	0.14	0.06	N.A.	N.A.	0.22
MGO	15.18	14.21	17.00	16.56	14.39	17.50	15.64	14.80	14.45	13.92
CAO	22.67	22.56	23.62	23.33	21.79	24.18	22.82	22.61	23.08	21.99
NA20	0.21	0.27	0.14	0.18	0.36	0.08	N.A.	0.34	0.64	0.26
K20	-	0.01	-	-	-	0.01	N.A.	0.05	0.05	-
TOTAL	99.22	99.44	98.75	99.80	99.46	99.22	99.57	99.22	100.21	99.54
ATOMIC FORMULA - ON BASIS OF 6 OXYGENS										
SI	1.903	1.877	1.940	1.953	1.873	1.950	1.937	1.905	1.886	1.850
TI	0.013	0.018	0.007	0.007	0.012	0.002	0.007	0.011	0.015	0.016
AL	0.155	0.169	0.069	0.086	0.181	0.045	0.091	0.145	0.146	0.203
FE	0.181	0.240	0.117	0.121	0.262	0.104	0.213	0.209	0.233	0.278
MN	0.005	0.006	0.003	0.004	0.008	0.004	0.002	-	-	0.007
MG	0.841	0.794	0.940	0.903	0.805	0.962	0.850	0.820	0.812	0.781
CA	0.903	0.906	0.939	0.915	0.872	0.956	0.909	0.904	0.921	0.887
NA	0.015	0.020	0.010	0.013	0.026	0.006	-	0.024	0.046	0.019
K	-	-	-	-	-	0.001	-	0.002	0.002	-
ATOMIC PROPORTIONS										
FE	9.43	12.38	5.88	6.25	13.51	5.14	10.80	10.82	11.91	14.30
MG	43.68	40.92	47.09	46.57	41.50	47.59	43.10	42.42	41.00	40.12
CA	46.90	46.70	47.03	47.18	44.98	47.27	46.09	46.76	47.09	45.58

TABLE A3.3 CLINOPYROXENES

	CP161	CP162A	CP162B	CP163	CP4771	CP4772	CP491	* CP581A	* CP581B	* CP582A
WEIGHT % OXIDE										
SIO2	50.96	50.24	50.38	50.17	50.63	49.69	51.56	52.84	51.37	50.53
TIO2	0.52	0.65	0.51	0.53	0.46	0.46	0.28	0.43	0.56	0.78
AL203	2.97	3.00	3.24	3.53	2.57	1.95	2.61	2.75	3.02	3.55
FEO	8.82	9.24	8.82	9.46	9.58	9.71	6.67	7.30	10.00	9.86
MNO	0.41	0.33	0.34	0.34	0.36	0.44	0.17	0.15	0.21	0.17
MGO	13.84	14.02	14.44	13.23	14.59	15.45	15.43	16.42	15.03	14.90
CAO	21.99	21.80	21.37	21.34	21.30	22.14	23.26	22.19	20.93	20.96
NA20	0.35	0.34	0.29	0.37	0.29	0.33	0.26	0.17	0.35	0.28
K20	-	0.01	0.01	0.01	0.02	0.02	0.01	0.01	-	0.01
TOTAL	99.86	99.64	99.41	99.54	99.80	100.18	100.26	102.26	101.48	101.02
ATOMIC FORMULA - ON BASIS OF 6 OXYGENS										
SI	1.909	1.892	1.894	1.892	1.903	1.874	1.909	1.911	1.895	1.874
TI	0.015	0.018	0.015	0.015	0.013	0.013	0.008	0.012	0.015	0.022
AL	0.131	0.133	0.144	0.157	0.114	0.087	0.114	0.117	0.131	0.155
FE	0.276	0.291	0.277	0.298	0.301	0.306	0.207	0.221	0.309	0.306
MN	0.013	0.011	0.011	0.011	0.012	0.014	0.005	0.002	0.007	0.005
MG	0.773	0.787	0.809	0.746	0.817	0.868	0.852	0.886	0.826	0.823
CA	0.882	0.880	0.861	0.882	0.858	0.895	0.923	0.861	0.828	0.833
NA	0.025	0.025	0.021	0.027	0.021	0.024	0.019	0.012	0.025	0.020
K	-	-	-	-	0.001	0.001	-	-	-	0.001
ATOMIC PROPORTIONS										
FE	14.30	14.86	14.24	15.48	15.24	14.80	10.44	11.22	15.72	15.59
MG	40.01	40.19	41.55	38.72	41.35	41.97	43.00	43.76	42.11	41.97
CA	45.69	44.95	44.21	45.80	43.41	43.23	46.61	45.02	42.17	42.44

TABLE A3.3 CLINOPYROXENES

	* CP582B	CP7A1	CP7A2	* CP131A	* CP131B	* CP132A	* CP132B	CP401A	CP401B	CP401C
WEIGHT % OXIDE										
SIO2	51.51	51.04	50.15	51.67	51.38	50.88	50.12	50.15	49.95	50.33
TIO2	0.58	0.37	0.49	0.47	0.47	0.55	0.45	0.58	0.53	0.47
AL203	3.27	2.32	3.17	3.52	3.41	3.45	3.43	3.63	3.31	2.47
FEO	10.84	6.43	7.27	8.65	9.26	8.84	5.80	10.01	9.20	10.71
MNO	0.25	0.10	0.07	0.32	0.33	0.34	0.33	0.23	0.18	0.32
MGO	14.28	15.34	15.09	15.84	15.91	15.46	15.53	14.19	14.04	14.43
CAO	20.81	23.65	23.55	20.79	19.76	20.70	21.16	21.09	21.53	20.60
NA20	0.41	0.18	0.17	0.27	0.31	0.28	0.29	0.39	0.37	0.38
K20	-	-	-	0.01	-	-	0.01	-	-	-
TOTAL	101.93	99.42	99.96	101.52	100.85	100.50	100.11	100.27	99.71	99.70
ATOMIC FORMULA - ON BASIS OF 6 OXYGENS										
SI	1.896	1.907	1.873	1.892	1.895	1.886	1.871	1.877	1.877	1.900
TI	0.016	0.010	0.014	0.013	0.013	0.015	0.013	0.016	0.015	0.013
AL	0.142	0.102	0.140	0.152	0.148	0.151	0.151	0.160	0.147	0.110
FE	0.334	0.201	0.227	0.265	0.286	0.274	0.275	0.314	0.289	0.338
MN	0.008	0.003	0.002	0.010	0.010	0.011	0.010	0.007	0.006	0.010
MG	0.784	0.854	0.840	0.864	0.874	0.854	0.864	0.792	0.820	0.812
CA	0.821	0.947	0.942	0.815	0.781	0.822	0.846	0.846	0.867	0.833
NA	0.029	0.013	0.013	0.019	0.022	0.020	0.021	0.028	0.027	0.028
K	-	-	-	-	-	-	-	-	-	-
ATOMIC PROPORTIONS										
FE	17.22	10.03	11.29	13.62	14.72	14.05	13.84	16.07	14.63	17.05
MG	40.44	42.67	41.80	44.45	45.05	43.79	43.53	40.57	41.49	40.94
CA	42.34	47.30	47.01	41.94	40.22	42.16	42.65	43.36	43.88	42.01

TABLE A3.3 CLINOPYROXENES

	CP402	* CP403A	* CP403B	* CP381	* CP771	CP772 / CP131	CP132	CP133	CP571A
WEIGHT % OXIDE									
SIO2	51.22	51.98	49.72	54.09	51.73	51.45	50.82	52.30	51.12	46.97
TIO2	0.51	0.26	0.51	0.17	0.34	0.23	0.36	0.22	0.44	0.76
AL2O3	1.53	-	2.66	1.61	3.00	2.64	3.16	1.38	2.54	4.48
FEO	9.21	5.03	8.38	5.34	6.43	6.18	6.02	4.56	9.10	8.91
MNO	0.24	-	-	0.17	0.17	0.16	0.17	0.18	0.36	0.23
MGO	15.59	16.91	15.35	16.72	15.47	15.82	15.41	17.05	15.10	13.83
CAO	21.14	22.96	21.19	23.69	24.06	23.92	23.30	23.38	20.41	21.45
NA2O	0.36	0.02	0.36	0.09	0.15	0.28	0.23	0.13	0.40	0.28
K2O	-	-	-	0.01	-	-	0.01	0.01	0.01	-
TOTAL	99.80	97.34	98.17	101.88	101.20	100.67	99.46	99.22	99.48	98.91
ATOMIC FORMULA - ON BASIS OF 6 OXYGENS										
SI	1.920	1.967	1.890	1.952	1.897	1.897	1.893	1.938	1.910	1.854
TI	0.014	0.007	0.014	0.005	0.009	0.006	0.010	0.006	0.012	0.022
AL	0.068	-	0.119	0.069	0.130	0.115	0.139	0.061	0.112	0.200
FE	0.289	0.159	0.266	0.161	0.197	0.191	0.187	0.141	0.285	0.282
MN	0.008	-	-	0.005	0.005	0.005	0.005	0.006	0.011	0.007
MG	0.871	0.954	0.870	0.899	0.846	0.870	0.855	0.942	0.843	0.780
CA	0.849	0.931	0.863	0.916	0.945	0.945	0.930	0.928	0.820	0.870
NA	0.026	0.015	0.026	0.006	0.013	0.020	0.017	0.009	0.029	0.021
K	-	-	-	-	-	-	0.001	-	-	-
ATOMIC PROPORTIONS										
FE	14.37	7.78	16.50	8.16	9.91	9.50	9.50	7.03	14.65	14.59
MG	43.36	46.67	41.90	45.50	42.54	43.36	43.36	46.82	43.28	40.39
CA	42.27	45.55	41.60	46.34	47.55	47.14	47.14	46.15	42.07	45.02

TABLE A3.3 CLINOPYROXENES

	CP1B1	CP1B2	CP1B3	CP1B4	CP361A	CP361B	CP362A	CP362B	CP881	CP581
WEIGHT % OXIDE										
SIO2	49.32	49.12	49.27	49.56	52.13	50.42	49.79	50.75	52.62	50.48
TIO2	0.70	0.72	0.62	0.71	0.29	0.51	0.63	0.37	0.17	0.41
AL203	3.88	4.31	4.47	4.26	2.25	3.33	3.55	3.11	1.46	2.98
CR203	0.04	0.02	0.04	0.02	0.21	0.01	0.06	0.05	0.31	0.03
FEO	9.84	9.88	9.46	10.03	6.04	9.21	9.20	7.52	4.60	6.85
MNO	0.36	0.30	0.23	0.29	0.17	0.37	0.30	0.20	0.16	0.22
MGO	12.86	13.10	13.24	12.60	16.01	13.76	13.75	15.09	16.80	15.13
CAO	21.59	21.65	21.83	21.61	21.80	21.21	21.53	22.26	23.14	23.35
NA20	0.39	0.41	0.37	0.37	0.19	0.34	0.37	0.24	0.15	0.40
K20	-	0.01	-	-	-	0.01	0.01	0.01	-	-
NIO	0.05	0.03	0.06	0.05	0.01	0.06	0.01	-	0.09	0.03
TOTAL	99.03	99.54	99.60	99.51	99.11	99.24	99.20	99.61	99.48	99.88
ATOMIC FORMULA - ON BASIS OF 6 OXYGENS										
SI	1.875	1.858	1.858	1.874	1.936	1.901	1.882	1.895	1.943	1.884
TI	0.020	0.021	0.018	0.020	0.008	0.015	0.018	0.010	0.005	0.012
AL	0.174	0.192	0.200	0.190	0.099	0.148	0.158	0.137	0.064	0.131
CR	0.001	0.001	0.001	0.001	0.006	0.001	0.002	0.001	0.009	0.001
FE	0.313	0.313	0.298	0.317	0.188	0.290	0.291	0.235	0.142	0.214
MN	0.012	0.010	0.007	0.009	0.005	0.012	0.010	0.006	0.005	0.007
MG	0.729	0.739	0.744	0.710	0.886	0.773	0.775	0.840	0.925	0.842
CA	0.879	0.877	0.882	0.875	0.868	0.857	0.872	0.891	0.916	0.934
NA	0.028	0.030	0.027	0.027	0.014	0.025	0.030	0.017	0.011	0.029
K	0.000	0.000	0.000	0.000	0.000	0.001	0.000	0.010	0.000	0.000
NI	0.002	0.001	0.002	0.002	0.000	0.002	0.000	0.000	0.003	0.001
ATOMIC PROPORTIONS										
FE	16.29	16.20	15.50	16.67	9.66	15.13	15.01	11.95	7.17	10.75
MG	37.94	38.30	38.66	37.31	45.65	40.26	39.98	42.73	46.45	42.31
CA	45.77	45.50	45.48	46.02	44.69	44.61	45.01	45.32	46.19	46.94

TABLE A3.3 CLINOPYROXENES

	CP5B2	CP5B3	CP101	CP102	CP103	CP561	CP562A	CP562B
WEIGHT % OXIDE								
SIO2	50.60	51.30	51.32	51.79	51.67	51.55	52.80	52.15
TIO2	0.43	0.27	0.50	0.49	0.54	0.47	0.23	0.37
AL2O3	3.59	2.45	2.55	3.12	3.11	3.31	2.44	2.84
CR2O3	0.02	-	-	-	0.02	0.03	0.17	0.04
FEO	6.64	6.47	8.24	8.14	8.14	8.40	4.96	7.63
MNO	0.25	0.20	0.44	0.33	0.38	0.32	0.16	0.23
MGO	14.87	15.07	14.98	14.57	14.43	14.92	15.85	14.99
CAO	23.35	23.33	20.45	21.09	21.15	20.91	23.04	21.57
NA2O	0.53	0.41	0.34	0.29	0.30	0.28	0.18	0.28
K2O	0.01	-	-	0.29	-	-	-	-
NIO	-	0.05	0.01	0.01	-	0.03	0.08	0.03
TOTAL	100.29	99.55	98.83	99.83	99.75	100.21	99.93	100.12
ATOMIC FORMULA - ON BASIS OF 6 OXYGENS								
SI	1.878	1.914	1.928	1.924	1.923	1.910	1.940	1.929
TI	0.012	0.008	0.014	0.014	0.015	0.013	0.006	0.010
AL	0.157	0.108	0.113	0.137	0.136	0.145	0.106	0.124
CR	0.000	0.000	0.000	0.200	0.001	0.001	0.005	0.001
FE	0.206	0.202	0.259	0.253	0.253	0.260	0.153	0.236
MN	0.008	0.006	0.014	0.011	0.012	0.010	0.005	0.007
MG	0.823	0.838	0.839	0.806	0.800	0.824	0.858	0.826
CA	0.929	0.933	0.823	0.839	0.843	0.830	0.907	0.855
NA	0.038	0.030	0.025	0.021	0.022	0.020	0.013	0.020
K	0.000	0.000	0.000	0.001	0.000	0.001	0.002	0.000
NI	0.000	0.001	0.000	0.000	0.000	0.001	0.002	0.001
ATOMIC PROPORTIONS								
FE	10.54	10.24	13.48	13.32	13.36	13.60	7.91	12.31
MG	42.02	42.48	43.66	42.47	42.18	43.03	45.03	43.10
CA	47.44	47.28	42.86	44.20	44.46	43.37	47.06	44.59

TABLE A3.4 PRIMARY AMPHIBOLES

	BH101	BH102	BH103	BH104	BH621	BH622A	BH622B	BH961	BH962	BH963
WEIGHT % OXIDE										
SIO2	41.76	41.04	41.49	41.62	39.68	40.28	38.75	40.47	39.00	40.57
TIO2	3.06	3.09	3.27	3.05	2.05	2.20	2.28	3.11	3.72	2.11
AL203	12.84	12.30	11.71	12.01	12.84	13.26	13.40	12.46	13.39	14.05
FEO	11.60	12.25	11.68	11.82	13.48	13.12	14.69	13.05	14.05	11.15
MNO	0.30	0.32	0.32	0.32	0.30	0.16	0.24	0.23	0.25	0.18
MGO	13.94	13.31	13.82	13.34	12.95	13.83	12.25	12.54	11.41	13.85
CAO	11.67	11.58	11.44	11.50	12.26	12.07	12.14	11.60	11.63	12.04
NA2O	2.36	2.24	2.38	2.40	2.01	2.12	2.03	2.53	2.37	2.41
K2O	1.09	1.20	1.10	1.08	1.65	1.45	1.45	1.23	1.49	1.09
TOTAL	98.64	97.34	97.22	97.18	97.23	98.48	97.24	97.24	97.31	97.45
ATOMIC FORMULA - ON BASIS OF 23 OXYGENS										
SI	6.115	6.121	6.176	6.197	5.999	5.979	5.892	6.079	5.902	6.012
TI	0.337	0.347	0.366	0.342	0.233	0.245	0.261	0.352	0.424	0.236
AL	2.218	2.163	2.056	2.109	2.289	2.321	2.402	2.207	2.390	2.455
FE2	1.421	1.529	1.454	1.471	1.704	1.628	1.868	1.639	1.779	1.382
MN	0.037	0.040	0.040	0.040	0.039	0.021	0.031	0.029	0.032	0.023
MG	3.042	2.960	3.065	2.960	2.918	3.060	2.775	2.807	2.574	3.058
CA	1.831	1.851	1.824	1.835	1.987	1.919	1.977	1.866	1.886	1.912
NA	0.670	0.649	0.686	0.694	0.590	0.611	0.597	0.738	0.696	0.692
K	0.203	0.228	0.209	0.206	0.318	0.274	0.282	0.237	0.288	0.206

TABLE A3.4 PRIMARY AMPHIBOLES

	BH964	BH7A1	BH7A2	BH7A3	BH571A	BH571B	BH572	BH573	BH151	BH152A
WEIGHT % OXIDE										
SIO2	40.05	38.81	39.10	39.32	40.98	41.15	41.48	41.56	41.41	43.12
TIO2	2.76	2.24	2.08	2.06	2.08	2.11	2.77	2.57	1.80	1.75
AL2O3	13.83	13.11	13.26	13.72	12.52	12.61	12.18	12.59	12.66	11.82
FEO	13.03	13.43	13.82	13.42	10.97	11.39	11.26	11.32	15.68	10.65
MNO	0.24	0.21	0.18	0.10	0.20	0.17	0.18	0.19	0.35	0.14
MGO	12.39	12.61	12.28	12.70	14.15	14.19	14.68	14.27	10.83	15.28
CAO	12.25	12.05	12.15	12.48	12.38	12.35	11.70	11.83	12.04	11.60
NA2O	2.38	2.11	2.12	2.06	2.54	2.42	2.42	2.40	2.09	2.28
K2O	1.16	1.45	1.43	1.59	0.65	0.63	0.58	0.62	0.68	0.69
TOTAL	98.09	96.02	96.42	97.45	96.46	97.24	97.24	97.35	97.55	97.23
ATOMIC FORMULA - ON BASIS OF 23 OXYGENS										
SI	5.964	5.940	5.964	5.925	6.129	6.123	6.141	6.146	6.232	6.333
TI	0.310	0.258	0.238	0.234	0.234	0.236	0.308	0.286	0.204	0.193
AL	2.429	2.367	2.386	2.438	2.207	2.212	2.126	2.196	2.246	2.048
FE2	1.622	1.720	1.763	1.692	1.372	1.417	1.395	1.399	1.973	1.308
MN	0.030	0.027	0.023	0.013	0.025	0.022	0.022	0.023	0.045	0.017
MG	2.749	2.876	2.792	2.853	3.154	3.146	3.238	3.144	2.429	3.344
CA	1.954	1.976	1.985	2.016	1.984	1.969	1.856	1.875	1.941	1.826
NA	0.688	0.625	0.628	0.603	0.737	0.699	0.695	0.688	0.611	0.640
K	0.220	0.284	0.278	0.306	0.123	0.120	0.110	0.117	0.132	0.112

TABLE A3.4 PRIMARY AMPHIBOLES

	BH152B	BH153	BH561	BH562	BH563	BH281	BH282	BH135	BH136	BH137
WEIGHT % OXIDE										
SIO2	42.20	42.15	41.48	42.55	42.03	42.99	41.05	41.29	42.56	42.40
TIO2	1.84	1.74	2.58	2.30	2.71	1.47	1.77	2.10	2.15	2.12
AL203	12.09	12.22	12.26	12.15	12.26	10.89	12.55	12.24	11.55	11.63
FEO	10.69	12.38	11.40	11.46	11.42	11.83	12.87	12.74	12.06	12.64
MNO	0.14	0.24	0.21	0.17	0.18	0.24	0.25	0.25	0.30	0.29
MGO	15.24	13.77	14.63	14.38	14.62	14.67	13.63	13.64	14.28	13.88
CAO	11.48	11.74	11.66	11.57	11.89	11.21	11.63	11.56	11.41	11.55
NA2O	2.14	2.21	2.18	2.34	2.43	2.24	2.12	2.27	2.31	2.57
K2O	0.60	0.59	0.68	0.61	0.73	0.73	0.94	0.60	0.54	0.58
TOTAL	96.42	97.03	97.19	97.62	98.28	96.27	96.83	96.70	97.18	97.68
ATOMIC FORMULA - ON BASIS OF 23 OXYGENS										
SI	6.259	6.267	6.149	6.260	6.161	6.420	6.158	6.186	6.308	6.281
TI	0.205	0.195	0.287	0.254	0.299	0.165	0.200	0.237	0.240	0.236
AL	2.115	2.142	2.142	2.108	2.120	1.914	2.218	2.161	2.017	2.030
FE2	1.326	1.539	1.413	1.411	1.400	1.477	1.614	1.596	1.495	1.566
MN	0.017	0.030	0.026	0.022	0.022	0.030	0.032	0.032	0.038	0.036
MG	3.368	3.050	3.232	3.153	3.195	3.265	3.048	3.046	3.153	3.065
CA	1.825	1.871	1.852	1.824	1.868	1.793	1.869	1.855	1.811	1.833
NA	0.615	0.637	0.627	0.669	0.692	0.648	0.616	0.659	0.664	0.738
K	0.113	0.111	0.129	0.115	0.136	0.139	0.180	0.115	0.102	0.110

TABLE A3.5 PLAGIOCLASES

	* F60131	* FL1131	* FL1132	FL331	FL332	FL431	FL1041	FL432
WEIGHT % OXIDE								
SIO2	56.36	58.91	59.90	55.77	56.84	53.74	54.92	53.88
AL2O3	28.74	26.44	25.34	27.25	26.33	27.55	28.67	27.51
FEO	0.68	0.91	0.87	N.A.	N.A.	1.01	0.37	1.01
CAO	11.10	9.33	8.01	10.28	9.17	11.81	10.87	11.23
NA2O	5.40	6.50	6.74	5.83	5.88	5.07	5.30	5.17
K2O	0.47	0.77	0.66	0.67	0.77	0.47	0.50	0.46
TOTAL	101.75	102.87	101.51	99.80	98.97	99.87	100.61	99.49
ATOMIC FORMULA - ON THE BASIS OF 8 OXYGE								
SI	2.484	2.587	2.649	2.523	2.584	2.453	2.469	2.464
AL	1.493	1.370	1.322	1.454	1.410	1.483	1.519	1.484
FE	0.025	0.034	0.320	0.000	0.000	0.039	0.014	0.039
CA	0.524	0.439	0.379	0.498	0.444	0.578	0.524	0.550
NA	0.462	0.554	0.578	0.512	0.518	0.449	0.462	0.459
K	0.026	0.043	0.037	0.039	0.045	0.027	0.028	0.027
MOLECULAR PROPORTIONS								
AN	51.77	42.38	38.13	47.54	44.16	54.84	51.65	53.12
AB	45.63	53.45	58.13	48.79	51.42	42.59	45.54	44.30
OR	2.60	4.17	3.74	3.67	4.42	2.57	2.81	2.58

TABLE A3.6 SPINELS

	SP131	SP132A	SP133	SP134	SP431	SP432	SP433	SP434	SP441	SP541
WEIGHT % OXIDE										
SIO2	0.43	0.49	0.56	0.50	2.53	2.62	2.19	3.77	1.21	2.94
TIO2	9.81	0.59	0.49	8.59	9.52	10.44	7.78	0.18	8.82	10.27
AL203	2.18	5.41	5.14	2.85	4.86	4.51	6.00	5.95	2.82	2.20
CR203	2.02	54.61	54.34	0.90	0.41	0.25	0.23	55.02	0.64	0.07
FE203	42.58	7.40	7.97	45.95	37.81	39.22	42.85	2.79	44.42	39.98
FEO	39.67	24.20	24.23	39.06	40.16	36.85	35.81	19.79	40.34	41.88
MNO	0.09	0.62	0.52	-	0.28	0.32	0.43	0.40	-	0.08
MGO	0.04	5.70	5.74	0.06	0.86	4.18	2.90	10.40	0.10	0.31
CAO	0.30	0.11	0.10	0.46	1.42	1.07	1.12	1.60	0.40	1.99
TOTAL	97.22	99.20	99.11	98.38	97.85	99.48	99.31	99.91	98.74	99.71
ATOMIC FORMULA										
SI	0.133	0.139	0.158	0.152	0.751	0.750	0.630	0.998	0.364	0.868
TI	2.277	0.125	0.104	1.966	2.126	2.244	1.684	0.036	2.005	2.287
AL	0.794	1.792	1.705	1.024	1.702	1.521	2.038	1.858	1.005	0.768
CR	0.494	12.118	12.082	0.217	0.097	0.058	0.053	11.519	0.153	0.016
FE3	9.892	1.563	1.687	10.522	8.448	8.434	9.281	0.555	10.103	8.906
FE2	10.243	5.681	5.700	9.940	9.972	8.806	8.620	4.384	10.198	10.368
MN	0.023	0.147	0.125	0.000	0.070	0.078	0.104	0.091	0.000	0.019
MG	0.020	2.385	2.408	0.027	0.382	1.780	1.246	4.104	0.043	0.138
CA	0.099	0.034	0.031	0.152	0.453	0.329	0.345	0.455	0.129	0.631

TABLE A3.6 SPINELS

	SP542	SP551	SP571	SP1131	SP1132	SP1133
WEIGHT % OXIDE						
SIO2	2.00	3.64	0.41	0.20	1.19	1.19
TIO2	6.29	3.56	0.14	5.56	1.75	1.74
AL203	3.06	3.18	9.78	4.69	0.63	0.63
CR203	0.13	0.16	51.51	0.08	0.03	0.08
FE203	49.95	51.87	7.73	51.42	61.95	61.41
FEO	39.06	33.15	19.36	36.36	33.29	32.84
MNO	0.13	0.38	0.49	0.32	0.27	0.23
MGO	0.33	2.59	8.80	0.06	0.05	0.05
CAO	0.78	2.05	0.23	0.12	0.52	0.71
TOTAL	101.71	100.59	98.57	98.79	99.68	98.86
ATOMIC FORMULA						
SI	0.584	1.050	0.111	0.059	0.362	0.365
TI	1.382	0.772	0.029	1.260	0.403	0.402
AL	1.054	1.080	3.122	1.668	0.226	0.228
CR	0.029	0.038	11.024	0.019	0.007	0.019
FE3	10.985	11.242	1.576	11.673	14.237	14.220
FE2	9.547	7.983	4.384	9.173	8.502	8.452
MN	0.032	0.093	0.112	0.081	0.071	0.060
MG	0.142	1.113	3.550	0.025	0.022	0.022
CA	0.245	0.632	0.068	0.040	0.170	0.234

TABLE A3.7 PRIMARY BIOTITES

	BI331	BI332
WEIGHT % OXIDE		
SIO2	36.93	36.48
TIO2	5.23	4.22
AL2O3	14.17	14.36
FEO	13.21	16.13
MNO	0.23	0.21
MGO	16.08	15.22
CAO	0.06	0.04
NA2O	0.51	0.27
K2O	8.99	8.12
TOTAL	95.42	95.04
ATOMIC FORMULA - ON BASIS OF 22 OXYGENS		
SI	5.479	5.477
TI	0.583	0.476
AL	2.480	2.543
FE	1.640	2.025
MN	0.030	0.026
MG	3.555	3.405
CA	0.009	0.007
NA	0.148	0.078
K	1.701	1.556

TABLE A3.8 SECONDARY AMPHIBOLES

	HB611	HB612	HB613	H614	HB615	HB491	HB492	HB493	HB161	HB162A
WEIGHT % OXIDE										
SIO2	46.37	52.20	43.56	52.32	44.33	45.60	44.19	47.82	48.49	51.37
TIO2	0.39	0.05	0.35	0.06	0.61	0.73	0.99	0.74	0.14	0.18
AL203	11.61	4.46	13.15	3.87	12.35	7.79	8.92	7.41	5.06	2.63
FEO	15.51	11.51	16.40	11.84	16.41	17.75	18.25	16.87	15.66	13.67
MNO	0.30	0.28	0.35	0.22	0.35	0.46	0.45	0.39	0.35	0.40
MGO	11.85	16.17	10.65	15.64	10.60	11.11	10.02	11.55	13.37	15.07
CAO	12.01	12.46	11.65	12.37	11.56	11.92	11.82	11.81	12.32	12.42
NA20	1.30	0.28	1.54	0.22	1.59	0.96	1.01	0.83	0.53	0.37
K20	0.23	0.10	0.19	0.08	0.19	0.58	0.82	0.48	0.12	0.07
TOTAL	99.56	97.50	97.85	96.62	97.99	96.89	96.46	97.90	96.03	96.18
ATOMIC FORMULA - ON BASIS OF 23 OXYGENS										
SI	6.707	7.504	6.467	7.593	6.566	6.903	6.757	7.083	7.277	7.593
AL4	1.293	0.496	1.533	0.407	1.434	1.077	1.243	0.917	0.723	0.407
AL6	0.687	0.260	0.770	0.256	0.723	0.293	0.366	0.377	0.173	0.052
TI	0.043	0.005	0.039	0.006	0.068	0.084	0.114	0.082	0.016	0.020
FE	1.876	1.384	2.037	1.437	2.032	2.247	2.335	2.090	1.966	1.690
MN	0.037	0.034	0.044	0.028	0.043	0.059	0.058	0.049	0.045	0.051
MG	2.555	3.463	2.357	3.382	2.431	2.506	2.284	2.550	2.991	3.320
CA	1.861	1.919	1.854	1.923	1.834	1.934	1.938	1.874	1.981	1.967
NA	0.363	0.077	0.445	0.061	0.457	0.281	0.300	0.238	0.153	0.105
K	0.042	0.018	0.037	0.015	0.036	0.112	0.159	0.091	0.022	0.013
STRUCTURAL FORMULA										
Z	8.00	8.00	8.00	8.00	8.00	8.00	8.00	8.00	8.00	8.00
Y	5.20	5.15	5.25	5.11	5.21	5.19	5.16	5.15	5.19	5.13
A+X	2.27	2.01	2.34	2.00	2.33	2.24	2.40	2.30	2.16	2.08

TABLE A3.8 SECONDARY AMPHIBOLES

	HB1628	HB771	HB772	HB1B1A	HB1B1B	HB1B2	HB1B3	HB4B1A	HB4B1B	HB4B2
WEIGHT % OXIDE										
SIO2	48.29	56.33	55.78	55.39	54.15	53.93	51.98	46.56	50.81	45.27
TIO2	0.02	0.01	0.01	-	0.03	-	-	0.25	0.14	0.50
AL203	4.62	1.11	1.80	0.78	0.77	1.89	3.37	8.09	4.61	8.69
FEO	17.94	6.44	5.21	10.45	12.36	8.88	12.12	15.96	12.89	16.77
MNO	0.33	0.19	0.17	0.18	0.22	0.20	0.17	0.31	0.34	0.37
MGO	12.10	20.53	20.88	17.06	16.72	18.04	15.48	13.63	15.39	12.36
CAO	12.34	13.50	13.54	12.56	12.54	13.03	12.82	12.20	12.77	12.41
NA20	0.53	0.17	0.25	0.22	0.21	0.30	0.43	0.93	0.46	1.05
K20	0.24	0.15	0.04	0.04	0.05	0.03	0.14	0.64	0.27	0.78
TOTAL	96.42	98.32	97.67	96.66	97.04	96.35	96.50	97.97	97.97	98.19
ATOMIC FORMULA - ON BASIS OF 23 OXYGENS										
SI	7.307	7.831	7.768	7.954	7.839	7.752	7.590	6.899	7.362	6.749
AL4	0.693	0.169	0.232	0.046	0.132	0.248	0.410	1.011	0.638	1.251
AL6	0.132	0.013	0.064	0.086	-	0.073	0.171	0.312	0.150	0.276
TI	0.003	0.001	0.001	-	0.003	-	-	0.028	0.016	0.056
FE	2.270	0.749	0.607	1.255	1.496	1.068	1.480	1.977	1.562	2.091
MN	0.043	0.022	0.020	0.020	0.026	0.024	0.022	0.039	0.041	0.050
MG	2.728	4.254	4.333	3.652	3.610	3.865	3.368	2.678	3.388	2.748
CA	2.001	2.011	2.020	1.932	1.934	2.008	2.005	1.937	1.982	1.983
NA	0.157	0.046	0.006	0.061	0.059	0.083	0.122	0.268	0.130	0.302
K	0.046	0.008	0.007	0.007	0.010	0.014	0.025	0.122	0.049	0.200
STRUCTURAL FORMULA										
Z	8.00	8.00	8.00	8.00	7.97	8.00	8.00	8.00	8.00	8.00
Y	5.18	5.04	5.02	5.14	5.13	5.03	5.04	5.23	5.16	5.22
A+X	2.20	2.06	2.09	2.00	2.00	2.10	2.15	2.33	2.16	2.48

TABLE A3.8 SECONDARY AMPHIBOLES

	HB4B3	HB3A1A	HB3A1B	HB3A2	HB8B1	HB8B2	HB8B3A	HB8B3B	HB6E1	B6E2
WEIGHT % OXIDE										
SIO2	50.15	51.08	54.73	51.30	51.82	48.16	50.61	51.86	43.14	43.86
TIO2	0.25	0.05	-	0.16	0.02	0.07	0.05	0.07	0.54	0.41
AL203	5.66	4.57	0.87	4.85	4.43	8.15	5.94	5.19	13.57	13.16
FEO	12.41	12.78	11.29	11.20	13.41	13.61	12.50	13.02	15.36	15.32
MNO	0.34	0.31	0.42	0.36	0.30	0.26	0.24	0.31	0.30	0.32
MGO	15.21	15.26	16.24	15.50	14.49	13.25	14.14	14.16	10.38	10.37
CAO	12.96	12.92	12.82	12.71	12.70	12.63	12.82	12.57	12.04	12.13
NA20	0.54	0.53	0.16	0.73	0.31	0.61	0.60	0.60	1.78	1.65
K20	0.30	0.12	0.04	0.14	0.17	0.33	0.23	0.23	0.35	0.34
TOTAL	97.83	97.62	96.57	96.95	97.64	97.07	97.13	98.02	97.46	97.55
ATOMIC FORMULA - ON BASIS OF 23 OXYGENS										
SI	7.271	7.416	7.921	7.440	7.516	7.077	7.367	7.482	6.422	6.510
AL4	0.729	0.584	0.079	0.560	0.484	0.923	0.633	0.518	1.578	1.490
AL6	0.239	0.198	0.070	0.269	0.274	0.490	0.387	0.365	0.804	0.814
TI	0.028	0.005	-	0.017	0.002	0.008	0.006	0.007	0.060	0.046
FE	1.505	1.552	1.366	1.359	1.627	1.672	1.522	1.570	1.912	1.901
MN	0.042	0.039	0.051	0.044	0.037	0.032	0.030	0.038	0.038	0.040
MG	3.287	3.301	3.504	3.350	3.131	2.901	3.068	3.044	2.304	2.294
CA	2.014	2.009	1.968	1.975	1.974	1.988	1.999	1.942	1.920	1.929
NA	0.153	0.150	0.046	0.206	0.089	0.175	0.170	0.163	0.513	0.475
K	0.056	0.023	0.007	0.025	0.031	0.062	0.042	0.041	0.067	0.065
STRUCTURAL FORMULA										
Z	8.00	8.00	8.00	8.00	8.00	8.00	8.00	8.00	8.00	8.00
Y	5.10	5.09	4.99	5.04	5.07	5.10	5.01	5.02	5.12	5.09
A+X	2.22	2.18	2.04	2.21	2.09	2.22	2.21	2.15	2.50	2.47

TABLE A3.8 SECONDARY AMPHIBOLES

	HB6E3	HB0A1A	HB0A1B	HB16A1	HB16A2	HB0KA1	HB05A2	HB4C1	HB4C2	HB29B1
WEIGHT % OXIDE										
SIO2	43.45	53.00	53.24	53.20	53.82	52.45	53.67	52.75	47.63	40.88
TIO2	0.38	0.06	0.05	-	-	0.04	-	0.06	0.29	0.87
AL203	13.91	3.08	2.76	2.62	2.32	3.40	2.76	3.68	7.20	13.14
FEO	15.54	14.30	14.52	11.66	9.15	12.75	11.31	11.64	15.37	18.66
MNO	0.35	0.31	0.37	0.26	0.23	0.38	0.30	0.35	0.36	0.38
MGO	10.43	13.68	13.79	16.32	17.86	14.65	16.43	15.48	12.65	8.23
CAO	11.99	12.41	12.62	12.82	13.15	13.44	12.59	12.70	12.71	12.22
NA20	1.72	0.32	0.23	0.35	0.33	0.41	0.40	0.36	0.79	1.27
K20	0.40	0.12	0.12	0.08	0.07	0.17	0.11	0.21	0.63	1.76
TOTAL	98.17	97.26	97.70	97.32	96.93	97.70	97.57	97.22	97.63	97.41
ATOMIC FORMULA - ON BASIS OF 23 OXYGENS										
SI	6.419	7.724	7.737	7.673	7.705	7.601	7.697	7.617	7.057	6.270
AL4	1.581	0.276	0.263	0.327	0.295	0.399	0.303	0.383	0.943	1.730
AL6	0.843	0.253	0.209	0.119	0.097	0.183	0.164	0.243	0.315	0.648
TI	0.042	0.006	0.006	-	-	0.005	-	0.006	0.033	0.100
FE	1.919	1.743	1.765	1.407	1.095	1.546	1.356	1.405	1.904	2.394
MN	0.044	0.038	0.046	0.032	0.028	0.047	0.037	0.043	0.046	0.049
MG	2.297	2.971	2.986	3.509	3.809	3.164	3.512	3.332	2.793	1.881
CA	1.899	1.938	1.966	1.981	2.018	2.067	1.935	1.964	2.018	2.008
NA	0.492	0.090	0.063	0.099	0.092	0.115	0.110	0.100	0.226	0.377
K	0.075	0.023	0.023	0.015	0.012	0.031	0.020	0.039	0.119	0.344
STRUCTURAL FORMULA										
Z	8.00	8.00	8.00	8.00	8.00	8.00	8.00	8.00	8.00	8.00
Y	5.14	5.01	5.01	5.07	5.03	4.94	5.07	5.03	5.09	5.07
A+X	2.47	2.05	2.05	2.09	2.12	2.23	2.06	2.10	2.36	2.73

TABLE A3.8 SECONDARY AMPHIBOLES

	HB2982	HB0M1	HB072	HB29A1	HB29A2	HB74B1	HB74B2	HB74B3	HB74B4	HB111
WEIGHT % OXIDE										
SIO2	41.61	50.67	50.61	43.58	43.96	51.42	49.98	47.43	41.99	51.24
TIO2	0.83	0.08	0.12	0.71	0.72	0.15	0.18	0.31	0.25	0.08
AL2O3	12.77	4.09	4.67	11.02	11.40	3.94	5.48	6.89	11.05	4.21
FEO	18.42	16.40	15.42	17.47	17.35	12.53	13.30	15.30	19.27	13.94
MNO	0.40	0.55	0.49	0.43	0.48	0.28	0.33	0.41	0.37	0.33
MGO	9.01	12.74	12.82	10.15	10.07	15.36	14.36	12.97	9.71	14.05
CAO	12.23	12.43	12.49	12.27	12.40	12.72	12.47	12.35	12.02	12.55
NA2O	1.29	0.29	0.38	0.99	0.98	0.47	0.59	0.76	1.59	0.50
K2O	1.51	0.20	0.14	1.14	1.26	0.19	0.32	0.31	1.22	0.16
TOTAL	98.07	97.45	97.15	97.76	98.61	97.07	97.00	96.74	97.46	97.05
ATOMIC FORMULA - ON BASIS OF 23 OXYGENS										
SI	6.315	7.490	7.465	6.566	6.560	7.491	7.328	7.077	6.439	7.509
AL4	1.685	0.510	0.535	1.434	1.440	0.581	0.672	0.923	1.561	0.491
AL6	0.601	0.204	0.278	0.524	0.566	0.169	0.277	0.288	0.436	0.236
TI	0.095	0.009	0.014	0.081	0.081	0.017	0.020	0.035	0.030	0.008
FE	2.338	2.027	1.902	2.201	2.165	1.527	1.631	1.909	2.471	1.709
MN	0.051	0.069	0.061	0.055	0.061	0.034	0.041	0.052	0.048	0.041
MG	2.038	2.807	2.818	2.278	2.239	3.336	3.138	2.884	2.220	3.068
CA	1.989	1.969	1.975	1.980	1.983	1.986	1.959	1.974	1.975	1.971
NA	0.380	0.083	0.109	0.290	0.283	0.134	0.168	0.221	0.473	0.142
K	0.293	0.037	0.027	0.220	0.241	0.036	0.060	0.060	0.238	0.030
STRUCTURAL FORMULA										
Z	8.00	8.00	8.00	8.00	8.00	8.00	8.00	8.00	8.00	8.00
Y	5.12	5.11	5.07	5.14	5.11	5.28	5.11	5.17	5.20	5.06
A+X	2.06	2.09	2.11	2.49	2.51	2.16	2.19	2.25	2.69	2.14

TABLE A3.8 SECONDARY AMPHIBOLES

	HB881	HB882	HB581	HB582	HB583	HB1681	HB1682	HB1683
WEIGHT % OXIDE								
SIO2	48.07	46.80	52.64	47.01	51.86	52.98	54.47	54.43
TIO2	0.12	0.23	0.36	0.34	0.12	-	0.02	0.07
AL2O3	6.38	8.94	3.48	8.64	4.20	2.91	1.90	1.99
CR2O3	0.13	-	0.02	0.02	0.05	0.10	0.17	0.13
FEO	15.11	14.09	7.31	10.55	6.60	9.58	8.60	9.05
MNO	0.35	0.30	0.27	0.28	0.22	0.33	0.24	0.27
NIO	0.16	-	0.04	0.05	0.01	-	-	0.02
MGO	12.95	12.62	19.65	15.71	19.42	17.11	18.29	18.35
CAO	12.55	12.54	13.04	13.25	13.46	12.79	12.69	12.81
NA2O	0.57	1.03	0.55	1.30	0.53	0.31	0.35	0.31
K2O	0.23	0.30	0.14	0.64	0.16	0.21	0.08	0.04
TOTAL	96.64	96.84	97.49	97.79	96.65	96.32	96.80	97.47
ATOMIC FORMULA - ON BASIS OF 23 OXYGENS								
SI	7.166	6.934	7.462	6.834	7.404	7.656	7.774	7.735
AL4	0.834	1.066	0.538	1.166	0.596	0.344	0.226	0.265
AL6	0.288	0.497	0.044	0.316	0.112	0.152	0.093	0.069
CR	0.016	0.000	0.002	0.003	0.006	0.012	0.019	0.014
TI	0.013	0.025	0.039	0.037	0.013	0.000	0.002	0.008
FE	1.883	1.746	0.867	1.282	0.788	1.158	1.026	1.076
MN	0.044	0.037	0.032	0.034	0.026	0.040	0.029	0.032
TI	0.019	0.000	0.005	0.006	0.002	0.000	0.000	0.002
MG	2.878	2.787	4.151	3.403	4.133	3.686	3.889	3.886
CA	2.005	1.991	1.980	2.063	2.039	1.980	1.940	1.950
NA	0.165	0.295	0.151	0.367	0.147	0.086	0.096	0.086
K	0.044	0.057	0.025	0.119	0.028	0.039	0.015	0.008
STRUCTURAL FORMULA								
Z	8.00	8.00	8.00	8.00	8.00	8.00	8.00	8.00
Y	5.14	5.09	5.14	5.08	5.08	5.05	5.06	5.09
A+x	2.21	2.34	2.16	2.55	2.21	2.10	2.05	2.04

TABLE A3.8 SECONDARY AMPHIBOLES

	HB112
WEIGHT % OXIDE	
SIO2	51.47
TIO2	0.06
AL203	4.30
FEO	13.26
MNO	0.32
MGO	14.75
CAO	12.50
NA2O	0.51
K2O	0.16
TOTAL	97.34
ATOMIC FORMULA - ON BASIS OF 23 OXYGENS	
SI	7.493
AL4	0.507
AL6	0.232
TI	0.006
FE	1.615
MN	0.040
MG	3.200
CA	1.951
NA	0.145
K	0.030
STRUCTURAL FORMULA	
Z	8.00
Y	5.09
A+X	2.13

TABLE A3.9 SECONDARY BIOTITES

	BI881	BI6B1	BI6B2	BI5B1	BI5B2	BI11B1	BI4B1 *	BU4B2 *	BI6A1	BI6A2
WEIGHT % OXIDE										
SIO2	36.47	37.77	38.96	38.83	39.65	38.83	37.31	36.82	37.23	37.81
TIO2	1.40	1.07	1.04	0.70	0.71	0.74	1.05	1.10	0.87	0.95
AL2O3	16.67	15.00	14.76	14.88	15.10	15.28	16.15	16.34	15.20	15.06
FEO	18.79	16.19	14.91	14.27	13.52	14.60	17.54	17.58	15.80	15.85
MNO	0.28	0.23	0.17	0.31	0.22	0.08	N.A.	N.A.	0.24	0.21
MGO	11.56	14.81	14.64	16.72	16.61	14.89	13.55	13.45	14.62	14.18
CAO	0.06	0.23	0.19	0.10	0.13	0.02	N.A.	N.A.	0.04	0.06
NA2O	0.01	0.01	0.01	-	0.11	-	N.A.	N.A.	0.11	0.11
K2O	9.32	8.72	9.41	10.30	10.16	9.89	9.71	9.70	9.67	9.20
TOTAL	94.55	94.02	94.08	96.21	96.25	94.33	95.31	94.98	93.77	93.43
ATOMIC FORMULA - ON BASIS OF 22 OXYGENS										
SI	5.582	5.719	5.861	5.737	5.812	5.827	5.628	5.582	5.682	5.765
AL4	2.418	2.281	2.139	2.263	2.188	2.173	2.372	2.418	2.318	2.235
AL6	0.591	0.398	0.480	0.329	0.422	0.531	0.502	0.503	0.418	0.473
TI	0.161	0.121	0.117	0.077	0.078	0.084	0.119	0.125	0.099	0.109
FE	2.403	2.050	1.875	1.764	1.658	1.832	2.213	2.229	2.016	2.020
MN	0.036	0.029	0.022	0.038	0.027	0.011	-	-	0.031	0.027
MG	2.637	3.341	3.283	3.682	3.629	3.330	3.246	3.039	3.324	3.222
CA	0.010	0.037	0.031	0.015	0.020	0.003	-	-	0.006	0.010
NA	0.002	0.003	0.003	-	0.031	-	-	-	0.032	0.033
K	1.820	1.684	1.806	1.912	1.901	1.894	1.869	1.875	1.883	1.789
STRUCTURAL FORMULA										
Z	8.00	8.00	8.00	8.00	8.00	8.00	8.00	8.00	8.00	8.00
Y	5.83	5.94	5.78	5.89	5.81	5.79	5.88	5.90	5.89	5.85
X	1.83	1.72	1.84	1.96	1.95	1.90	1.87	1.88	1.92	1.83

TABLE A3.9 SECONDARY BIOTITES

	BI0A1	BI0A2	BI05A1	BI29B1	B14C1	BI74B1	BI74B2	BI11	BI12
WEIGHT % OXIDE									
SIO2	36.64	36.70	37.94	37.19	37.44	36.64	36.69	36.03	36.24
TIO2	0.88	0.90	1.29	1.65	1.01	1.57	1.41	0.83	0.63
AL203	15.90	16.01	14.70	15.89	16.18	15.55	15.67	15.99	15.98
FEO	19.59	19.29	15.62	18.00	16.79	17.32	17.21	18.82	18.84
MNO	0.29	0.22	0.21	0.28	0.23	0.23	0.22	0.26	0.37
MGO	11.24	11.03	13.96	12.04	13.87	13.60	13.55	12.27	12.39
CAO	0.03	0.02	0.12	0.06	0.03	0.06	0.08	0.07	0.06
NA2O	-	-	-	0.04	0.01	0.11	0.11	0.01	0.06
K2O	9.44	10.20	9.93	9.53	9.71	9.62	9.60	10.09	10.00
TOTAL	94.01	94.36	93.76	94.68	95.26	94.70	94.54	94.36	94.57
ATOMIC FORMULA - ON BASIS OF 22 OXYGENS									
SI	5.670	5.672	5.782	5.666	5.635	5.582	5.594	5.568	5.585
AL4	2.330	2.322	2.218	2.334	2.365	2.418	2.406	2.432	2.415
AL6	0.572	0.596	0.425	0.522	0.508	0.377	0.411	0.483	0.491
TI	0.103	0.105	0.148	0.189	0.115	0.179	0.162	0.096	0.073
FE	2.535	2.493	1.991	2.294	2.114	2.207	2.194	2.433	2.428
MN	0.038	0.029	0.027	0.037	0.029	0.029	0.028	0.034	0.049
MG	2.592	2.540	3.172	2.735	3.111	3.088	3.079	2.826	2.846
CA	0.005	0.004	0.020	0.009	0.005	0.010	0.014	0.011	0.010
NA	-	-	-	0.013	0.003	0.032	0.031	0.004	0.018
K	1.863	2.010	1.931	1.852	1.864	1.870	1.867	1.990	1.966
STRUCTURAL FORMULA									
Z	8.00	8.00	8.00	8.00	8.00	8.00	8.00	8.00	8.00
Y	5.84	5.77	5.76	5.78	5.88	5.88	5.87	5.87	5.89
X	1.87	2.01	1.95	1.87	1.87	1.91	1.91	2.00	1.99

TABLE A3.10 CHLORITES

	* CH381	* CH382	CH75B1	CH75B2	CH881	CH882	CH11B1	CH361	* CH581	* CH582
WEIGHT % OXIDE										
SIO2	26.56	26.16	27.55	27.57	25.83	28.82	28.80	26.80	28.31	28.56
TIO2	-	N.A.	0.02	0.05	0.09	0.29	-	0.03	N.A.	N.A.
AL2O3	17.58	17.71	19.79	18.95	20.23	18.47	17.51	15.42	18.10	17.88
FEO	27.77	27.96	13.73	15.07	22.36	23.94	15.81	30.65	21.69	21.30
MNO	-	N.A.	0.39	0.37	0.39	0.39	0.17	0.39	N.A.	N.A.
MGO	15.34	15.57	23.73	23.36	17.56	15.50	24.11	11.68	19.37	19.35
CAO	-	-	0.43	0.10	0.10	0.09	0.02	0.15	N.A.	N.A.
NA2O	-	N.A.	0.03	-	N.A.	-	-	0.02	N.A.	N.A.
K2O	-	N.A.	0.01	0.53	0.03	0.11	-	0.03	N.A.	N.A.
TOTAL	87.24	87.40	85.68	86.00	86.53	87.58	86.26	85.18	87.46	87.08
ATOMIC PROPORTIONS - ON BASIS OF 28 OXYGENS										
SI	5.706	5.624	5.593	5.639	5.442	6.008	5.859	6.022	5.845	5.906
AL4	2.294	2.376	2.407	2.362	2.558	1.992	2.141	1.978	2.155	2.094
AL6	2.159	2.115	2.332	2.210	2.469	2.549	2.023	2.111	2.251	2.267
FE	4.992	5.028	2.332	2.578	3.939	4.173	2.690	5.760	3.744	3.683
MN	0.000	0.000	0.067	0.064	0.069	0.068	0.029	0.075	0.000	0.000
MG	4.914	4.987	7.182	7.119	5.512	4.815	7.312	3.911	5.958	5.963
CA	0.000	0.000	0.094	0.022	0.022	0.021	0.004	0.037	0.000	0.000
NA	0.000	0.000	0.010	0.000	0.000	0.000	0.000	0.010	0.000	0.000
K	0.000	0.000	0.003	0.139	0.008	0.030	0.000	0.010	0.000	0.000
TI	0.000	0.000	0.003	0.007	0.015	0.041	0.000	0.005	0.000	0.000
STRUCTURAL FORMULA										
Z	8.00	8.00	8.00	8.00	8.00	8.00	8.00	8.00	8.00	8.00
Y	12.06	12.13	12.02	12.14	12.03	11.70	12.06	11.92	11.95	11.91

TABLE A3.10 CHLORITES

	* CH481	* CH4B2	* CH131	* CH101	* CH102	CH6E1	CH4C1	CH29A1	CH29A2	CH541
WEIGHT % OXIDE										
SIO2	26.35	26.34	26.69	28.62	26.72	26.16	26.45	26.25	26.55	28.35
TIO2	N.A.	N.A.	N.A.	N.A.	N.A.	0.02	0.03	0.04	0.04	0.05
AL203	20.02	20.19	18.76	14.45	17.29	19.45	19.74	18.27	18.85	16.92
FEO	20.47	20.95	28.68	31.63	32.13	20.82	19.36	23.86	23.66	22.26
MNO	N.A.	N.A.	N.A.	N.A.	0.49	0.27	0.30	0.47	0.49	0.32
MGO	19.83	19.87	14.52	13.81	12.69	17.97	20.64	17.04	17.20	17.59
CAO	N.A.	N.A.	N.A.	N.A.	N.A.	-	0.04	0.08	0.03	0.28
NA20	N.A.	N.A.	N.A.	N.A.	N.A.	-	-	-	-	N.A.
K20	N.A.	N.A.	N.A.	N.A.	N.A.	0.01	0.01	N.A.	N.A.	N.A.
TOTAL	86.66	87.35	88.64	88.52	89.32	84.70	86.57	86.03	86.85	85.76
ATOMIC PROPORTIONS - ON BASIS OF 28 OXYGENS										
SI	5.474	5.441	5.653	6.172	5.745	5.584	5.482	5.623	5.613	6.009
AL4	2.536	2.559	2.347	1.828	2.255	2.416	2.518	2.377	2.387	1.991
AL6	2.379	2.361	2.339	1.848	2.130	2.479	2.307	2.237	2.322	2.230
FE	3.557	3.620	5.080	5.705	5.778	3.716	2.355	4.274	4.183	3.945
MN	0.000	0.000	0.000	0.000	0.000	0.050	0.053	0.086	0.088	0.057
MG	6.139	6.119	4.585	4.438	4.068	5.716	6.373	5.440	5.419	5.557
CA	0.000	0.000	0.000	0.000	0.000	0.000	0.010	0.019	0.008	0.064
NA	0.000	0.000	0.000	0.000	0.000	0.000	0.000	0.000	0.000	0.000
K	0.000	0.000	0.000	0.000	0.000	0.004	0.002	0.000	0.000	0.000
TI	0.000	0.000	0.000	0.000	0.000	0.003	0.005	0.007	0.006	0.008
STRUCTURAL FORMULA										
Z	8.00	8.00	8.00	8.00	8.00	8.00	8.00	8.00	8.00	8.00
Y	12.07	12.10	12.00	11.99	12.07	11.97	12.10	12.06	12.03	11.87

TABLE A3.10 CHLORITES

CH441

WEIGHT % OXIDE

SIO2	28.49
TIO2	0.01
AL2O3	18.71
FEO	22.74
MNO	0.15
MGO	15.68
CAO	0.18
NA2O	N.A.
K2O	N.A.
TOTAL	87.06

ATOMIC PROPORTIONS - ON BASIS OF 28 OXYGENS

SI	6.136
AL4	1.864
AL6	2.892
FE	4.095
MN	0.027
MG	5.032
CA	0.410
NA	0.000
K	0.000
TI	0.003

STRUCTURAL FORMULA

Z	8.00
Y	12.09

TABLE A3.11 EPIDOTES

	EP6A1A	EP6A1B	EP6A2	EP0A1	EP0A2	EP29B1	EP29B2	EP381 *	EP382 *	EP881
WEIGHT % OXIDE										
SIO2	37.10	36.73	37.22	38.39	38.40	37.57	38.31	37.42	37.73	37.65
TIO2	0.04	0.03	0.05	0.10	0.07	0.13	0.12	N.A.	N.A.	0.06
AL203	22.81	21.70	22.90	26.93	26.27	24.65	24.92	21.41	22.22	26.54
FE203	13.51	14.87	14.07	7.90	8.53	10.81	10.72	15.71	15.54	8.73
MNO	0.21	0.17	0.23	0.15	0.19	0.15	0.13	N.A.	N.A.	0.12
MGO	0.01	0.02	0.04	0.03	0.03	0.02	0.04	N.A.	N.A.	0.06
CAO	23.71	23.40	23.73	23.34	23.55	23.68	23.94	23.71	23.86	23.97
NA20	-	-	N.A.	N.A.	N.A.	-	-	N.A.	N.A.	-
K20	-	N.A.	N.A.	N.A.	N.A.	0.01	0.01	N.A.	N.A.	0.01
TOTAL	97.39	96.92	98.24	96.84	97.04	97.02	98.19	98.25	99.35	97.13
ATOMIC PROPORTIONS - ON BASIS OF 25 OXYGENS										
SI	5.966	5.966	5.942	6.049	6.059	5.995	5.008	6.002	5.975	5.958
AL4	0.034	0.034	0.058	0.000	0.000	0.005	0.000	0.000	0.025	0.042
AL6	4.492	4.123	4.254	5.004	4.889	4.634	4.609	4.050	4.125	4.907
FE	1.635	1.818	1.690	0.937	1.013	1.298	1.329	1.896	1.852	1.039
MN	0.029	0.023	0.031	0.020	0.025	0.020	0.017	0.000	0.000	0.017
MG	0.002	0.005	0.010	0.007	0.007	0.005	0.009	0.000	0.000	0.013
CA	4.086	4.072	4.059	3.940	3.981	4.049	4.023	4.075	4.048	4.064
NA	0.000	0.000	0.000	0.000	0.000	0.000	0.000	0.000	0.000	0.000
K	0.000	0.000	0.000	0.000	0.000	0.002	0.002	0.000	0.000	0.002
TI	0.005	0.004	0.006	0.012	0.008	0.016	0.014	0.000	0.000	0.007
STRUCTURAL FORMULA										
Z	6.00	6.00	6.00	6.05	6.06	6.00	5.01	6.00	6.00	6.00
Y	5.93	5.94	5.94	5.94	5.90	5.97	5.98	5.97	5.98	5.95
X	4.12	4.10	4.11	3.98	4.02	4.05	4.02	4.07	4.05	4.11

TABLE A3.11 EPIDOTES

	EP882	EP0181	EP0182	EP1181	EP1182	EP6B1	EP6B2	EP5B1	EP4B1 *	EP4B2 *
WEIGHT % OXIDE										
SIO2	37.85	38.19	38.17	37.28	37.16	37.03	37.22	36.73	38.03	37.70
TIO2	0.12	0.03	0.05	0.19	0.02	0.10	0.09	0.03	N.A.	N.A.
AL203	26.12	27.19	26.22	21.99	22.47	21.88	21.61	22.20	22.66	23.49
FE203	9.04	7.35	7.78	14.39	14.53	15.41	15.95	14.76	14.11	14.13
MNO	0.17	0.13	0.17	0.06	0.07	0.28	0.28	0.15	N.A.	N.A.
MGO	0.08	0.01	0.01	0.02	0.02	0.06	0.05	0.06	N.A.	N.A.
CAO	23.40	22.92	23.44	23.03	23.20	22.61	22.18	23.44	23.41	24.12
NA20	-	-	-	-	0.03	-	-	-	N.A.	N.A.
K20	0.01	-	-	-	-	-	0.01	0.04	N.A.	N.A.
TOTAL	96.79	95.83	95.84	96.96	97.50	97.37	97.09	97.58	98.21	99.44
ATOMIC PROPORTIONS										
SI	5.994	6.062	6.084	6.024	5.974	5.981	6.010	5.926	6.050	5.937
AL4	0.006	0.000	0.000	0.000	0.026	0.019	0.000	0.074	0.000	0.063
AL6	4.872	5.086	4.927	4.188	4.233	4.309	4.058	4.150	4.251	4.299
FE	1.067	0.878	0.933	1.749	1.758	1.874	1.915	1.791	1.689	1.675
MN	0.023	0.017	0.022	0.009	0.010	0.038	0.038	0.020	0.000	0.000
MG	0.019	0.003	0.003	0.006	0.004	0.015	0.012	0.015	0.000	0.000
CA	3.971	3.896	4.003	3.988	3.998	3.913	3.838	4.052	3.399	4.070
NA	0.000	0.000	0.000	0.000	0.001	0.000	0.000	0.000	0.000	0.000
K	0.002	0.000	0.000	0.000	0.001	0.001	0.002	0.008	0.000	0.000
TI	0.014	0.004	0.006	0.023	0.003	0.007	0.011	0.004	0.000	0.000
STRUCTURAL FORMULA										
Z	6.00	6.06	6.08	6.02	6.00	6.00	6.01	6.00	6.05	6.00
Y	5.94	5.96	5.86	5.95	5.99	6.18	5.97	5.94	5.94	5.97
X	4.03	3.92	4.03	4.03	4.02	3.98	3.90	4.10	3.99	4.07

TABLE A3.11 EPIDOTES

	EP3A1	EP541	EP441	EP431
WEIGHT % OXIDE				
SIO2	37.66	37.69	37.77	37.49
TIO2	0.04	0.02	0.03	0.01
AL203	22.30	23.00	22.14	22.19
FE203	14.73	12.51	13.68	14.18
MNO	0.10	N.A.	N.A.	N.A.
MGO	-	0.22	0.10	0.04
CAO	22.79	22.98	22.90	22.14
NA2O	0.01	0.07	0.31	N.A.
K2O	-	N.A.	N.A.	N.A.
TOTAL	97.45	96.47	96.93	96.41
ATOMIC PROPORTIONS ON BASIS OF 25 OXYGENS				
SI	6.036	6.015	6.085	6.063
AL4	0.000	0.000	0.000	0.000
AL6	4.215	4.329	4.207	4.233
FE	1.777	1.660	1.659	1.718
MN	0.016	0.000	0.000	0.000
MG	0.000	0.000	0.024	0.096
CA	3.914	3.930	3.953	3.837
NA	0.003	0.022	0.097	0.000
K	0.000	0.000	0.000	0.000
TI	0.005	0.002	0.004	0.001
STRUCTURAL FORMULA				
Z	6.04	6.01	6.08	6.06
Y	5.99	6.03	5.89	6.06
X	3.94	3.95	4.05	3.84

TABLE A3.12 SECONDARY FELDSPARS

	FL161 *	FL162 *	FL163 *	FL164 *	FL165 *	FL491	FL74B1	FL9A1	FL9A2	FL4C1
WEIGHT % OXIDE										
SIO2	63.17	51.85	55.92	51.91	52.55	52.43	68.15	58.71	57.74	60.82
AL2O3	21.37	28.15	24.99	28.15	27.97	28.94	20.32	25.74	26.52	24.31
FEO	N.A.	0.06	1.01	0.75	0.71	0.86	N.A.	0.17	0.11	N.A.
CAO	3.50	12.71	7.74	12.30	12.20	12.25	1.02	8.10	8.11	6.05
NA2O	9.76	4.64	5.28	4.58	4.97	4.50	11.11	7.16	7.20	7.46
K2O	N.A.	N.A.	1.96	0.37	N.A.	0.16	N.A.	0.18	0.14	0.10
TOTAL	97.81	98.30	96.91	98.07	98.40	99.13	100.60	99.78	99.82	98.74
ATOMIC FORMULA - ON BASIS OF 8 OXYGENS										
SI	2.849	2.406	2.608	2.413	2.429	2.406	2.961	2.631	2.591	2.727
AL	1.136	1.541	1.374	1.543	1.525	1.566	1.041	1.360	1.404	1.286
FE	0.000	0.037	0.039	0.029	0.028	0.033	0.000	0.007	0.004	0.000
CA	0.169	0.632	0.387	0.612	0.604	0.602	0.048	0.375	0.390	0.291
NA	0.854	0.417	0.478	0.413	0.446	0.400	0.936	0.622	0.627	0.648
K	0.000	0.000	0.467	0.022	0.000	0.009	0.000	0.010	0.008	0.006
MOLECULAR PROPORTIONS										
AN	16.54	60.22	39.42	58.45	57.55	59.52	4.82	37.24	38.06	30.77
AB	83.46	39.78	48.68	39.43	42.44	39.57	95.18	61.76	61.17	68.62
OR	-	-	11.91	2.12	-	0.90	-	1.00	0.77	0.61

TABLE A3.12 SECONDARY FELDSPARS

	FL0A1	FL0A2	FL5A1	FL5A2	FL8B1	FL8B2	FL8B3	FL071	FL111	FL6E1
WEIGHT % OXIDE										
SIO2	67.83	67.39	67.57	68.17	68.05	65.27	64.90	62.88	67.02	68.09
AL203	19.58	20.05	20.05	20.33	20.30	19.06	18.45	18.94	19.89	19.84
FEO	N.A.	N.A.	N.A.	N.A.	N.A.	N.A.	N.A.	N.A.	0.10	N.A.
CAO	0.44	0.49	0.56	0.27	0.87	0.12	0.03	0.03	0.76	0.09
NA20	11.70	11.61	11.64	12.20	11.51	0.25	0.21	1.21	11.30	11.80
K20	0.08	0.07	0.06	0.05	0.07	15.91	16.15	14.79	0.06	0.03
TOTAL	99.92	99.61	99.88	101.04	100.79	100.61	99.74	97.86	99.14	99.85
ATOMIC FORMULA - ON BASIS OF 8 OXYGENS										
SI	2.970	2.961	2.961	2.957	2.956	2.988	3.001	2.961	2.960	2.980
AL	1.027	1.039	1.037	1.040	1.040	1.029	1.007	1.052	1.036	1.024
FE	0.000	0.000	0.000	0.000	0.000	0.000	0.000	0.000	0.004	0.000
CA	0.021	0.023	0.026	0.013	0.041	0.006	0.002	0.001	0.036	0.004
NA	0.993	0.989	0.989	1.026	0.969	0.022	0.019	0.111	0.968	1.001
K	0.004	0.004	0.004	0.003	0.004	0.929	0.953	0.888	0.003	0.002
MOLECULAR PROPORTIONS										
AN	2.05	2.26	2.57	1.22	4.00	0.61	0.17	0.15	3.58	0.43
AB	97.52	97.34	97.08	98.51	95.64	2.31	1.92	11.06	96.08	99.41
OR	0.44	0.40	0.35	0.28	0.36	97.08	97.91	88.79	0.34	0.16

TABLE A3.12 SECONDARY FELDSPARS

	FL6E2	FL6E3	FL9B1	FL9B2
WEIGHT % OXIDE				
SIO2	67.64	68.81	57.11	57.07
AL2O3	20.64	19.81	27.22	27.13
FEO	N.A.	N.A.	N.A.	N.A.
CAO	0.36	0.35	9.09	9.65
NA2O	11.75	11.76	4.91	5.16
K2O	0.07	0.04	0.09	0.13
TOTAL	100.47	100.77	99.02	99.14
ATOMIC FORMULA - ON BASIS OF 8 OXYGENS				
SI	2.947	2.984	2.573	2.571
AL	1.061	1.013	1.446	1.442
FE	0.000	0.000	0.000	0.000
CA	0.017	0.016	0.468	0.466
NA	0.993	0.989	0.429	0.451
K	0.004	0.002	0.005	0.007
MOLECULAR PROPORTIONS				
AN	1.67	1.63	51.84	50.45
AB	97.97	98.14	47.56	48.77
OR	0.37	0.23	0.60	0.78

TABLE A3.13 SECONDARY MAGNETITES

	MG 74B	MG 5A1	MG5A3	MG491	MG492	MG5B1	MG771	MG5A2	MG3A1	MG3A2
WEIGHT % OXIDE										
SIO2	0.23	2.36	0.76	0.18	0.14	N.A.	N.A.	0.97	0.67	0.44
TIO2	0.08	4.21	1.58	0.12	0.26	0.21	0.08	0.14	0.11	0.21
AL203	0.16	0.35	0.32	0.27	0.11	N.A.	N.A.	0.43	0.15	0.16
CR203	N.A.	N.A.	0.98	0.24	0.25	0.51	N.A.	0.78	1.81	4.33
FE203	68.32	55.53	63.39	67.36	68.19	67.71	68.72	64.61	64.73	63.09
FEO	31.13	33.99	33.31	31.01	31.37	30.81	30.79	31.81	31.24	31.42
MNO	0.20	-	0.27	0.21	0.26	0.26	0.27	0.28	0.30	0.33
MGO	0.02	0.08	0.16	0.01	0.02	N.A.	N.A.	0.12	0.20	0.12
CAO	0.14	3.35	N.A.	N.A.	N.A.	N.A.	N.A.	N.A.	N.A.	N.A.
TOTAL	100.30	99.89	100.75	99.39	100.62	99.50	99.86	99.13	99.22	100.10
ATOMIC FORMULA										
SI	0.072	0.708	0.230	0.054	0.043	0.000	0.000	0.298	0.208	0.135
TI	0.019	0.951	0.360	0.028	0.060	0.048	0.020	0.032	0.026	0.047
AL	0.060	0.124	0.116	0.097	0.039	0.000	0.000	0.158	0.056	0.057
CR	0.000	0.000	0.235	0.060	0.062	0.125	0.000	0.191	0.442	1.048
FE3	15.760	12.556	14.471	15.679	15.694	15.780	15.962	14.991	15.034	14.532
FE2	7.981	8.542	8.450	8.022	8.024	7.980	7.950	8.203	8.066	8.043
MN	0.052	0.000	0.069	0.054	0.069	0.068	0.070	0.074	0.078	0.086
MG	0.011	0.037	0.071	0.066	0.010	0.000	0.000	0.053	0.091	0.053
CA	0.046	1.079	0.000	0.000	0.000	0.000	0.000	0.000	0.000	0.000

TABLE A3.14 PREHNITES

	PR631	PR632
WEIGHT % OXIDE		
SIO2	42.56	43.31
AL2O3	23.77	23.04
FEO	1.09	1.48
MGO	0.33	0.22
CAO	26.64	26.59
NA2O	0.11	0.13
K2O	0.05	0.04
TOTAL	94.55	94.82
ATOMIC FORMULA - ON BASIS OF 22 OXYGENS		
SI	5.954	6.046
AL	3.922	3.792
FE	0.128	0.173
MG	0.069	0.047
CA	3.993	3.978
NA	0.030	0.036
K	0.008	0.007

APPENDIX 4

OXYGEN ISOTOPE ANALYSIS

A4:1 Oxygen extraction

Separation of minerals was first carried out using conventional heavy liquids and magnetic techniques. It was possible to separate the minerals pyroxene, magnetite, amphibole (secondary), feldspar and epidote, from some samples, to the required purity of 95% or greater. This was tested for by X-ray diffraction and optical examination.

Oxygen extraction from whole-rocks and silicate or oxide minerals was achieved using the BrF_5 method of Clayton & Mayeda (1963). In this system, about 10-20 milligrams of finely crushed sample are loaded in Ni reaction vessels, and reacted with excess BrF_5 for 12-15 hours at 500-600^{o}C. When the reaction is complete, oxygen is reacted with pure carbon to form CO_2 (Taylor & Epstein, 1962) and the volume of gas measured by a manometer. In this way, the oxygen yield can be calculated to check for any incompleteness of reaction or leakage. The CO_2 gas is then sealed in a glass tube to await mass spectrometric analysis. Carbon dioxide from calcite was liberated by reacting a whole-rock aliquot with 100% phosphoric acid at 25.4^{o}C for 24 hours (McCrea, 1950). In this method, only two-thirds of the oxygen bound in $CaCO_3$ is released as CO_2, but knowledge of the isotopic fractionation for the reaction allows correction for the isotopic shift in CO_2 composition.

A4:2 $^{18}O/^{16}O$ ratio determination

The $^{18}O/^{16}O$ ratio, and $\delta^{18}O$ value (Chapter 8), is obtained by analysing the CO_2 gas by mass spectrometer. These determinations

were carried out for the writer by Dr. K. Muehlenbachs, since no mass spectrometer was available in 1975 when the writer visited the University of Alberta. The type of machine used is a 60^{o} sector, dual gas feed and double collecting mass spectrometer as described by McKenney et al. (1950). This allows simultaneous comparison of sample and standard (SMOW) to be made, resulting in high precision. Since CO_2 and not oxygen gas is measured, corrections are made for ^{13}C, as well as mass-44 tail effects and valve mixing (Craig, 1957).

The analyses made are tabulated in Table 8.1. These all gave quantitative oxygen yields. Accuracy, as determined from analyses of standards (with good oxygen yields), is estimated to be about $\pm$ $0.3^{o}/oo$. This is adequate for the purposes of this study.

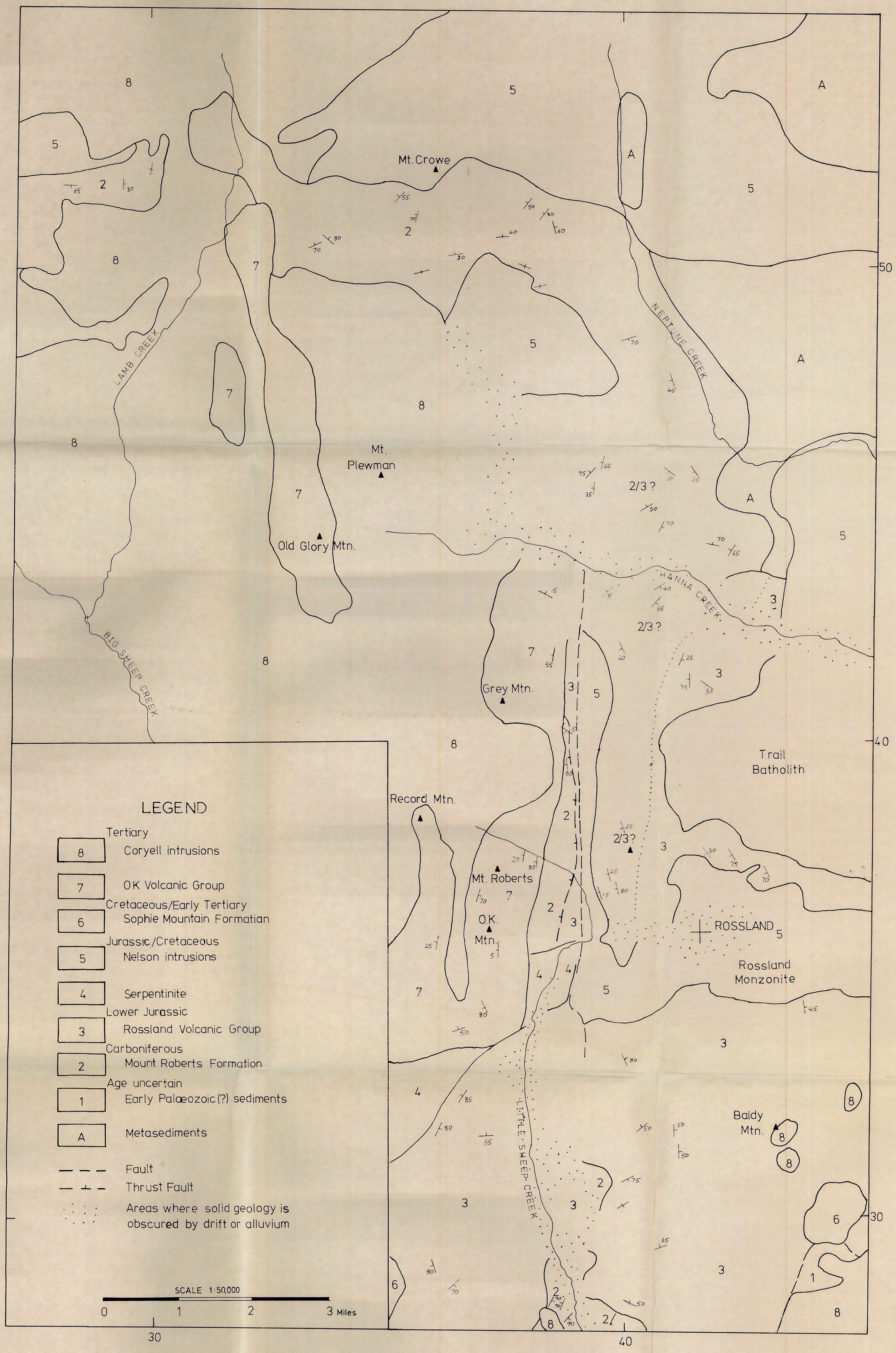

FIG. 1.1 (SHEET 2).

GEOLOGY OF THE ROSSLAND AREA, B.C.

(Based on G S C Map 23-1963 and B.C. Dept. of Mines & Petroleum Resources Prelim. Map no. 4.)

FIG. 1.1 (SHEET 1).

GEOLOGY OF THE SALMO AREA, SOUTHERN BRITISH COLUMBIA.

(Based on G.S.C. maps 1145A, 1144A, 52-13A, 62-2A)

Legend

CENOZOIC

Tertiary

- 10 — CORYELL PLUTONIC ROCKS
- 9 — SHEPPARD PLUTONIC ROCKS

MESOZOIC

Upper Jurassic and Cretaceous

- 8 — NELSON PLUTONIC ROCKS (a 'Pseudodiorite'; b Syenite; c Pyroxenite; d Silver King Porphyry)
- 7 — ROSSLAND MONZONITE

Middle and (?) Upper Jurassic

- 6 — UPPER ROSSLAND GROUP

Lower and Middle Jurassic

- 5 — HALL FORMATION

Lower Jurassic

- 4 — ELISE FORMATION / ROSSLAND VOLCANIC GROUP
- 3 — ARCHIBALD FORMATION

Lower Jurassic and (?) Upper Triassic

- 2 — YMIR GROUP

PALAEOZOIC AND OLDER

- 1 — PRE-MESOZOIC ROCKS
- A — METASEDIMENTS

Bedding (inclined, vertical)

Fault

Thrust fault (tick on downdip side)

Geological boundary

Rivers, lakes

Town

Sample location

Area where solid geology is obscured by drift

One Thousand Metre Universal Transverse Mercator Grid zone = 11 — 100,000 m Square identification = ME

SCALE 1:50000

0 1 2 3 Miles

70 80 90

80 70 60 50 40

50 60 70 80 90

KOOTENAY L. — NELSON — KOOTENAY RIVER — HALL CREEK — SALMO RIVER — EERIE CREEK — ARCHIBALD CREEK — HELLROARING CREEK — COLUMBIA RIVER — KELLY CREEK — BEAVER CREEK — PEND D'OREILLE

Toad Mtn. — Mt. Elise — Dominion Mtn. — Keystone Mtn. — Eerie Mtn. — Mt. Kelly — Blizzard Mtn. — Lake Mtn.

YMIR — SALMO — PARKS — FRUITVALE — TRAIL — Champion Lakes

5430 000 mN

450 000 mE.